

Tracking Orai1, Adenylyl Cyclase Type 8, and STIM1 Activity in Triple Negative Breast Cancer

Tiffany Au¹, Moana Hala'ufia², and David L. Roman²

¹Diamond Bar High School, ²Department of Pharmaceutical Sciences and Experimental Therapeutics

Introduction

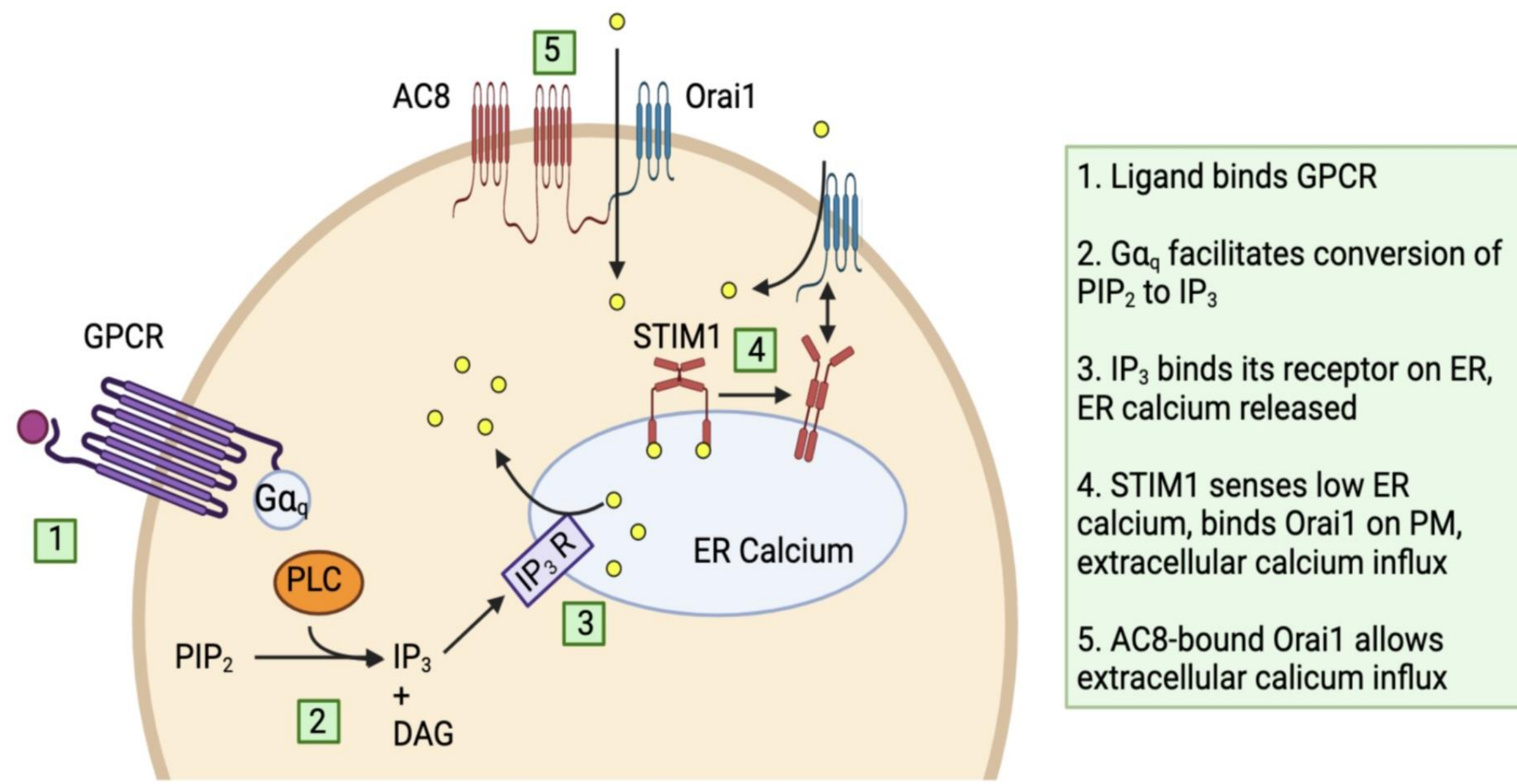


Figure 1: Store Operated Calcium Entry. STIM1 senses calcium depletion in ER and activates Orai1. Interaction between AC8 and Orai1 leads to calcium influx.

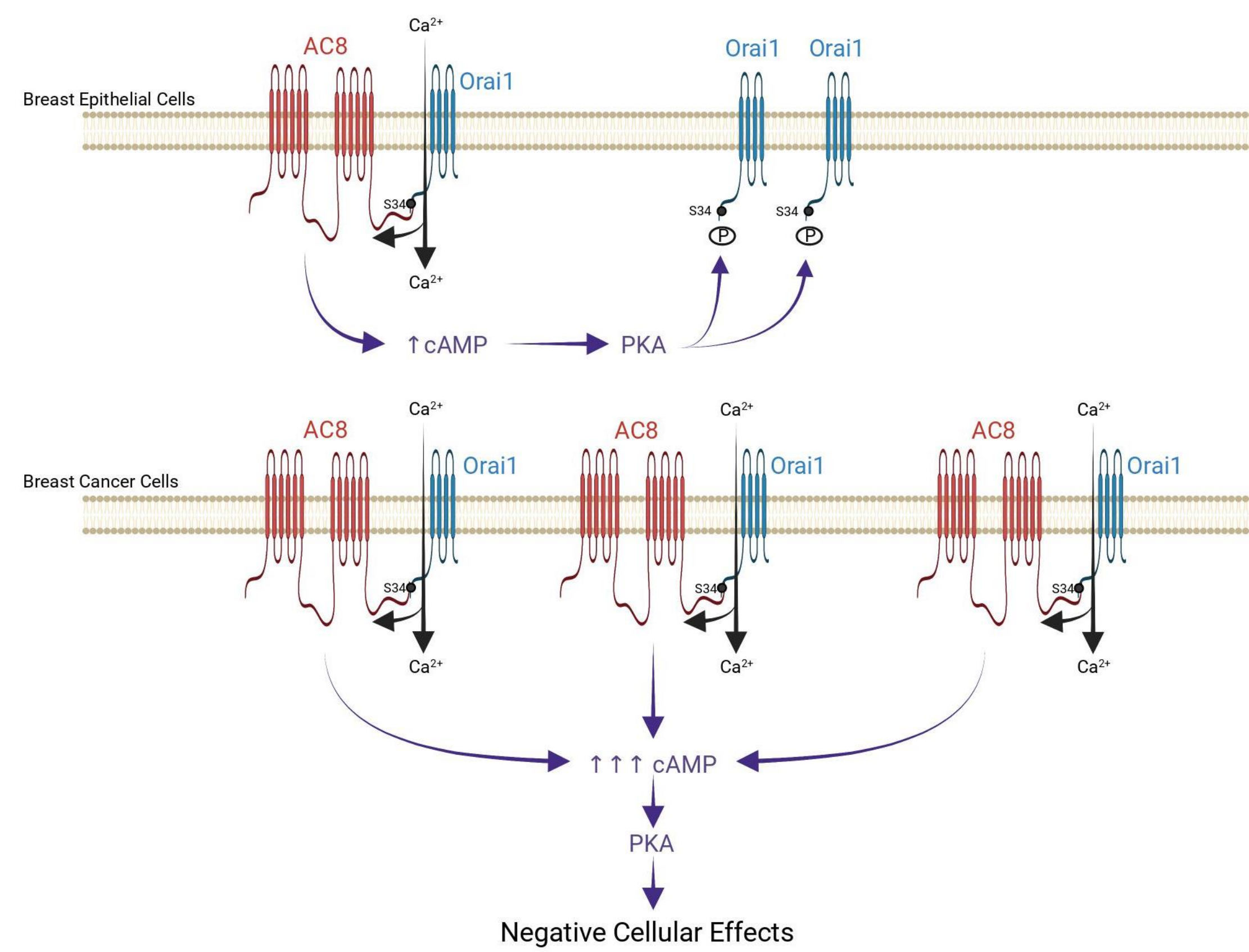


Figure 2: Interplay of AC8 and Orai1 in Cancerous Cells. Orai1 is incapable of being phosphorylated and inactivated due to overexpression of AC8. Surplus of calcium elicits various cellular responses including migration and proliferation of breast cancer.

Research Objectives

- Analyze the effect Zegocractin has on STIM1's coupling to Orai1 via NanoBiT
- Examine how Forskolin impacts AC8's binding to Orai1 via NanoBiT
- Verify that AC8 and Orai1 protein are overexpressed in triple negative breast cancer cell lines (MDA-MB-231 and MDA-MB-157) using anti-Orai1 and anti-AC8 antibodies and a fluorescently tagged secondary antibody

Results

NanoBiT Protein Tagging

Increasing concentrations of Zegocractin dose-dependently inhibits the interaction between Orai1 and STIM1

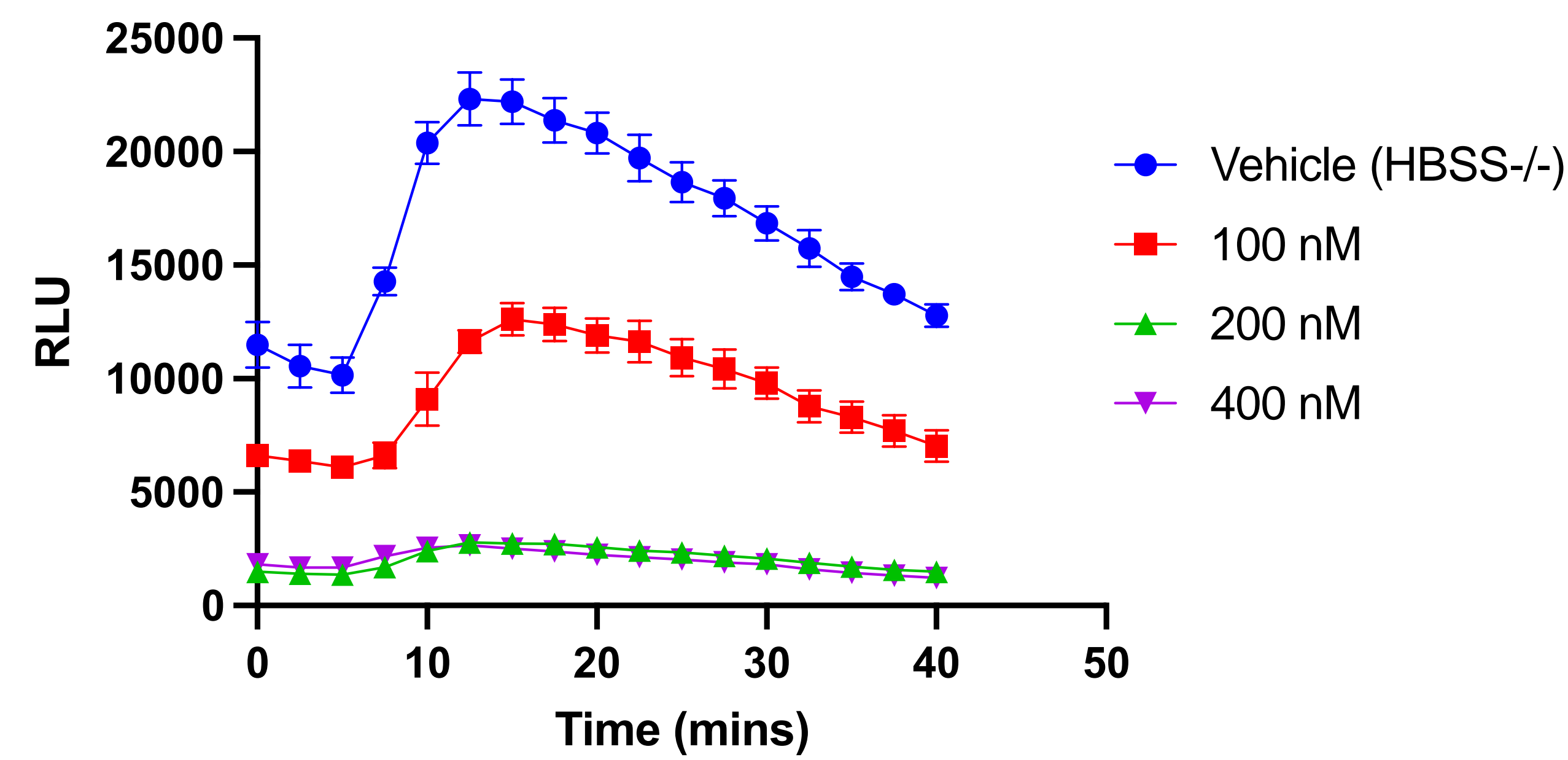


Figure 3: Zegocractin is a specific inhibitor to the Orai1 and STIM1 protein-protein interaction. Smaller increases in RLU values demonstrate lack of STIM1 binding to Orai1. N=3

Increasing concentrations of Forskolin dose-dependently inhibits the interaction between Orai1 and AC8

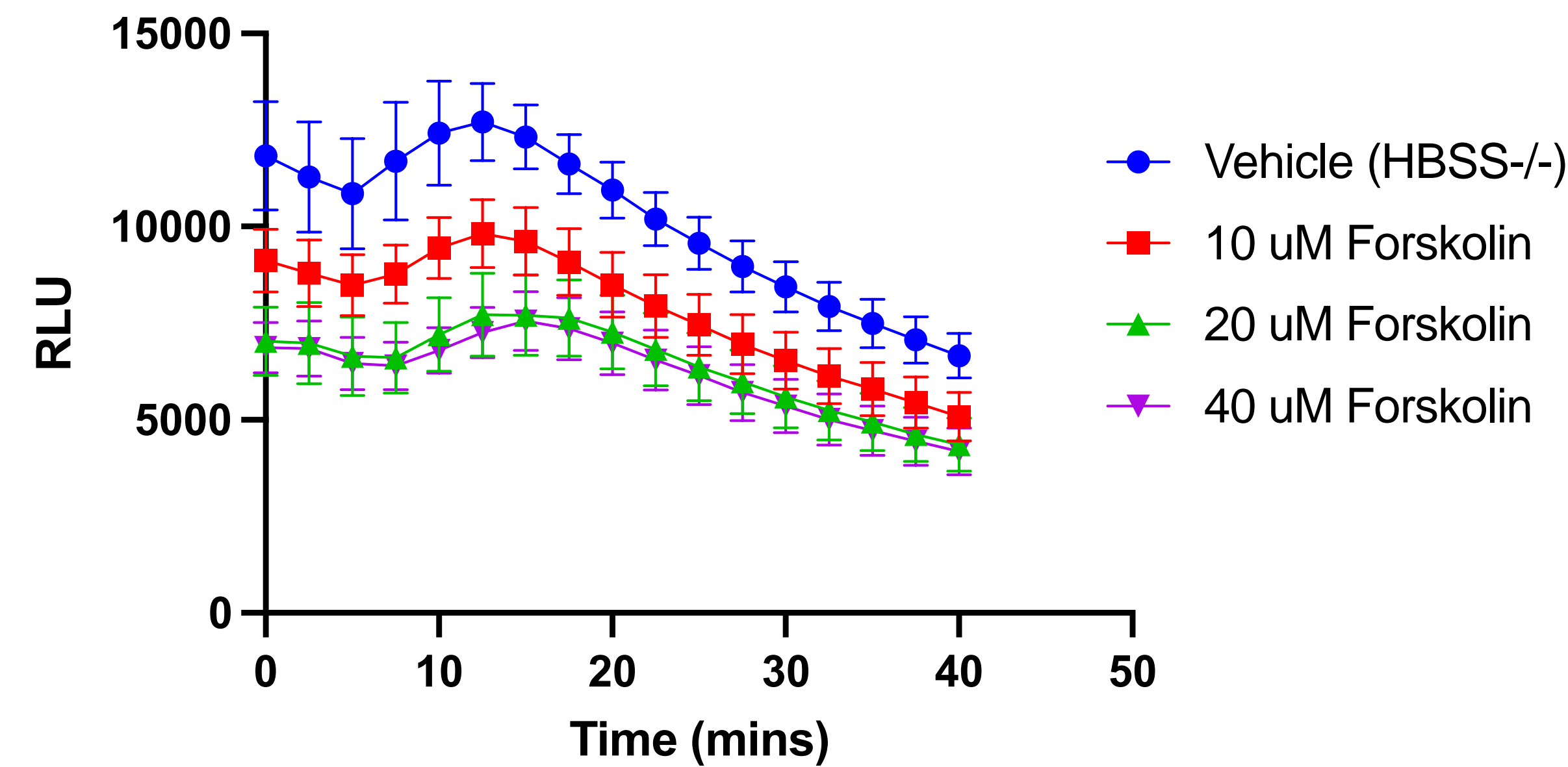


Figure 4: Forskolin is a potent activator of AC8. Decreases in RLU values indicate that forskolin debilitates the AC8 and Orai1 interaction. N=3

Western Blots

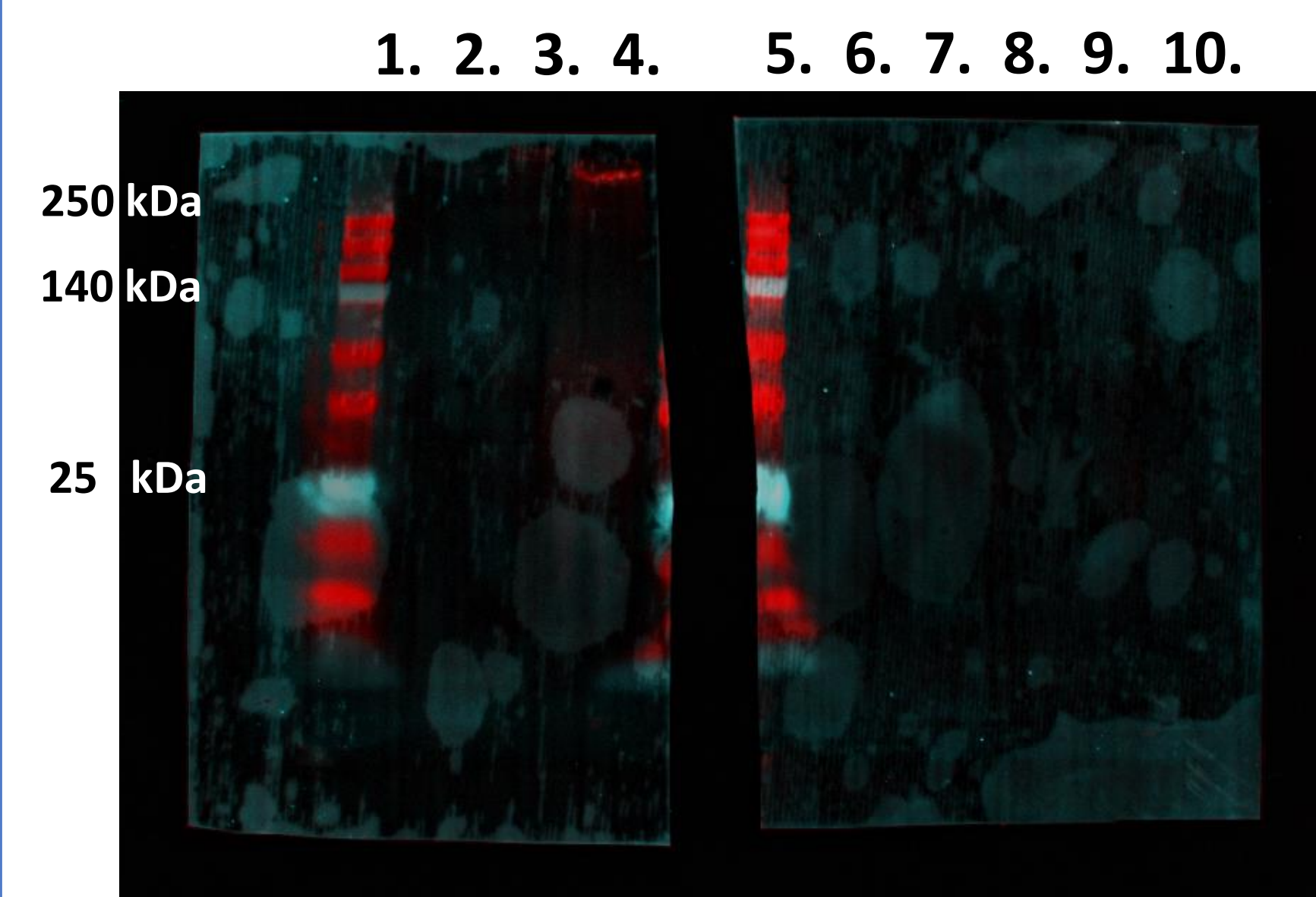


Figure 5: Transfected HEK293T Cells. PDVF membrane from HEK293T cells transfected to overexpress AC8 and Orai1. Successful binding of AC8 primary and secondary antibodies (lane 4); AC8 didn't migrate to correct molecular weight (140 kDa). Anti-Orai1 primary didn't detect Orai1 (lanes 6-10)

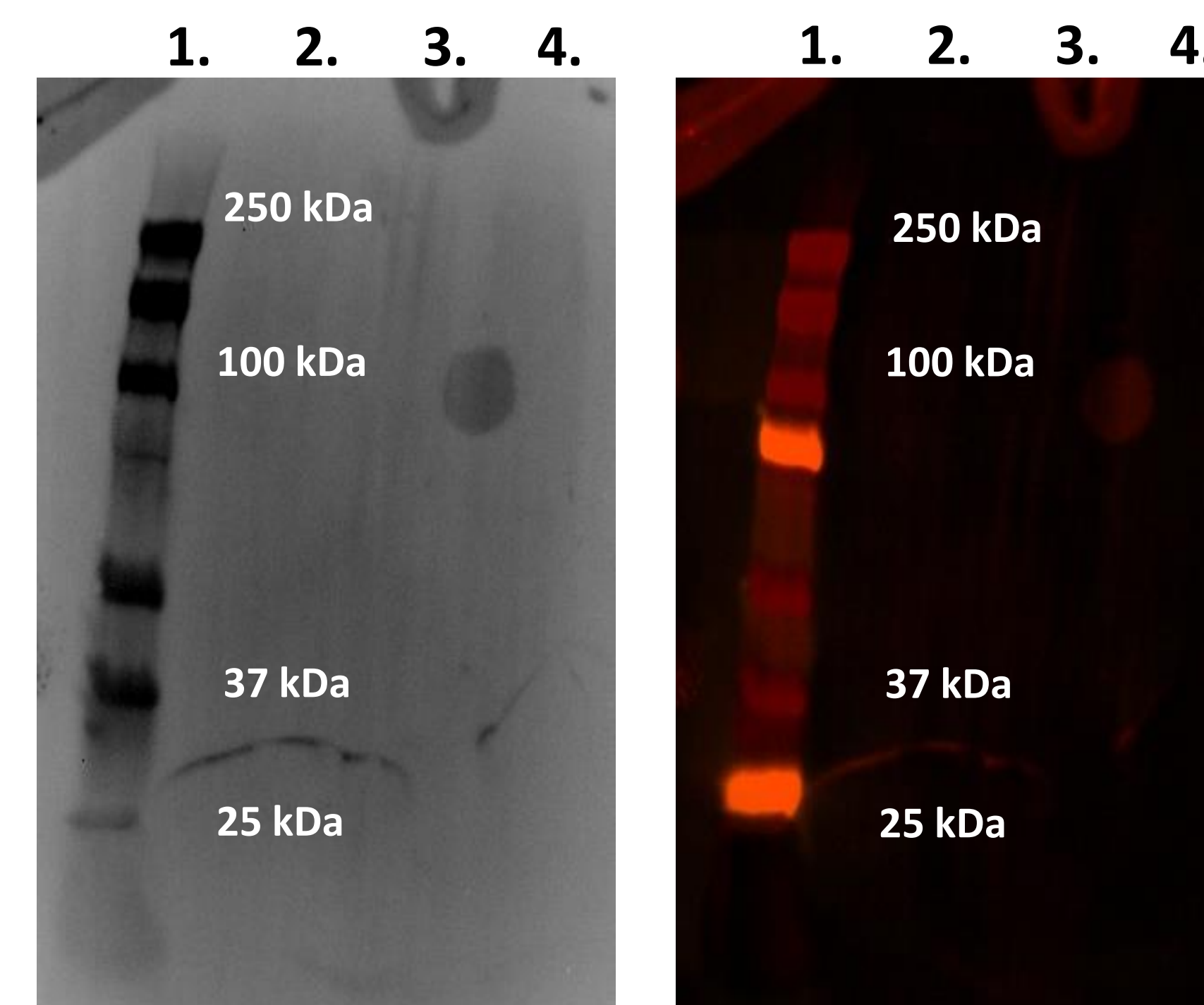


Figure 6: MDA-MB-231/MDA-MB-157 (TNBC cells). Orai1 is overexpressed (33 kDa) in TNBC cells (lanes 1 & 2) in relation to MCF12 cells (normal breast epithelial, lane 4). Anti-Orai1 primary antibody binds to Orai1 and is detected by goat anti-rabbit secondary antibody

Methods

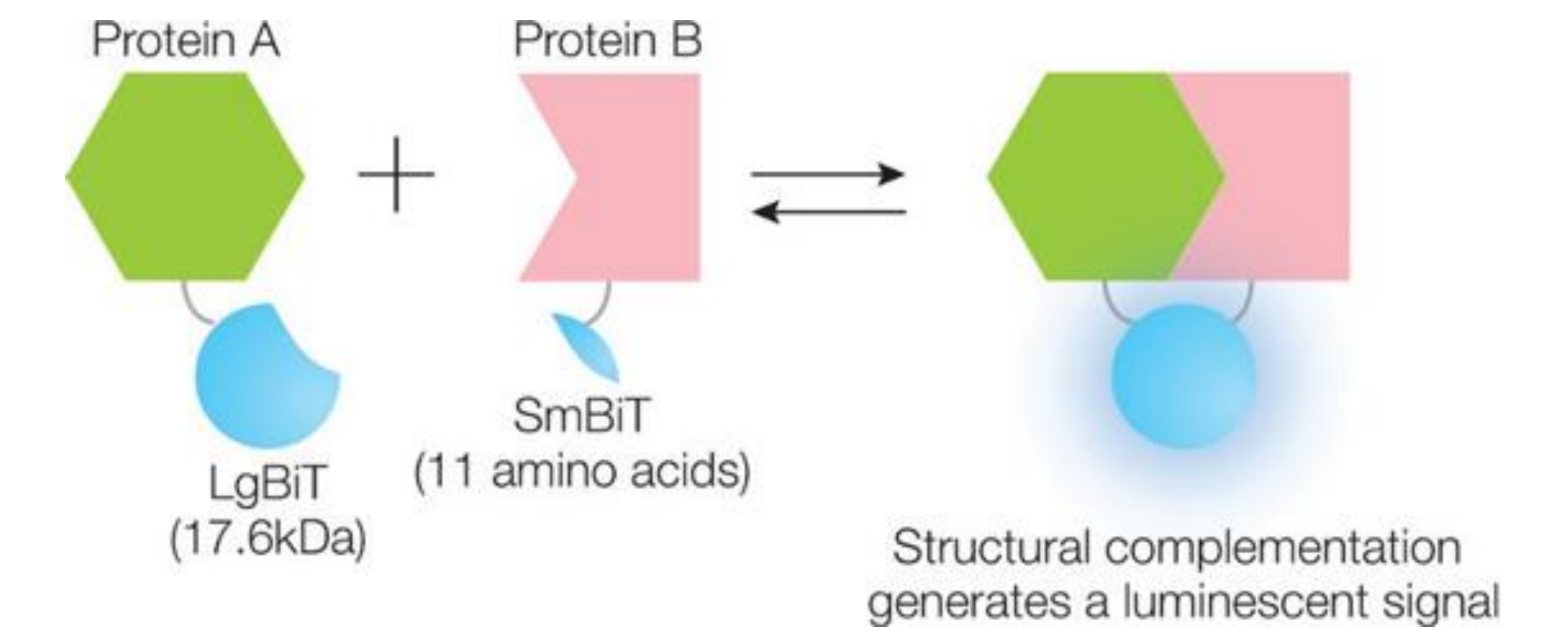


Figure 7: NanoBiT Protein Tagging: A bright luminescent signal is detected as LgBiT functionalizes with SmBiT on the protein of interest

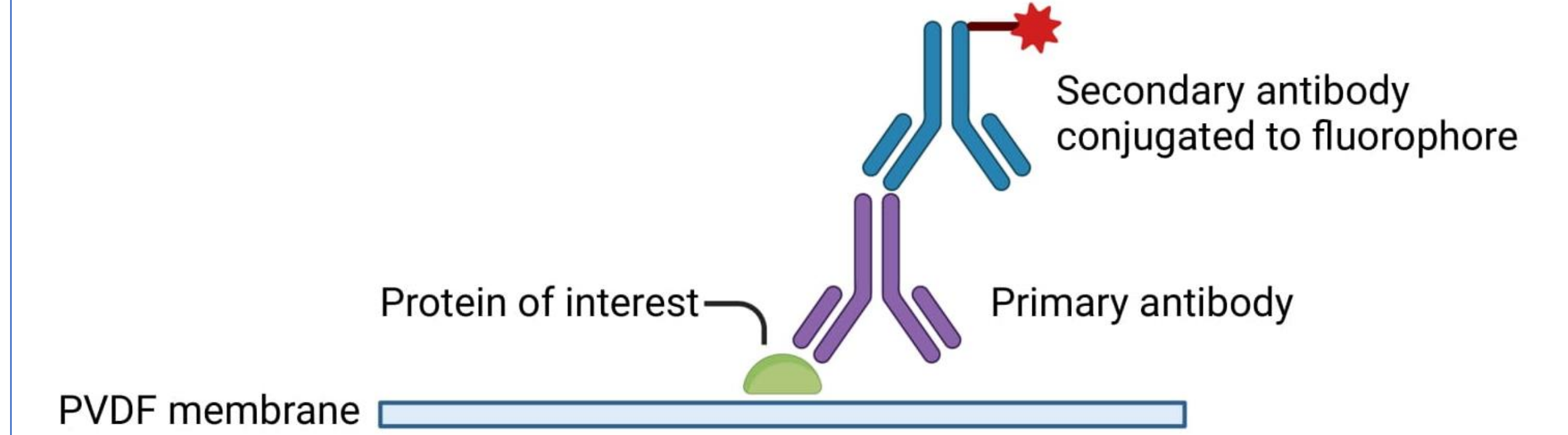


Figure 8: Antibody Detection in Western Blots. Primary antibody binds to the protein of interest. Secondary antibody with fluorescence signal detects primary antibody.

Conclusions/Implications

- Zegocractin significantly inhibits STIM1 and Orai1 interaction
- Forskolin diminishes luminescent signal between AC8 and Orai1
- Run NanoBiT protein assay with forskolin on Orai1 and STIM1
- Use immunoprecipitation before running western blot to isolate Orai1 or AC8 from lysate

References

- Jardin, I., Lopez, J. J., Sanchez-Collado, J., Gomez, L. J., Salido, G. M., & Rosado, J. A. (2022). Store-operated calcium entry and its implications in cancer stem cells. *Cells*, 11(8), 1332. <https://doi.org/10.3390/cells11081332>
- Sánchez-Collado, J., López, J. J., & Rosado, J. A. (2021). The orai1-AC8 interplay: How breast cancer cells escape from orai1 channel inactivation. *Cells*, 10(6), 1308. <https://doi.org/10.3390/cells10061308>
- NanoBiT protein:protein interaction system - promega. (n.d.). Retrieved July 24, 2022, from <https://www.promega.com/-/media/files/resources/protocols/technical-manuals/101/nanobit-protein-protein-interaction-system-protocol.pdf?la=en>

Acknowledgments

I would like to express my gratitude to Moana Hala'ufia, Dr. Roman, and Joshua C. Wilkinson for their guidance throughout this project. Special thanks to SSTP and the Belin-Blank Center for this amazing opportunity.

Raspberry Pi Based Data Acquisition System (DAQ) for a Colorectal Cancer SiNW Array-based Biosensor

Sneha Chakraborty¹, Luke Huang², Brady Lin,³ Daniel Keefe,⁴ Fatima Toor⁴

¹Irvington High School, Fremont, CA, USA; ²New Canaan High School, New Canaan, CT, USA; ³Tianjin Experimental High School, Tianjin, China; ⁴Electrical and Computer Engineering Department, University of Iowa, Iowa City, IA, USA

Motivation and Project Goals

Project Goals:

- The purpose of this project is to create an **efficient Data Acquisition System (DAQ) for the Colorectal Cancer (CRC) SiNW Array Biosensor** to facilitate its use as a point of care test.

Significance and Motivation:

- Colorectal Cancer (CRC)** is the **third leading cause of death** for both women and men worldwide.
- Tracking common CRC Protein biomarkers** (i.e., CEA) is beneficial in identifying possible CRC patients, **raising 5-year survival rates** by nearly 91%.
- Common approach** for CRC tracking/detection is **enzyme-linked immunosorbent assay (ELISA)** but high-cost and need for trained personnel **limits its use as point-of-care (POC) device**

Why Silicon Nanowire Array Biosensor?

Fig.1 NWs are very sensitive detectors because of extremely high surface area to volume ratio.

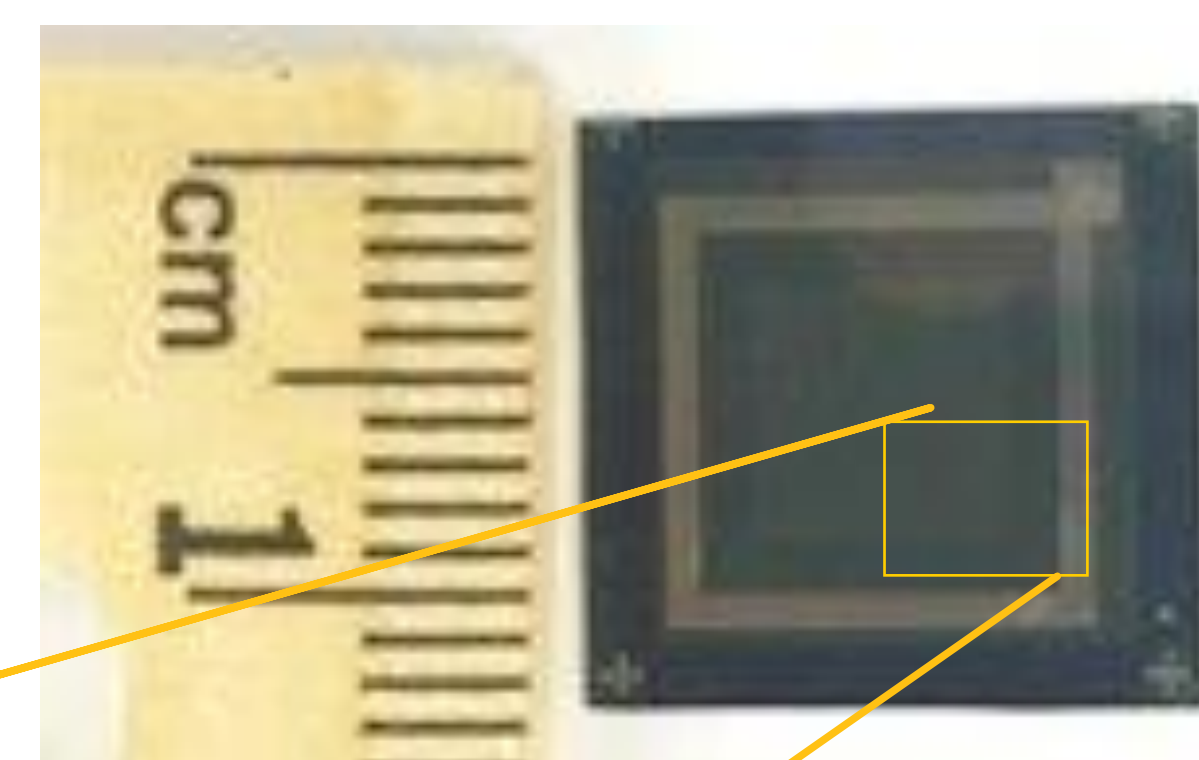
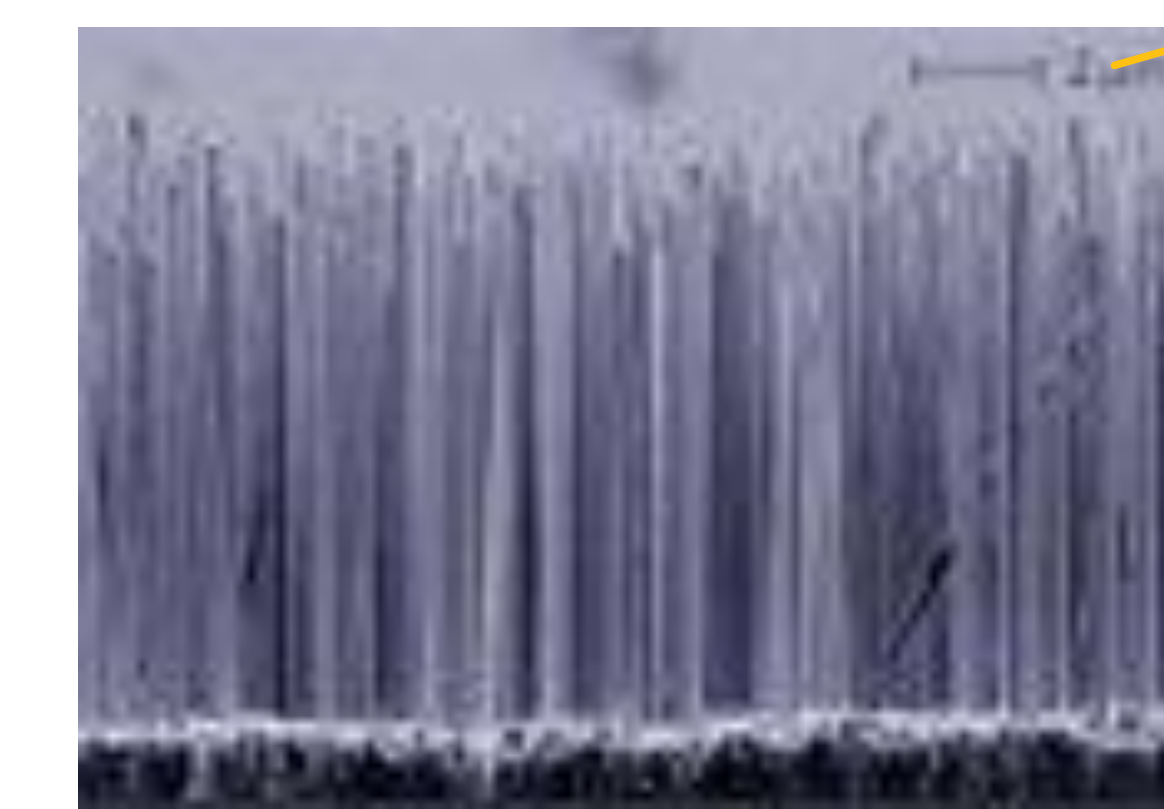
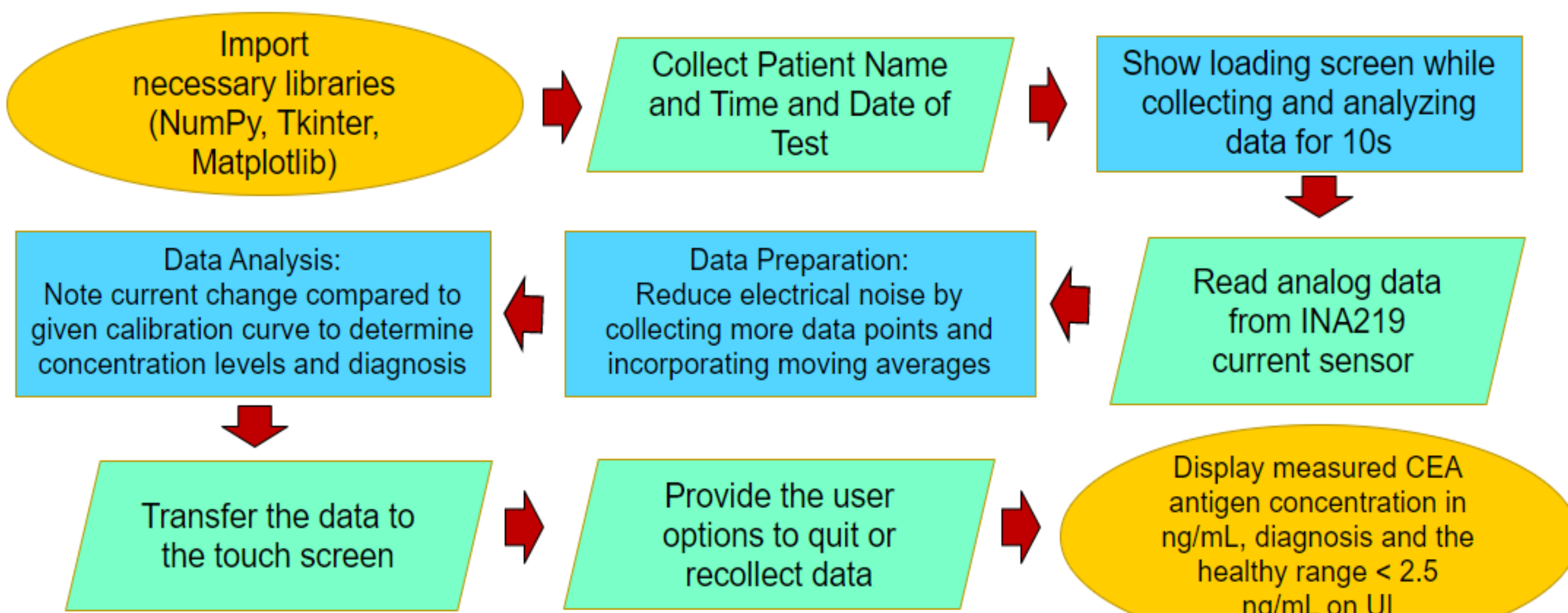


Fig.2 The final Silicon Array is portable, and this allows it to be easily scalable



DAQ Flowchart



Results

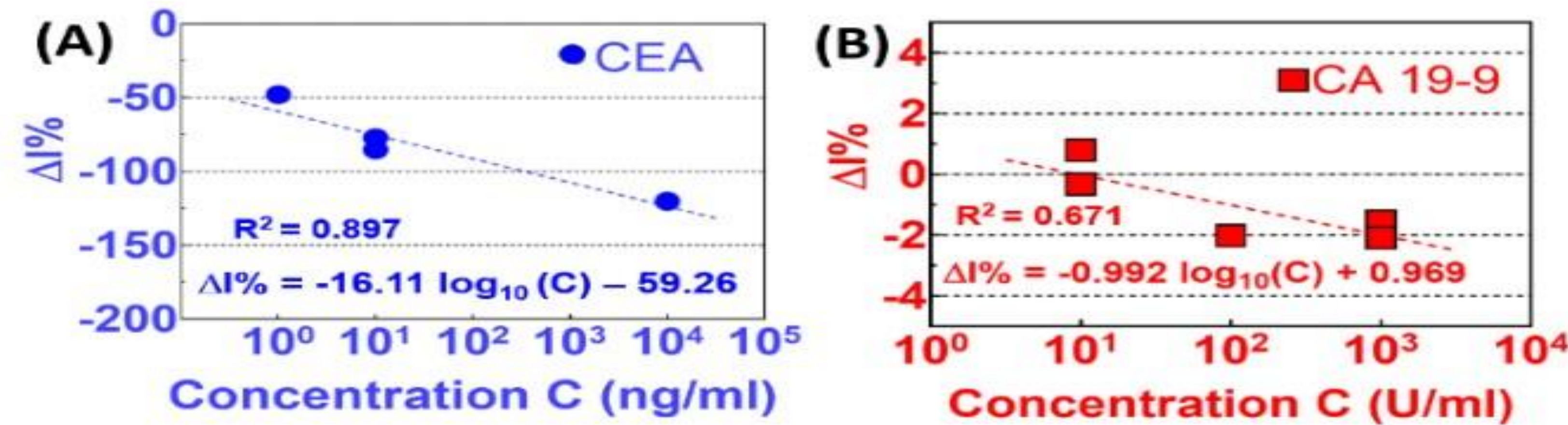
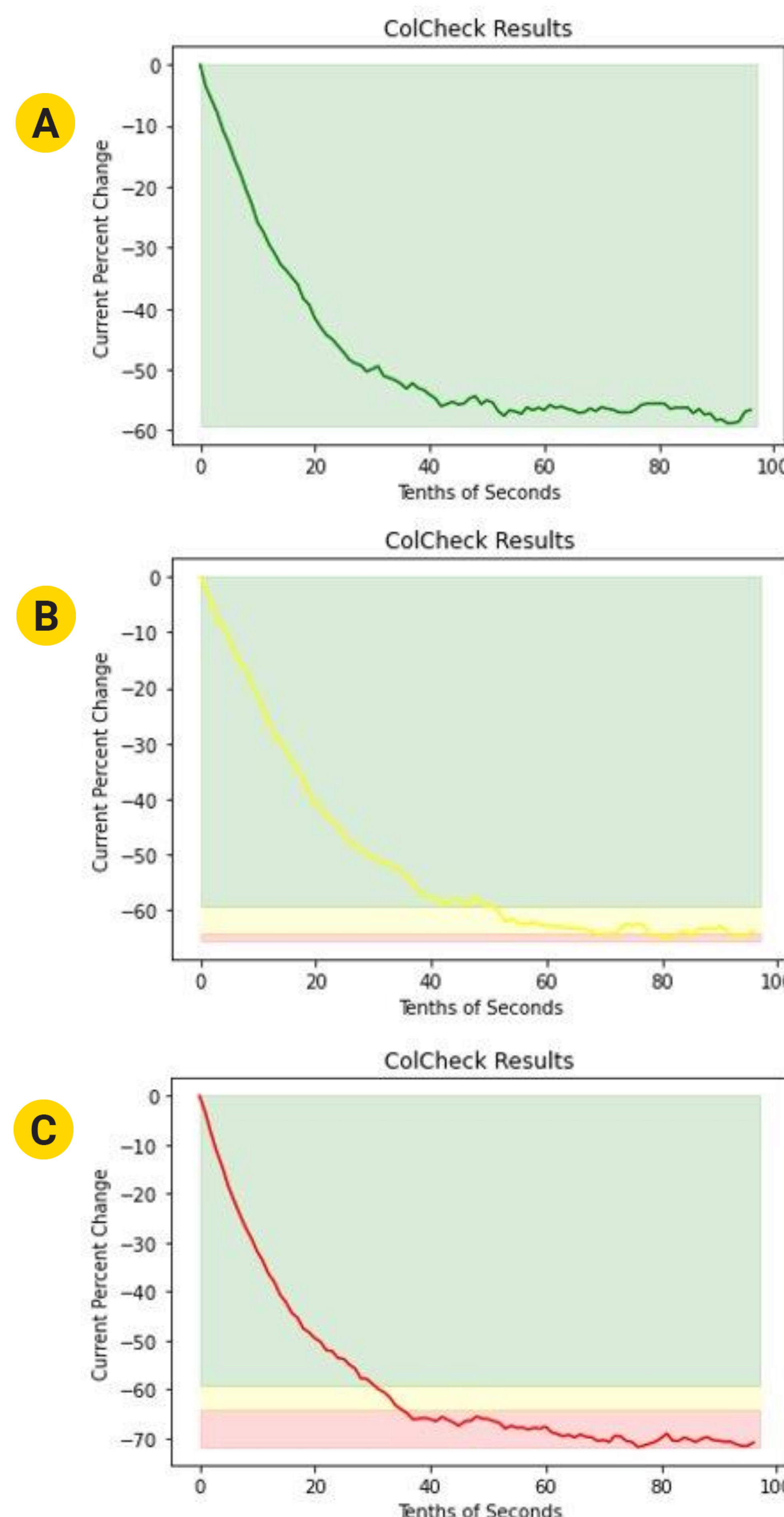
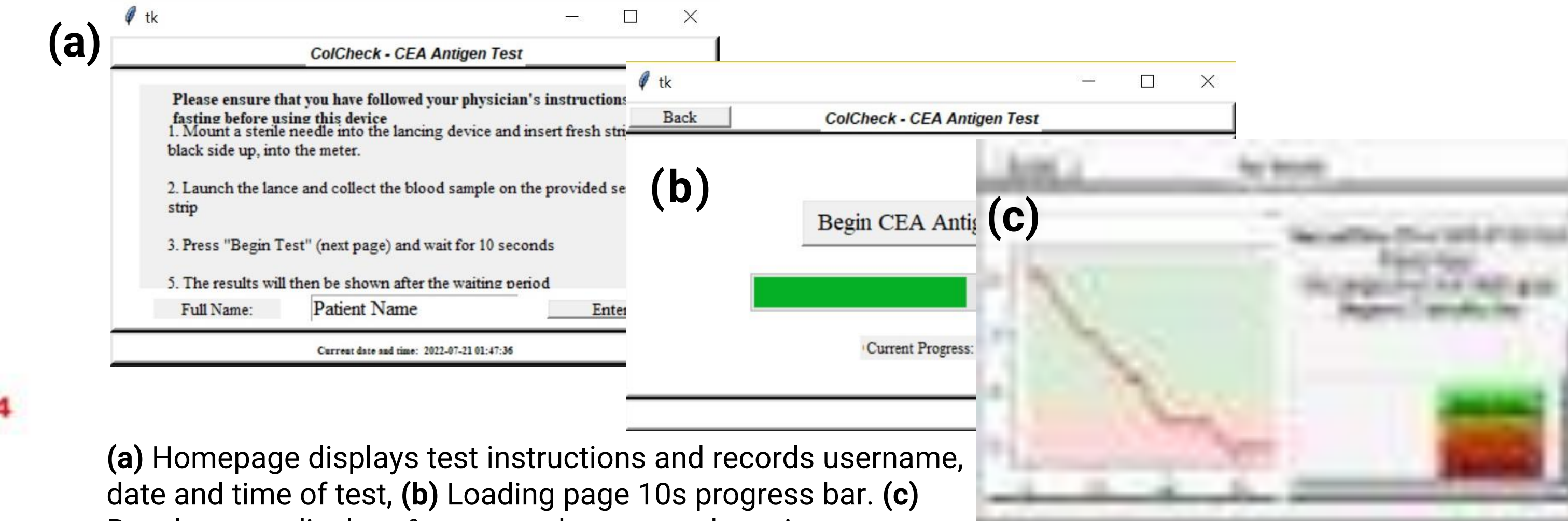


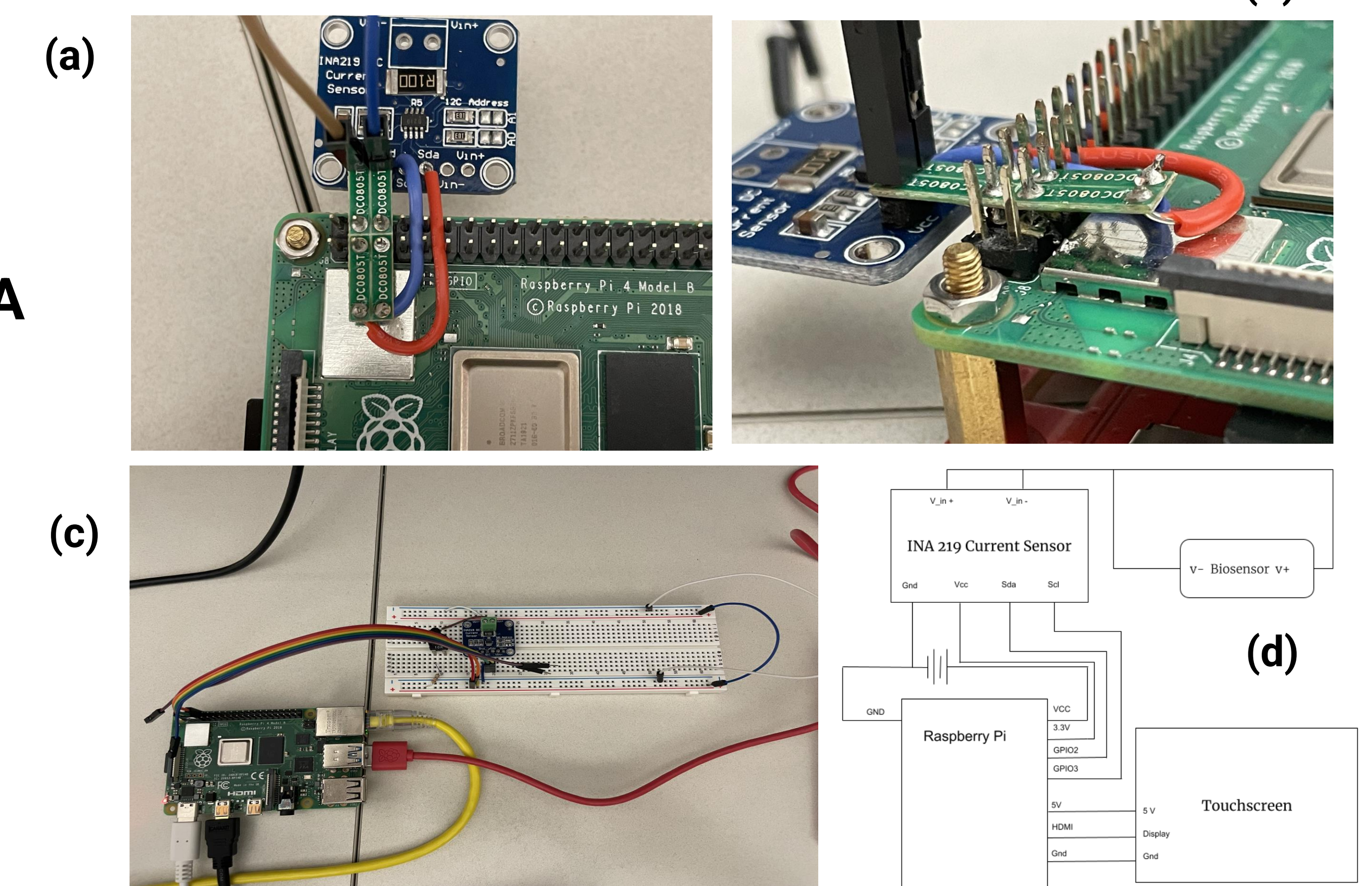
Fig.4 Semi-log data plots of $\Delta I\%$ as a function of CEA concentration level (A) and as a function of CA 19-9 (B) R^2 squared values for the regression confirm a strong correlation between the $\Delta I\%$ and antigen concentration.



Graphical User Interface (GUI)



Raspberry Pi Setup



Future Work

As of now, our results have been based on current changes generated by an **Analog Potentiometer** rather than the actual vSiNW-diode-based biosensor. For **future work**, we plan to test our DAQ by connecting our current sensor to the **actual vSiNW-diode-based sensor** and introduce a **compact casing** for our hardware.

Reference(s)

- Smith, R., Gao, B., Malkawi, W. I., Keefe, D. W., Geary, S., Kasi, P. K., Salem, A., Toor, F., Member, & IEEE. (in press). Vertically-Oriented Silicon Nanowires Array-based Biosensor Platform for Label-Free Detection of Protein and ctDNA Colorectal Cancer Biomarkers. IEEE Sensors Council.

Microneedle-Assisted Delivery of Caffeine Gels to Treat Apnea of Prematurity

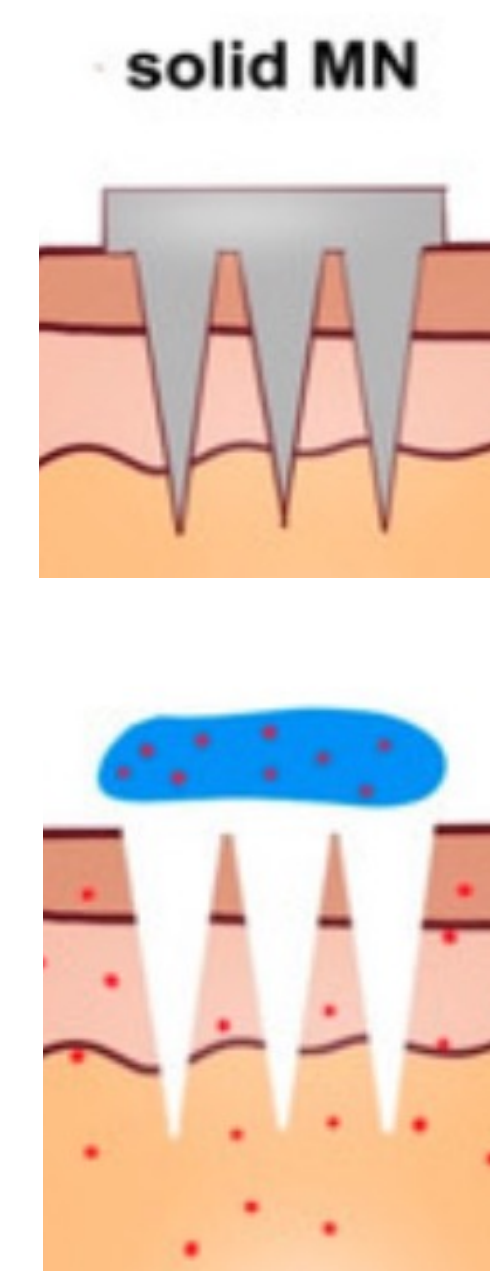
Rachel Y. Chan¹, Heeva V. Maithania², Nicole K. Brogden^{2,3}

¹Monta Vista High School, Cupertino, CA, ²Department of Pharmaceutical Sciences and Experimental Therapeutics, University of Iowa, Iowa City, ³Department of Dermatology, University of Iowa Hospitals, Iowa City, IA



Introduction

- Apnea of prematurity (AOP) is a serious sleep disorder wherein premature neonates stop breathing > 15-20s at a time due to an underdeveloped brainstem (the part of the central nervous system that controls breathing).
- Recent studies show that caffeine can stimulate the brainstem. However, caffeine is a hydrophilic, small molecule that does not have ideal physiochemical properties for absorption through the skin. Hence, microneedle-assisted drug delivery of caffeine through topical gel represents an innovative approach for AOP.



Objective

The goal of this work is to formulate caffeine-loaded gels with hydroxyethyl cellulose (HEC) as a polymer carrier and characterize viscosity, in vitro drug release, and permeation through microneedle-treated skin.

Materials and Methods

In Vitro Release and Permeation Study



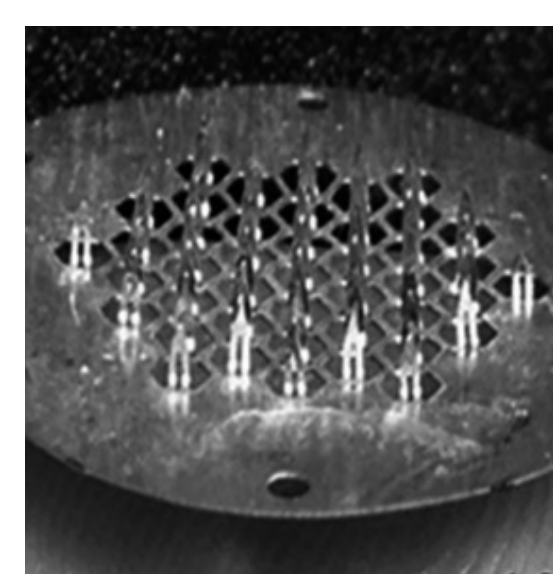
Diffusion cells: In-line diffusion cells with 1.76 cm² diffusion area (PermeGear)

Donor: 500 μL of caffeine base (1.3% w/v) with HEC (1.5% and 2.5% w/v) at pH 5, 6.5, and 7.4 (n = 3)

Receiver: HEPES buffer (pH 7.4) prewarmed to 37°C

Membrane:

- Release study: cellulose dialysis membrane (Snakeskin® Dialysis Tubing, 10K MWCO)
- Permeation study: dorsal skin from Yucatan miniature pigs



Stainless steel MN array (650 μm, 50 MNs)

Analysis: Samples were analyzed with HPLC-UV

Results

Solubility Study

Table 1. Solubility of caffeine base in citrate phosphate buffer at pH 5, 6.5, and 7.4 represented as mean ± SD (n = 3).

Solution pH	Caffeine Solubility (mg/mL)
pH 5	15.721 ± 0.044
pH 6.5	14.420 ± 0.014
pH 7.4	13.209 ± 0.131
water	19.095 ± 0.015

Viscosity Study

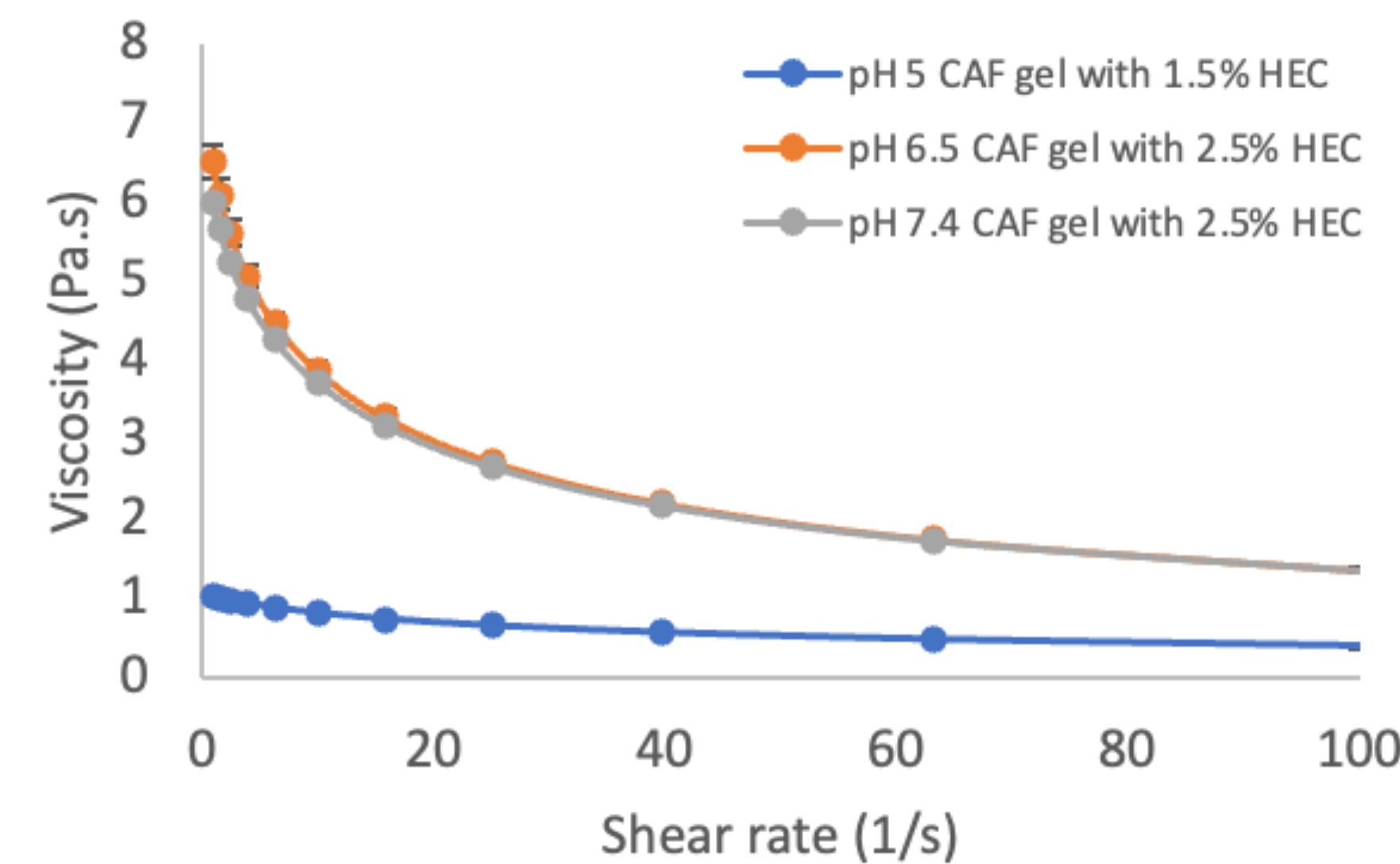


Figure 1. Flow curve of caffeine base (1.3% w/v) loaded gel at pH 5, pH 6.5, and pH 7.4 represented as mean ± SD (n = 3).

Table 2. Viscosity of caffeine base (1.3% w/v) loaded gel at pH 5, pH 6.5, pH 7.4 represented as mean ± SD (n = 3).

Gel pH	Viscosity (Pa.s)
pH 5	1.036 ± 0.02
pH 6.5	6.510 ± 0.211
pH 7.4	5.994 ± 0.191
water	6.584 ± 0.263

In Vitro Release Study

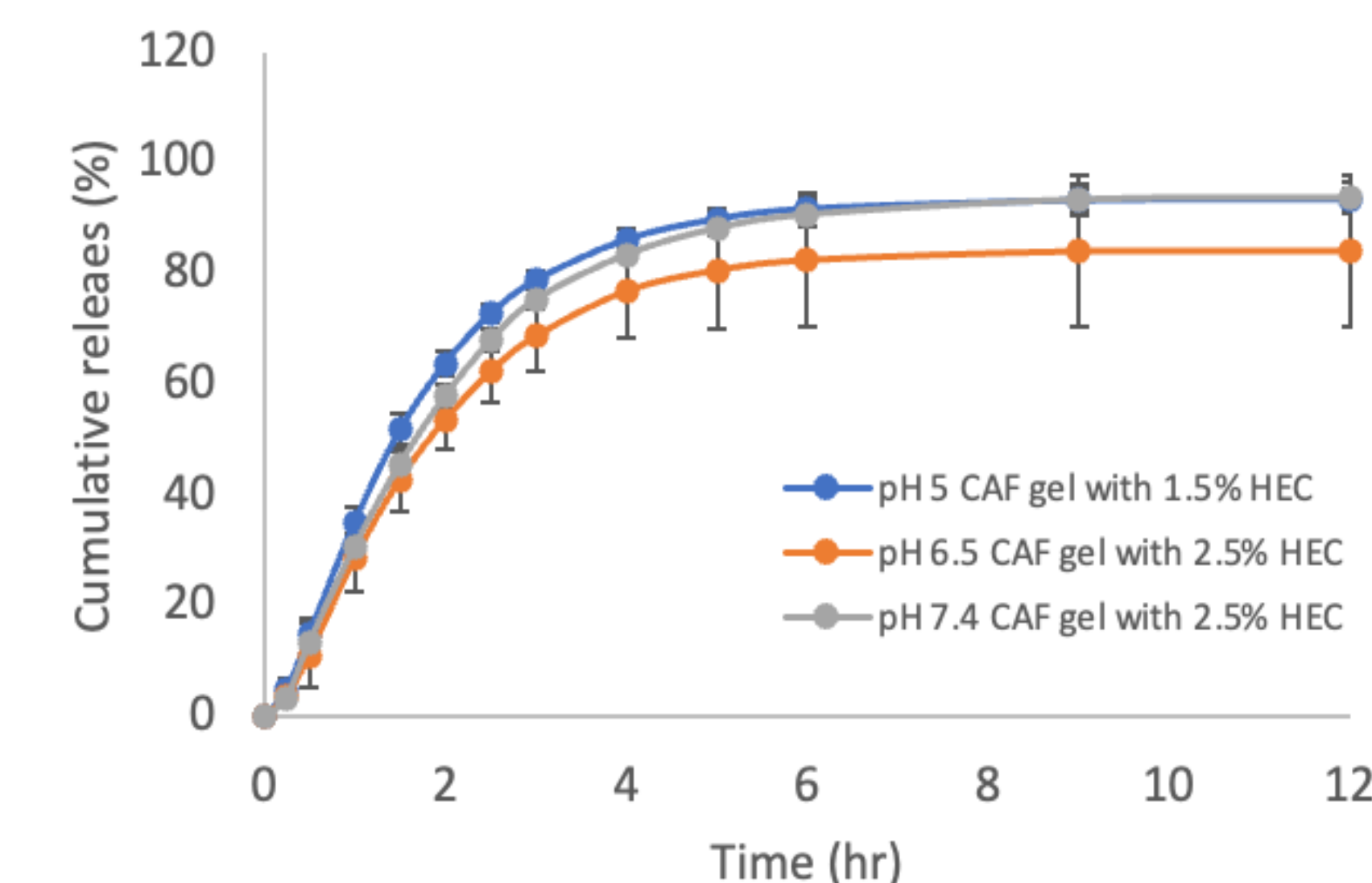


Figure 2. Cumulative release of caffeine base (1.3% w/v) loaded gel at pH 5, 6.5 and 7.4, represented as mean ± SD (n = 3).

In Vitro Permeation Study: intact skin

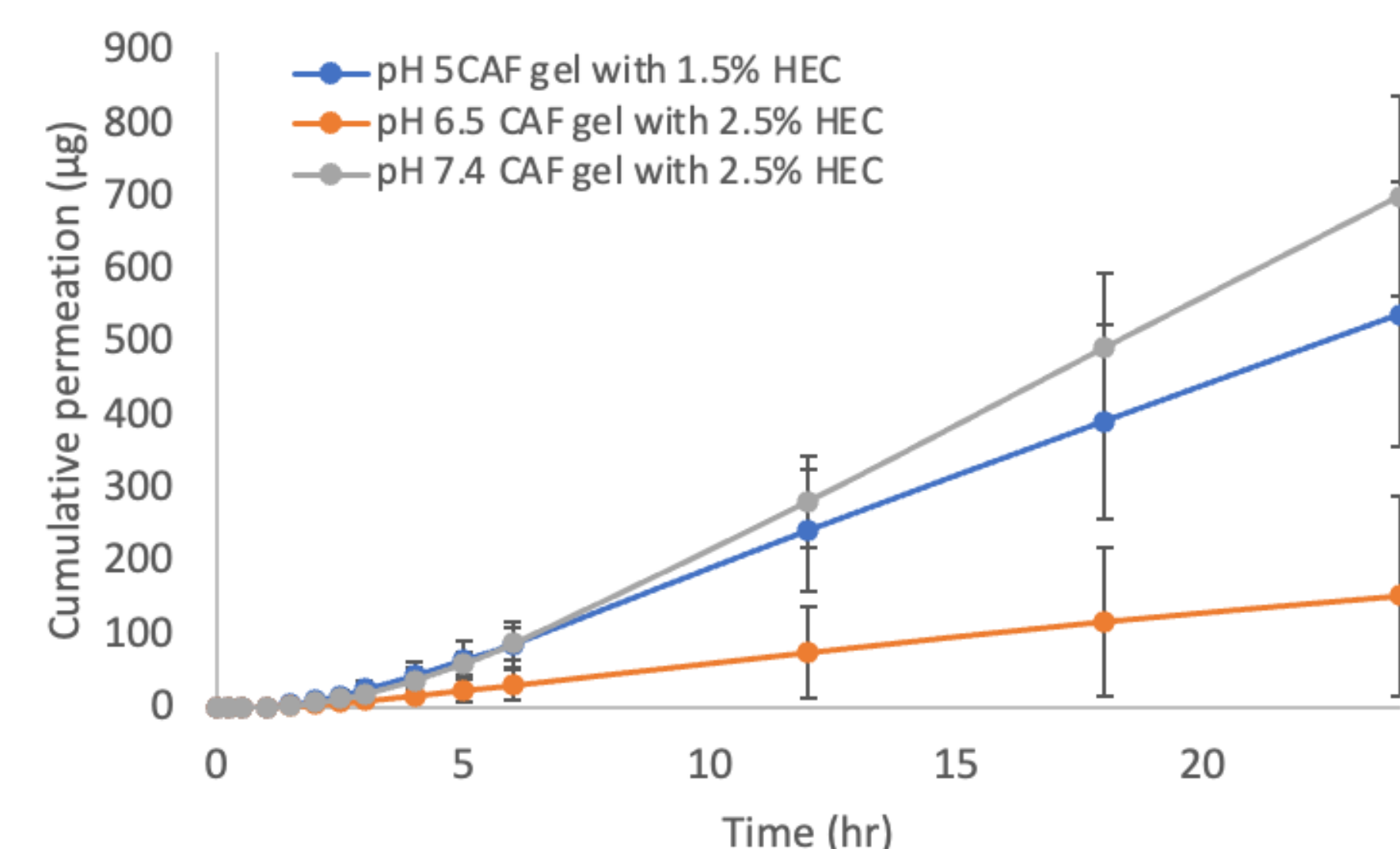


Figure 3. Cumulative permeation of caffeine base (1.3% w/v) loaded gel at pH 5, 6.5 and 7.4 through dorsal skin from Yucatan miniature pigs, represented as mean ± SD (n = 3).

In Vitro Permeation Study: MN-treated skin

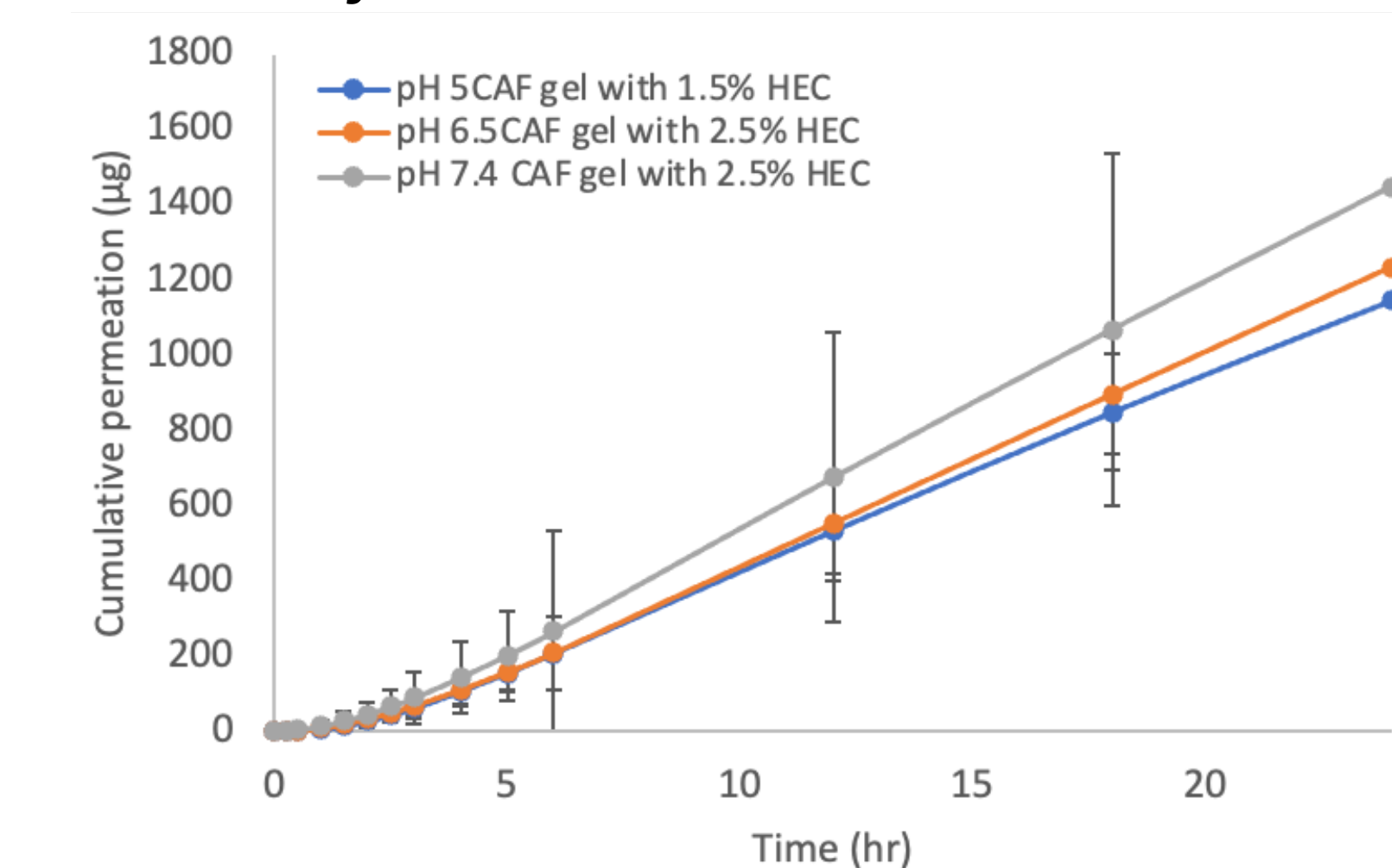


Figure 4. Cumulative permeation of caffeine base (1.3% w/v) loaded gel at pH 5, 6.5 and 7.4 through MN-treated dorsal skin from Yucatan miniature pigs, represented as mean ± SD (n = 3).

Table 3. Cumulative delivery, lag time, and steady-state flux of caffeine base (1.3% w/v) loaded gel (1.5% w/v and 2.5% w/v HEC) at pH 5, 6.5, and 7.4 represented as mean ± SD. Q₂₄: cumulative permeation over 24 hours; J_{ss}: steady state flux

Group	Gel pH	Q ₂₄ (μg)	Lag time (hr)	J _{ss} (μg/cm ² /hr)
Intact skin	pH 5	539.59 ± 181.70	2.11 ± 0.97	13.99 ± 4.73
	pH 6.5	154.30 ± 38.75	1.68 ± 0.91	4.01 ± 1.56
	pH 7.4	701.03 ± 137.07	3.86 ± 0.37	19.76 ± 3.54
MN-treated skin	pH 5	1145.76 ± 702.18	1.85 ± 1.07	22.01 ± 16.66
	pH 6.5	1232.63 ± 155.10	2.28 ± 1.06	32.20 ± 2.86
	pH 7.4	1446.78 ± 469.12	1.99 ± 0.12	36.56 ± 9.47

Conclusion

- 62.35-72.80% of the drug was released in the first 2.5 hours, suggesting immediate release of caffeine base from gel
- Drug release was not statistically different at various pH levels
- With MN pretreatment, a significant increase in steady-state flux was observed compared to intact skin
- Decrease in the absorption lag time for pH 5 and pH 7.4 through microneedle-assisted delivery represents a quicker onset of action

Acknowledgements

I would like to thank Dr. Heena Maithania for her mentorship and guidance, Dr. Nicole K. Brogden for the opportunity to conduct research in her lab, as well as the entire Brogden Lab and the University of Iowa College of Pharmacy. Special thanks to Belin-Blank for making this opportunity possible.

References

- Dobson NR, Hunt CE. Pharmacology Review: Caffeine Use in Neonates: Indications, Pharmacokinetics, Clinical Effects, Outcomes. *NeoReviews*. 2014; 11: 540-550.
- Sollami A, Marino L, Fontechiari S, Fornari M, Tirelli P, Zenuhaj E. Strategies for pain management: a review. *Acta Biomed*. 2015; 86 Suppl 2: 150-157.
- Tobin, K.V.; Fiegel, J.; Brogden, N.K. Thermosensitive Gels Used to Improve Microneedle-Assisted Transdermal Delivery of Naltrexone. *Polymers* 2021, 13, 933. <https://doi.org/10.3390/polym13060933>

Utilization of rTg4510 mouse model in Alzheimer's disease and related dementias

Audrey Chen¹, Utsav Mukherjee^{2,3,4}, Snehajyoti Chatterjee^{2,3}, Ted Abel^{2,3}

¹Leland High School, San Jose, CA, ²Department of Neuroscience and Pharmacology, Carver College of Medicine, University of Iowa, Iowa City, IA, ³Iowa Neuroscience Institute, University of Iowa, Iowa City, IA, ⁴Interdisciplinary Graduate Program in Neuroscience, University of Iowa, Iowa City, IA

Introduction

Alzheimer's disease (AD) is a progressive medical condition which is classified as a type of dementia. This disorder disrupts the function of the brain by killing the neurons and causing the brain to shrink, also known as brain atrophy. The hippocampus is affected in the early stage of AD. It destroys the ability to think, learn, and memorize.

Mechanisms of AD

- The main causes of Alzheimer's disease are the two abnormal protein build-ups: amyloid precursor protein (APP) and tau protein.
- APP generates amyloid beta polypeptides which forms amyloid plaques around neurons.
- Tau protein often leads to neurofibrillary tangles (NFTs) in the brain.
- NFTs are a major hallmark in AD as they affect the communication between neurons and are often found in severe Alzheimer's disease brain tissues.
- However, there is no effective treatment for long-term memory deficits in Alzheimer's disease and related dementias (ADRD).

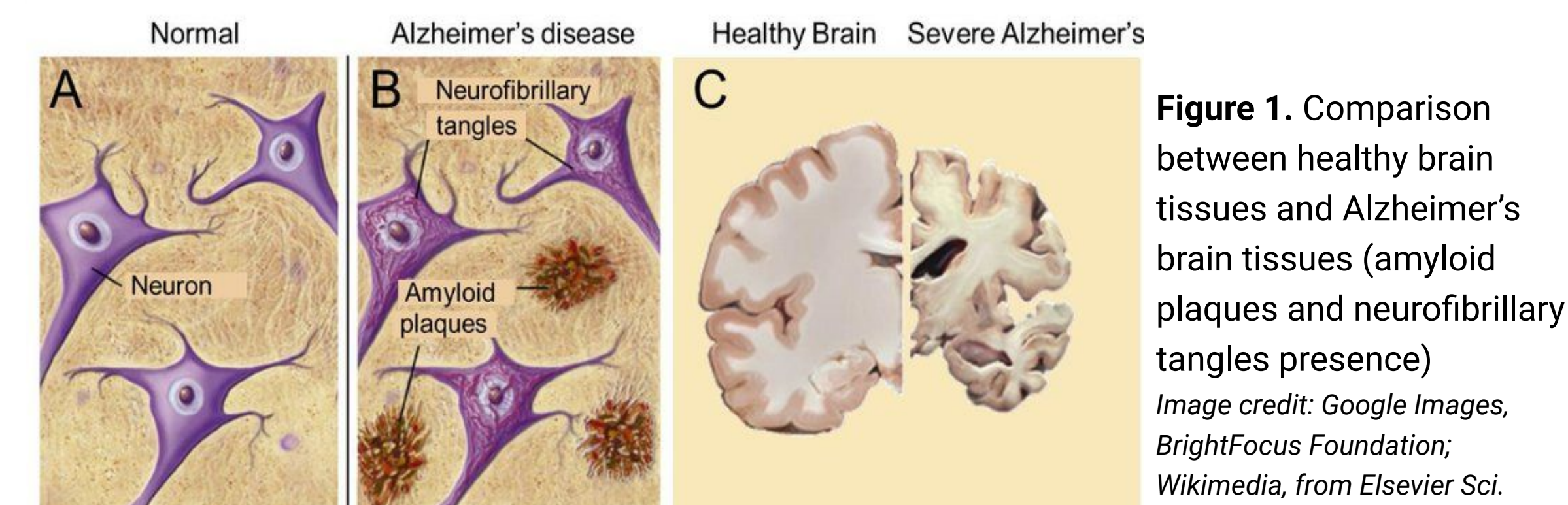
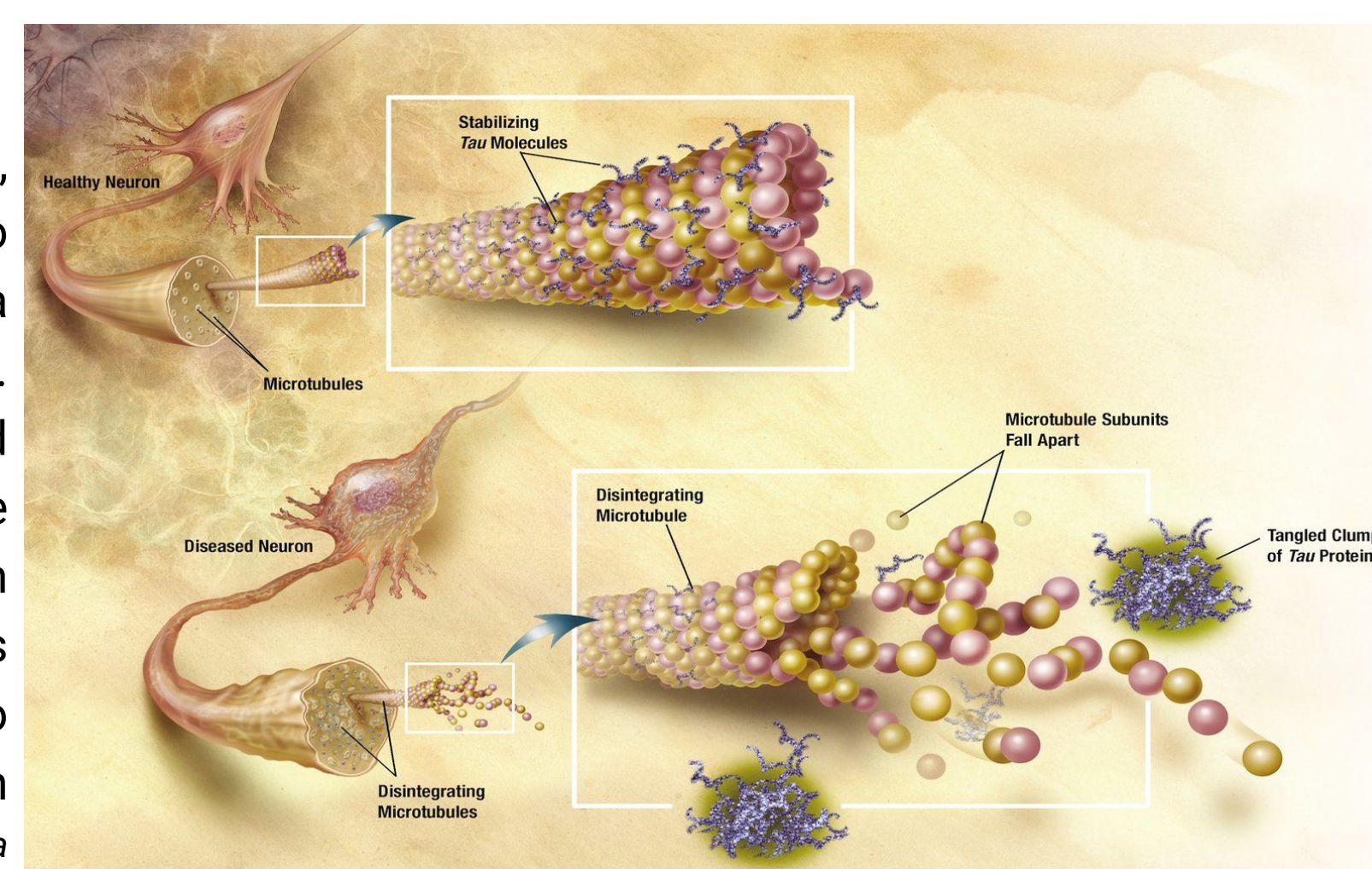


Figure 1. Comparison between healthy brain tissues and Alzheimer's brain tissues (amyloid plaques and neurofibrillary tangles presence)
Image credit: Google Images, BrightFocus Foundation, Wikimedia, from Elsevier Sci.

Figure 2. In a healthy brain, tau proteins bind to microtubules with a stabilized phosphorylation. In Alzheimer's, depolarized microtubules disintegrate as the tau proteins form neurofibrillary tangles around the neurons due to hyperphosphorylation
Image credit: Wikipedia



Objectives

- Assess the effectiveness of using tau-based rTg4510 mouse to model the neurofibrillary tangles present in ADRD.
- Discuss implications of the rTg4510 mouse model on clinical research for ADRD.

Methods

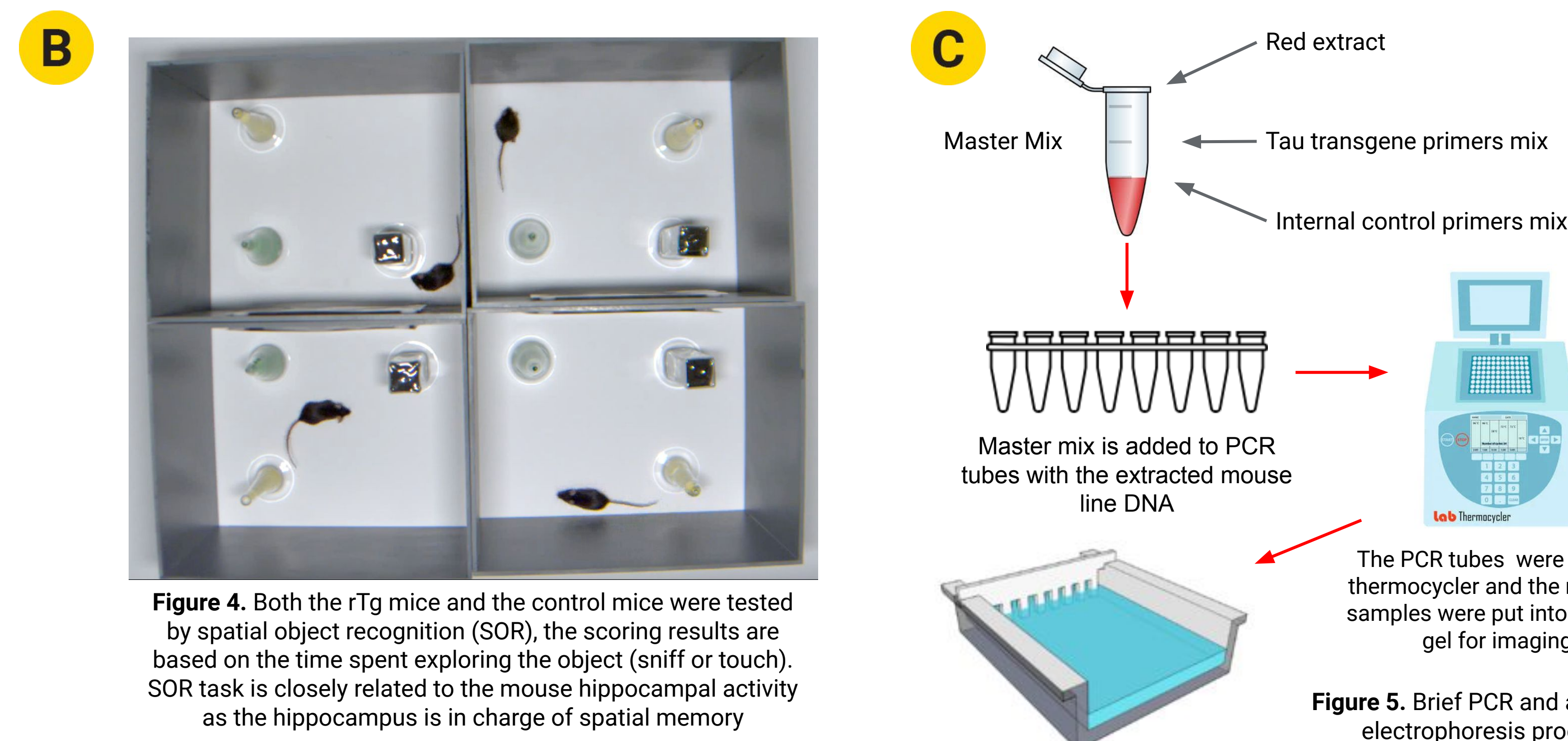
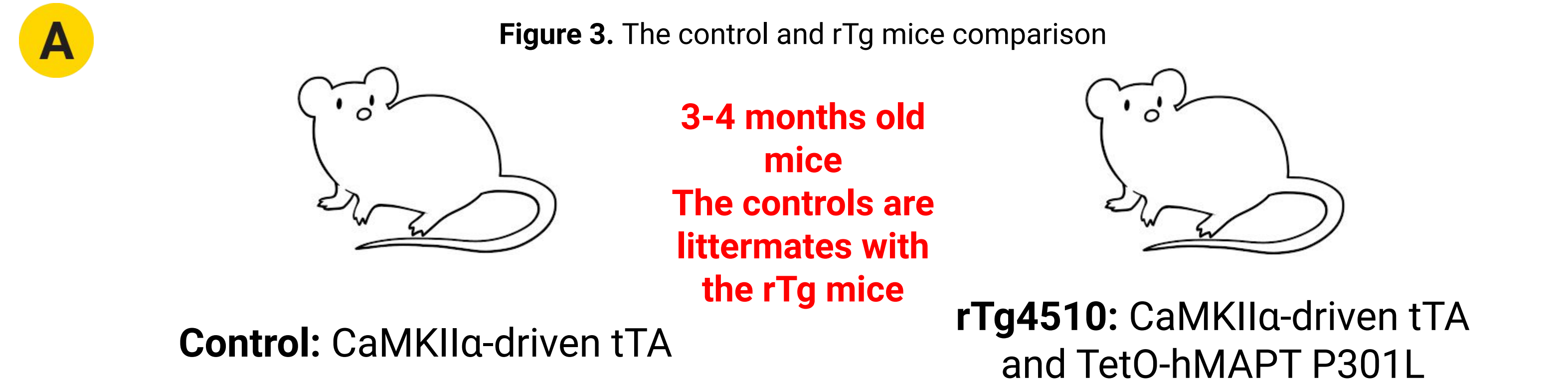


Figure 4. Both the rTg mice and the control mice were tested by spatial object recognition (SOR), the scoring results are based on the time spent exploring the object (sniff or touch). SOR task is closely related to the mouse hippocampal activity as the hippocampus is in charge of spatial memory

Figure 5. Brief PCR and agarose gel electrophoresis procedure

Results

Figure 6.1. TetO-hMAPT Tau

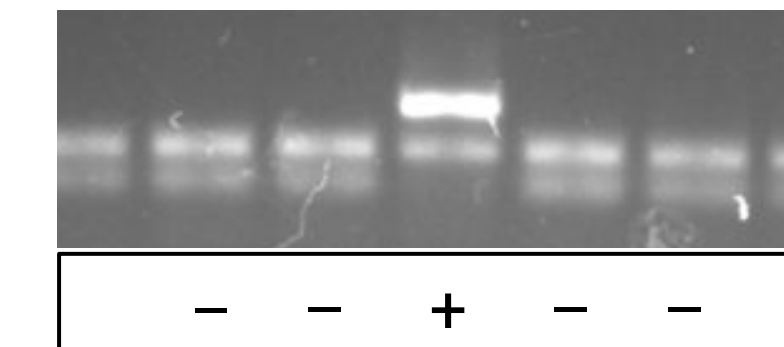


Figure 6.2. CaMKIIα-tTA

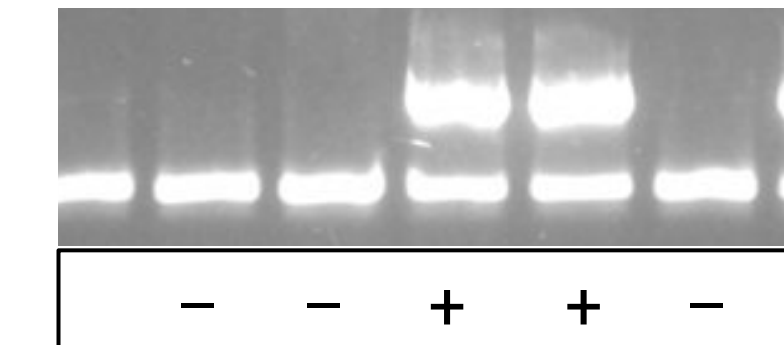


Figure 6. Validation of transgene presence in rTg mice
The mouse line DNA was run in PCR and agarose gel electrophoresis after the behavior tests, which validates the gene expression in both rTg and control mice. As shown in figure 6.1., the top line band shows the presence of tau gene, while in figure 6.2. the top line band shows the presence of tTA gene in the mouse. According to the methodology, if the mouse expresses both tau and tTA genes, then it is a rTg4510 mouse; if the mouse only expresses one band, then it is control. This helps validate the SOR scoring results in our experiment.

Figure 7. SOR task scoring results
The graph shows the spatial object recognition task results in terms of the time spent exploring the displaced object. In the training session, the control and rTg mice both spent around 30% of the time exploring the displaced object. However, in the testing session, the control mice spent significantly more time than the rTg mice, lining out a major comparison in our study.

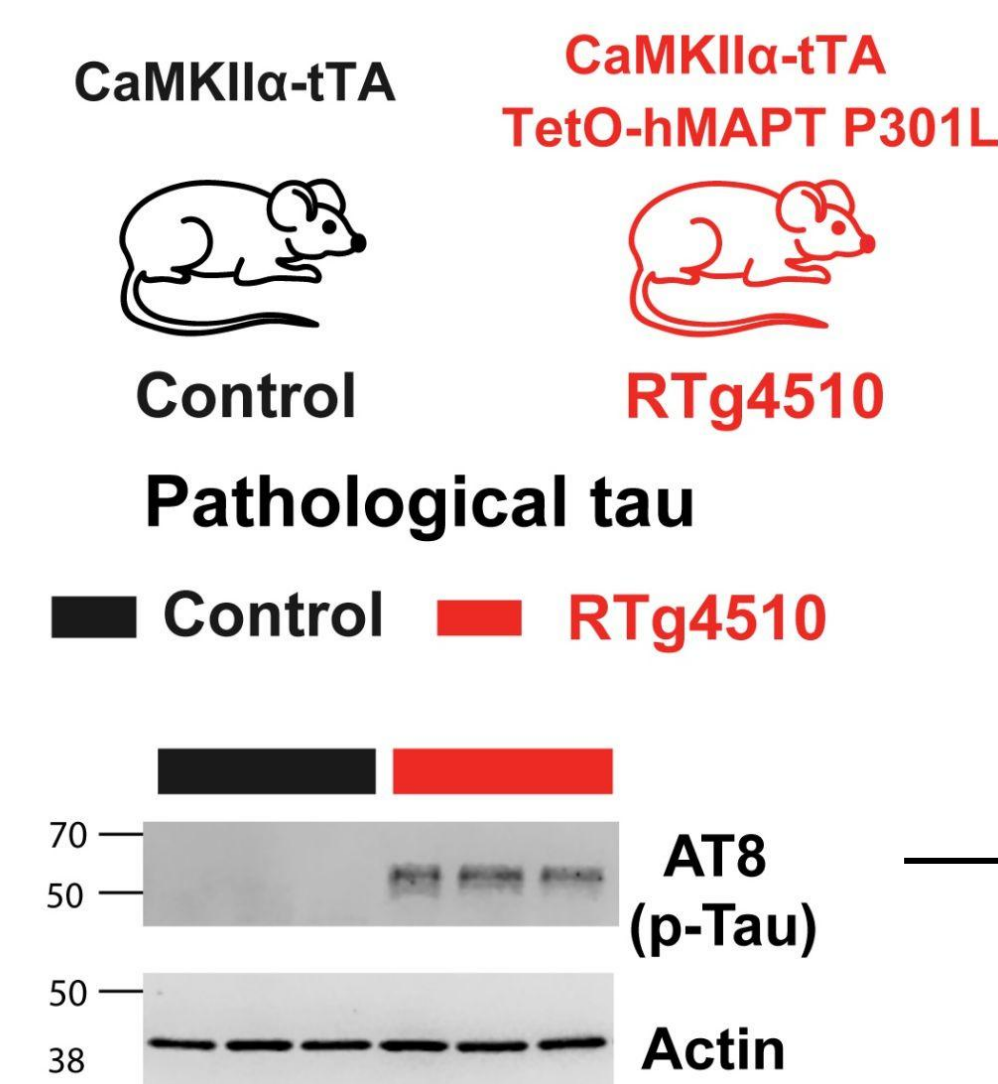
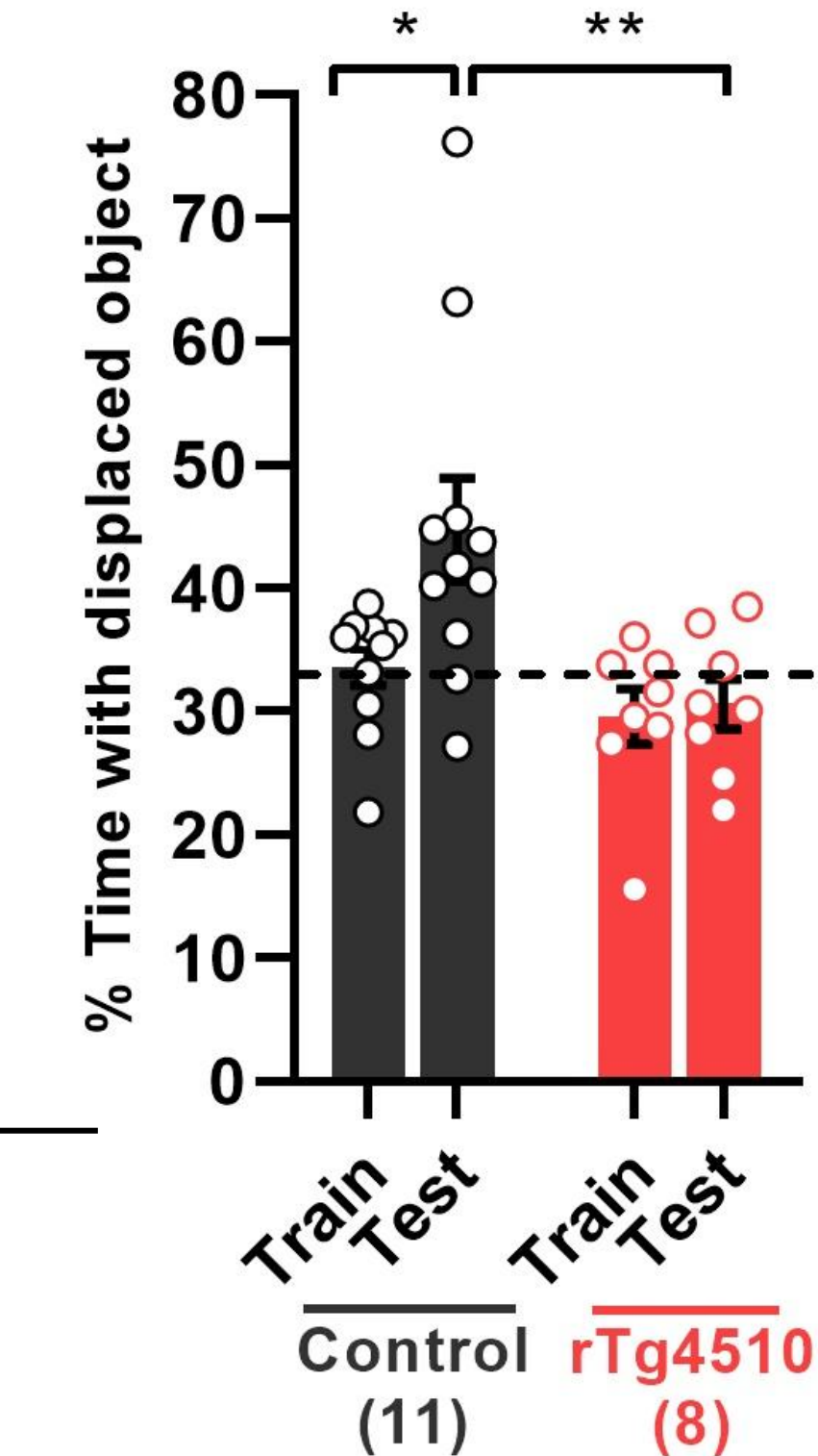


Figure 8. Western blots results in control and rTg mice
The top of this figure illustrates a simplified representation of the control mouse with only the CaMKIIα-tTA gene and the rTg4510 mouse with CaMKIIα-tTA and TetO-hMAPT P301L gene. The image below is the western blots of tau protein phosphorylation in the mouse dorsal hippocampus. The proteins are extracted from the hippocampus due to the fact that the hippocampus is essential for forming memories. As reflected in figure, both control and rTg express actin protein. On the other hand, only rTg mice exhibit AT8 phosphorylated tau protein.

Conclusions

- The time spent exploring represents the preference the mouse expresses towards the objects.
- The control mice exhibit preference towards the displaced object. In contrast, the rTg mice did not show a clear preference.
- The mouse's preference suggests their ability to identify objects in space, which corresponds to the function of the hippocampus. If they do not exhibit clear preference, meaning the mice do not remember the location of the object after 24 hours. This shows that the rTg mice exhibit long-term memory deficits and impaired memory consolidation.
- The PCR and Western blotting results verify the genotype of each mouse and validate the SOR scoring, demonstrating that the rTg mice form neurofibrillary tangles in brain.

Implications

- These findings suggest that rTg4510 mouse model could be used to simulate medical conditions in ADRD.
- Our study provides an alternative method to research the mechanisms for memory loss.
- Future studies should seek to approach ADRD clinically using our mouse model.

Acknowledgments

Special thanks to Utsav Mukherjee, Dr. Snehajyoti Chatterjee, Dr. Ted Abel, all members from Ted Abel lab as well as the University of Iowa Carver College of Medicine for mentoring and guiding me on this project. I would also like to thank the SSTP program for providing me with this opportunity.

References

- Chatterjee, S., Bahl, E., Mukherjee, U., Walsh, E. N., Shetty, M. S., Yan, A. L., Vanrobaeys, Y., Lederman, J. D., Giese, K. P., Michaelson, J., & Abel, T. (2022). Endoplasmic reticulum chaperone genes encode effectors of long-term memory. *Science Advances*, 8(12). <https://doi.org/10.1126/sciadv.abm6063>
- Chatterjee, S., Walsh, E. N., Yan, A. L., Giese, K. P., Safe, S., & Abel, T. (2020). Pharmacological activation of NR4A rescues age-associated memory decline. *Neurobiology of Aging*, 85, 140–144. <https://doi.org/10.1016/j.neurobiolaging.2019.10.001>
- Shetty, M. S., Ris, L., Schindler, R. F., Mizuno, K., Fedele, L., Giese, K. P., Brand, T., & Abel, T. (2021). Mice lacking the cAMP effector protein POPDC1 show enhanced hippocampal synaptic plasticity. *Cerebral Cortex*. <https://doi.org/10.1093/cercor/bhab426>

Does Factor VIII deficiency (Hemophilia A) cause increased neuroinflammation?

Hadil El-Genedy¹, Kendall Cornick², Danielle York³, Janice Staber, MD³

¹Rivermont Collegiate; ²Carver College of Medicine, University of Iowa; ³Department of Pediatrics, University of Iowa Stead Family Children's Hospital

Background

- Hemophilia A is a genetic bleeding disorder that prevents blood from properly clotting due to the lack of clotting factor VIII (FVIII).
- Patients with hemophilia A receive FVIII protein replacement therapy, greatly improving their life expectancy and quality of life.
- However, those suffering with hemophilia A have neurophenotypic differences such as increased rates of anxiety and depression, decreased brain volumes, and increased cerebral microbleeds.
- Preliminary studies from the Staber Lab have shown that mice with hemophilia A experience behavioral differences compared to wild type mice.
- These neuropathologic differences including the increased rates of anxiety and depression and the behavioral differences could be caused by neuroinflammation.

Objectives

- This study aims to characterize the neuroinflammatory response in a mouse model of hemophilia A by measuring microglial activation and gene expression levels of neuroinflammatory markers (CD206, iNOS, TNF- α , IL-4R α , IL-1 β , IL-6, TGF- β , IL-4R α , and IL-10).
- Microglial activity was measured by analyzing microglial morphology in the hippocampus, cortex, and thalamus of hemophilia A and wild type mice as well as quantifying microglia in different stages of activation.
- We hypothesize that FVIII deficient (hemophilia A) mice will have increased expression of pro-inflammatory markers and increased microglial activity compared to controls.

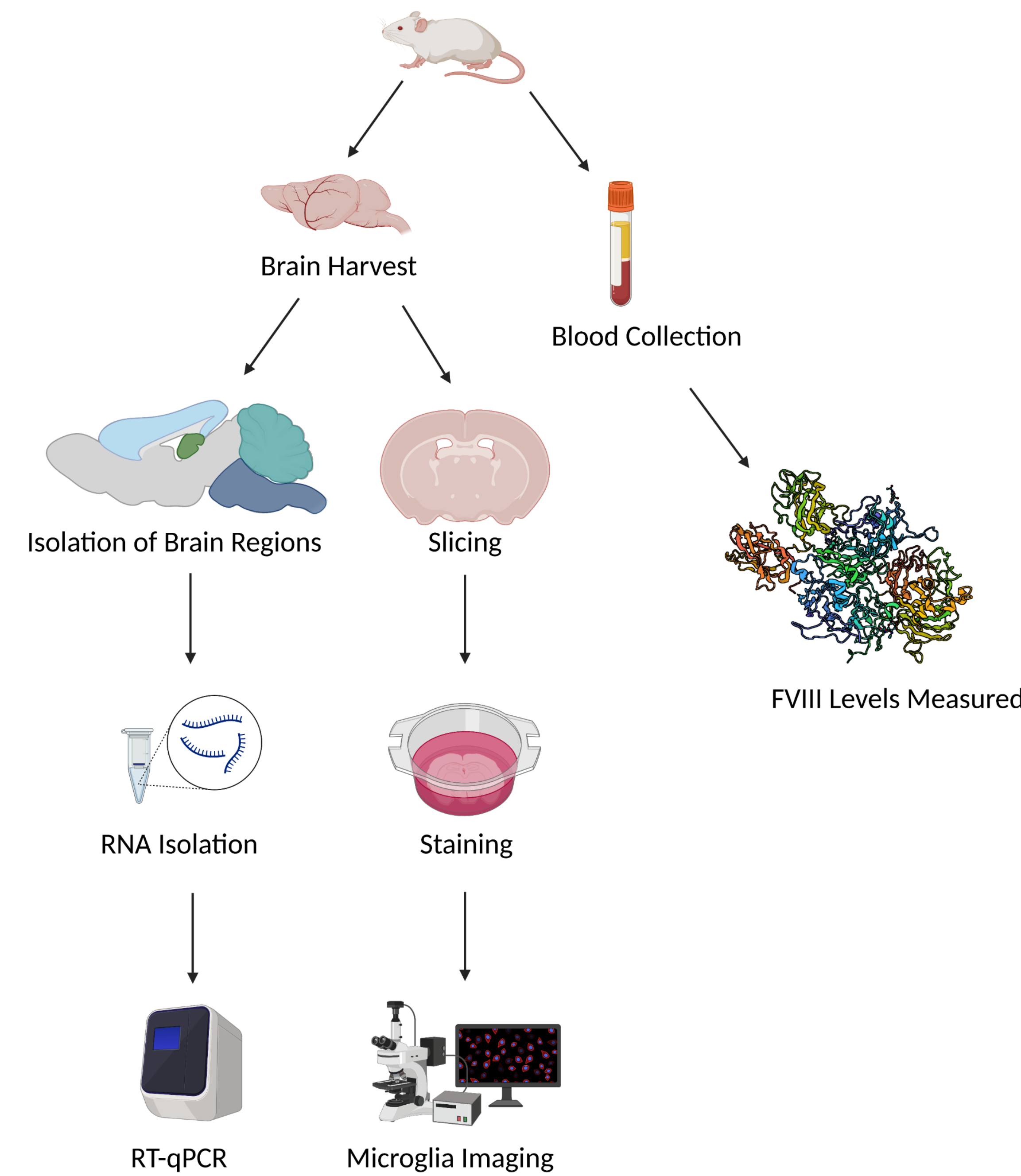
Microglia Classification

Microglia	Classification	Image
Ramified	"Resting" microglia surveying immunity	
Rodlike	Microglia at the beginning of activation	
Bushy	Activated microglia	
Ameboid	Post-activation microglia	

Figure 1. Microglia Classifications

Microglia classifications form a spectrum from ramified, "resting" microglia, to ameboid, microglia post-activation. This spectrum can be broken down into four broad classifications, with each classification corresponding to a different level of activation and a distinct morphology.

Methodology



- Hemophilia A (HA) and wild type (WT) mice on a Bl6/C57 background were used for these studies.

FVIII Levels Measured

- Blood was collected from 6-month-old mice via a retroorbital eye bleed.
- Blood was spun down in a centrifuge to separate and obtain plasma.
- FVIII levels were measured using the plasma in order to determine severity of hemophilia in the hemophilic mice (data not shown).

Microglia Activity

- Brains from 6-month-old HA and WT mice were harvested.
- The brains are then sectioned and stained using immunofluorescence.
- Immunofluorescent staining included Iba-1 and CD68, markers of microglial activation.
- After slides are stained, they are imaged under a confocal microscope in order to determine differences in microglial quantity, activity, and morphology.

Gene Expression of Neuroinflammatory Markers

- 6-month-old hemophilic and wild type mice brains were harvested.
- The cortex, brainstem, and cerebellum were isolated from these brains and used for RNA isolation.
- From the isolated RNA, cDNA was generated to run RT-qPCR and measure gene expression.
- Neuroinflammatory markers measured include CD206, iNOS, TNF- α , IL-4R α , IL-1 β , IL-6, TGF- β , IL-4R α , and IL-10.
- GraphPad Prism will be used to preform statistical analysis such as a one-way ANOVA and a Tukey's post-hoc test (once data is completely collected). GraphPad Prism was used to graph data.

Results

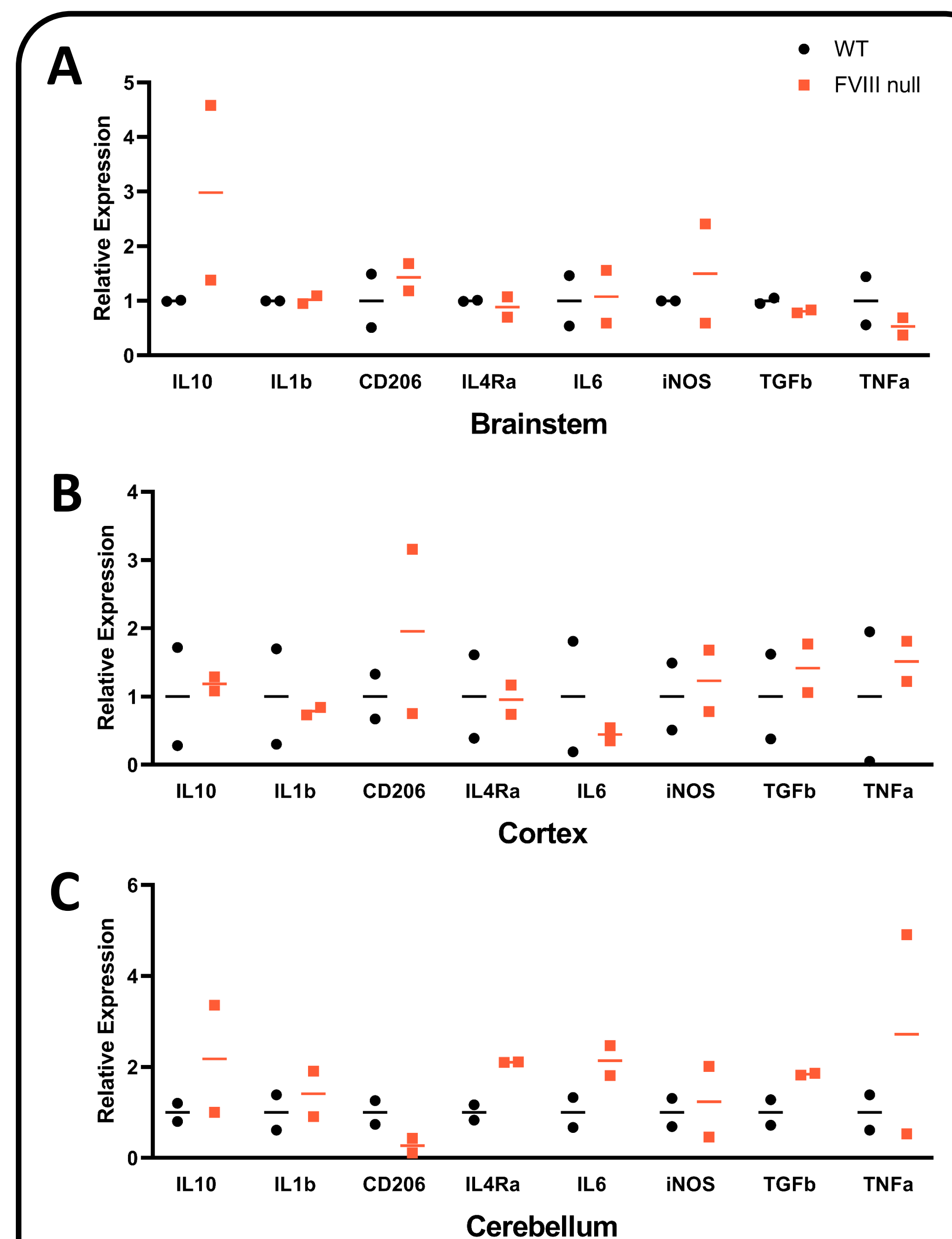
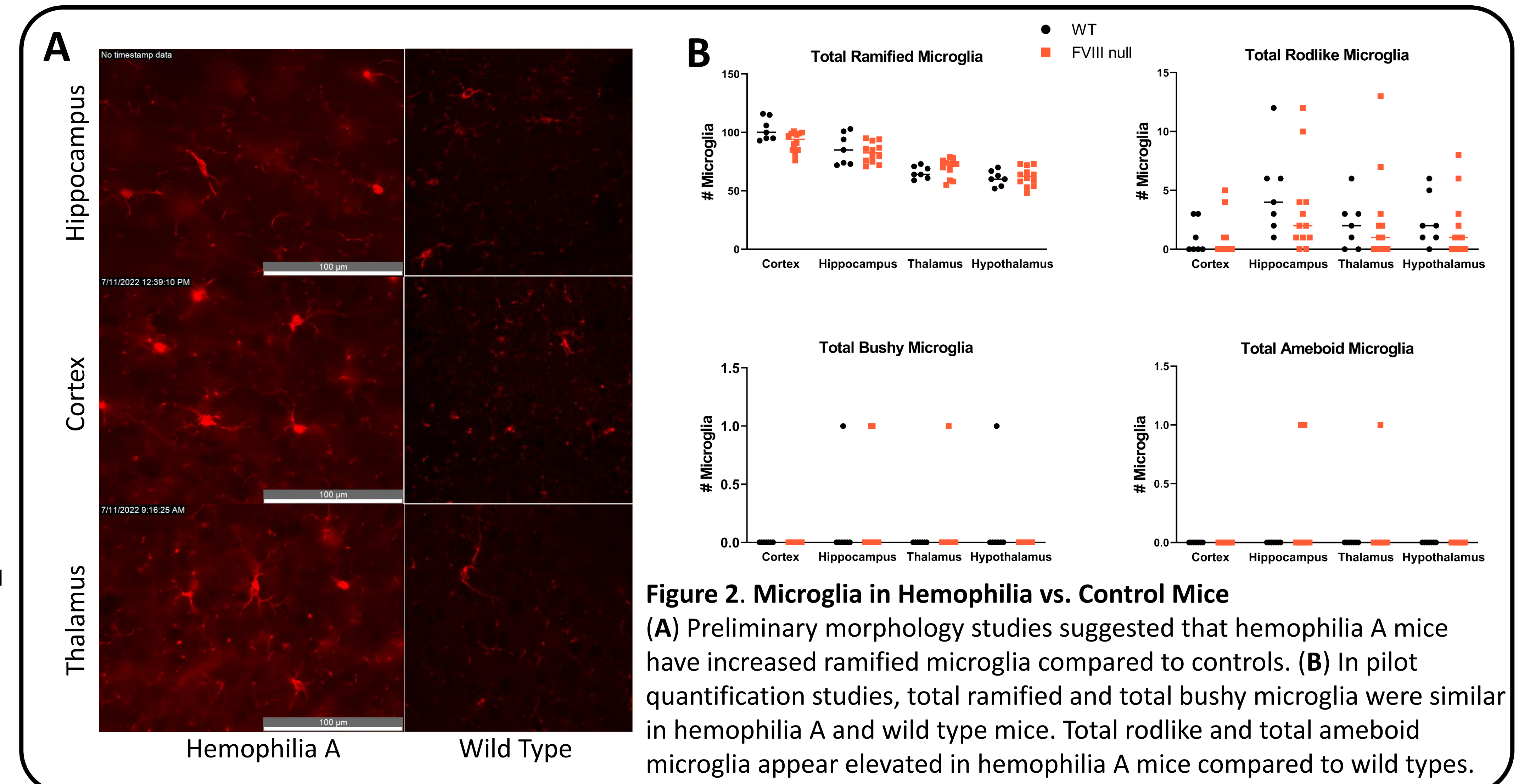


Figure 3. Relative Gene Expression in Hemophilia vs. Controls
(A) Relative expression of IL-10, CD206, and iNOS appear elevated in the brainstems of HA mice. **(B)** CD206 is elevated in the cortex of one HA mouse, but altogether expression appears similar between HA and WT. **(C)** IL-10, IL-1 β , IL-4R α , IL-6, iNOS, TGF- β , and TNF- α appear elevated in the cerebellum of HA mice compared to WT.

Conclusions

- Confirming our hypothesis, expression of neuroinflammatory markers remained similar between wild type and hemophilia A mice in the cortex.
- In the brainstem and cerebellum of HA mice, three and seven markers (respectively) showed elevation compared to WT mice, indicating activation of neuroinflammatory pathways.
- Total rodlike and ameboid microglia appear elevated in HA mice, indicating elevated microglial activity.
- The activation of microglia and neuroinflammatory pathways could be correlated with the increased mental health disorders and decreased neurocognition seen in patients with HA.

Acknowledgements

I would like to thank the SSTP program and everyone at the Belin-Blank Center for this opportunity. Special thanks to Dr. Staber, Danielle York, and Kendall Cornick for welcoming me in the lab, allowing me to take on their project, and for their gracious mentoring.

References

- Chang, C. F., Wan, J., Li, Q., Renfro, S. C., Heller, N., & Wang, J. (2017). Alternative activation-skewed microglia/macrophages promote hematoma resolution in experimental intracerebral hemorrhage. *Neurobiology of Disease*, 103, 54-69. 10.1016/j.nbd.2017.03.016
- Cherry, J. D., Olschowska, J. A., & O'Banion, M. K. (2014). Neuroinflammation and M2 microglia: the good, the bad, the inflamed. *Journal of Neuroinflammation*, 11(1). <https://doi.org/10.1186/1742-2094-11-98>
- Kumar, A., Barrett, J. P., Alvarez-Croda, D. M., Stoica, B. A., Faden, A. I., & Loane, D. J. (2016). NOX2 drives M1-like microglial/macrophage activation and neurodegeneration following experimental traumatic brain injury. *Brain, Behavior, and Immunity*, 58, 291-309. 10.1016/j.bbi.2016.07.158
- Leng, F., & Edison, P. (2021). Neuroinflammation and microglial activation in Alzheimer disease: where do we go from here? *Nature Reviews: Neurology*, 17(3), 157-172. 10.1038/s41582-020-00435-y
- Rauf, A., Badoni, H., Abu-Izneid, T., Olatunde, A., Rahman, M., Painuli, S., Semwal, P., Wilairatana, P., & Mubarak, M. S. (2022). Neuroinflammatory Markers: Key Indicators in the Pathology of Neurodegenerative Diseases. *Molecules*, 27(10). doi:10.3390/molecules27103194
- Biorender. BioRender. (n.d.). Retrieved July 25, 2022, from <https://biorender.com/>

Introduction

The abstract concept of number is a common dimension seen in daily interactions with the physical world. While once thought to be a uniquely human skill, numerosity can also be perceived by nonhuman animals such as pigeons and bees.

Many theories have proposed that number is correlated with nonnumerical magnitudes such as the total area of all stimulus elements (Lourenco and Aulet, 2022). Research has also shown that numerosity is used as a discriminative stimulus when other cues are made irrelevant (Kubo, 2020).

In this study, three different relations between the total area of the stimulus elements and numerosity were devised to identify the interdependence among these quantities: confounded, matched, and conflicting.

- Confounded** : More items, More Area
- Matched** : More items, Equal Area
- Conflicting** : More Items, Less Area

Methods

Subjects (n=4) were trained to discriminate numerosity. In some trials, choice of the larger number was correct, and on other trials, choice of the smaller number was correct depending on the color of the items.

Training Phase:

- Confounded Area
- Matched Area

Testing Phase:

- Training Phase Areas
- Conflicting Area

Experimental Setup

For each trial, a peck to the start stimulus was followed by two response options on either side of the screen. Food pellet reinforcement followed correct responses, but not following incorrect responses.

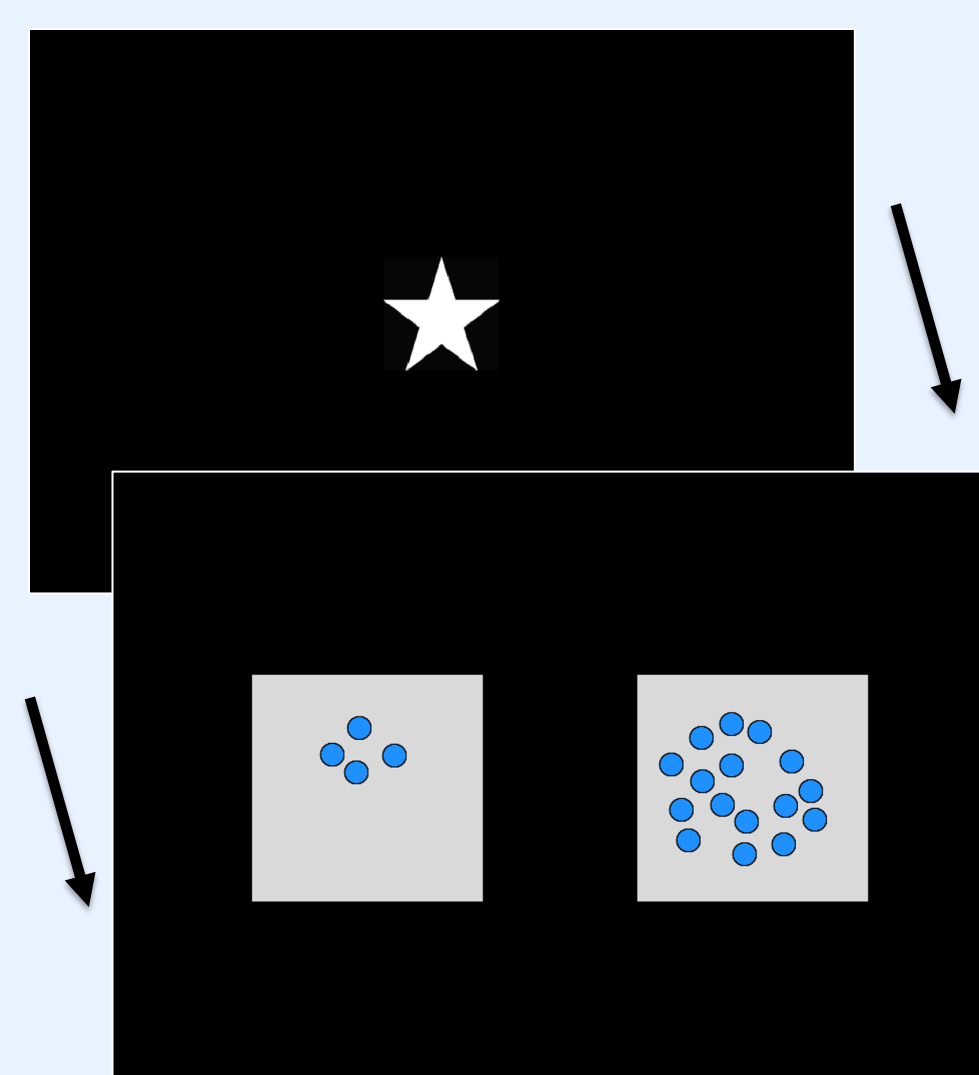


Figure 1. Trial sequence

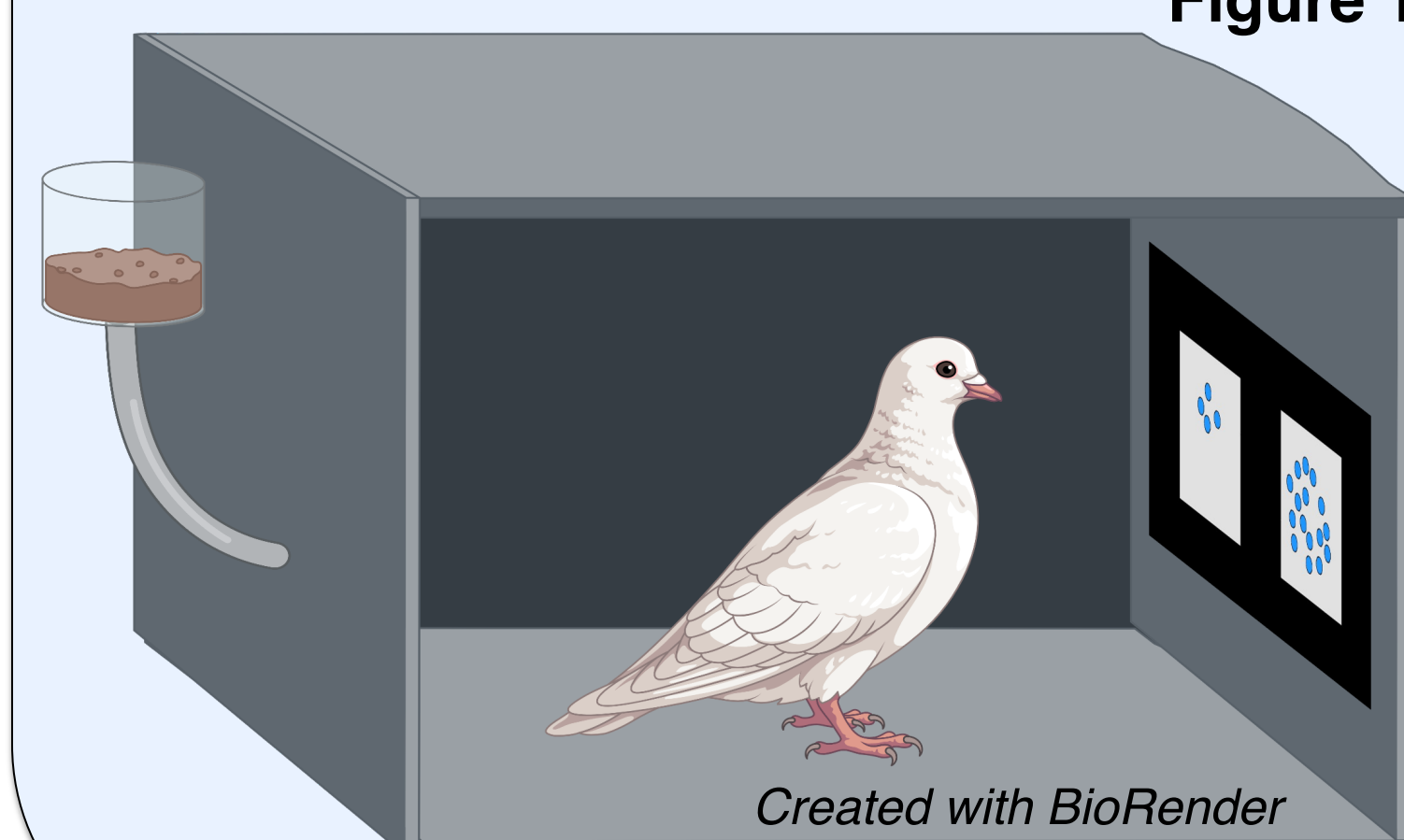


Figure 2. Experimental Setup

Area Manipulation

Training Phase

Confounded	60 Trials
Match Many	60 Trials
Match Few	60 Trials
Conflicted	N/A
Total Trials	180 Trials

Testing Phase

Confounded	60 Trials
Match Many	60 Trials
Match Few	60 Trials
Conflicted	20 Trials
Total Trials	200 Trials

Figure 3. Trial Layout in Training and Testing Phases: During Training, pigeons were given 180 trials equally divided among five numerosity ratios (1:1 to 4) and two tasks (choose more/choose fewer). During Testing, 20 conflicting trials were added.

Confounded Area

Matched Area

Conflicting Area

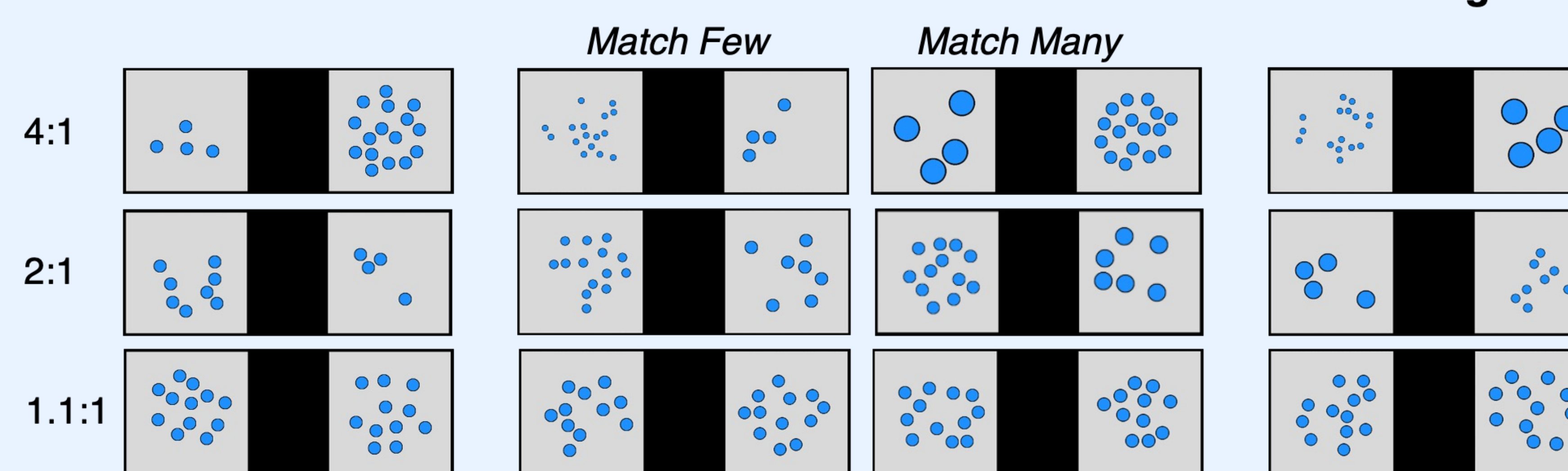


Figure 5. Various Numerosity Ratios: To assess the pigeons' ability to discriminate number, five numerosity ratios were presented: 1:1.1, 1:1.5, 1:2, 1:3, and 1:4. Three area manipulations were presented. In the Confounded Area, total element area was positively correlated with numerosity. Matched Area modified the total area on one side to match the other depending on the trial type (Match Many or Match Few). For Conflicting Area, the ratio of the area was the opposite to that of numerosity.

Results

Training Phase

Figure 6. Effect of Numerosity Ratio: As the ratio between the stimuli's numerosity rose, the pigeons' accuracy improved significantly from near chance to 90% correct. Bars represent mean accuracy and error bars ± SEM.

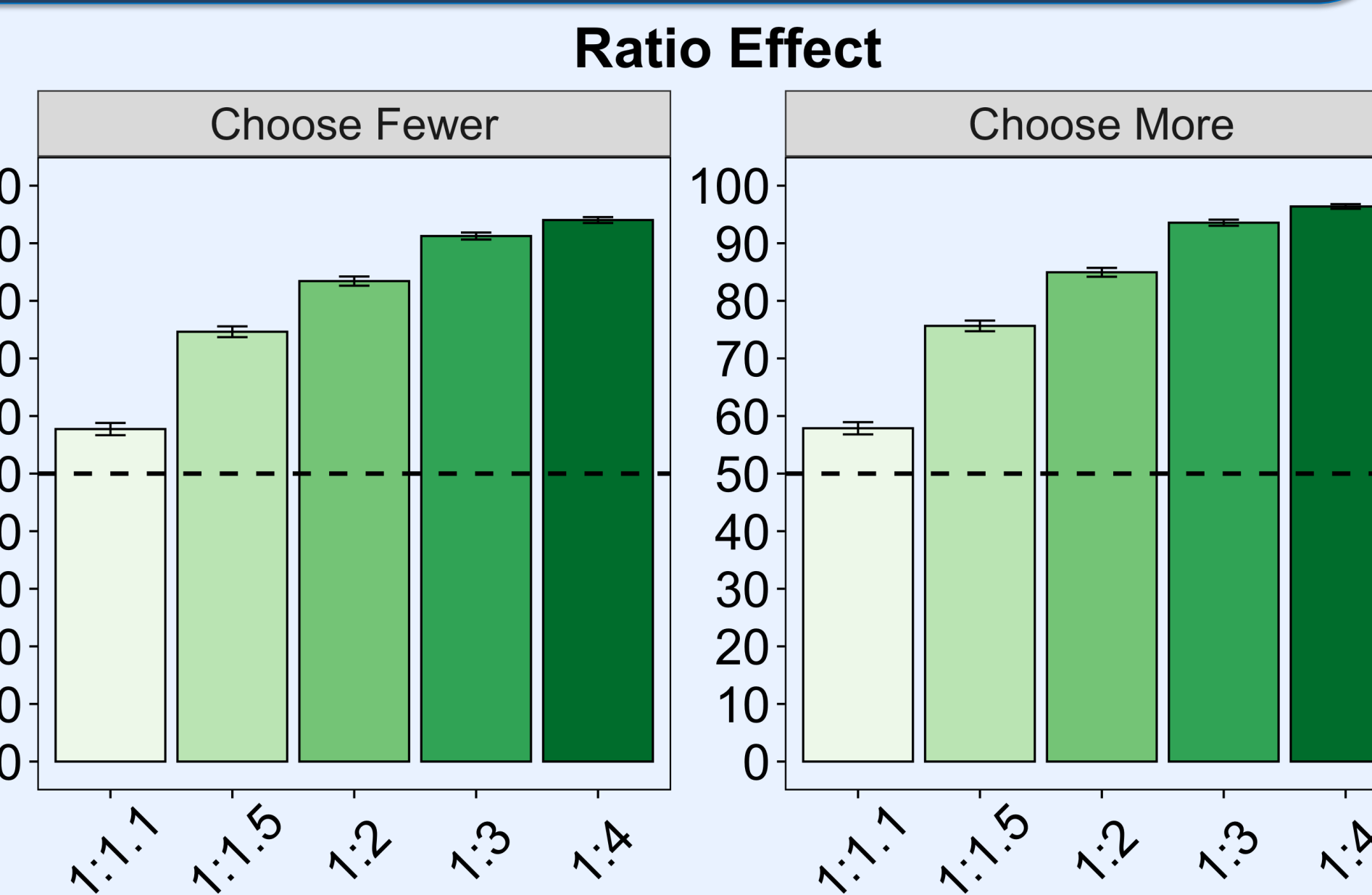
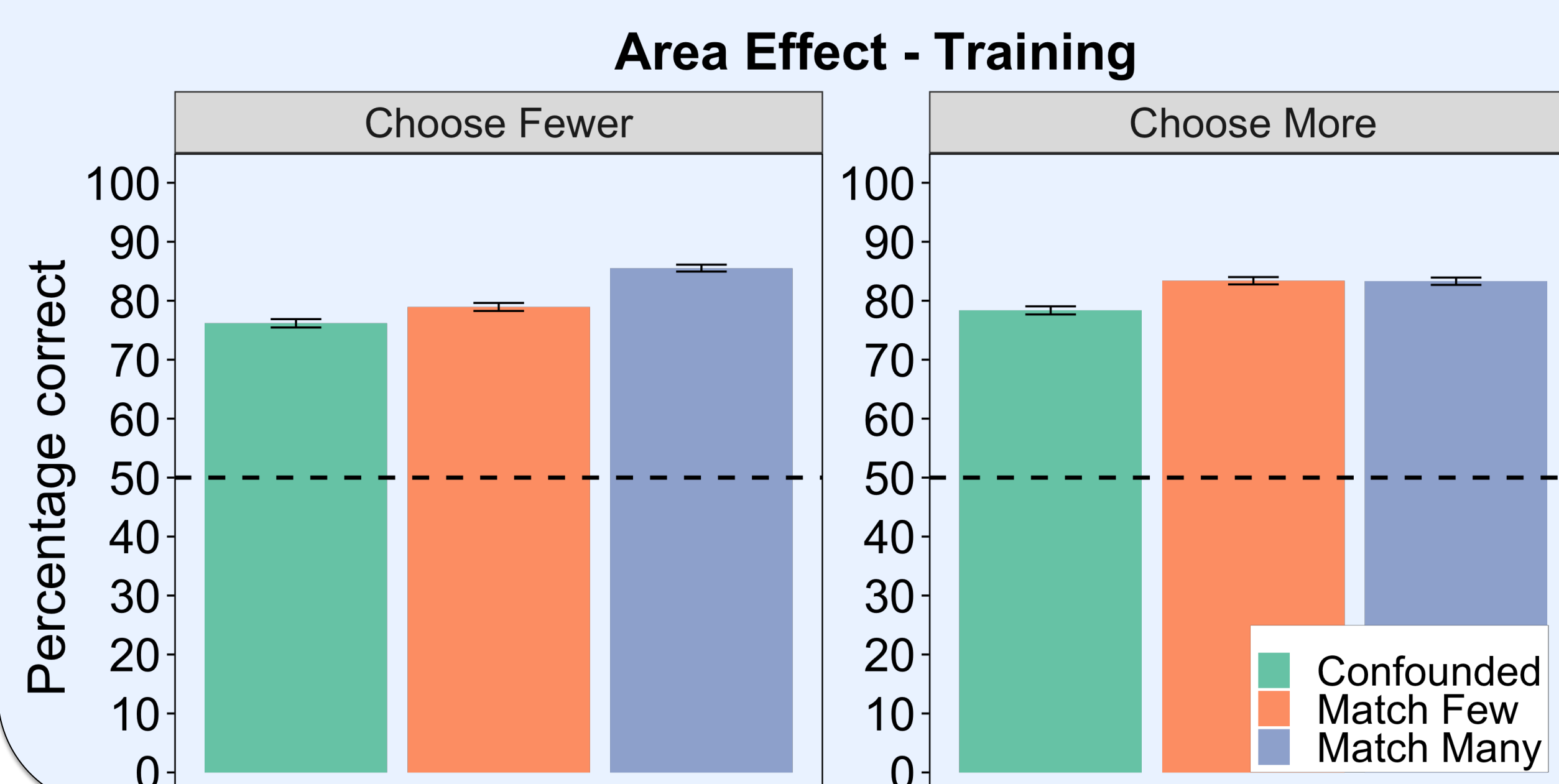


Figure 7. Area Manipulation during Training: Pigeons demonstrated similar accuracy when the total area of the elements was either matched on both sides of the screen or when positively correlated with numerosity. Bars represent mean accuracy and error bars ± SEM.

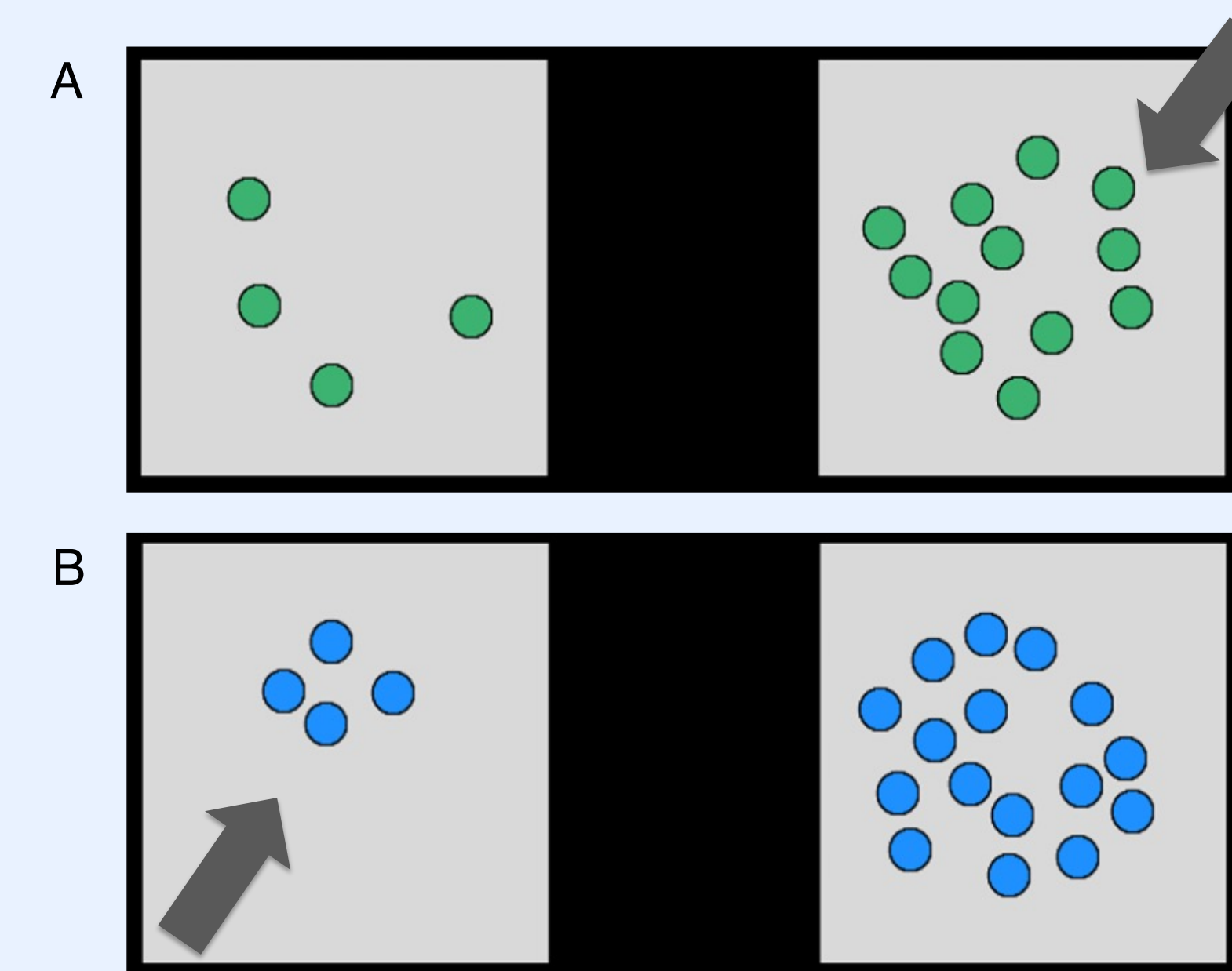


Figure 4. Task: The color distinctions were used to instruct the subjects to peck either the array with more or fewer items (task assignments were counterbalanced among subjects).

Testing Phase

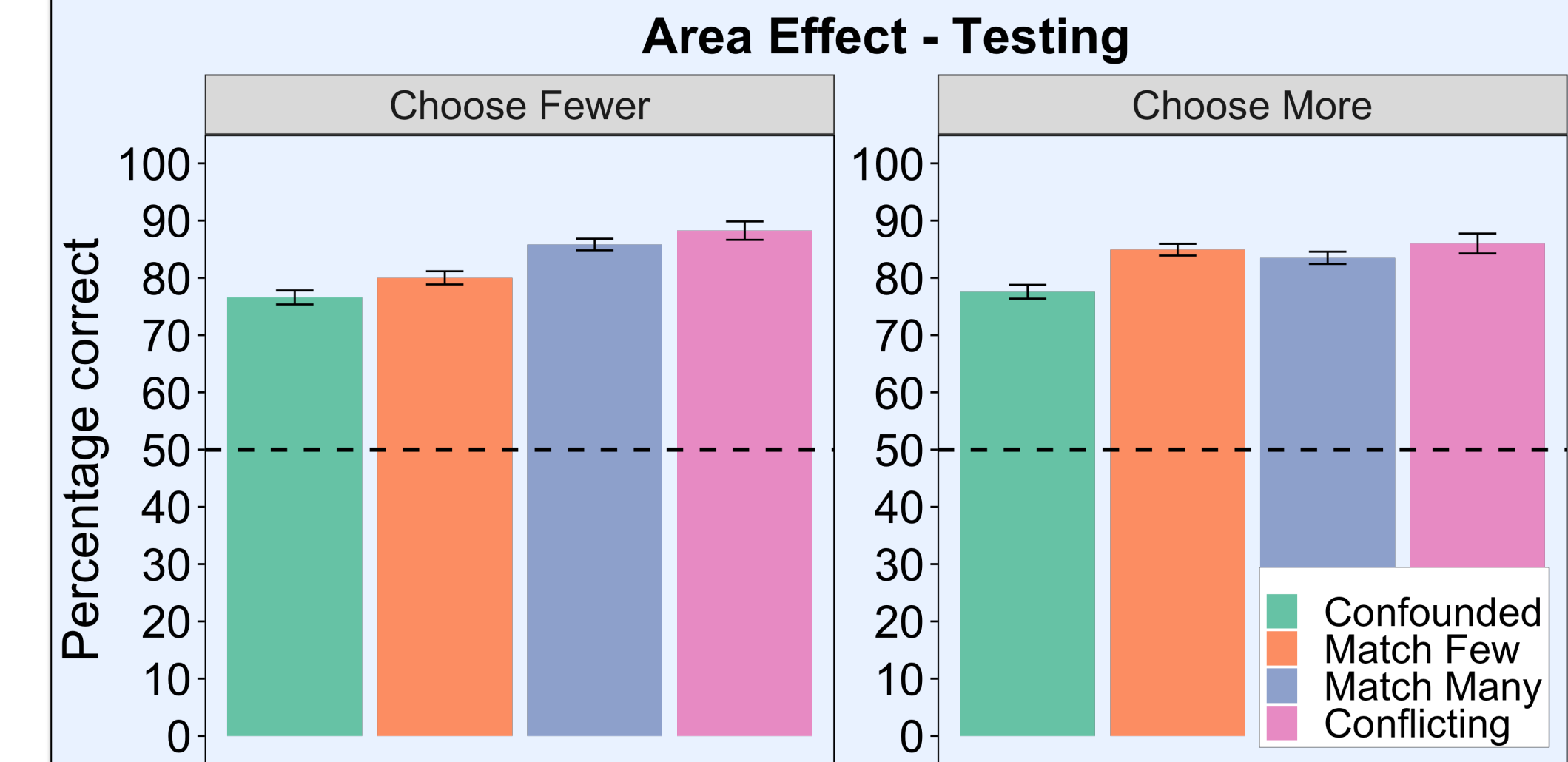


Figure 8. Area Manipulation during Testing: Critical testing trials with conflicted area and number yielded extremely high accuracy scores, unlike the below-chance scores which should have been produced if the birds were controlled by area alone. Bars represent mean accuracy for different trial types, and error bars ± SEM.

Conclusions

The pigeons exhibited excellent numerical accuracy scores under all manipulations of element area. These results imply strong control by number rather than area.

1. Pigeons learned to discriminate number, showing sensibility to numerical disparities.
2. Manipulated element areas didn't impair pigeons' abilities to discriminate number.

Future experiments should further explore the interactions with number and area, without training with matched area. Additionally, other visual cues that could impact stimulus discrimination in pigeons is also worth investigating (DeWind, Bonner, and Brannon, 2020).

References

DeWind, N. K., Bonner, M. F., & Brannon, E. M. (2020). Similarly oriented objects appear more numerous. *Journal of Vision*, 20(4), 4. <https://doi.org/10.1167/jov.20.4.4>

Kubo, N. (2020). Changes in Pigeons' Responses to Numerical Stimuli Depending on Total Element Area Differences between Stimuli. *Psychological Record* 72, (33–41). <https://doi.org/10.1007/s40732-020-00437-8>

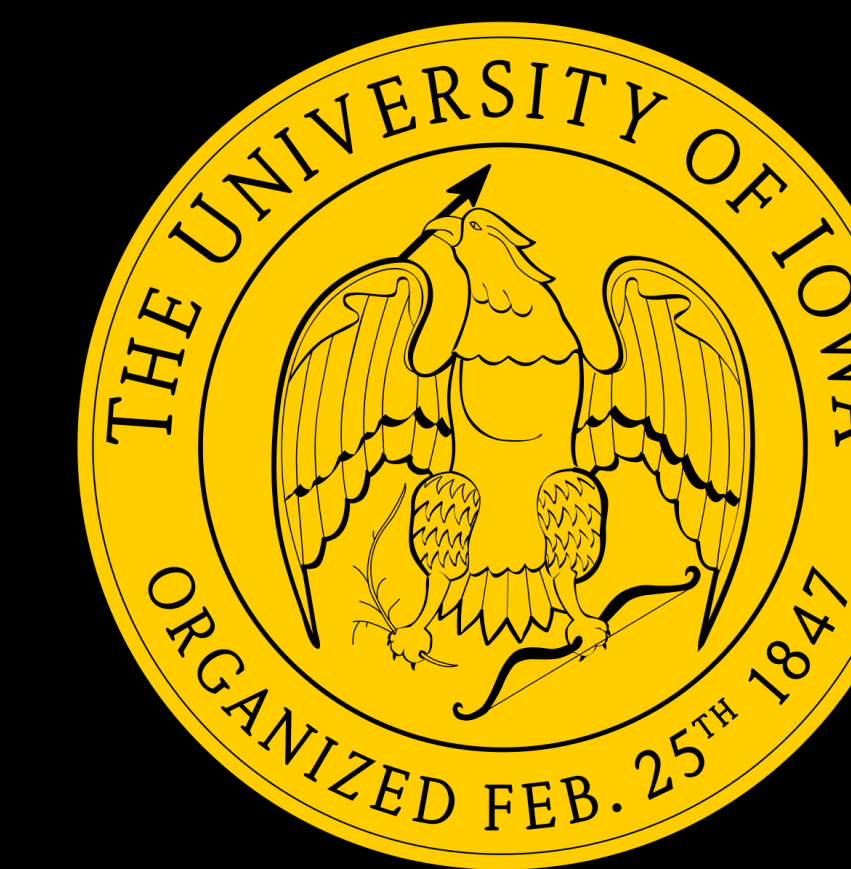
Lourenco, S. F., & Aulet, L. S. (2022). A Theory of Perceptual Number Encoding. *Psychological Review*. <https://doi.org/10.31234/osf.io/p7rqn>

Pyridine Activation Strategies: Synthesis of 4-Alkyl Pyridines

Developing Methods in Organic Chemistry

Jonah Hanson, Soe Tun, F. Christopher Pigge

Department of Chemistry, University of Iowa

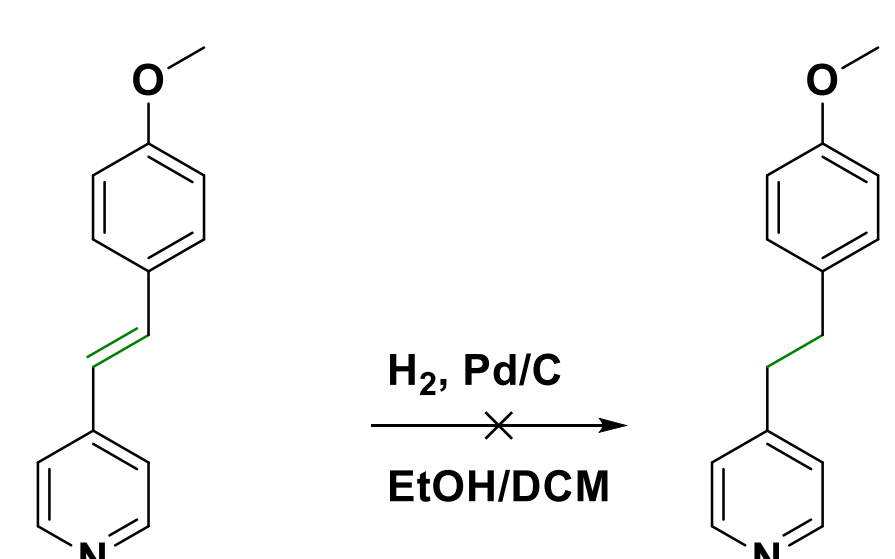
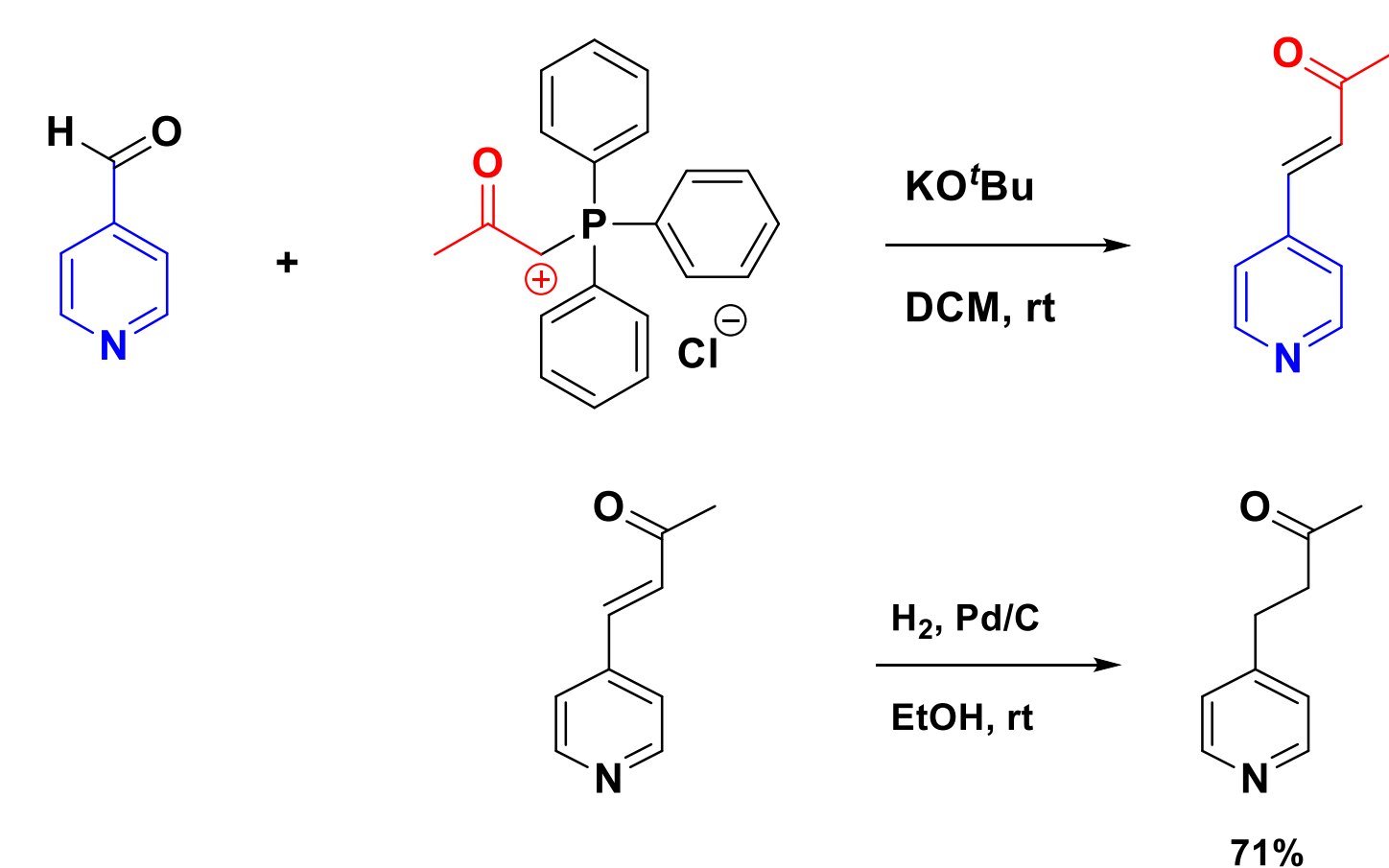
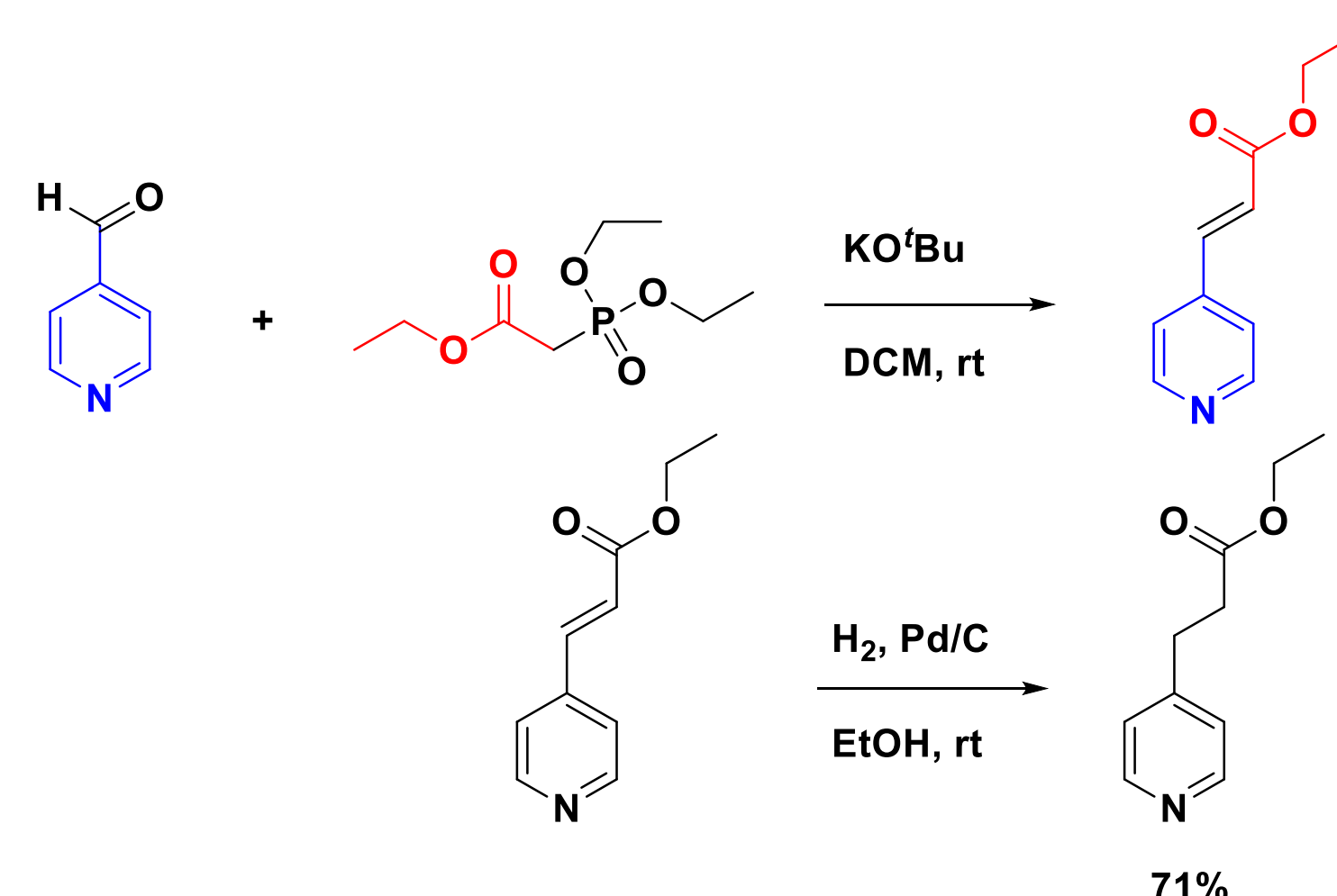


Introduction

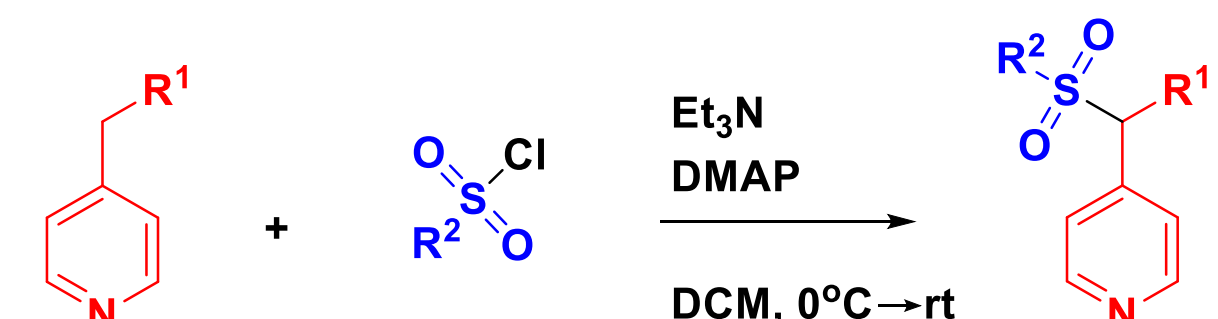
The crux of this project is to develop new methods for creating building blocks for pharmaceuticals. We found that 4-alkyl pyridine derivatives can readily undergo sulfonylation using various sulfonyl chloride derivatives under mild conditions. These methods can be used to create parts of pharmaceutical drugs.

Synthesis of 4-Alkyl Pyridine Precursors

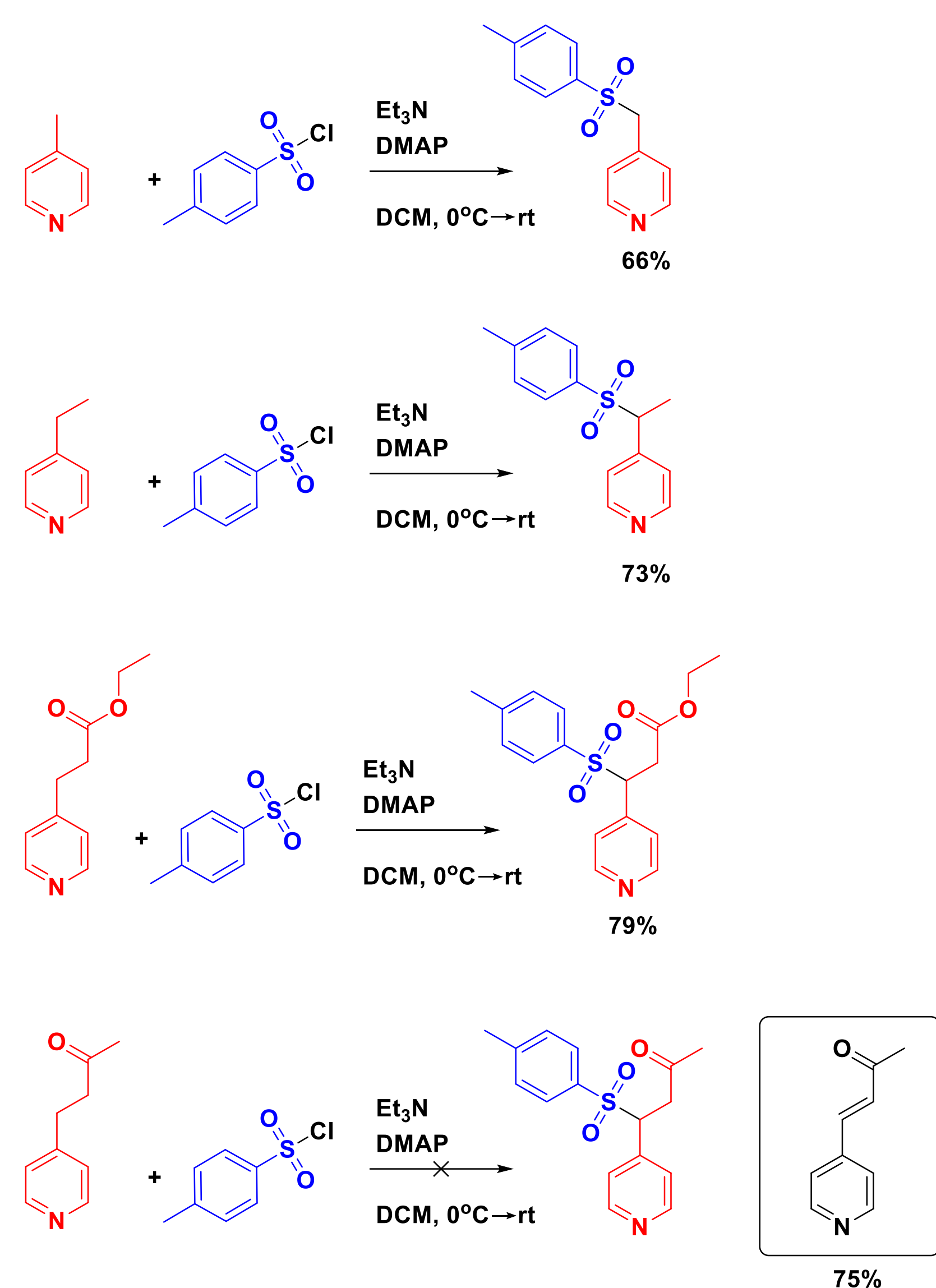
Synthesis of precursors was achieved either by Horner-Wadsworth-Emmons (HWE) reaction or Wittig reaction followed by hydrogenation. The resulting compounds were used to test the scope of the reaction using sulfonyl chloride in a later step.



Sulfonylation of 4-Alkyl Pyridines: General Reaction Scheme



Exploring Scopes and Limitations

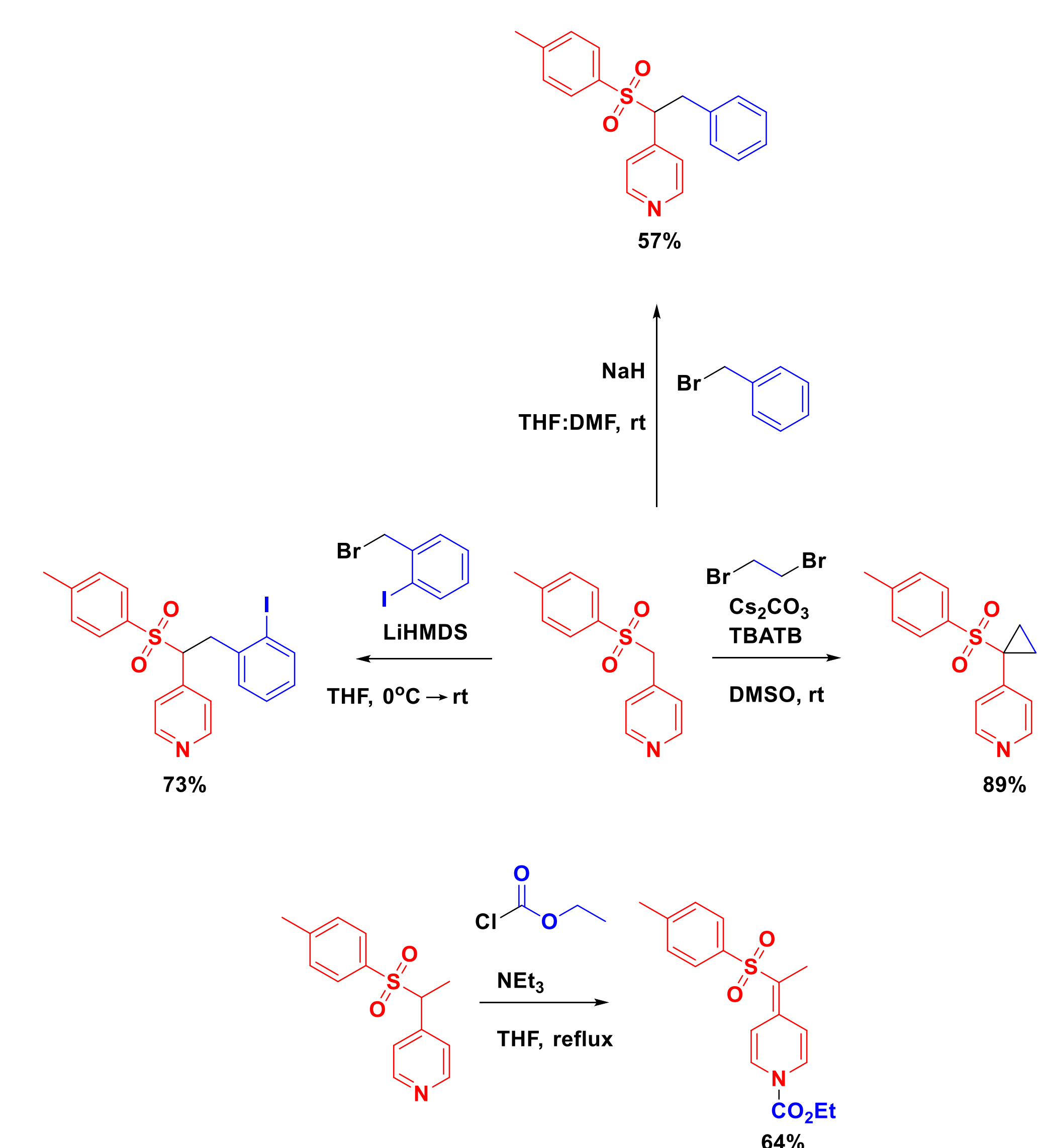


Purification

- Acid-Base Extraction
- Recrystallization
- Flash Column Chromatography

Post-Synthetic Modification of 4-(Tosylmethyl) Pyridine

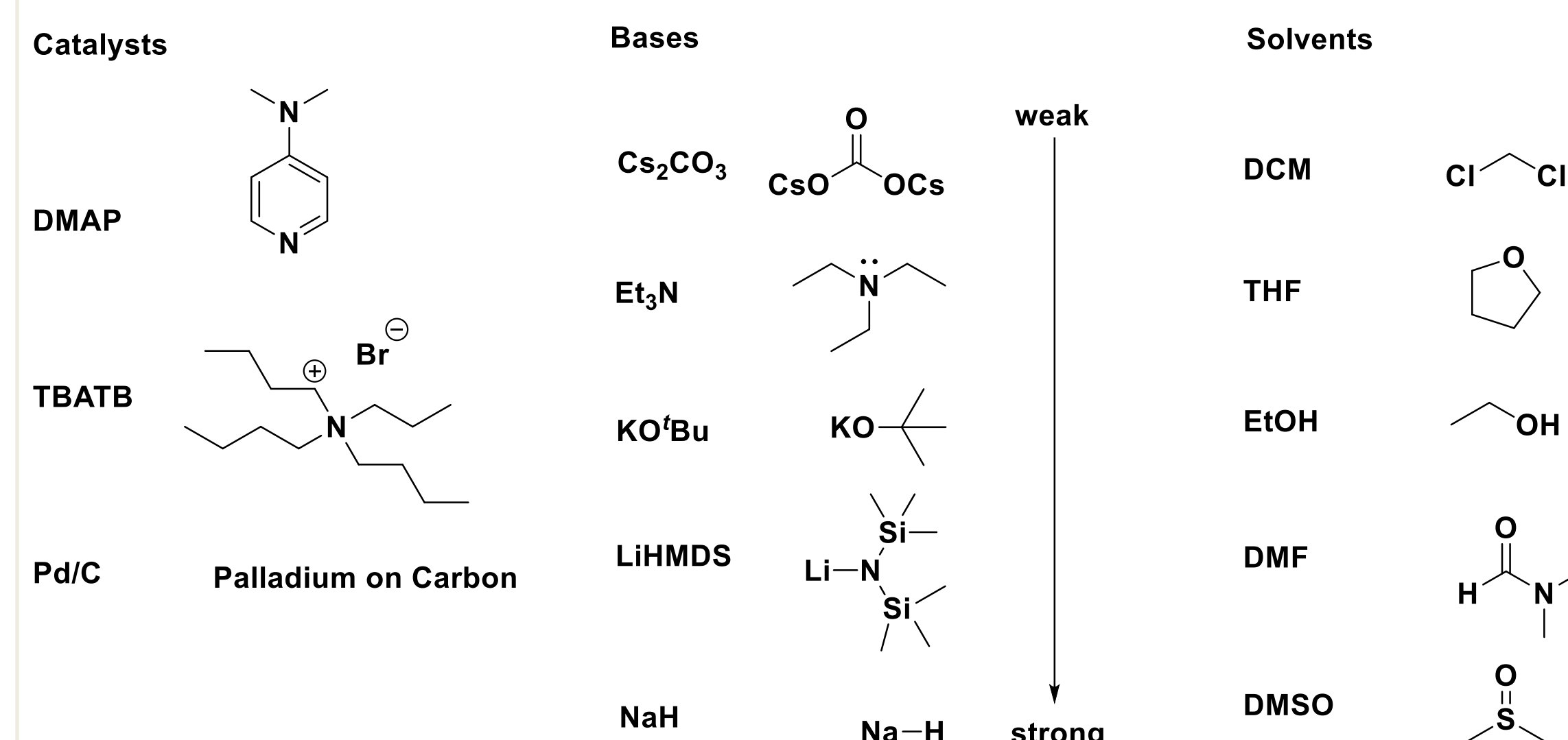
To show the application of our newly synthesized compounds, we further treated one of our targeted products (4-(tosylmethyl) pyridine) with different reagents.



Characterization

- Melting Point tells us how strong our compound's intermolecular forces are and how pure it is
- Nuclear Magnetic Resonance (NMR) gives information about how many unique hydrogens and carbons are in our compound
- Mass Spectrometry gives information about the chemical composition of the compound

Catalysts, Bases, and Solvents Used

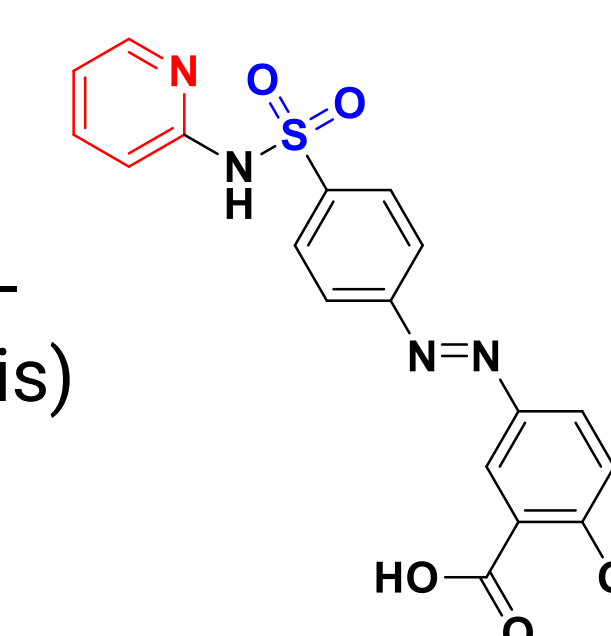


- Each reaction performed better using certain bases, solvents, and catalysts
- Stronger bases are more dangerous to use due to high reactivity
- Some bases and solvents reacted together which inhibits the reaction
- Certain solvents were harder to remove in the purification process

Pharmaceutical Potential

The compounds we created can be further manipulated to gain access to complex synthetic intermediates in pharmaceutical drugs more readily. They have been clinically shown to treat cancers, malaria, arthritis, tuberculosis, and other serious conditions. This project streamlines the drug manufacturing process by developing more efficient methods to synthesize building blocks of crucial pyridine-containing drugs.

Sulfasalazine
disease-modifying anti-rheumatic drug (arthritis)



Acknowledgments

I would like to thank the Secondary Student Training Program and the University of Iowa for giving me this great research opportunity.

IOWA

Time-of-day-dependent seizure mortality in a mouse model of Dravet Syndrome

Ariana Hernández-Vázquez¹, Benjamin L Kreitlow²⁻⁶, and Gordon F Buchanan²⁻⁶

¹Secondary Student Training Program, ²Medical Scientist Training Program, ³Interdisciplinary Graduate Program in Neuroscience, ⁴Iowa Neuroscience Institute, ⁵Department of Neurology, ⁶Carver College of Medicine, Iowa City, IA, USA

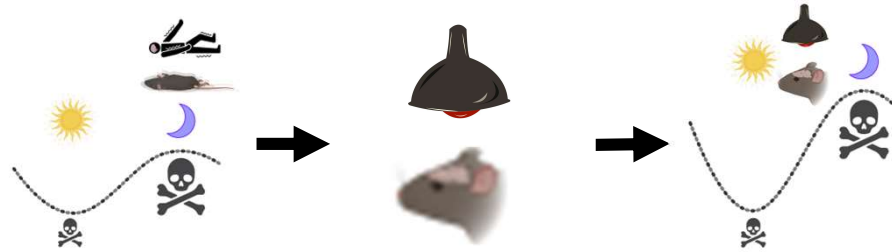


Introduction

- Epilepsy is a neurological disease characterized by spontaneous seizures.
- The phenomenon where a person dies due to a seizure is known as **sudden unexpected death in epilepsy (SUDEP)**¹
- SUDEP happens more during the night in both humans and rodent models^{2,3}
- Nighttime SUDEP risk appears to have a circadian rhythm component⁴
- Dravet Syndrome is a form of epilepsy that starts early in life and has a high risk of SUDEP⁵

Graphical Abstract

HYPOTHESIS: *Scn1a*^{R1407X/+} mice are more likely to die following heat-induced seizures during the night.



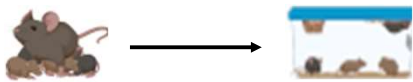
Discussion/Conclusion

- SUDEP is more likely to occur during the night.
- Although spontaneous deaths in the *Scn1a*^{R1407X/+} have been shown to occur more often during the night, whether or not this is true for heat-induced seizures is unknown.
- Preliminary evidence from this study demonstrates that **heat-induced seizures that occur during the night are more likely to be fatal.**
- However, it is not clear which mechanisms contribute to this nighttime risk.
- Two potential contributors are the suprachiasmatic nucleus, the body's circadian pacemaker or oscillating neurotransmitters, such as serotonin.

Materials and Methods

Mouse Model: *Scn1a*^{R1407X/+} mouse model of Dravet Syndrome. These mice experience potentially fatal seizures shortly after development and are susceptible to heat-induced seizures^{6,7}

- Mice were genotyped by routine PCR
- Mice were weaned at post-natal day 21



- Radio telemeters were implanted into the subcutaneous space to measure temperature
- Throughout the studied, animals were monitored for spontaneous seizure-associated death



- Animals were subject to a single heat induced seizure at *Zeitgeber Time* (ZT) 6 or 18
- Animals were allowed to acclimate to the chamber for 10 minutes with their temperature held at 37.5 °C before increasing their temperature by 0.5 °C every couple of minutes⁷.
- Temperature and video was analyzed *post-hoc*

Results

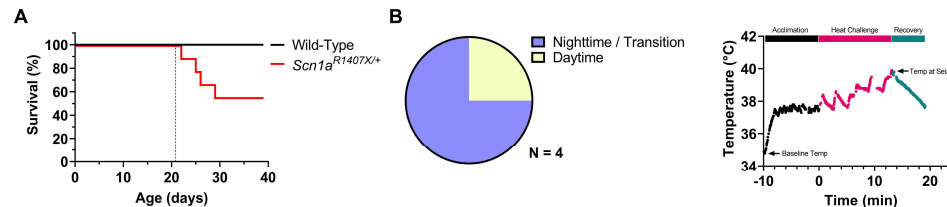


Fig 1. The *Scn1a*^{R1407X/+} mouse model of Dravet Syndrome experiences spontaneous, seizure-associated death. Shortly after weaning (post-natal day 21; hashed line), mice experience spontaneous, seizure-associated death (A). Mice were housed in a 12:12 light-dark cycle (lights on at 6 AM, off at 6 PM) and monitored throughout the day (7:30 AM until 4:30 PM). Deaths that occurred during this time were considered daytime deaths, while those outside of this window were groups as nighttime or transition (within 1.5 hours of light cycle change). Three of the four observed deaths occurred during the nighttime or transition period (B). Animals that were euthanized or died following a heat-induced seizure were excluded from analysis.

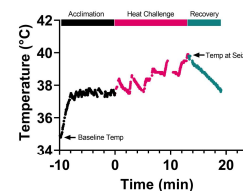


Fig 2. Representative temperature recording during a heat-induced seizure trial. Mice were acclimated for 10 min at 37.5 °C and then slowly warmed up with a heat lamp until experiencing a seizure.

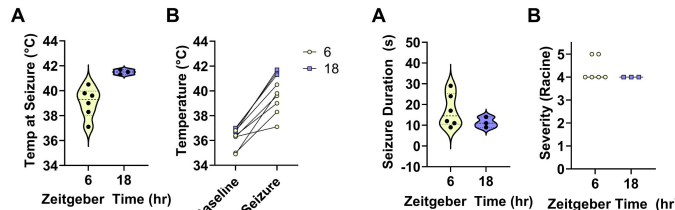


Fig 3. Core body temperature at time of seizure. Seizures induced during the day are associated with a lower temperature required to induce a seizure and increased variability compared to those induced at night (A). However, when comparing baseline temperature, mice have higher core body temperature during the night (B).

Fig 4. Duration and severity of heat-induced seizures does not appear to be influenced by time of day. Video collected from infrared cameras were analyzed *post hoc* to determine the duration and severity of heat-induced seizures.

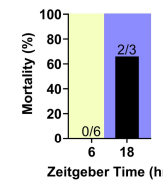
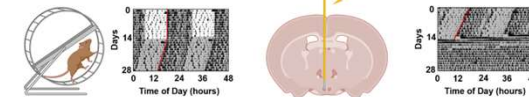


Fig 5. Heat-induced seizures appear to be more fatal during the night. While seizures induced during the day were never fatal, 2/3 of seizures resulted in death.

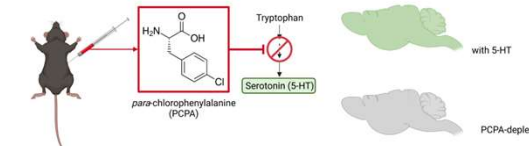
Future Directions

Will the rhythm of death persist if:

1. The brain's circadian pacemaker is destroyed?



2. Serotonin neurons are eliminated from the brain?



Acknowledgements

This work was supported by the NIH/NIGMS T32 CM007337 (to Iowa MSTP), NIH/NINDS R01 NS095842 (to GFB), and the Beth L. Tross Epilepsy Professorship (to GFB). Data was analyzed using GraphPad Prism 9. Vector images created in BioRender.

References

- Nashef, L, et al. 2012. *Epilepsia*. 53(2): 227 – 233.
- Ryvlin, P, et al. 2013. *Lancet Neurol*. 12(10): 966-977.
- Purnell, B. S., et al. 2018. *Front Neurol*. 9: 1079.
- Purnell, B. S., et al. 2021. *J Physiol*. 599(6): 1885-1899.
- Dravet, C, et al. 2011. *Epilepsia*. 52 Suppl 2: 3 – 9.
- Teran, F. A, et al. 2019. *Front Neurol*. 10: 278.
- Oakley, J. C, et al. 2009. *PNAS*. 106(10): 3994-3999.

A Raspberry Pi based Data Acquisition System for a Colorectal Cancer SiNW Array-based Biosensor

Luke Huang¹, Sneha Chakraborty², Brady Lin³, Daniel Keefe⁴, Fatima Toor⁴

²New Canaan High School, New Canaan, CT, USA; ²Irvington High School, Fremont, CA, USA; ³Tianjin Experimental High School, Tianjin, China;

⁴Electrical and Computer Engineering Department, University of Iowa, Iowa City, IA, USA



Motivation and Project Goals

Significance and Motivation:

- CRC is the third leading cause of cancer related death in the US but also one of the most easily preventable form of cancer.
- Point of care testing reduces unnecessary deaths from people avoid screening out of embarrassment.

Project Goals:

- Create an efficient data acquisition system (DAQ) for the colorectal cancer (CRC) SiNW array biosensor silicon.
- Facilitate the biosensor's use as point of care test.

Why Silicon Nanowire Array Biosensor?

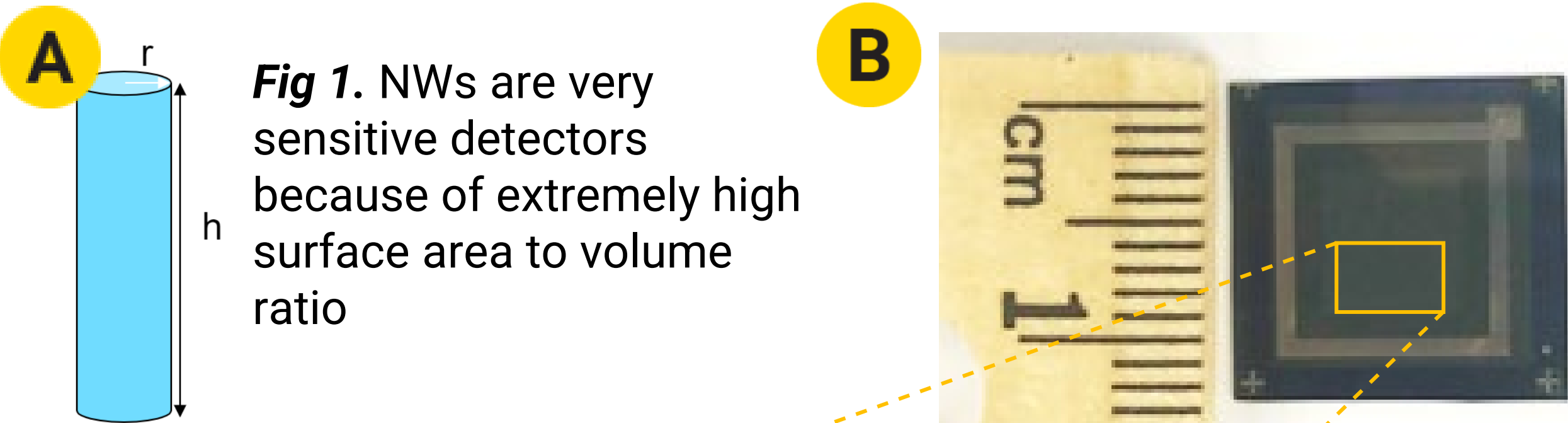


Fig 1. NWs are very sensitive detectors because of extremely high surface area to volume ratio

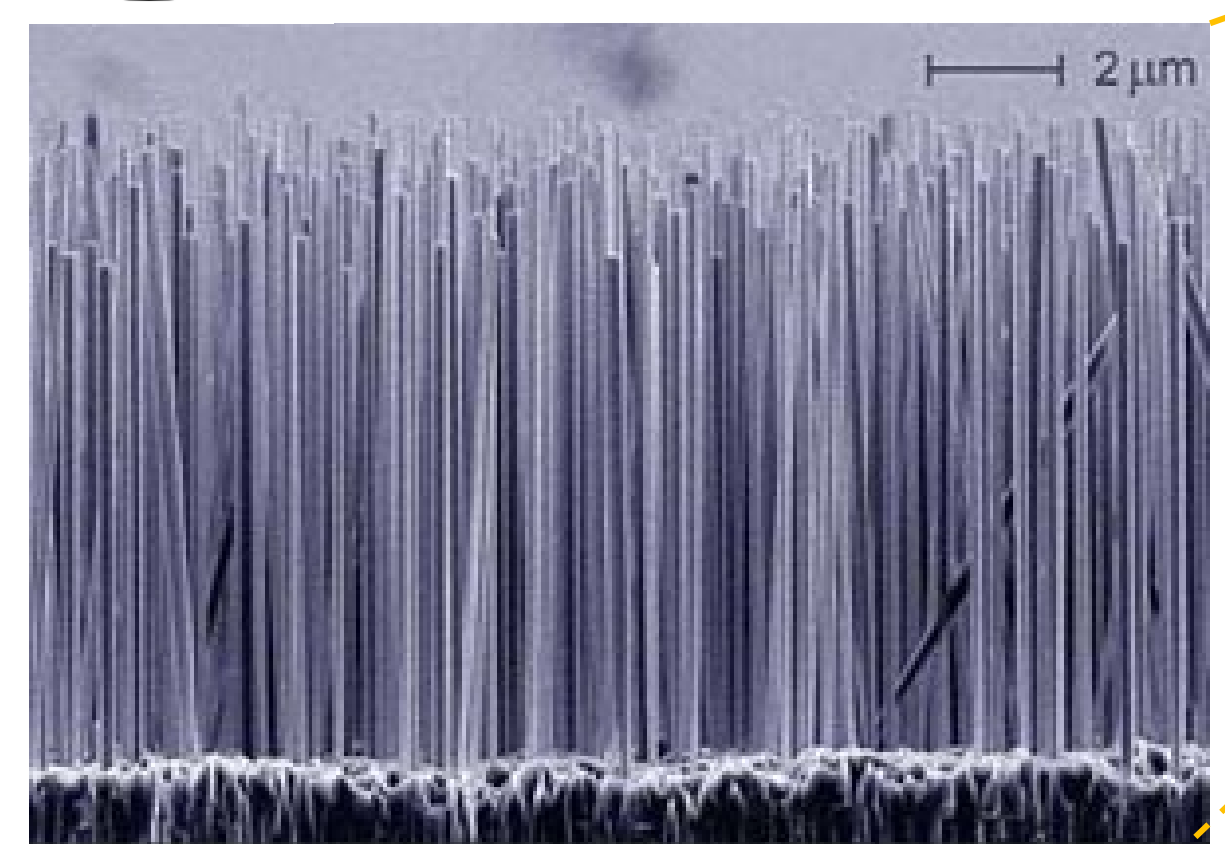
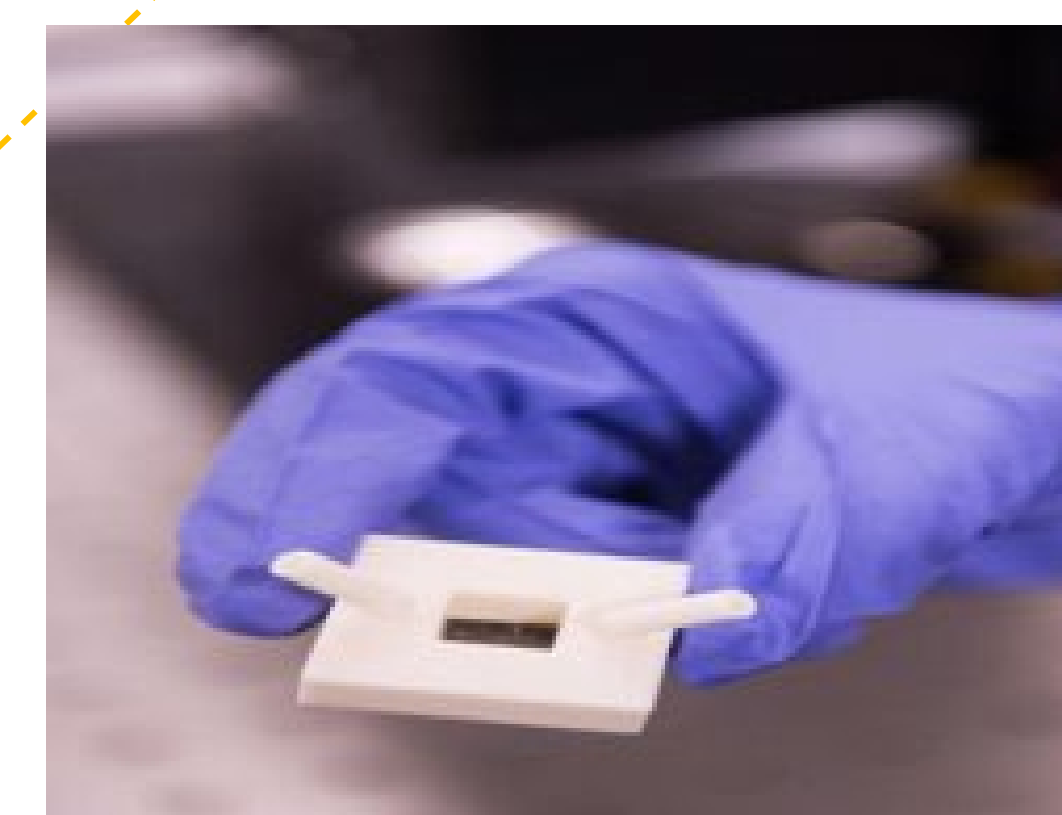
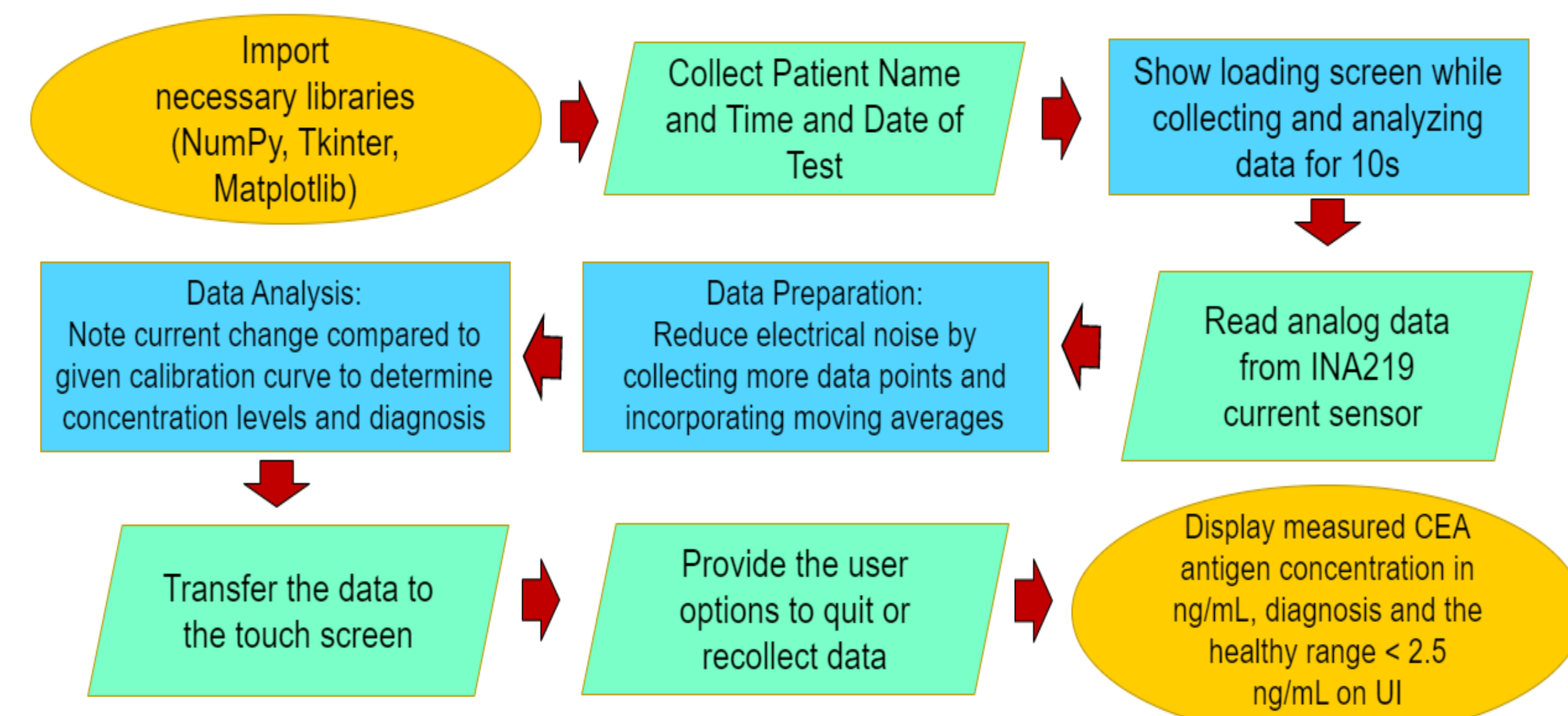


Fig 2. The final silicon array biosensor is portable, and this allows it to be easily scalable.



DAQ Flowchart



Results

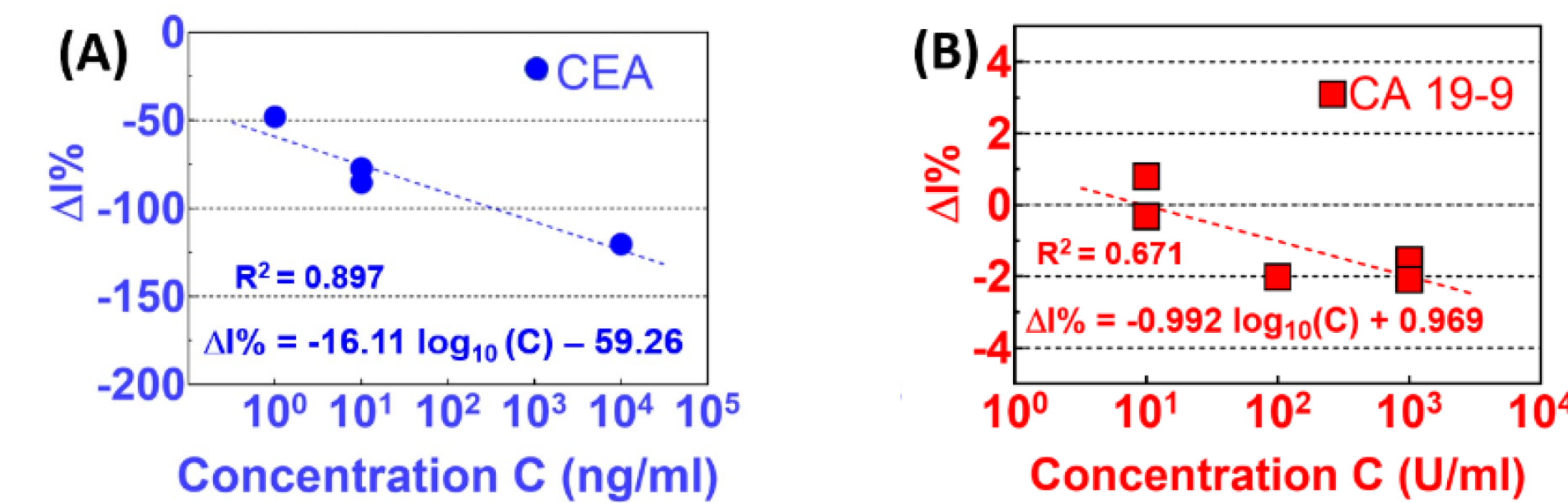
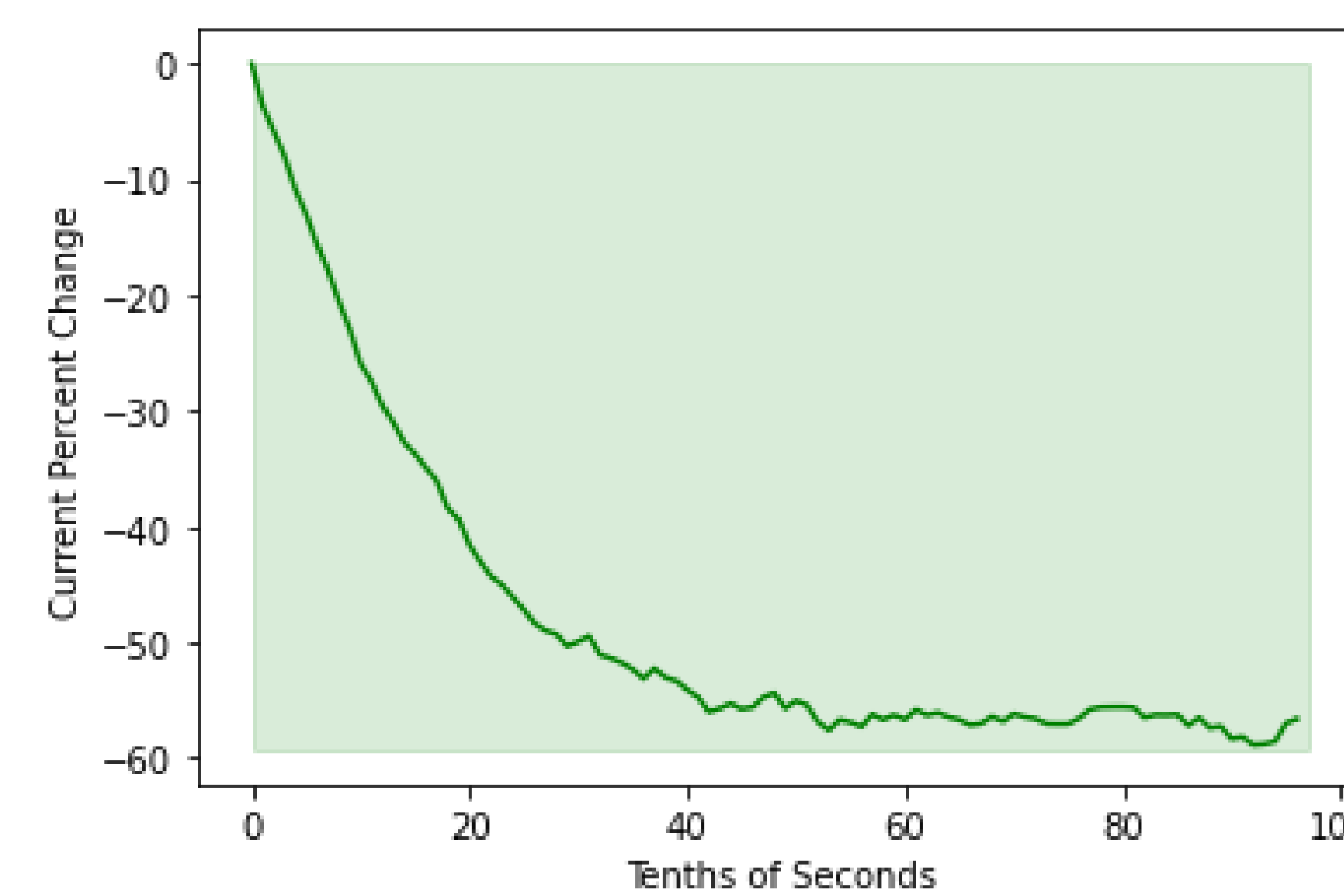
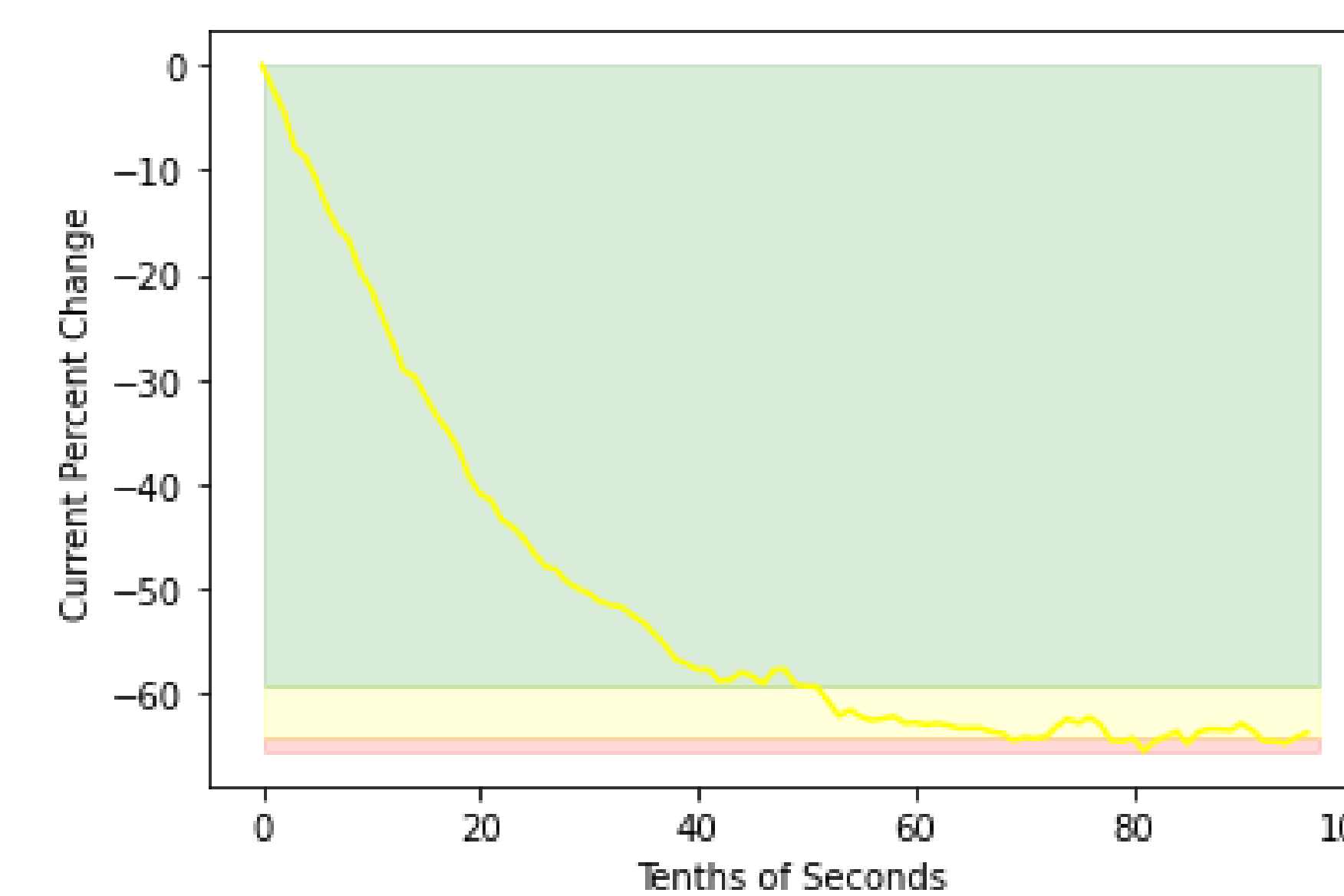


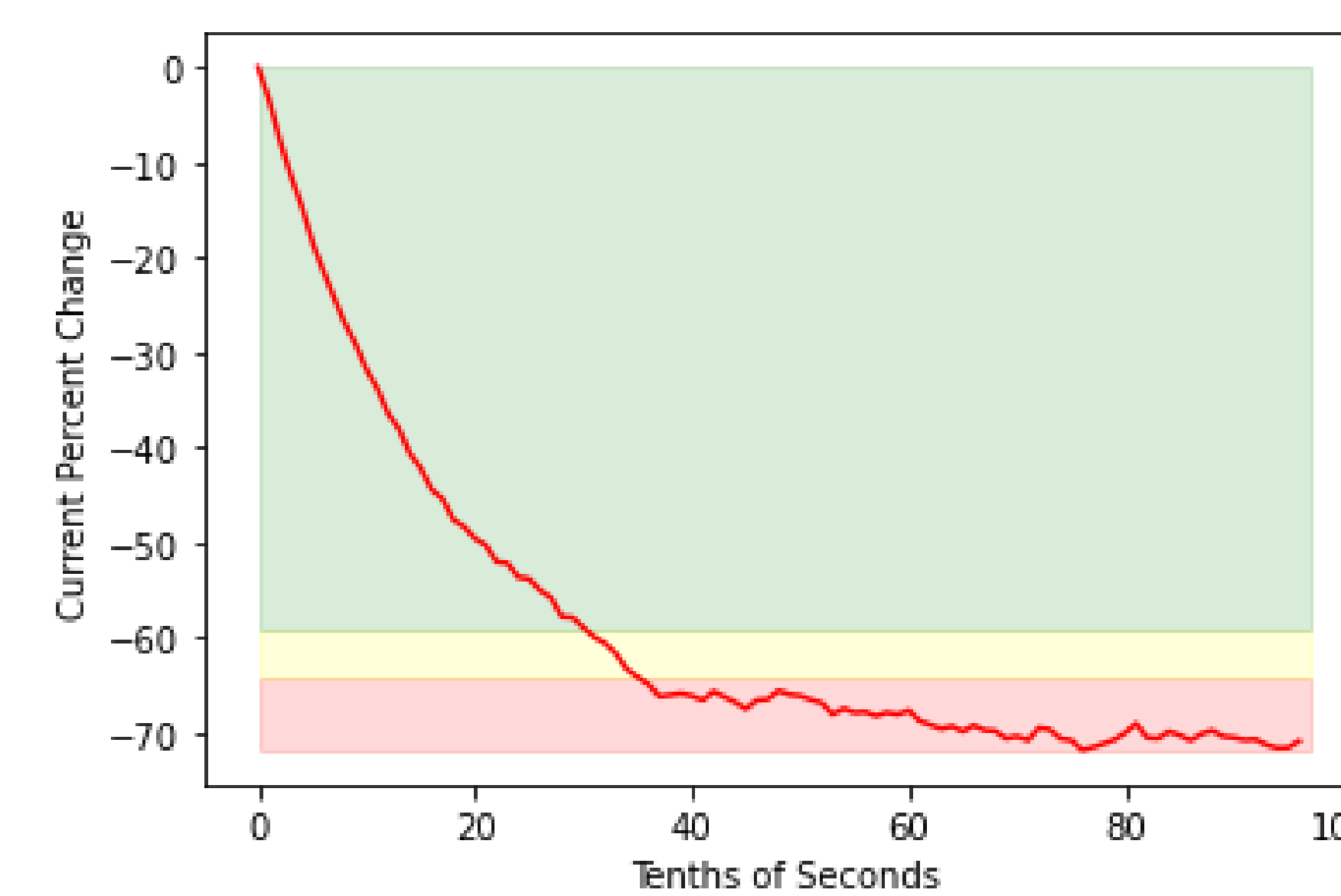
Fig 4. Semi-log data plots of $\Delta I\%$ as a function of CEA concentration level (a) and as a function of CA 19-9 (B). R-squared values for the regression expressions confirm a strong correlation between $\Delta I\%$ and antigen concentration



Healthy
< 1.0 ng/mL
CEA Concentration

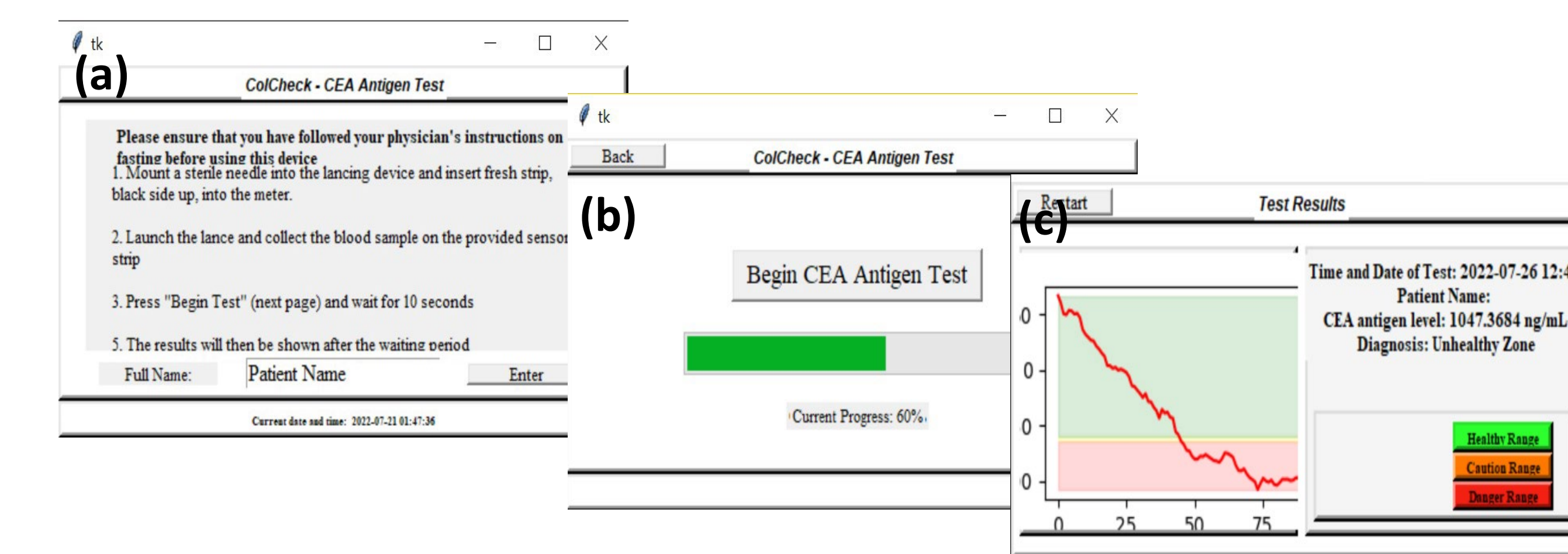


Warning
1.0 – 2.5 ng/mL
CEA Concentration



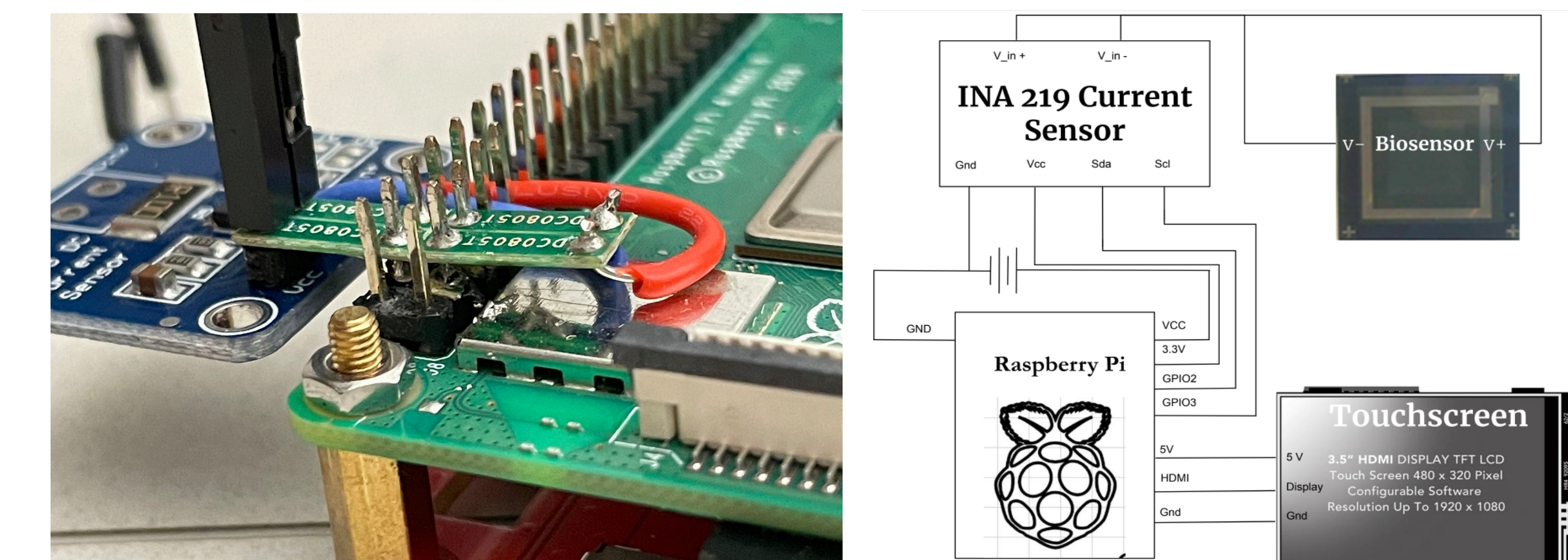
Unhealthy
> 2.5 ng/mL
CEA Concentration

Graphical User Interface (GUI)



(a) Homepage displays test instructions and records username, date and time of test, (b) Loading page 10s progress bar. (c) Results page displays % current-change graph, antigen concentration level and patient diagnosis

Raspberry Pi based DAQ System



Left: Image of Raspberry and INA 219 Current Sensor combined hardware. Right: Circuit diagram of the Data Acquisition System.

Future Work

As of now, our results have been based on current changes generated by an analog potentiometer rather than the actual SiNW-diode-based biosensor. For future work, we plan to test our DAQ by connecting our current sensor to the actual SiNW based biosensor and introduce a compact casing for our hardware.

References

1. Smith, R., Gao, B., Malkawi, W. I., Keefe, D. W., Geary, S. M., Kasi, P. M., Salem, A. K., & Toor, F. (2022). Vertically-Oriented Silicon Nanowires Arraybased Biosensor Platform for Label-Free Detection of Protein and ctDNA Colorectal Cancer Biomarkers [Unpublished manuscript]
2. Toor, F. (2019). Surface modified doped silicon nanowire based solar cells for applications in cancer antigen detection [PowerPoint slides] College of Electrical and Computer Engineering, University of Iowa

Background

Endometrial Cancer (EC) one of few cancers with cases on a rise in recent years. It is the most common gynecological malignancy equating to around 12,000 deaths each year.

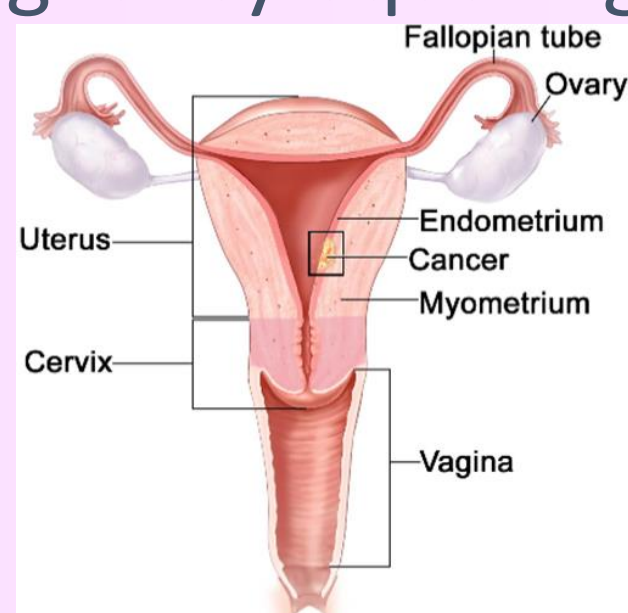


Fig. 1 an image of the female reproductive organs showing the location of endometrial cancer.

SETDB1 is a H3K9 methyltransferase involved in gene silencing. It has been identified as an oncogene in various cancers creating a need to better understand its mechanisms of amplification, overexpression, and activation. It is usually overexpressed and correlates with the worst EC patient prognosis.

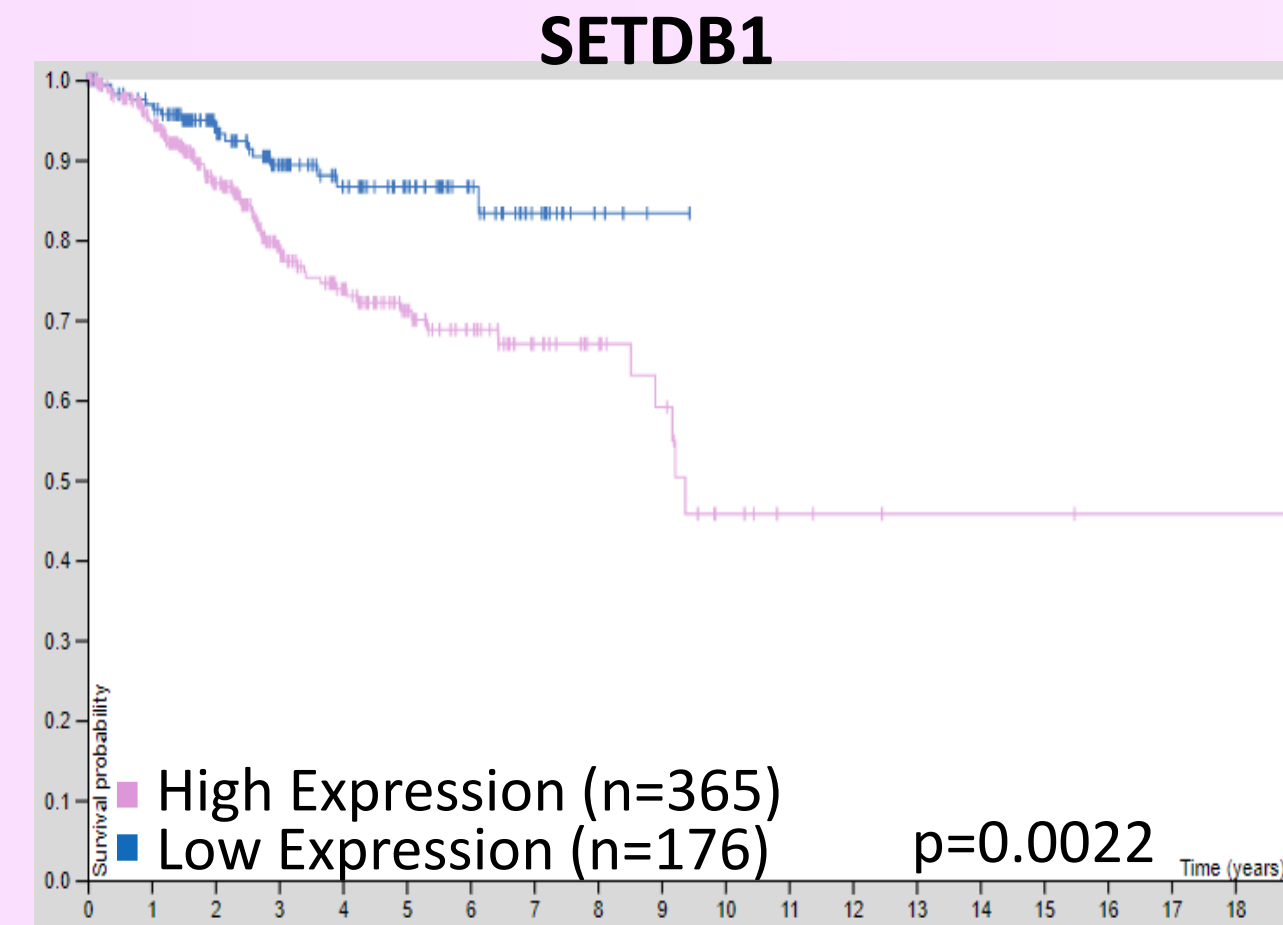


Fig. 2 an image of SETDB1 expression and prognosis in EC patients.

Taken from the Human Protein Atlas

mCherry is a member of the mFruits family and is a basic red fluorescent protein. The protein has been used to visualize genes and analyze their function. It glows red when exposed to green light.

KDM4A is a lysine specific demethylase that demethylates H3K9/36. It has been identified as an oncogene and is usually overexpressed correlating with EC progression and poorer patient prognosis.

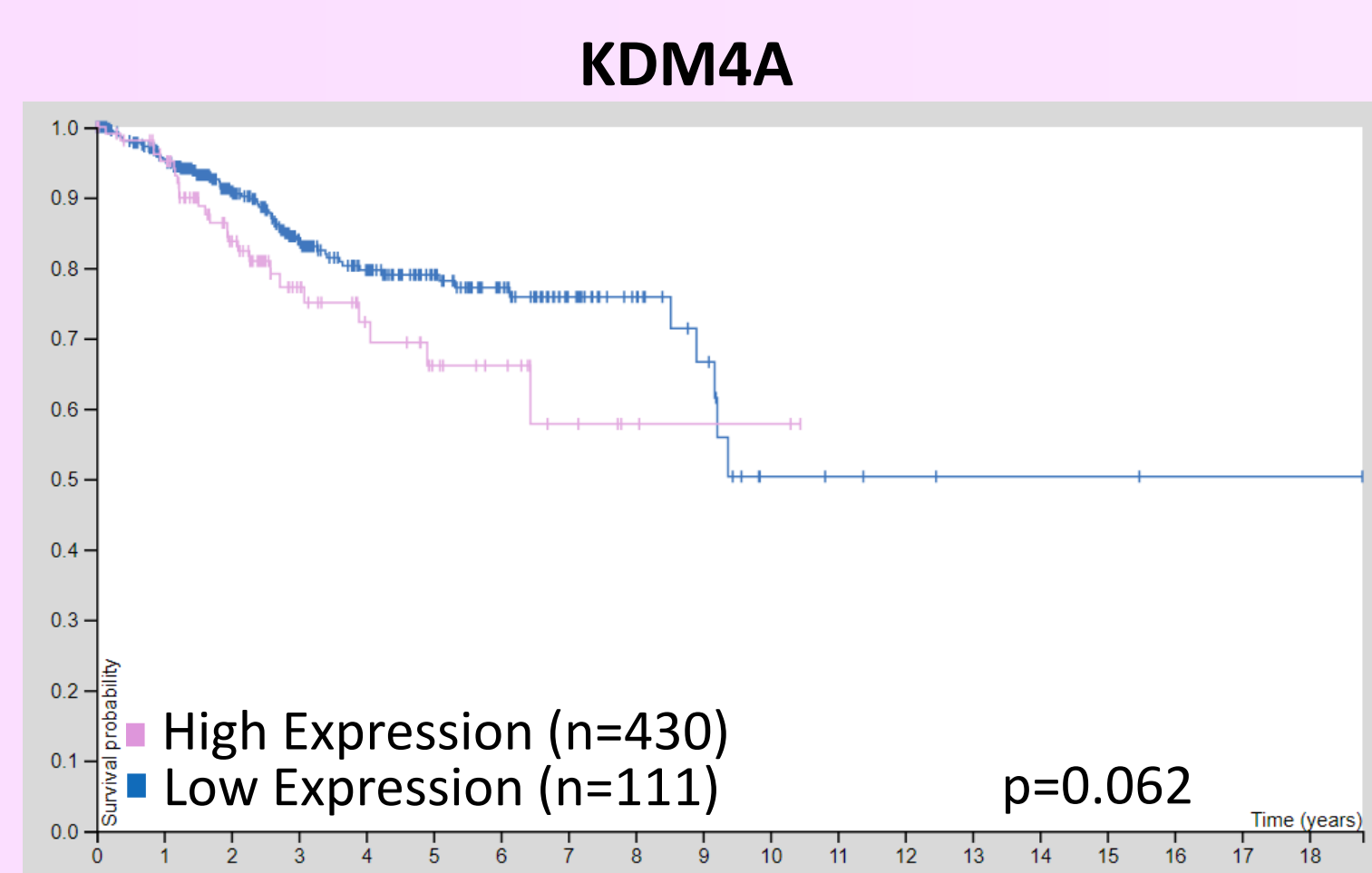


Fig. 3 an image of KDM4A expression and prognosis in EC patients.

Taken from the Human Protein Atlas

GFP is the green fluorescent protein. It is often used to monitor gene expression and glows green when exposed to blue light.

Objectives

- Verify mCherry as a stable SETDB1 reporter in ECC1, Hec50 and ISH cells
- Study how overexpression of KDM4A-GFP correlates with SETDB1 expression

Methods

SETDB1 Reporter (mCherry)

- Method 1** transfect ECC1, Hec50, and Ishikawa cells with SETDB1 ex22 sgRNA-lentCRISPR v1 and SETDB1 reporter gene (SETDB1-hygro-mCherry)

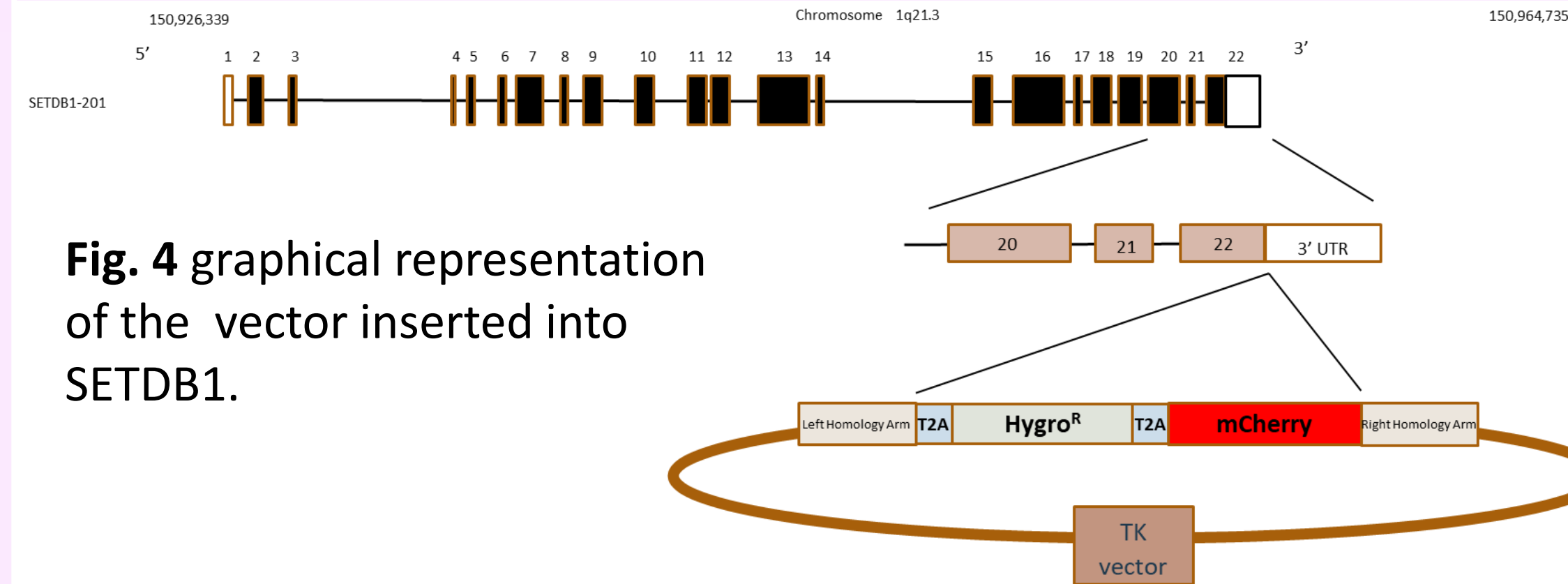


Fig. 4 graphical representation of the vector inserted into SETDB1.

- Method 2** determine which single clone has correct SETDB1 reporter insertion in gDNA using PCR to identify the clone. Then run an agarose gel and use chemidoc to check gel bands for insertion.



Fig. 5 diagram of PCR tube set up that was used to check for SETDB1 reporter insertion.

- Method 3** grow positive clones into spheroids and use a fluorescent microscope to visualize reporter expression.

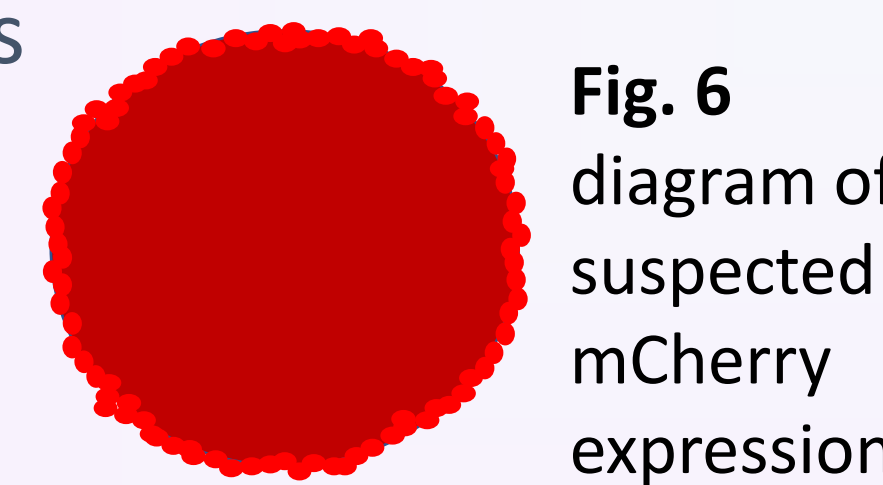
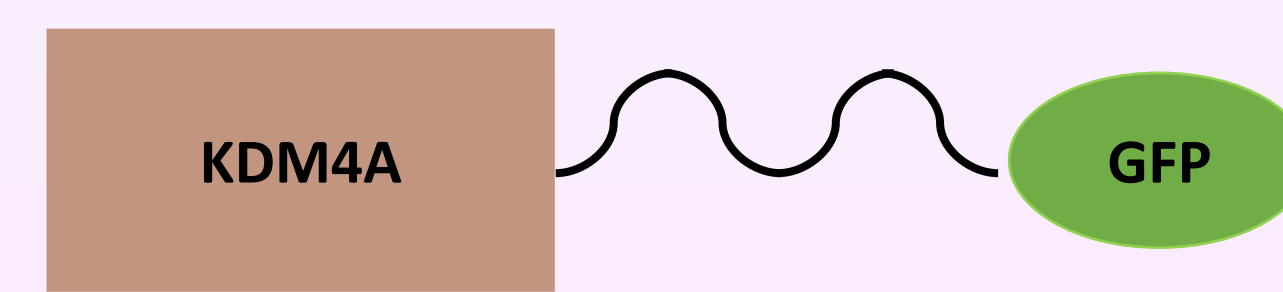


Fig. 6 diagram of suspected mCherry expression.

KDM4A Overexpression

- Method 1** transfect reporter positive clones with KDM4A – GFP at two different densities (10k and 20k)

Fig. 7 graphical representation of KDM4A-GFP that was transfected.



- Method 2** grow clones into spheroids and use a fluorescent microscope to visualize SETDB1 and KDM4A expression.



Fig. 8 diagram of mCherry expression.



Fig. 9 diagram of GFP expression.



Fig. 10 diagram of merged expression.

Acknowledgements

I would like to thank Dr. Yang for the opportunity to work in her lab. I would also like to thank Kiarash Salari for his mentorship and guidance as well as Matthew Wells and Johnathan Schultz and the entire Yang lab. Lastly, I would like to thank the Belin Blank Center and SSTP program for this research opportunity. Funding for this project was supported by NIH R37-CA238274 (SY) and the Department of Pathology Start-Up Fund (SY).

Results

SETDB1 Reporter (mCherry)

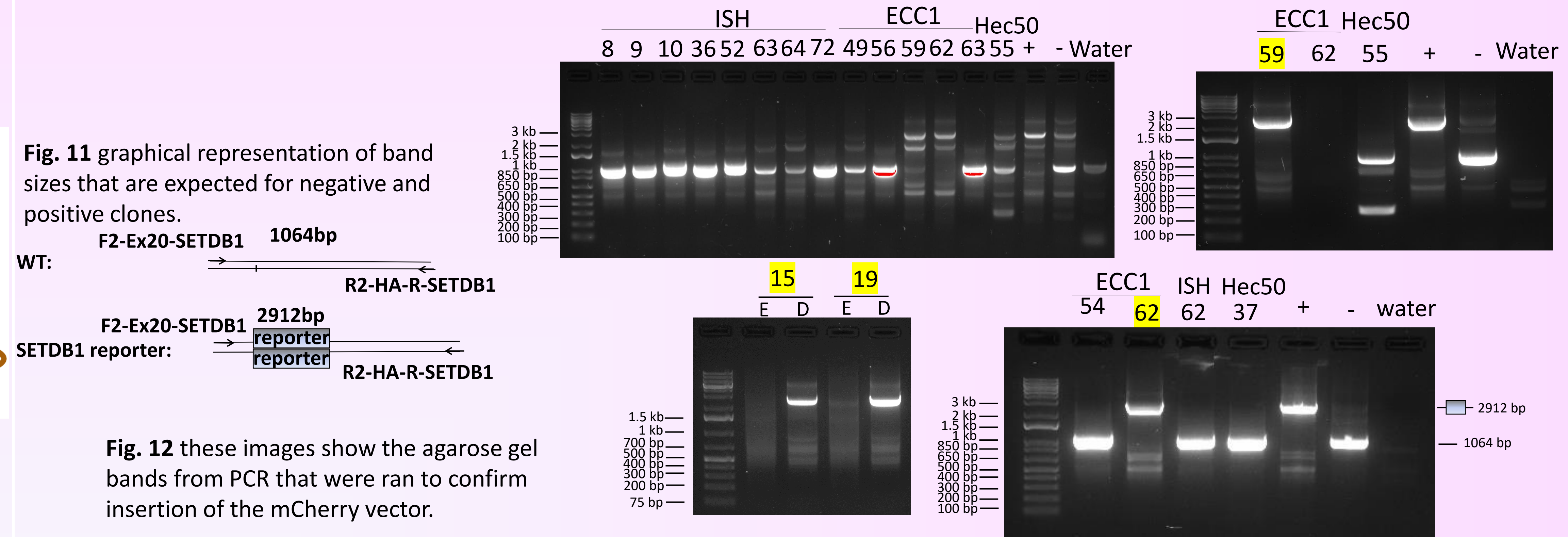


Fig. 11 graphical representation of band sizes that are expected for negative and positive clones.

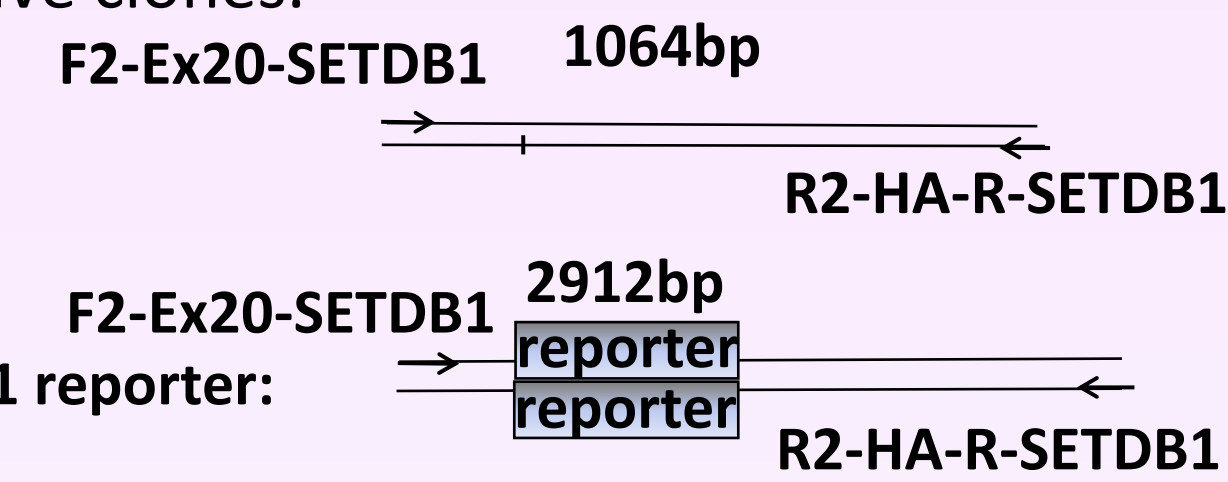


Fig. 12 these images show the agarose gel bands for PCR that were ran to confirm insertion of the mCherry vector.

KDM4A Overexpression

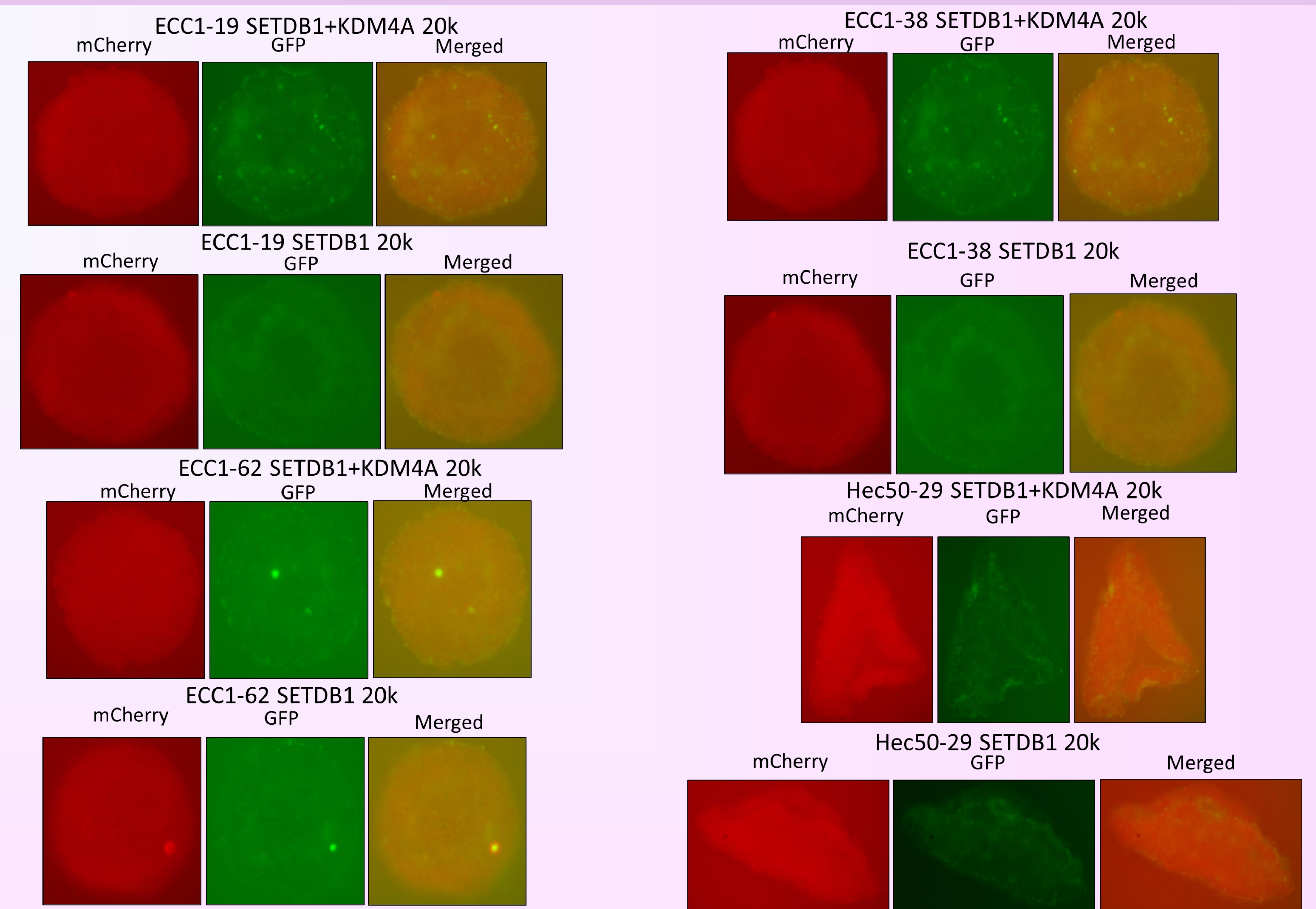


Fig. 13 these images show the spheroids of cells that were transfected with SETDB1 reporter and KDM4A-GFP. They were taken using a fluorescent microscope.

Conclusion

- SETDB1 reporter was verified in ECC1 and Hec50 cells

Future Directions

- Continue work to verify SETDB1 reporter in ISH cells
- Continue work to verify upregulation of SETDB1 with KDM4A-GFP overexpression

References

Lazaro-Camp, V. J., Salari, K., Meng, X., & Yang, S. (2021). SETDB1 in cancer: overexpression and its therapeutic implications. *American Journal of Cancer Research*, 11(5), 1803–1827. <https://www.ncbi.nlm.nih.gov/pmc/articles/PMC8167684/>

Mishra, S., Van Rechem, C., Pal, S., Clarke, T. L., Chakraborty, D., Mahan, S. D., Black, J. C., Murphy, S. E., Lawrence, M. S., Daniels, D. L., & Whetstone, J. R. (2018). Cross-talk between lysine-modifying enzymes controls site-specific DNA amplifications. *Cell*, 174(4). <https://doi.org/10.1016/j.cell.2018.06.018>

Subach, F. V., Patterson, G. H., Manley, S., Gillette, J. M., Lippincott-Schwartz, J., & Verkhusha, V. V. (2009). Photoactivatable mCherry for high-resolution two-color fluorescence microscopy. *Nature Methods*, 6(2), 153–159. <https://doi.org/10.1038/nmeth.1298>

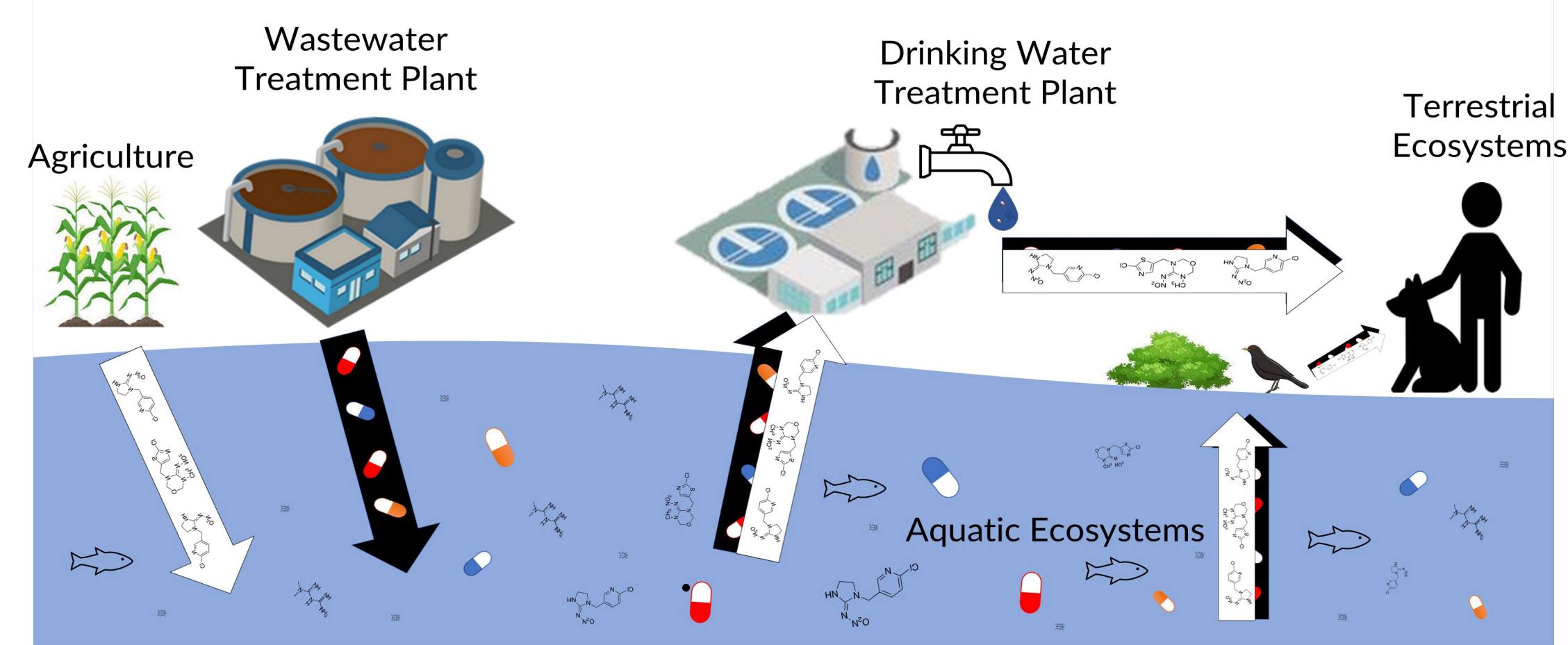
Wang, C., Xia, Z., Li, Z., Ye, F., Ji, S., Lu, C., & Zhang, H. (2021). Expression of SET domain bifurcated histone lysine methyltransferase 1 and its clinical prognostic significance in hepatocellular carcinoma. *Journal of Clinical Laboratory Analysis*, 36(1). <https://doi.org/10.1002/jcla.24090>

Macroinvertebrates Bioaccumulate Pharmaceuticals and Neonicotinoids in an Effluent-Dominated Stream: A Tale of Bugs on Drugs

Krishna Kapoor, Grant Hemphill, Alyssa Mianeki, & Gregory LeFevre

Introduction

- Waterbodies receive high amounts of neonicotinoids and pharmaceuticals from runoff and wastewater
- The purpose of this study is to investigate if macroinvertebrates are bioaccumulating neonicotinoids and pharmaceuticals



Experimental Design

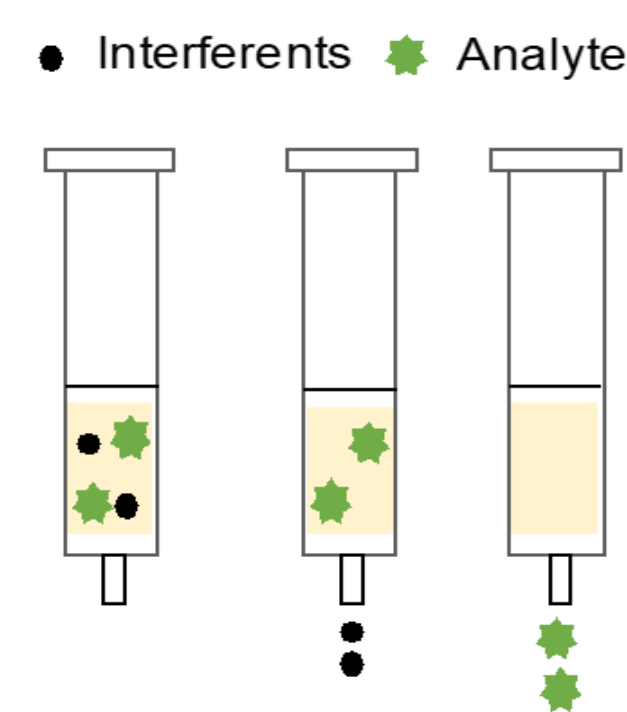
In-field sampling at Muddy Creek, Iowa

- 1 L and 500 mL water collection at US1, Effluent, and 5km Downstream
- 1-hour bug collection at US1 and Effluent



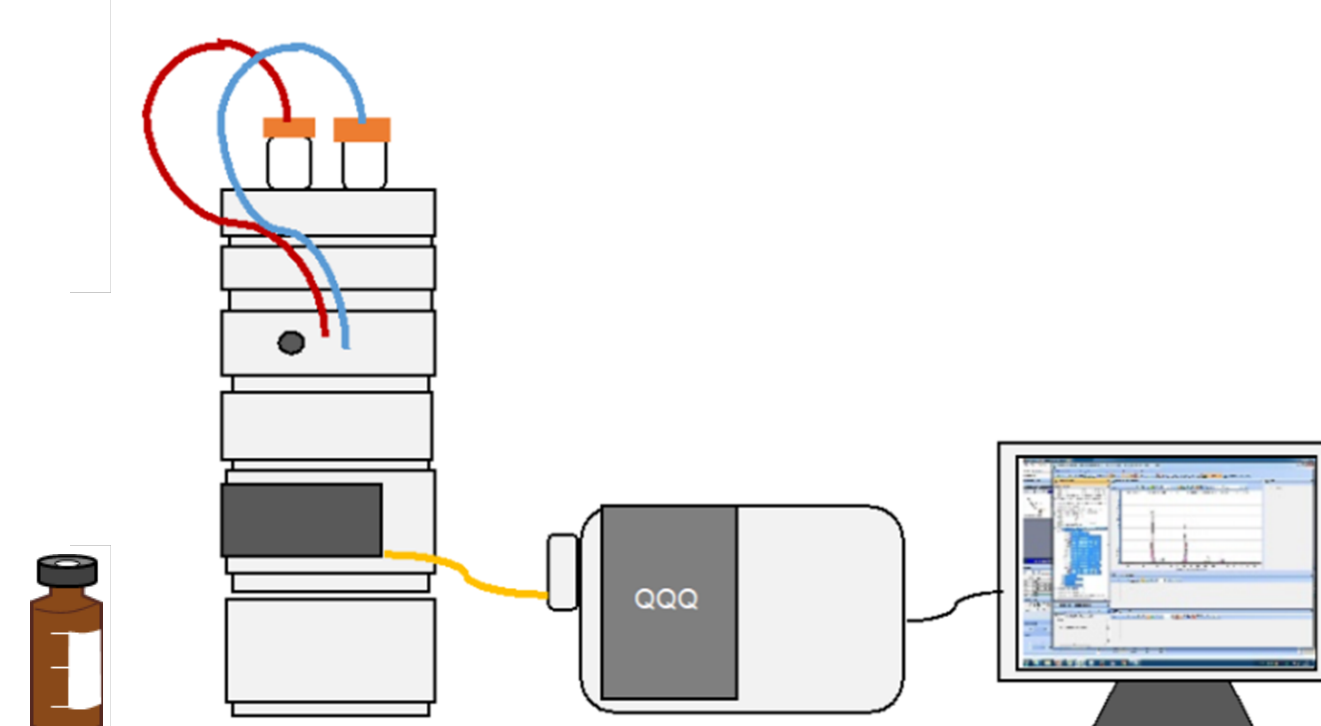
In-lab extraction

- Water extracted with solid phase extraction (SPE)
- Bugs extracted with a series of solvents



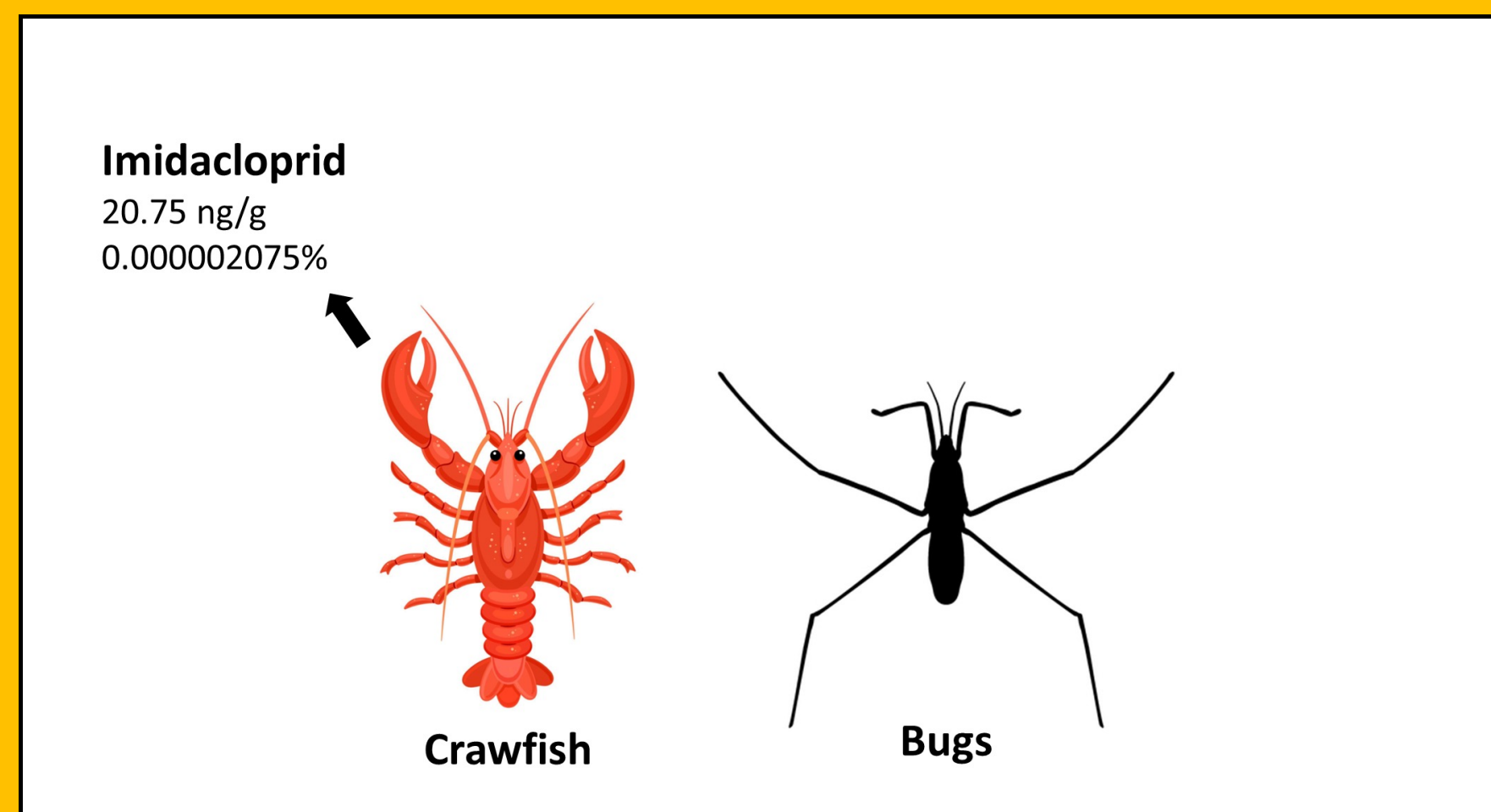
Instrumental Method

- Samples analyzed using LC-MS/MS

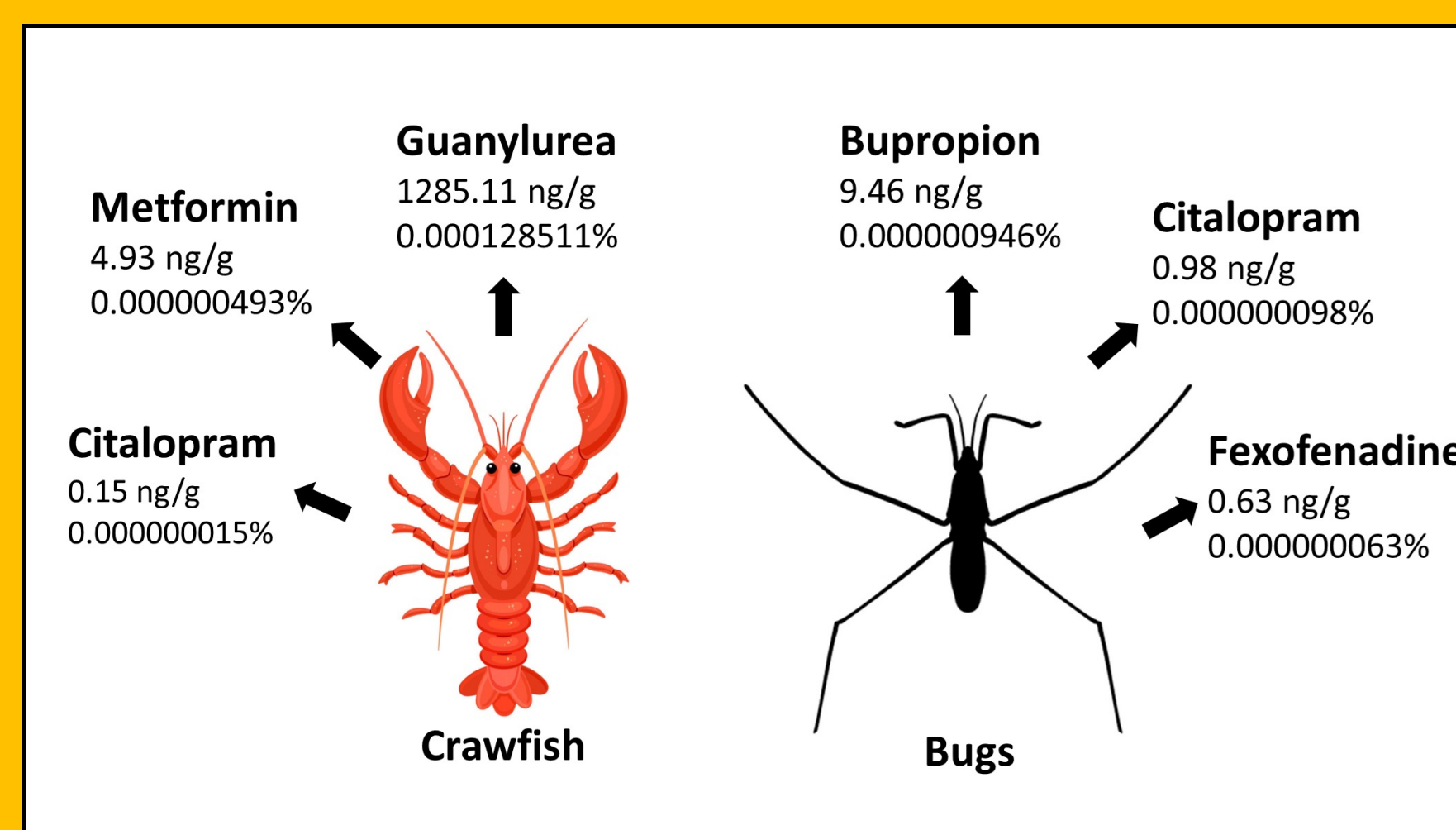


Results

Upstream Biota Concentrations

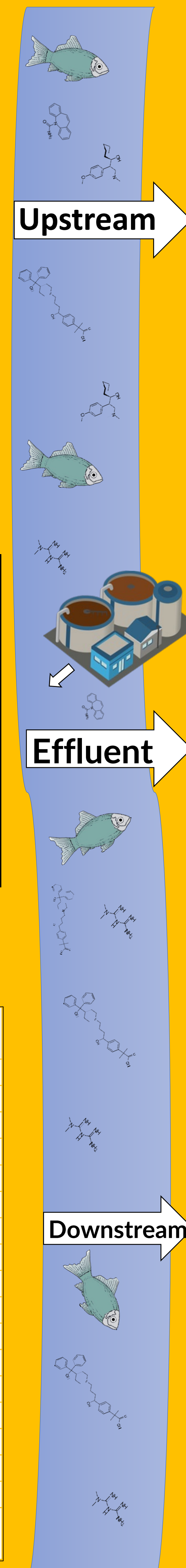


Effluent Biota Concentrations

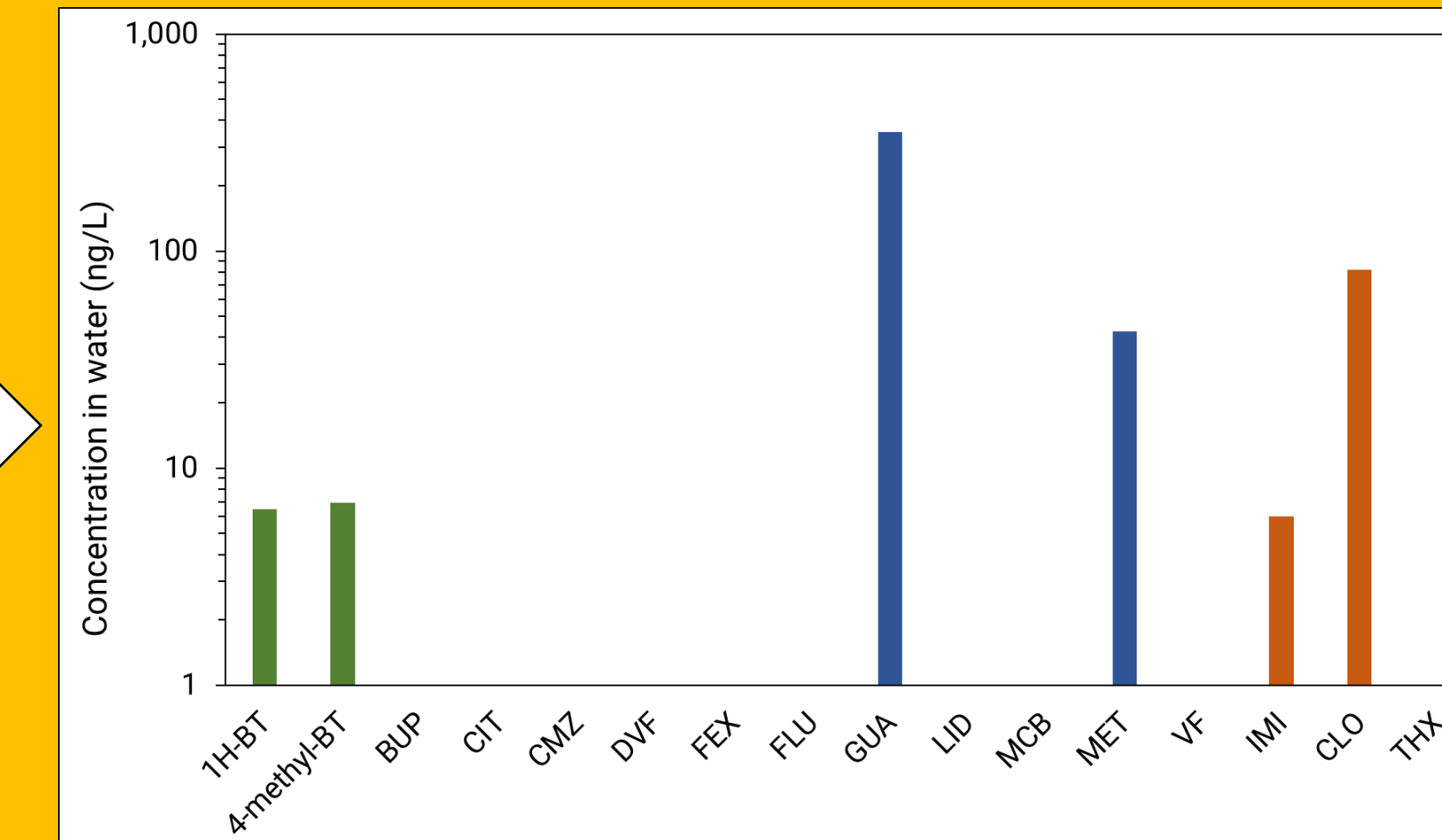


Pharmaceuticals and

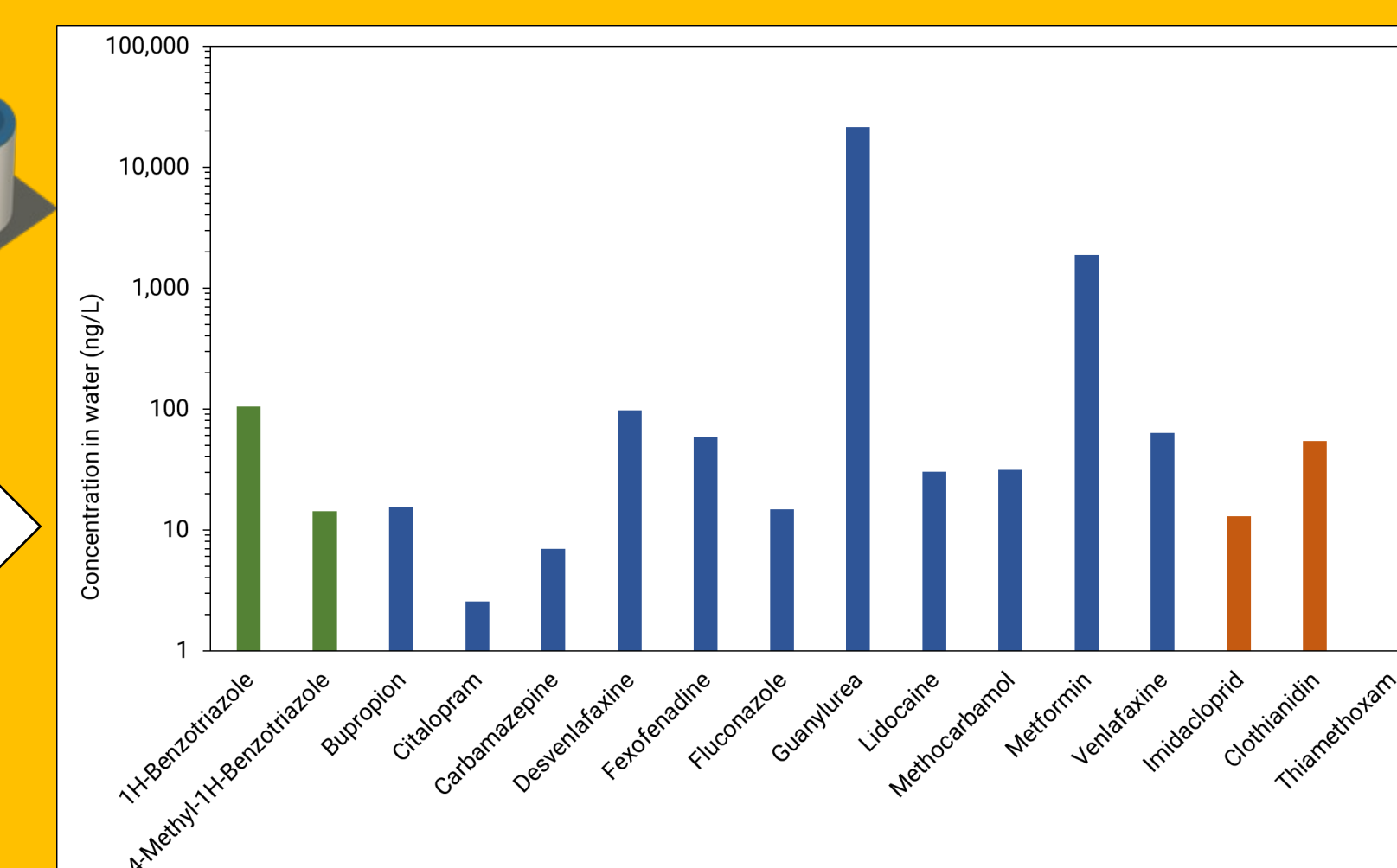
Compound	Description	m/z
Thiamethoxam	Neonicotinoid Insecticide	292.0266
Imidacloprid	Neonicotinoid Insecticide	256.0595
Clothianidin	Neonicotinoid Insecticide	250.0160
Atenolol	Beta-blocker	267.1703
Bupropion	Antidepressant	240.1150
Carbamazepine	Anti-seizure	237.1022
Citalopram	Antidepressant	325.1711
Desvenlafaxine	Antidepressant	264.1958
Fexofenadine	Antihistamine	502.2952
Fluconazole	Antifungal	307.1113
Guanylurea	Metformin metabolite	103.0614
Lidocaine	Local numbing agent	235.1805
Metformin	Antidiabetic	130.1087
Methocarbamol	Muscle Relaxant	242.1023
Sulfamethoxazole	Antibiotic	254.0594
Venlafaxine	Antidepressant	278.2115
1H-Benzotriazole	Corrosion Inhibitor	120.0556
4-Methyl-1H-Benzotriazole	Corrosion Inhibitor	134.0713



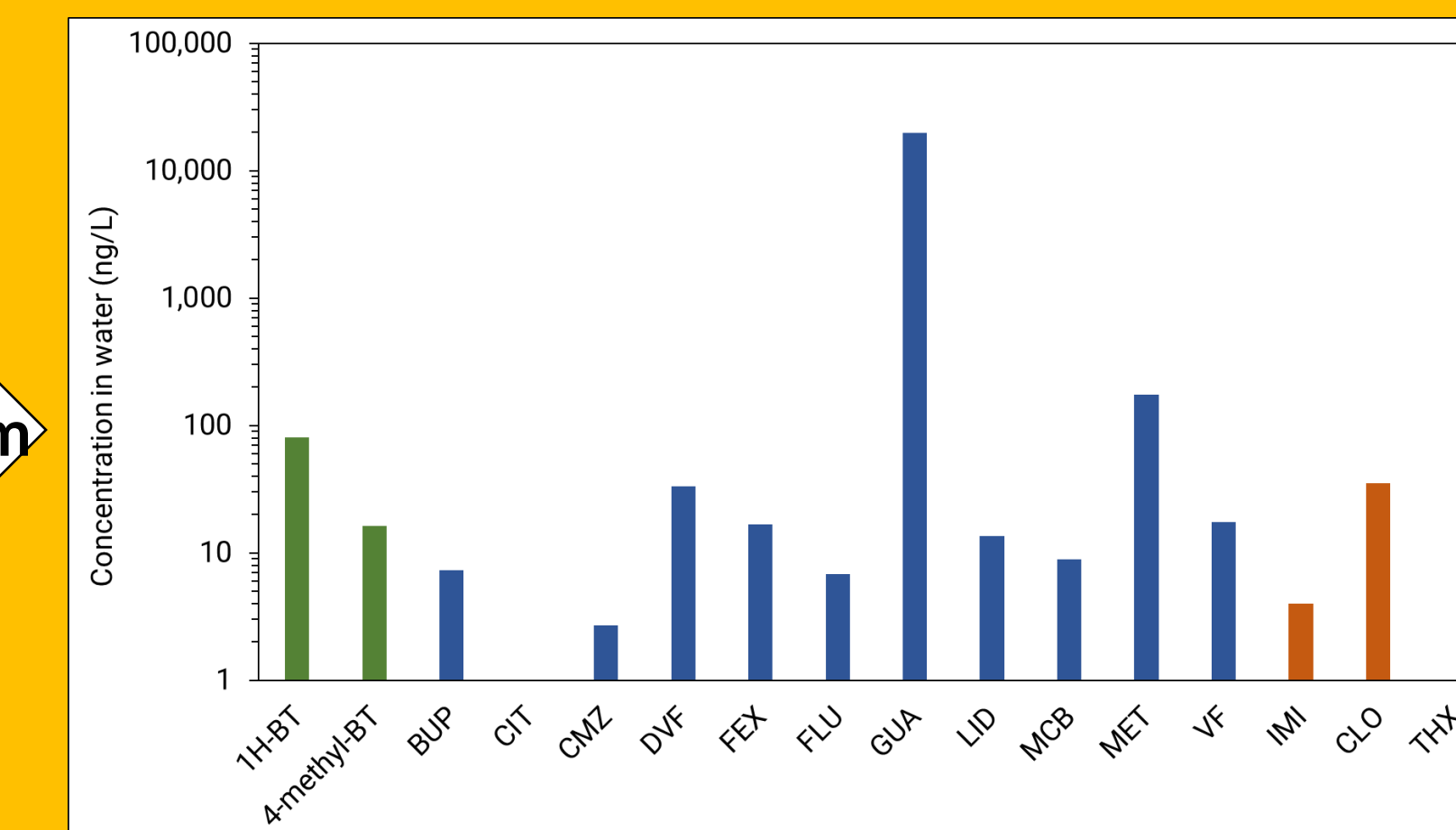
Upstream Water Concentrations



Effluent Water Concentrations



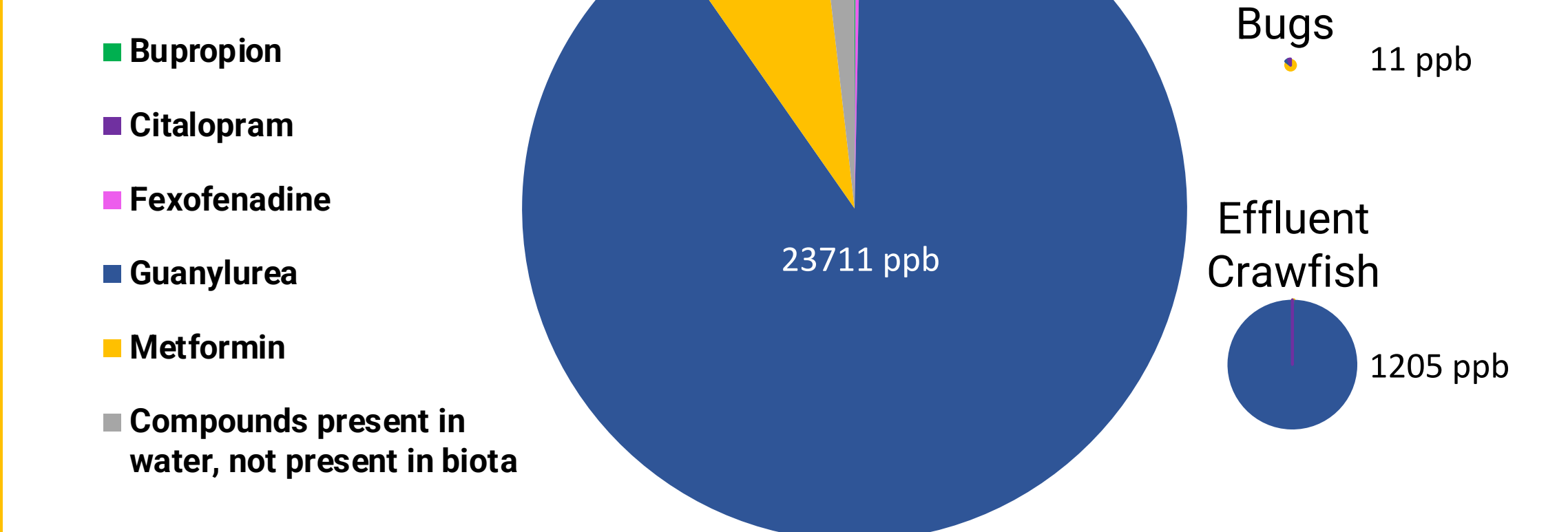
5km Downstream Water Concentrations



**We picked the highest concentration of any compound in samples that had duplicates
 **These are all below the level of quantitation (LOQ). The calculated numbers are prone to error and could be variable from the reported concentrations

Data Analysis

Effluent Water



**These pie charts are proportional to the total concentration of chemicals in the water and in the biota

Conclusion

Pharmaceuticals and neonicotinoids bioaccumulate in macroinvertebrates

- Imidacloprid was found in upstream crawfish
- No pollutants were found in upstream bugs
- Metformin, citalopram, and guanylurea were found in effluent crawfish
- Bupropion, citalopram, and fexofenadine were found in effluent bugs

Pollutants in the macroinvertebrates have a higher abundance at the effluent site

- The upstream biota concentration range is non-detect (n.d.) to 20.75 ppb
- The effluent biota concentration range is n.d. to 1285 ppb

The Big Picture

- Water quality has degraded due to climate change and urbanization
- Other organisms in aquatic and terrestrial ecosystems are likely exposed to these pollutants
- Manmade pollutants may be present in drinking water downstream of pollutant sources

References

- Webb DT; Zhi H; Kolpin DW; Klaper RD; Iwanowicz LR; LeFevre GH; (2021). Municipal wastewater as a year-round point source of neonicotinoid insecticides that persist in an effluent-dominated stream. Environ. Sci. Process. Impacts.
- Zhi, H., Kolpin, D. W., Klaper, R. D., Iwanowicz, L. R., Meppelink, S. M., & LeFevre, G. H. (2020). Occurrence and spatiotemporal dynamics of pharmaceuticals in a temperate-region wastewater effluent-dominated stream Environ. Sci. Tech., 54(20), 12967-12978.

INTRODUCTION

Collagen in the skin

- Collagen is an abundant protein in the skin necessary for maintaining structural integrity
- Determining collagen content is required in clinical practice to characterize tissues and determine disease states
- Current methods for determining collagen content are invasive and usually require biopsies of the skin that are >25cm²
- Hydroxyproline comprises >15% of the amino acid composition in collagen
- Collagen content is commonly measured using biochemical hydroxyproline assays, computer-aided histomorphometric analyses of histological sections, and sodium dodecyl sulfate-polyacrylamide gel electrophoresis (SDS-PAGE)

Optical Coherence Tomography (OCT)

- OCT is a noninvasive optical imaging modality that provides high resolution and cross-sectional imaging
- Allows for collagen estimation using attenuation and surface reflectivity values
- Overcomes the need for biopsies and >24 hr. analytical testing times
- Has not been validated or quantified

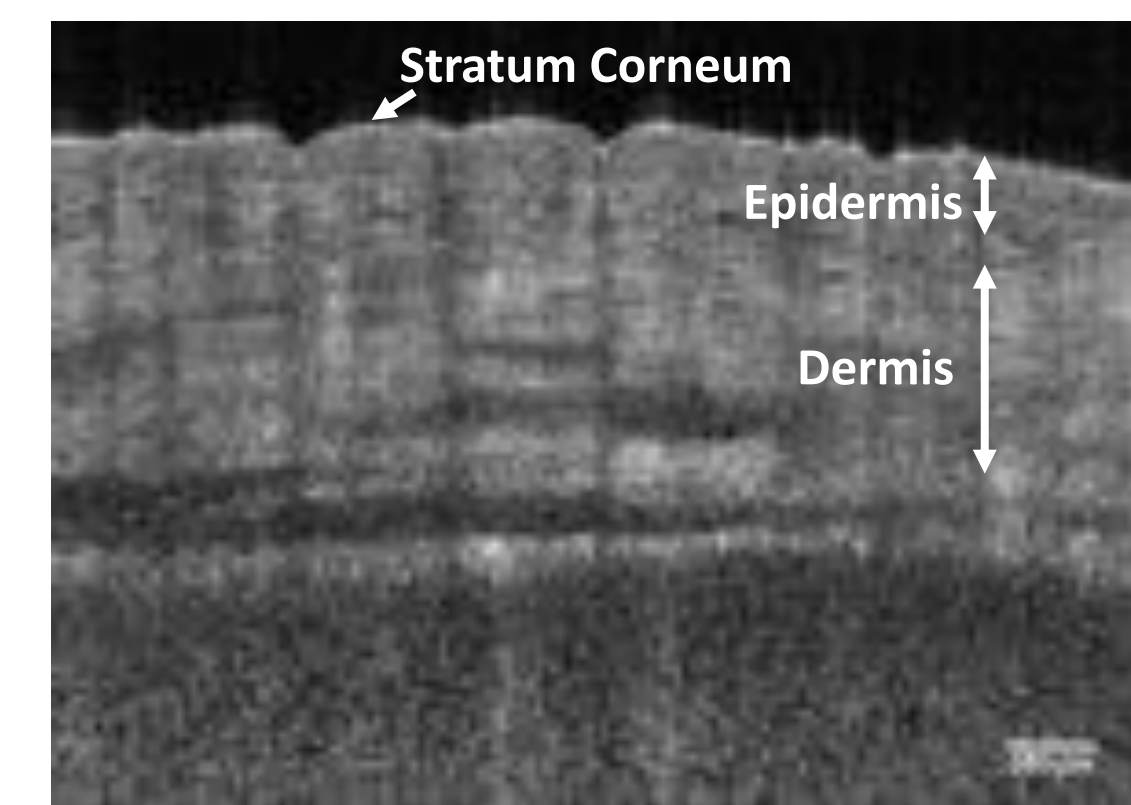


Figure 1. OCT image of excised abdominal skin.

Objective

The goal of this research is to quantify total collagen in excised skin samples and study its correlation to attenuation and surface reflectivity values obtained using optical coherence tomography.

MATERIALS AND METHODS

Optical Coherence Tomography

- Collected attenuation coefficient and surface reflectivity values using a 3x3 mm section at 250 frames. Scanned in three different locations.

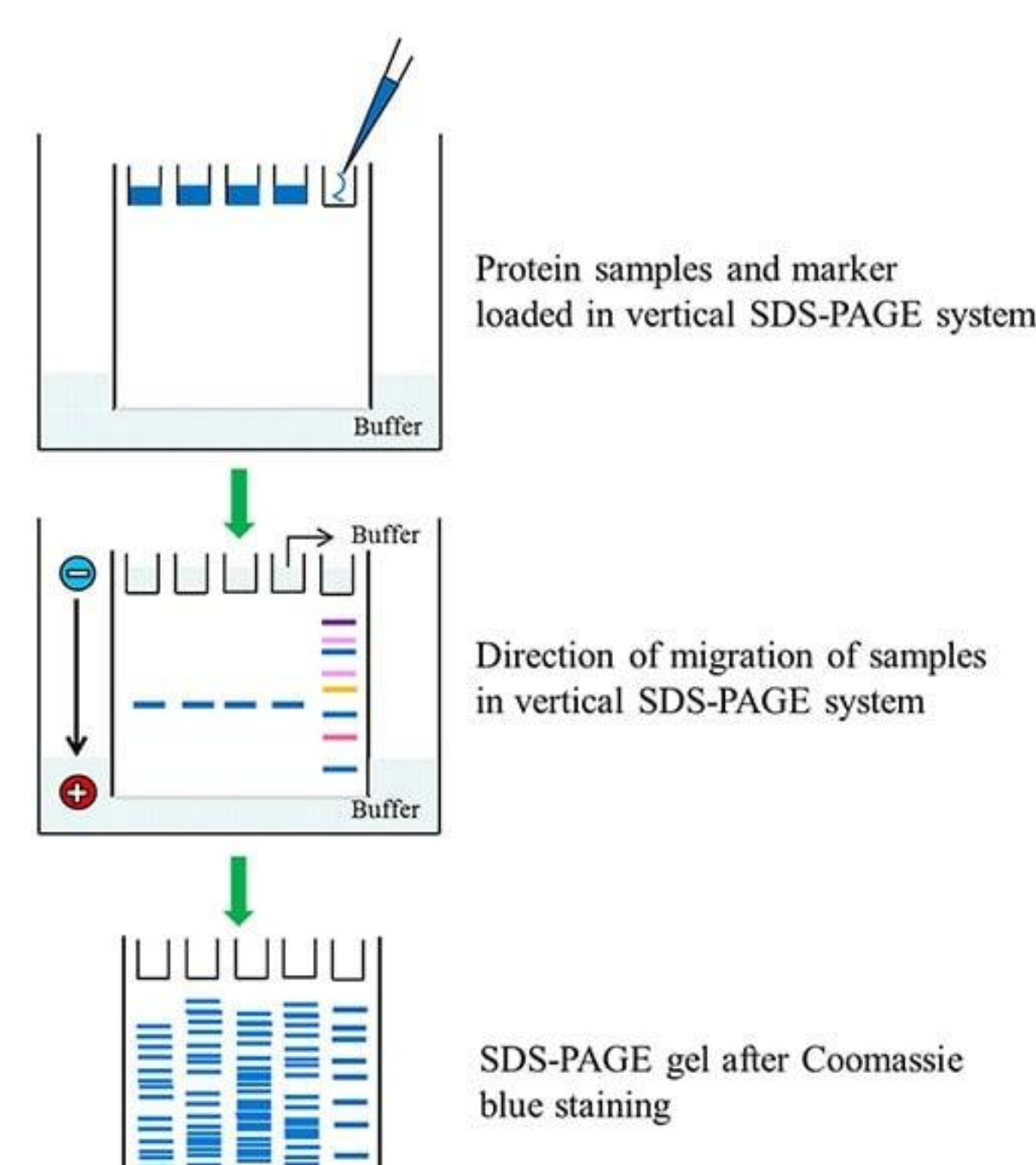
Hydroxyproline assay

- Subcutaneous fat and connective tissue was removed from human skin samples prior to hydrolysis
- Hydroxyproline calibration curve was prepared to interpolate unknown concentrations from skin samples

Bicinchoninic assay (BCA)

- Total protein content in human skin samples was measured to determine loading quantities in SDS-PAGE gels

SDS-PAGE



- SDS-PAGE separates proteins in a mixture by molecular weight

- Band width and optical intensity as measured by ImageJ software is used to determine protein content

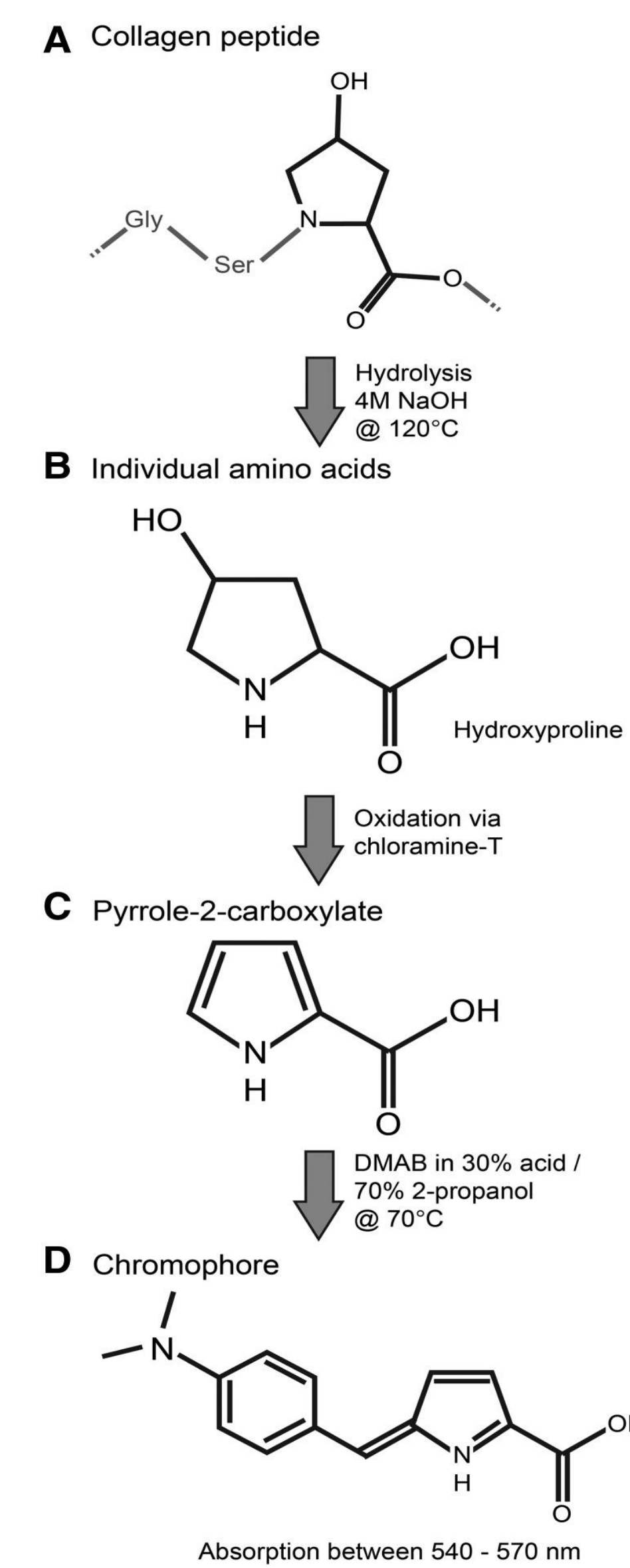


Figure 2. Overview of the hydroxyproline assay. Collagen peptides are first hydrolyzed to individual amino acids including hydroxyproline. Oxidation then yields a pyrrole that reacts with DMAB (para-Dimethylaminobenzaldehyde) to produce a chromophore with peak absorption of light with wavelengths between 540 and 570 nm.

RESULTS

A positive correlation was found between hydroxyproline content and attenuation/surface reflectivity in human skin & porcine skin

Human skin

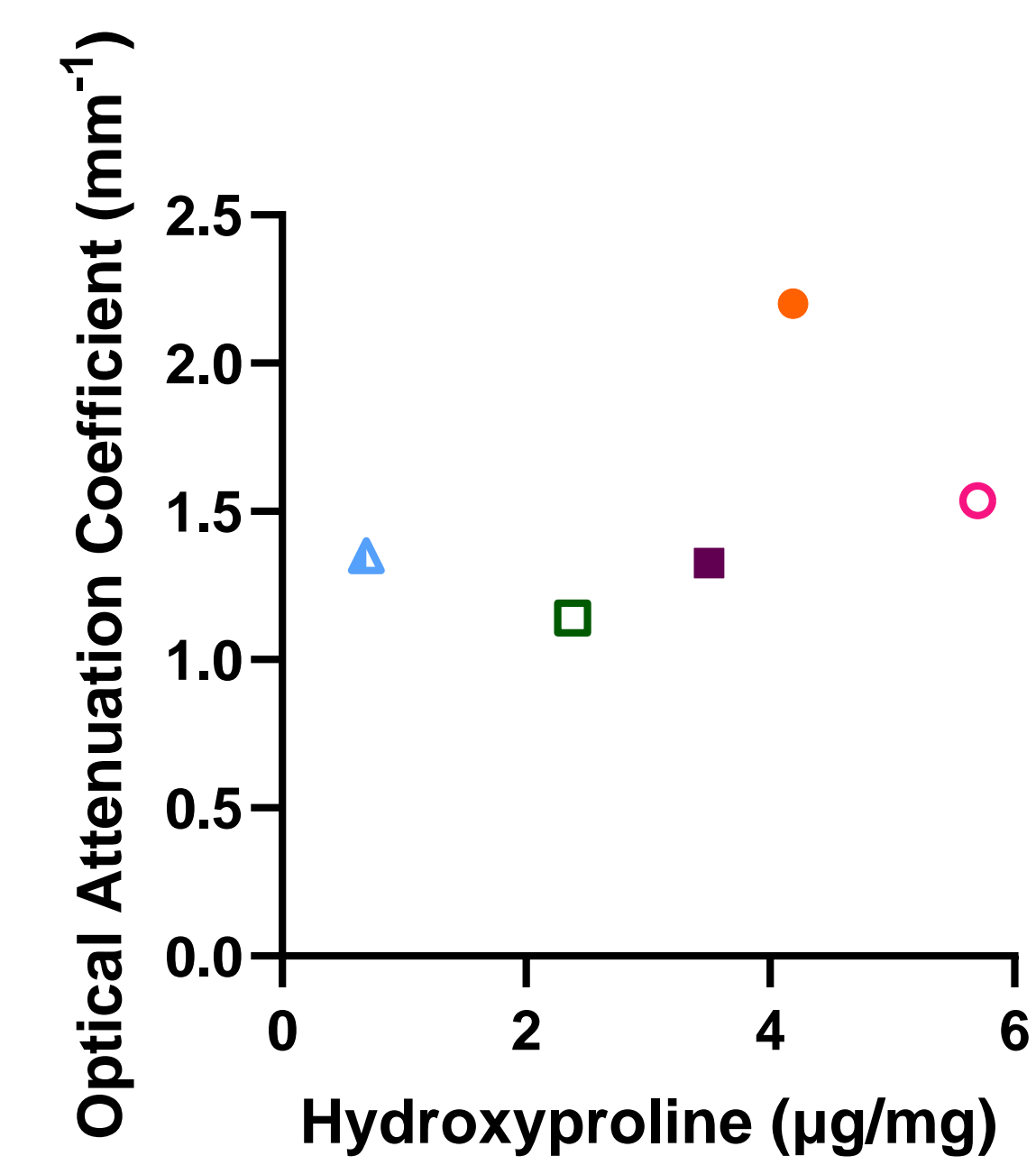


Figure 3. Human skin hydroxyproline content (µg/mg) vs optical attenuation coefficient (mm⁻¹). Mean of absorbance repeated in triplicate. Each data point represents an individual donor. Matching shapes indicate samples from the same patient.

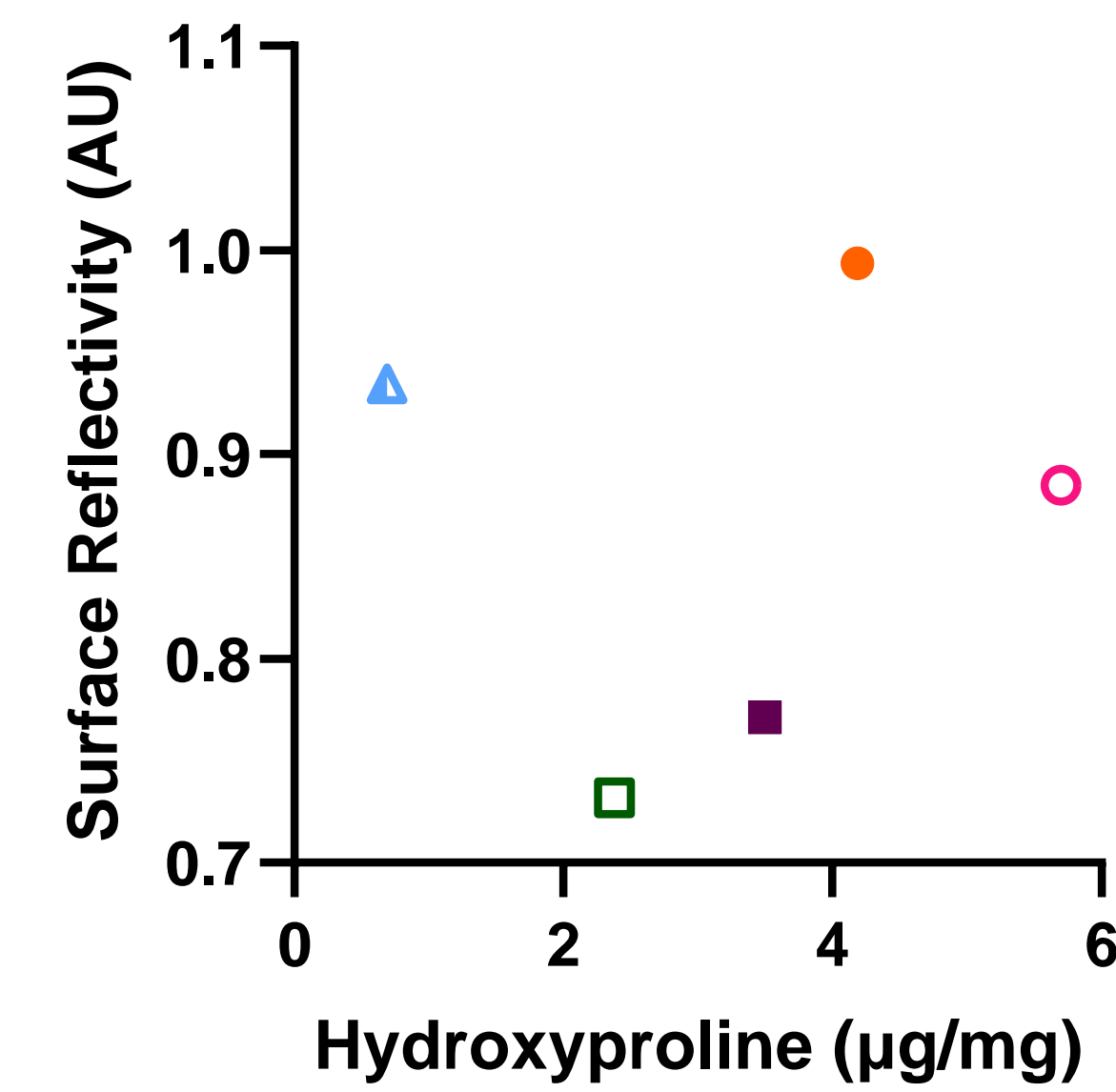


Figure 4. Human skin hydroxyproline content (µg/mg) vs surface reflectivity (AU). Mean of absorbance values repeated in triplicate. Each data point represents an individual donor. Matching shapes indicate samples from the same patient.

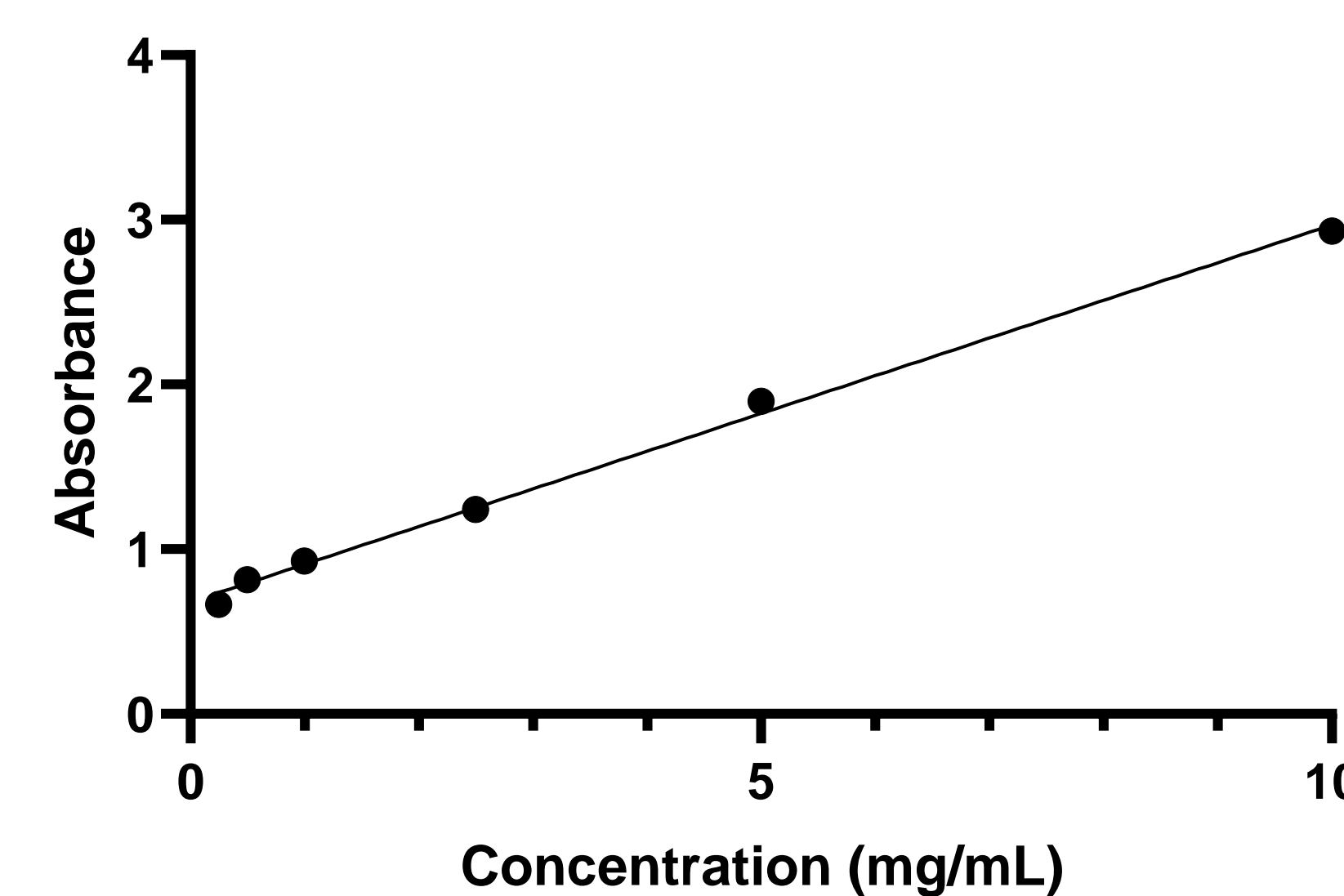


Figure 5. Sample calibration curve for hydroxyproline content measurements.

Porcine skin

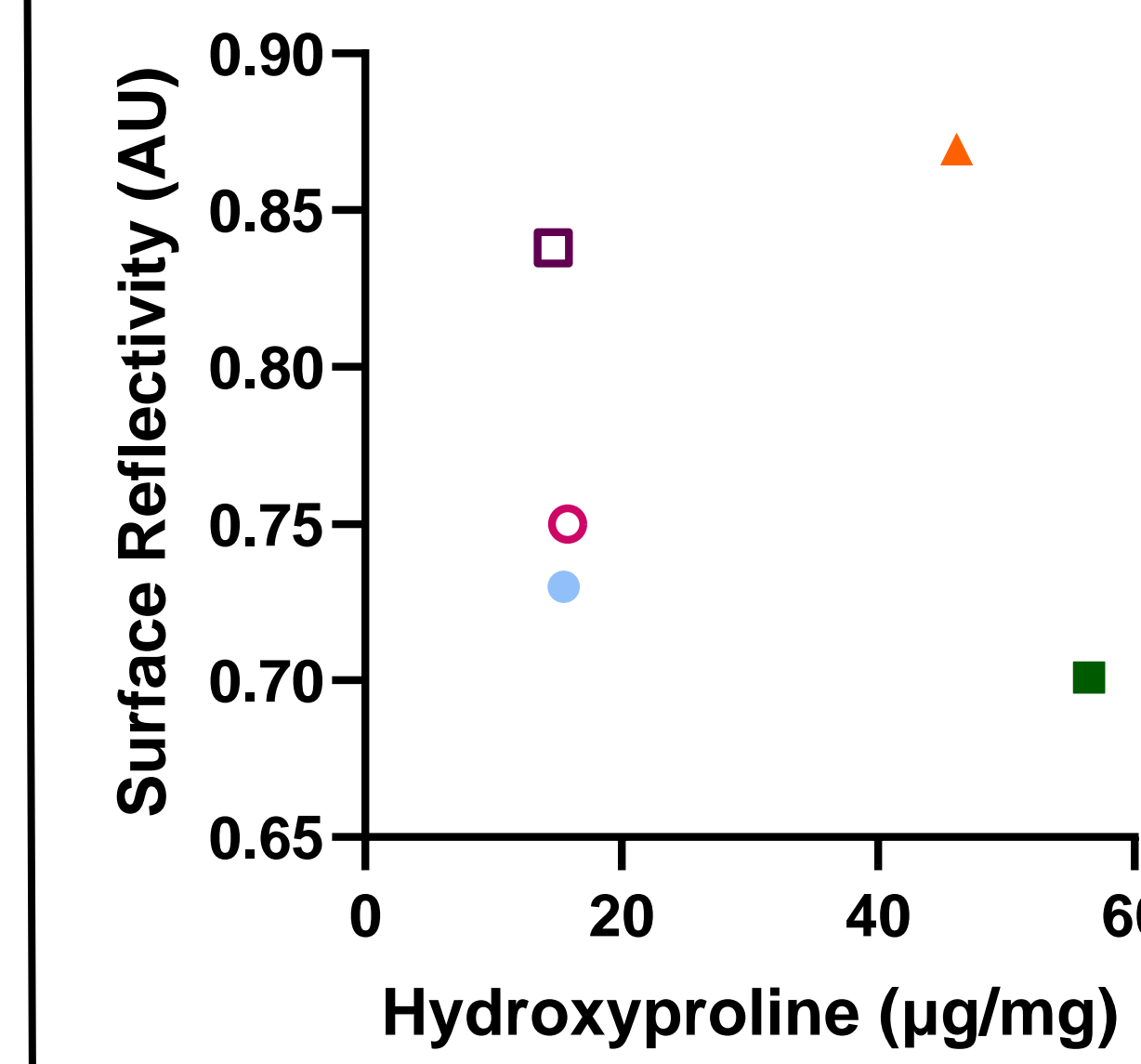


Figure 6. Porcine skin hydroxyproline content (µg/mg) vs surface reflectivity (AU). Mean of absorbance values repeated in triplicate. Each data point represents an individual donor. Matching shapes indicate samples from the same anatomical site.

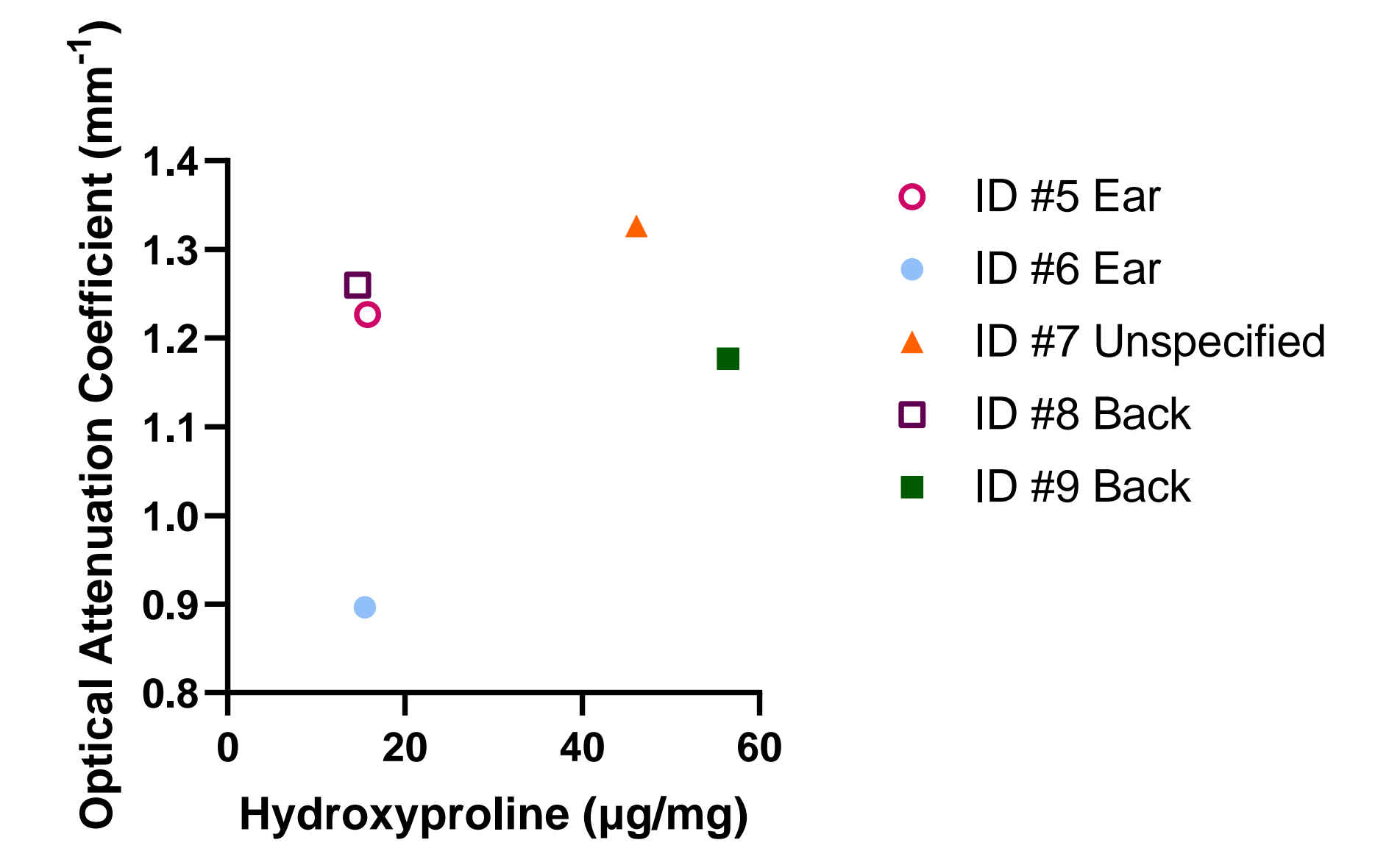


Figure 7. Porcine skin hydroxyproline content (µg/mg) vs optical attenuation coefficient (mm⁻¹). Mean of absorbance values repeated in triplicate. Each data point represents an individual donor. Matching shapes indicate samples from the same anatomical site.

Visible bands from SDS-PAGE indicate the presence of type I collagen in human skin

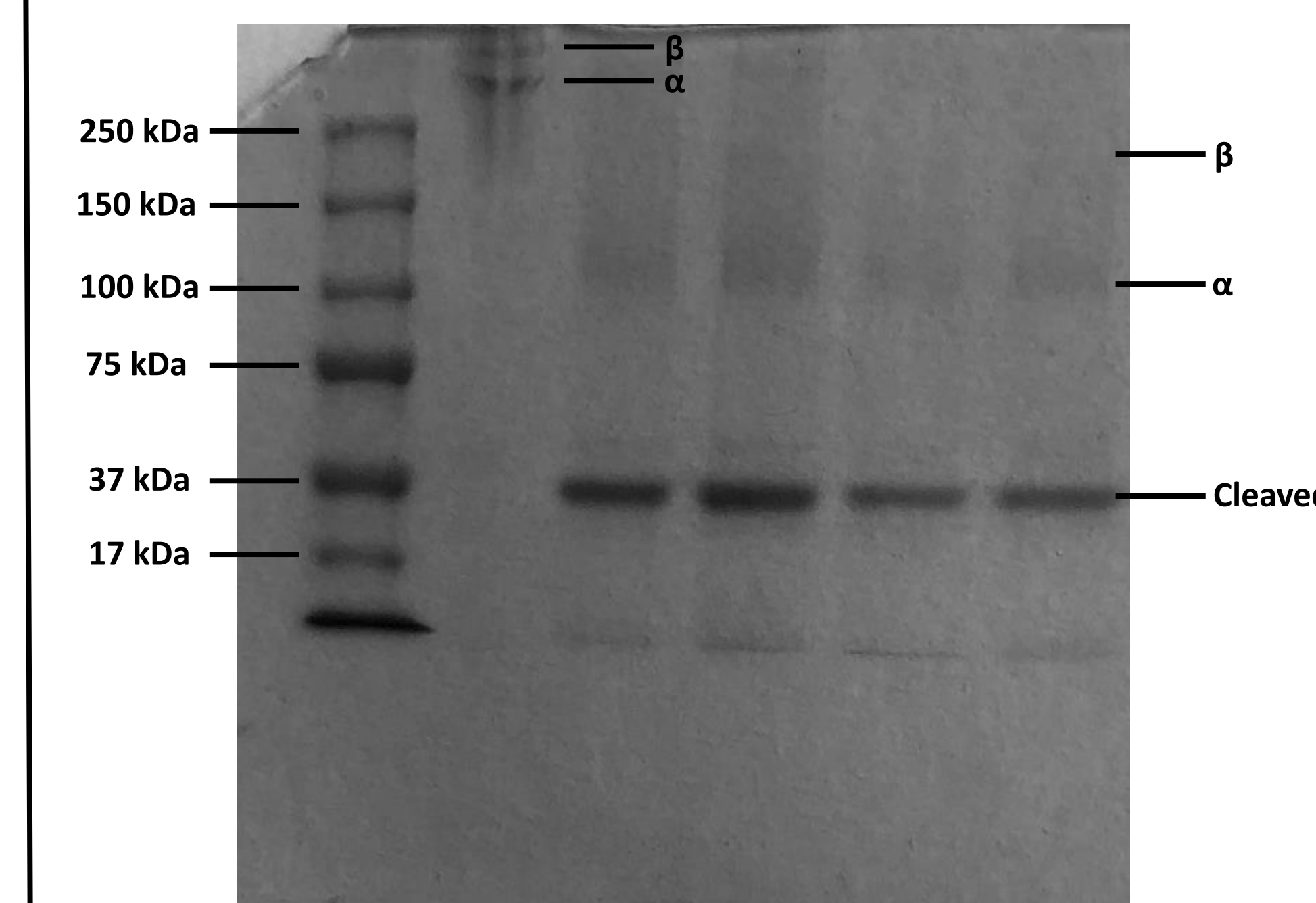


Figure 8. SDS-PAGE of extracted collagen from human skin. Lane 1: molecular weight marker. Lane 2: collagen control from rat tail. Lane 3: Back 1. Lane 4: Abdomen 1. Lane 5: Back 2. Lane 6: Abdomen 2.

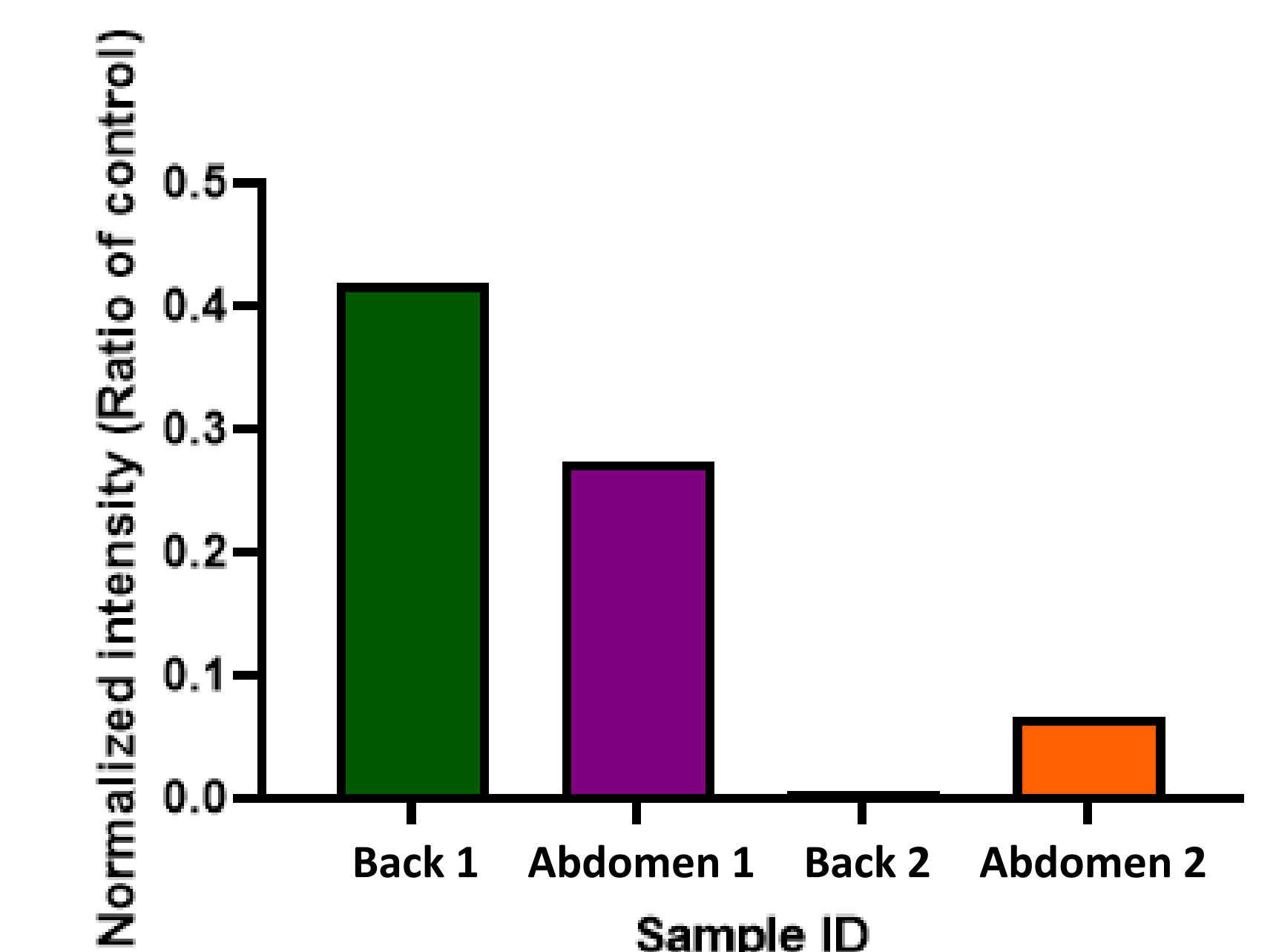


Figure 9. Type I collagen content in human skin determined using SDS-PAGE. ImageJ software was used to determine normalized intensity.

CONCLUSIONS

- A positive correlation was found between hydroxyproline content and OCT measurements
- Care must be taken to ensure digested skin sample falls within the linear range of the hydroxyproline calibration curve
- OCT is a promising technique for the noninvasive determination of collagen content in human skin

FUTURE STUDIES

- Positive correlation of hydroxyproline content to attenuation and surface reflectivity values will be verified with a greater number of skin samples
- SDS-PAGE will be rerun to accurately correlate protein to hydroxyproline content

ACKNOWLEDGMENTS

Nishant Lahiri would like to thank the Secondary Student Training Program at the University of Iowa and the Belin Blank Center for Gifted Education for the opportunity to conduct research. Nishant thanks the University of Iowa Tissue Procurement Core for the human skin samples and Dr. Ethan Anderson for the Chloramine-T reagent. Nishant would like to acknowledge the Brogden lab members for their guidance, especially Ms. Valeria Cota for teaching various laboratory techniques and analysis, and Professor Nicole Brogden for her mentorship and support.

REFERENCES

- Blair, M. J., Jones, J. D., Woessner, A. E., & Quinn, K. P. (2020). Skin structure–function relationships and the wound healing response to intrinsic aging. *Advances in Wound Care*, 9(3), 127-143. <https://doi.org/10.1089%2Fwound.2019.1021>
- Cissell, D. D., Link, J. M., Hu, J. C., & Athanasiou, K. A. (2017). A modified hydroxyproline assay based on hydrochloric acid in ehrlich's solution accurately measures tissue collagen content. *Tissue Engineering Part C: Methods*, 23(4), 243-250. <https://doi.org/10.1089%2Ften.tec.2017.0018>
- Francis, M., & Macmillan, D. C. (1971). The extraction of polymeric collagen from biopsies of human skin. *Biochimica Et Biophysica Acta (BBA) - Protein Structure*, 251(2), 236-245. [https://doi.org/10.1016/0005-2795\(71\)90107-3](https://doi.org/10.1016/0005-2795(71)90107-3)
- Inanc, S., Keles, D., & Oktay, G. (2017). An improved collagen zymography approach for evaluating the collagenases mmp-1, mmp-8, and mmp-13. *BioTechniques*, 63(4), 174-180. <http://dx.doi.org/10.2144/000114597>
- Ricard-blum, S. (2010). The collagen family. *Cold Spring Harbor Perspectives in Biology*, 3(1), a004978. <https://doi.org/10.1101%2Fcsfperspect.a004978>

Evaluation of optimal threshold settings for use of UBO Detector automated segmentation software for assessment of White Matter Lesions on FLAIR imaging Magnetic Resonance Imaging

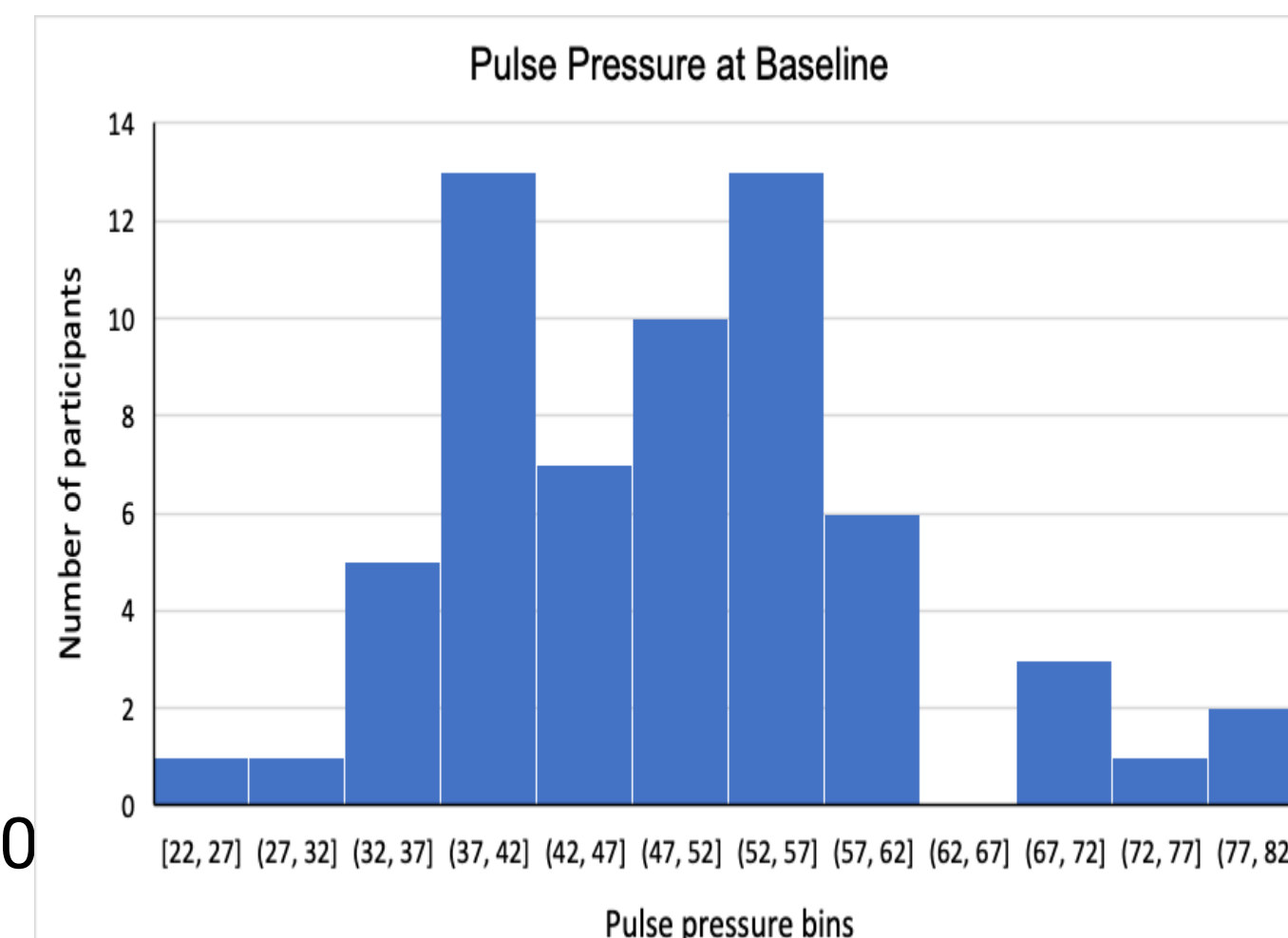
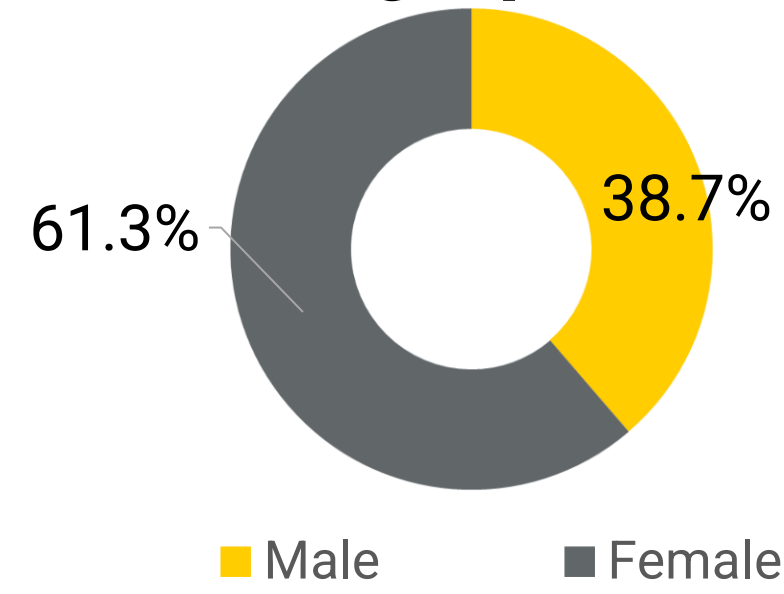
John LaMasters, Shivangi Jain PhD, Kelsey Baller, Jenna Springer, Michelle W. Voss PhD

Introduction

The field of study investigating aging and the brain specifically in the area regarding the relationship between hypertension and white matter lesions requires assessment of MRI imaging primarily using FLAIR imaging (Wardlaw, Forte, Badji).

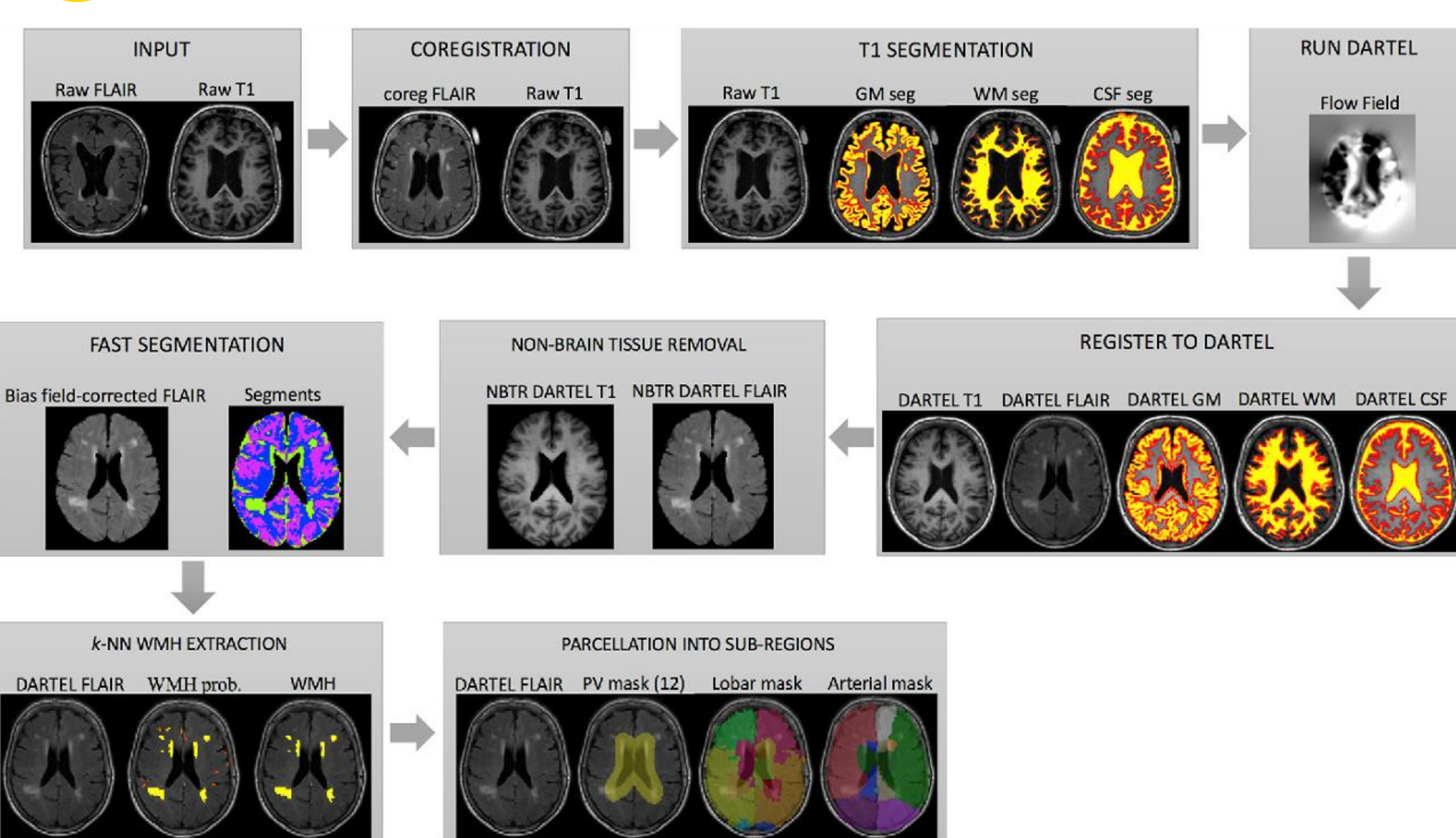
- Further study of the impact of aging and the brain including the impact of exercise and hypertension require evaluation of WML on FLAIR imaging MRI (Voss, Aghjayan).
- Gold standard technique of human evaluation of WML on FLAIR MRI is labor intensive and time consuming.
- Several software programs have been evaluated for automated segmentation however no specific program has been determined to be the reference standard.
- UBO Detector has been previously validated (Jiang, Hotz, Vanderbecq) for automated segmentation. There is potential for error introduced due to background signal "noise" in the MRI scans. Different threshold settings are available to adjust the sensitivity.
- The optimal settings for use of the UBO Detector software have not previously been determined.
- This study was performed to compare the results of 0.5 and 0.7 thresholds for automated segmentation of the UBO Detector to the gold standard of human interpretation.
- The threshold is a percentage of voxels detected to be defined as a WML.

Demographics



Ave Age 63 yo; Range 55-80

A Transformation of images for segmentation

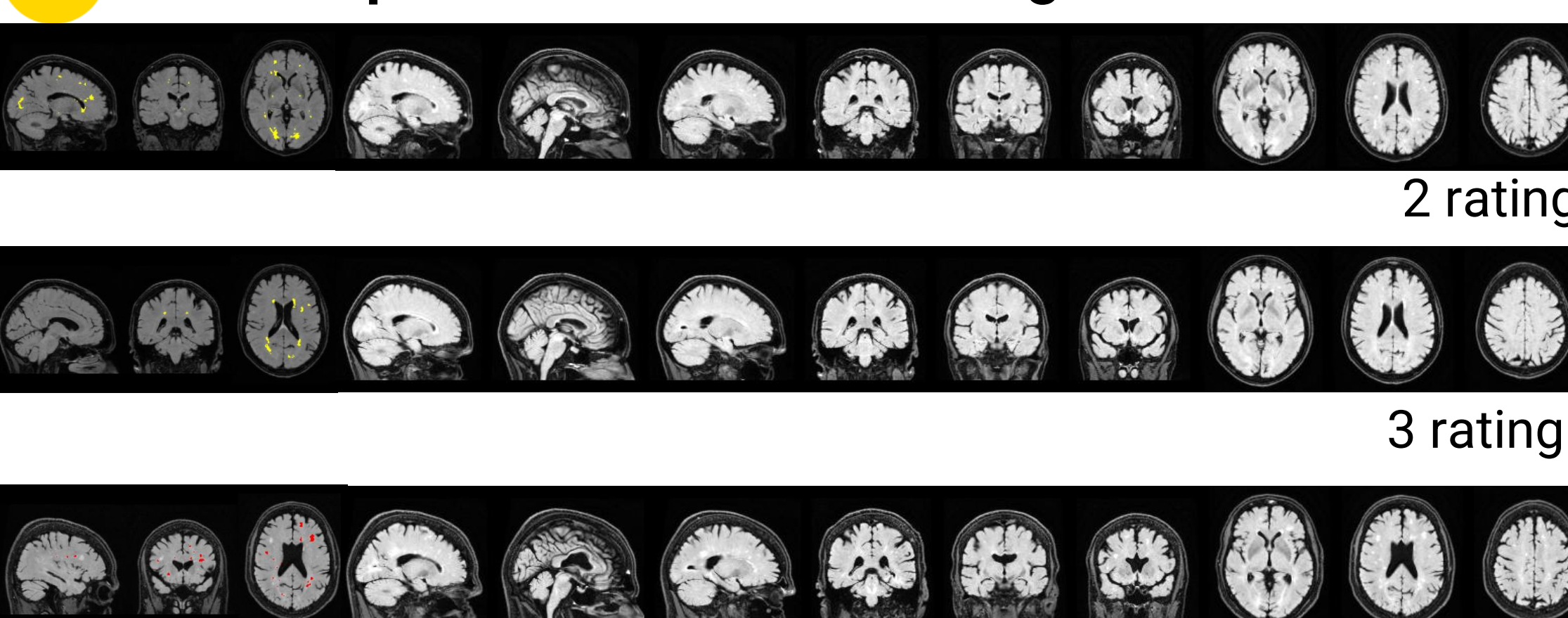


Methods

Assessment of WML was performed using FLAIR MRI images by 3 separate independent observers. We performed automatic segmentations with settings 0.5 and 0.7 using the UBO Detector software (Jiang). We used observation by human researchers as the gold-standard.

- 98 participants scans were evaluated
- Results of thresholding with the automated segmentations at 0.5 and 0.7 were rated by human reviewers and graded on a 1 to 3 integer scale for performance (1 = good, 2= adequate, 3= poor)
- Pulse Pressure (PP) =Systolic-Diastolic Pressure
- The masks given rating of 1 by two of three observers were compiled into two intensity maps based on their pulse pressure (PP) group (High PP >50, Low PP <=to 50)
- Mask overlay of the two pulse pressure groups was performed to evaluate degree of overlap

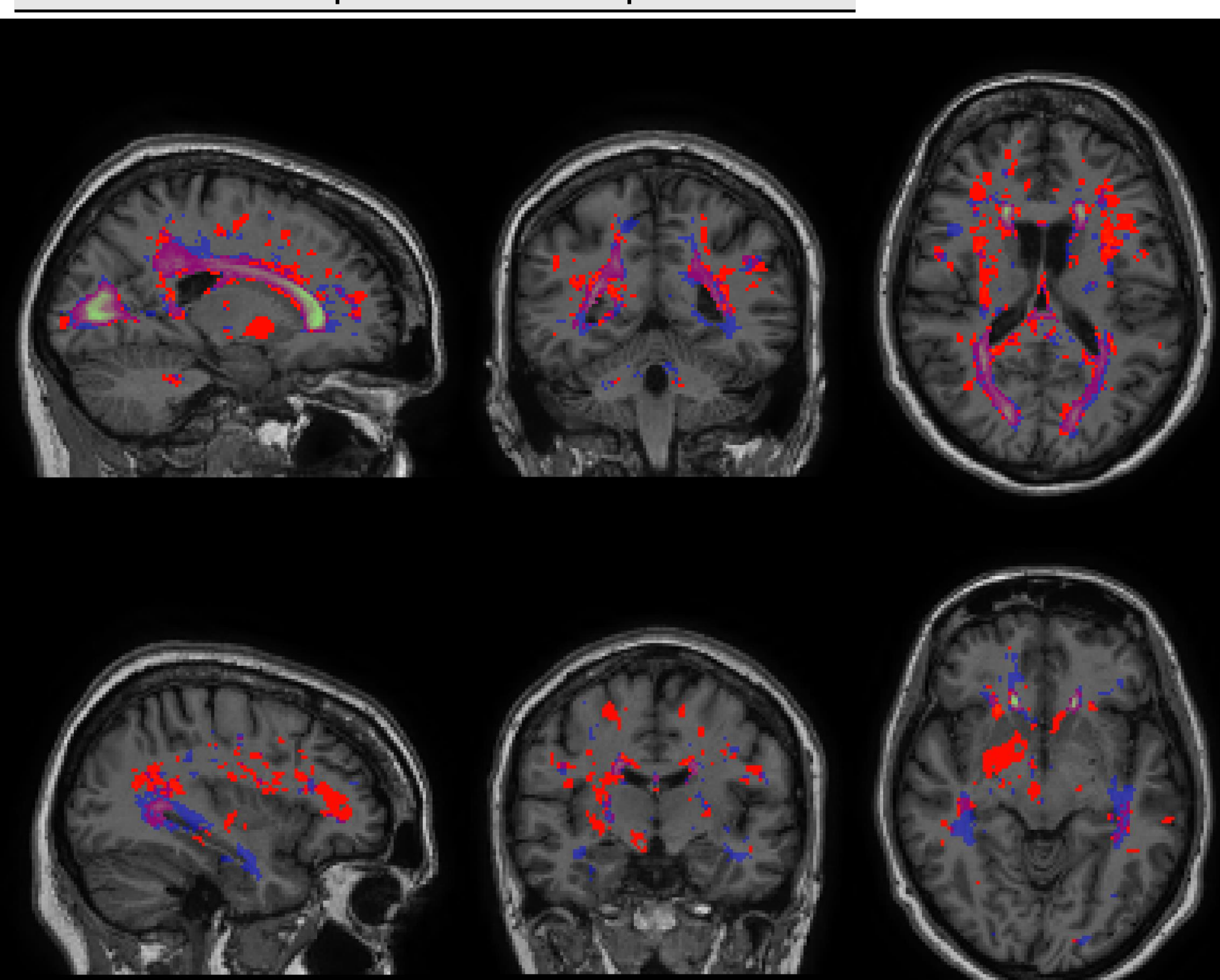
B Examples of FLAIR mask ratings



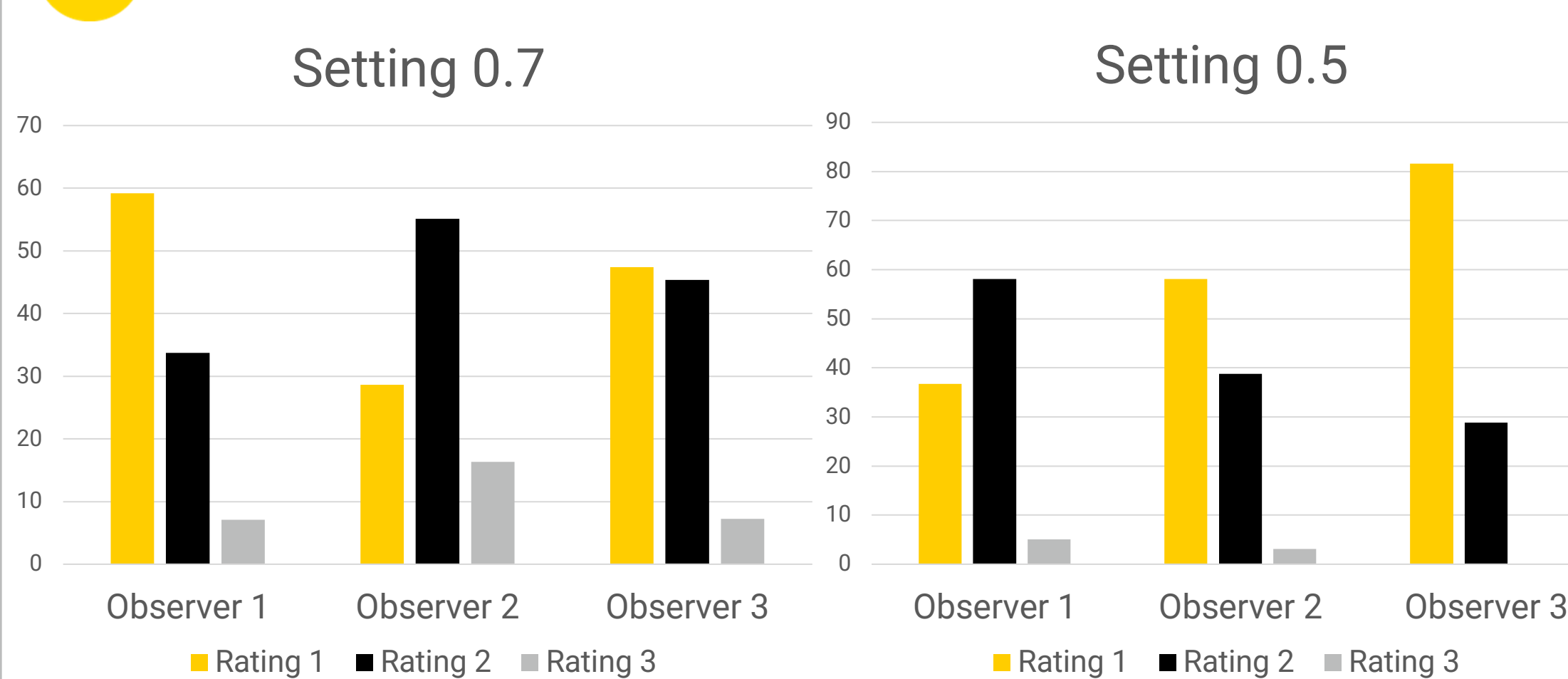
C Combined High and Low Pulse Pressure groups

Legend- Colors

- Red = High PP
- Blue = Low PP
- Green/White/Purple = Overlap



D Ratings of Observers



Results

Analysis of setting 0.5 and 0.7 of UBO Detector automatic segmentation assessment of white matter lesions on FLAIR MRI were compared to human interpretation by 3 observers.

- Of the 98 masks rated, 64 were rated acceptable at grade 1 by at least 2 of 3 observers
- Data from 2 participants were excluded due to missing pulse pressure data
- 29 of the acceptable grade masks were from the high pulse pressure group and 33 were from the low pulse pressure group
- WML were more widely dispersed in participants with high pulse pressure (PP)

Discussion

This study was performed to further validate the UBO Detector automated segmentation software technology that may be used to make the process of assessment of white matter lesions (WML) on FLAIR imaging MRI more efficient than the previous method of human observer interpretation.

- Several automated segmentation software programs have been validated previously (Jiang, Hotz, Vandenberg)
- No standard reference of automated segmentation software has been determined.
- Error in automated segmentation software can be introduced due to background signals of the MRI scan
- Threshold Settings of 0.5 and 0.7 of the UBO Detector software were evaluated for congruence to gold standard manual human interpretation to identify the most accurate settings.
- Results indicate future investigation of threshold 0.3 may prove to be more accurate.

If a reference standard was able to be determined for automated segmentation software programs and specific threshold settings, it would assist researchers with efficiency and better comparability of results for future study.

Conclusion

The performances we report of both UBO Detector threshold settings 0.7 and 0.5 is variable and moderate accuracy but acceptable, with most readings receiving a rating of 1 or 2.

- Both settings consistently underestimated WML volume and had some images with a rating of 3. This suggests more work is needed to improve performance of automated algorithms for WML automated segmentation.
- Similar to other studies, both threshold settings 0.7 and 0.5 were acceptable but lower than human interpretation and no clear reference standard was identified
- High PP is associated with microvascular disease and the effects of WML are more diffusely located throughout the brain compared with low pulse pressure

Acknowledgments

I would like to thank Dr. Michelle Voss in the Psychological and Brain Sciences who was my mentor for this research project.

I would also like to thank my lab colleagues, Dr. Shivangi Jain, Kelsey Baller, Jenna Springer, Bryan Madero, and Will Daniels for support in data collection and interpretation.

References

1. Wardlaw, J. M., Valdés Hernández, M. C., & Muñoz-Maniega, S. (2015). What are white matter hyperintensities made of? Relevance to vascular cognitive impairment. *Journal of the American Heart Association*, 4(6), 001140. <https://doi.org/10.1161/JAHA.114.001140>
2. Forte, G., & Casagrande, M. (2020). Effects of Blood Pressure on Cognitive Performance in Aging: A Systematic Review. *Brain sciences*, 10(12), 919. <https://doi.org/10.3390/brainsci10120919>
3. Badji A, Cohen-Adad J and Girouard H (2022) Relationship Between Arterial Stiffness Index, Pulse Pressure, and Magnetic Resonance Imaging Markers of White Matter Integrity: A UK Biobank Study. *Front. Aging Neurosci.* 14:856782. doi: 10.3389/fnagi.2022.856782
4. Voss, M. W., & Jain, S. (2022). Getting Fit to Counteract Cognitive Aging: Evidence and Future Directions. *Physiology (Bethesda, Md.)*, 37(4), 0. <https://doi.org/10.1152/physiol.00038.2021>
5. Aghjayan, S. L., Bourmias, T., Kang, C., Zhou, X., Stillman, C. M., Donofry, S. D., Kamarck, T. W., Marsland, A. L., Voss, M. W., Fraundorf, S. H., & Erickson, K. I. (2022). Aerobic exercise improves episodic memory in late adulthood: a systematic review and meta-analysis. *Communications medicine*, 2, 15. <https://doi.org/10.1038/s43856-022-00079-7>
6. Jiang, J., Liu, T., Zhu, W., Koncz, R., Liu, H., Lee, T., Sachdev, P. S., & Wen, W. (2018). UBO Detector - A cluster-based, fully automated pipeline for extracting white matter hyperintensities. *NeuroImage*, 174, 539–549. <https://doi.org/10.1016/j.neuroimage.2018.03.050>
7. Hotz, I., Deschwanden, P. F., Liem, F., Ménilat, S., Malagurski, B., Kollias, S., & Jäncke, L. (2022). Performance of three freely available methods for extracting white matter hyperintensities: FreeSurfer, UBO Detector, and BIANCA. *Human brain mapping*, 43(5), 1481–1500. <https://doi.org/10.1002/hbm.25739>
8. Vanderbecq, Q., Xu, E., Ströer, S., Couvy-Duchesne, B., Diaz Melo, M., Dormont, D., Colliot, O., & Alzheimer's Disease Neuroimaging Initiative (2020). Comparison and validation of seven white matter hyperintensities segmentation software in elderly patients. *NeuroImage. Clinical*, 27, 102357. <https://doi.org/10.1016/j.nicl.2020.102357>

Research Objective

To investigate the effects of isoform-specific *prickle* mutations on the neurological dysfunction of *prickle* larvae, mainly short-term memory and movement

Introduction

Prickle encodes two adult protein isoforms of the Planar Cell Polarity (PCP) complex, and mutations in both isoforms have been associated with neurological disorders. For instance, when the *prickle-spiny-legs* (*sple*) isoform is mutated, the fly exhibits seizures and locomotor defects that mimic those found in human *PRICKLE* patients (Ehaideb et al., 2016). Conversely, when the *prickle-prickle* isoform (*pk*) is mutated, preliminary data reveals widespread neurodegeneration in the mutant brains, and *pk/pk* mutants show a pronounced reduction in lifespan. Finally, when a mutation affects the entire gene (*pk-sple13*) intermediate phenotypes between *sple/sple* and *pk/pk* are observed.

While individuals with *PRICKLE* mutations can present with seizures, they also have an increased likelihood of presenting with an autism spectrum disorder (ASD) that includes intellectual disability (i.e., learning and memory deficits) (Paemka et al., 2013). Preliminary data in the Manak laboratory has shown that adult *sple* mutants, in addition to manifesting seizures, show learning deficits (Figure 1a). Therefore, we wanted to determine whether locomotor or learning deficits were also manifest in earlier life stages of development of the *sple* mutants (i.e., larvae; Fig. 1b).

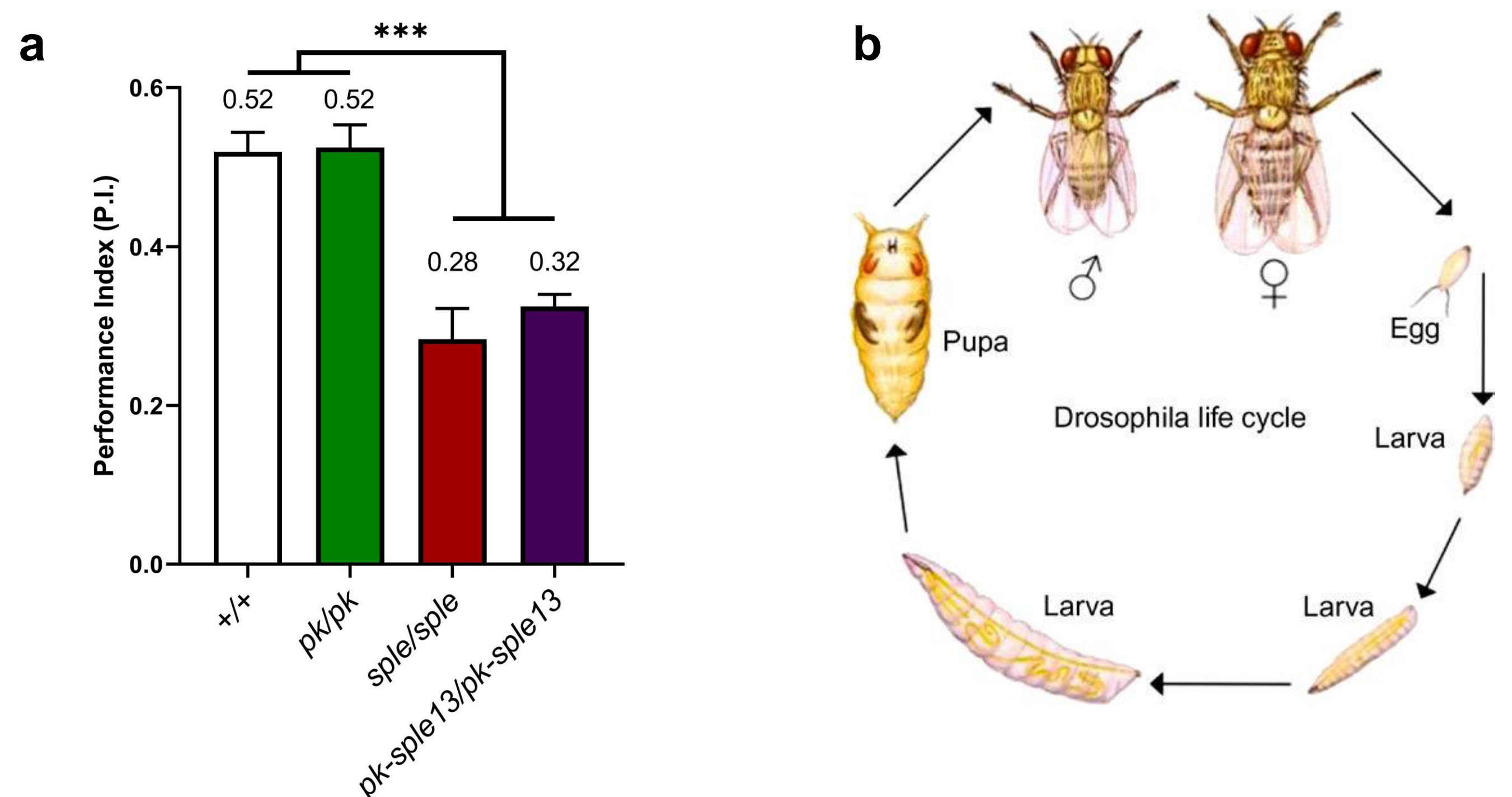


Figure 1: Adult *Drosophila prickle* mutants show a decreased ability to learn. a) The Performance Index (P.I.) indicates how well the adult fly learns to associate smell with an electric shock. *pk/pk* mutants showed no change when compared to controls; however, both the *sple/sple* and *pk-sple13/pk-sple13* mutants show a significant decrease in short-term learning ability. n = 225 adult flies each (assayed in 3 batches of 75). *** p < 0.001. One Way ANOVA
b) Illustration of the *Drosophila* life cycle.

Methods and Materials

Genotypes (All outcrossed to a *w¹¹¹⁸* background)

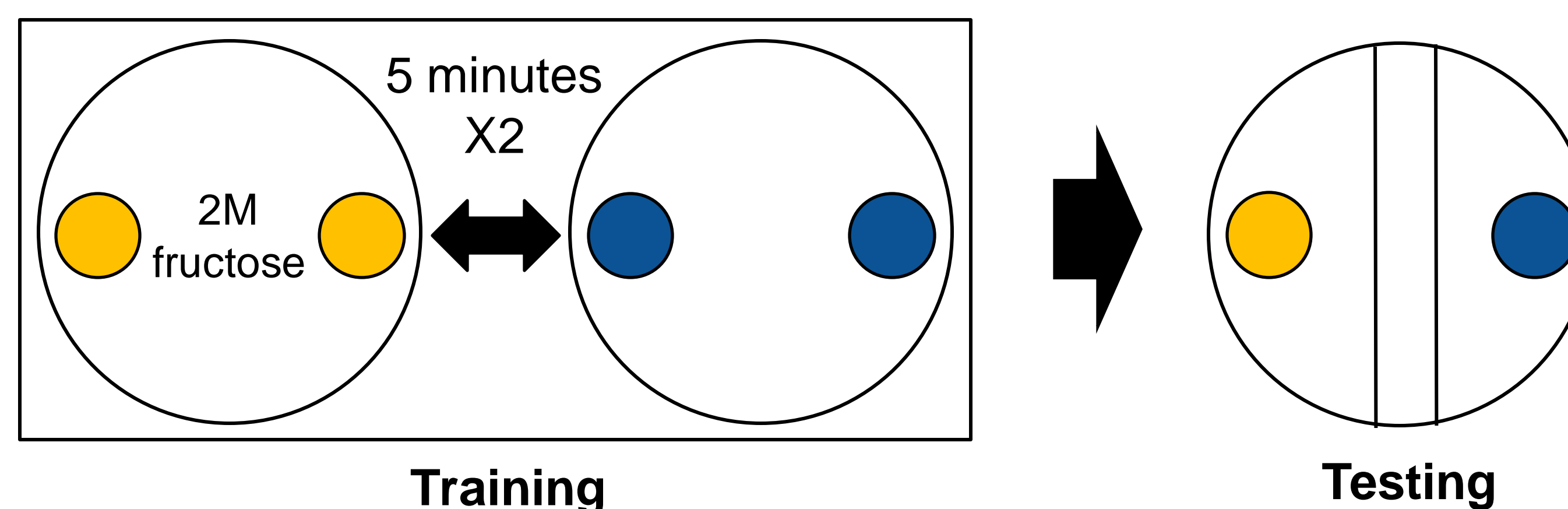
- *WT* (+/+)
- *pk^{sple1}/pk^{sple1}* (*sple/sple*) – null mutation of the *spiney-legs* isoform, seizure-prone
- *pk^{pk1}/pk^{pk1}* (*pk/pk*) – null mutation of the *prickle* isoform, exhibits neurological degeneration and shortened lifespan
- *pk^{pk-sple13}/pk^{pk-sple13}* (*pk-sple13/pk-sple13*) – null mutation for the *prickle* gene

Larvae Crawling Assay

1. L3 larvae were individually placed onto an 85 mm 2.5% agarose plate. 30 seconds of active crawling were recorded to track the larval movement. (Canon High Definition Vixia HFM31 Camcorder with zoom [resolution 1920 × 1080] for higher resolution). Motion was assessed using a Manual Tracking plugin of FIJI software

Larval Olfactory Learning Assay

1. L3 larvae were trained on 2M fructose agarose plates with 2 caps of either 1:100 OCT or 1:25 MCH (shown below) for 5 minutes.
2. The larvae were then transferred onto an agarose plate without fructose with 2 caps of the opposite scent for 5 minutes.
3. Steps 1 and 2 were repeated
4. Larvae were immediately placed in the center of the testing plate, which contained 1 cap of each scent. After 5 minutes, the position of each larvae was recorded.
5. The performance index was then calculated.



Results

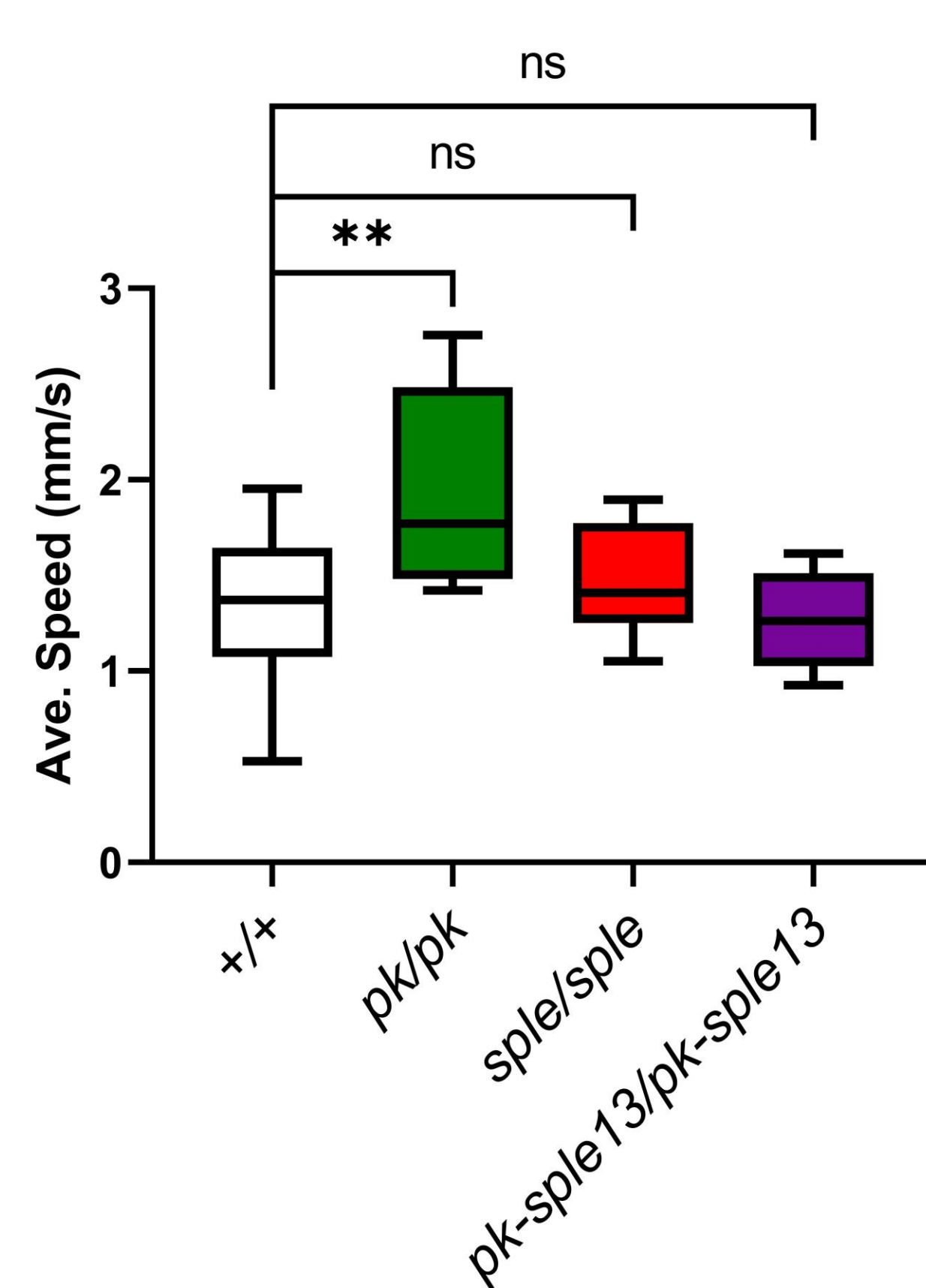


Figure 2: *pk* mutant larvae, but not *sple* mutant larvae, show an increase in locomotor speed. Note the wide variance of velocities for the *pk/pk* mutants in comparison to the other isoforms. However, the median speed for *pk/pk* is higher than the other isoforms and shows a statistically significant increase in velocity. Notably, the *sple/sple* mutant velocities are not significantly different than control, suggesting that the *sple* mutant larvae do not have a locomotor defect. n = 12 for +/+ larvae, 10 for *pk/pk* larvae, 11 for *sple/sple* larvae, and 10 for *pk-sple13/pk-sple13* larvae. * p < 0.05, ** p < 0.01. One-way ANOVA

Results

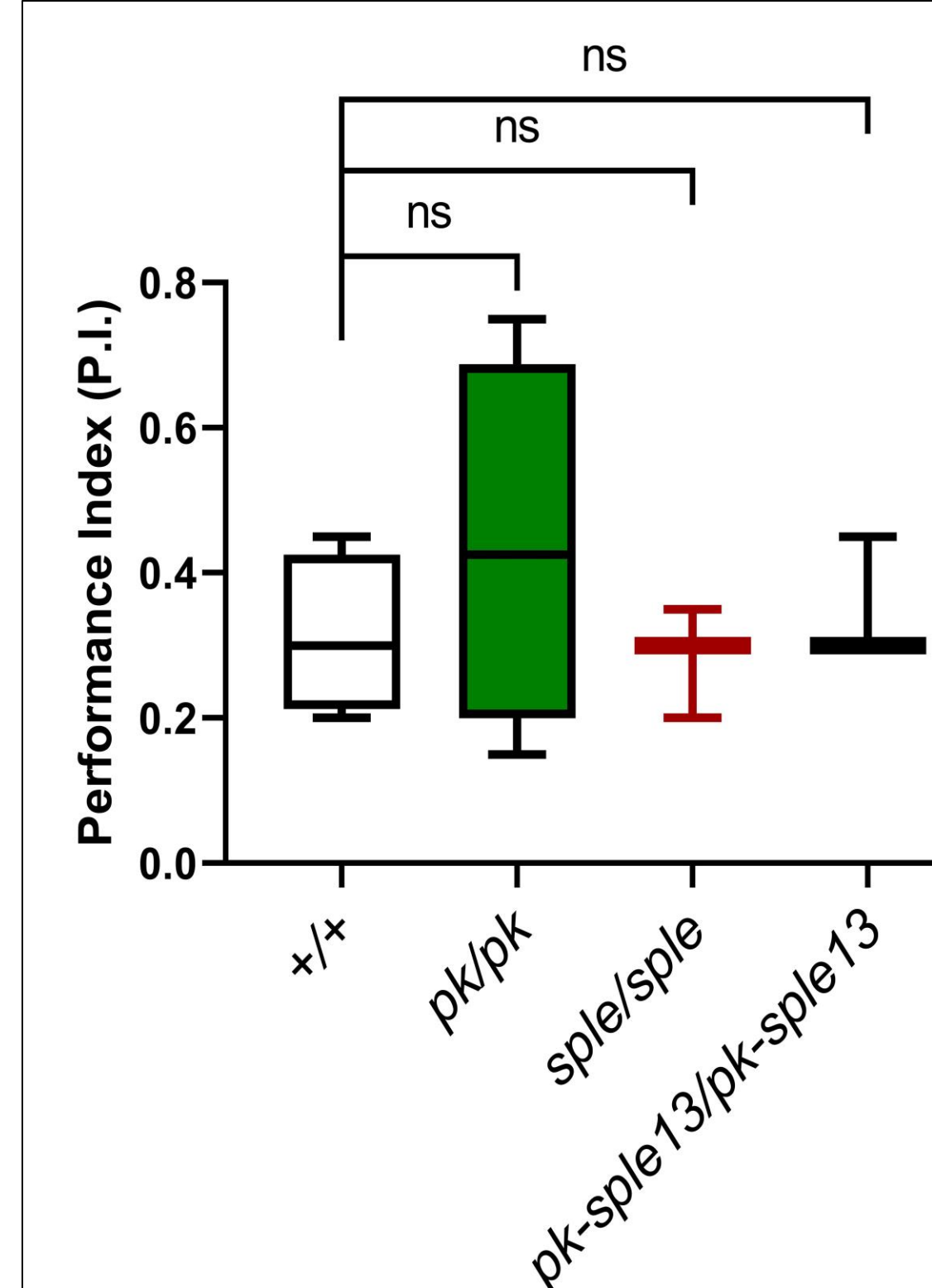


Figure 3: *Drosophila L3 sple* mutant larvae do not exhibit learning deficits. Preliminary data reveals that *sple* mutant larvae can associate a scent with an attractive stimulus (fructose) similar to controls. This suggests the *sple* mutation does not drastically impact the ability of *Drosophila* larvae to form and retain short-term memories. n = 30 for all lines. Kruskal-Wallis test.

Conclusions

- *sple* mutant larvae do not show obvious locomotor defects as assessed by the crawling assay.
- Notably, these data suggest that *sple* mutants only show locomotor defects as adults.
- *sple* mutant larvae do not show learning deficits as assessed by the larval olfactory learning assay.
- Similar to the locomotor assay results, *sple* mutants only show learning deficits as adults.

Future Directions

- Increase the sample size for each strain for both experiments.
- Explore automating movement tracking to standardize tracking and allow for assessing more detailed tracking parameters.
- Employ the learning assays with an aversive rather than attractive stimulus (NaCl or Quinine) to determine whether learning ability differs between control and mutants.

Acknowledgements

- This work was supported by a grant from the Stead Family Department of Pediatrics, Carver College of Medicine to JRM.
- I would like to thank Dr. Manak and everyone in the Manak lab for their time, help, and input over this summer.

References

1. Ehaideb, S. N., Wignall, E. A., Kasuya, J., Evans, W. H., Iyengar, A., Koerselman, H. L., Lilienthal, A. J., Bassuk, A. G., Kitamoto, T., & Manak, J. R. (2016). Mutation of orthologous *prickle* genes causes a similar epilepsy syndrome in flies and humans. *Annals of Clinical and Translational Neurology*, 3(9), 695–707. <https://doi.org/10.1002/acn3.334>
2. Tao, H., Manak, J. R., Sowers, L., Mei, X., Kiyonari, H., Abe, T., Dahdaleh, N. S., Yang, T., Wu, S., Chen, S., Fox, M. H., Gunnert, C., Montine, T., Bird, T., Shaffer, L. G., Rosenfeld, J. A., McConnell, J., Madan-Khetarpal, S., Berry-Kravis, E., ... Bassuk, A. G. (2011). Mutations in *prickle* orthologs cause seizures in flies, mice, and humans. *The American Journal of Human Genetics*, 88(2), 138–149. <https://doi.org/10.1016/j.ajhg.2010.12.012>
3. Ehaideb, S. N., Iyengar, A., Ueda, A., Iacobucci, G. J., Cranston, C., Bassuk, A. G., Gubb, D., Axelrod, J. D., Gunawardena, S., Wu, C.-F., & Manak, J. R. (2014). *prickle* modulates microtubule polarity and axonal transport to ameliorate seizures in flies. *Proceedings of the National Academy of Sciences*, 111(30), 11187–11192. <https://doi.org/10.1073/pnas.1403357111>
4. Apostolopoulou, A. A., Widmann, A., Rohwedder, A., Pfitzenmaier, J. E., & Thum, A. S. (2013). Appetitive associative olfactory learning in *Drosophila* larvae. *Journal of Visualized Experiments*, (72). <https://doi.org/10.3791/4334>
5. Scherer, S., Stocker, R. F., & Gerber, B. (2003). Olfactory learning in individually assayed *Drosophila* larvae. *Learning & Memory*, 10(3), 217–225. <https://doi.org/10.1101/m.57903>
6. Paemka, L., Mahajan, V. B., Skeie, J. M., Sowers, L. P., Ehaideb, S. N., Gonzalez-Alegre, P., Sasaoka, T., Tao, H., Miyagi, A., Ueno, N., Takao, K., Miyakawa, T., Wu, S., Darbro, B. W., Ferguson, P. J., Pieper, A. A., Britt, J. K., Wemmie, J. A., Rudd, D. S., ... Bassuk, A. G. (2013). Prickle1 interaction with synapsin I reveals a role in autism spectrum disorders. *PLoS ONE*, 8(12). <https://doi.org/10.1371/journal.pone.0080737>

Impact of Placental *Igf-1* Overexpression on Angiogenesis in Embryonic Mouse Brain

Aidan Lin¹, Annemarie Carver^{2,3,4}, Robert Taylor^{3,4}, and Hanna Stevens^{2,3,4}

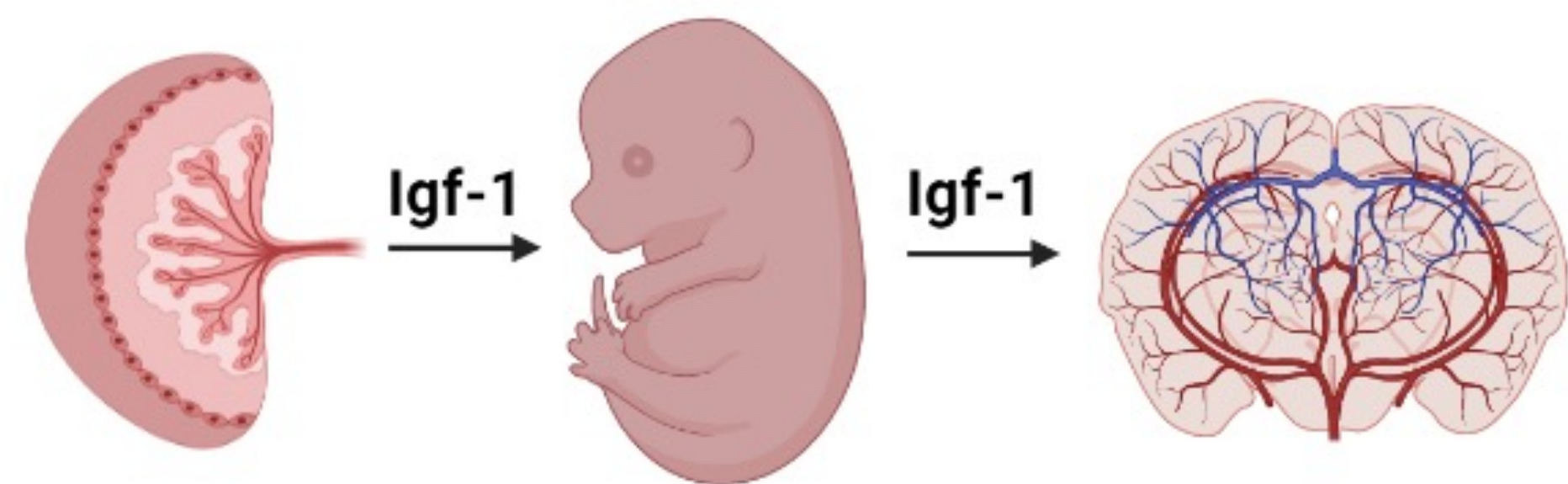
Brophy College Preparatory¹, Interdisciplinary Graduate Program in Genetics², Department of Psychiatry³, Iowa Neuroscience Institute⁴
Carver College of Medicine, University of Iowa, Iowa City, Iowa

Introduction

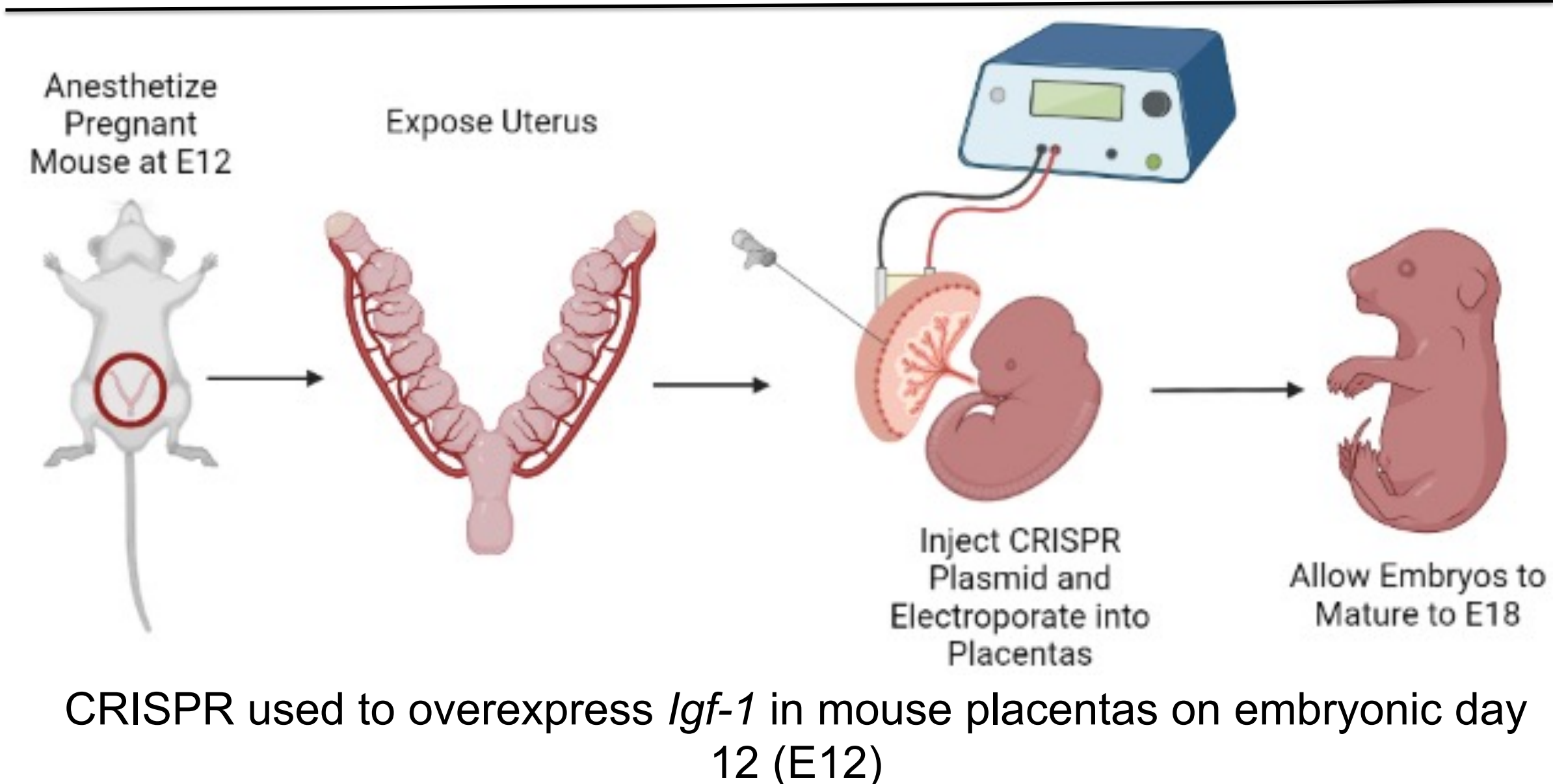
2.3%  1 in 44

- Autism Spectrum Disorder (ASD) is found in around 1 in 44 children (CDC)
 - Common traits are challenges with social skills, repetitive behaviors, speech and nonverbal communication¹
- Igf-1* is an important growth factor/hormone for neuron formation (neurogenesis) and blood vessel development (angiogenesis)^{2,3}
 - Placenta is main source of *Igf-1* prior to birth⁴
- Some people with ASD have altered expression of *IGF-1*⁵
- Recent findings show people with ASD have abnormal angiogenesis in the brain⁶

We hypothesize that overexpression of *Igf-1* in the placenta will cause abnormal blood vessel development in the brain.



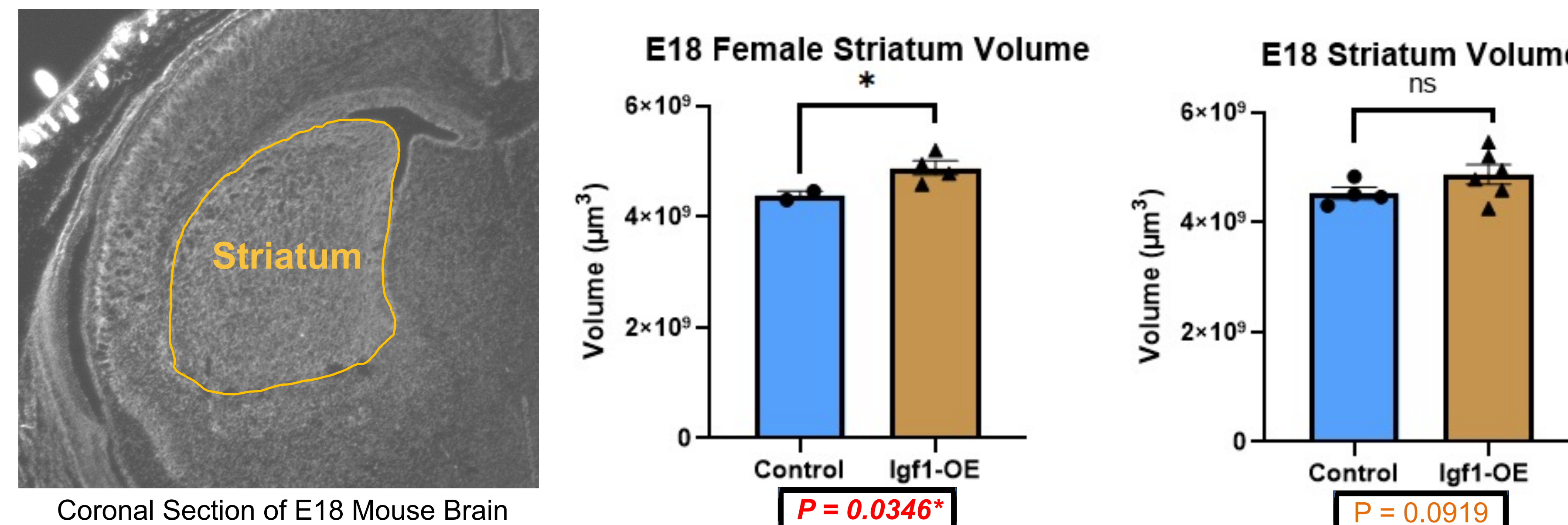
Methods



- Immunohistochemistry:** Stained E18 coronally-sectioned brains with Isolectin B4 to visualize vasculature
- Microscopy and Stereology:** Measured striatal volume & counted blood vessels and branch points
- Statistics:** T-test to analyze embryonic angiogenesis in control and *Igf-1* overexpression samples

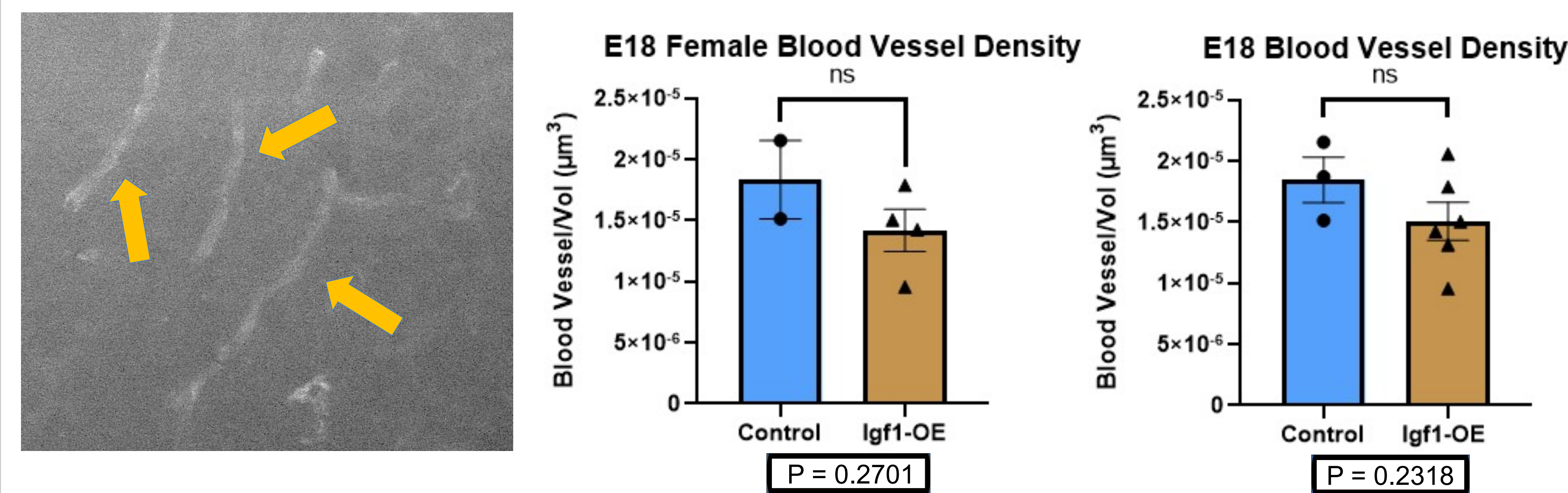
Results

Striatal Volume



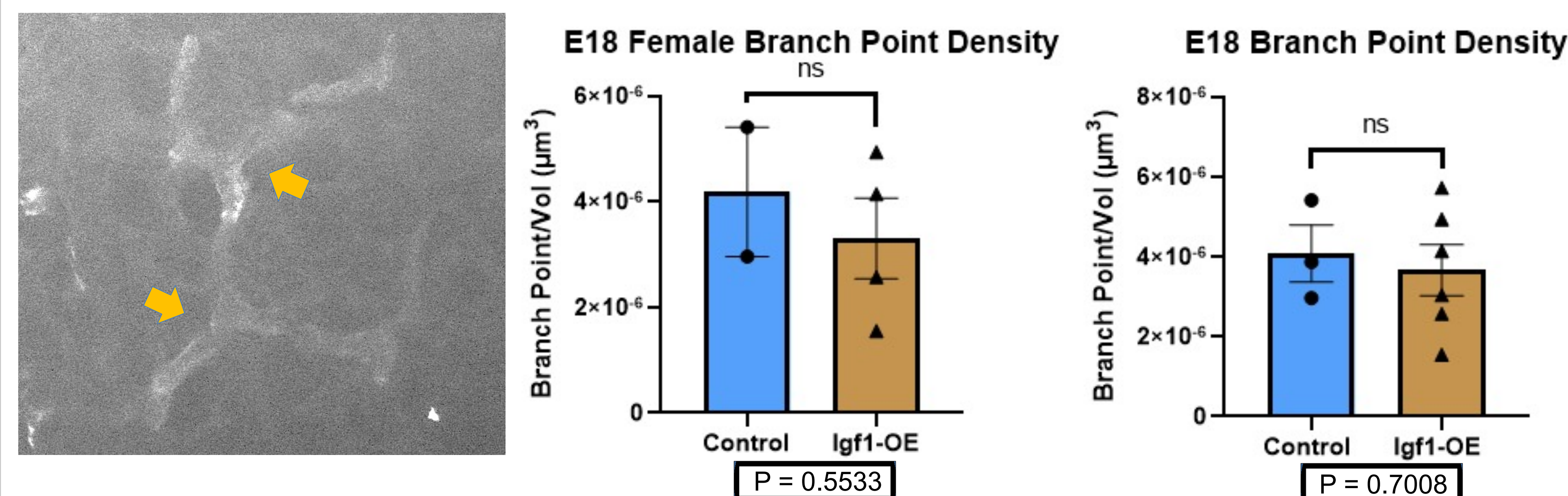
Significant increase in E18 female striatal volumes and trending increase with males

Striatal Blood Vessels



No significant difference in number of striatal blood vessels regardless of sex or placental *Igf-1* expression

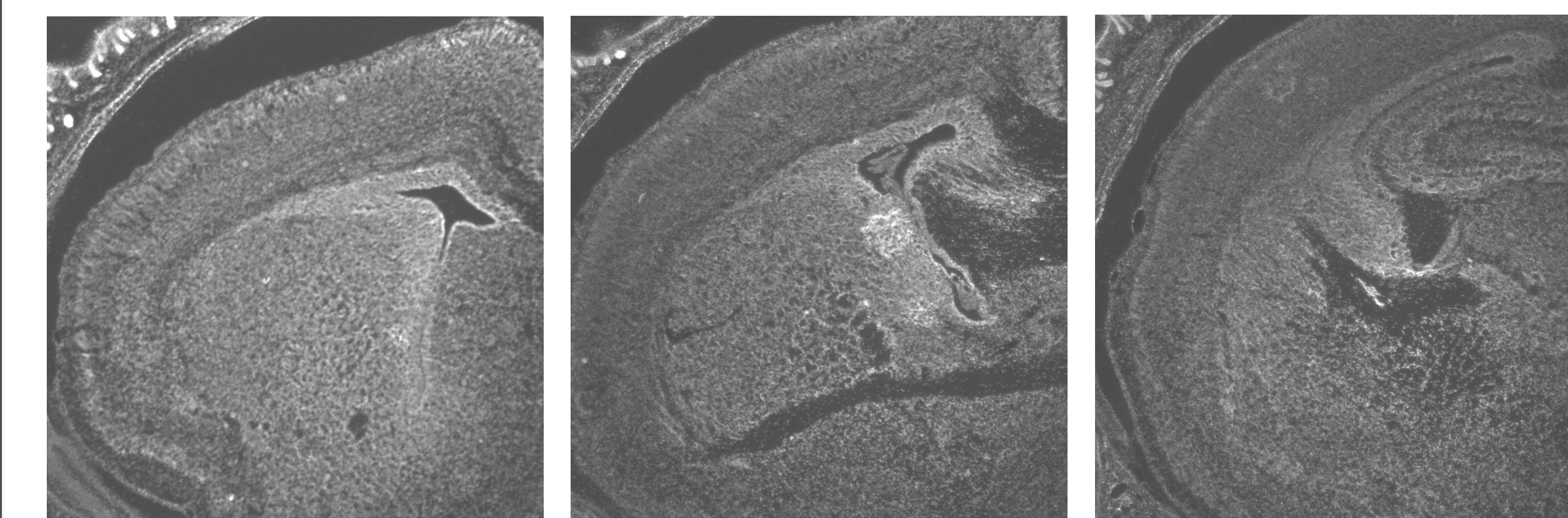
Striatal Branch Points



No significant difference in number of striatal blood vessel branch points regardless of sex or placental *Igf-1* expression

Conclusions

- Significant increase in striatal volume in females with a trending increase in males and females combined
 - This result recapitulates previous findings from our lab, demonstrating that placental *Igf-1* levels impact neurogenesis
- No difference in blood vessels or branch points regardless of sex or *Igf-1* placental expression
- Some people with ASD have an enlarged striatum⁷
 - The E18 female striatum volumes from our study also show this finding
 - Enlarged striatum can contribute to the development of ASD as the striatum controls restrictive and repetitive behaviors⁷
- Previous work has shown that individuals with ASD do not show structural differences in blood vessels but show abnormal blood vessel organization and proliferation⁶
 - Our study replicates this and shows no structural difference in blood vessels



Serial Coronal Sections of E18 Mouse Brain

Future Directions

- Continue to investigate impact of placental *Igf-1* overexpression on angiogenesis in the brain
- Further explore brain vascular development
 - Splitting/Intussusceptive
 - Proliferation of blood vessels
- Look into other time points such as E14, E16, and post-birth
- Investigate placental angiogenesis

References and Funding Sources

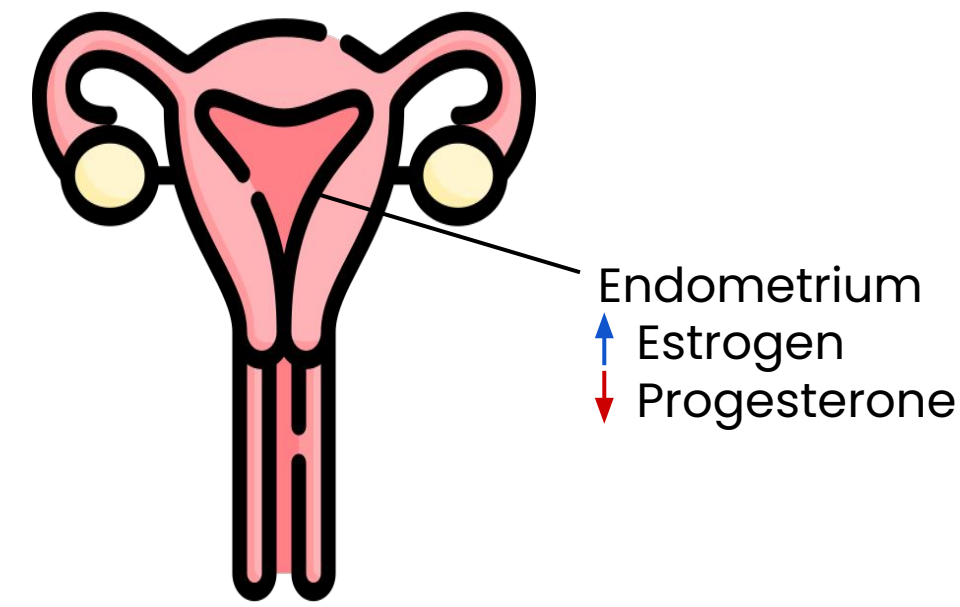
- Hus, Y., & Segal, O. (2021). Challenges Surrounding the Diagnosis of Autism in Children. *Neuropsychiatric disease and treatment*, 17, 3509–3529. <https://doi.org/10.2147/NDT.S282569>
- Steinman G. (2020). The putative etiology and prevention of autism. *Progress in molecular biology and translational science*, 173, 1–34. <https://doi.org/10.1016/bs.pmbts.2020.04.013>
- Rabinovsky, E. D., & Draghia-Akli, R. (2004). Insulin-like growth factor I plasmid therapy promotes in vivo angiogenesis. *Molecular therapy: the journal of the American Society of Gene Therapy*, 9(1), 46–55. <https://doi.org/10.1016/j.ymthe.2003.10.003>
- Chellakootty, M., Skibsted, L., Skouby, S. O., Andersson, A. M., Petersen, J. H., Main, K. M., Skakkebaek, N. E., & Juul, A. (2002). Longitudinal study of serum placental GH in 455 normal pregnancies: correlation to gestational age, fetal gender, and weight. *The Journal of clinical endocrinology and metabolism*, 87(6), 2734–2739. <https://doi.org/10.1210/jcem.87.6.8544>
- Wrigley, S., Arafa, D., & Tropea, D. (2017). Insulin-Like Growth Factor 1: At the Crossroads of Brain Development and Aging. *Frontiers in cellular neuroscience*, 11, 14. <https://doi.org/10.3389/fncel.2017.00014>
- Azmilia, E. C., Saccomano, Z. T., Alzoobae, M. F., Boldrini, M., & Whitaker-Azmitia, P. M. (2016). Persistent Angiogenesis in the Autism Brain: An Immunocytochemical Study of Postmortem Cortex, Brainstem and Cerebellum. *Journal of autism and developmental disorders*, 46(4), 1307–1318. <https://doi.org/10.1007/s10803-015-2672-6>
- Langen, M., Bos, D., Noordermeer, S. D., Nederveen, H., van Engeland, H., & Durston, S. (2014). Changes in the development of striatum are involved in repetitive behavior in autism. *Biological psychiatry*, 76(5), 405–411. <https://doi.org/10.1016/j.biopsych.2013.08.013>

R01 MH122435 and NIH T32GM008629

PHB2 reduction increases progesterone receptor (PR) expression in endometrial cancer cells

Background

- Endometrial cancer is one of the few cancers with an increasing number of cases in recent years
 - Estrogen and progesterone are two hormones that regulate endometrial growth through interactions with their receptors
 - Estrogen promotes endometrial growth while progesterone limits endometrial growth



- Progesterone receptor (PR) is significantly downregulated in endometrial cancer patients
- PHB2 is an oncogene that can inhibit production of apoptotic proteins such as caspases 3 and 8
- PHB2 is correlated with higher rates of tumorigenesis and is negatively correlated with PR expression (Fig. 1)

- Previous experiments have shown dramatic increases in PR expression by knocking down PHB2
- sgRNA and shRNA, once integrated in viruses can be used to lower the expression of mRNA and proteins
- shRNA turns into siRNA upon insertion into target cells marks proteins for degradation
- sgRNA guides CRISPR Cas9 to cleave target sequences out of host genomes

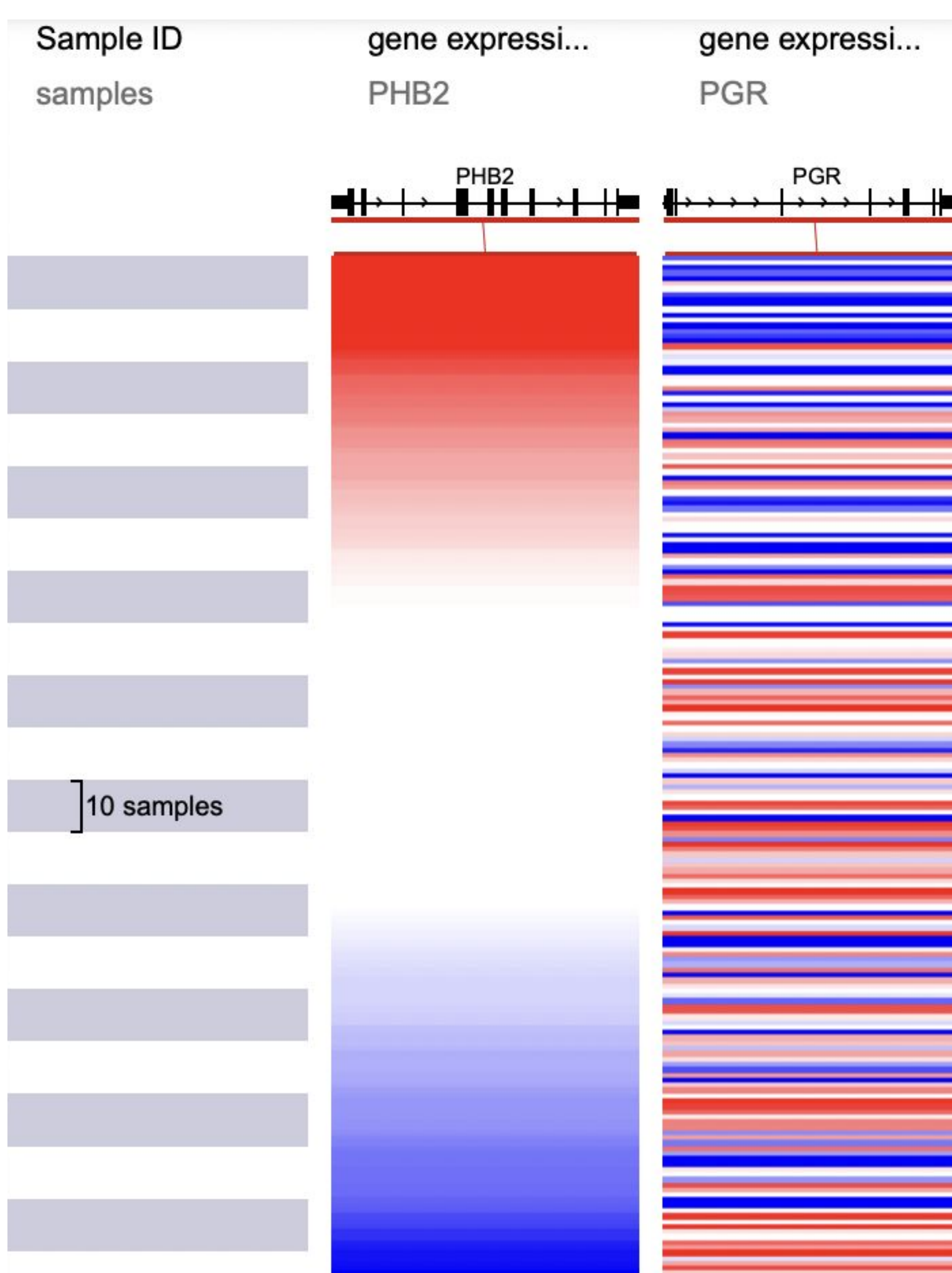


Figure 1: relationship between PHB2 and PR. The red sections represent high expression and blue represents low expression.

	shRNA name	region	Cell	Knockdown	Exon
1	PHB2-1	CDS	A549	98%	5
2	PHB2-2	CDS	A549	95%	4
3	PHB2-3	CDS	A549	83%	8
4	PHB2-4	CDS	A549	92%	7-8
5	PHB2-5	CDS	A549	79%	4

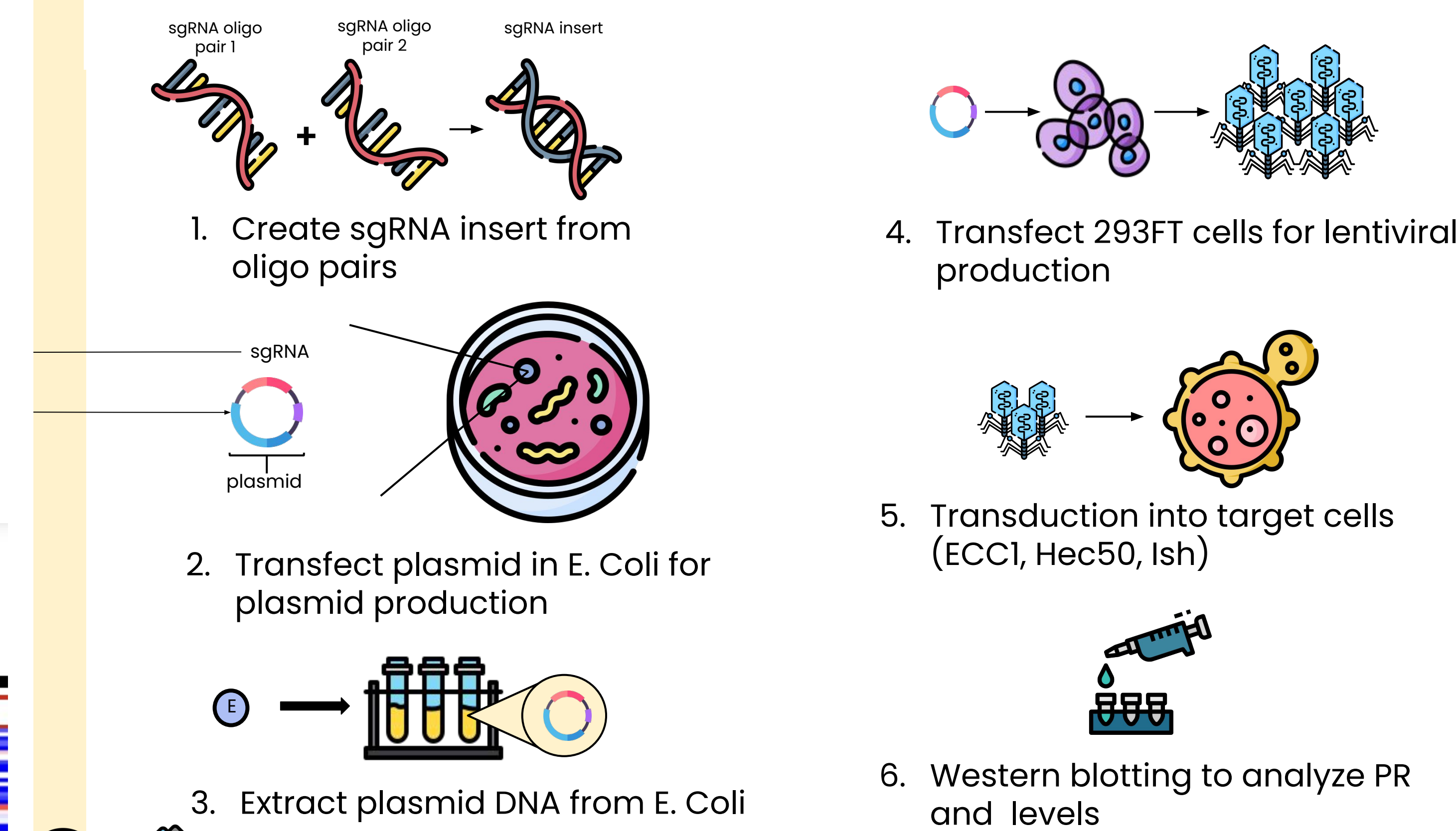
- The PHB2 gene is located on chromosome 12p13.31
- The available shRNA sequences target four of the ten PHB2 exons

Figure 2: shRNA product information. Two sequences target exon 4, one targets exon 5, one targets exon 7, and two target exon 8.

Objectives

- Generate PHB2 knockdown and knockout cells
- Analyze the change in PR expression in PHB2 knockdown and knockout cells
- Evaluate whether PHB2 is a potential target treatment oncogene

Methods



Results

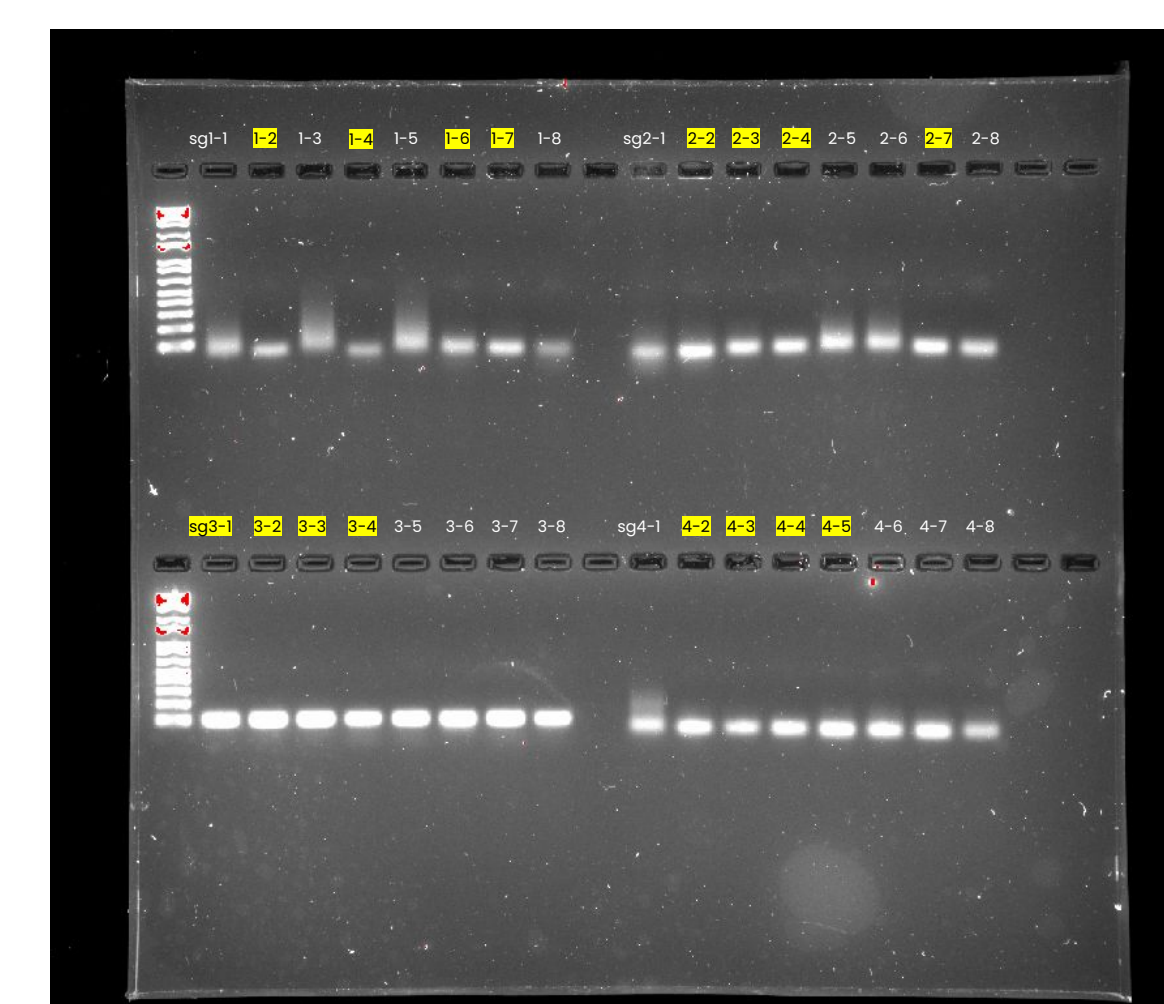


Figure 3: results of sgRNA vector PCR amplification. All of the E. coli clones selected had the correct sgRNA sequence.

PHB shRNA	concentration (ug/uL)	A260/A280
PHB-sh1	0.1933	1.92
PHB-sh2	0.4630	1.91
PHB-sh3	0.4004	1.91
PHB-sh4	0.2124	1.90
PHB-sh5	1.543	1.91

Figure 4: results of plasmid DNA extraction from shRNA-transfected E. Coli. The midprep samples of shRNA had a concentration around 0.200 - 1.50 ug/uL. All the samples were pure.

PHB sgRNA	concentration (ug/uL)	A260/A280
PHB-sg1-2	0.2932	1.87
PHB-sg1-4	0.3381	1.89
PHB-sg1-6	0.3578	1.88
PHB-sg1-7	0.2549	1.85
PHB-sg2-2	0.2783	1.86
PHB-sg2-3	0.3339	1.86
PHB-sg2-4	0.2576	1.86
PHB-sg2-7	0.3404	1.87
PHB-sg3-1	0.3616	1.88
PHB-sg3-2	0.3543	1.93
PHB-sg3-3	0.3264	1.87
PHB-sg3-4	0.3518	1.87
PHB-sg4-2	0.3655	1.87
PHB-sg4-3	0.3241	1.86
PHB-sg4-4	0.2747	1.85
PHB-sg4-5	0.4358	1.87

Figure 5: results of plasmid DNA extraction from sgRNA-transfected E. Coli. The miniprep samples of sgRNA all had a concentration of about 0.250 - 0.450 ug/uL. All the samples were pure.

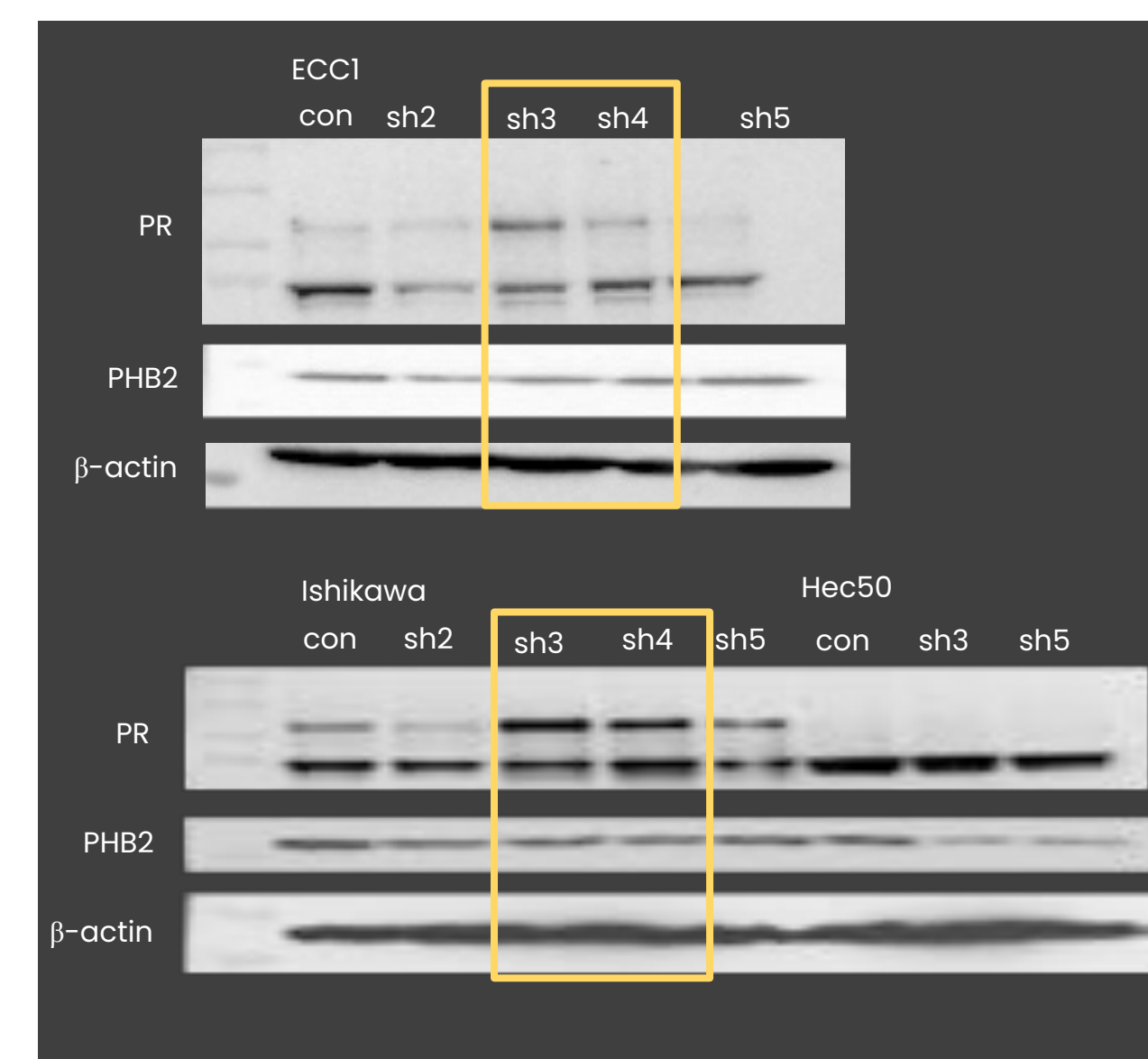


Figure 6: PHB2 knockdown western blot for PR expression. Target cells generally expressed a spectrum of percent increases in PR expression ranging from 50-200% compared to control cells. The reduction in PHB2 expression is also visualized to be about 25% in ECC1 and Ishikawa cells, and around 50% in Hec50 cells.

Conclusions/Implications

- Consistent PHB2 knockout and knockdown cells can be successfully created using sgRNA and shRNA
 - Survival rates were lower in current knockout cells than knockdown cells
- A reduction in PHB2 led to an increase in PR expression by an average of 100% in ECC1 and Ish endometrial cancer cell lines
- Knocking down with shRNA-3 and shRNA-4 resulted in the highest increase of PR expression in ECC1 and Ish cells
 - Increased by around 200%
- Targeting exon 8 of PHB2 gene resulted in high PR level increases
- PHB2 is a potential cancer treatment target oncogene

Future Directions

From our results, we discovered that targeting exon 8 for PHB2 knockdown was highly effective, but the exact function and mechanisms of exon 8 are yet unknown. Future studies should aim to discover the significance of exon 8 in endometrial cancer. Our lab will continue analyzing the effect of PHB2 knockdown using sgRNA in endometrial cancer cells on PR expression. Other directions of PHB2 research should focus on analyzing the different functions and mechanisms of PHB2 in cancer patients and the reasoning behind the variability in the correlation between PHB2 expression and tumorigenesis. Additionally, PHB2 research should explore the effects of PHB2 reduction on non-target cells and how the effects of PHB2 reduction can be mediated within non-target host cells.

Acknowledgements

A special thank you to the Belin Blank Center for providing this amazing opportunity and to Tianyue Li, Dr. Meng, and Dr. Yang for your patience and guidance in these five weeks.

References

- Alavi, M. V. (2019). Targeted OMA1 Therapies for Cancer. *International Journal of Cancer*, 145(9), 2330-2341. <https://doi.org/10.1002/ijc.32177>
- Artal-Sanz, M., & Tavernarakis, N. (2009). Prohibitin and mitochondrial biology. *Trends in Endocrinology & Metabolism*, 20(8), 394-401. <https://doi.org/10.1016/j.tem.2009.04.004>
- Flaticon. (2020). *Flaticon*. Flaticon. <https://www.flaticon.com/>
- Rodriguez, A. C., Blanchard, Z., Maurer, K. A., & Gertz, J. (2019). Estrogen Signaling in Endometrial Cancer: A Key Oncogenic Pathway with Several Open Questions. *Hormones and Cancer*, 10(2-3), 51-63. <https://doi.org/10.1007/s12672-019-0358-9>
- Yang, S., Jia, Y., Liu, X., Winters, C., Wang, X., Zhang, Y., Devor, E. J., Hovey, A. M., Reyes, H. D., Xiao, X., Xu, Y., Dai, D., Meng, X., Thiel, K. W., Domann, F. E., & Leslie, K. K. (2014). Systematic dissection of the mechanisms underlying progesterone receptor downregulation in endometrial cancer. *Oncotarget*, 5(20), 9783-9797. <https://doi.org/10.18632/oncotarget.2392>

PERFORMANCE SIMULATION OF A RADIATION TOLERANT QUARTZ BASED HIGH GRANULARITY CALORIMETER

P. Loranger, J. Wetzel *The University of Iowa - Dept. of Physics and Astronomy*

Problem

As particle colliders race towards higher energies, a variety of problems arise when trying to design and build new detectors, particularly when designing calorimeters used in the very forward (VF) region of a collider:

- Scintillators take too long to reset, creating pile-up
- VF detectors are exposed to by extreme amounts of radiation, scintillators are not tolerant enough.
- Current VF detectors have lower energy resolution compared to primary detectors; VF data is not used in cutting edge research.

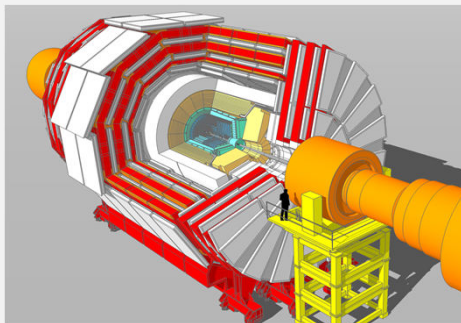


Fig 1. Cutaway diagrams of CMS detector by Tai Sakuma

Solution

Quartz calorimeters are the perfect candidate for VF detector designs in higher luminosity particle colliders.

- High radiation tolerance
- High energy resolutions
- Detects and 'reads' events very quickly

Methodology

- Layers of iron absorber and quartz cubes, backed by SiPMs
- 4x4x4, 3x3x3, 3x3x21
- Simulation written in C++ using GEANT4 simulation toolkit.
- Over 1,000,000 individual simulations ran on Argon HPC!

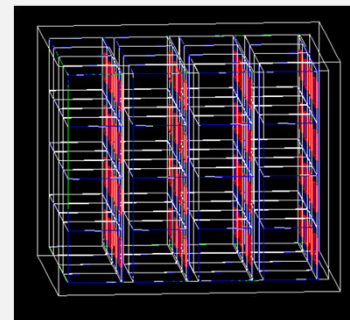


Fig 2. Rendering of 4x4x4 calorimeter

Results

- CERN's ROOT HEP data analysis toolkit and Python
- 4x4x4 preforms better than 3x3x7
- See QR code for full dataset & graphs

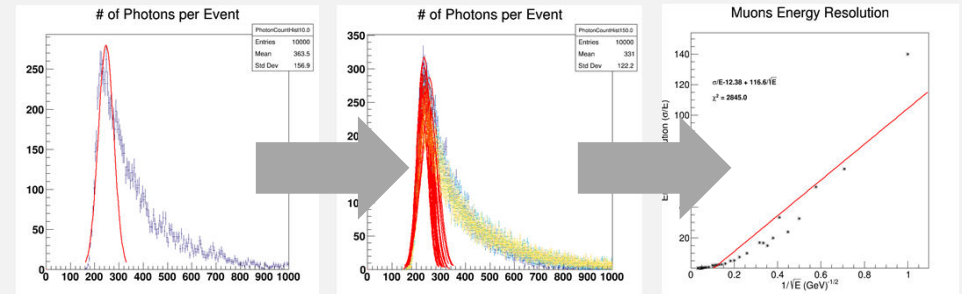


Fig 3, 4, & 5. (left to right) 4x4x4 10 GeV # of photons per energy graph, layered 4x4x4 # of photons per energy graph, 4x4x4 muons energy resolution graph

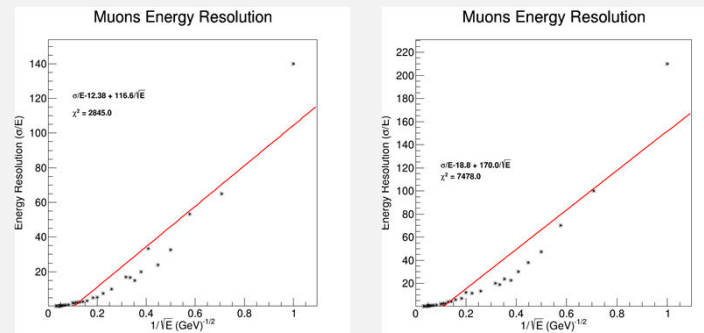


Fig 6 & 7. (left to right) 4x4x4 muons energy resolution graph, 3x3x7 muons energy resolution graph. These are 2 out of the 9 energy resolution graphs we made.



Fig 8. QR code for updated poster and full dataset

Conclusion

As of time of writing, our simulations are still running and we do not have a complete set of data, particularly for the very promising 3x3x21 calorimeter. Use the QR code above to read the updated version of this poster our complete set of data.

Acknowledgments

I would like to thank Professor Wetzel for guiding me in my research and my parents for their never-ending support.

Data Analysis and Prediction for DMQMC

Save computing resources by interpolating data across $\Delta\tau$

Songhang Man, Gabriel Smith, William Van Benschoten, James Shepherd

Introduction

Density Matrix Quantum Monte Carlo, DMQMC, stochastically samples the thermal Density Matrix, $\hat{\rho}(\beta)$, where $\beta = (k_b T)^{-1}$, to yield exact-on-average energies for the system.

In DMQMC, $\hat{\rho}(\beta)$ is rewritten as:

$$\hat{\rho}(\beta) \rightarrow \hat{f}(\tau) = \sum_{ij} f_{ij}(\tau) |D_i\rangle \langle D_j|$$

with each iteration of the simulation sampling:

$$f_{ij}(\tau + \Delta\tau) = f_{ij}(\tau) [1 + \Delta\tau S] - \frac{\Delta\tau}{2} \sum_k [H_{ik} f_{kj}(\tau) + f_{ik}(\tau) H_{kj}]$$

DMQMC simulations with small $\Delta\tau$ produce high accuracy results but with high computation cost.

We are looking for a method to save computer resource in calculation while still retaining a relatively high accuracy.

Research Question

Can spline interpolations be used to predict accurate small $\Delta\tau$ DMQMC data using low-cost large $\Delta\tau$ data?

Methods

Data analysis was done on the stretched H_6 linear chain.

The interpolations were tested by:

- Extracting evenly spaced points from the original dataset.
- Comparing different degree interpolations to the original dataset.
- For cubic spline, altering number of data points in interpolation.

Predicting small $\Delta\tau$ data with large $\Delta\tau$ data:

- Comparing original large $\Delta\tau$ and small $\Delta\tau$ datasets.
- Comparing large $\Delta\tau$ interpolations with small $\Delta\tau$ dataset.
 - Altering the high $\Delta\tau$ interpolation with weighting and smoothing factors.

Python Libraries

- **Data processing:** Pandas, NumPy
- **Interpolation:** scipy.interpolate.UnivariateSpline
- **Plotting:** Matplotlib

Variables

- Degree of polynomial in interpolation
- Percentage of data used in interpolation

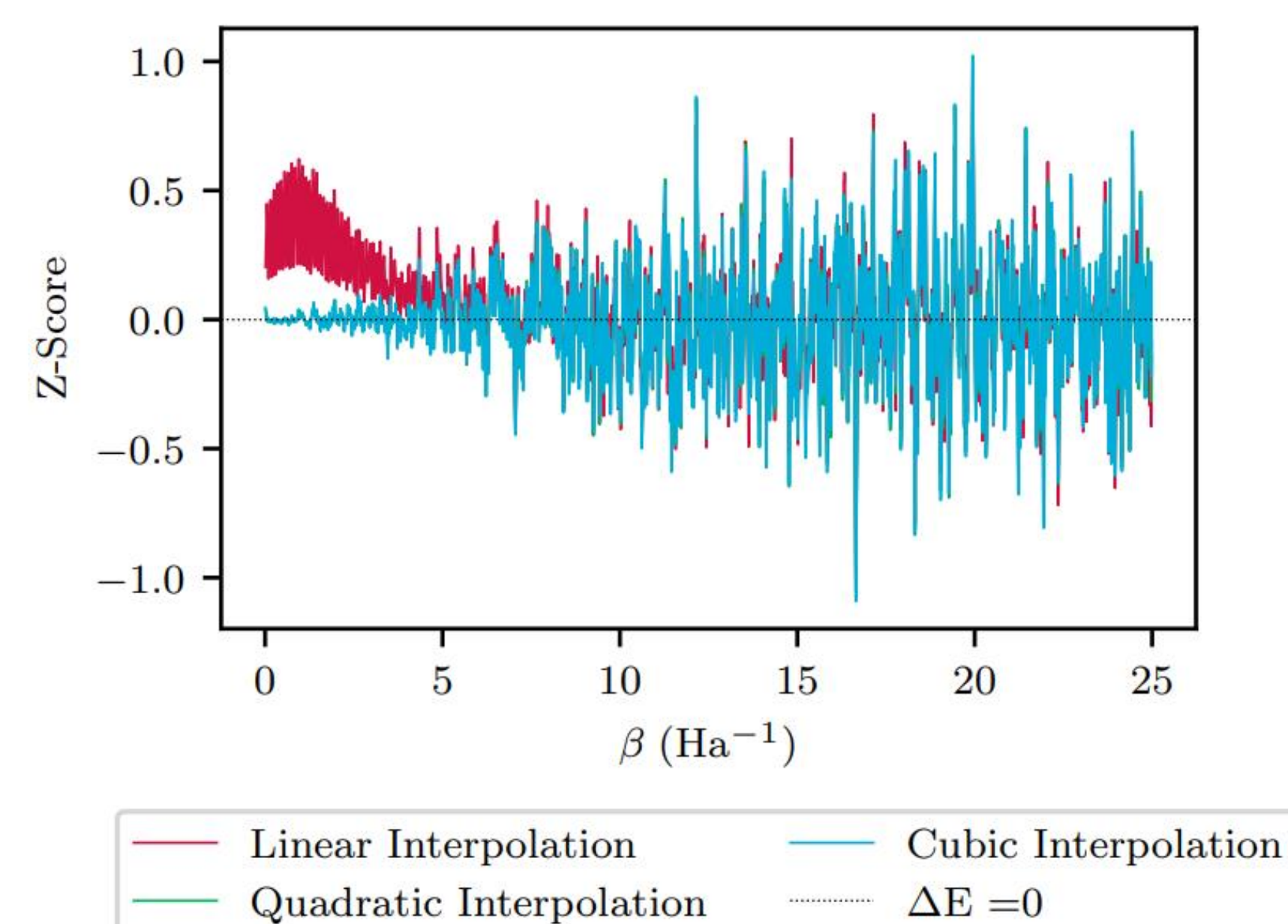


Figure 1. Normalized difference between the interpolated and original values under different degrees of interpolation with 20% of the data points used in interpolation.

2 Amount of Data in Interpolation

- Using cubic interpolations:
 - The amount of data points can be reduced to 1.25% while containing the residual within 2σ
 - Outliers in a peak at the first few interpolation points.
- Interpolations can yield good predictions with few datapoints.

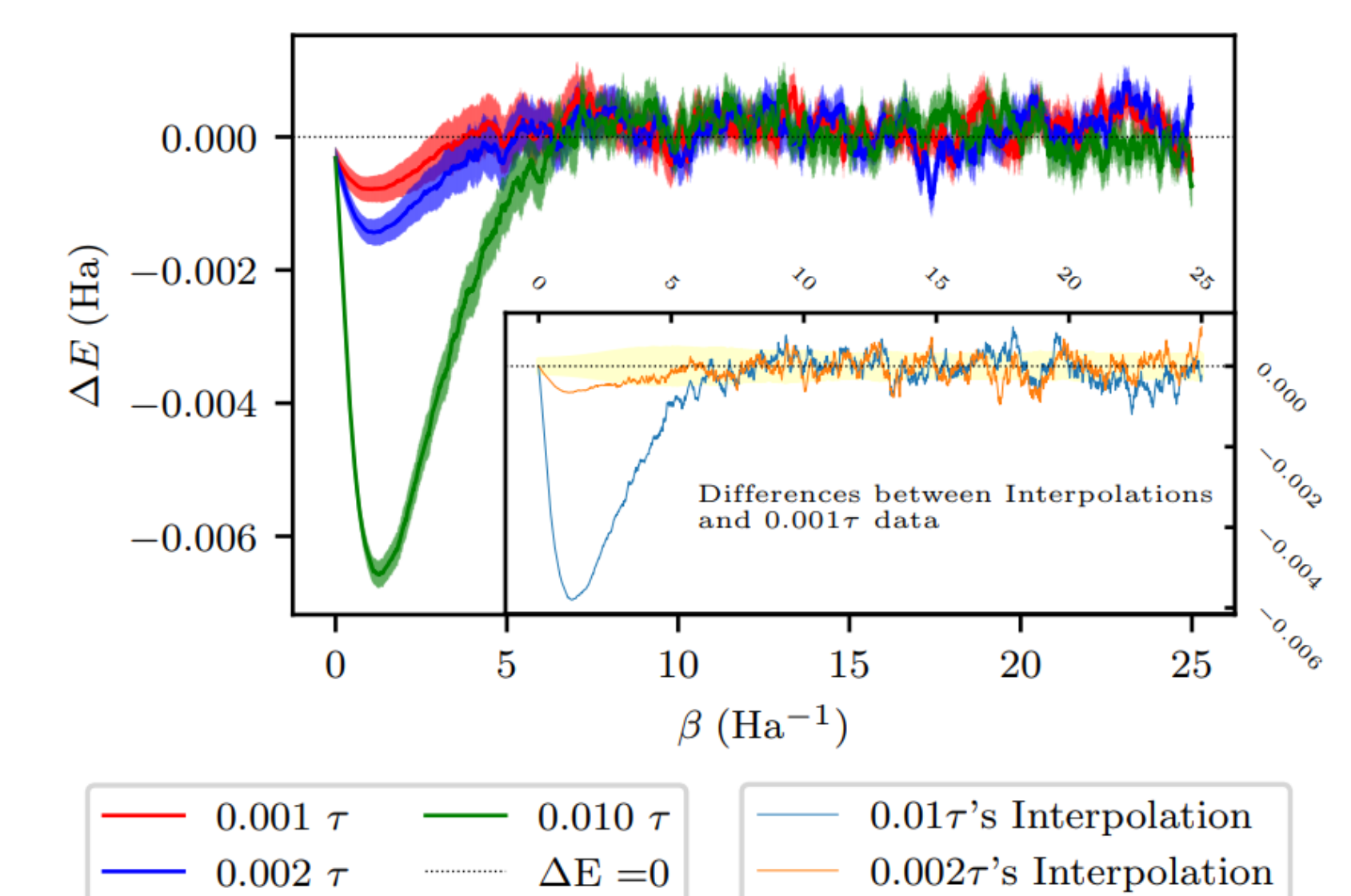


Figure 3. (Main Plot) Energy differences between the, $0.001\Delta\tau$, $0.002\Delta\tau$, $0.010\Delta\tau$ dataset and ft-FCI. (Inset) Energy difference between the Interpolation of high $\Delta\tau$ data and $0.001\Delta\tau$ data.

4 Weighting and Smoothing

- The manipulations in weight and smoothing have not reduced the difference in the low beta area
- The lines with different smoothing factors overlap on this scale.
 - We speculate that the smoothing factor has reached a threshold that results in a single 5th degree curve. The smoothing is a topic for future investigation.

1 Different Degree of Interpolation

- Higher degree interpolations have a better fit to the original data.
- Linear interpolations suffer systemic errors in low-beta range.
- The difference between high and low degree interpolation is most exemplified as a low percentage of the data is used to make interpolation.

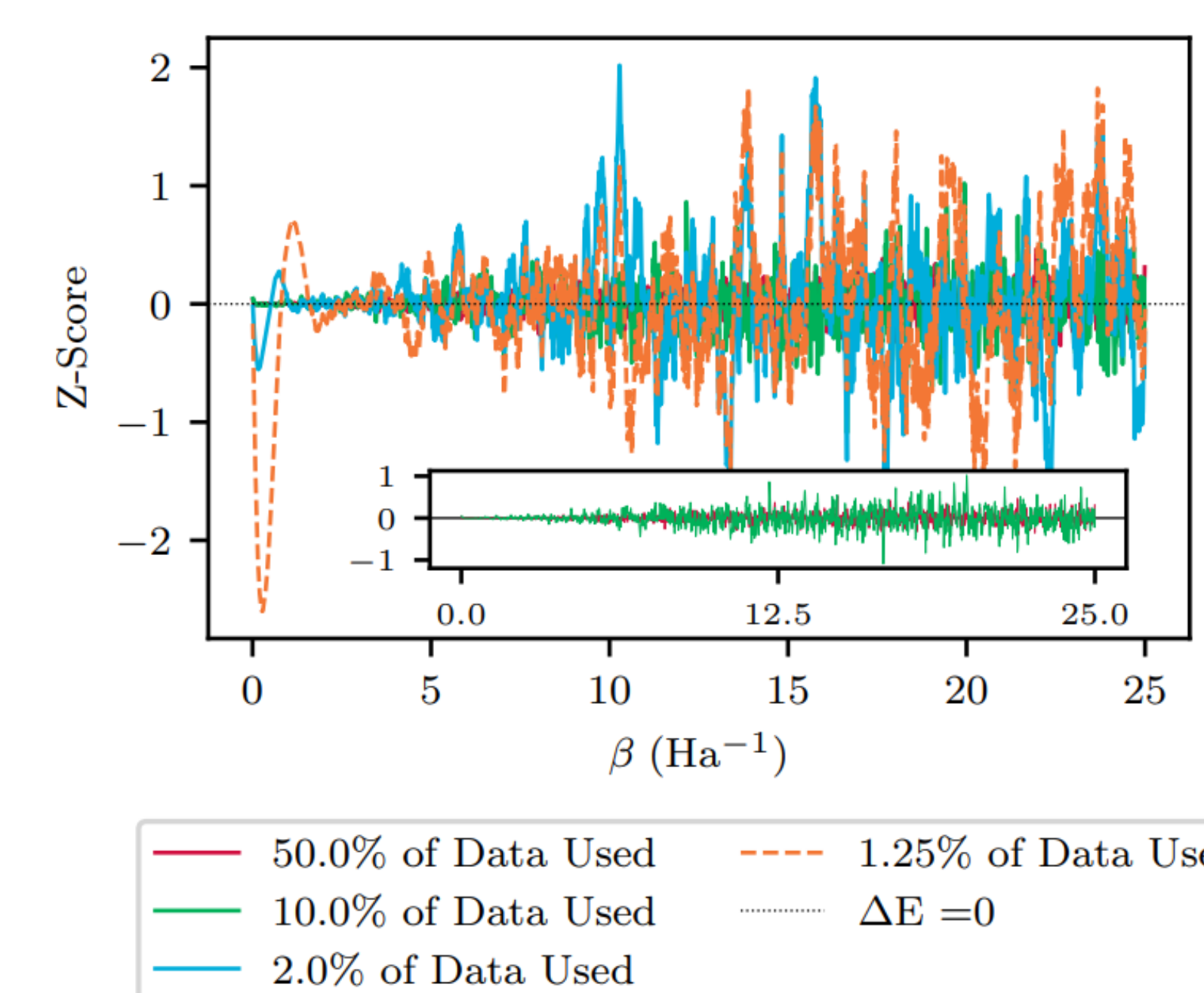


Figure 2. Normalized difference between the interpolated and original values under different density of data used in interpolation.

3 Large Delta tau vs Small Delta tau

- The large $\Delta\tau$ data systematically underestimate system energies in low beta range, which may be caused by time-step error or other errors exacerbated in the high $\Delta\tau$ setting.
- In high beta range, $0.01\Delta\tau$ displays a similar error magnitude to exact data compares to $0.001\Delta\tau$.
- Interpolation by itself does not help reconciling the gap

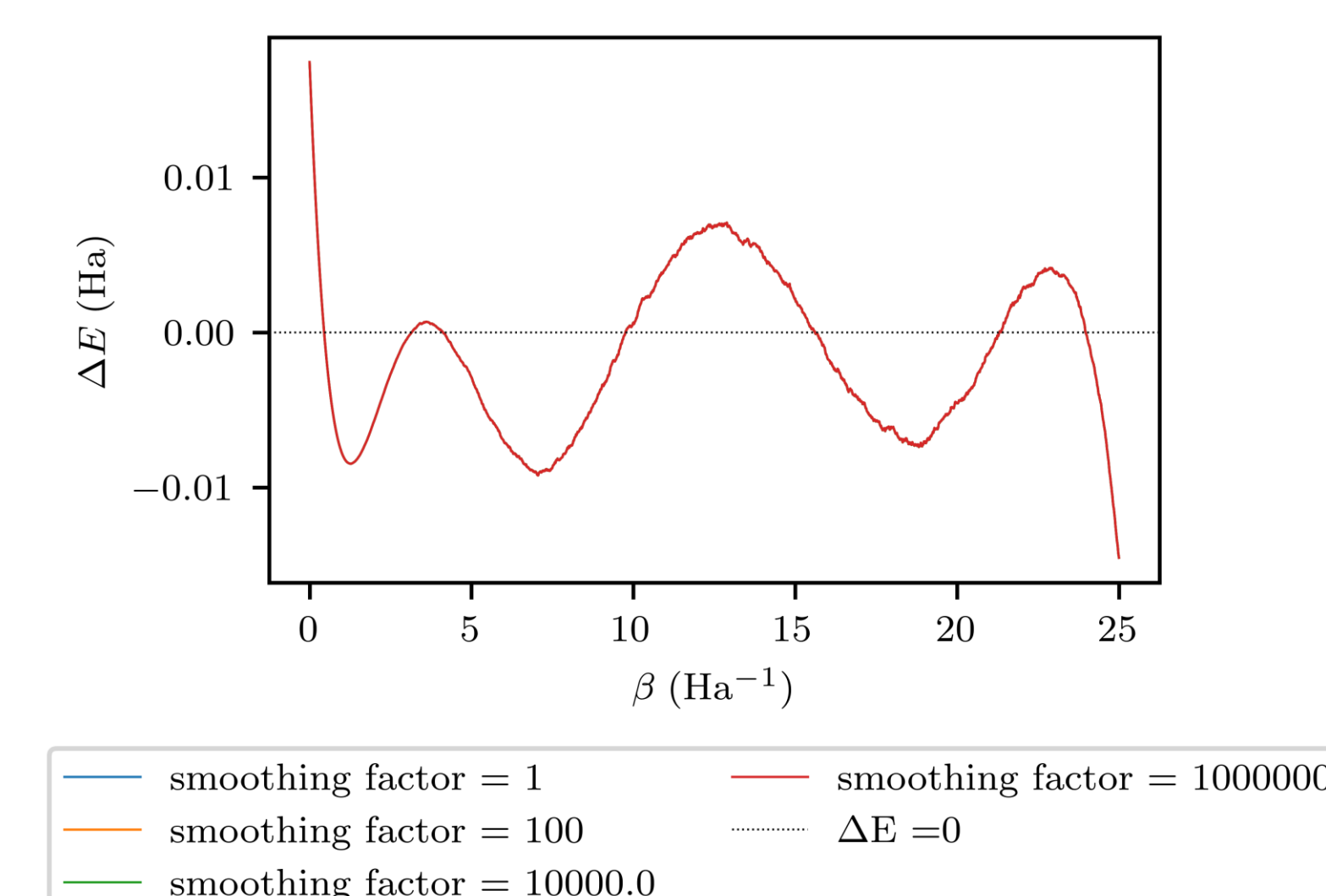


Figure 4. Energy difference between the weighted (inversely related to the residual in figure 3) interpolation and $0.001\Delta\tau$ data with various smoothing factor.

Summary of Findings

- Interpolations can predict the original data set, even with few data points.
 - Higher degree interpolating splines have a better fit, in general, to the data.
 - Cubic interpolations of 2% of the dataset results in residuals within 2σ
- Large $\Delta\tau$ data systematically underestimate the energies in the low- β range.
 - Interpolation alone does not reconcile this ΔE .
 - Weighting and smoothing factors have not shrunk the ΔE .
- In the high- β range, large $\Delta\tau$ displays similar ΔE to exact compared to small $\Delta\tau$.

Future Work

To further investigate into the datasets and resolve the time-step error in low beta range, we will take the following approaches:

- **Find out the error source:** Investigate the original DMQMC algorithm to identify the source of error, run calculations to calculate the error.
- **Filter the data:** Investigate in the point where the error magnitudes of high and low τ data converge to isolate the high quality τ data from the low beta range low quality data.
- **Better model:** Investigate in other models/operations that can fit the data better, such as applying Inverse Laplace Transform on the spline of the datapoints. According to our result in step 4, the 5th degree polynomial curve seems to have a relatively good fit to the data, which can also be investigated.

Acknowledgments

I would like to express my gratitude to Gabe Smith and Professor Shepherd for mentoring and giving constructive helps during my project, and all other researchers in Shepherd Group for providing a welcoming and friendly environment. I would also like to thank the Belin-Blank Center and the SSTP for this research opportunity.

References

- Blunt, N. S., Rogers, T. W., Spencer, J. S., & Foulkes, W. M. C. (2014). Density-matrix quantum Monte Carlo method. *Physical Review B*, 89(24). <https://doi.org/10.1103/physrevb.89.245124>
- Petras, H. R., Ramadugu, S. K., Malone, F. D., & Shepherd, J. J. (2020). Using Density Matrix Quantum Monte Carlo for Calculating Exact-on-Average Energies for *ab Initio* Hamiltonians in a Finite Basis Set. *Journal of Chemical Theory and Computation*, 16(2), 1029–1038. <https://doi.org/10.1021/acs.jctc.9b01080>

Lipid Nanoparticles as a Delivery System for CST6-encoding mRNA for Bone Regeneration Applications

Sami Panyam¹, Pornpoj Phruttivanichakun², Aliasger Salem²

¹Conestoga High School, Berwyn, PA

²College of Pharmacy, University of Iowa, Iowa City, IA

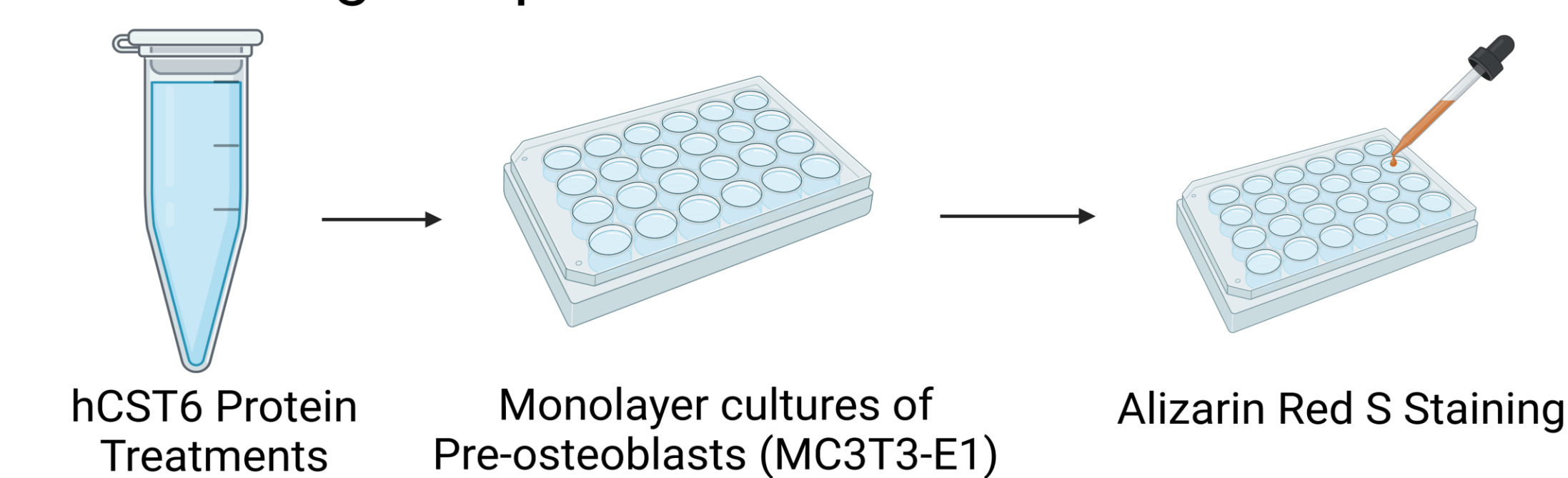
Contact information: aliasger-salem@uiowa.edu, pornpoj-phruttivanichakun@uiowa.edu

PURPOSE

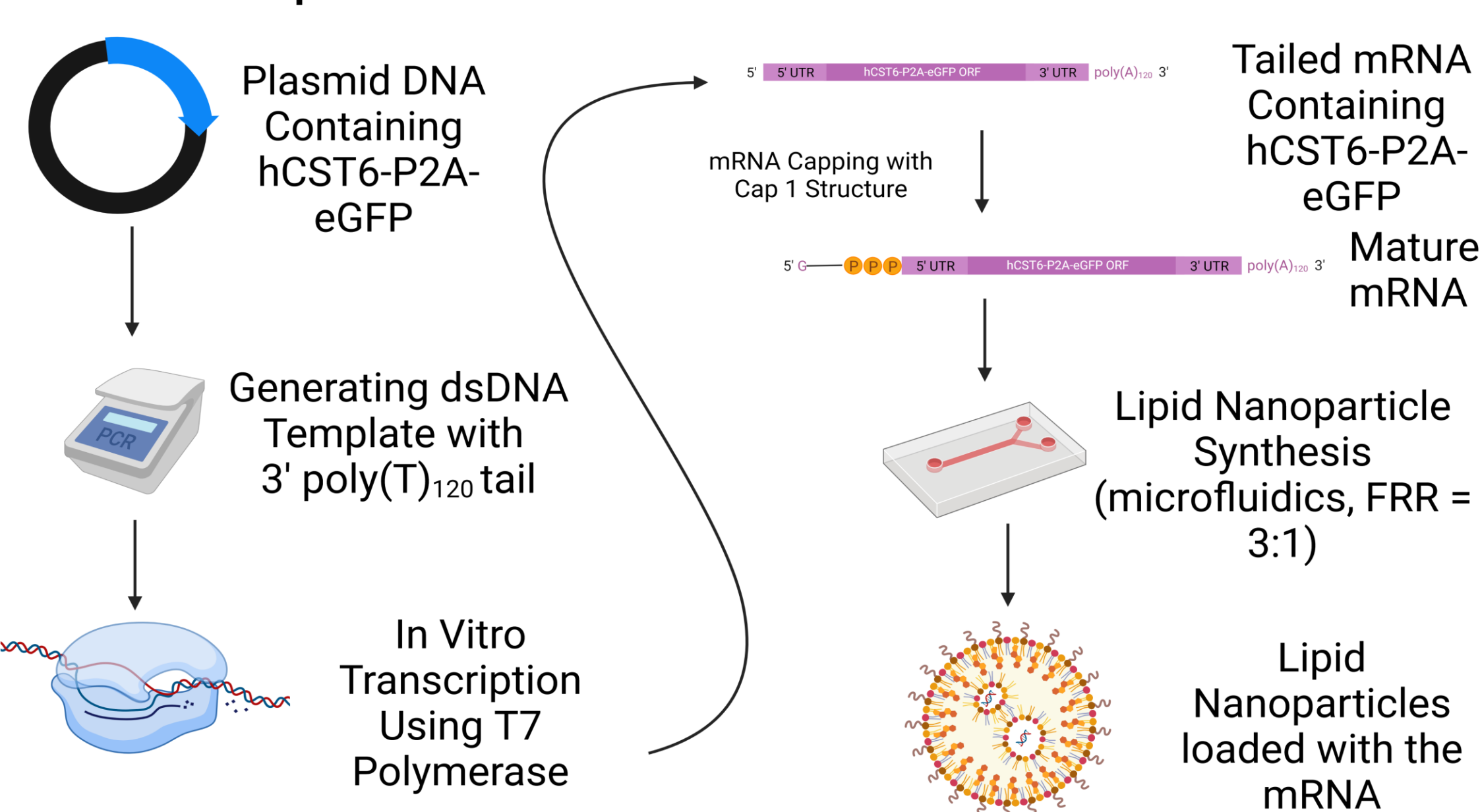
- Cystatin E/M (CST6) has been associated with the inhibition of osteoclast differentiation (Li et al., 2021). We proposed that CST6 might promote osteogenic differentiation.
- Different doses of CST6 protein may promote osteogenic differentiation of the pre-osteoblastic MC3T3-E1 cells. Mineralization of the differentiated cells can be visualized at the end of the study using Alizarin Red S Staining (2.1).
- SM102-based lipid nanoparticles can be fabricated using a microfluidic device to encapsulate CST6-encoding mRNA to deliver the mRNA to cells (2.2).
- Use of modified nucleosides like pseudouridine and N1-methyl pseudouridine can affect the translation of the mRNA transcript. We tested this using eGFP as a reporter gene to assess the nucleosides' impact on transfection (2.3).

METHODS

2.1 Osteogenic promotion of hCST6



2.2 Nanoparticle Formulation



2.3 Transfection of MC3T3-E1 cells

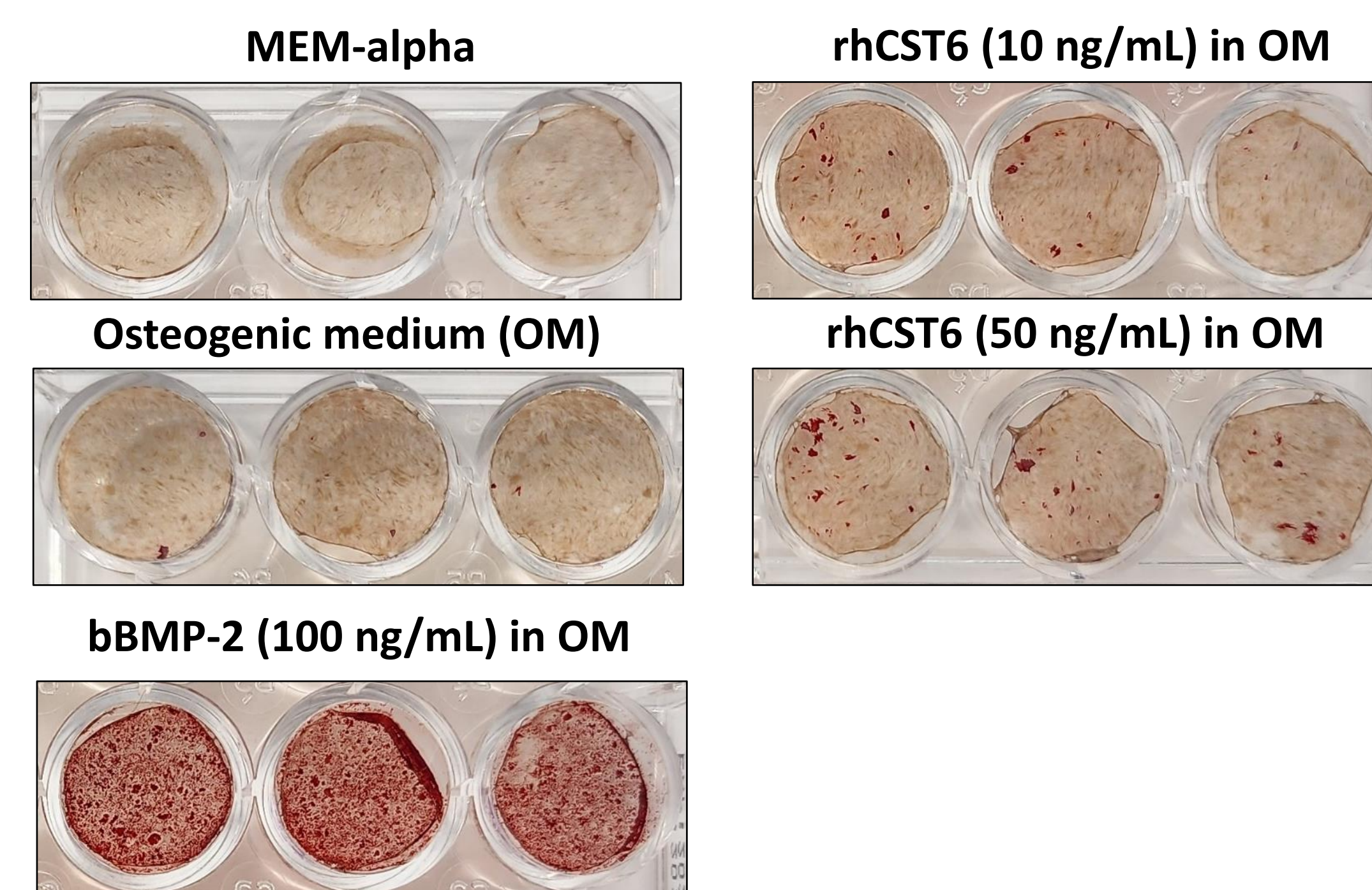
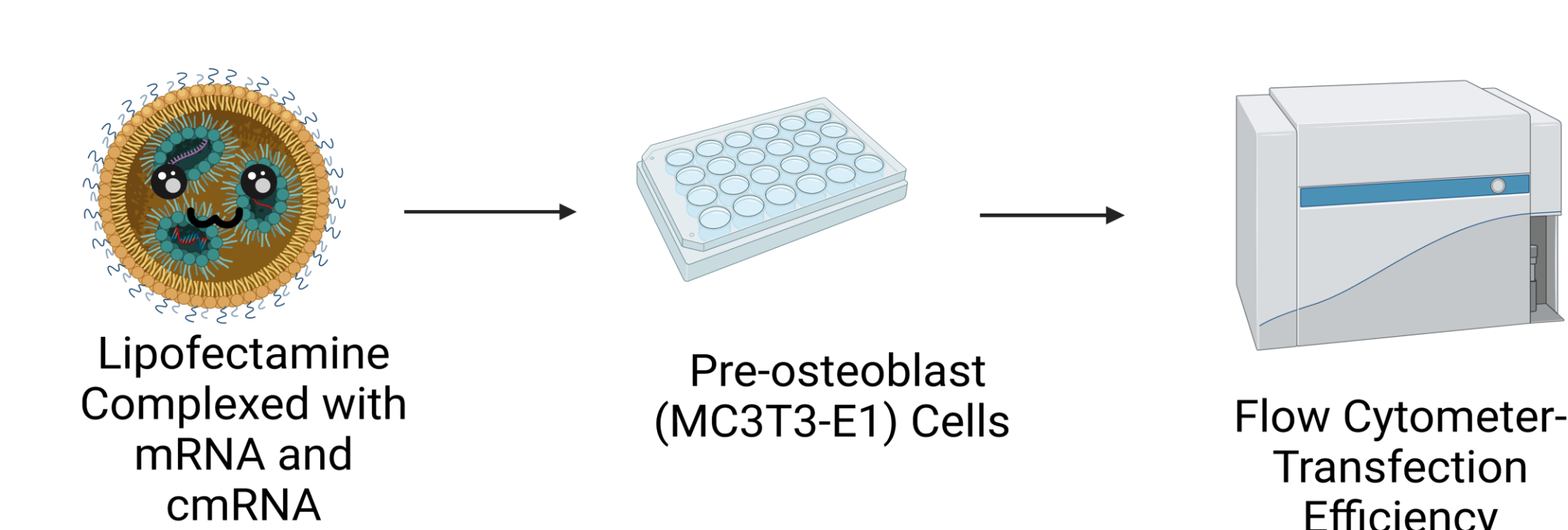


Figure 1. Alizarin Red S Staining of MC3T3-E1 (subclone 4) cells after 21 days of osteogenesis induction. The cells were treated at confluency with bovine bone morphogenic protein (bBMP-2, 100 ng/mL) in osteogenic medium or recombinant human CST6 protein (rhCST6, 10 ng/mL or 50 ng/mL) in complete MEM-alpha medium containing osteogenic supplements.

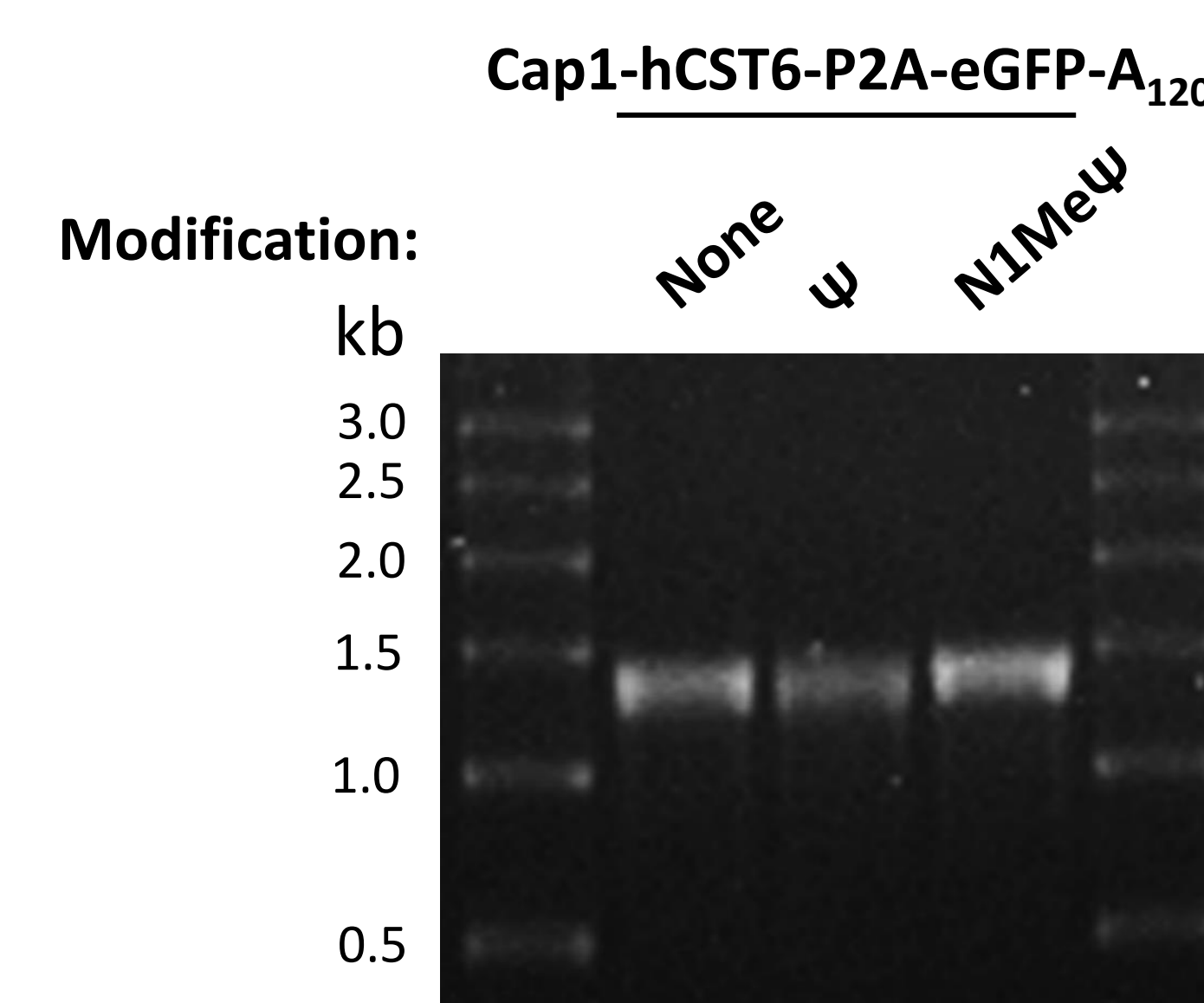


Figure 2. Denaturing 1.5% agarose gel electrophoresis of aliquots of in-vitro transcribed Cap1-hCST6-A₁₂₀ containing no modified nucleoside (None), total pseudouridine replacement (Ψ), and total N1-methylpseudouridine replacement (N1MeΨ). The expected size of the complete mRNA transcript was 1,425 nt.

RESULTS

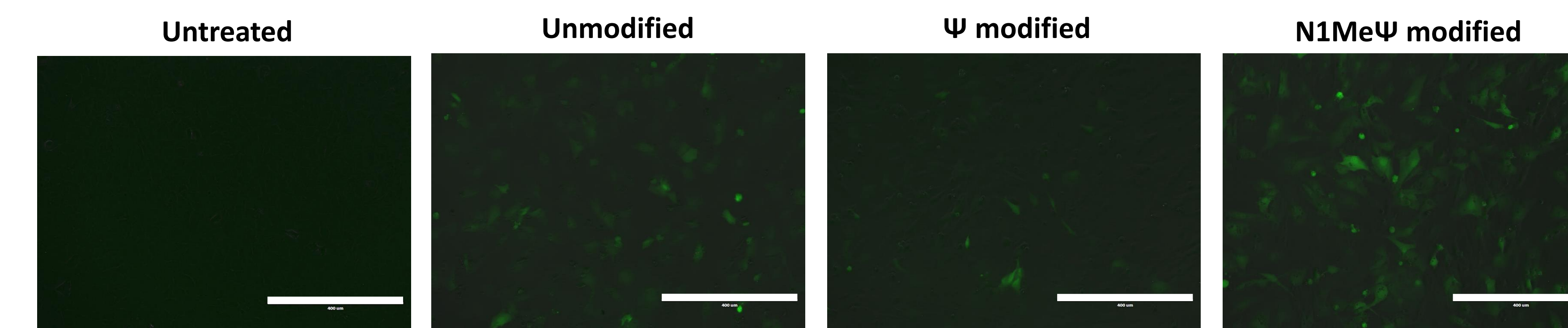


Figure 3. Representative fluorescence micrographs of MC3T3-E1 (subclone 4) cells at 24 hours after transfection with 0.5 μg of Cap1-hCST6-eGFP-A₁₂₀ cmRNA using Lipofectamine 2000 (cmRNA: Lipofectamine 2000: ratio = 1:2). Cells were seeded into 24-well plates at the density of 50,000 cells per well and left to attach for 24 hours prior to experiment. Scale bars represent 400 μm.

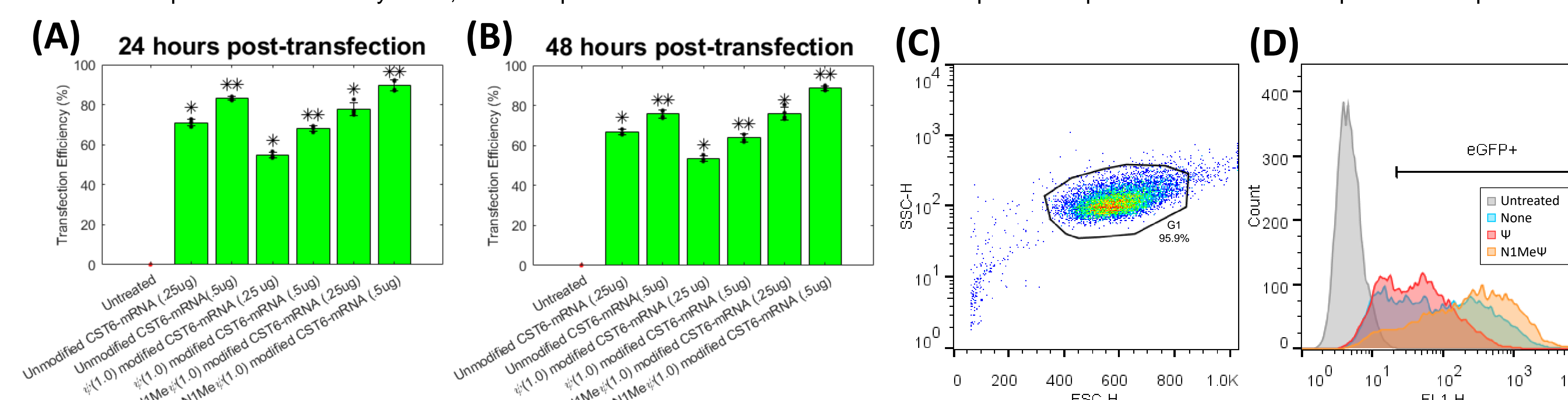


Figure 4. Transfection efficiency in MC3T3-E1 (subclone 4) cells transfected with in vitro-transcribed Cap1-P2A-eGFP-A₁₂₀ mRNAs. The eGFP expression was assessed using flow cytometry and Lipofectamine 2000 was used as the transfection agent (cmRNA: Lipofectamine 2000: ratio = 1:2). (A) and (B) show the transfection efficiency at 24 hours and 48 hours after transfection (n = 4 per group). Statistical analysis was done one-way ANOVA with multiple comparison tests using Turkey's test. *p < 0.05 between different base modifications at 0.25 μg-mRNA dose, and **p < 0.05 between different base modifications at 0.5 μg-mRNA dose. (C) and (D) show representative flow cytometry data with (C) depicting the gating of the target population and (D) showing representative transfection data.

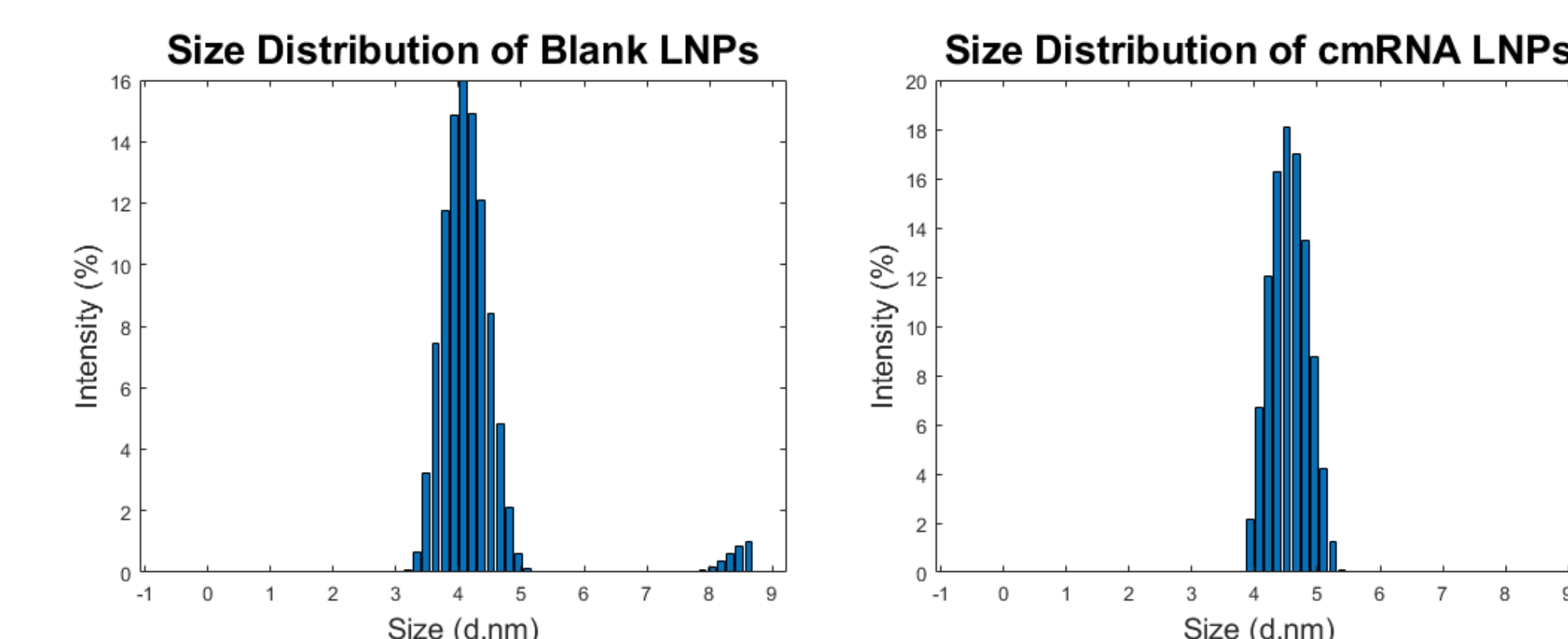


Figure 5. The particle size distribution of SM102-based lipid nanoparticles from Dynamic Light Scattering (DLS) data. The lipid nanoparticles were loaded with either hCST6-P2A-eGFP-A₁₂₀ mRNA (mRNA LNPs) or were formed without payload (Blank LNPs).

Parameter	Blank LNPs	mRNA LNPs
Hydrodynamic Diameter (nm)	60.53 ± 1.18	90.79 ± 2.12
Polydispersity Index	0.189 ± 0.025	0.079 ± 0.008
Zeta Potential (mV)	-2.05 ± 0.15	-2.58 ± 1.67
Entrapment Efficiency (%)	-	68.52%

Table 1. Characterization of SM102-based lipid nanoparticles using Dynamic Light Scattering (DLS). The lipid nanoparticles were loaded with either hCST6-P2A-eGFP-A₁₂₀ mRNA (mRNA LNPs) or were formed without payload (Blank LNPs).

CONCLUSION

- The cells treated with recombinant human CST6 protein produced noticeable calcium deposits after Alizarin Red S staining.
- We were able to formulate lipid nanoparticles encapsulating Cap1-CST6-P2A-eGFP-A₁₂₀ mRNA with desirable physical characteristics.
- We found that the replacement of uridine base in the mRNA transcript with N1-methyl pseudouridine yielded better transfection efficiency in MC3T3-E1 cells than the non-modified mRNA and the pseudouridine-modified cmRNA.

ACKNOWLEDGEMENTS

I would like to give special thanks to Dr. Salem and Pornpoj Phruttivanichakun for mentoring me and giving me the opportunity to work in a lab. I would also like to thank the Belin Blank center and Secondary Student Training Program for providing me with the resources and ability to perform research in a professional setting.

REFERENCES

Li, X., Liang, Y., Lian, C., Peng, F., Xiao, Y., He, Y., Ma, C., Wang, Y., Zhang, P., Deng, Y., Su, Y., Luo, C., Kong, X., Yang, Q., Liu, T., & Hu, G. (2021). CST6 protein and peptides inhibit breast cancer bone metastasis by suppressing CTSB activity and osteoclastogenesis. *Theranostics*, 11(20), 9821-9832. <https://doi.org/10.7150/tno.62187>

The figure used in Methods section was created with BioRender.com.

Neuroanatomical Correlates of Noun and Verb Retrieval in the Controlled Oral Word Association Test

Eliza Podvalny¹, Carolina Deifelt Streese^{2,3}, Jax Skye^{2,5}, Joel Bruss², Daniel Tranel^{2,4}

¹The Hackley School, NY; ²Department of Neurology, University of Iowa; ³Department of Neurosurgery, University of Iowa

⁴Department of Psychological and Brain Sciences, University of Iowa; ⁵Department of Psychiatry, University of Iowa

Introduction

- Previous neuroimaging studies show a double dissociation between nouns and verbs^[1]
 - Verbs -- frontal lobe^[1-2]
 - Nouns -- temporal lobe^[1-2]
- Controlled Oral Word Association (COWA) test is a verbal fluency test where participants have 1 minute to say as many words as possible that begin with a given letter.
- **Hypothesis:** Can parts-of-speech analysis of COWA data be used with the lesion method to offer new perspectives on the double dissociation between nouns and verbs in the brain?

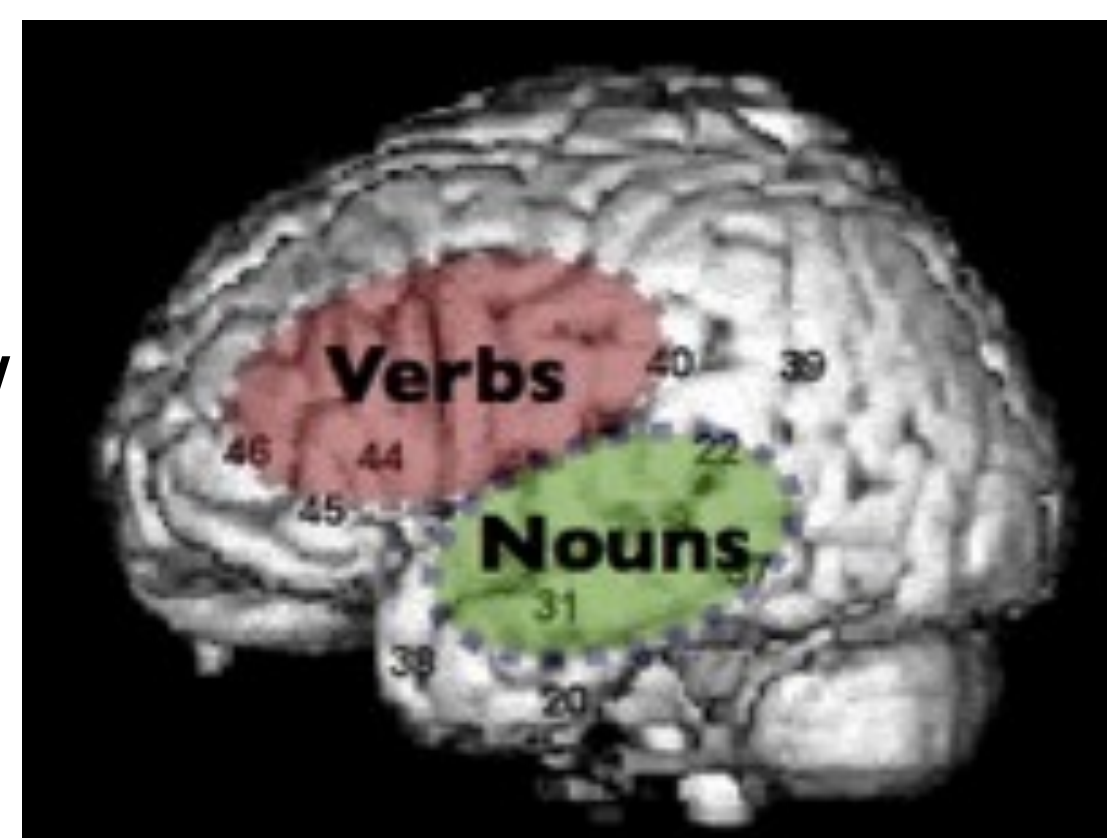


Fig. 1. Neural models regarding the process of nouns and verbs.²

Methods

- **Participants:** 226 patients with focal, stable, acquired brain lesions from the Iowa Neurological Patient Registry.

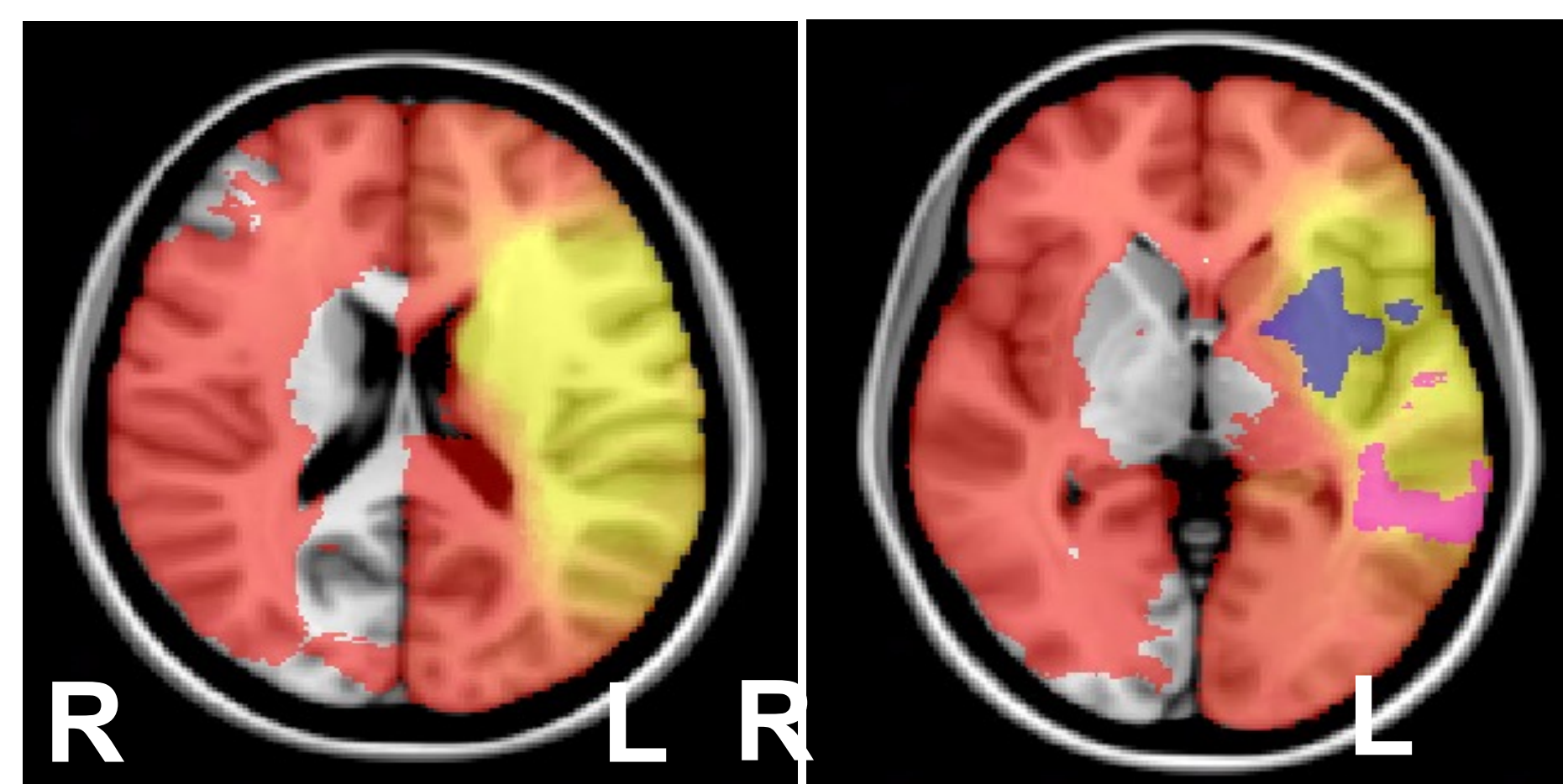


Fig. 2.1. Lesion overlap map from an axial cut. Blue and pink represent our ROIs and are lesions of participants in a separate study.¹

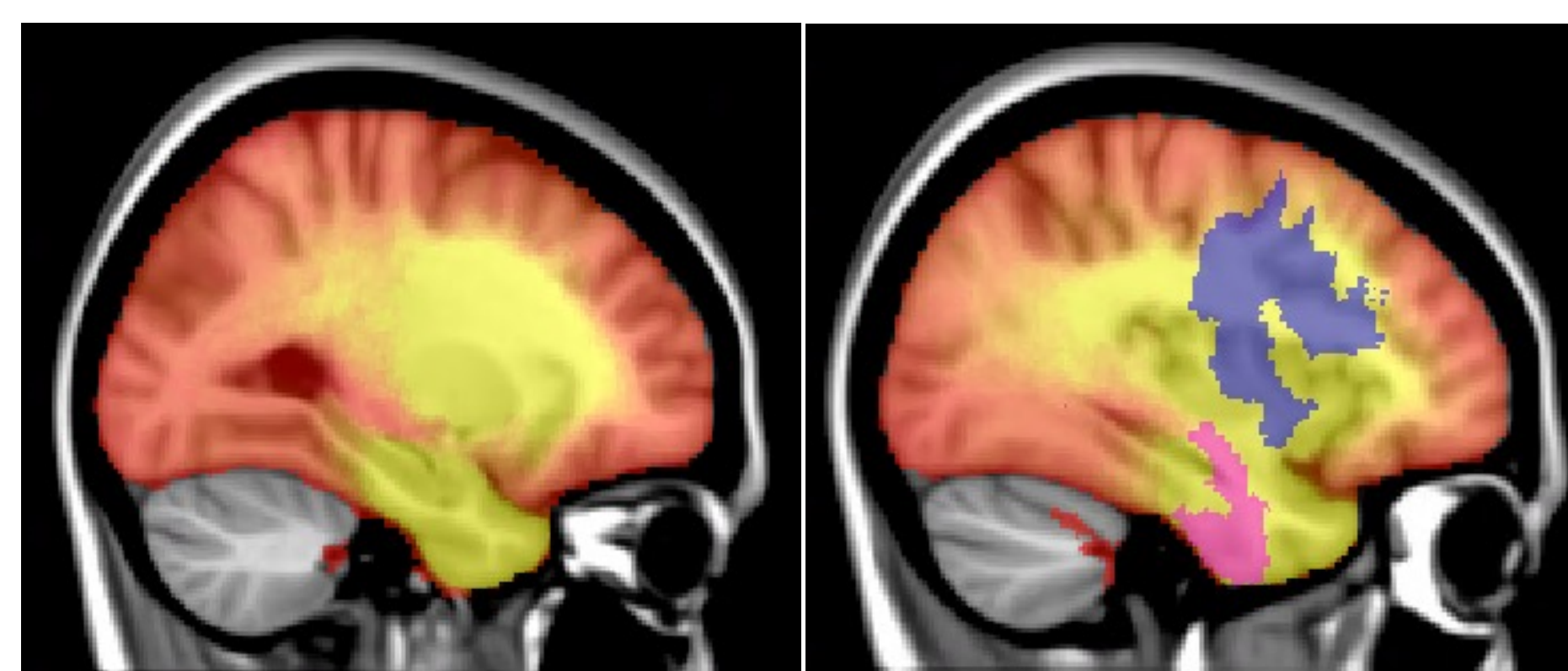


Fig. 2.2. Lesion overlap map in a sagittal cut.

1. Structural neuroimaging scans obtained 3 months or more after the lesion onset.
- List of words from the **COWA test**
- **Parts of Speech Analysis** - total number of nouns and verbs (calculated noun-to-verb ratio)
- **Neuroanatomical Correlates** – LESYMAP Analysis

Results

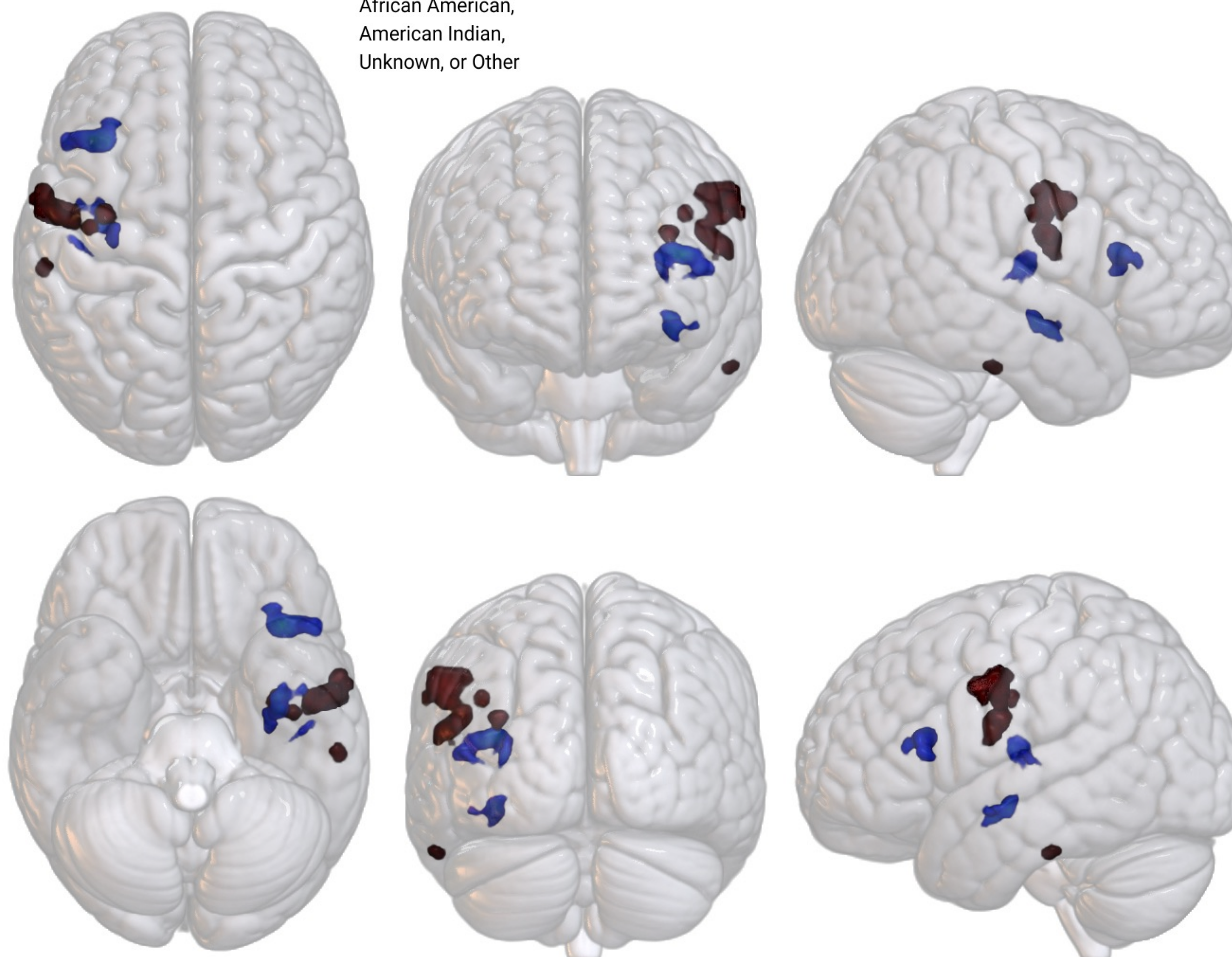
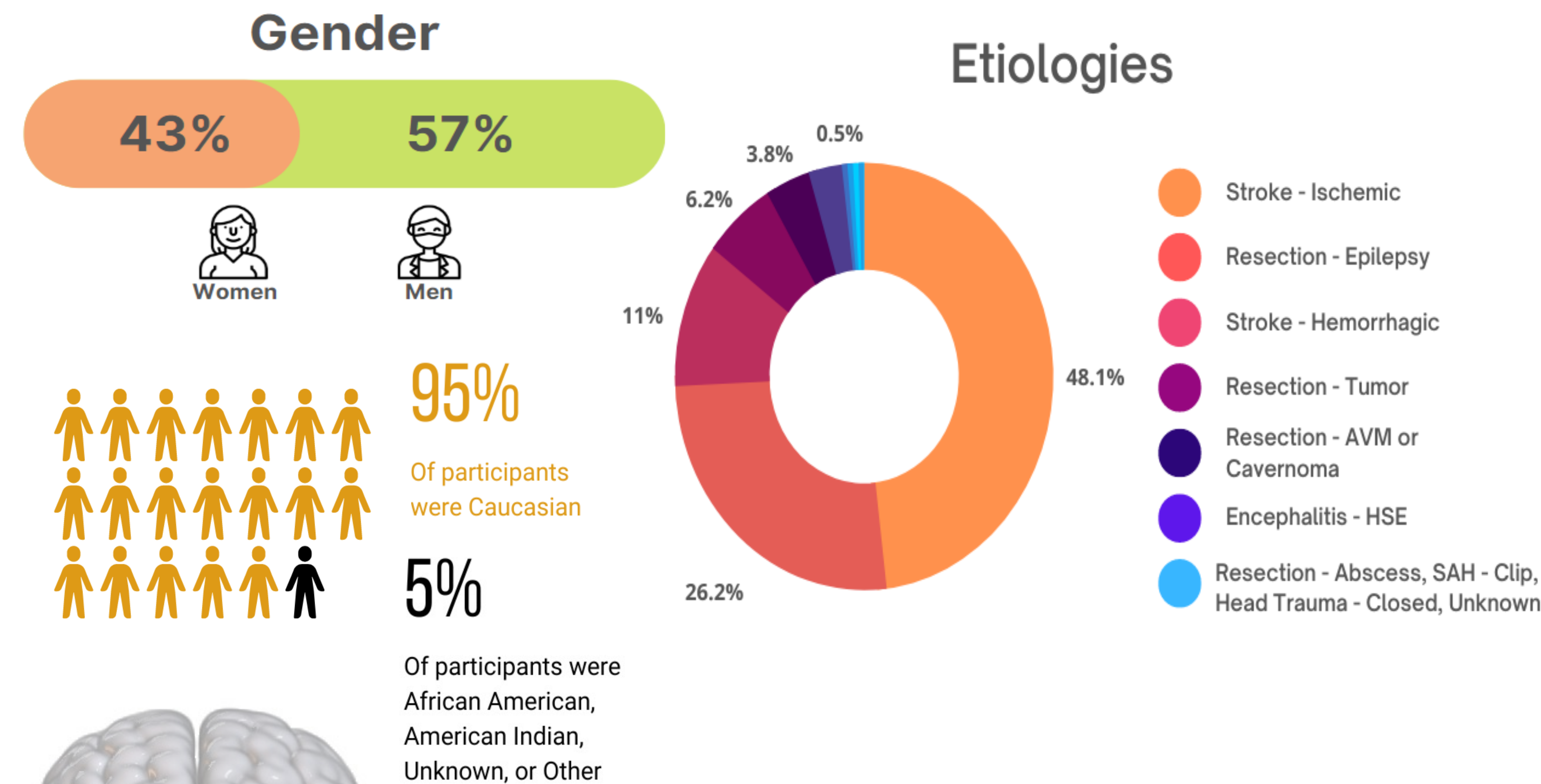


Fig. 3. Results overlaid on a 3-Dimensional MNI152 Brain. Red regions are associated with verb retrieval and blue regions are associated with noun retrieval.

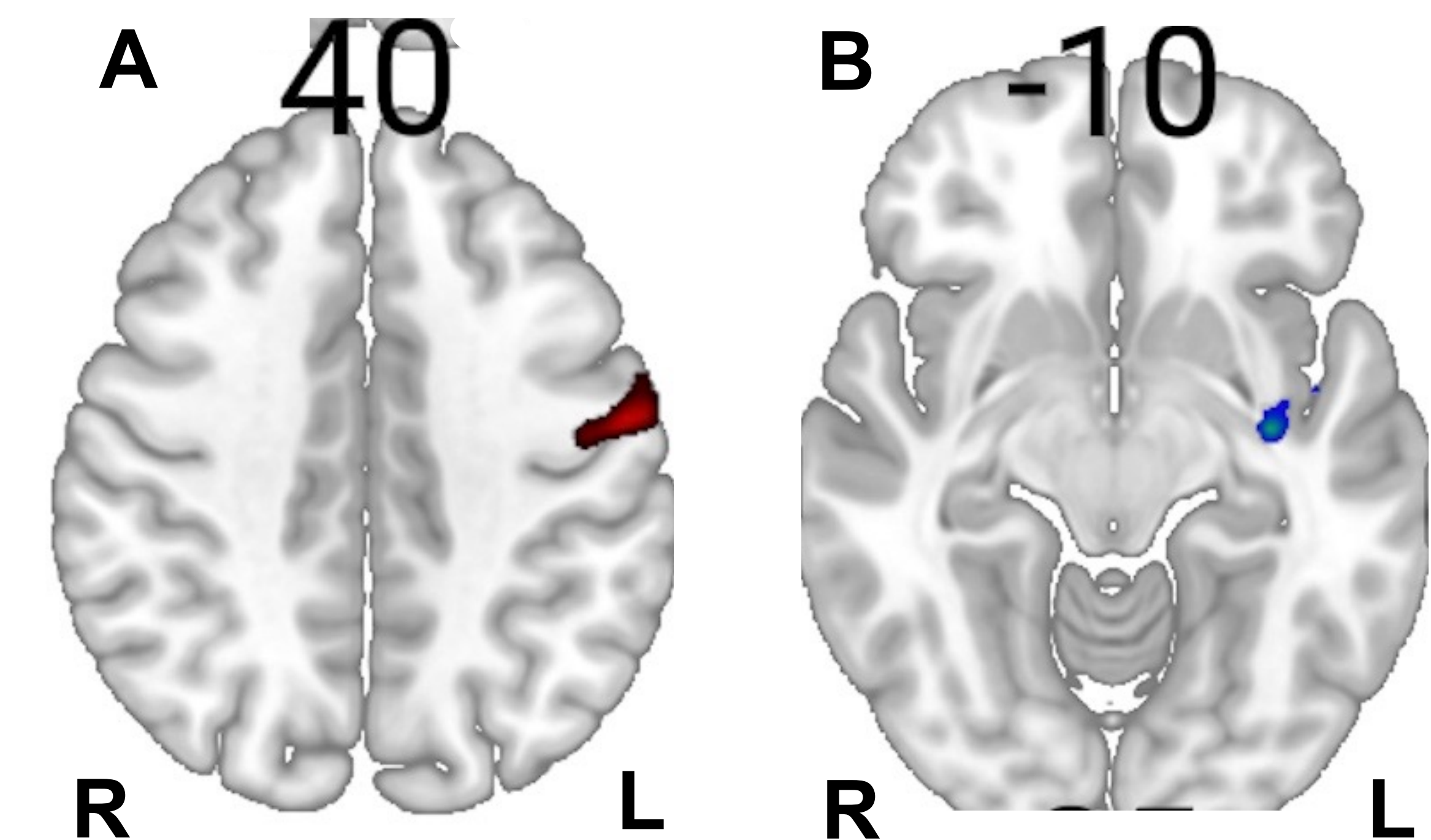


Fig. 4. Results overlaid on MNI152 brain slices at z = 40mm and z = -10mm in radiographic orientation. (A) Bias against verb retrieval is associated with damage to the precentral gyrus. (B) Bias against noun retrieval is associated with damage to white matter

Discussion

- Replicated previous results that showed differentiation between nouns and verbs
- Limitation with homographs, POS tagger, and lost 5% of words due to illegibility

Future Directions

- Full brain analysis
- Use modeling approach that gives likelihood, not fixed categories
- Explore other parts of speech (e.g. adjectives)

Acknowledgments

Special thanks to Dr. Tranel and Dr. Deifelt Streese for their guidance and continued support on this project. I would also like to thank Belin-Blank and SSTP for this amazing research opportunity.

References

1. Damasio, A. R., & Tranel, D. (1993, January 7). Nouns and verbs are retrieved with differently distributed neural systems. *Proceedings of the National Academy of Sciences of the United States of America*, 90, 4957-4960
2. Vigliocco, G., Vinson, D. P., Druks, Judit., Barber, Horacio., Cappa, S. F. (2011, January). Nouns and verbs in the brain: A review of behavioural, electrophysiological, neuropsychological and imaging studies. *Neuroscience & Behavioral Reviews*, 35(3), 407-426, <https://doi.org/10.1016/j.neubiorev.2010.04.00>

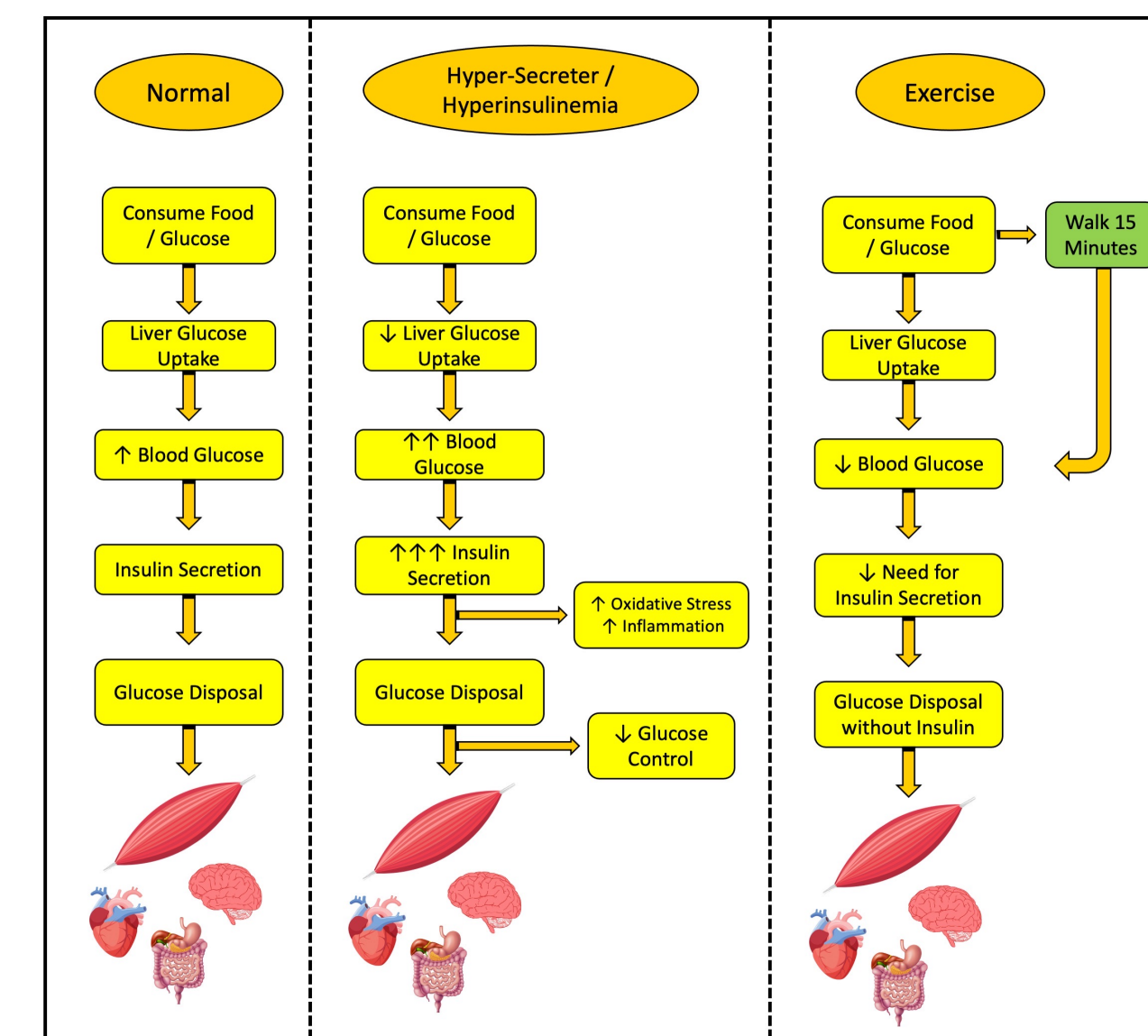
Does Electrically Induced Exercise During Stance Attenuate Peak Metabolic Biomarkers in People With and Without Spinal Cord Injury?

Sophia Ramaraju, Anjali Sanghvi, Olga Dubey, Jinhyun Lee, Kristin A. Johnson, Michael A. Petrie, and Richard K. Shields

Department of Physical Therapy and Rehabilitation Science, Carver College of Medicine
University of Iowa, Iowa City, IA

Introduction

The lack of physical activity increases the likelihood of developing non-communicable diseases including type two diabetes and cancer.^{1,2} While life-style recommendations, like exercise, are plausible for people with intact central nervous systems (CNS), it is challenging for people with paralysis because they cannot volitionally “turn on” their paralyzed muscles.



After muscle paralysis people with metabolic disease lose their sensitivity to insulin and are unable to move glucose out of the bloodstream leading to diabetes. Recent research supports that only 15 minutes of exercise after a meal removes glucose from the blood stream requiring less need for insulin.³ We sought to understand if standing with or without “electrically induced” exercise, increases HR and reduces key biomarkers, like insulin, in people with and without paralysis from spinal cord injury (SCI).

Purpose and Hypothesis

We aim to determine if passive and active stance triggers an increase in heart rate (HR) and regulates metabolic biomarkers in individuals with and without SCI. We expect that passive and active stance will both increase HR and attenuate peak insulin and glucose levels in people with and without SCI.

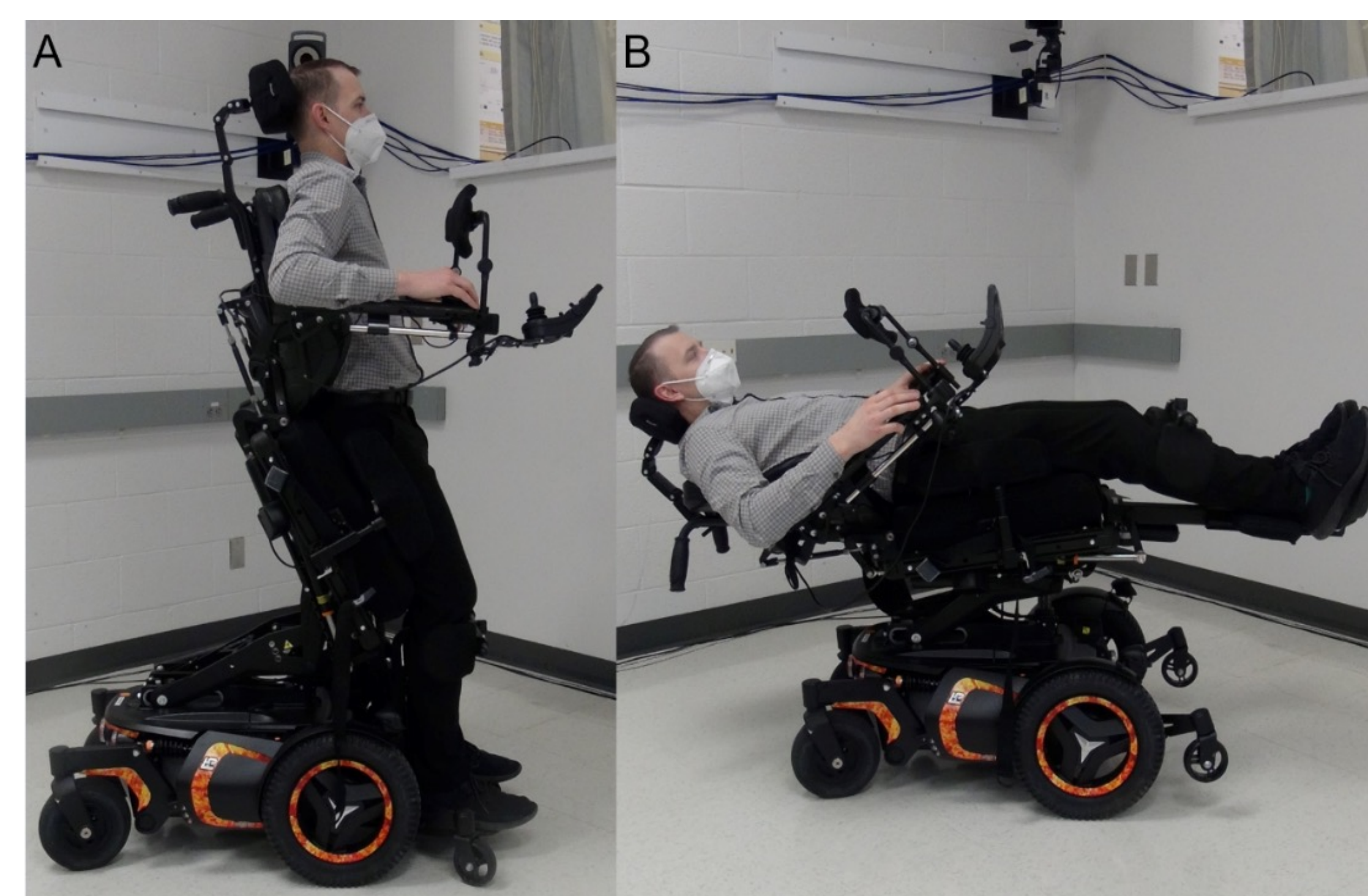
Methods

Participants: One male (age XX) without SCI and one male (age xx) with SCI.

Design: Two Sessions of Stance: with or without exercise of the quad/HS muscles before and after a balanced meal

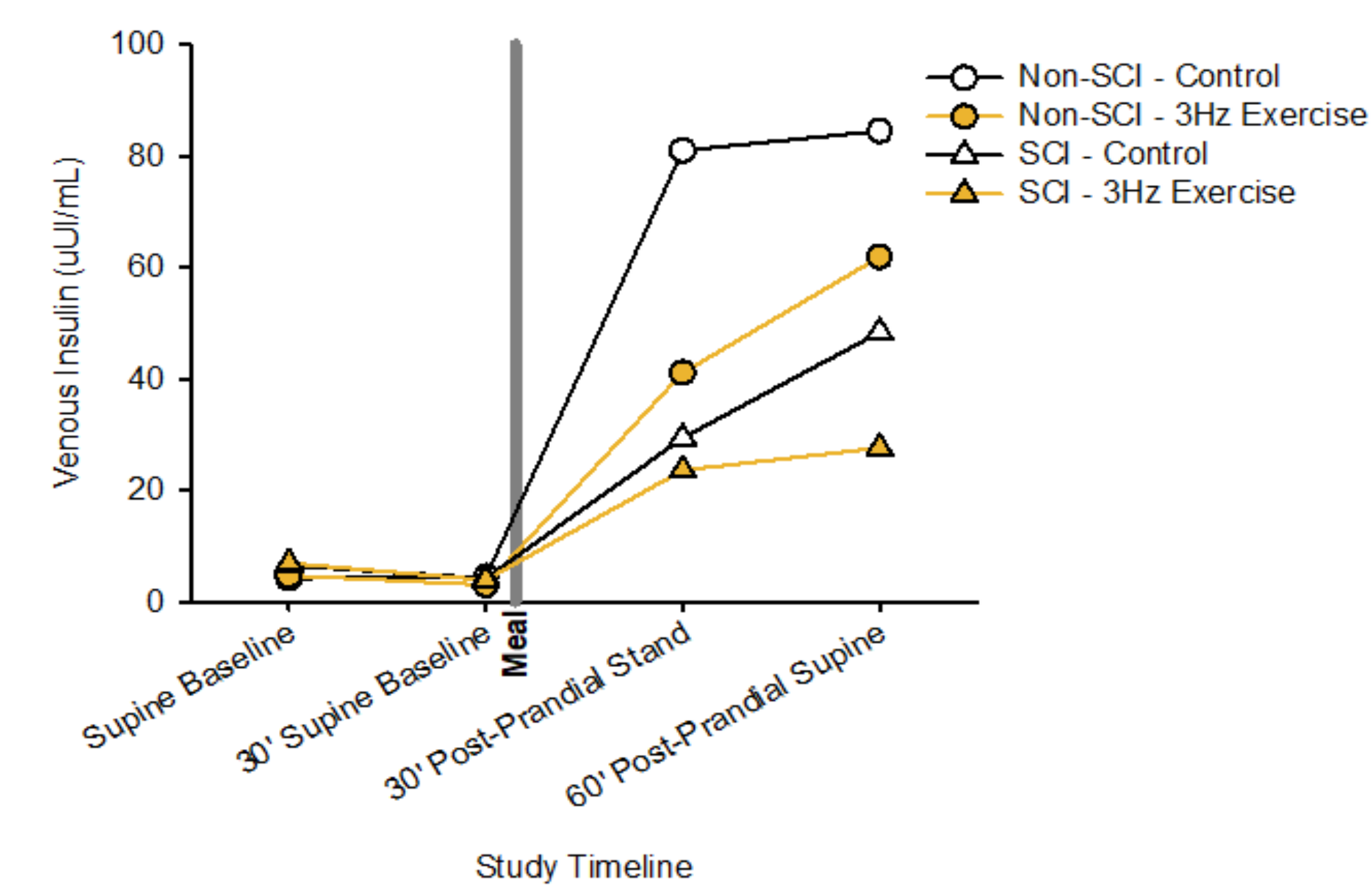
Exercise: Electrically induced using 3 Hz frequency and ~ 100 milliamps intensity.

Outcome measures: HR, LF/HF, Insulin, and Glucose

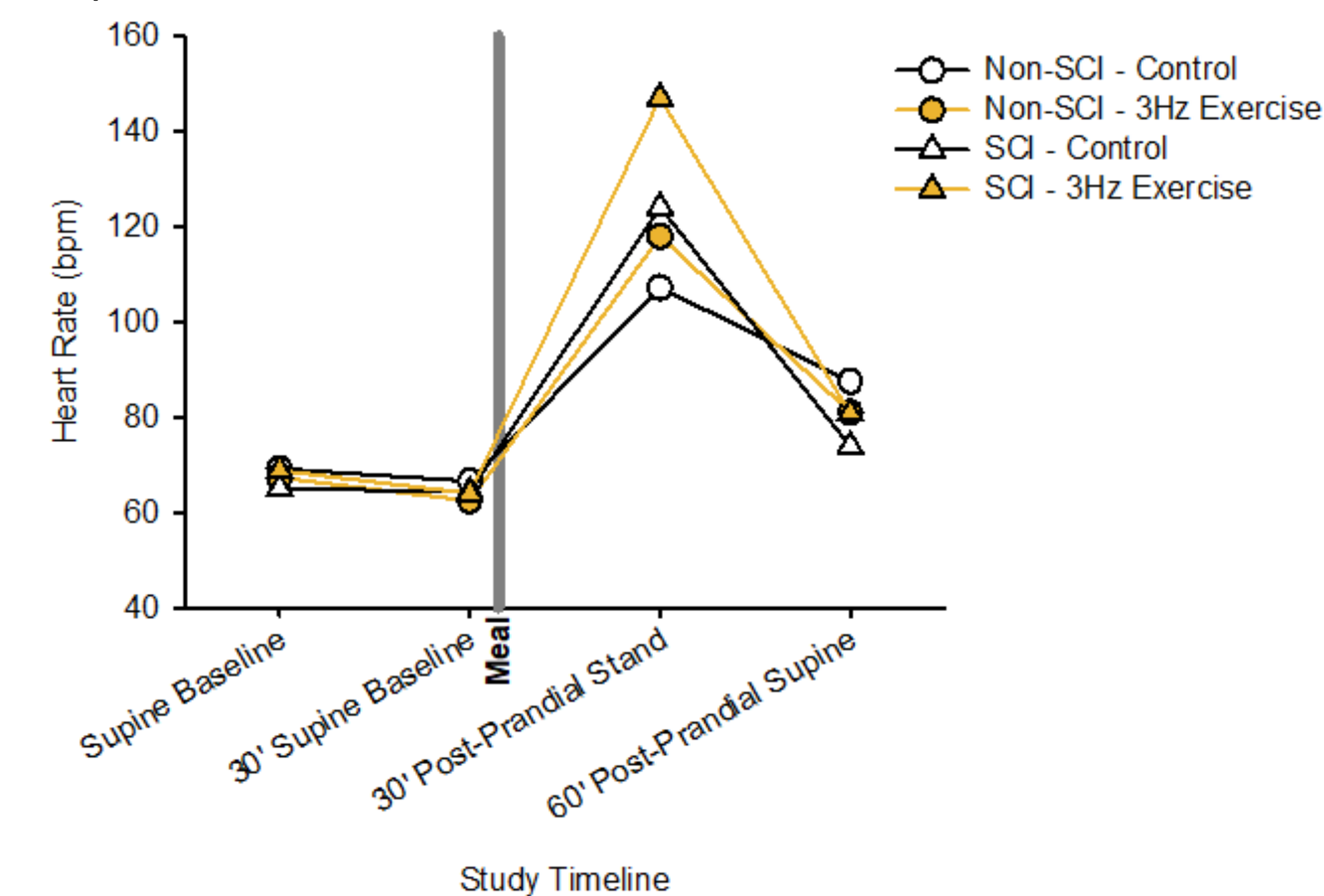


Instrumented wheelchair to introduce electrically induced exercise in the supine and upright stance positions. Note the identical lower extremity joint angles in upright (A) and supine (B) conditions offering the first valid comparison about systemic upright cardiovascular stress and electrically induced exercise on HR and metabolic biomarkers (insulin and glucose).

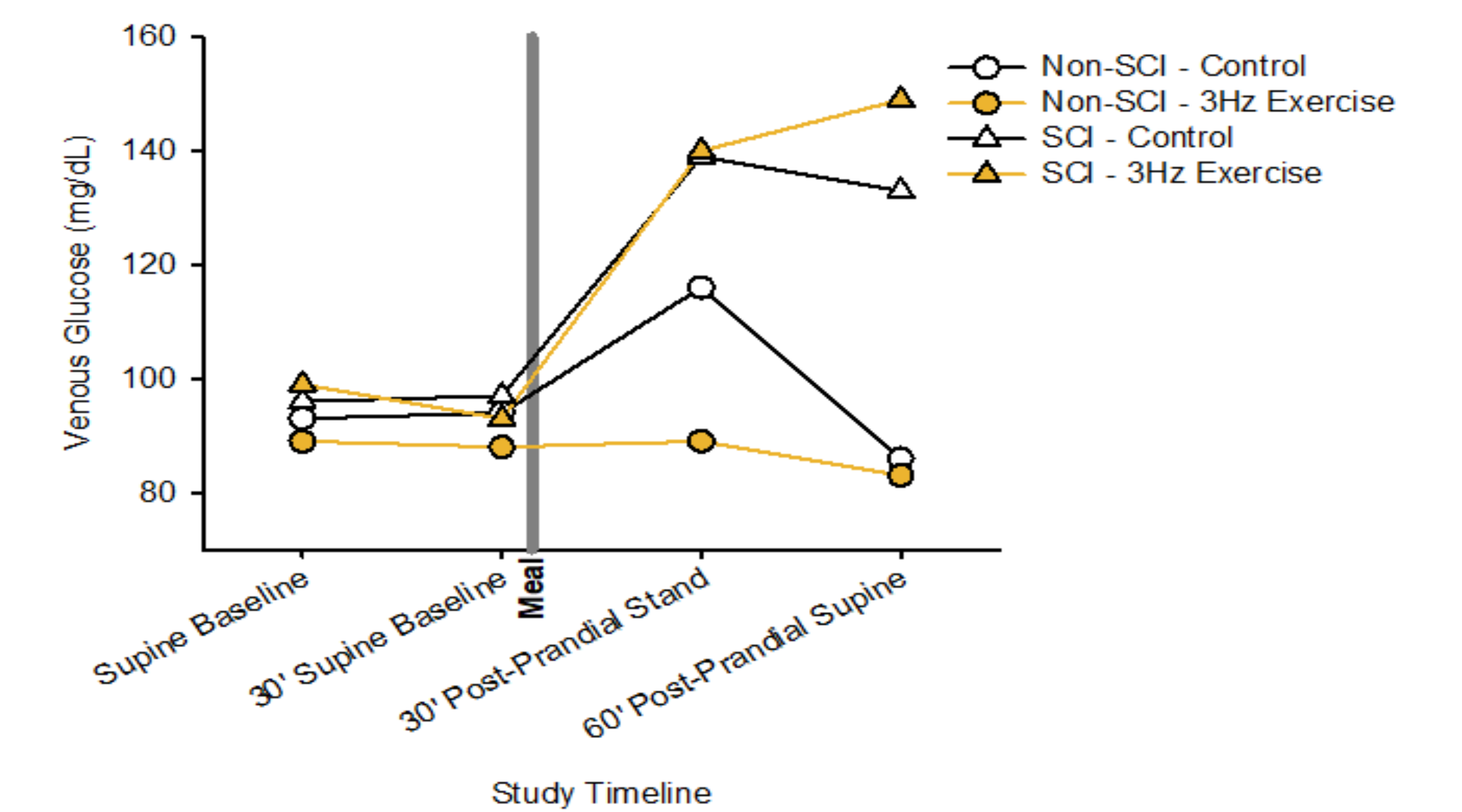
Results



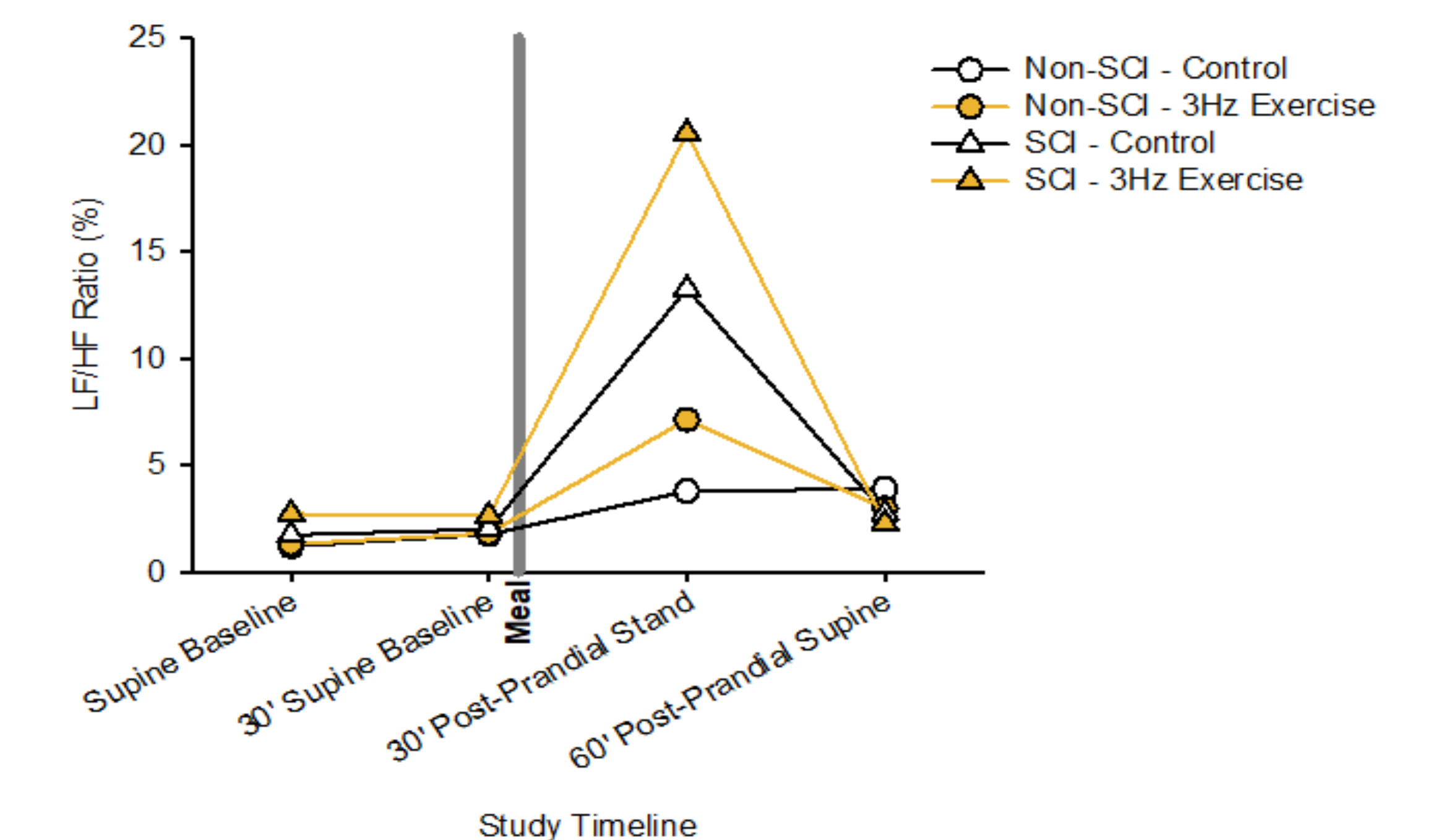
Insulin levels after a meal are reduced during stance and 3 Hz exercise as compared to stance without exercise in both participants.



Heart rate with stance and 3 Hz exercise is increased in both participants.



Glucose levels after a meal are reduced with stance and 3 Hz exercise but only in participant without SCI.



LF/HF, as an index of sympathetic vagal tone, is greatest with stance and 3 Hz exercise in both participants.

Conclusions and Clinical Implications

The first major finding of this preliminary “proof of concept” study is that stance and electrically induced exercise increased HR, LF/HF, and attenuated peak insulin levels following a meal in a person with SCI. The second important discovery is that when the stance was combined with electrically induced exercise there was an even greater reduction in insulin compared with stance alone. A limitation is that we do not know if the electrical stimulation in supine would yield a similar outcome as stance, and that is the focus of an ongoing trial. These preliminary results offer the first metabolic analysis of stance with and without electrically induced exercise in a person with SCI.

References and Acknowledgements

- Shields, R. K. (2021). Precision Rehabilitation: How lifelong Healthy Behaviors Modulate Biology, Determine Health, and Affect Populations. *Physical Therapy*, 102(1). <https://doi.org/10.1093/ptj/pzab248>
- Barker, K., & Eickmeyer, S. (2020). Therapeutic Exercise. *Medical Clinics of North America*, 104(2), 189–198. <https://doi.org/10.1016/j.mcna.2019.10.003>
- Gillen JB, et al. (2021). Exercise and Nutrient Interactions for Post-Prandial Glucose Control. *Appl. Physiol. Nutr. Metab.* 46:856-865.

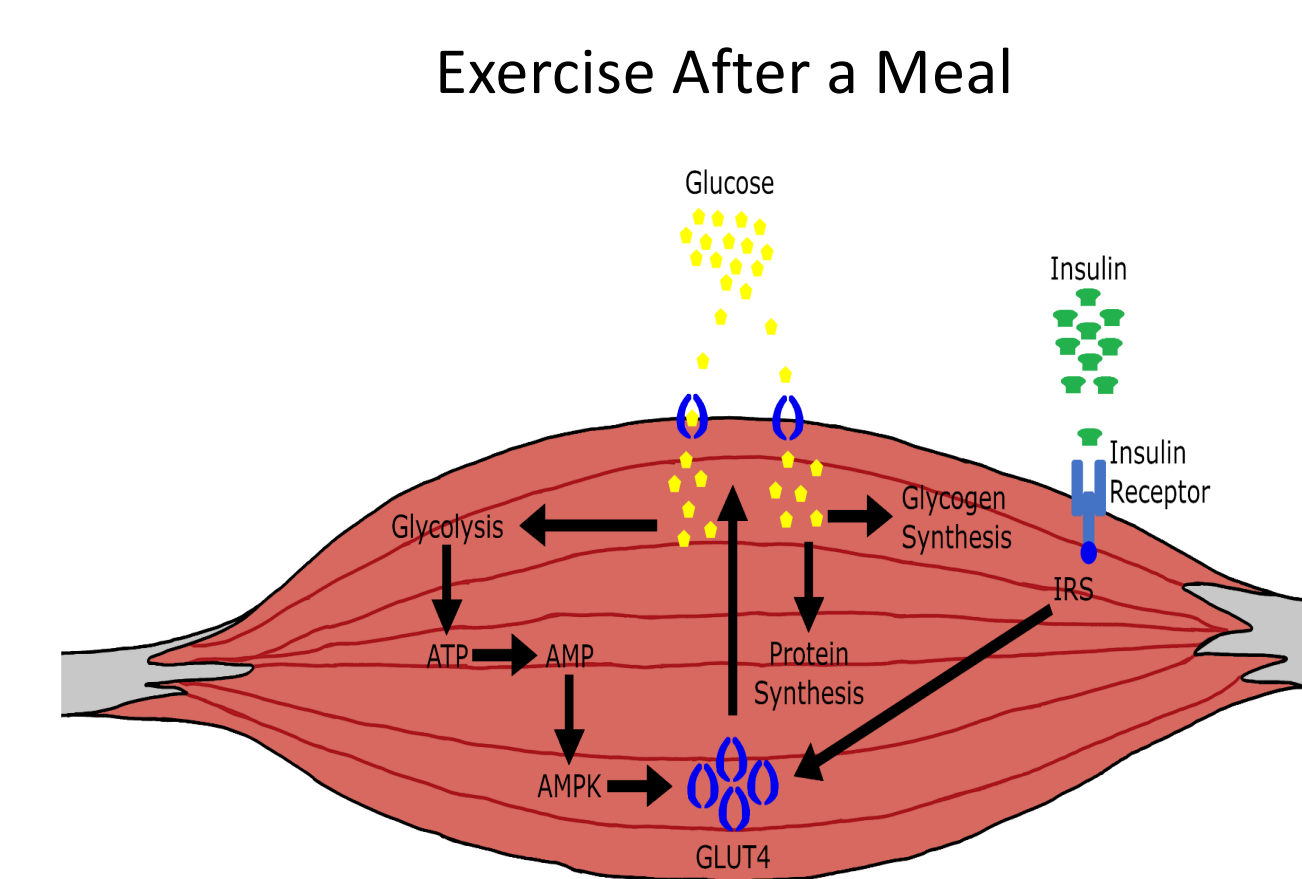
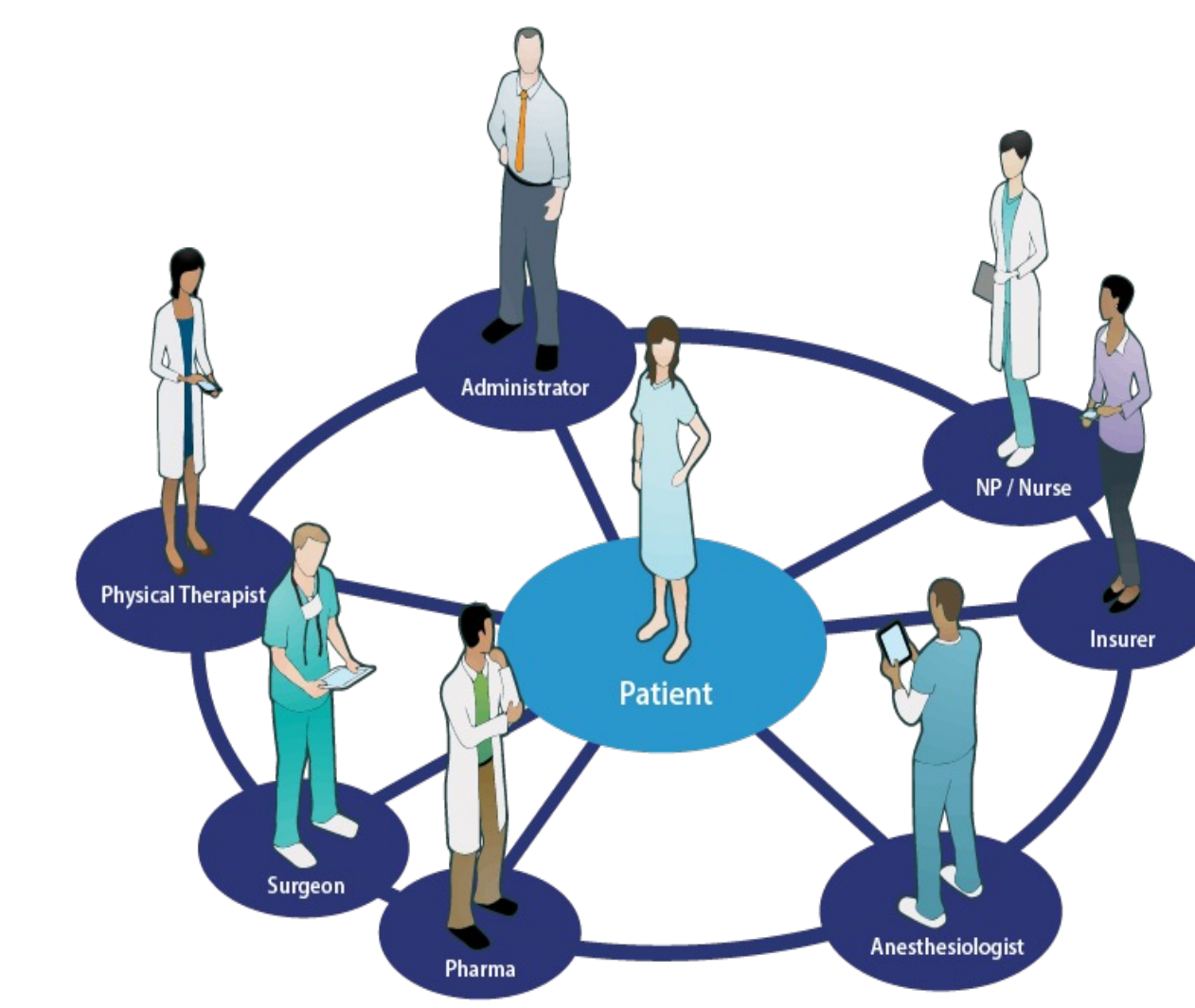
This study was funded by the National Center for Medical Rehabilitation Research within the National Institutes of Health: Grants R01-HD084645 and R01-HD082109 We thank the Secondary Student Training Program (SSTP) for providing us the opportunity to do research with Dr. Shields and his lab.

Do Healthcare Practitioners Prescribe Exercise After Meals In Patients With Metabolic Impairment?

Introduction

The lack of physical activity increases the likelihood of developing non-communicable diseases including type two diabetes and cancer.^{1,2} Metabolic disease is a primary predictor of all cause mortality. The emphasis in medicine on prescriptive drugs may overshadow a “patient centered” lifestyle approach, including exercise, for patients with metabolic disease.^{1,2} We sought to survey physicians and rehabilitation specialists to determine if exercise is prescribed for people with metabolic impairment and the type of exercise that is recommended.

Insulin opens the “door” for glucose to leave the bloodstream and enter external organs, like muscle. People with metabolic disease lose their sensitivity to insulin and are unable to remove glucose out of the bloodstream after a meal. Recent research supports that only 15 minutes of exercise after a meal removes glucose from the blood in the absence of insulin.³ We sought to survey physicians and rehabilitation specialists to determine if they prescribe exercise after meals to reduce the need for insulin.



Purpose and Hypothesis

The aims of this study are to determine the dose of exercise that healthcare providers (physicians and physical therapists) recommend, and whether the timing of exercise is related to eating for people with metabolic impairment. We expect that healthcare providers (physicians and physical therapists) recommend exercise consistently, but that neither healthcare specialty considers time of meals when prescribing exercise.

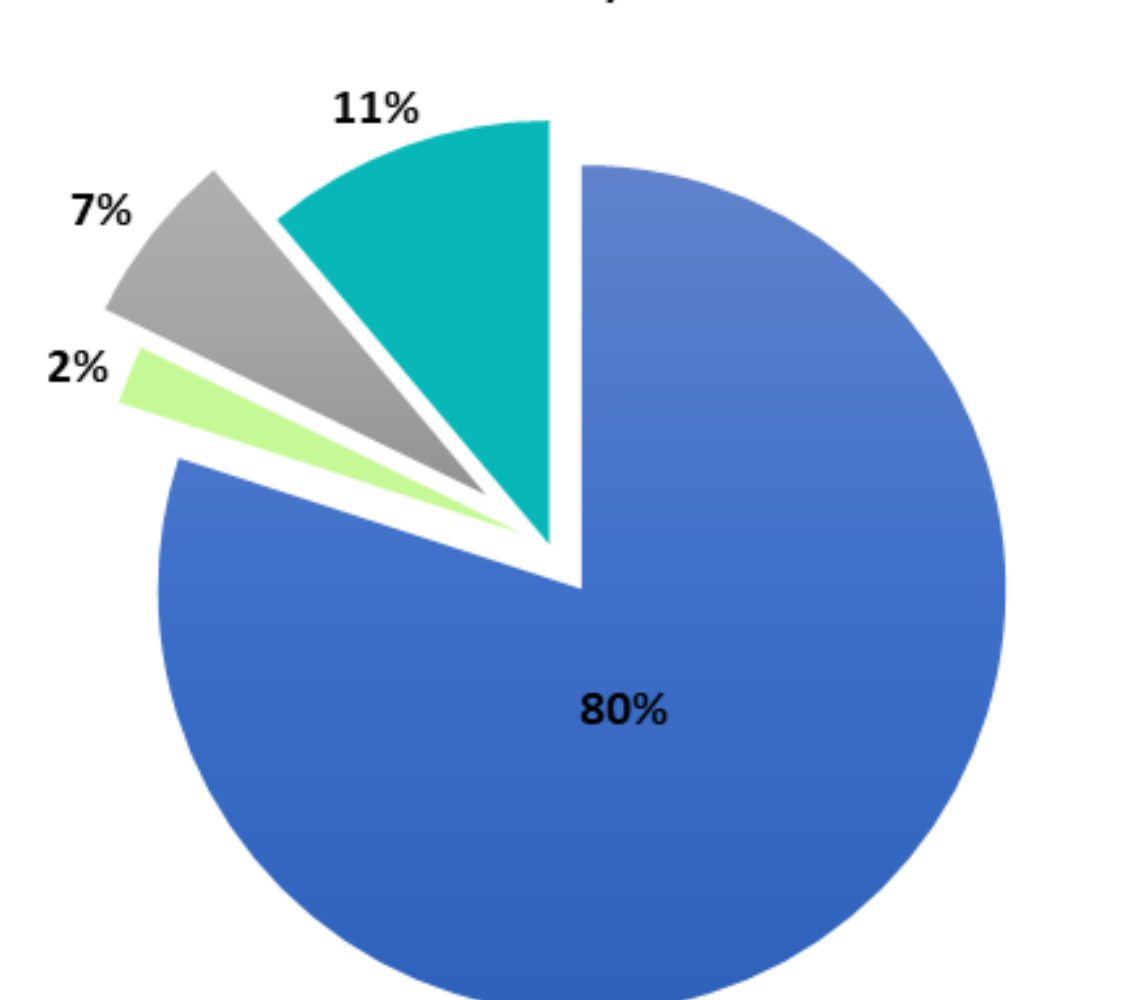
Methods

Participants:

- 59 English-speaking healthcare providers
- Seven MD departments (40)
- One Rehabilitation department of physical therapists (PT) (19)

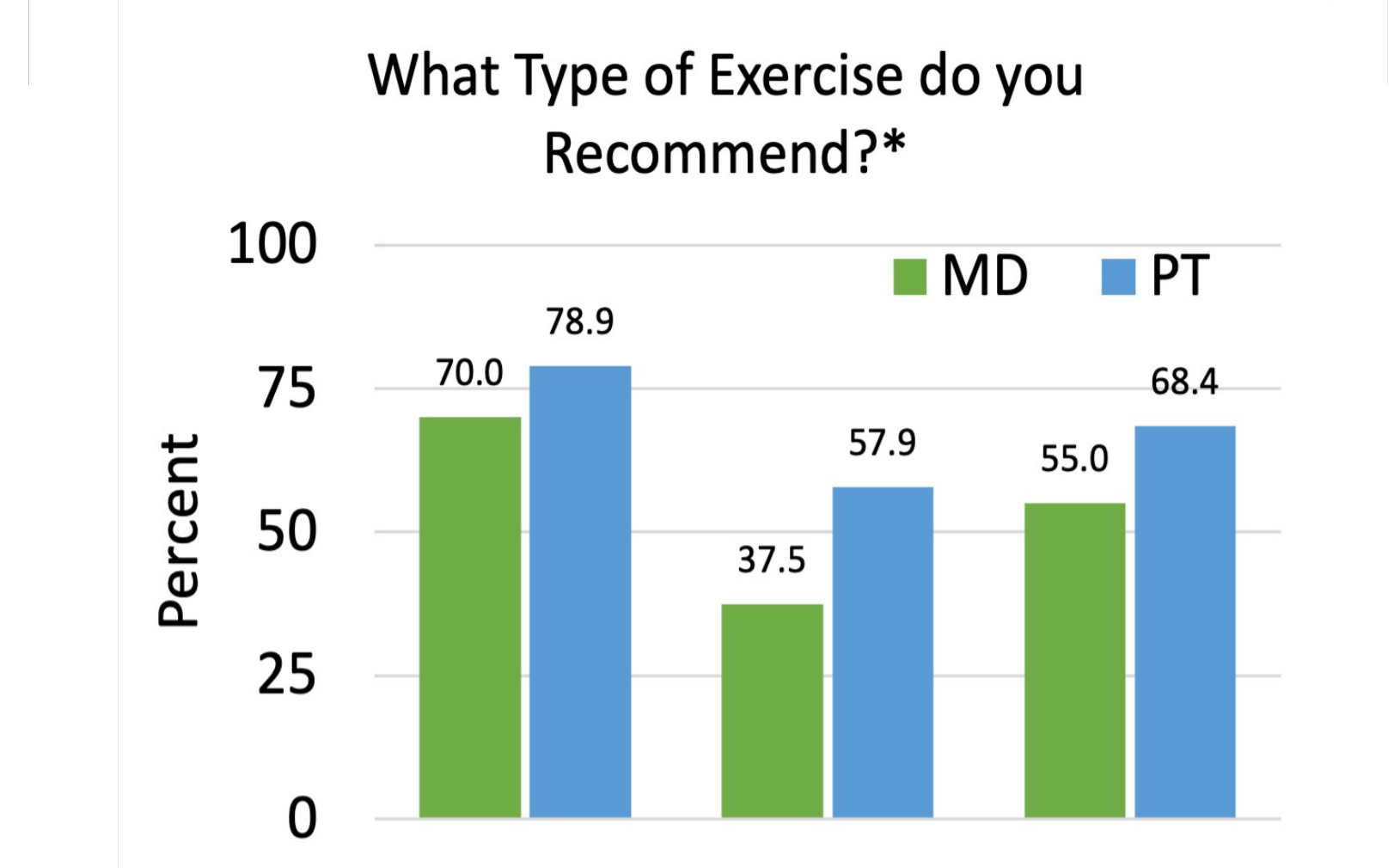
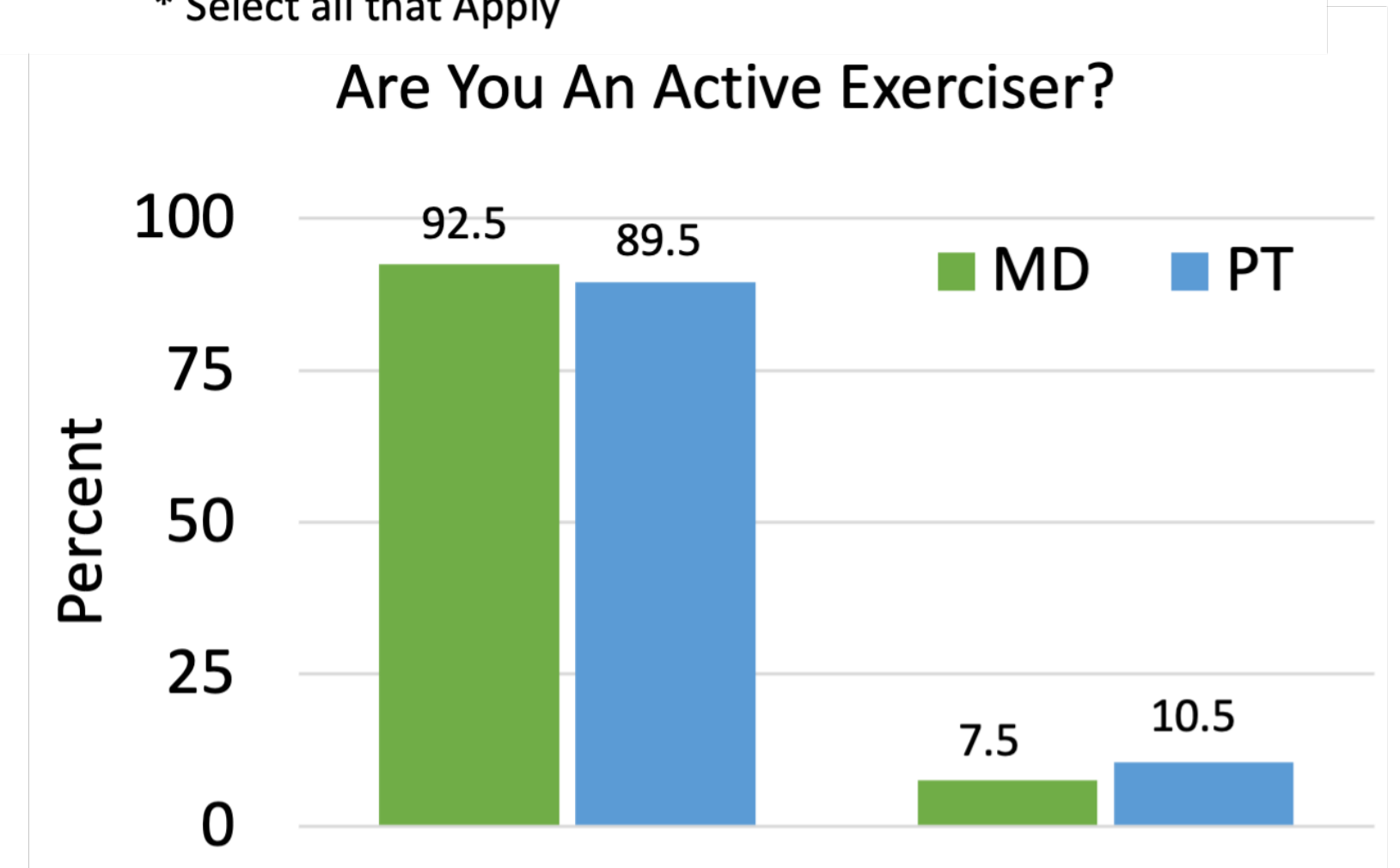
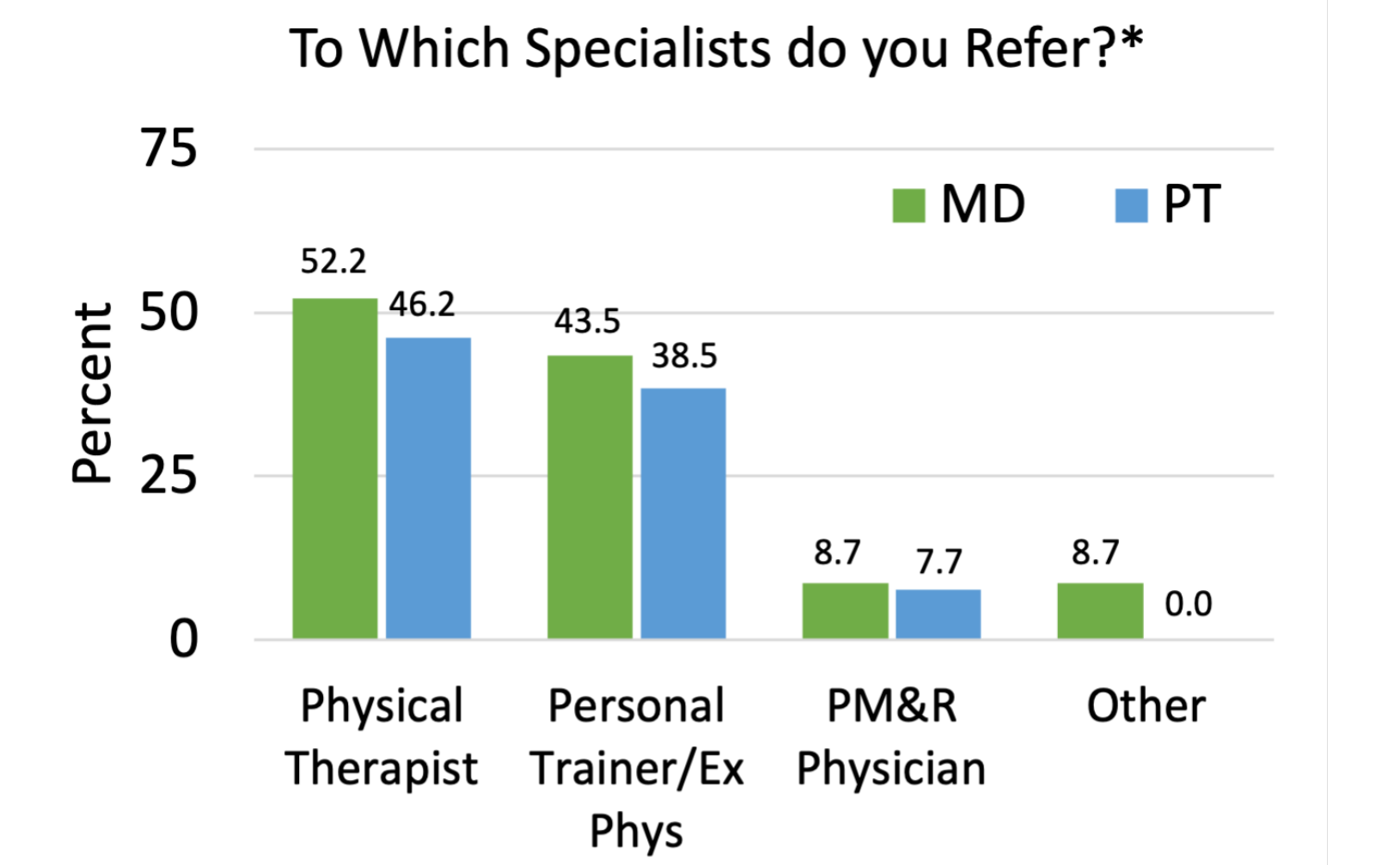
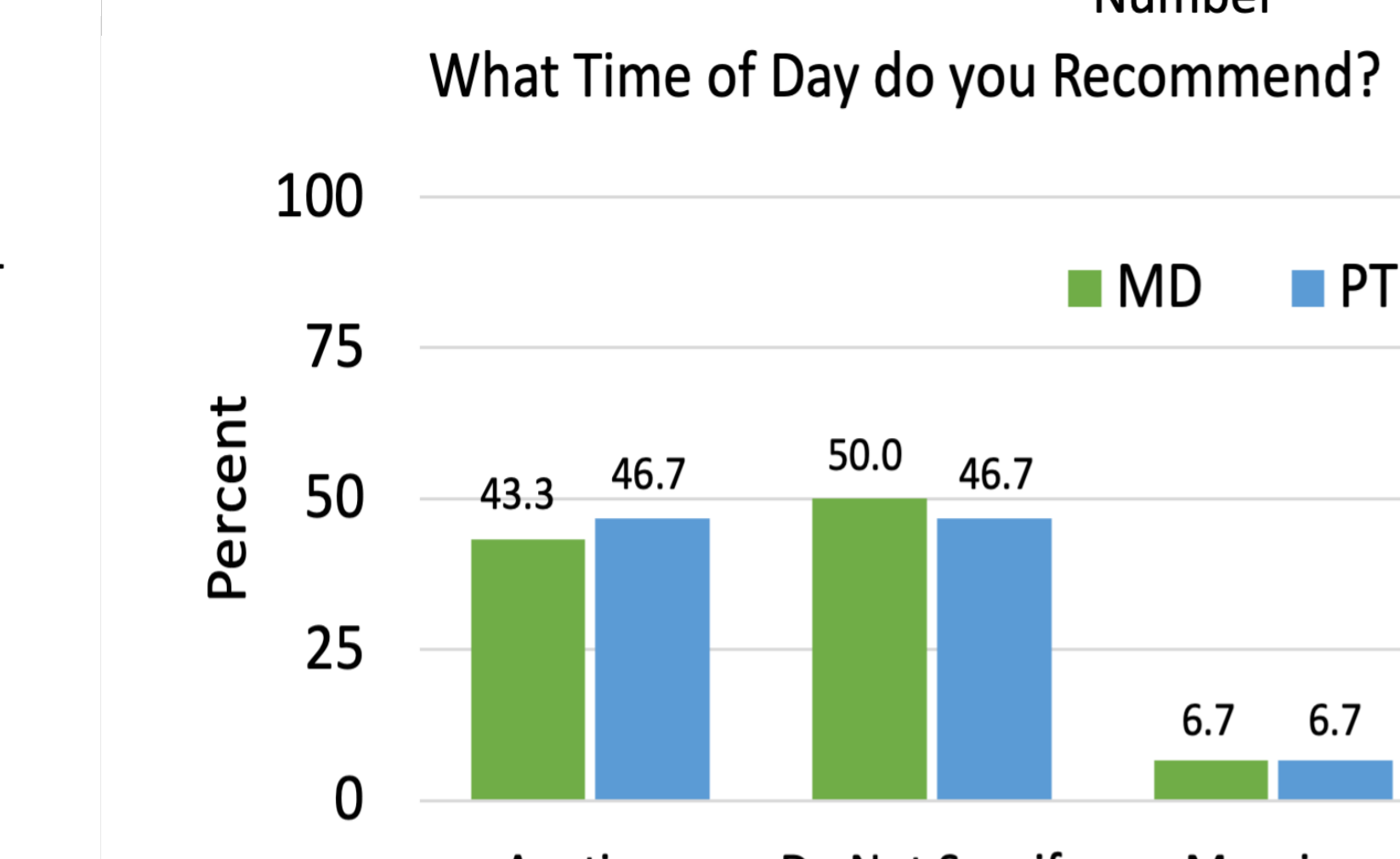
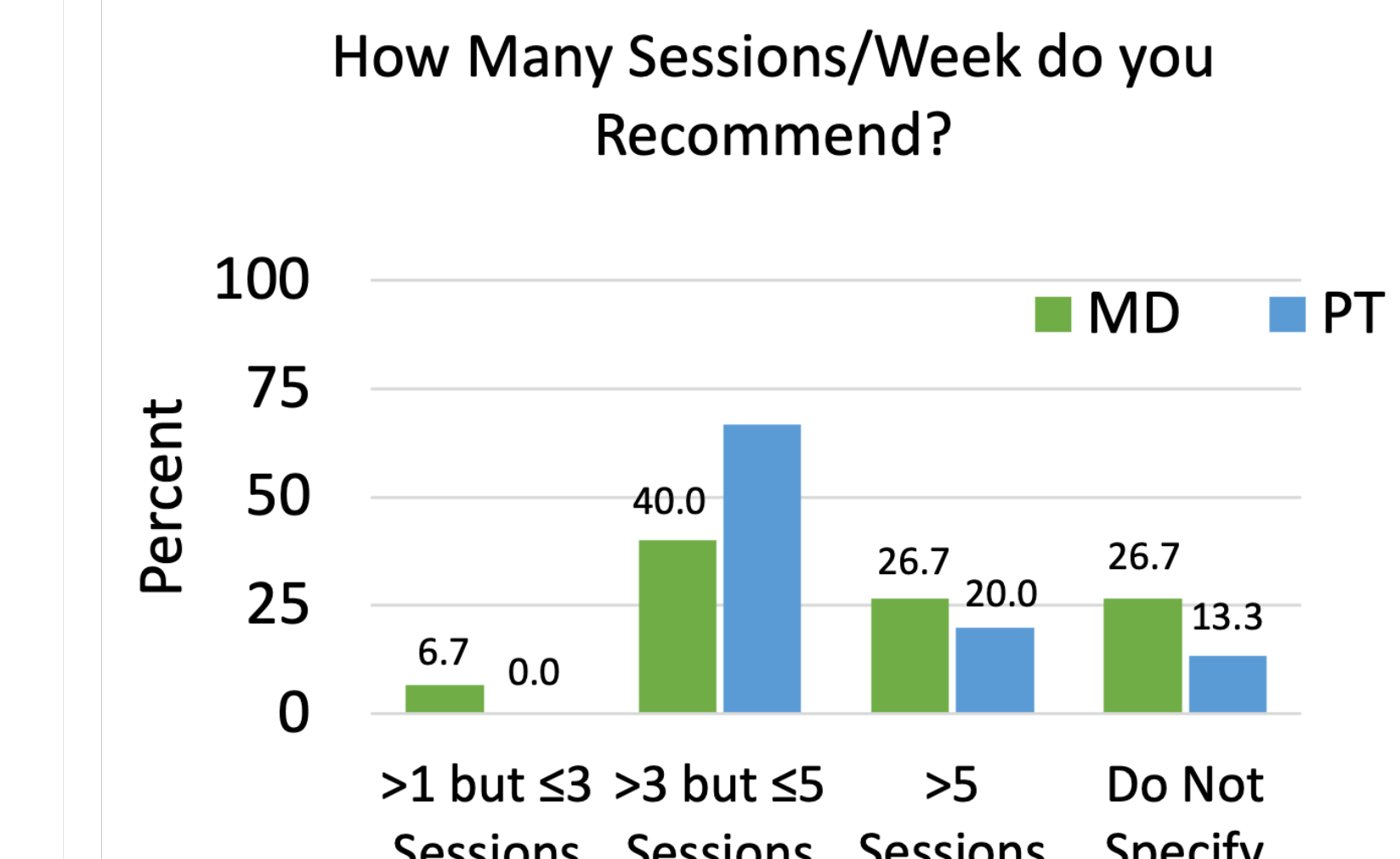
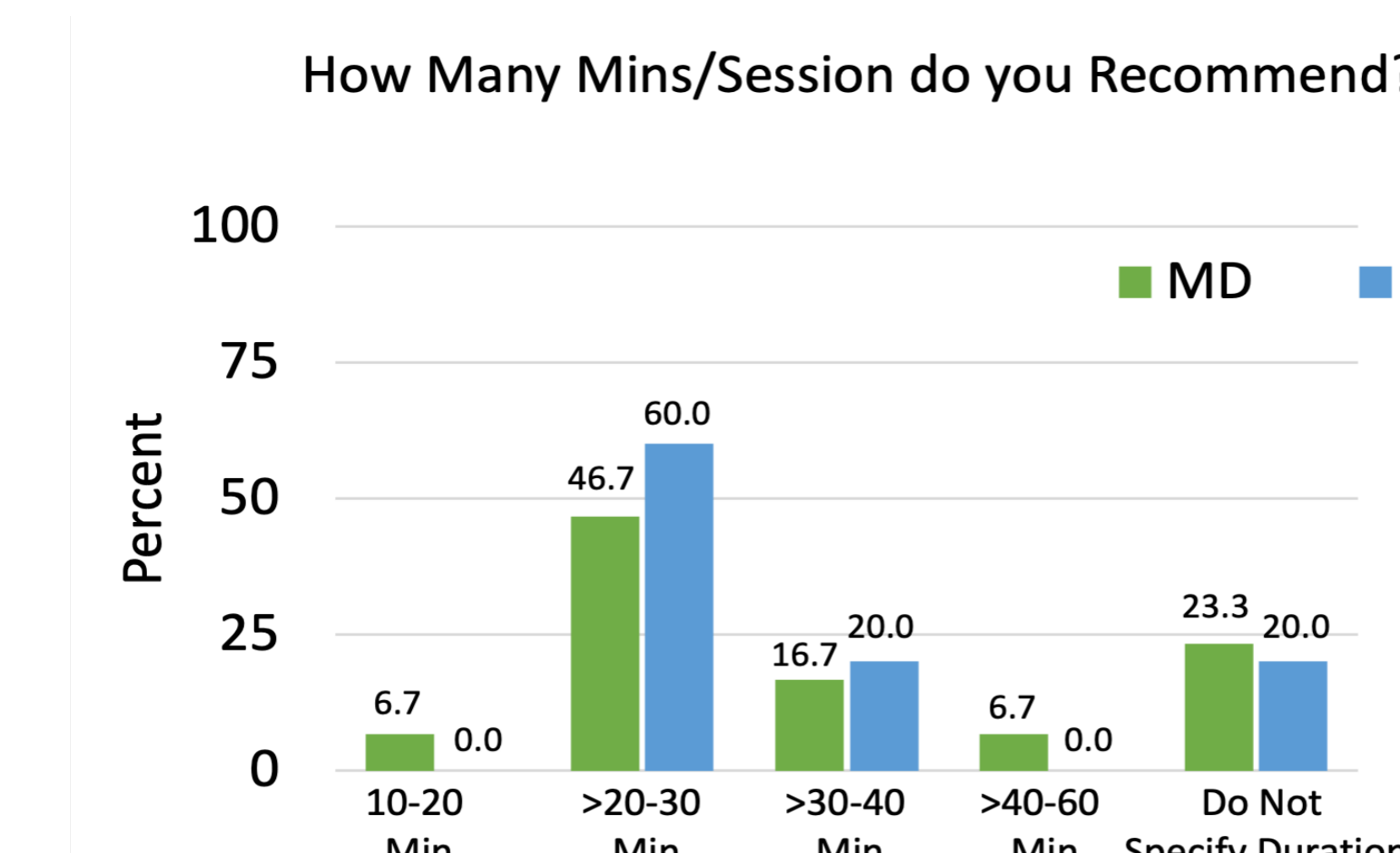
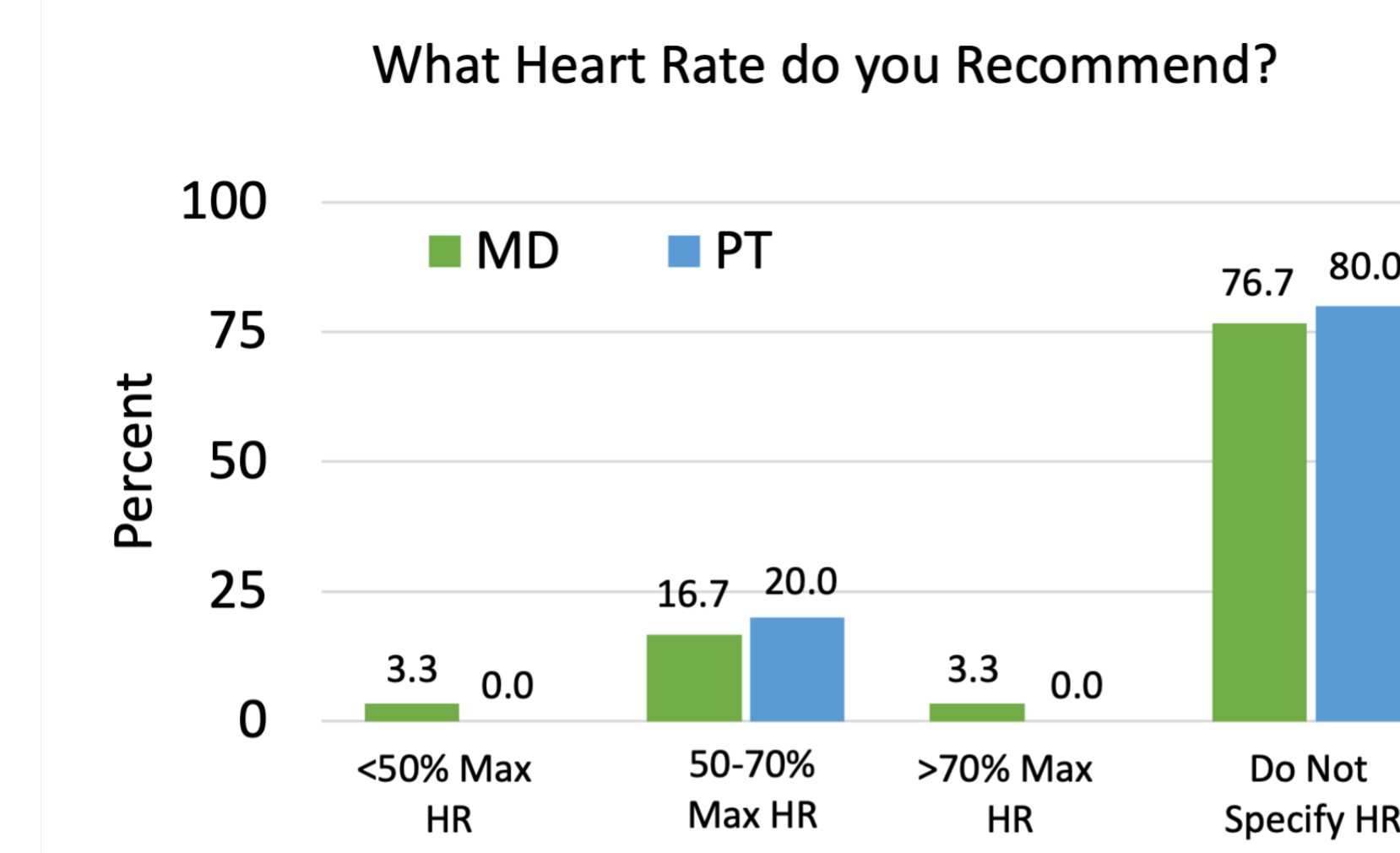
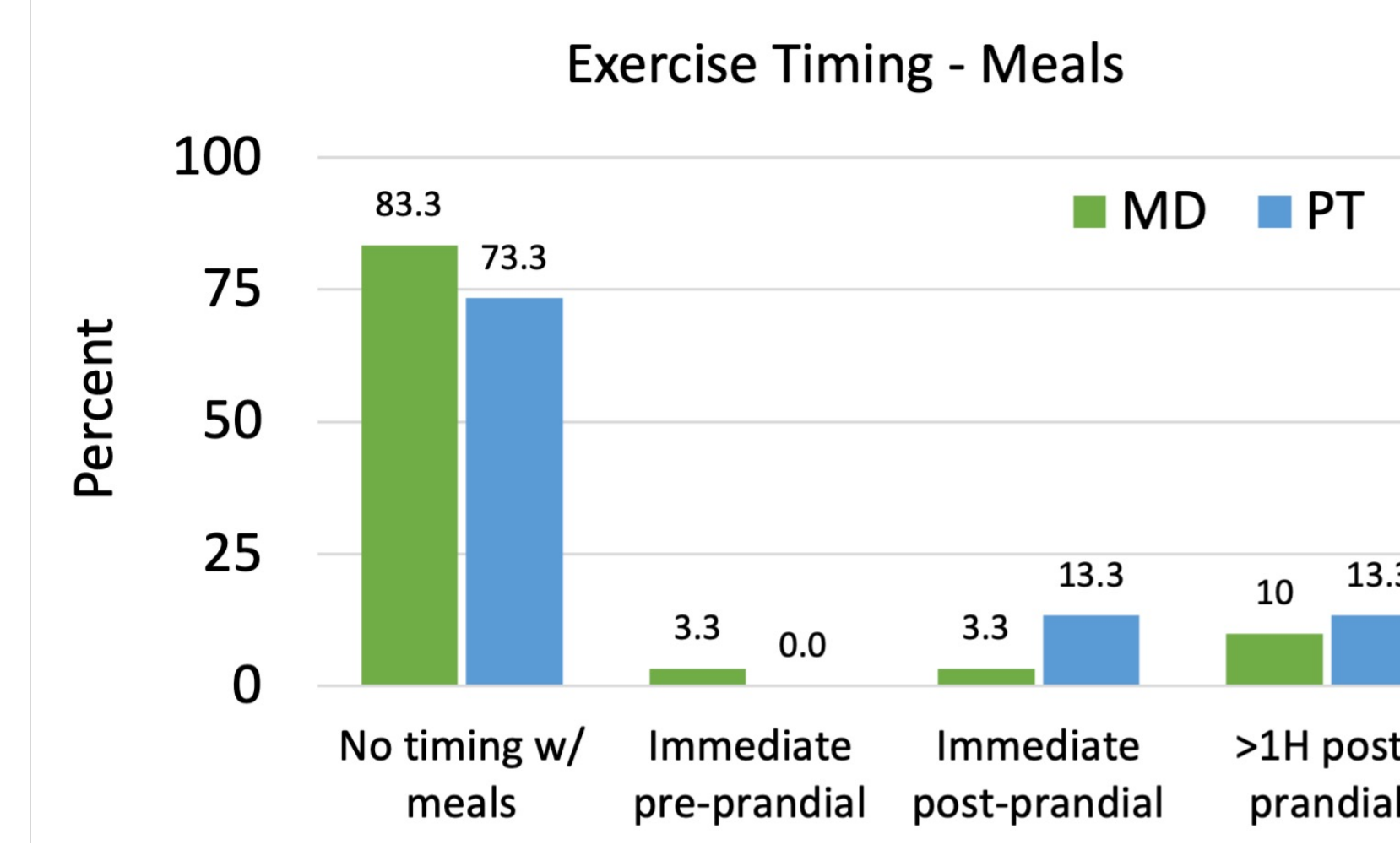
Data Collection and Analysis: Each healthcare provider completed a 10-question survey regarding their standard recommendations on exercise including the time of day and relation to meals. As demonstrated in the figure, 80% of all healthcare providers DO NOT recommend exercise based on the time of a meal. Only 7% of all participants recommended exercise immediately after a meal.

If you advise your patients about exercise, do you typically recommend that they exercise:



■ I Do Not Recommend Exercise Based on Time of a Meal
■ Right Before Having a Meal
■ Immediately After Having a Meal
■ Greater than 1 Hour After a Meal

Results



Conclusions and Clinical Implications

The first major finding of this study is that neither rehab specialists or physicians recommend exercise following a meal. This finding suggests healthcare practitioners are not aware of the contemporary research supporting that 15 minutes of exercise following a meal significantly reduces post-prandial insulin levels.³ A second major finding is that rehabilitation specialists recommend 20% more anaerobic exercise and 13% more general activity as compared with physicians. Lastly, there is internal consistency between rehab specialists and physicians among several aspects of exercise prescription. Methods to translate new research findings into the clinic may be needed for all healthcare specialties.

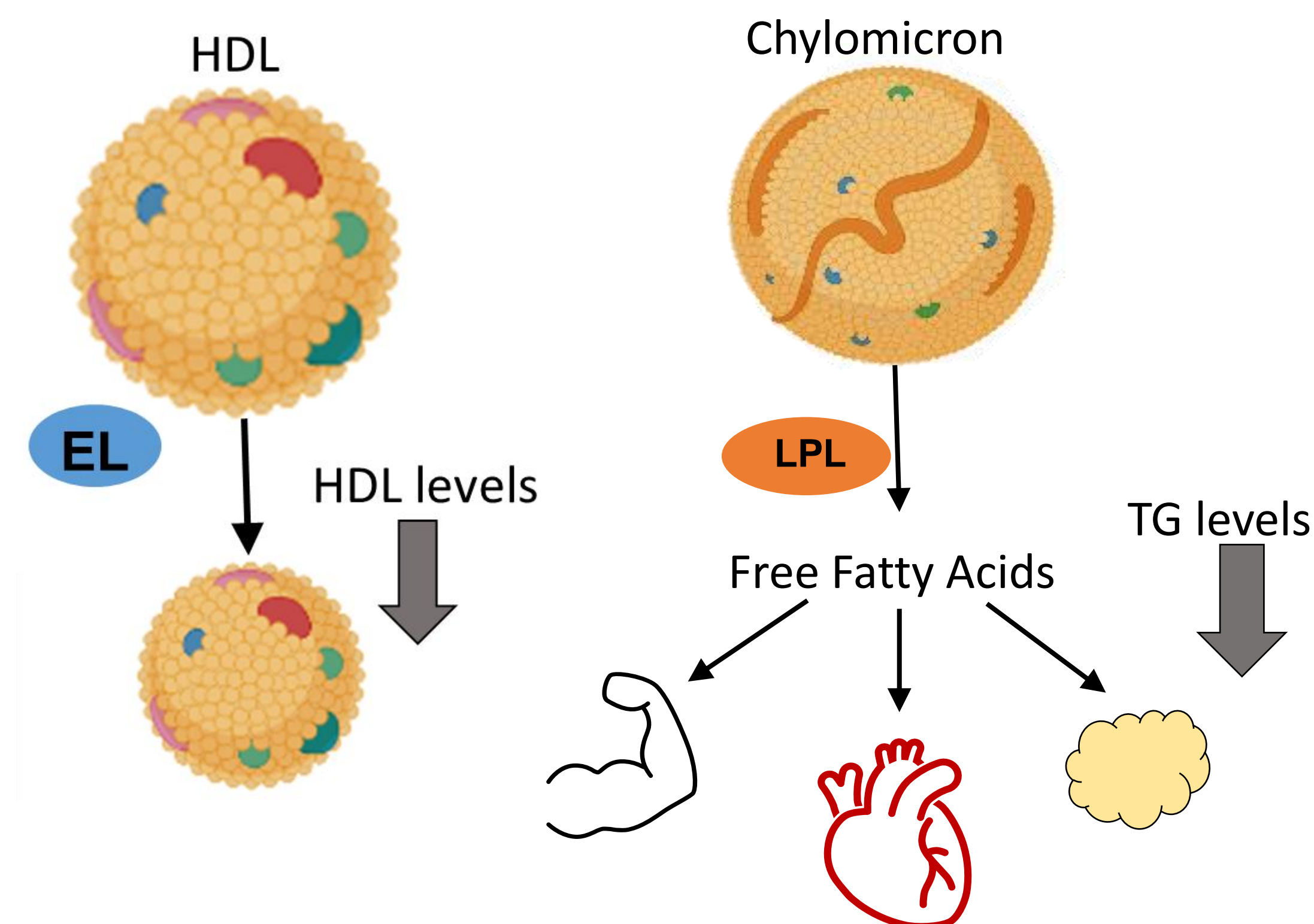
References and Acknowledgements

1. Shields, R. K. (2021). Precision Rehabilitation: How lifelong Healthy Behaviors Modulate Biology, Determine Health, and Affect Populations. *Physical Therapy*, 102(1). <https://doi.org/10.1093/ptj/pzab248>
2. Barker, K., & Eickmeyer, S. (2020). Therapeutic Exercise. *Medical Clinics of North America*, 104(2), 189–198. <https://doi.org/10.1016/j.mcna.2019.10.003>
3. Gillen JB, et al. (2021). Exercise and Nutrient Interactions for Post-Prandial Glucose Control. *Appl. Physiol. Nutr. Metab.* 46:856-865.

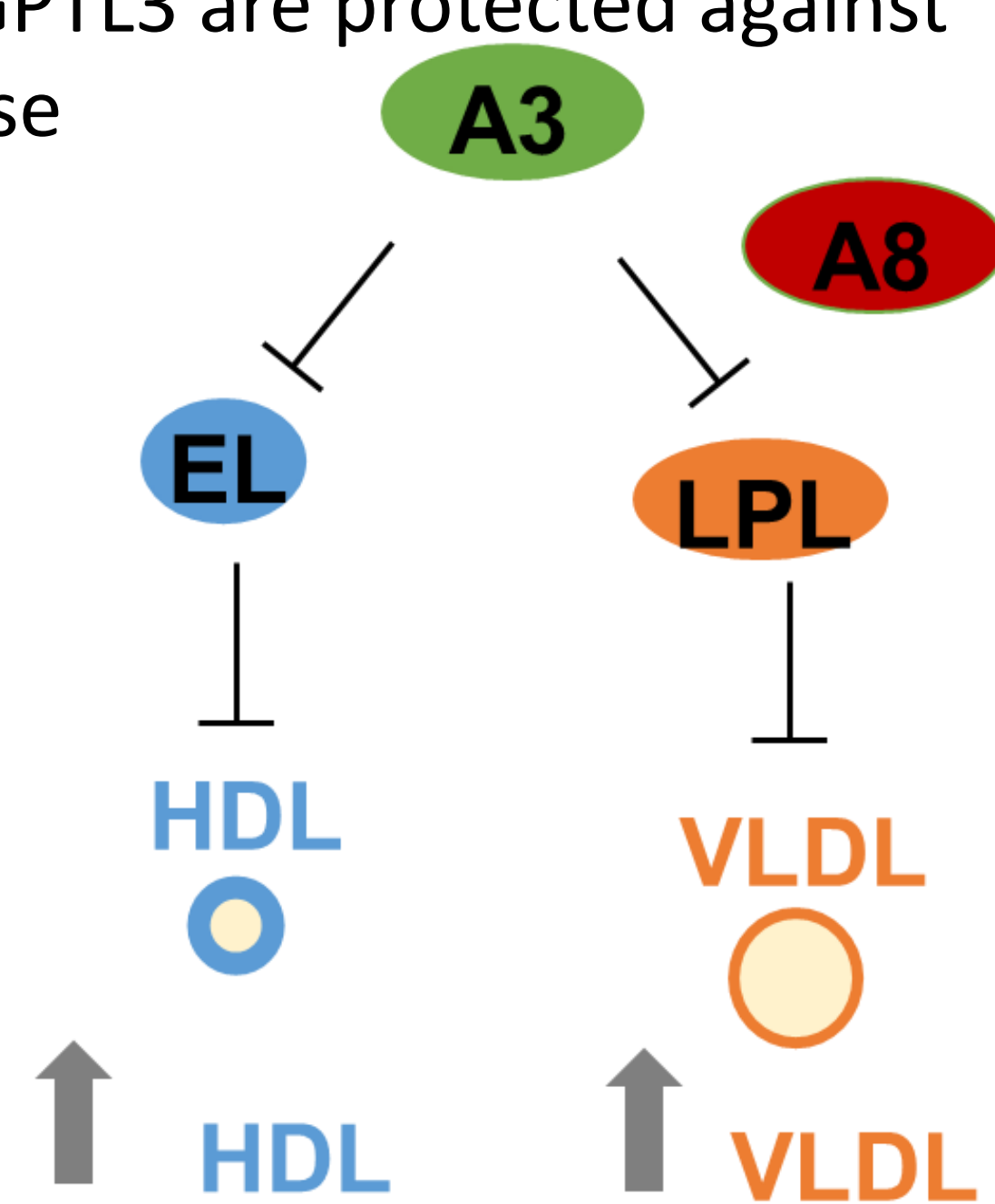
This study was funded by the National Center for Medical Rehabilitation Research within the National Institutes of Health: Grants R01-HD084645 and R01-HD082109. We thank the Secondary Student Training Program (SSTP) for providing us the opportunity to do research with Dr. Shields and his lab.

Background

- Chylomicrons/Very high-density lipoproteins (VLDL) transport fats to tissues (heart, muscle, adipose).
- High density lipoprotein (HDL) carries cholesterol to liver. High levels of HDL = lower risk of heart disease
- Endothelial lipase (EL) regulates and reduces HDL
- Lipoprotein lipase (LPL) is a critical enzyme that clears and reduces fat in the bloodstream.



- Angiotensin-like 3 (ANGPTL3) binds and inhibits EL causing an increase of HDL cholesterol in the bloodstream
- ANGPTL3 can form a complex with ANGPTL8 to bind and inhibit LPL and causes more fat to remain in the bloodstream
- Humans lacking ANGPTL3 are protected against cardiovascular disease



Objective

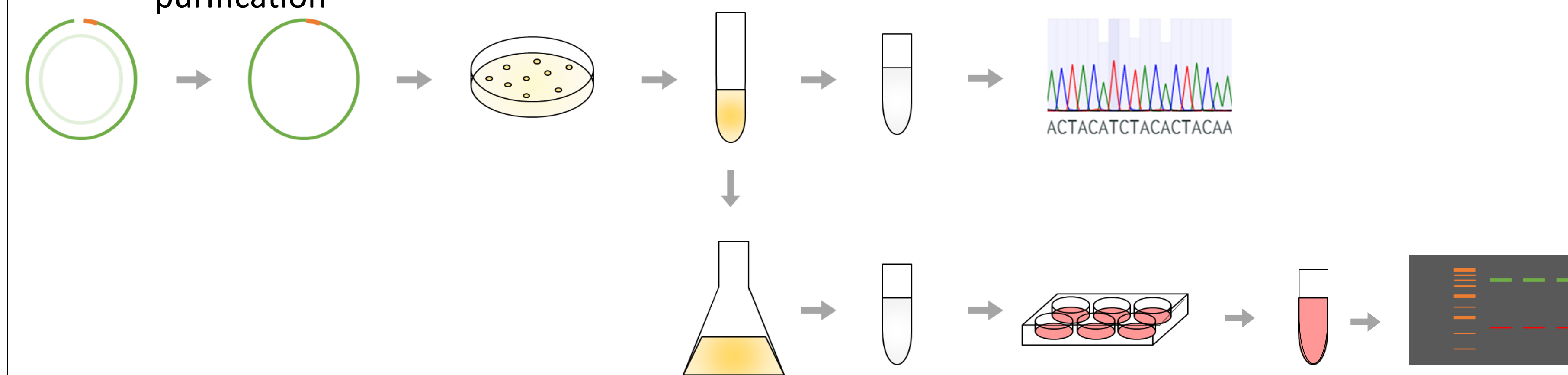
To identify regions and residues of ANGPTL3 required for binding and inhibition of LPL and EL



Mutation Goal
(amino acids 17-35)

Methods

1. Site-directed mutagenesis
 - PCR
 - Ligation
 - Transformation
 - Culture
 - Plasmid purification
 - Sequencing
 - Large scale plasmid purification
2. Protein Expression
 - Culture cells
 - Transfection
 - Harvesting
 - Western blot
3. Functional characterization
 - EL inhibition assay
 - LPL inhibition assay
 - EL binding assay



Results

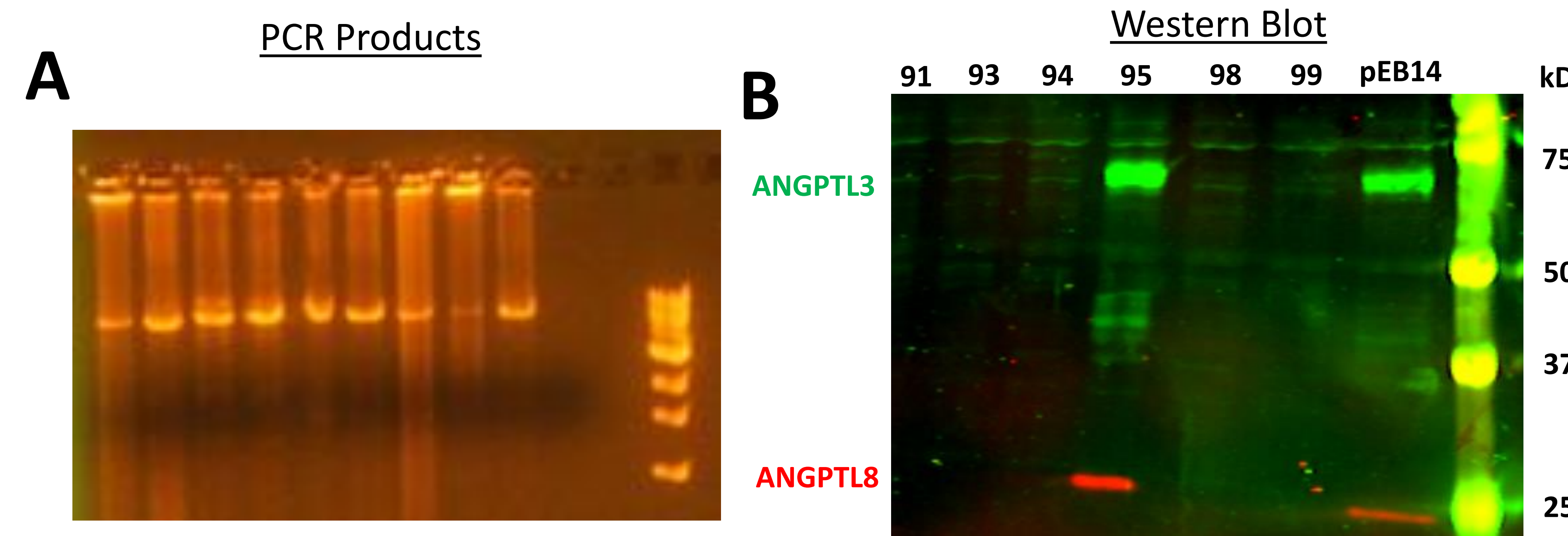


Figure 1. (A) PCR results mutants pA3A91-99. (B) Western blot set 1 cell media results. Protein was only expressed in mutant pA3A95 (S25A F26A) and wild-type ANGPTL3 (pEB14).

EL and LPL Inhibition Results

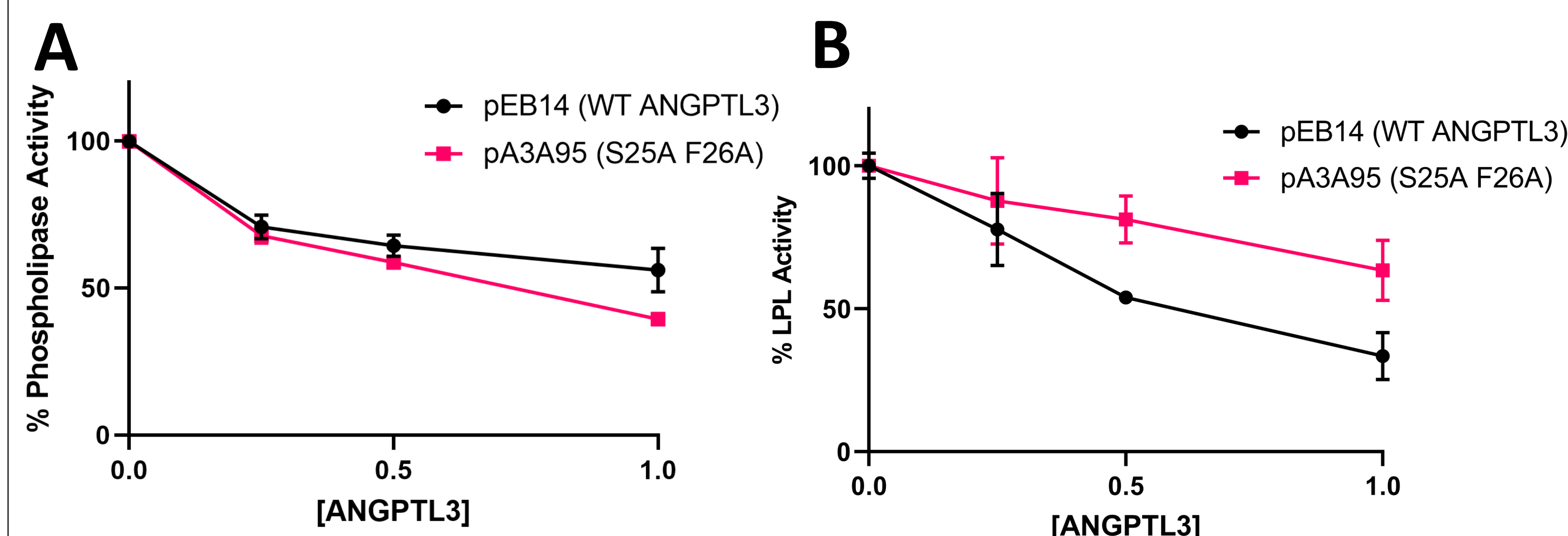


Figure 2. (A) Phospholipase activity of EL after incubation at 37 C for 30 minutes with increasing concentrations of wild-type or mutant ANGPTL3 (B) LPL activity after incubation with increasing concentrations of ANGPTL3 or ANGPTL3 (S25A F26A) in complex with ANGPTL8

EL Binding Assay Results

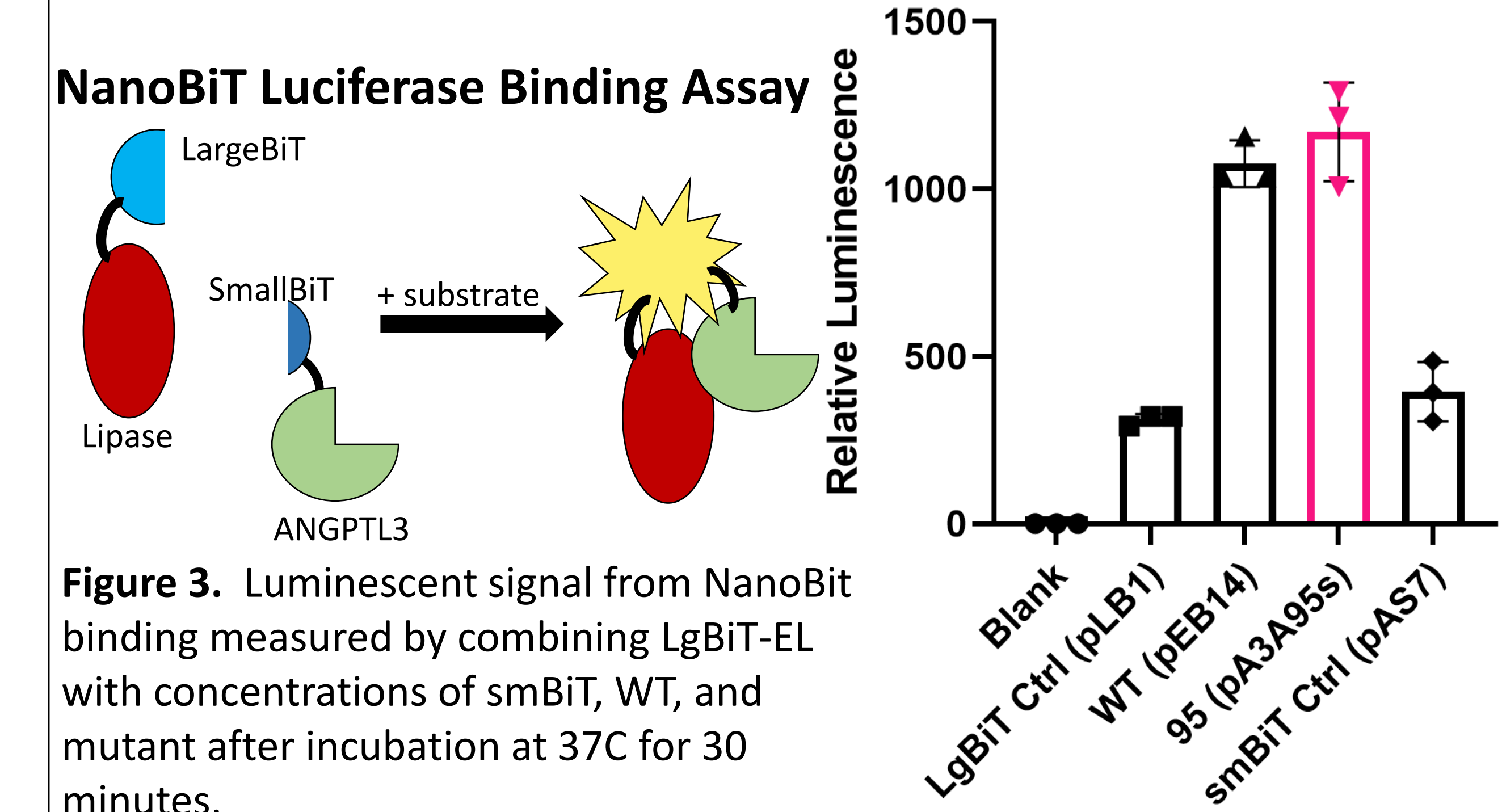


Figure 3. Luminescent signal from NanoBiT binding measured by combining LgBiT-EL with concentrations of smBiT, WT, and mutant after incubation at 37C for 30 minutes.

Conclusion

- ANGPTL3 mutant (S25A F26A) is defective against LPL inhibition
- Retains binding and inhibition of EL

Future directions

- Perform LPL binding assays
- Finish 9 mutants of N-terminal domain and combine data already collected by the lab to map out important residues.
- Test interesting mutants on mouse models to test the physiological effects

Acknowledgments



References

- Davie, K. L. (2021). The regulation of endothelial lipase and lipoprotein lipase by ANGPTL3 and ANGPTL8. *PhD Thesis*. <https://doi.org/10.17077/etd.006244>
- Li, Y., He, P.-P., Zhang, D.-W., Zheng, X.-L., Cayabyab, F. S., Yin, W.-D., & Tang, C.-K. (2014). Lipoprotein lipase: From gene to atherosclerosis. *Atherosclerosis*, 237(2), 597–608. <https://doi.org/10.1016/j.atherosclerosis.2014.10.016>
- Preiss-Landl, K., Zimmermann, R., Hämmerle, G., & Zechner, R. (2002). Lipoprotein lipase: The regulation of tissue specific expression and its role in lipid and energy metabolism. *Current Opinion in Lipidology*, 13(5), 471–481. <https://doi.org/10.1097/00041433-200210000-00002>
- Sylvers-Davie, K. L., & Davies, B. S. (2021). Regulation of lipoprotein metabolism by ANGPTL3, ANGPTL4, and ANGPTL8. *American Journal of Physiology-Endocrinology and Metabolism*, 321(4). <https://doi.org/10.1152/ajpendo.00195.2021>
- Wang, H., & Eckel, R. H. (2009). Lipoprotein lipase: From gene to obesity. *American Journal of Physiology-Endocrinology and Metabolism*, 297(2). <https://doi.org/10.1152/ajpendo.90920.2008>

PLANT UPTAKE RATES OF XENOBIOTIC COMPOUNDS WITH HIGHLY ELECTRONEGATIVE FUNCTIONAL GROUPS

Kaitlyn Roach¹, Dr. Gregory LeFevre², Sraboni Chowdhury²

¹Miramonte High School, Orinda, CA, ²Department of Civil and Environmental Engineering, University of Iowa

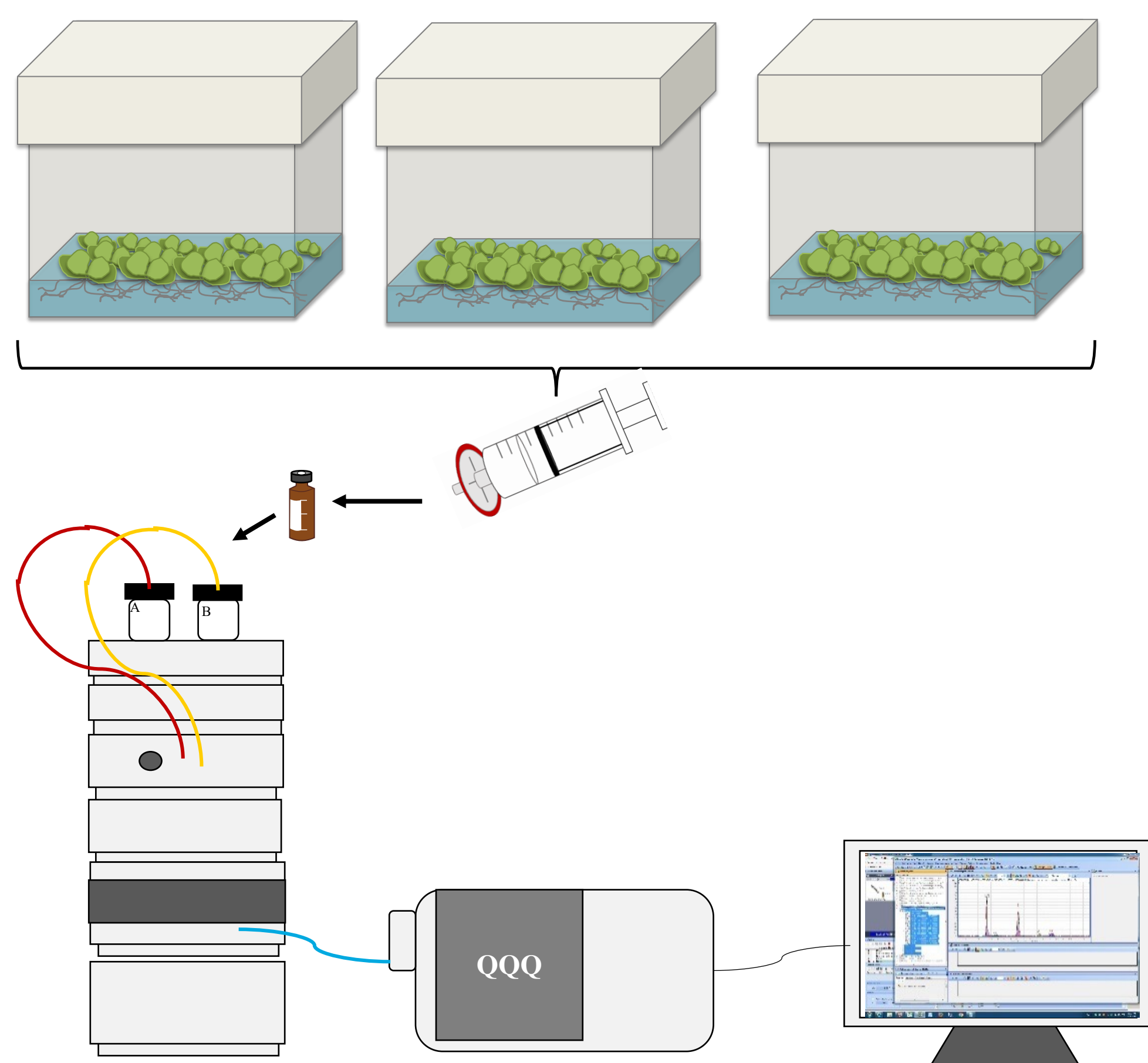
Introduction

Toxic chemicals and pollutants in stormwater runoff pose a large environmental threat, as they can degrade ecosystems, pollute drinking water, and lead to animal and human digestion of harmful chemicals. Plants are often used in storm water infrastructure to remove harmful compounds, and sometimes crops will be irrigated with recycled water containing such contaminants. For this reason, understanding plant uptake of such chemicals is important not only for the fate of the environment but also to comprehend what happens if chemicals are later consumed by humans. Plants can take up compounds from the environment using transpiration, but they also contain specialized transporters to uptake nutrients and xenobiotics at faster rates.

However, there is a lack of information regarding how plant uptake of xenobiotics varies based on a chemical's functional group position and electrostatic nature. The purpose of this study was to explore plant uptake of compounds with highly electronegative electron withdrawing groups.

Method

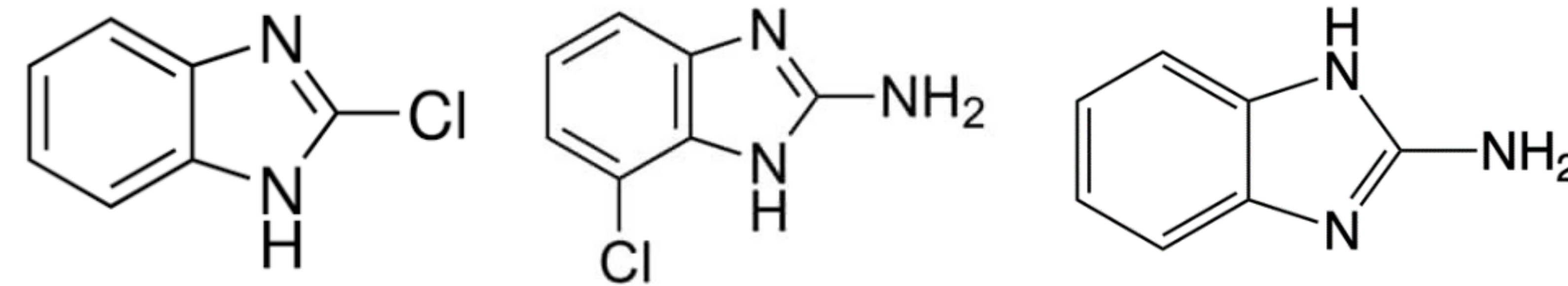
- *Arabidopsis thaliana* seeds were sterilized and grown in autoclaved Magenta boxes with a growth medium for 10 days
- For each chemical (2-Chlorobenzimidazole, 2-Amino-7-chloro-1H-benzimidazole, or 2-Amino benzimidazole), there were
 - 4 boxes of plants with spiked growth medium
 - 3 boxes used as negative controls (no plants)
 - 3 boxes of plants used for sorption experiment
- Growth medium with spiked chemicals was sampled every couple of hours over a 48-hour time period
- Samples were analyzed using an LC-MS/MS machine



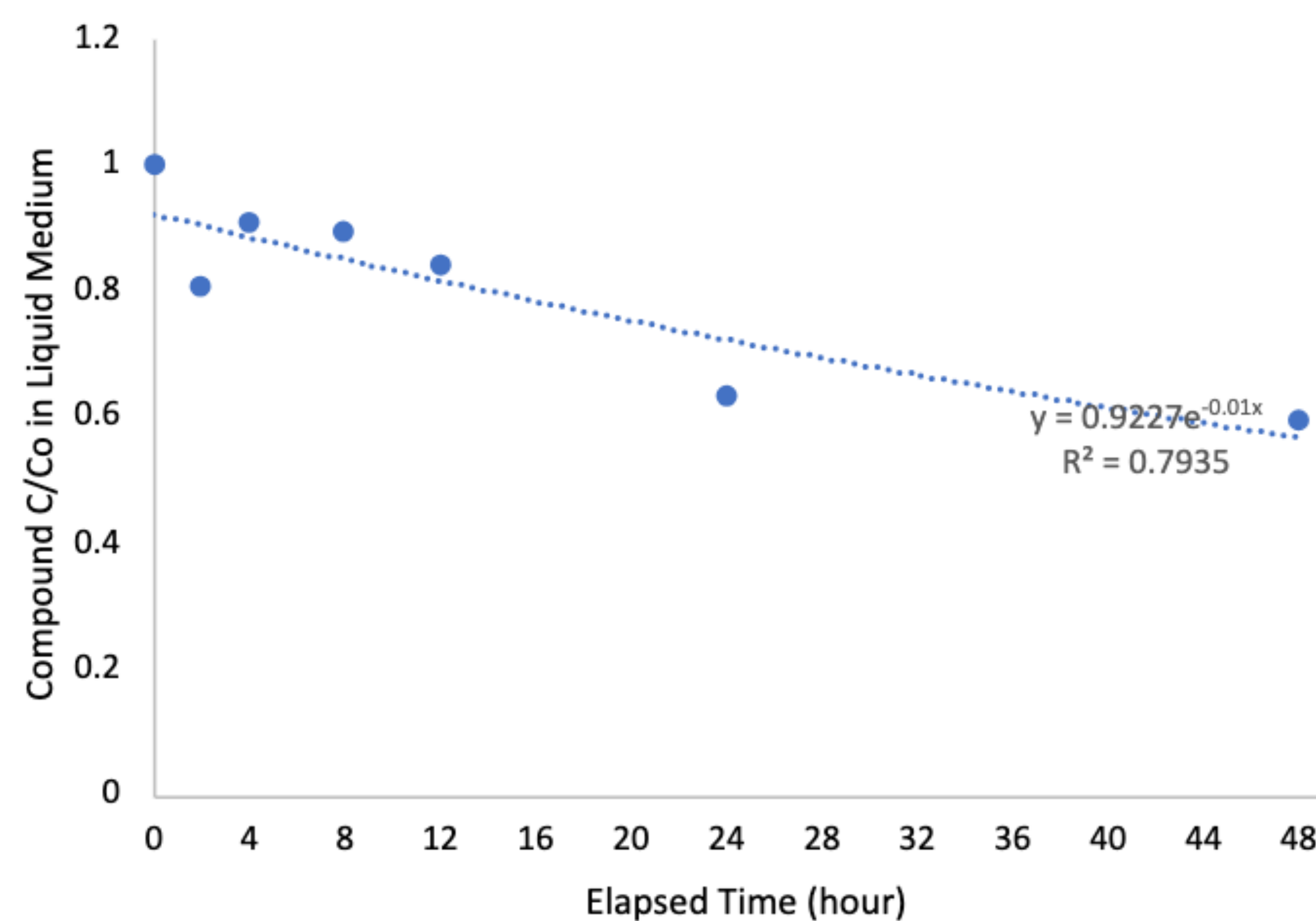
Results

Chemicals tested in this study:

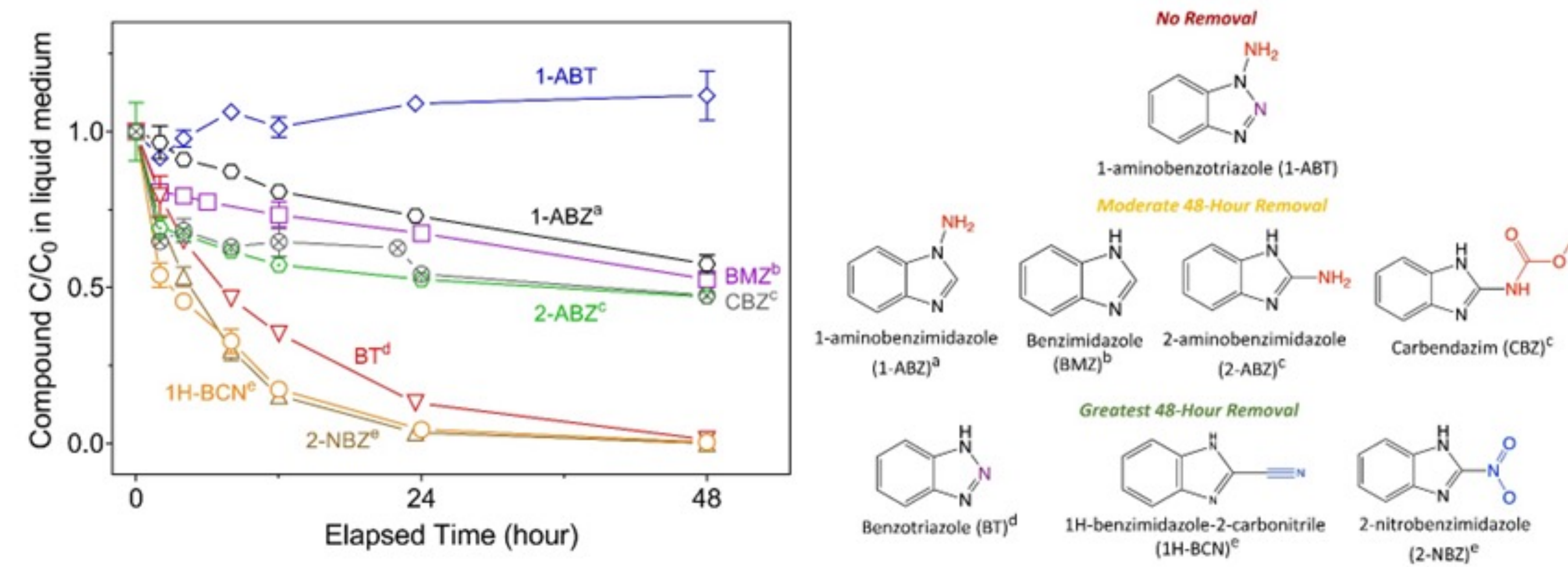
2-chlorobenzimidazole 2-Amino-7-chloro-1H-benzimidazole 2-Amino benzimidazole



Plant Uptake Rate of 2-Chlorobenzimidazole

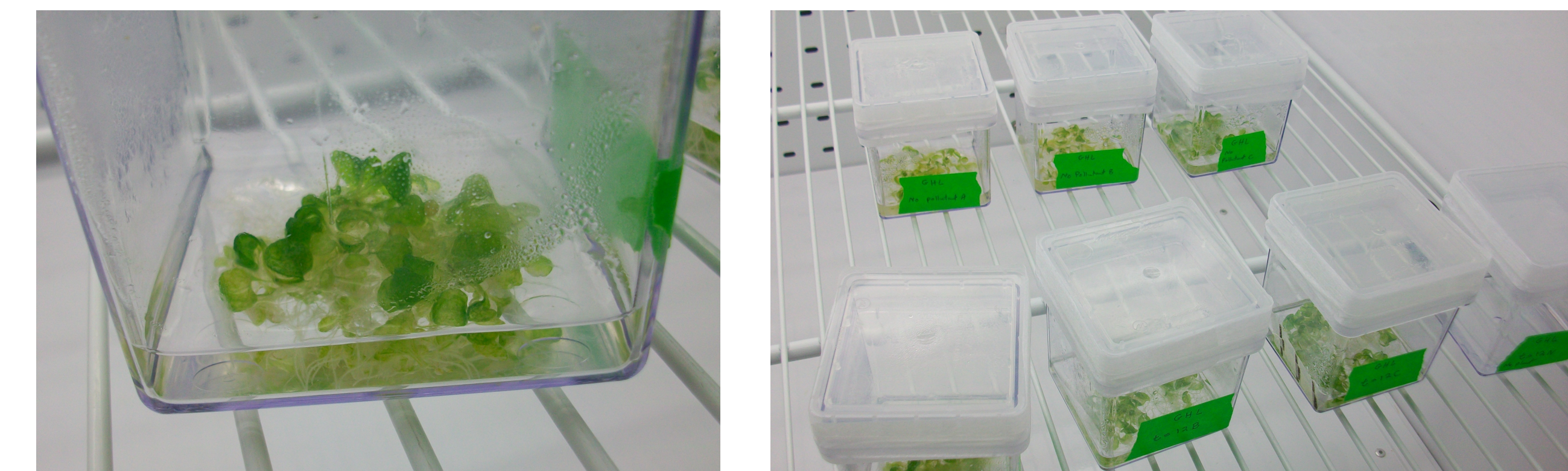


Plant Uptake Rates of Benzimidazoles Over Time – Previous Lab Research



Conclusion

- The position and electrostatic nature of functional groups play an important role in the rate at which plants uptake chemicals
- Specifically, compounds with highly electronegative electron withdrawing groups are taken in rapidly by plants
- This information can help create future plant uptake models, which will allow for more informed phytoremediation efforts and increased understanding about human exposure to toxic chemicals when plants are grown with recycled water



Future Research

- Extracted plant tissue from the experiment should be tested to determine what metabolites were created after plants took up chemicals from the growth medium, since plants often transform chemicals into glycosylated or amino acid conjugates
- Plant uptake measurements for benzimidazoles with highly electronegative withdrawing groups should be thoroughly compared with plant uptake measurements for benzimidazoles with functional groups in different positions and differing electrostatic natures
- Using such comparisons, a model should be created in order to predict how plants will uptake a wide variety of contaminants based on their chemical structures

References

- Kepler, S., Huynh, K., Reinhold, D., & Bornhorst, G. M. (2021). Fate of Phytometabolites of Antibiotics during In Vitro Digestion and Implications for Human Health. *Journal of Agricultural and Food Chemistry*, 69(43), 12598–12607. <https://doi.org/10.1021/acs.jafc.1c03934>
- LeFevre, G. H., Müller, C. E., Li, R. J., Luthy, R. G., & Sattely, E. S. (2015). Rapid Phytotransformation of Benzotriazole Generates Synthetic Tryptophan and Auxin Analogs in Arabidopsis. *Environmental Science & Technology*, 49(18), 10959–10968. <https://doi.org/10.1021/acs.est.5b02749>
- Muerdter, C. P., Wong, C. K., & LeFevre, G. H. (2018). Emerging investigator series: the role of vegetation in bioremediation for stormwater treatment in the built environment: pollutant removal, hydrologic function, and ancillary benefits. *Environmental Science: Water Research & Technology*, 4(5), 592–612. <https://doi.org/10.1039/c7ew00511c>



Gene-Based and Pathway-Based Analysis of GWAS Data Identifies Candidate Genes and Processes Involved in Non-syndromic Orofacial Clefts of African Populations

Anmol Singhal^{1,2}; Azeez Alade¹, BS, DDS, MS; Tamara Busch¹, BS, MS; Abimbola Oladayo¹, DDS, MS; Waheed Awotoye¹, DDS, PhD; Emmanuel Aladenika¹, BS, DDS; Anjolaoluwa Awe¹; Jorge Ceballos¹, BS; Lord Gowans¹, MS, PhD; Mekonen Eshete¹, MD, PhD; Lanre Adeyemo¹, DDS, PhD; Azeez Butali¹, DDS, PhD

¹Department of Oral Pathology, Radiology, and Medicine, University of Iowa, ²Mira Loma High School

Introduction

- Non-syndromic orofacial clefts include cleft lip only (CLO), cleft lip and palate (CLP) and cleft palate only (CPO). Collectively, these are the most common craniofacial birth defects in humans, affecting approximately 1/800 live births worldwide (Rahimov, Jugessur, and Murray, 2012).
- Genome-wide association study (GWAS) is an approach used to search for small variations called single-nucleotide polymorphisms (SNPs) that are associated with a phenotype within a population.
- GWAS does not completely reveal the genetic etiology of orofacial clefts, so additional strategies including gene and pathway-based analysis are currently being employed (Mishra and MacGregor, 2015).
- We utilized the African cleft GWAS summary data (Butali et al., 2019) to identify genes and pathways involved in the pathogenesis of orofacial clefts.

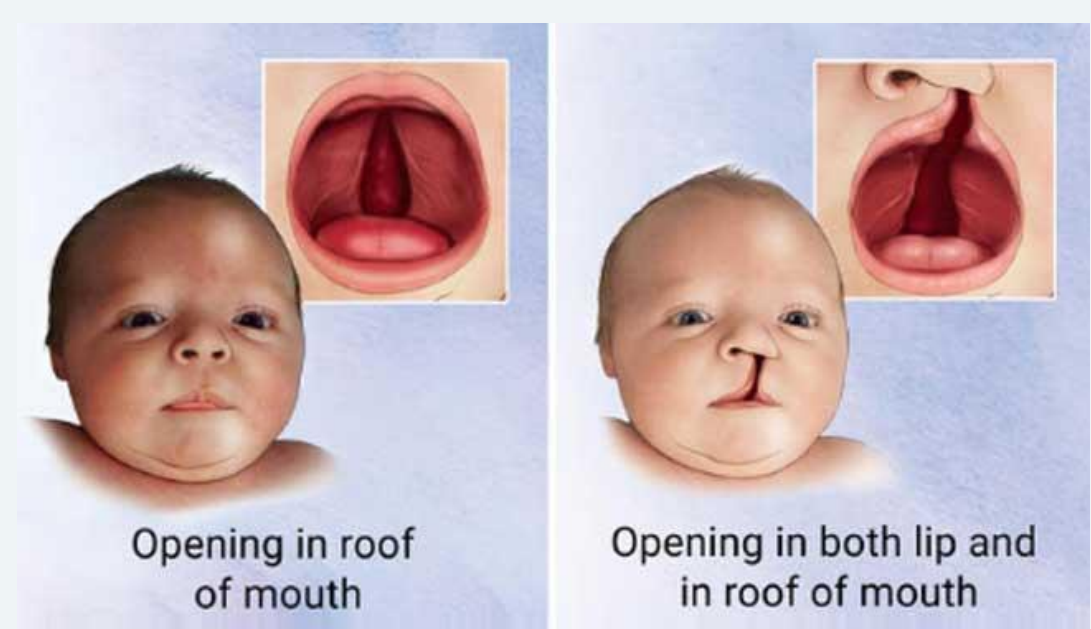
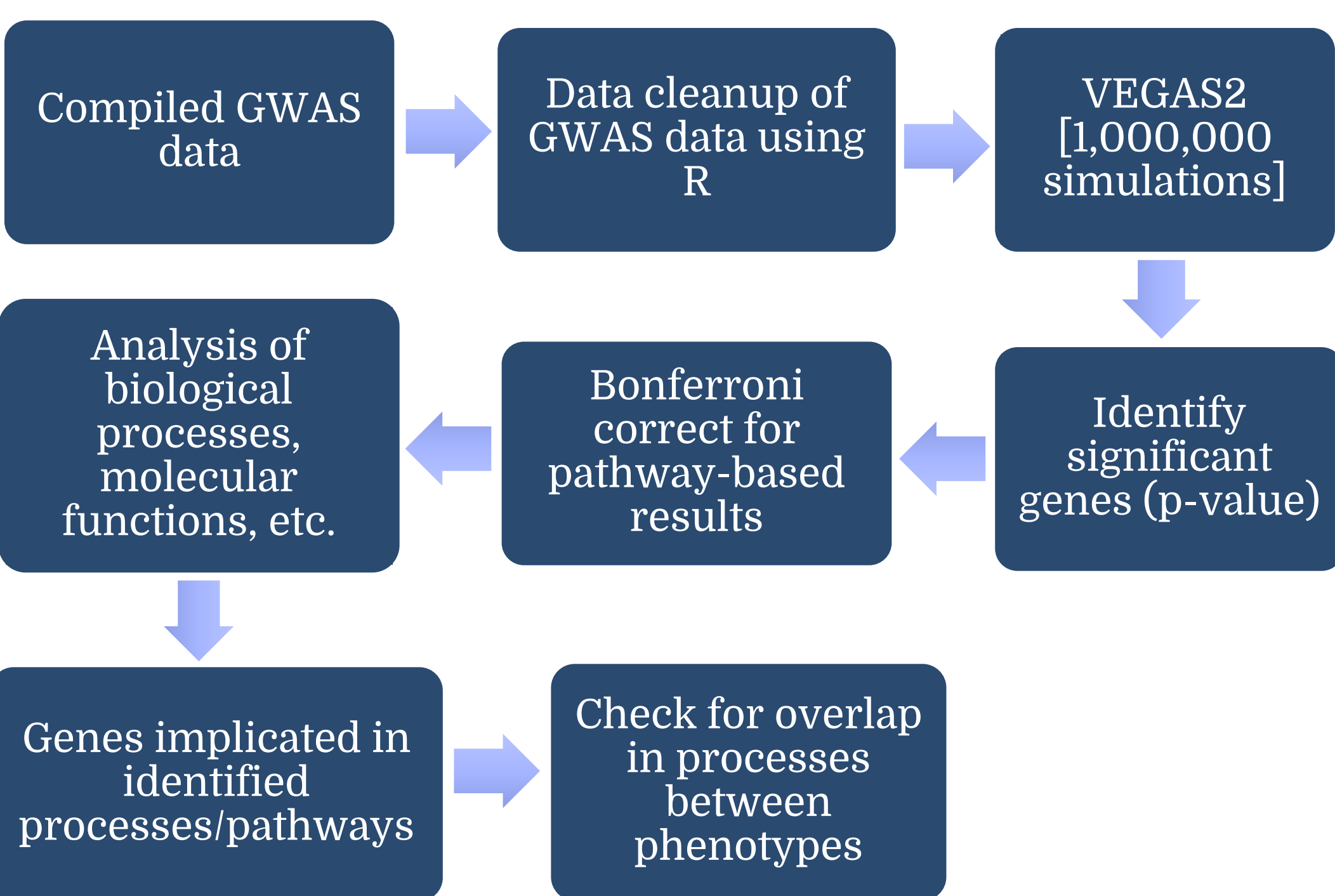


Figure 1: Images displaying the physical appearance of cleft palate only (CPO) (left) and cleft lip or cleft lip and palate (CL/P) (right)

Image Credit: Apollo Hospital

Methods



VEGAS2 Software

Versatile Gene-Based Association Study - 2 [VEGAS2]

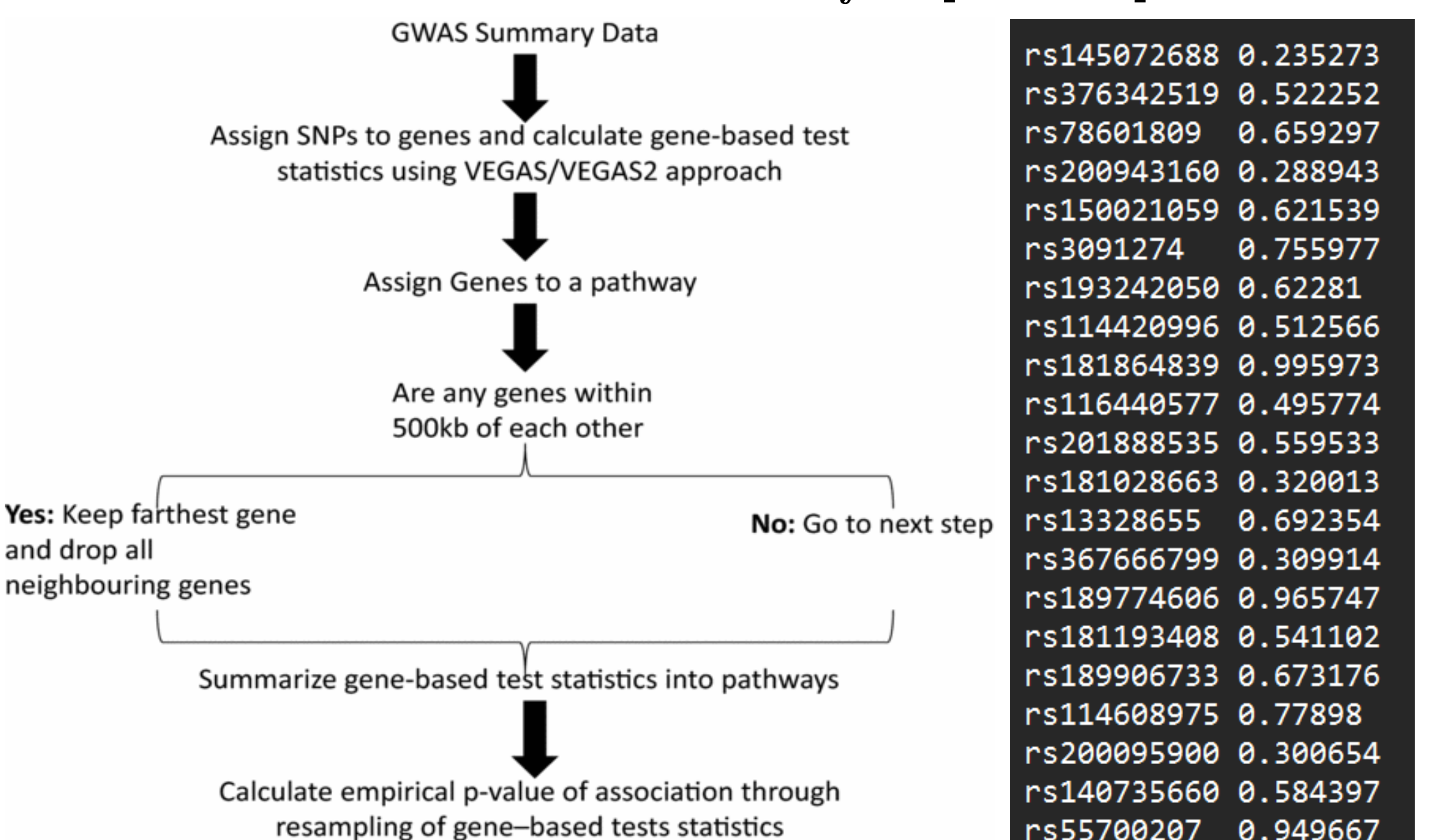


Figure 2a: This pathway outlines how VEGAS2 processes the inputted GWAS data.

Figure 2b: Sample input file (.txt) of processed GWAS data (SNP id on the left, associated p-value on the right)

Image Credit: Mishra and MacGregor, 2017

Results

Gene-Based

Significant Genes Involved in CL/P				
Gene	nSNPs	p-value	TOPSNP	TOPSNP.Pvalue
CTDSP2	4	4.10E-05	rs75066937	2.02E-05
VPS45	19	4.70E-05	rs112640811	7.06E-06
ALG14	3	7.10E-05	rs149853734	7.41E-05
N4BP2L1	3	7.40E-05	rs206323	4.83E-05
IFT22	7	8.80E-05	rs115968752	4.46E-05

Table 1: Candidate genes for CL/P with significant p-values**

Significant Genes Involved in CPO				
Gene	nSNPs	p-value	TOPSNP	TOPSNP.Pvalue
SULT2A1	4	1.00E-06	rs62529857	7.84E-08
LRMP	5	3.00E-06	rs115543267	1.16E-06
OPALIN	4	4.00E-06	rs11597348	3.66E-07
DNTT	8	5.00E-06	rs2273891	6.73E-07
LOC643542	2	8.00E-06	rs77554717	2.68E-07
WDR64	3	8.00E-06	rs12565867	4.43E-06
PPP2R2C	10	8.00E-06	rs73207824	8.33E-07

Table 2: Candidate genes for CPO with significant p-values**

Pathway-Based

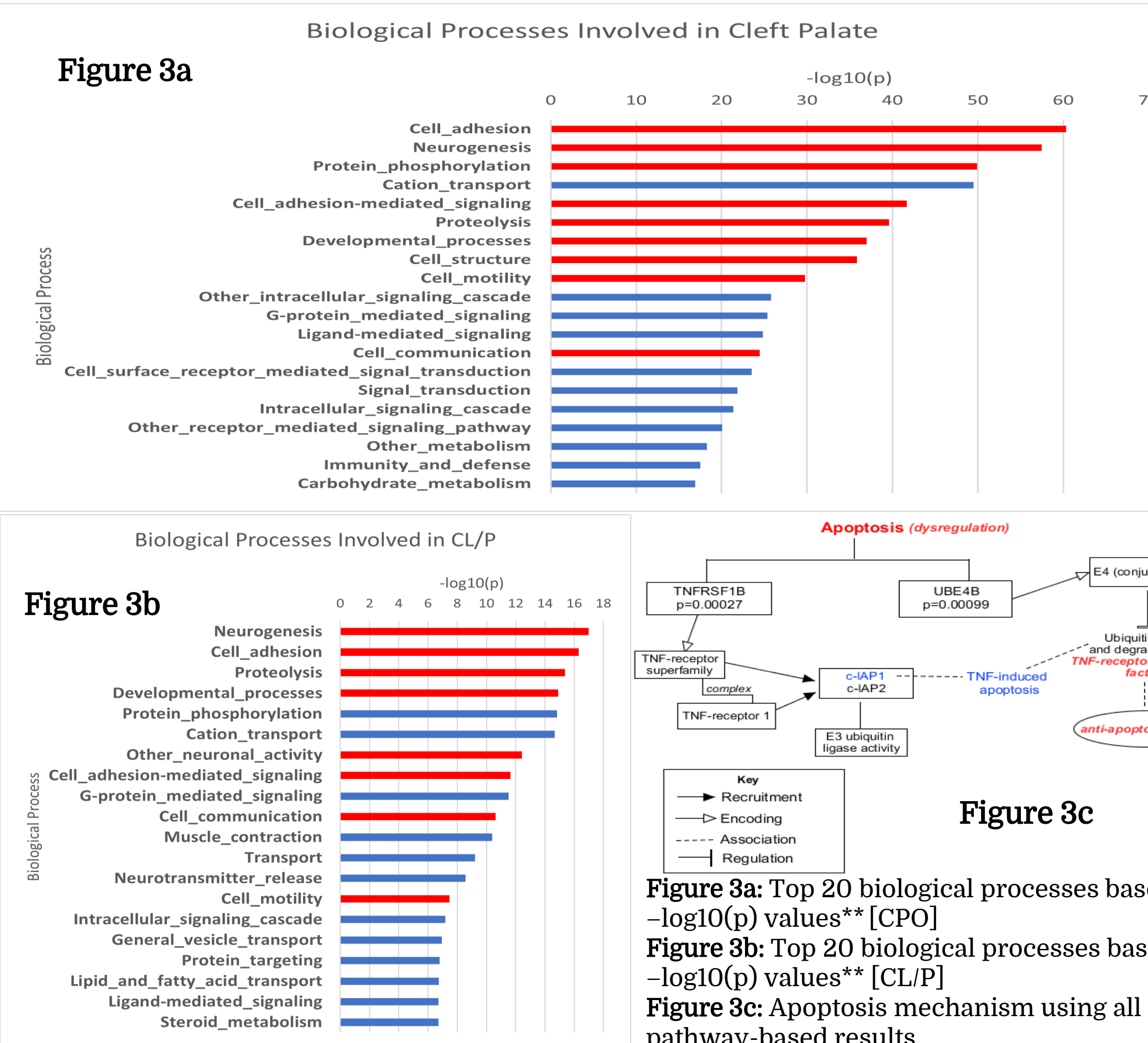


Figure 3a

Figure 3b

Figure 3c

Overlaps in Processes Between CL/P and CPO

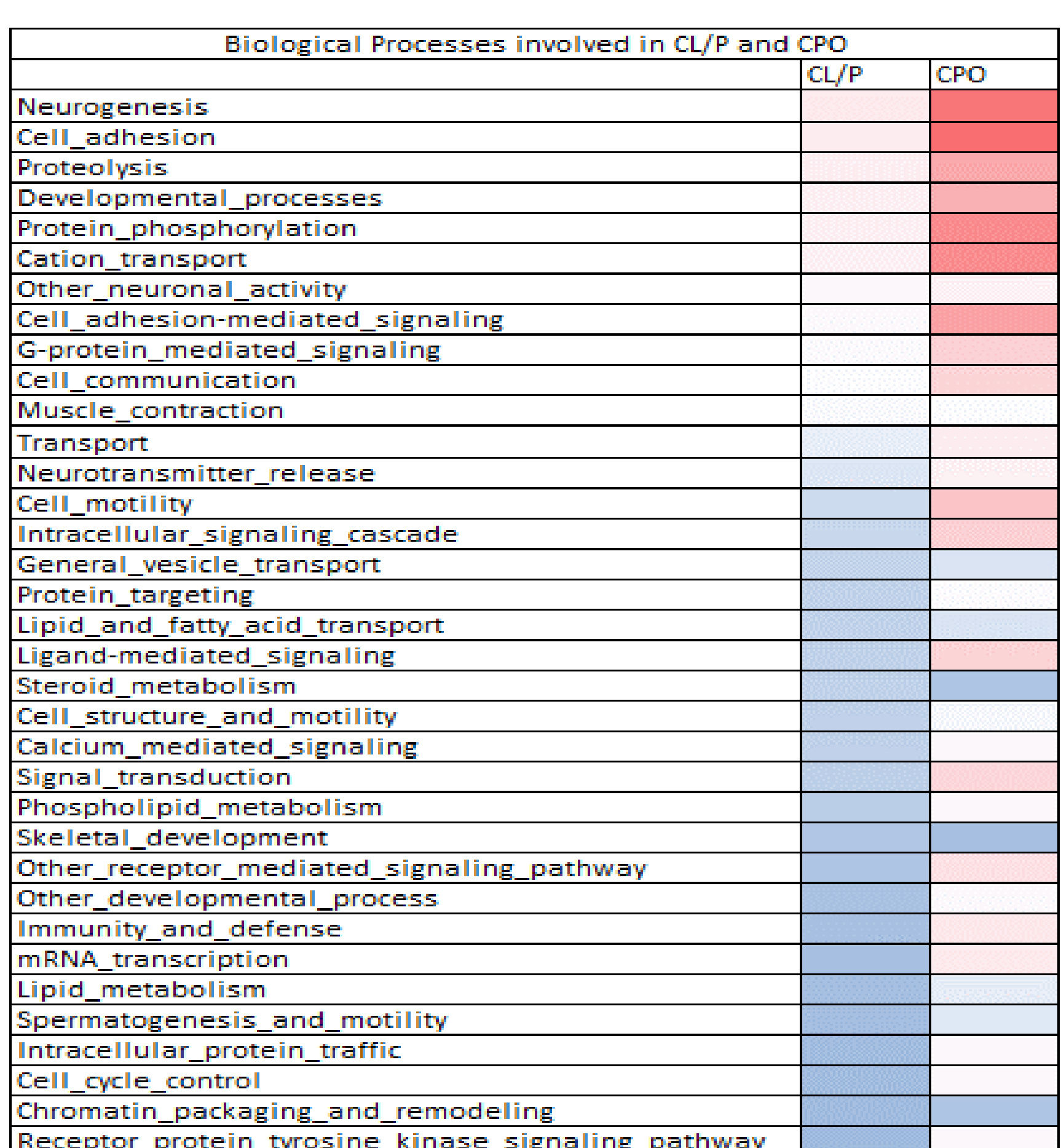


Figure 4a: Comparison of biological processes involved in CL/P and CPO

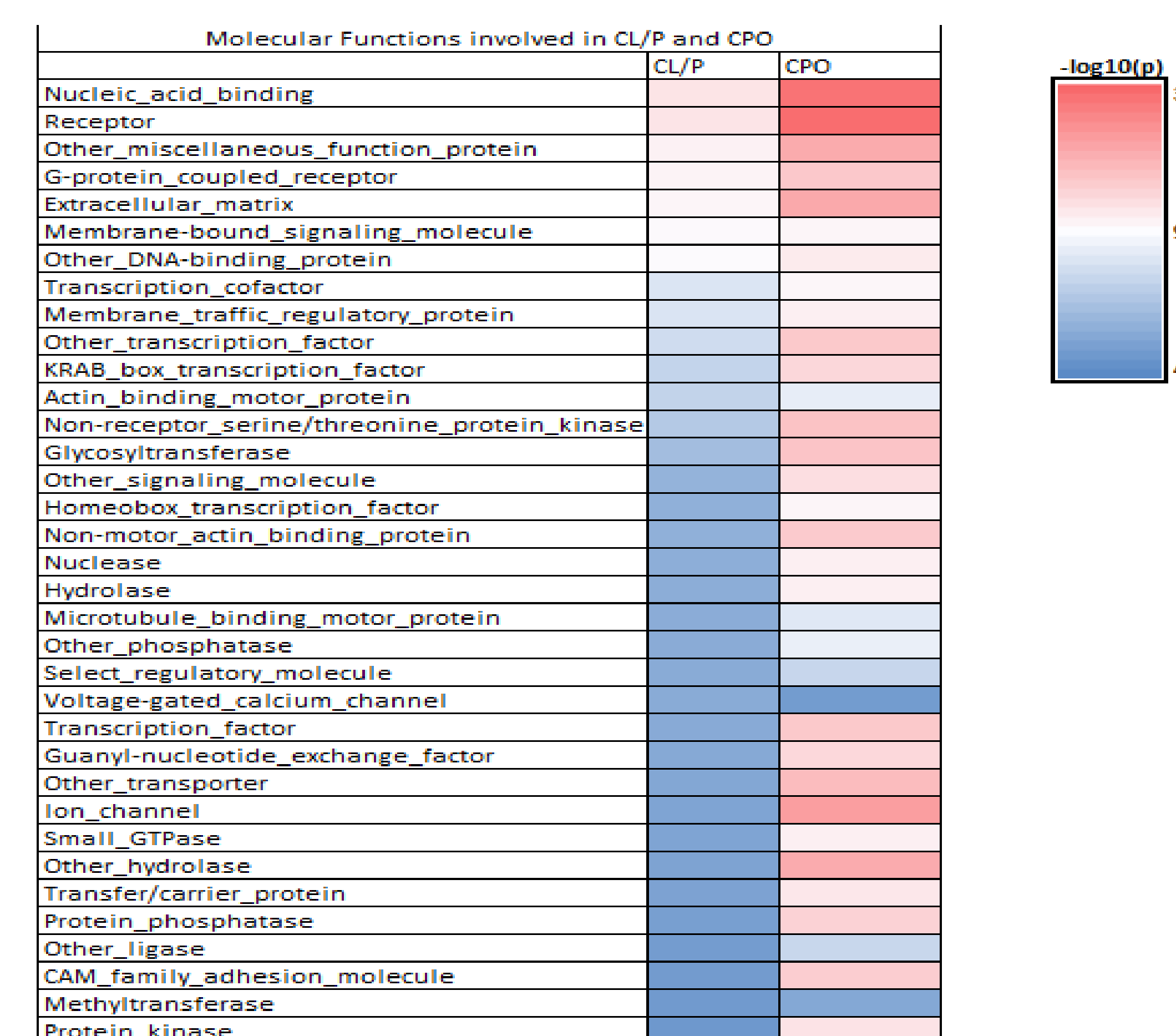


Figure 4b: Comparison of molecular functions involved in CL/P and CPO

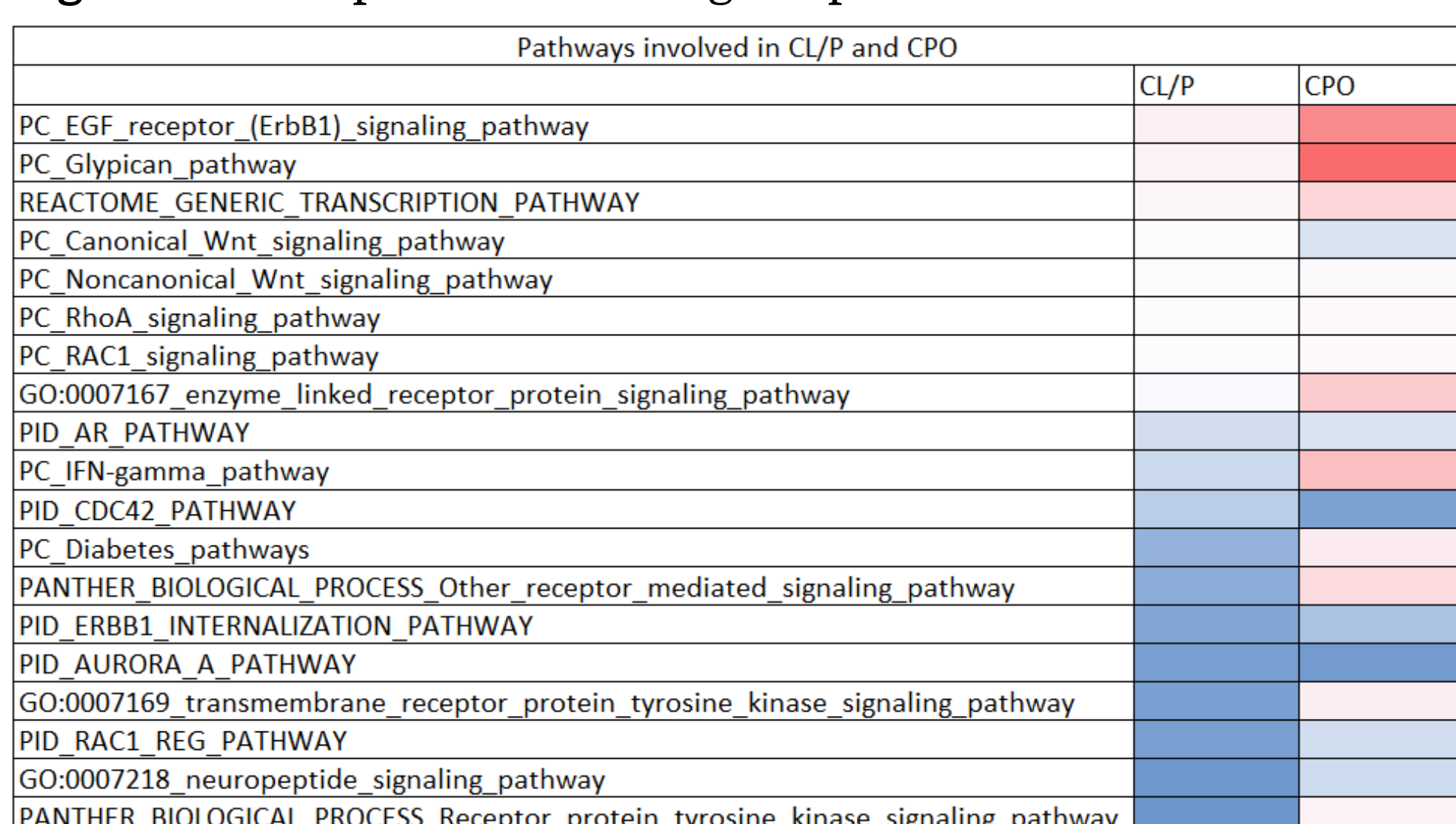


Figure 4c: Comparison of pathways involved in CL/P and CPO

Trend: Majority of the processes show stronger association with CPO than CL/P. In gene-based results, more genes showed association with CPO compared to CL/P. This translates to having more pathway genes in CPO than CL/P. **Example - Neurogenesis CL/P:** 9 genes involved **CPO:** 30 genes involved **Limitation:** To compare phenotypes, the list of genes should be of equal length

Processes previously noted in literature to be associated with orofacial clefts (PMID)
Cell adhesion (32725806, 35205020)
Neurogenesis (28106045)
Developmental process (28106045)
Cell motility (32725806)
Proteolysis (32725806)
Cell adhesion mediated signaling (35205020)
Cell communication (32666711)



For supplementary materials such as additional data, scan the QR code on the left.

**For more graphs, tables, detailed pathway diagrams see supplementary data folder

Conclusion

- Pathway-based analysis of genome-wide association study data confirm known pathways and genes involved in orofacial clefts.
- Data shows that disease is polygenic and multiple genes work together to express the function of a specific process, ultimately causing malformations in the embryonic development stage.
- Performing pathway analysis allows us to identify novel biological processes and map out the cause of orofacial clefts, allowing us to intervene at the pathway level.
- Certain genes may only be associated with specific developmental processes (palatal, cleft lip only, both palate and lip), so the difference in strength of association of processes is due to the varying genetic etiology between the cleft phenotypes.

Limitation

This approach searches for genes associated with a SNP in a set haplotype block of 500kb around the targeted SNP. Specifying stringent boundaries, however, may not fully capture regulatory regions or those SNPs in high LD with variants in the gene (Liu et al., 2010).

Future Directions

- Gene knockout models
- Novel therapeutic approaches
- Mechanistic intervention
- Establish markers to identify abnormalities
- Prenatal diagnosis and genetic counseling

Acknowledgements

Special thanks to Azeez Alade, Tamara Busch, Dr. Butali, and the Butali Lab on their guidance in my research experience. Thank you to the Belin-Blank Center and SSTP for their exceptional hospitality outside of research hours. This project was supported by NIH/NIDCR DE028300.

References

Butali, A., Mossey, P. A., Adeyemo, W. L., Eshete, M. A., Gowans, L., Busch, T. D., Jain, D., Yu, W., Huan, L., Laurie, C. A., Laurie, C. C., Nelson, S., Li, M., Sanchez-Lara, P. A., Magee, W. P., Magee, K. S., Auslander, A., Brindopke, F., Kay, D. M., Caggana, M., ... Adeyemo, A. A. (2019). Genomic analyses in African populations identify novel risk loci for cleft palate. *Human molecular genetics*, 28(6), 1038–1051. <https://doi.org/10.1093/hmg/ddy402>

Liu, J. Z., McRae, A. F., Nyholt, D. R., Medland, S. E., Wray, N. R., Brown, K. M., AMFS Investigators, Hayward, N. K., Montgomery, G. W., Visscher, P. M., Martin, N. G., & Macgregor, S. (2010). A versatile gene-based test for genome-wide association studies. *American journal of human genetics*, 87(1), 139–145. <https://doi.org/10.1016/j.ajhg.2010.06.009>

Mishra, A., & Macgregor, S. (2015). VEGAS2: Software for More Flexible Gene-Based Testing. *Twin Research and Human Genetics*, 18(1), 80–91. [doi:10.1017/thg.2014.79](https://doi.org/10.1017/thg.2014.79)

Mishra, A., & Macgregor, S. (2017). A Novel Approach for Pathway Analysis of GWAS Data Highlights Role of BMP Signaling and Muscle Cell Differentiation in Colorectal Cancer Susceptibility. *Twin Research and Human Genetics*, 20(1), 1–9. [doi:10.1017/thg.2016.100](https://doi.org/10.1017/thg.2016.100)

Rahimov, F., Jugessur, A., & Murray, J. C. (2012). Genetics of nonsyndromic orofacial clefts. *The Cleft palate-craniofacial journal: official publication of the American Cleft Palate-Craniofacial Association*, 49(1), 73–91. <https://doi.org/10.1597/10-178>

Improving Polygenic Risk Prediction by Accounting for Ancestral Background

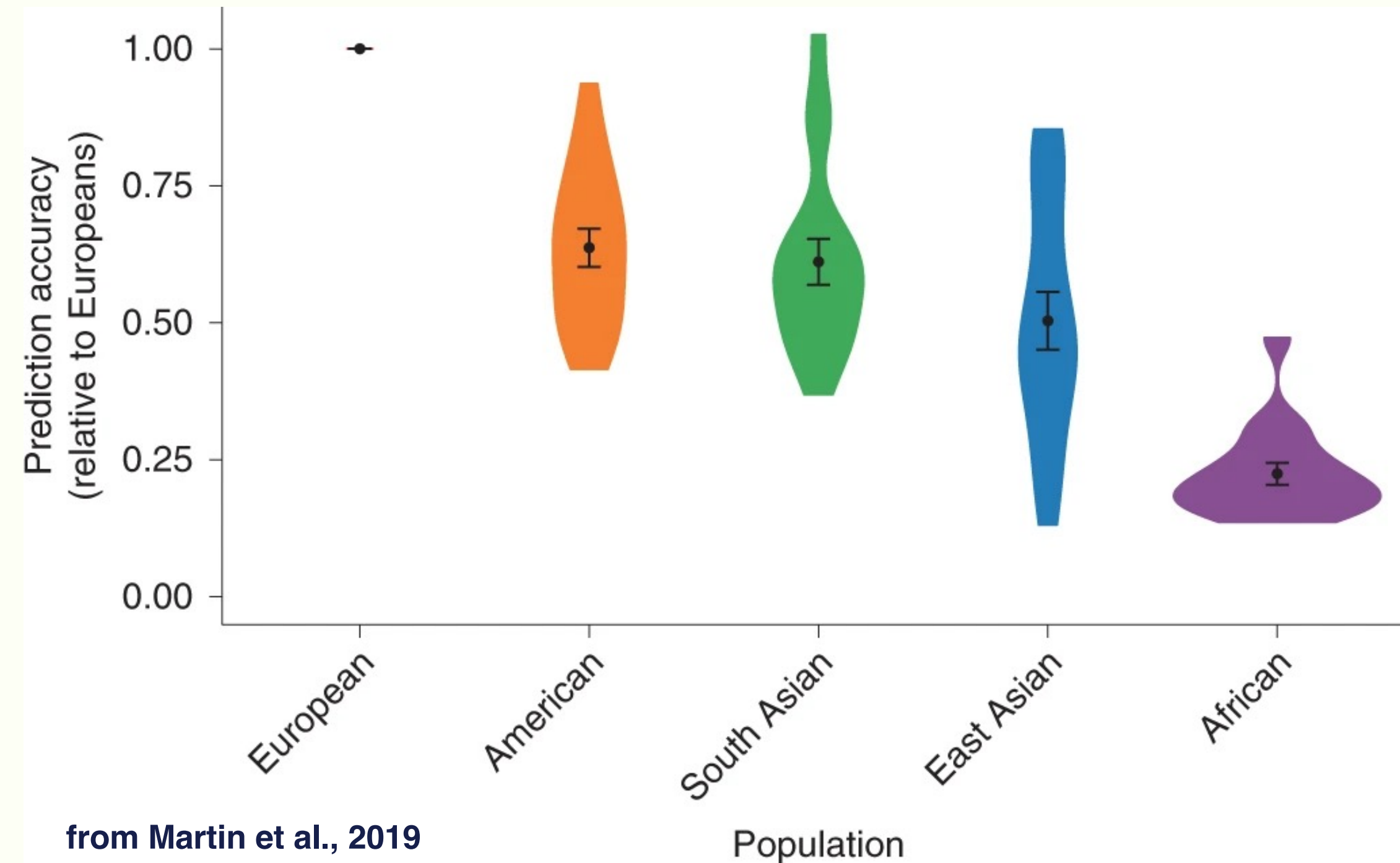
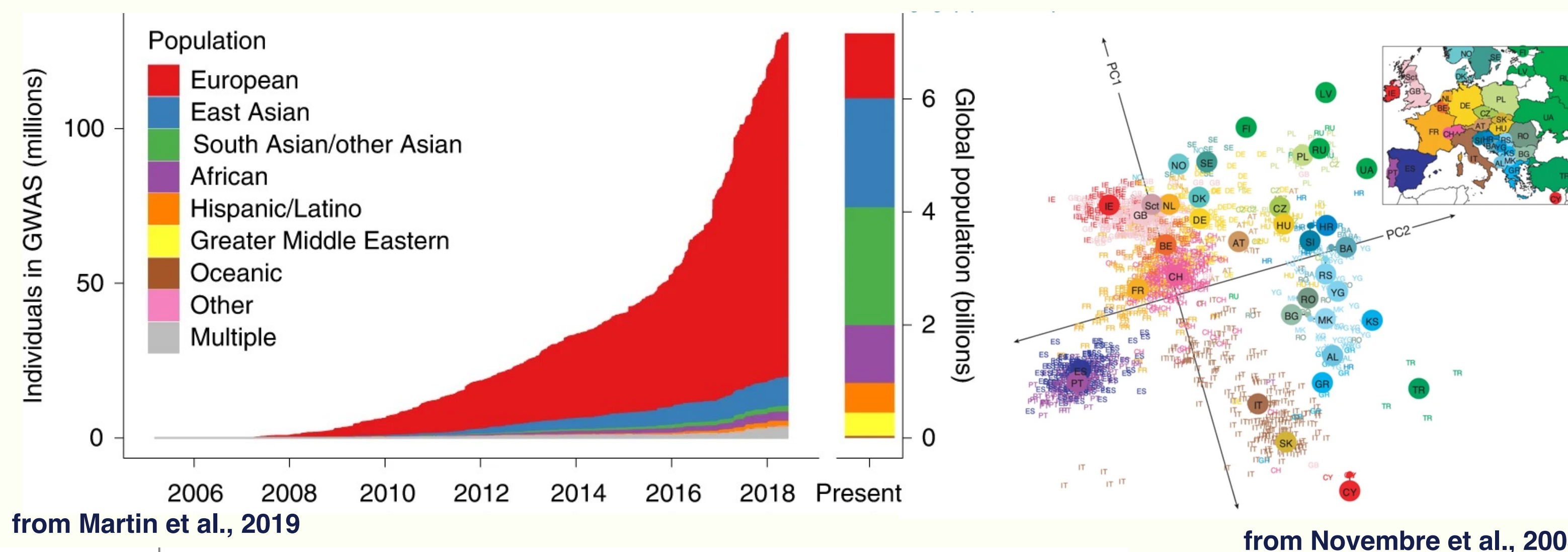
^aBriarcliff High School, NY
^bDepartment of Psychiatry
^cDepartment of Communication Sciences and Disorders
^dIowa Neuroscience Institute
 University of Iowa

IOWA

Mirabel Solomon^a, Lucas Casten^b, Ethan Bahl^b,
 Jacob J. Michaelson^{b,c,d}

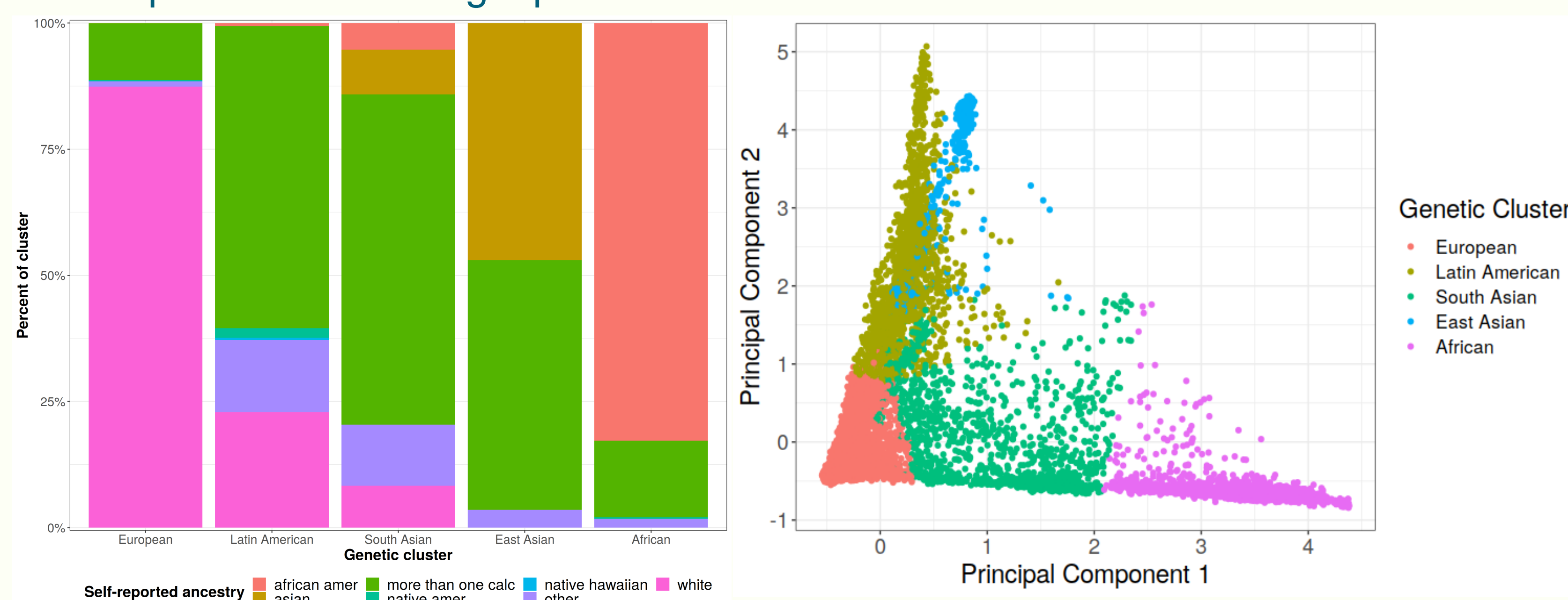
Background

- Calculating polygenic risk scores is a useful method for determining whether someone is at a high risk of developing a certain disease based on their genetic makeup.
- There is a **lack of diversity** in GWAS samples that has a much higher proportion of European samples than the actual makeup of the world population.
- There is a correlation between geographic and genetic distributions of people
- This leads to a **higher prediction accuracy in people of European descent** than people of other ethnicities.
- How can polygenic risk scores be more accurate for people of not just European descent?



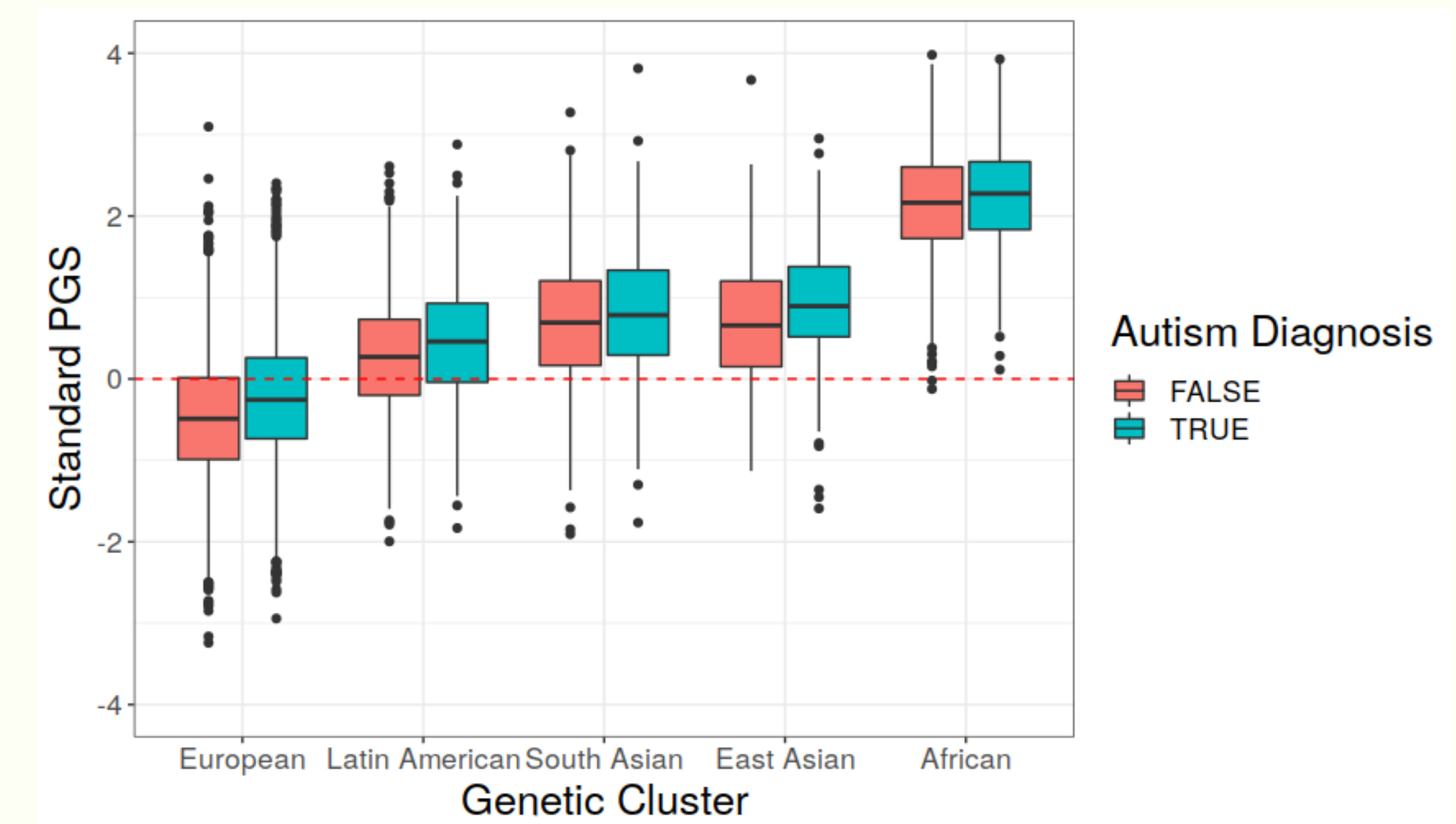
Methods

- The **SPARK cohort** facilitates studies involving large numbers of participants diagnosed with autism spectrum disorder (ASD). The **ABCD cohort** studies brain development and child health in the United States
- The ABCD cohort was genotyped on the Affymetrix NIDA SmokeScreen Array³ and processed through standard QC steps, such as removing low quality SNPs in samples. The quality-controlled set of SNPs were then imputed to the TopMed reference panel⁴
- The remaining individuals were **stratified into five “clusters” based on their principal components (PCs) from the combined HapMap and 1000 Genomes PCs⁵**
- Polygenic scores were then calculated from the imputed data using LDpred2⁶ and the bigsnpr tools in R



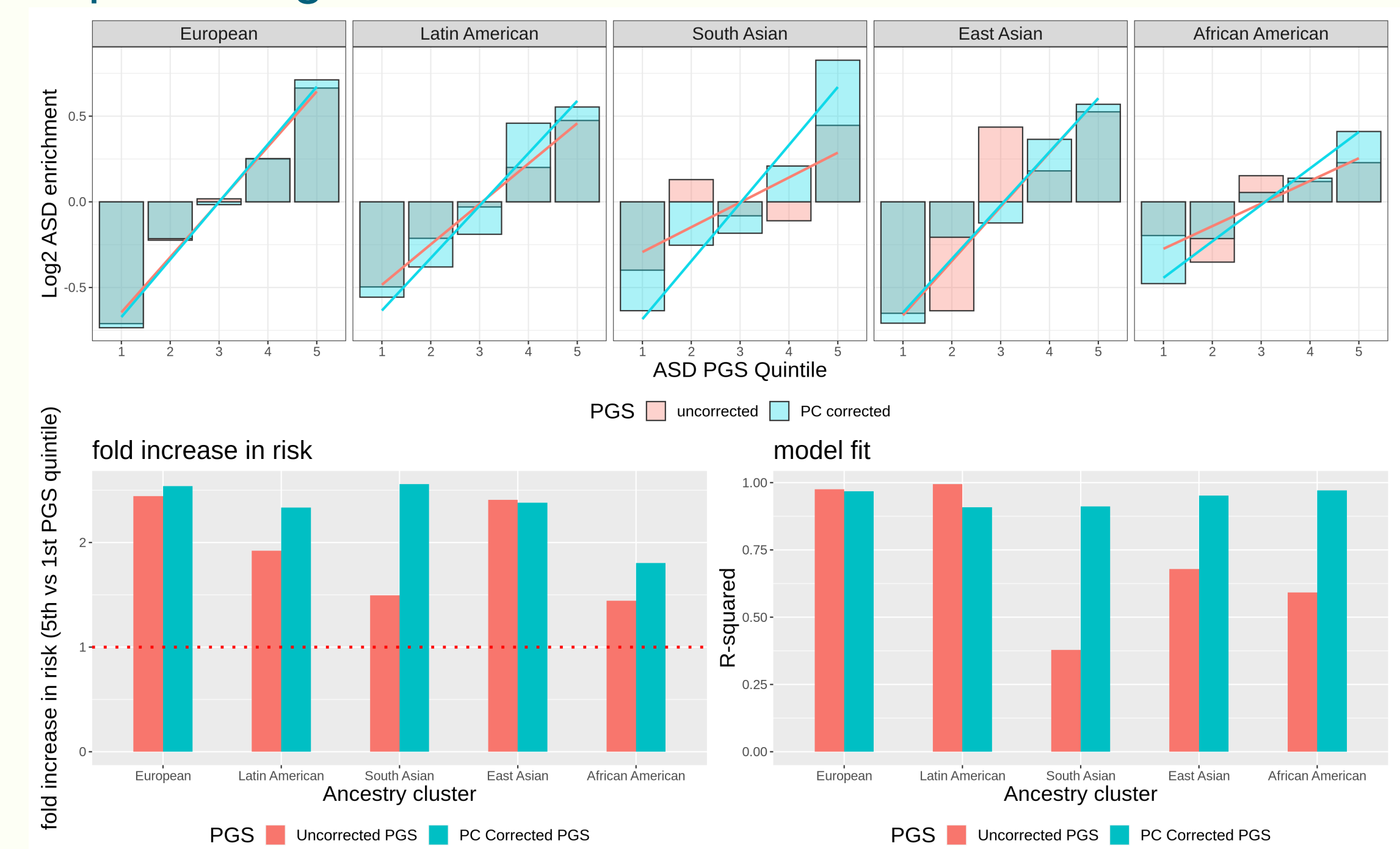
Standard PGS for Each Genetic Cluster

- Polygenic scores are **not equally distributed among all five clusters** – significantly higher for African Americans
- Every cluster should ideally be centered near the red reference line of zero
- There is **bias** due to the lack of GWAS diversity



Results

- After correcting for genetic ancestry, the **results showed significant improvement**, especially among those of non-European descent.
- Those with lower PGS had fewer autism cases, and those with higher PGS had an increased number of autism cases. This remained true for all five clusters.
- The greater the effect size, the more predictive the polygenic risk scores were in predicting autism



- Uncorrected PGS p-value is very low, representing a significant cluster-PGS interaction
- PC Corrected PGS p-value is much closer to one, showing that it is **less significant and has less bias**

	Uncorrected PGS p-values	Corrected PGS p-values
Cluster	2.2e-16	2e-16
Polygenic Score	2.2e-16	2e-16
Cluster and PGS Interaction	0.001201	0.9109

Conclusion

- Polygenic scores are clearly biased towards Europeans, but this can be fixed to a certain extent by **correcting for genetic ancestry**. This information is necessary in order to increase accuracy in genetic studies among diverse populations.
- An important step for the future would be to **increase the diversity of participants included in genetic studies**, such as GWAS, so that genetic information for those underrepresented groups can be more easily accessible for research.

References

- Martin, A.R., Kanai, M., Kamatani, Y. et al. Clinical use of current polygenic risk scores may exacerbate health disparities. *Nat Genet* 51, 584–591 (2019). <https://doi.org/10.1038/s41588-019-0379-x>
- Novembre, J., Johnson, T., Bryc, K. et al. Genes mirror geography within Europe. *Nature* 456, 98–101 (2008). <https://doi.org/10.1038/nature07331>
- Privé, F., Arbel, J., & Vilhjálmsson, B. J. LDpred2: better, faster, stronger. *Bioinformatics*, 36(22-23), 5424–5431 (2020). <https://doi.org/10.1093/bioinformatics/btaa1029>
- Privé, F., Aschard, H., Ziyatdinov, A., & Blum, M. Efficient analysis of large-scale genome-wide data with two R packages: bigstatsr and bigsnpr. *Bioinformatics*, 34(16), 2781–2787 (2018). <https://doi.org/10.1093/bioinformatics/bty185>
- Taliun, D., Harris, D.N., Kessler, M.D. et al. Sequencing of 53,831 diverse genomes from the NHLBI TOPMed Program. *Nature* 590, 290–299 (2021). <https://doi.org/10.1038/s41586-021-03205-y>
- Thomas, T.R., Koomar, T., Casten, L.G. et al. Clinical autism subscales have common genetic liabilities that are heritable, pleiotropic, and generalizable to the general population. *Transl Psychiatry* 12, 247 (2022). <https://doi.org/10.1038/s41398-022-01982-2>

Acknowledgements

Special thanks to Dr. Jacob Michaelson, Lucas Casten, Ethan Bahl, and the entire Michaelson lab for mentoring me through this amazing experience. I would also like to thank SSTP and the Belin Blank Center for providing me with this opportunity.

Contact

michaelson.lab.uiowa.edu
 jacob-michaelson@uiowa.edu



Monitoring Mealtime Intake Behavior in Residents with Dementia at Nursing Homes

Wendy Song, Heather Suh MPH, Wen Liu PhD

Palo Alto High School, University of Iowa College of Nursing

Introduction

- In 2022, around 6.5 million Americans aged 65 and older are expected to have dementia, and 10.7% of people aged 65 and older have dementia (Alzheimer's Association, 2022).
- Patients exhibit resistive behaviors and lower quality of life when their intake is compromised.
- Caregivers currently perform task-centered care due to work demands and focus solely on feeding, allowing the patient little autonomy and independence.
- OPTIMAL intervention protocol contains RECIPE principles promoting person-centered care: showing respect, creating environment, offering choices, supporting independence, acknowledging preferences, contains maintaining engagement.

SEM (Social Ecological Model)

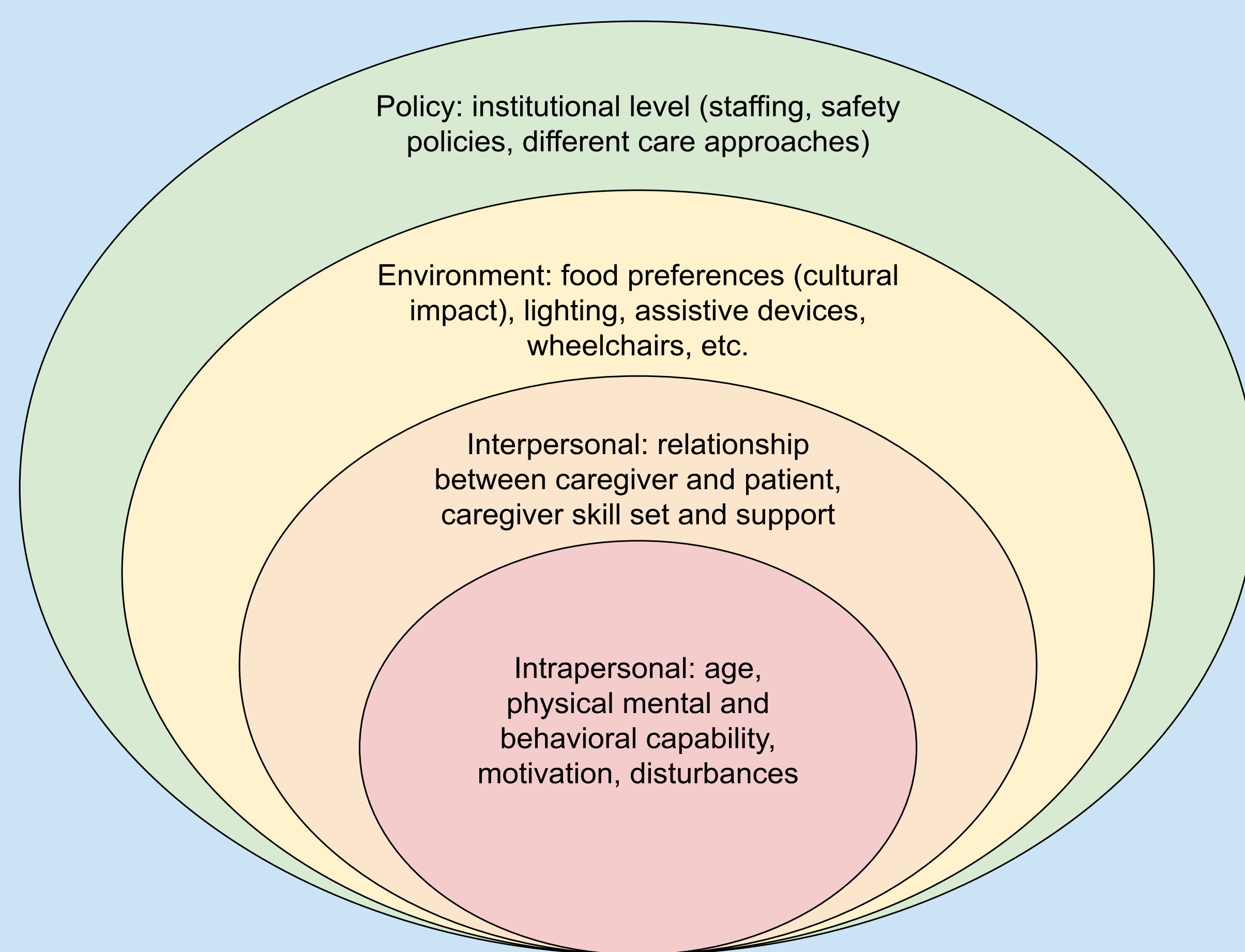


Figure 1. SEM (Social Ecological Model) depicting factors that typically influence mealtime behavior and eating performance.

Objectives

- Evaluate the impact that factors such as type of meal and food have on the food intake process.
- Hypothesize the impact that person-centered care administered through didactic training for caregivers has on the intake process.

Methods

- 6 meals evaluated per resident; staff and resident verbal and nonverbal behaviors as well as the food intake process were measured.
 - Resident positive, neutral behaviors: 8 verbal (ex. asking for help/cooperation), 5 nonverbal (ex. wiping away oral spillage/drool).
 - Resident challenging behaviors: 4 verbal (ex. interrupting/changing topic), 22 nonverbal, categories: chewing and swallowing difficulties (ex. holds food in mouth) with 4 items, functional impairment (ex. difficulty using utensil) with 5 items, resistiveness to care (ex. doesn't open mouth) with 6 items.
- Intake process: 0 for an unsuccessful intake attempt, 1 for solid food, 2 for liquid food. 0 if staff initiated the intake attempt, 1 if resident initiated with or without help of staff.

Results

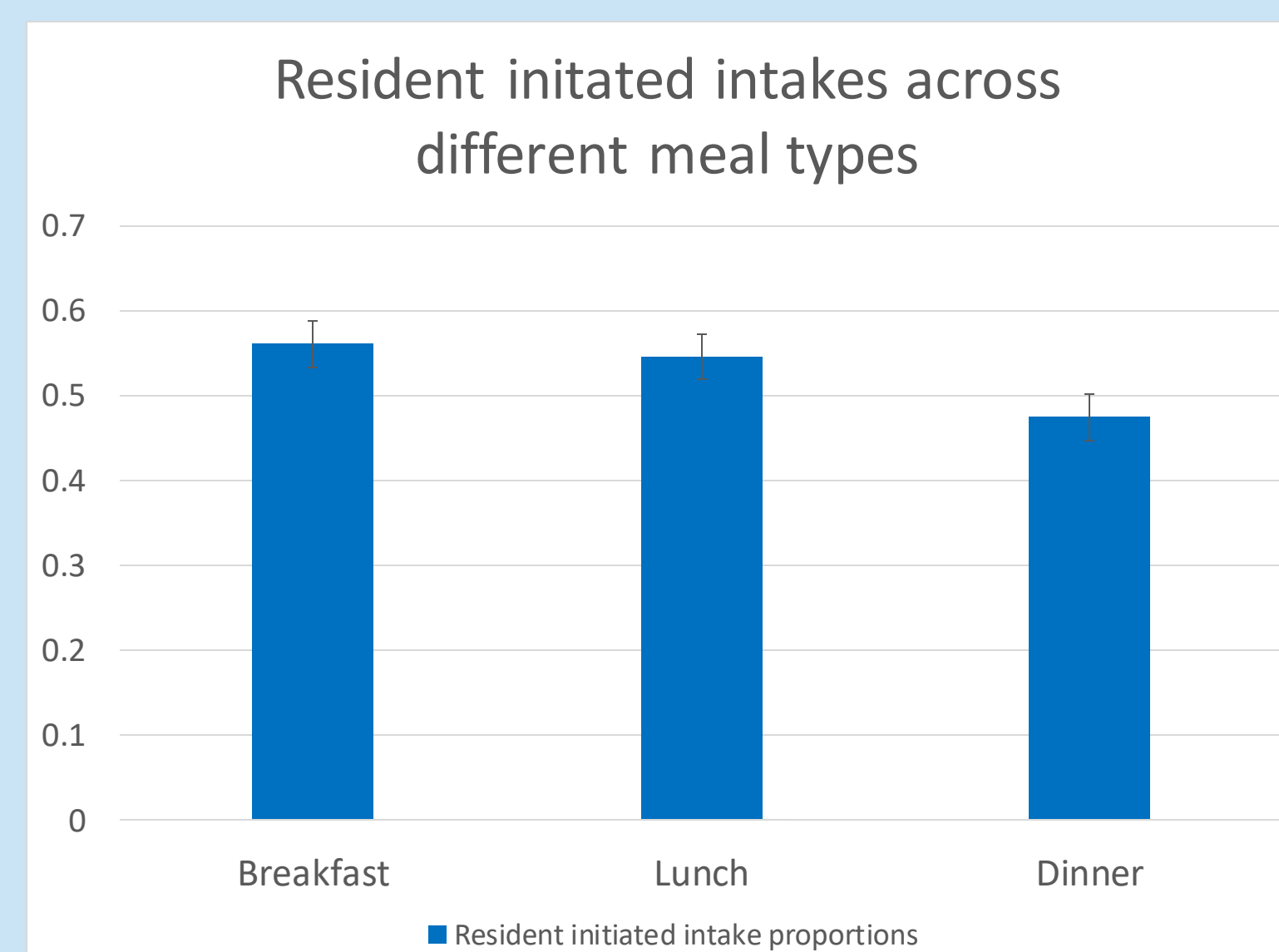


Figure 2. Proportion of resident-initiated intakes across breakfast, lunch, and dinner.

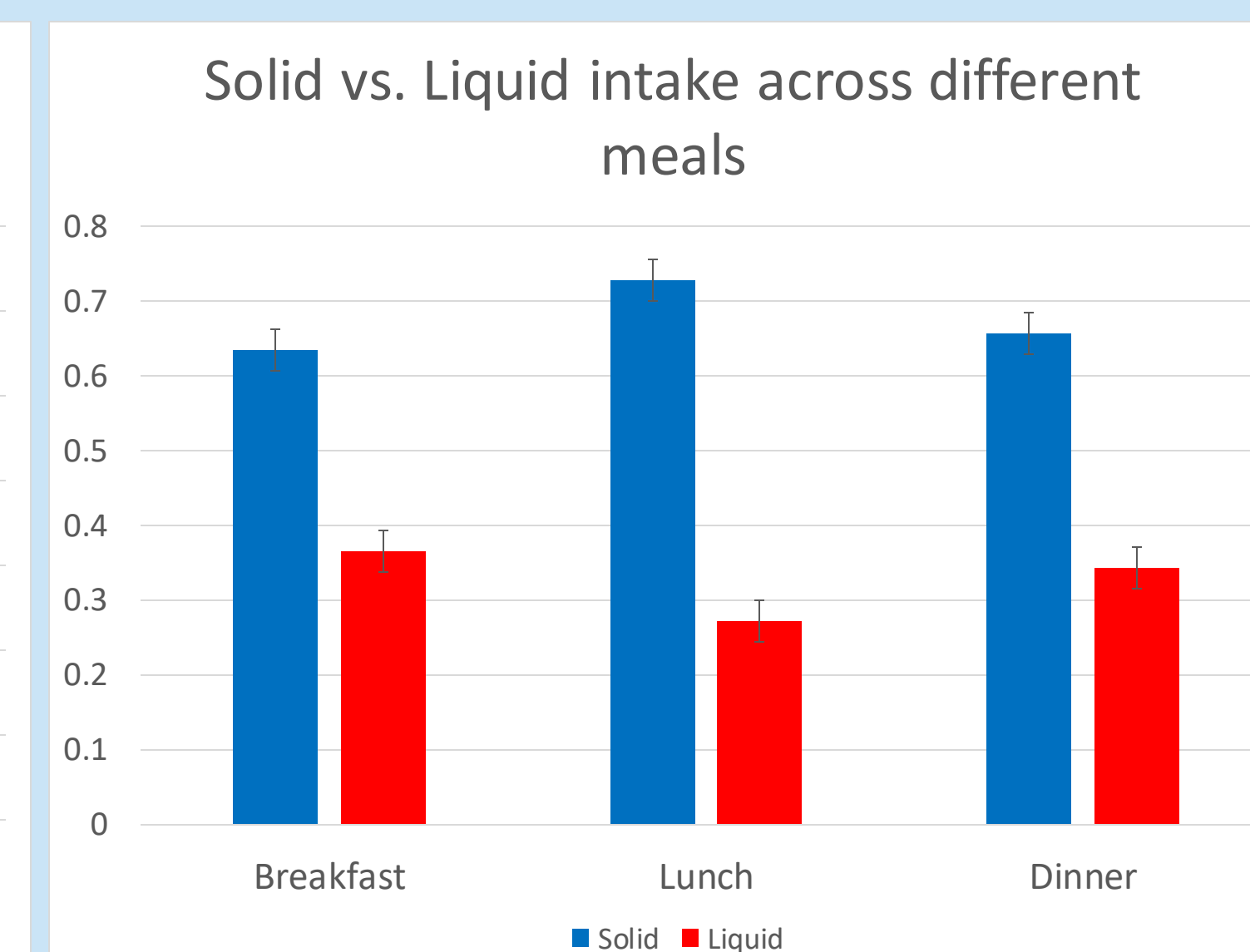


Figure 3. Proportion of solid vs. liquid intake among successful intake attempts during breakfast, lunch, and dinner.

Percent of Resident Initiated Intakes		
Breakfast	Lunch	Dinner
56.05%	54.63%	47.43%

Table 1. Table representation of the graph on the left above. The lowered proportion of intakes observed during dinner is statistically significant.

- Residents have a decreased ability to initiate intakes during dinner and later in the day.
- Residents consistently intake around twice as much solid food (63.4%, 72.8%, and 65.7%) when compared to liquid food (36.6%, 27.2%, and 34.2%).
- Only baseline data (T1) has been collected so far.

Discussion

During mealtime, dementia is the primary cause of challenging behaviors such as initiation of an intake attempt, getting food into the mouth, chewing and swallowing, or getting distracted and attempting to leave the dining table (Liu et al., 2014). This resistance negatively affects the intake amount and process, which are measured through checklists. The proportion of resident-initiated intakes is around 50% for all meals, suggesting the need for improved person-centered care to encourage resident autonomy. This data is representative of conditions before intervention and provides a strong baseline of residents' natural behaviors. Furthermore, staff use of verbal and nonverbal strategies correlates with residents' challenging behaviors (Liu et al., 2022), so a staff behavioral changes will impact resident behavior and therefore change the intake process and amount.

Future Directions

- Understand how the impact of dementia-induced behaviors on breakfast, lunch, and dinner differ.
- Explore the impact of other conditions related to old age on intake behavior.
- Further the current data by understanding the connections between different dementia aids and the intake process to develop stronger intervention tactics.
- Recognize the prevalence of person vs. task centered care, and the caregiver's role in the intake process.

Acknowledgments

I would like to thank Heather Suh, my mentor, for providing me with the study materials and ability to conduct the research and data analysis. Additionally, I would also like to thank Dr. Wen Liu for allowing me to be a part of this study.

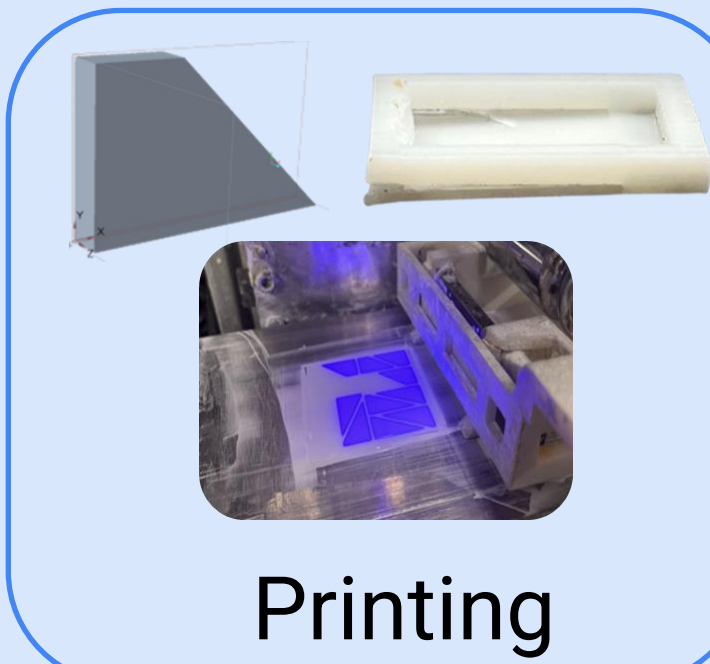
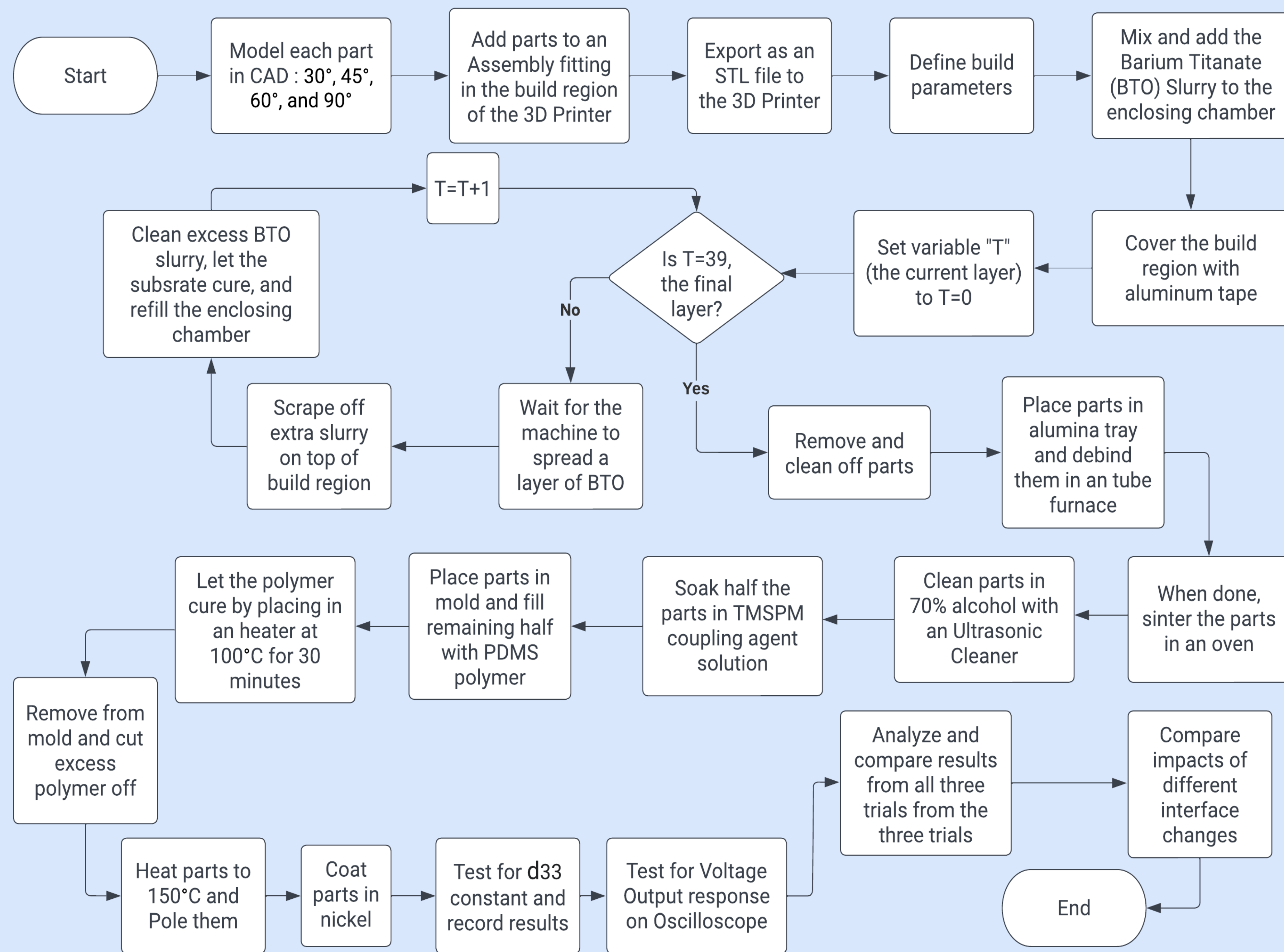
References

1. 2022 Alzheimer's disease facts and figures. (2022). *Alzheimer's & Dementia*, 18(4), 700–789. <https://doi.org/10.1002/alz.12638>
2. Liu, W., Cheon, J., & Thomas, S. A. (2014). Interventions on mealtime difficulties in older adults with dementia: A systematic review. *International Journal of Nursing Studies*, 51(1), 14–27. <https://doi.org/10.1016/j.ijnurstu.2012.12.021>
3. Liu, W., Perkhounkova, Y., Williams, K., Batchelor, M., & Hein, M. (2022). Mealtime nonverbal behaviors in nursing home staff and residents with dementia: Behavioral analyses of videotaped observations. *Geriatric Nursing*, 44, 112–124. <https://doi.org/10.1016/j.gerinurse.2022.01.009>

Background

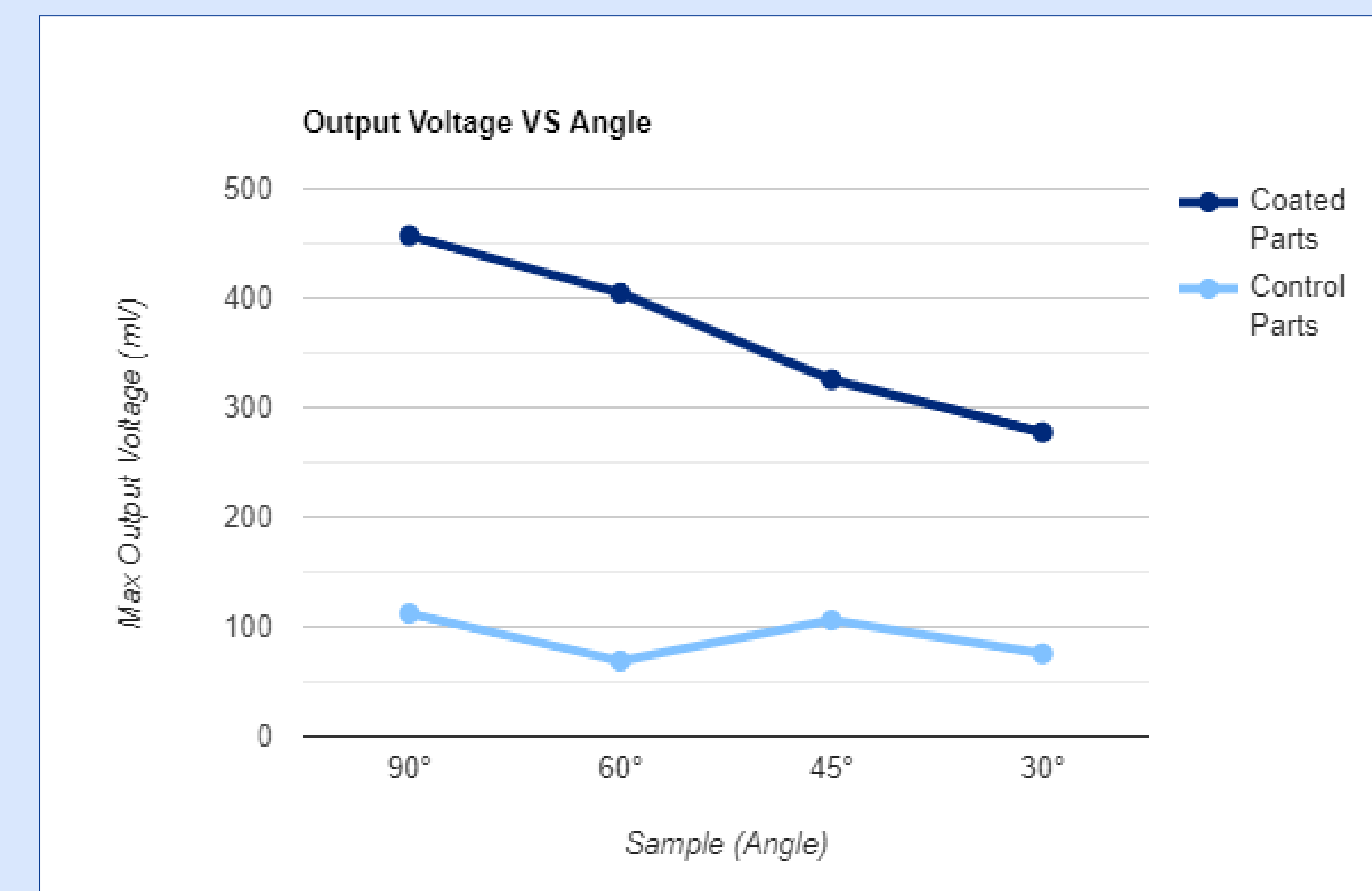
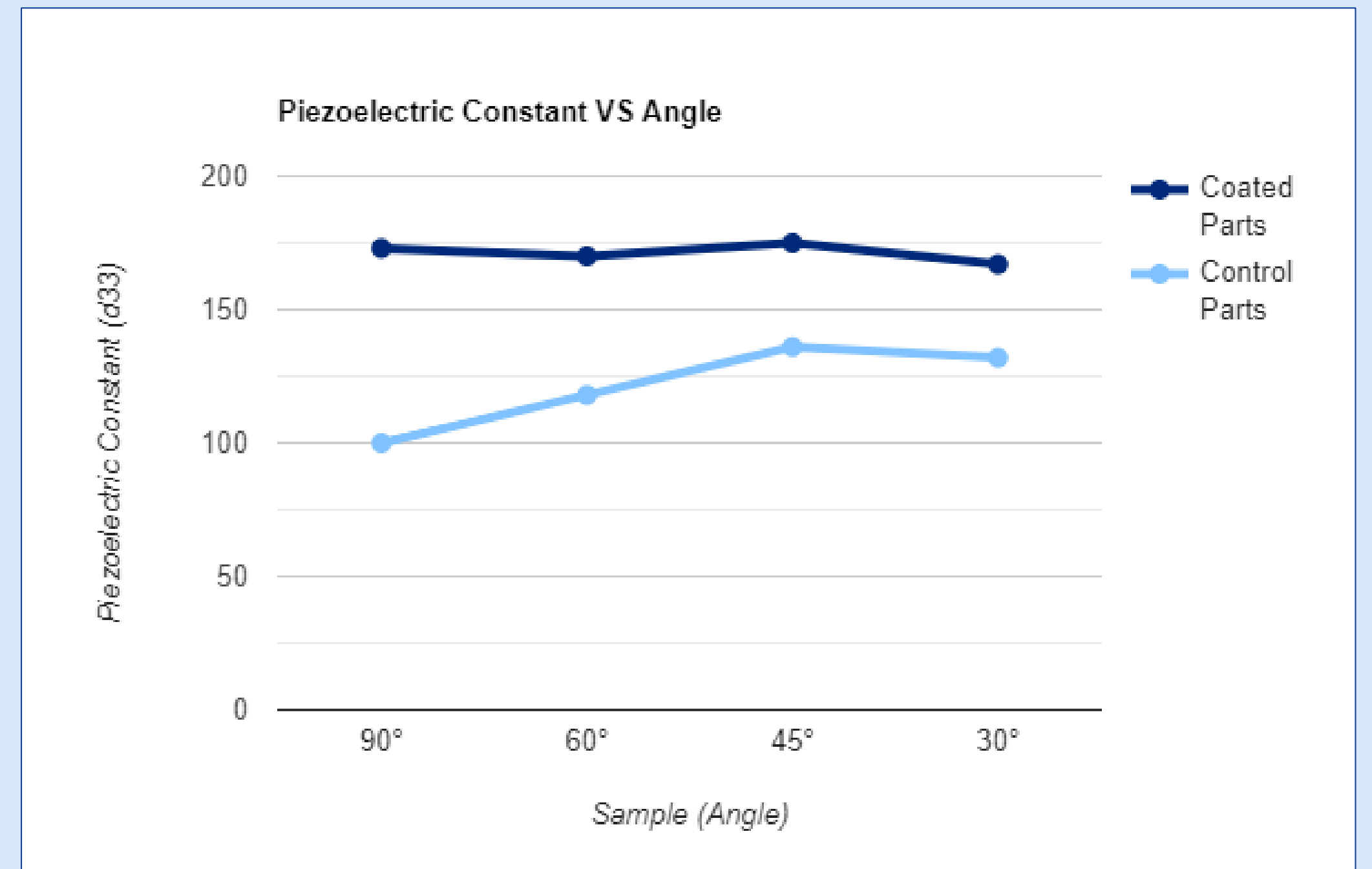
The capacity of some materials to produce an electric charge in response to applied mechanical stress is known as piezoelectricity. These piezoelectric properties can be optimized through various manipulations: material alteration, interface changes, polymeric bonding strength, among many others. The objective of this project was to determine the impact of different polymer bonding strengths and angle alterations of the contact surface between the polymer and ceramic phase, on final piezoelectric properties in additively manufactured Barium Titanate parts.

Methods

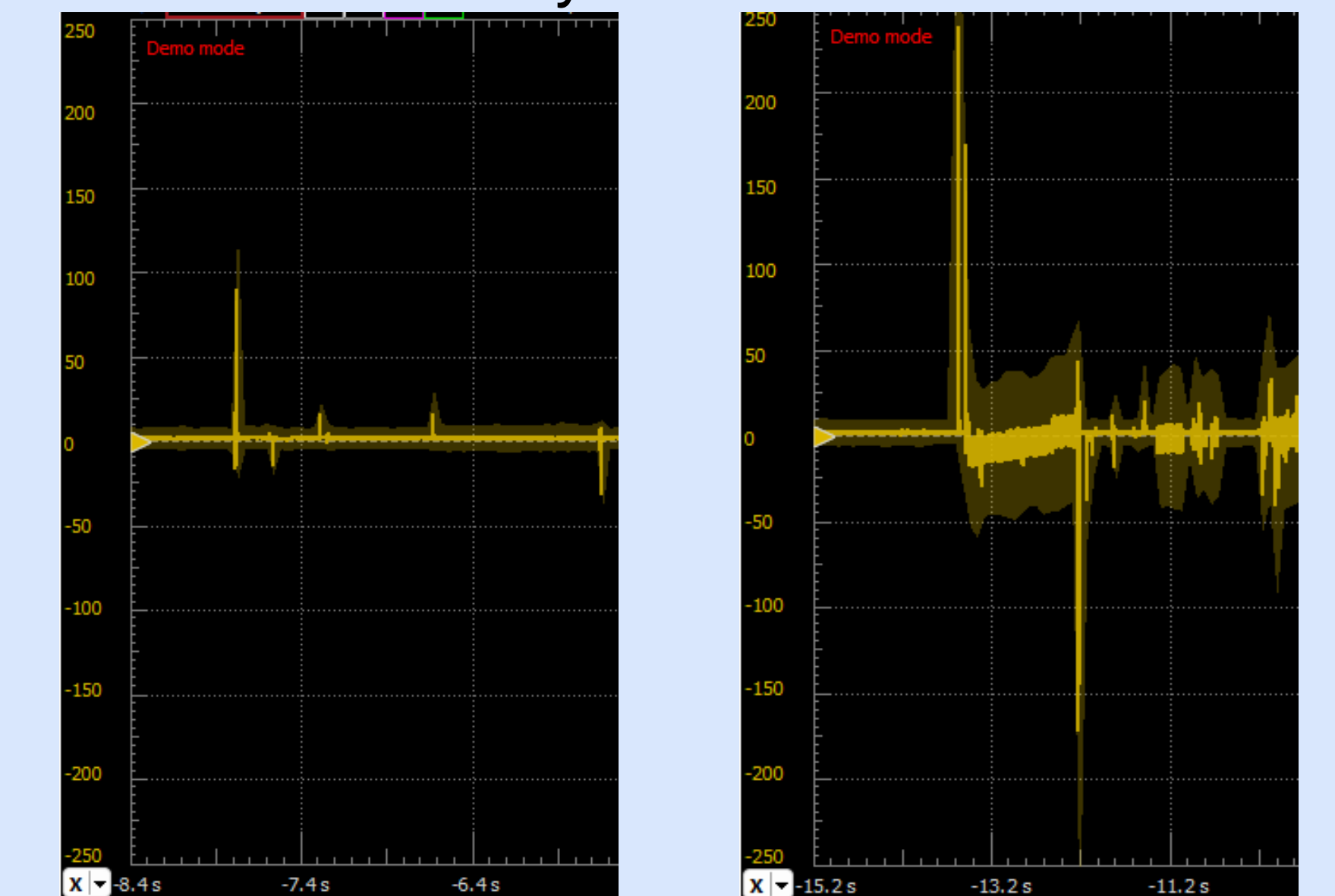


Results

Part Description	Average Piezoelectric Constant (d33)	Average Max Output Voltage (mV)
30°, Uncoated	132	75.39
45°, Uncoated	136	106.14
60°, Uncoated	118	68.78
90°, Uncoated	100	112.34
30°, Coated	167	277.57
45°, Coated	175	325.56
60°, Coated	170	404.35
90°, Coated	173	457.2



Electric Output Voltage Response when Polymer is Pressed



Conclusion

There is a significant increase in both the piezoelectric constant and the output voltage in the parts coated with TMSPM compared to those that were uncoated. Furthermore, it can be shown that alterations in the angle of the interface between the polymer and the ceramic piece results in a slight change of piezoelectric properties, where a decrease in the angle correlates to a decrease in coated parts' output voltages and an increase in uncoated parts' piezoelectric constant.

Implications

This research demonstrates different ways to optimize piezoelectric properties within parts of ceramic and polymers. By utilizing the information found in the research, future researchers can use this as a starting point in developing even further ceramics or materials with super-piezoelectric properties, as well as additionally increasing knowledge within the field on how certain physical alterations impact piezoelectricity.

Acknowledgment

Thank you for the guidance and support of Levi Kirby and Dr. Xuan Song throughout this process as well as the Belin-Blank Center and AMPRL at the University of Iowa for this opportunity. Additional thanks to NSF for funding this research and project.

References

Song, X., He, L., Yang, W., Wang, Z., Chen, Z., Guo, J., Wang, H., & Chen, L. (2019). Additive Manufacturing of Bi-Continuous Piezocomposites With Triply-Periodic Phase Interfaces for Combined Flexibility and Piezoelectricity. *Journal of Manufacturing Science and Engineering*, 141(11). <https://doi.org/10.1115/1.4044708>

Kim, K., Zhu, W., Qu, X., Aronson, C., McCall, W., Chen, S., & Sirbully, D. (2014). 3D Optical Printing of Piezoelectric Nanoparticle-Polymer Composite Materials. *ACS Publications*. <https://pubs.acs.org/doi/full/10.1021/nn503268f?cookieSet=1>

Su, J., & Zhang, J. (2015). Remarkable enhancement of mechanical and dielectric properties of flexible ethylene propylene diene monomer (EPDM)/barium titanate (BaTiO3) dielectric elastomer by chemical modification of particles. *RSC Advances*, 5(96), 78448–78456. <https://doi.org/10.1039/c5ra14047a>



Introduction

Epilepsy

- Epilepsy is a neurological disorder characterized by repeated seizures and affects over 50 million people worldwide¹.
- Current anti-epileptic drugs have limited efficacy in 33% of patients and often lead to adverse long-term side effects².

prickle

- The *prickle* gene in *Drosophila* (fruit flies) produces an adult isoform called *prickle-spiny-legs*(*pk^{sple}*)³.
- Mutations in the *pk^{sple}* isoform cause spontaneous myoclonic seizures, similar to those observed in humans with *PRICKLE* mutations⁴.

Oxidative Stress

- Previous work in the Manak laboratory shows that loss of the *pk^{sple}* isoform leads to increased expression of genes that encode proteins that mitigate oxidative stress.
- Oxidative stress in the nervous system contributes to the pathogenesis of epilepsy⁵.
- Curcumin, a polyphenol and antioxidant, has been shown to be effective in reducing oxidative stress and improving outcomes of disease processes involving oxidative stress⁶.
- Aspirin, an anti-inflammatory drug with antioxidant properties, increases lifespan and improves locomotor function in *Drosophila*⁷.

Research Objectives

The purpose of this study is to test whether treating seizure-prone *pk^{sple}* mutant flies with two compounds that have antioxidant properties, curcumin and aspirin, suppresses the *prickle*-mediated seizures.

Methods

Drosophila Stocks:

- The *pk^{sple}* mutation was backcrossed into a *Canton-S^{JD}* (*CS^{JD}*) background. *pk^{sple}* (*CS^{JD}*) and *CS^{JD}* control flies were used in all experiments.

Dietary Feeding of Curcumin and Aspirin:

- Drug food was made by combining standard cornmeal molasses *Drosophila* medium with aspirin and curcumin (dissolved in ethanol) to final concentrations of 1μM and 25μM, respectively.
- Vehicle-only food was made for aspirin and curcumin by dissolving appropriate amounts of ethanol in standard *Drosophila* medium.
- Adult flies were allowed to lay on the drug or vehicle-only medium and the developing larvae were grown on the same medium.
- Adult flies were switched to fresh drug- or vehicle-infused food every five days.

Spontaneous Seizure Assay:

- Freshly eclosed control and *pk^{sple}* flies (*CS^{JD}*) were aged 7-10 days at 25°C.
- 8-10 female and male flies per experimental condition were mouth-pipetted into circular chambers, and their behavior was recorded for five minutes under high-resolution videography.
- The videos were manually analyzed for spontaneous seizure events as previously reported³.



Figure 1: Mouth pipetting the flies.

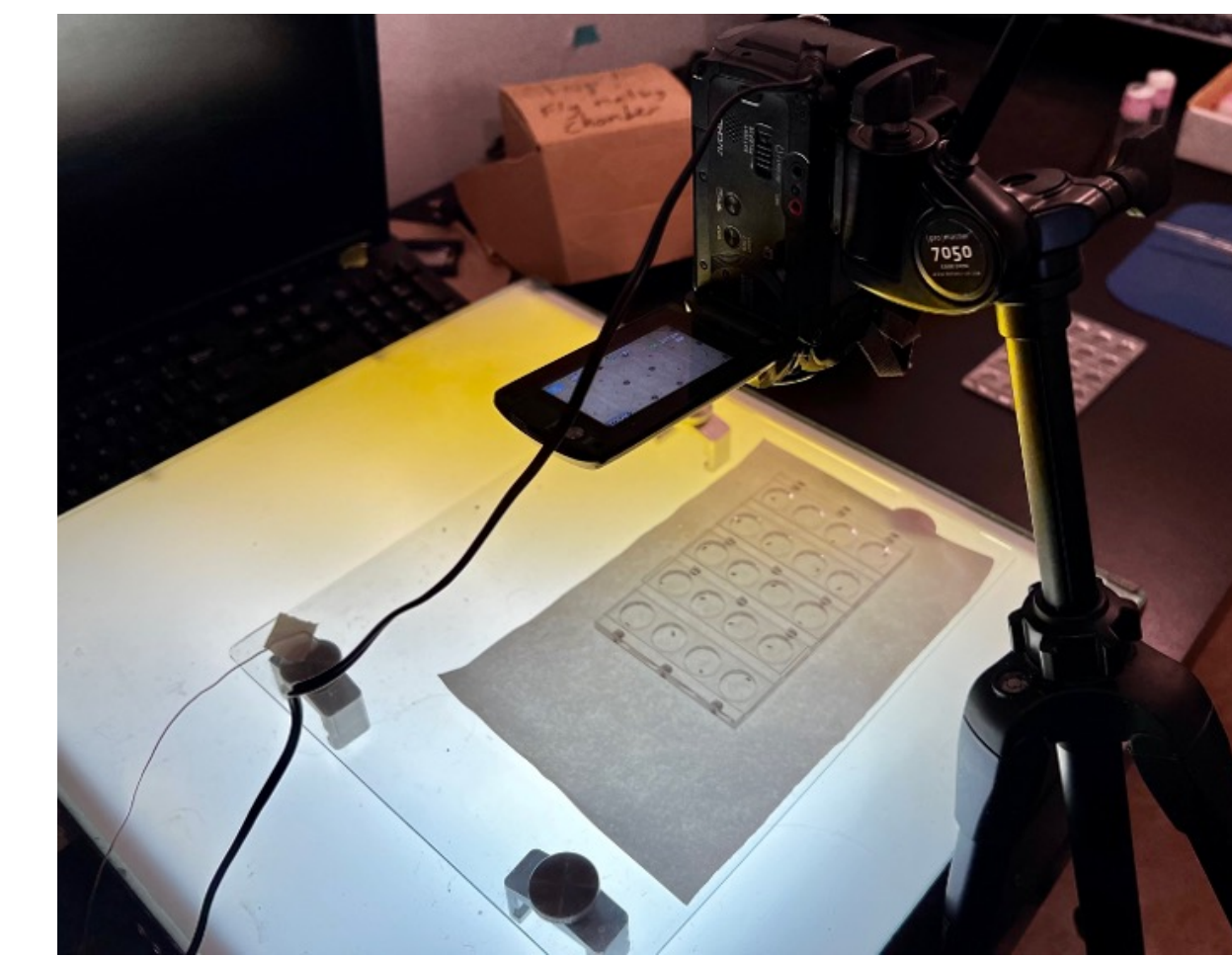


Figure 2: Apparatus for the Spontaneous Seizure Assay.

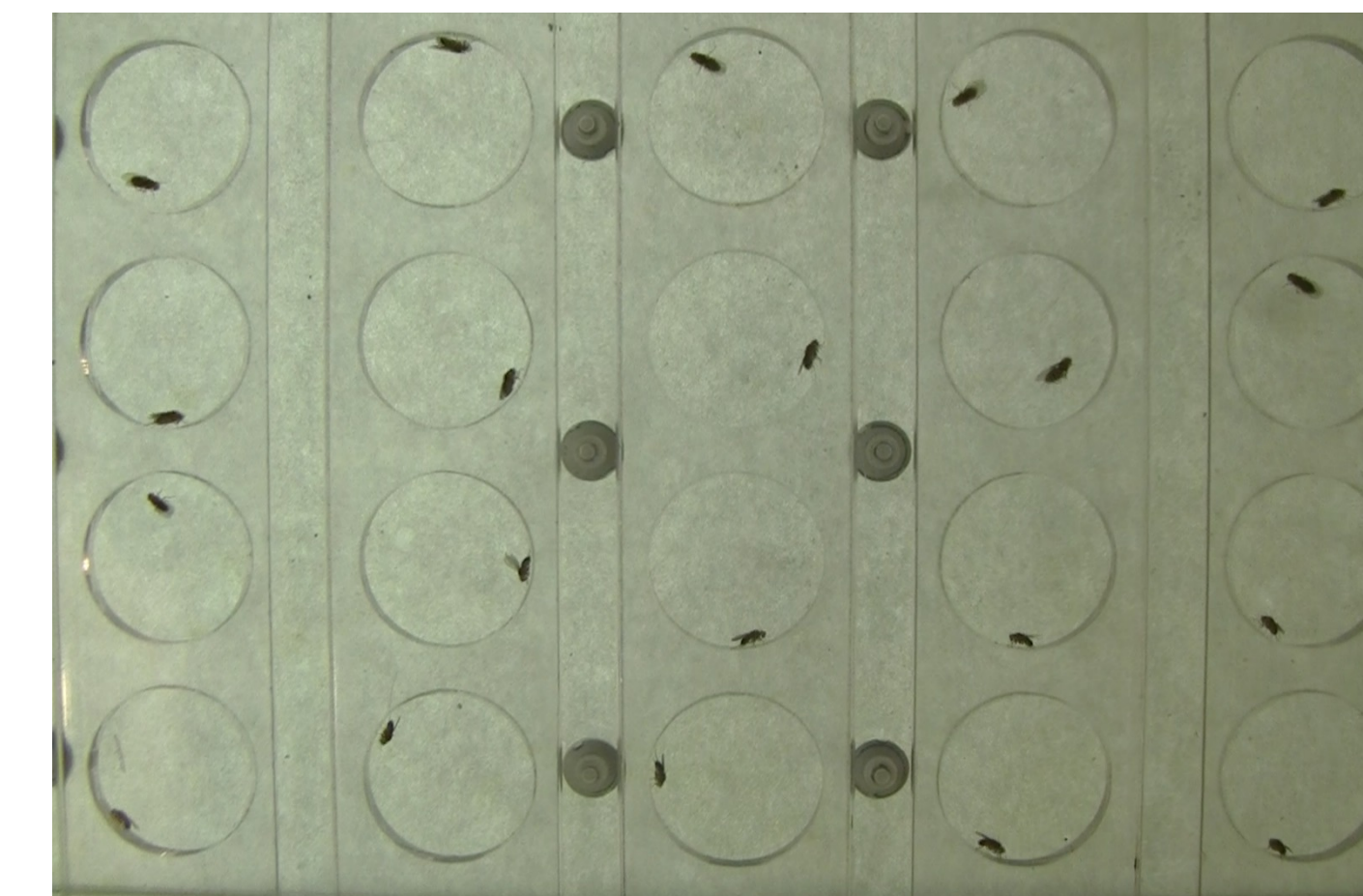


Figure 3: Recorded videos of the flies' behavior.

Results

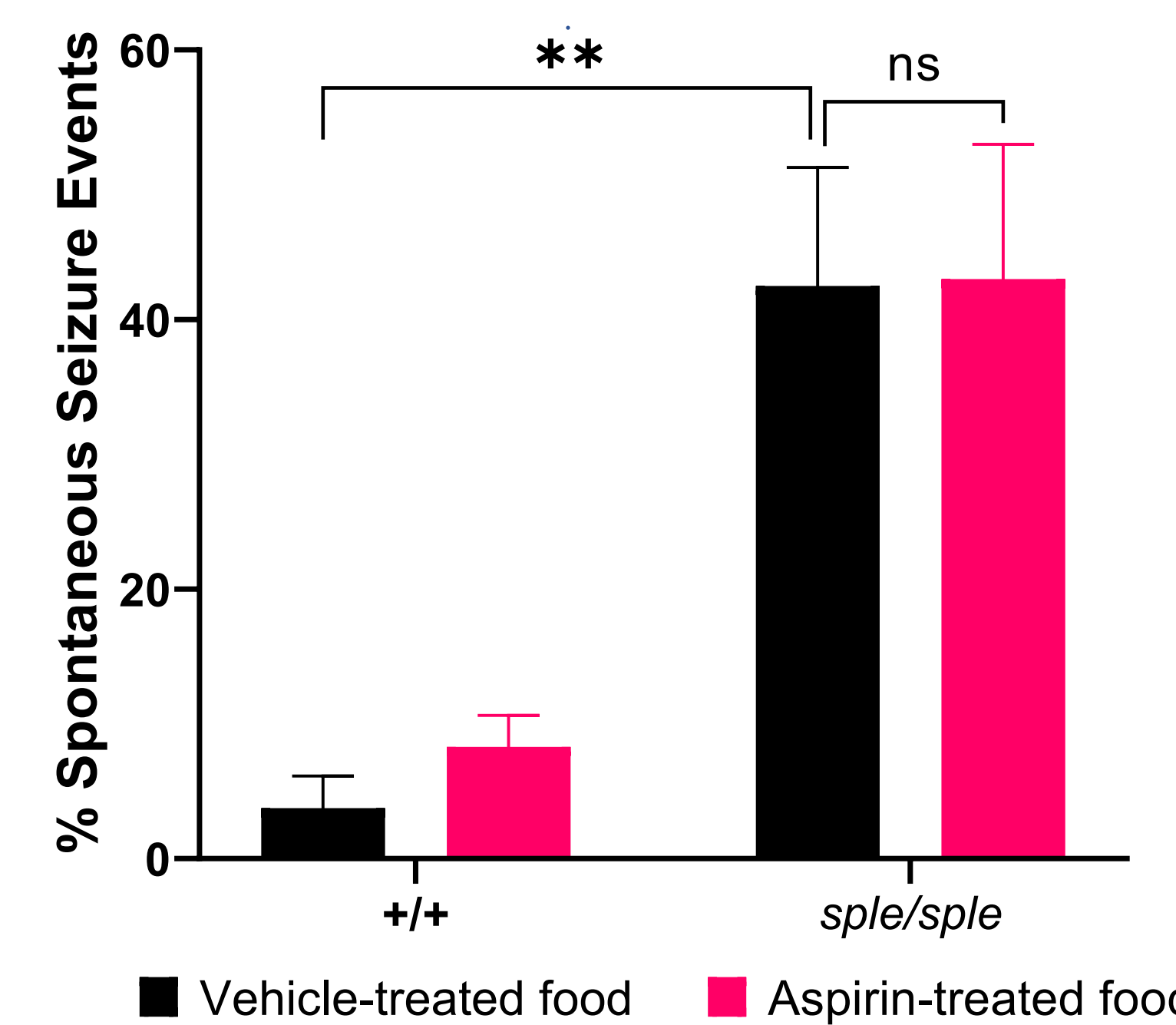


Figure 4: Aspirin-enriched diet does not decrease spontaneous seizure activity in *pk^{sple}* mutants. Quantification of spontaneous seizure events in +/+ and *sple/sple* grown on either an aspirin or vehicle medium. ** $p < 0.01$, ns = not significant. Two-way ANOVA, Error bars: SEM, $n \geq 5x$, 8-10 flies per genotype/treatment.

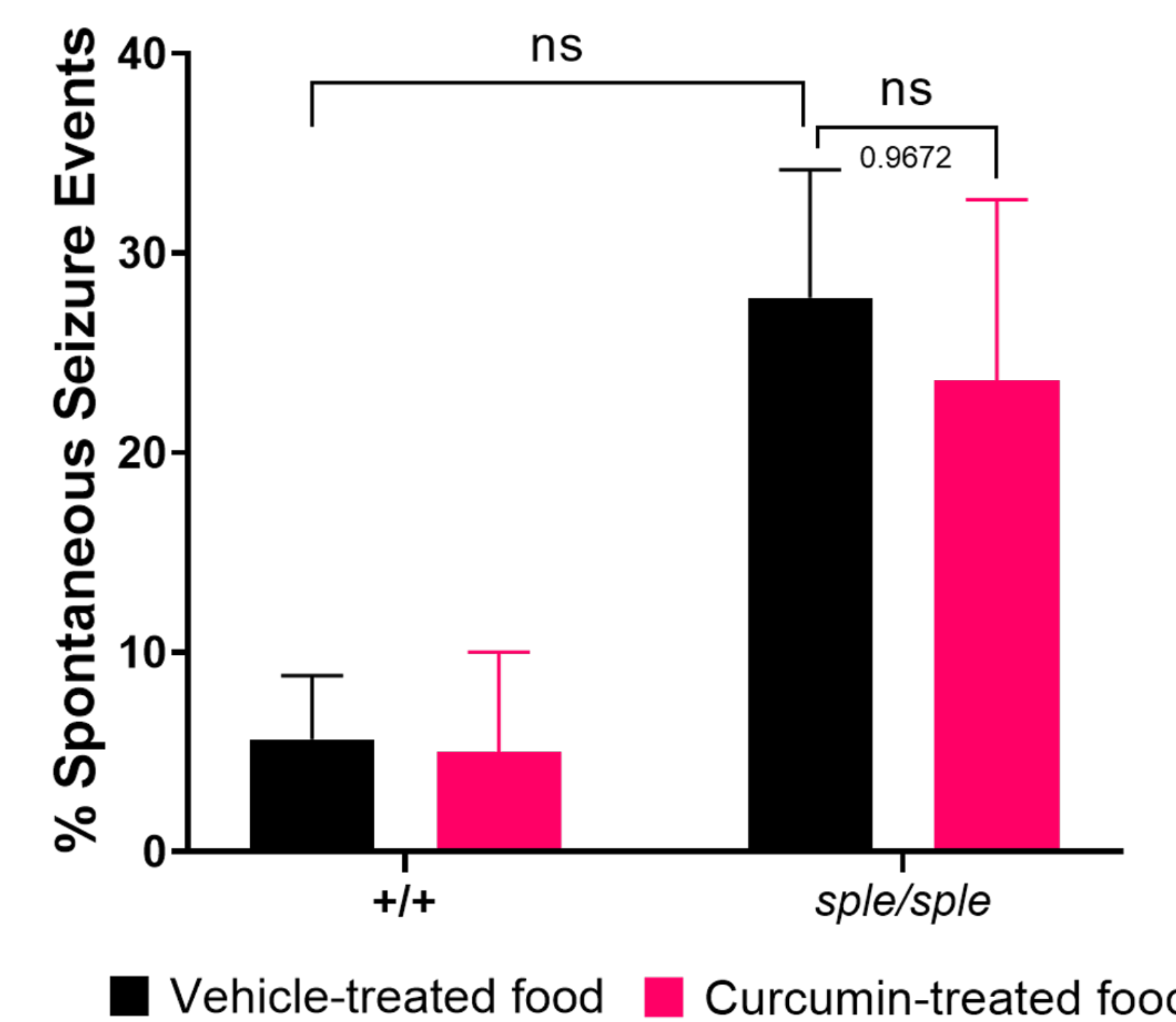


Figure 5: Curcumin-enriched diet shows a non-significant decrease in spontaneous seizure activity in *pk^{sple}* mutants. Quantification of spontaneous seizure events in +/+ and *sple/sple* grown on either a curcumin or vehicle medium. ns = not significant. Two-way ANOVA, Error bars: SEM, $n \geq 5x$, 8-10 flies per genotype/treatment.

Conclusions

- Adult *pk^{sple}* mutants exhibit a non-significant reduction of seizures when on a curcumin-enriched diet; increasing the power may yield statistical significance.
- Adult *pk^{sple}* mutants experienced no suppression in seizures when aspirin was added to their diet.
- These results suggest that while aspirin has no impact on suppressing epileptic seizures in *pk^{sple}* mutants, curcumin has promising potential as a compound for treating seizure disorders.

Future Directions

- Determine whether antioxidants increase the lifespan of *pk^{sple}* mutants.
- Determine whether classic antioxidants such as Vitamin C and Vitamin E show promise in reducing seizures in the *pk^{sple}* model of epilepsy.
- Improve statistical power by increasing the sample size of control and *pk^{sple}* mutants analyzed with the spontaneous seizure assay.

References

- Song, C., Zhu, C., Wu, Q., Qi, J., Gao, Y., Zhang, Z., Gaur, U., Yang, D., Fan, X., & Yang, M. (2017). Metabolome analysis of effect of aspirin on *drosophila* lifespan extension. *Experimental Gerontology*, 95, 54–62. <https://doi.org/10.1016/j.exger.2017.04.010>
- Dhir, A. (2018). Curcumin in epilepsy disorders. *Phytotherapy Research*, 32(10), 1865–1875. <https://doi.org/10.1002/ptr.6125>
- Ehaideb, S. N., Wignall, E. A., Kasuya, J., Evans, W. H., Iyengar, A., Koerselman, H. L., Lilienthal, A. J., Bassuk, A. G., Kitamoto, T., & Manak, J. R. (2016). Mutation of orthologous *prickle* genes causes a similar epilepsy syndrome in flies and humans. *Annals of Clinical and Translational Neurology*, 3(9), 695–707. <https://doi.org/10.1002/acn3.334>
- Parker, L., Howlett, I. C., Rusan, Z. M., & Tanouye, M. A. (2011). Seizure and epilepsy: Studies of seizure disorders in *drosophila*. *International Review of Neurobiology*, 1–21. <https://doi.org/10.1016/b978-0-12-387003-2.00001-x>
- Danilov, A., Shaposhnikov, M., Shevchenko, O., Zemskaya, N., Zhavoronkov, A., & Moskalev, A. (2015). Influence of non-steroidal anti-inflammatory drugs on *drosophila melanogaster* longevity. *Oncotarget*, 6(23), <https://doi.org/10.18632/oncotarget.5118>
- Abolaji, A. O., Fasae, K. D., Iwezor, C. E., Aschner, M., & Farombi, E. O. (2020). Curcumin attenuates copper-induced oxidative stress and neurotoxicity in *drosophila melanogaster*. *Toxicology Reports*, 7, 261–268. <https://doi.org/10.1016/j.toxrep.2020.01.015>
- Zhu, Y., Cai, Q., Zheng, X., Liu, L., Hua, Y., Du, B., Zhao, G., Yu, J., Zhuo, Z., Xie, Z., & Ji, S. (2021). Aspirin positively contributes to *drosophila* intestinal homeostasis and delays aging through targeting IMD. *Aging and Disease*, 12(7), 1821. <https://doi.org/10.14336/ad.2020.1008>

Acknowledgements

I would like to thank Krishna M. Nukala for his mentorship and advice, Dr. Manak for his guidance, and the entirety of the Manak Lab for support. Special thanks to the University of Iowa and SSTP program for giving me this opportunity. This work was supported by a research grant from The Stead Family Department of Pediatrics at the Carver College of Medicine to JRM.

The effect of corticosterone and 5-HT_{2C} receptors on seizure suppression and mortality in amygdala kindled mice

Lydia Tong¹, Katelyn G. Joyal^{2,3,4}, Nicole A. Boodhoo^{2,4}, Gordon F. Buchanan^{2,4}

¹Bellaire High School, 5100 Maple St, Bellaire, TX, 77401; ²Iowa Neuroscience Institute; ³Interdisciplinary Graduate Program in Neuroscience;

⁴Department of Neurology, Carver College of Medicine, University of Iowa, Iowa City, IA, 52242

Introduction

- Sudden unexpected death in epilepsy (SUDEP), the leading cause of death in patients with epilepsy, are at the greatest risk for the 35% of patients with epilepsy who will not achieve seizure freedom¹
- Mice lacking the 5-HT_{2C} receptor are significantly more seizure susceptible than wild-type controls²
- Prior research in the lab found that a high dose of MK-212 caused death following seizures in mice
- The 5-HT_{2C} receptor agonist MK-212 was found to increase corticosterone, a stress hormone in rodents³

Previous pilot experiments suggested CORT-113176, a corticosterone antagonist, and a high dose of MK-212 can result in seizure suppression in wild type animals.

Hypothesis

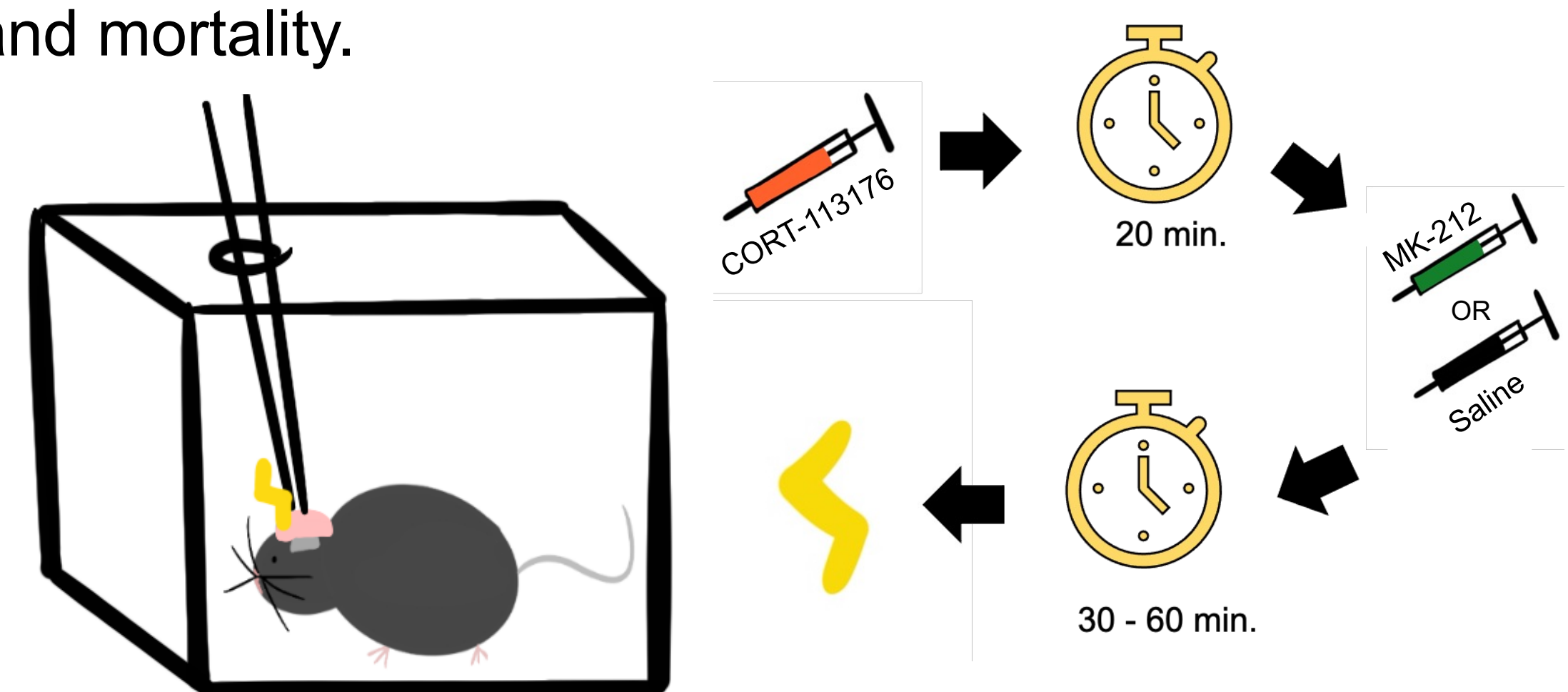
5-HT_{2C} receptor activation is necessary for the seizure suppression induced by the combination of CORT-113176 and MK-212.

Methods

Surgery: 8 adult 5-HT_{2C} knockout mice were implanted with EEG, EMG, and an electrode into the right basolateral amygdala (AP: -1.3mm; ML: -2.8mm; DV: -4.7mm).

Kindling: Afterdischarge threshold was determined, and each animal's threshold current was delivered twice daily until consistent convulsive seizures occurred.

Trials: Animals were injected (*i.p.*) with 70 mg of CORT-113176. After 20 minutes, mice were injected (*i.p.*) with 30 mg/kg MK-212 or saline (vehicle). After 30–60 minutes, we induced a seizure using the threshold pulse amplitude and evaluated measuring seizure severity and mortality.



Results

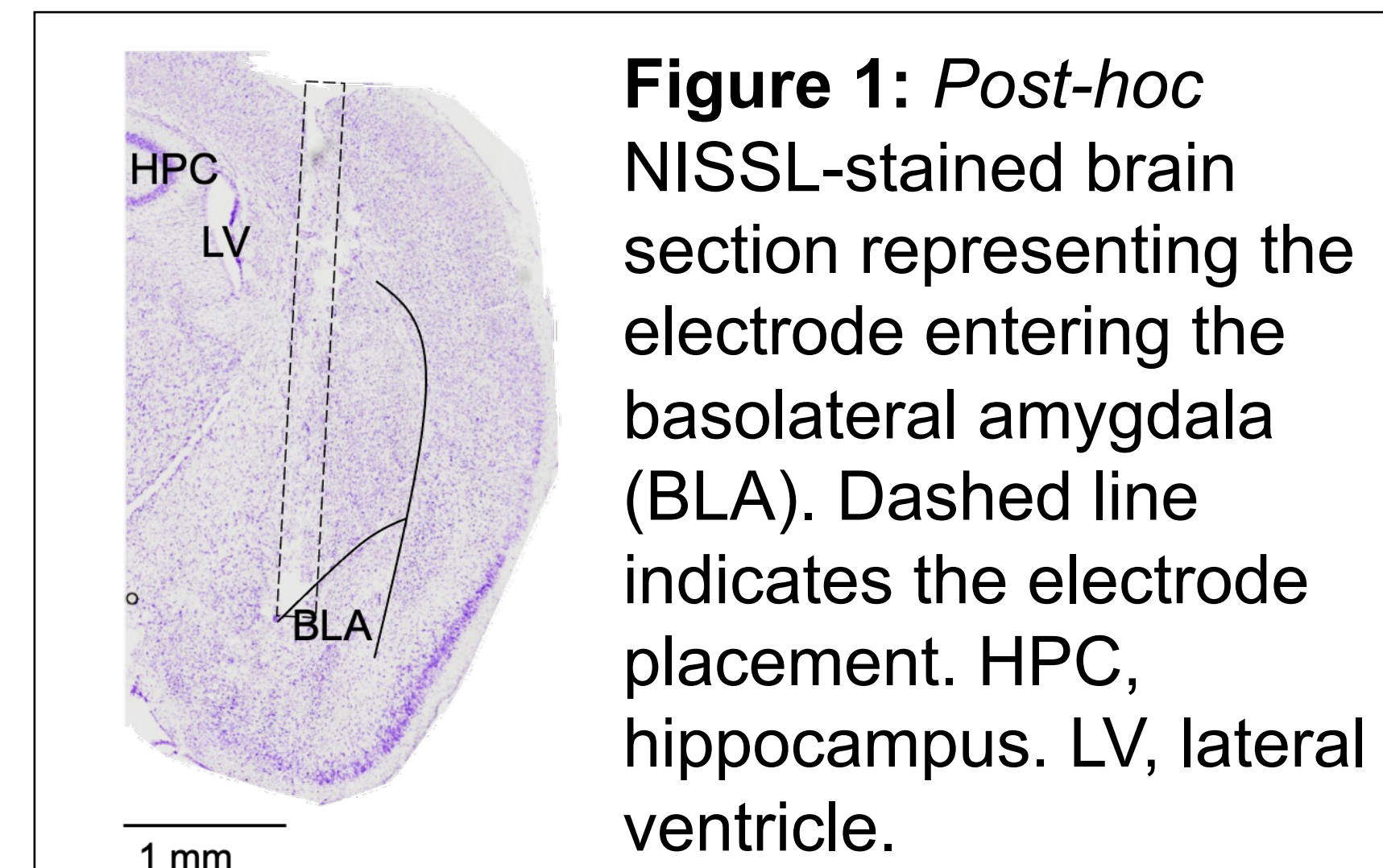


Figure 1: Post-hoc NISSL-stained brain section representing the electrode entering the basolateral amygdala (BLA). Dashed line indicates the electrode placement. HPC, hippocampus. LV, lateral ventricle.

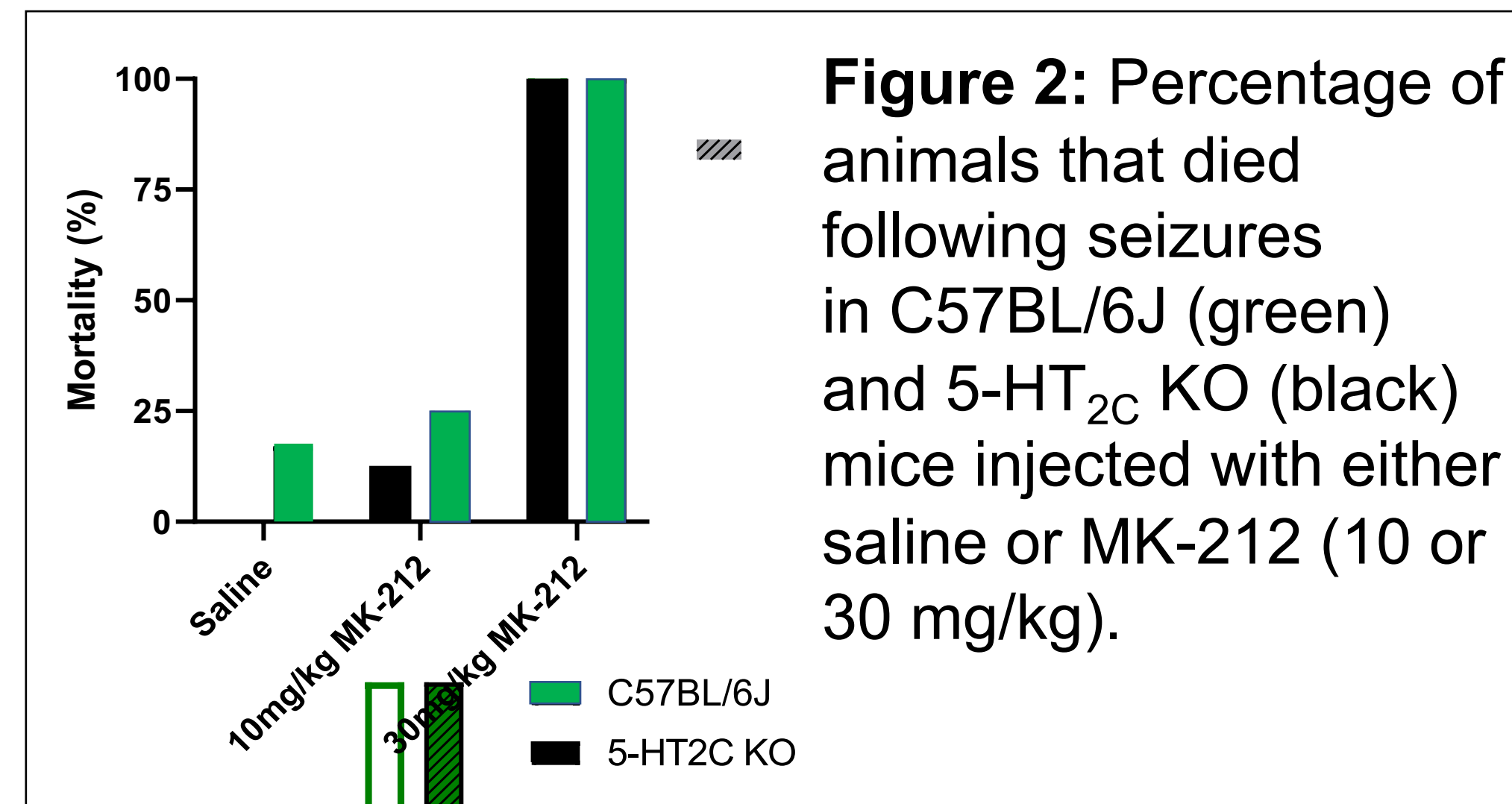


Figure 2: Percentage of animals that died following seizures in C57BL/6J (green) and 5-HT_{2C} KO (black) mice injected with either saline or MK-212 (10 or 30 mg/kg).

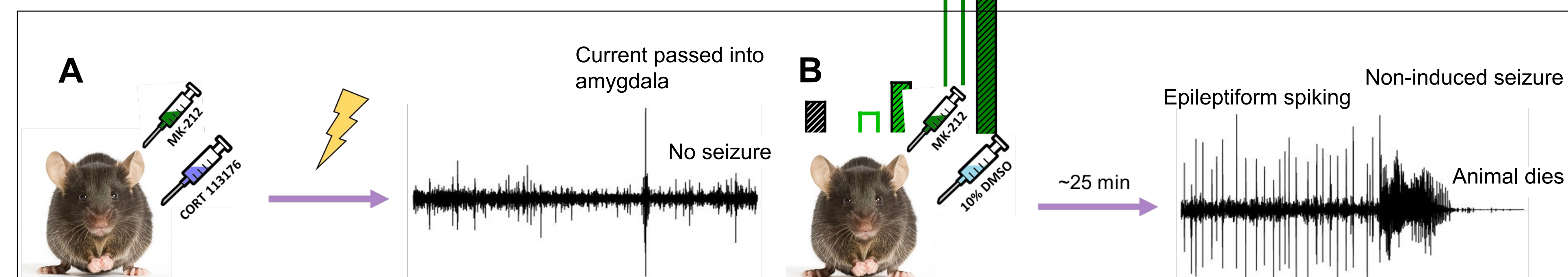


Figure 3: Pet1-Cre mice EEG traces from pilot experiments injected with either CORT-113176 and MK-212 (A) or 10% DMSO and MK-212 (B). Lightning bolt represents the time of electrical stimulation.

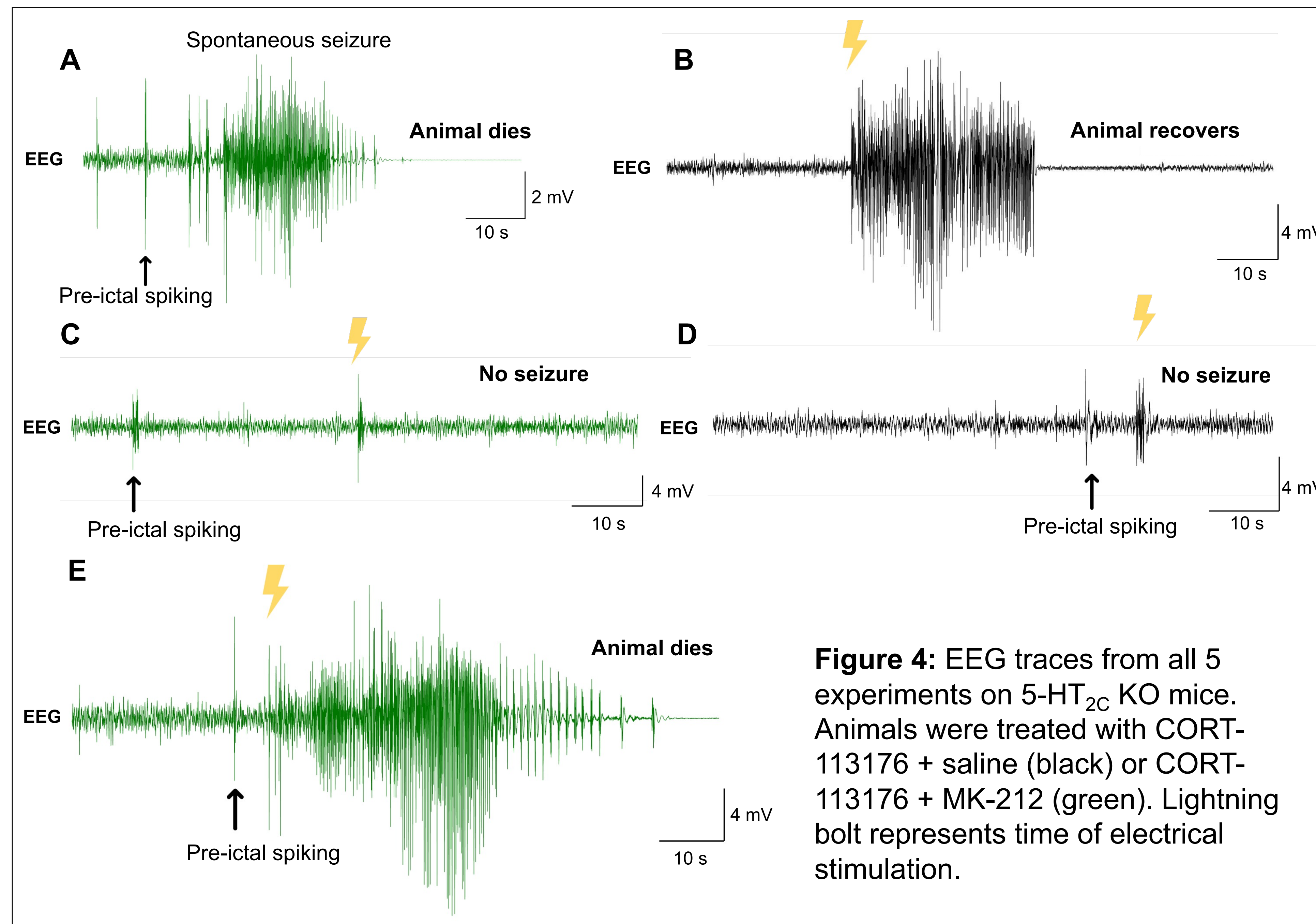


Figure 4: EEG traces from all 5 experiments on 5-HT_{2C} KO mice. Animals were treated with CORT-113176 + saline (black) or CORT-113176 + MK-212 (green). Lightning bolt represents time of electrical stimulation.

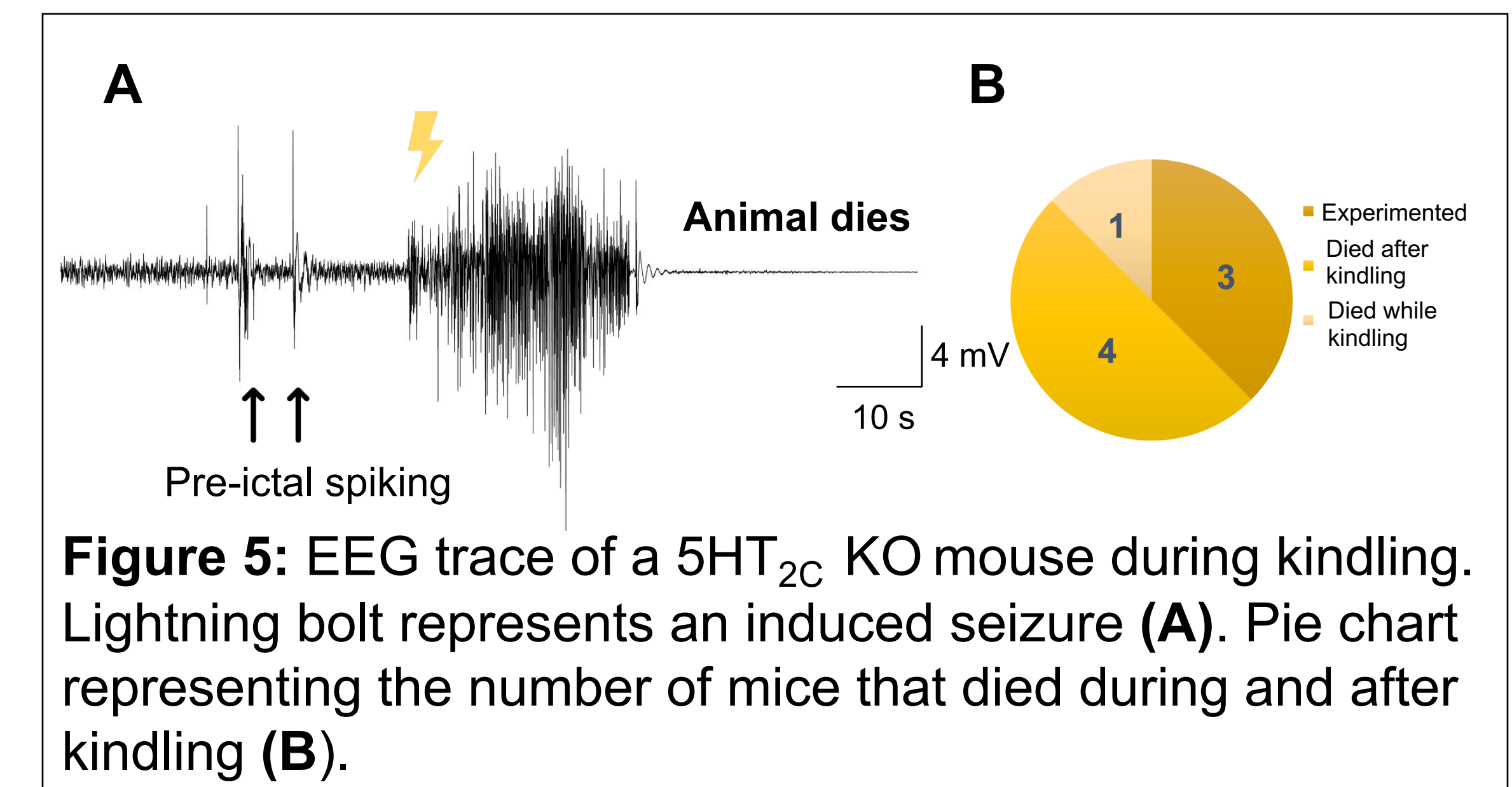


Figure 5: EEG trace of a 5HT_{2C} KO mouse during kindling. Lightning bolt represents an induced seizure (A). Pie chart representing the number of mice that died during and after kindling (B).

Conclusions

- The combination of CORT-113176 and MK-212 can suppress seizures in some animals
- 5-HT_{2C} receptor activation may not be necessary for seizure suppression
- 5-HT_{2C} KO mice are especially prone to seizure-induced death, which is consistent with previous findings in the literature

Future Directions

- Implant and complete trials on a cohort of animals
- Perform a dose response with corticosterone on a large pool of mice
- Explore more off-target effects that could potentially be from MK-212
- Perform different combinations of CORT-113176 and MK-212 to identify the best therapeutic windows to reduce SUDEP

Acknowledgements

This work was supported by the Belin Blank Center, NIH/NINDS R01 NS095842, and the Beth L. Tross Epilepsy Professorship

References

- Petrucci et al. (2020). *Exp Neurol.* 325: 113145.
- Applegate & Tecott. (1998). *Exp Neurol.* 154: 522-530.
- Kuznetsova et al. (2006). *Bull Exp Biol Med.* 142(5): 594-7.

Ellipsometry-Assisted Reactive Ion Etching for Reflection Grating Fabrication

Don Wong¹, Cecilia Fasano¹, Casey DeRoo¹

¹Diamond Bar High School; ²University of Iowa, Department of Physics and Astronomy

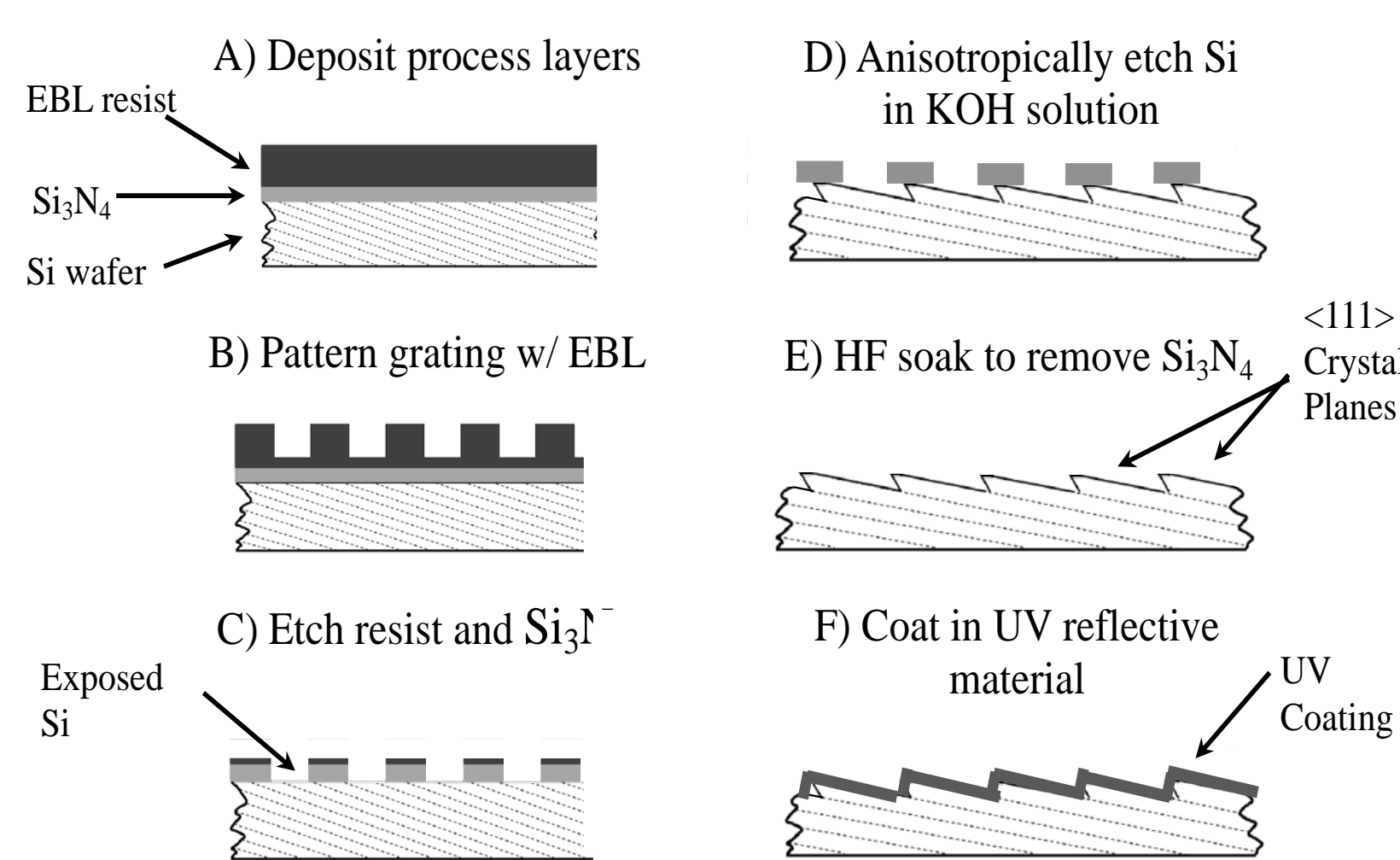
Abstract

Studying the light emitted by astronomical objects allows us to understand the chemical compositions, physical conditions, astronomical processes, and, fundamentally, the physics of what happens light years away. To enable detailed spectroscopic analysis – the study of specific wavelengths of light – high-resolution and cost-efficient reflection gratings must be fabricated. With nanoimprint lithography (NIL) being a precise and low-cost method to replicate reflection gratings for use in astronomical instruments, this study focuses on characterizing the crucial reactive ion etching (RIE) step of making gratings following NIL patterning. Using ellipsometry techniques, atomically thin layers can be measured with extremely high precision, allowing us to calculate RIE etch rates through these layers. This work enables astrophysicists to determine appropriate etch times for ongoing reflection grating fabrication projects, propelling the development of future spectroscopic missions.

Reflection Grating Fabrication

Recent advancements in the replication of reflection gratings have been made via microfabrication techniques such as **nanoimprint lithography (NIL)**.

NIL involves using a master grating as a mold to imprint itself onto a resist-coated wafer using high temperatures and pressures.

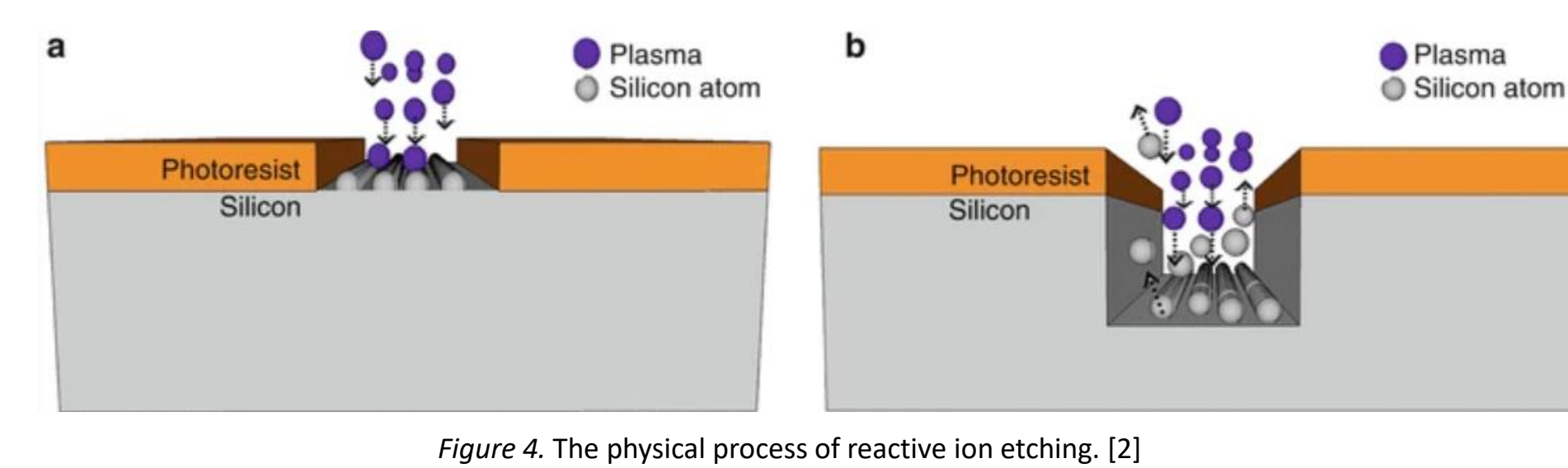


Process flow of nanoimprint lithography. This study focuses on **Step C** (Figure 2) of the NIL process.

Reactive Ion Etching

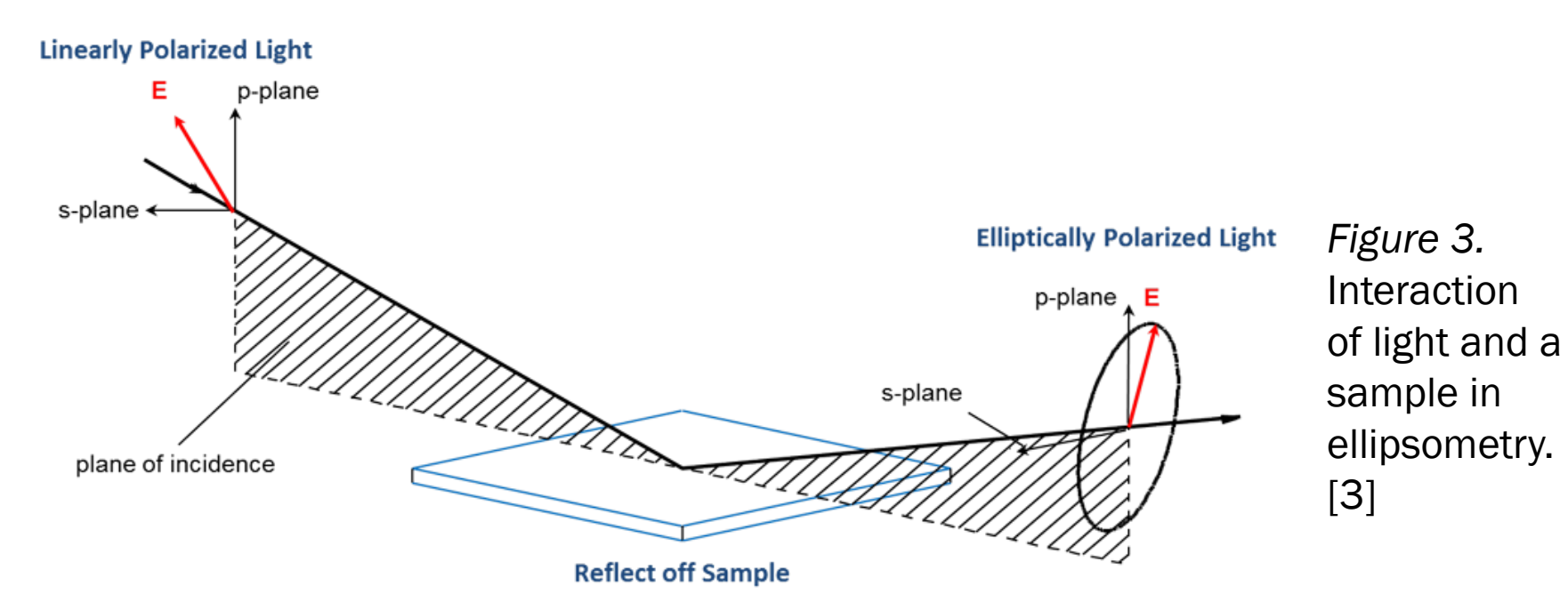
For grating fabrication, reactive ion etching (RIE) is required in order to transfer an imprinted pattern permanently.

RIE exposes bare silicon openings that will allow for the subsequent potassium hydroxide (KOH) wet-etching step. **The critical challenge for RIE is determining the “step time” required to create a successful etch – no under or over etching.**



Ellipsometry

With the help of optical techniques, ellipsometry can help **determine optical constants, thicknesses, and indexes of refraction** of thin films up to the nanometer scale. The instrument used for ellipsometry is the **ellipsometer**.



Science Case: The Missing Baryon Problem

From a census of the cosmic microwave background (CMB), astrophysicists find a discrepancy between the number of baryons in the early universe and the present day.

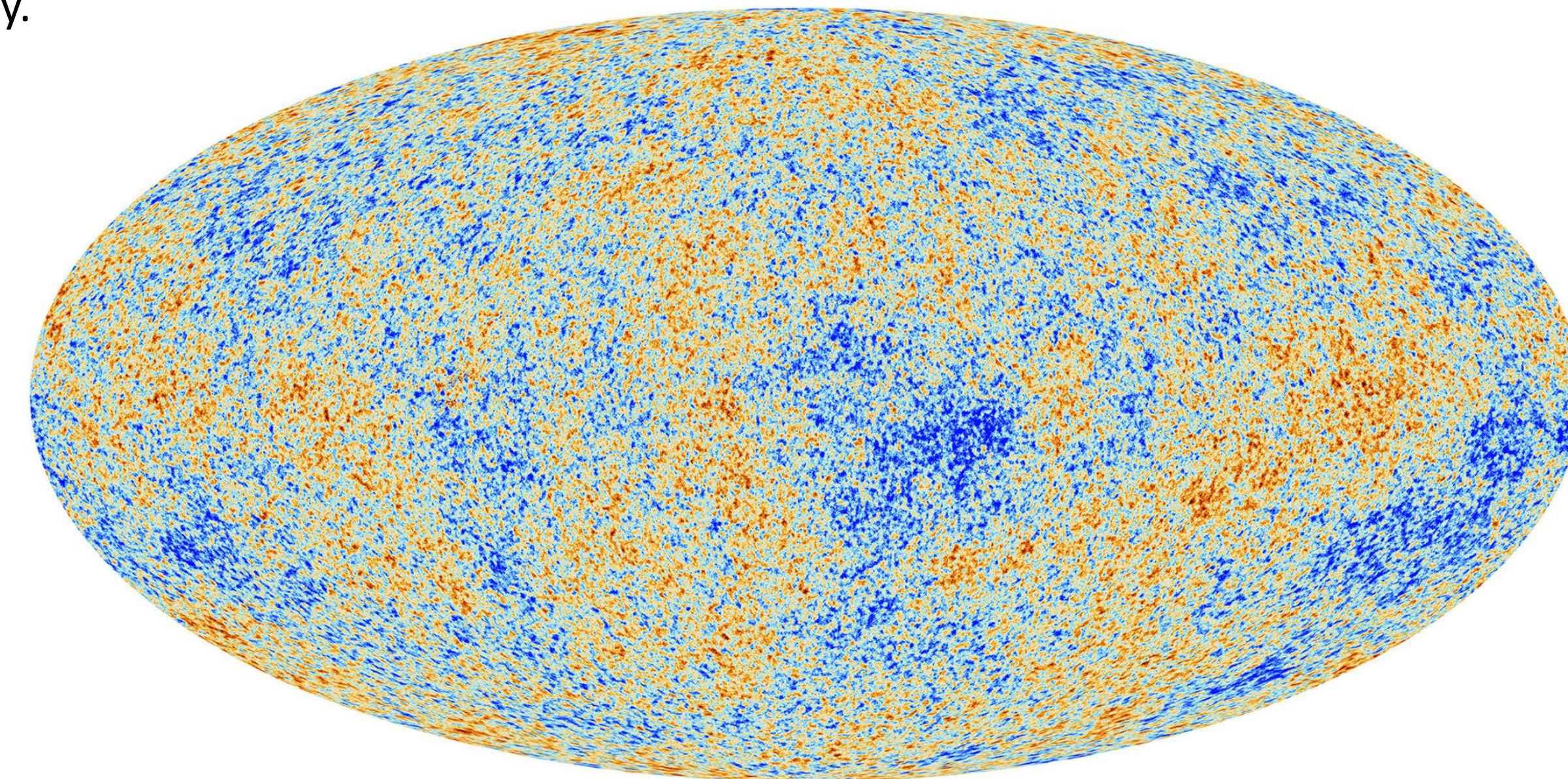


Figure 1. The Cosmic Microwave Background, as observed by the European Space Agency's Planck Observatory. [1]

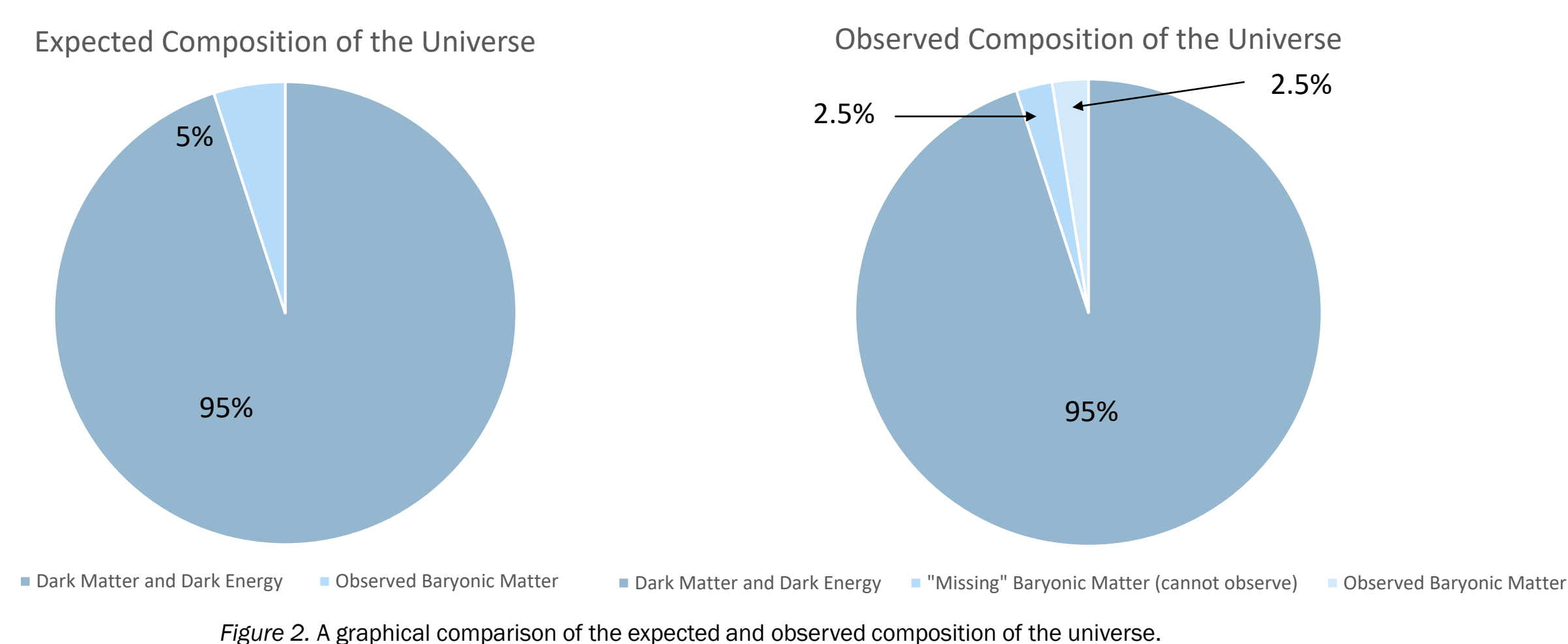


Figure 2. A graphical comparison of the expected and observed composition of the universe.

In order to conduct a more intensive survey for these “missing baryons”, said to be hidden in the Warm-Hot Intergalactic Medium (WHIM), further spectroscopy in the soft x-ray spectrum is needed. The currently active X-ray observatories, *Chandra* and *XMM-Newton*, do not have the physical capabilities to make such refined observations of the WHIM. (See Bregman 2007, Bregman et al. 2015, and references therein.)

In order to conduct a more comprehensive survey of the universe's baryons, a **new generation of more refined, high-resolution diffraction gratings must be fabricated.**

Methodology

Subject:

- Eight NXR-1025-coated wafer samples
- Eight SiN_x-coated wafer samples

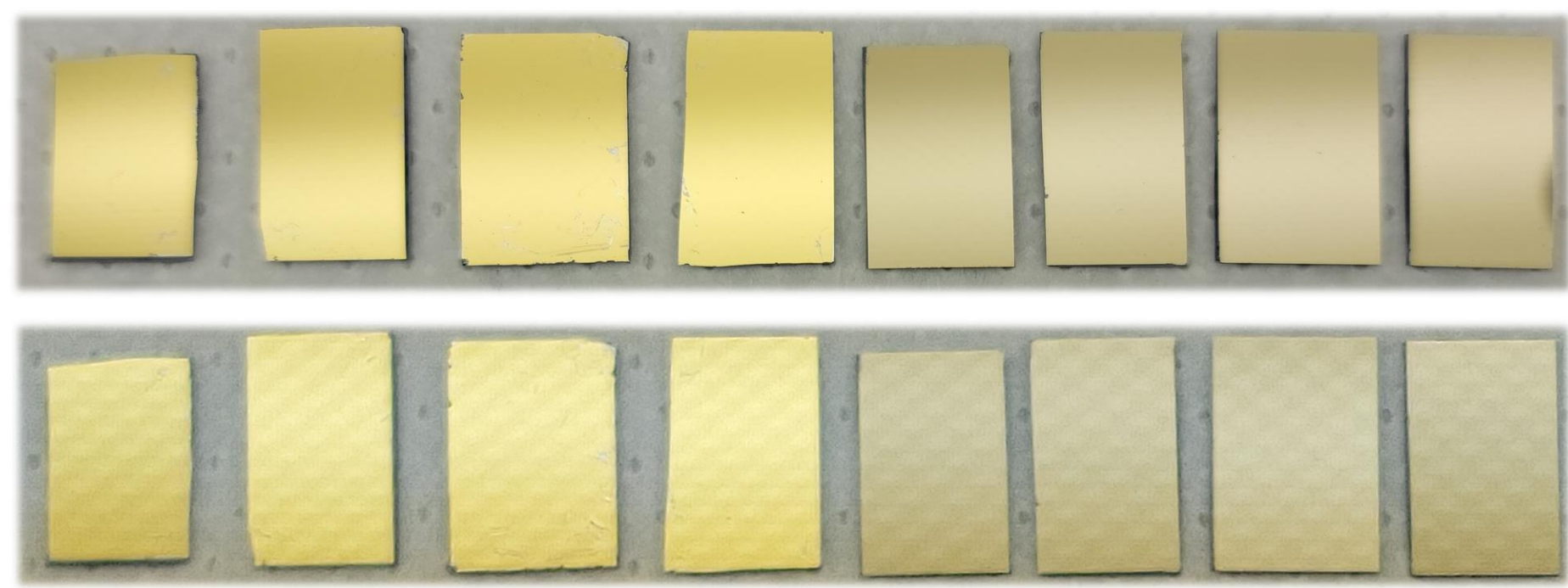


Figure 4. (Top) Four NXR-1025 coated wafer samples and four SiN_x-coated wafer samples. (Bottom) Four NXR-1025 coated wafer samples after RIE and four SiN_x-coated wafer samples after RIE.

Treatment:

- Reactive Ion Etching (RIE) – CHF₃/O₂ and Ar/O₂ etch recipes with increasing step times

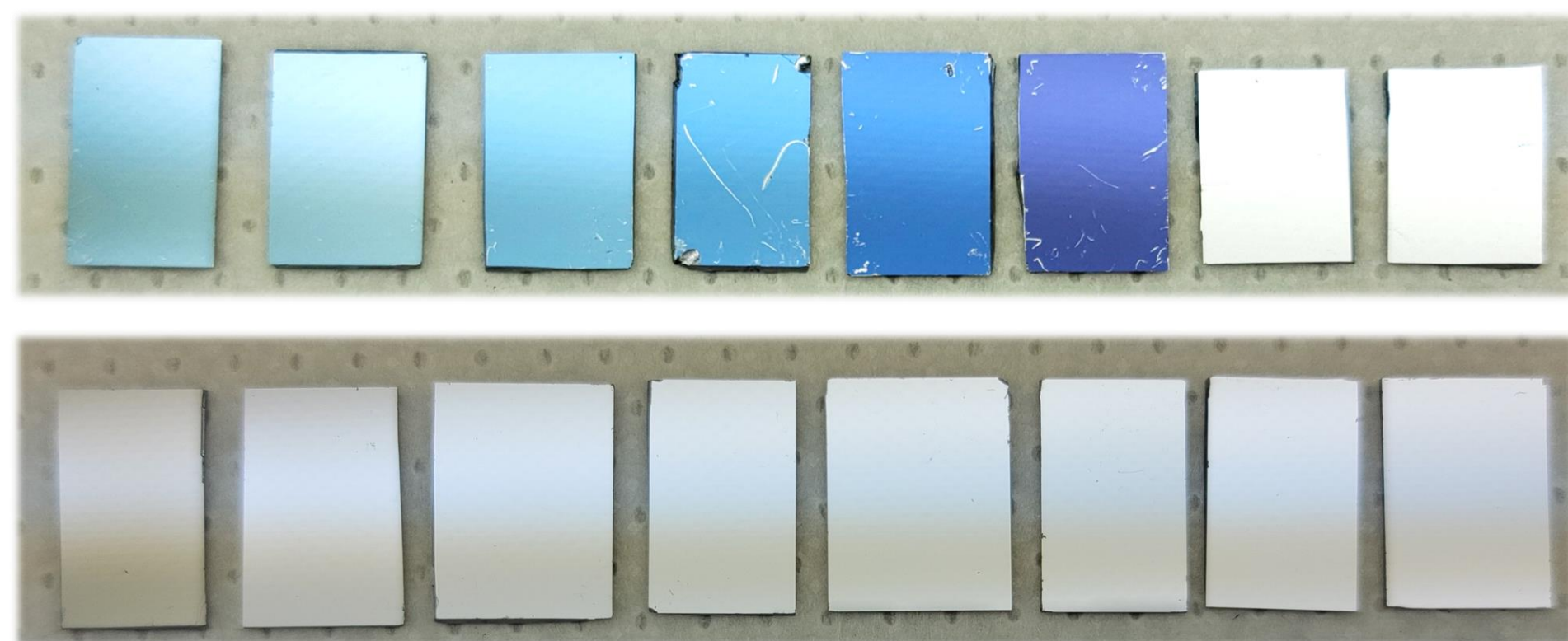


Figure 5. (Top) Eight NXR-1025 coated wafer samples after RIE. (Bottom) Eight SiN_x-coated wafer samples after RIE.

Data Analysis:

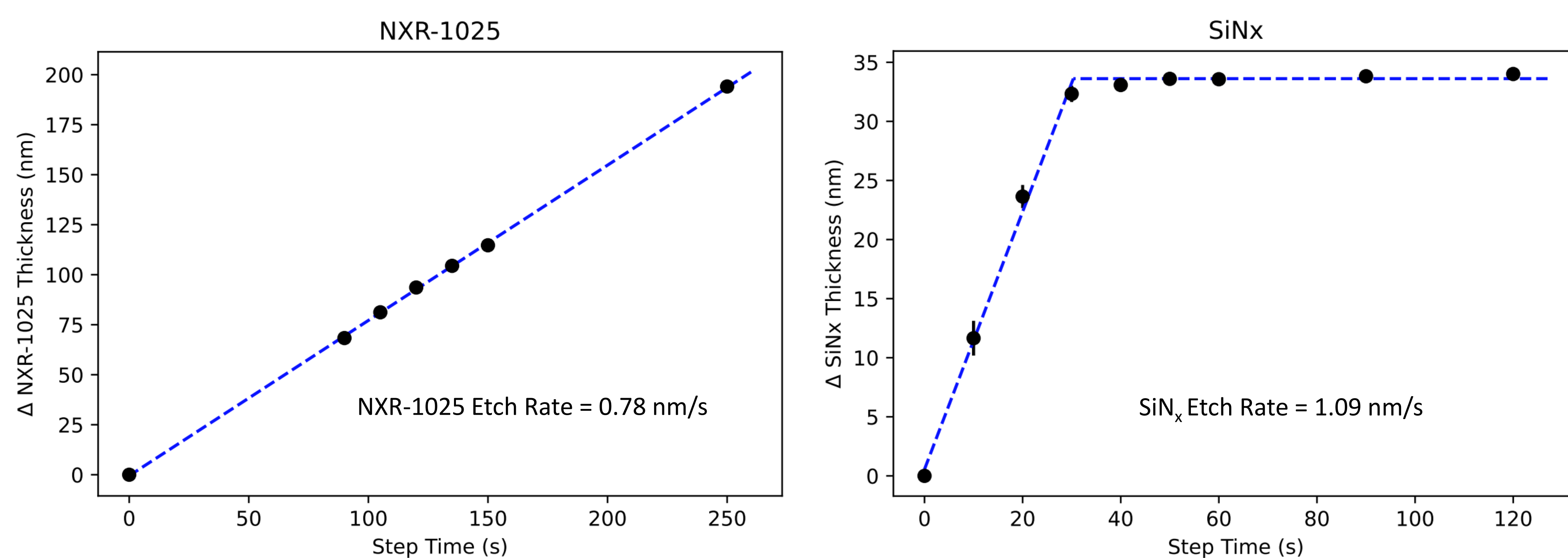
- Ellipsometer
- Graphs created with Python



Figure 7. Ellipsometer from J.A. Woollam.

Results

After plotting the change in thin film thicknesses vs. the respective step times, **etch rates for NXR-1025 and silicon nitride (SiN_x) were successfully determined.**



Conclusion

This study has shown that using ellipsometry-based techniques to determine thicknesses of thin films can successfully produce etch rates for reactive ion etching.

Future work can be further developed regarding this project. We can refine etch rate accuracy by testing more step times and executing the subsequent KOH wet etching step.

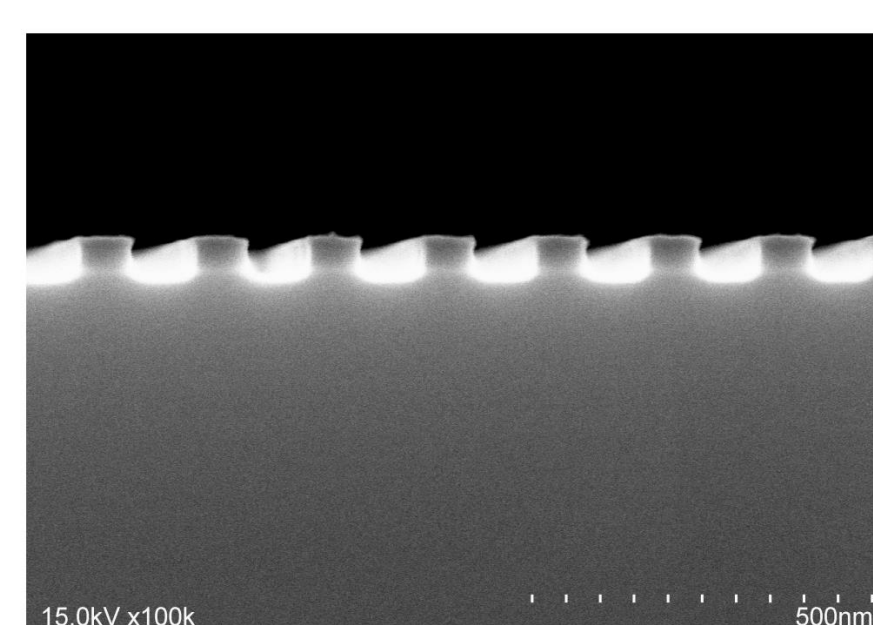


Figure 8. Silicon wafer sample after post-reactive ion etching. [4]

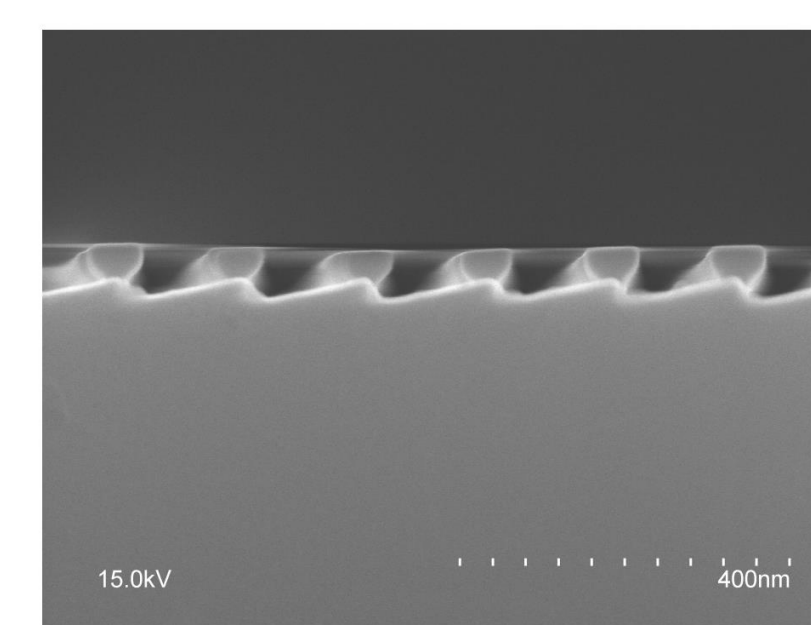


Figure 9. Silicon wafer sample after post-KOH wet etching. [4]

References

- ¹Planck Collaboration 2013
- ²Nayak et al. 2012
- ³J.A. Woollam Ellipsometry Website 2014
- ⁴DeRoo 2015

Support

This work was funded by NASA grants 80NSSC22K0159, 80NSSC21K1937 and internal funding from University of Iowa.

Purpose Statement

The purpose of this study is to understand how public health measures affect the geographical and temporal distributions of Omicron and Delta variants in university settings.

Introduction

Since the first emergence of SARS-CoV-2 in Wuhan, Hubei Province, China, and its ensuing spread across the globe, public health responses from the international to the institutional level have been implemented to mitigate the size and severity of SARS-CoV-2 outbreaks. However, the effects of these policies to limit the spread of virus have not been fully assessed. Importantly, phylogenetic analysis of viral genomes, which has revealed the origins, timeline, and dispersal of SARS-CoV-2 lineages, could aid in determining the effectiveness of specific interventions in different contexts.

University campuses have potential for increased viral transmission due to communal living, large student populations, and frequent travel. With a massive student population and international community, Purdue University surmounted these challenges through their comprehensive "Protect Purdue Plan" in the summer of 2020, which implemented regular testing, de-densification of classrooms and living spaces, and international and domestic travel regulations (Ciubotariu *et al.*)

In light of high vaccination rates, Purdue has returned to many pre-COVID policies. Therefore, the present study applied a phylogenetic approach to analyze SARS-CoV-2 genomes from Purdue University and determine how the university's loosened COVID regulations affect the transmission patterns and origins of SARS-CoV-2 lineages on campus. Such phylogenetic analysis can help determine whether cases were due to independent introductions from distinct geographical locations, or linked transmission through adjacent communities.

Our dataset includes Omicron and Delta viral genomes from Purdue University, as well as related sequences from GISAID. We applied a Bayesian coalescent approach to generate a Maximum Clade Credibility (MCC) phylogenetic tree. In order to make phylogeographic inferences, we performed a pairwise estimate of parsimony scores to estimate the association between Purdue sequences and sequences from certain geographical areas, allowing for us to assess the patterns of migration and transmission.

Methods

Genomic Dataset

In order to determine the geographical locations outside of the university from which clades of SARS-CoV-2 originated, we found related sequences in GISAID, making our dataset total to 142 sequences. GISAID is an open access database where genomes of viruses which require prompt responses may be published. Thus, GISAID houses the greatest number of SARS-CoV-2 genomes.

Sequence Alignment

When comparing many RNA sequences, insertions and deletions (indels) occur due to errors when sequencing the viral genome or due to mutations acquired in nature. Such indels result in frameshift mutations that can result in the comparison of different loci and must be corrected. We performed a multiple sequence alignment through NextAlign CLI via the command line, which aligns sequences with respect to parsimony and gap penalty.

BEAST MCC Tree

We used the Bayesian Evolutionary Analysis Sampling Trees (BEAST) software package to generate the Maximum Clade Credibility (MCC) phylogenetic tree. BEAST uses a Markov chain Monte Carlo (MCMC) technique to sample the posterior distributions of model parameters; we used a Markov chain length of 100 million steps. We used the HKY substitution model, which accounts for variation in the nucleotide base frequencies and different rates of transitions and transversions, combined with a gamma distribution to model site-rate heterogeneity. A strict clock was used, which assumes that all branches have the same rate of evolution; we fixed this clock to a substitution rate of 8E-4 subs./site/year

Parsimony Score Analysis

To elucidate the origins of the viral lineages, we performed pairwise estimates of Parsimony Scores (PS) in the BaTS software. PS are calculated by determining the number of character changes between nodes and tips on a tree, and reflect the number of geographical transitions. We subtracted the PS value of joint and independent categorizations of Purdue and state X, and determined the number of independent introductions based on significant delta values.

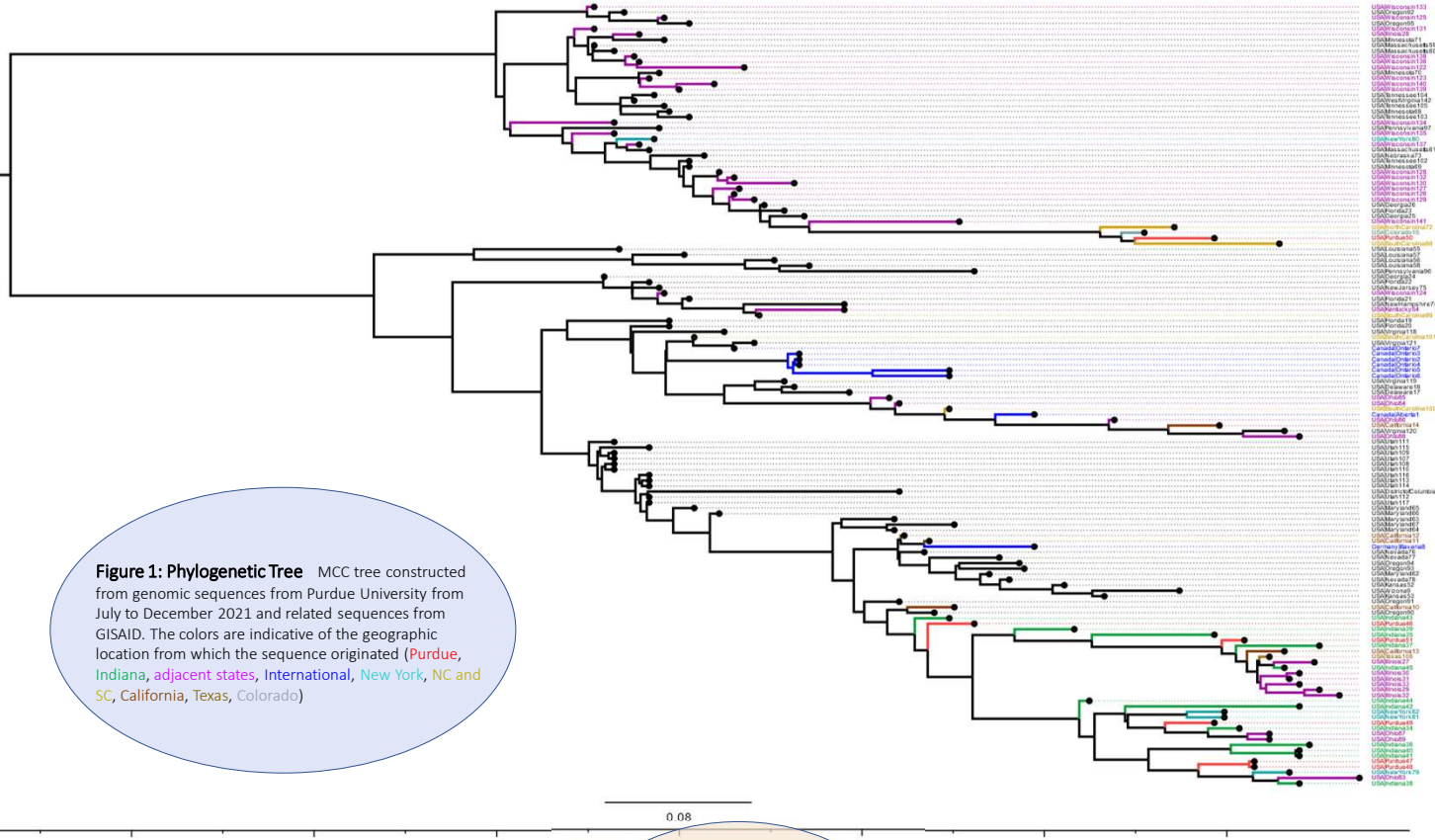


Figure 1: Phylogenetic Tree MCC tree constructed from genomic sequences from Purdue University from July to December 2021 and related sequences from GISAID. The colors are indicative of the geographic location from which the sequence originated (Purdue, Indiana, adjacent states, International, New York, NC and SC, California, Texas, Colorado)

Results

Based on our pairwise estimates of PS, we hypothesize 6 introductions from the following geographic locations:

- Significant migration: Indiana
- Some Migration: Colorado, Illinois, New York, Ohio, South Carolina
- Possible migration: California, North Carolina, Texas, and Wisconsin

From this data, there is no evidence of lineages being sourced directly from international locations.

Figure 2: BaTS Parsimony Scores The table below depicts the pairwise estimates of Parsimony Scores (PS) for 13/33 geographic locations from our data, which are states that are either adjacent, international, or differ significantly in delta values. PS is the number of character changes on the tree between "Purdue" & "non-Purdue" when:

- PS3: Purdue and StateX considered as independent characters
- PS2: Purdue-StateX are considered as a joint character.

	Indiana	Illinois	Kentucky	Ohio	Wisconsin	California	Texas	Colorado	NY	NC	SC	Germany	Canada
3-State	13.647	10.196	7.000	12.062	20.049	10.930	7.000	7.000	9.000	7.000	9.990	7.000	8.945
2-State	10.328	9.838	7.000	11.735	20.006	10.886	6.933	6.846	8.778	6.909	9.501	7.000	8.945
PS3-PS2	3.319	0.358	0.000	0.327	0.043	0.044	0.067	0.154	0.222	0.091	0.489	0.000	0.000

References:

Chen, J., Wang, R., Gilby, N. B., & Wei, G. W. (in press). Omicron Variant (B.1.1.529): Infectivity, Vaccine Breakthrough, and Antibody Resistance. *Journal of Chemical Information and Modeling*.
 Ciubotariu, I. I., Dorman, J., Perry, N. M., Gorenstein, L., Kattar, J. J., Feki, A. A., Zine, A., Hendrix, G. R., Wilkes, R. P., Kitchen, A., & Carpi, G. (in press). Genomic Surveillance of SARS-CoV-2 in a University Community: Insights into Tracking Variants, Transmission, and Spread of Gamma (P.1) Variant. *Open Forum Infectious Diseases*.

Acknowledgments:

I would like to thank Dr. Kitchen and the members of the Evolutionary Anthropology lab for guidance throughout the project, Faculty and staff of the Secondary Student Training Program for the opportunity to research, and the Carpi Lab at Purdue University for sharing viral genome sequences.

Conclusion and Discussion

- While in-state and adjacent state migration remain dominant (Ciubotariu *et al.*), interestingly, our analyses also support relatively distant migration from non-adjacent states: South Carolina, New York, and Colorado.
- Widespread origins of viral lineages in our analyses may be attributed to various factors, such as the lifting of travel restrictions at Purdue prior to our study, and Omicron's higher transmissibility (Chen *et al.*)
- Because our analyses are based on a subset of Purdue sequences, larger analyses are needed to definitively elucidate the origins of the campus's viral lineages by confirming which locations have the strongest associations, aiding in determining which travel regulations are necessary.

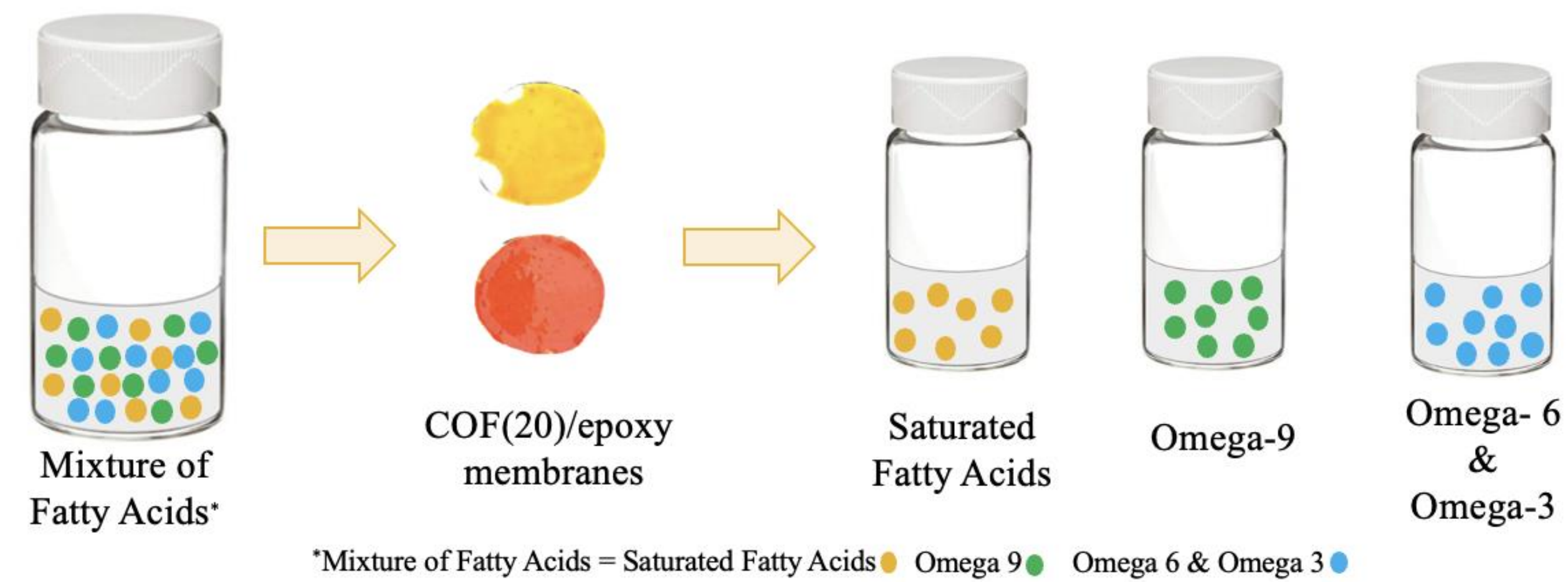
Highly Effective Separation of Fatty Acids Derived from Vegetable Oils Using COF Incorporated Epoxy Membranes

Nathan Xiong¹, Nimesh P. R Ranasinghe Arachchige², Ned B. Bowden²
¹The Bishop's School, ²Department of Chemistry, University of Iowa

Introduction

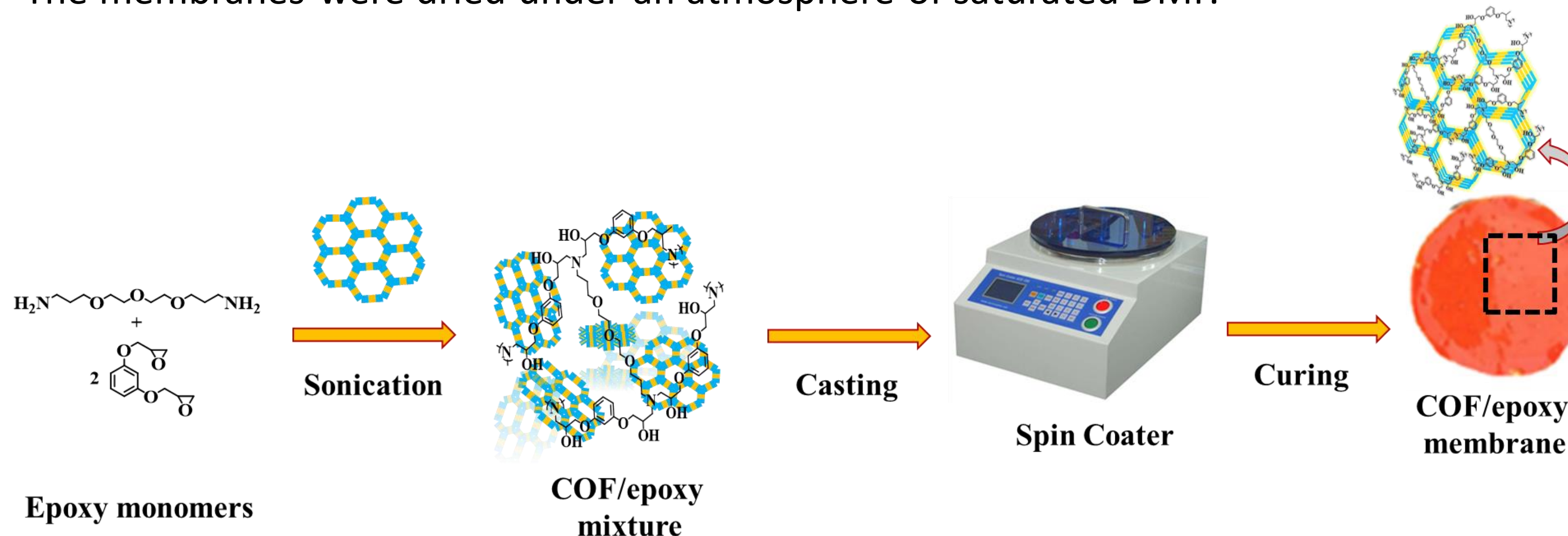
Over 200 million tons of vegetable oils produced each year, and this amount is increasing by 5% each year. Vegetable oils are usually a mixture of saturated and polyunsaturated fatty acids that individually are very valuable but are difficult to separate from each other.

Membrane separations offer an inexpensive alternative to traditional methods of purification such as distillation and column chromatography, and it is accessible to many organic chemicals that are currently difficult to purify. In this work, we report the development of a mixed matrix membrane using covalent organic frameworks (COFs) incorporated within an epoxy polymer (COF(n)/epoxy) that can separate fatty acids from each other by utilizing highly ordered structures and uniform crystalline pores in COFs.



Preparation of COF(20)/epoxy membrane

These highly flexible, hybrid membranes were fabricated via solution casting method: The membranes were dried under an atmosphere of saturated DMF.



Fluxes and relative flux of different fatty acids using COF(20)/epoxy membranes

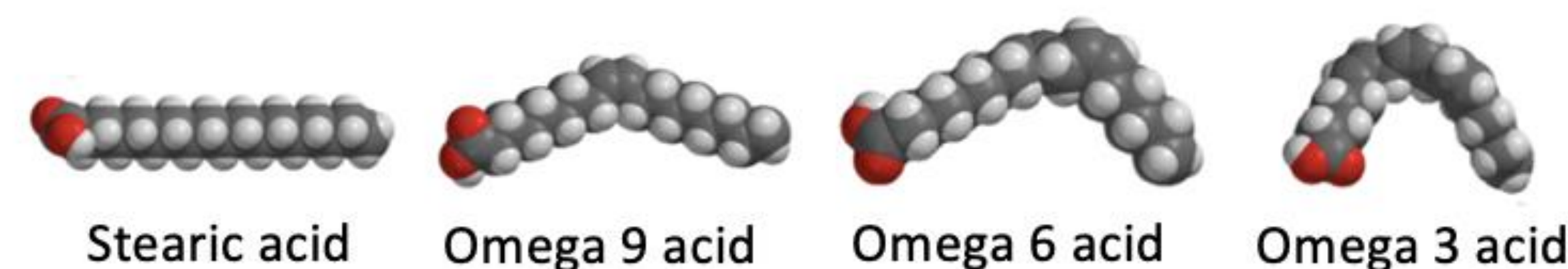
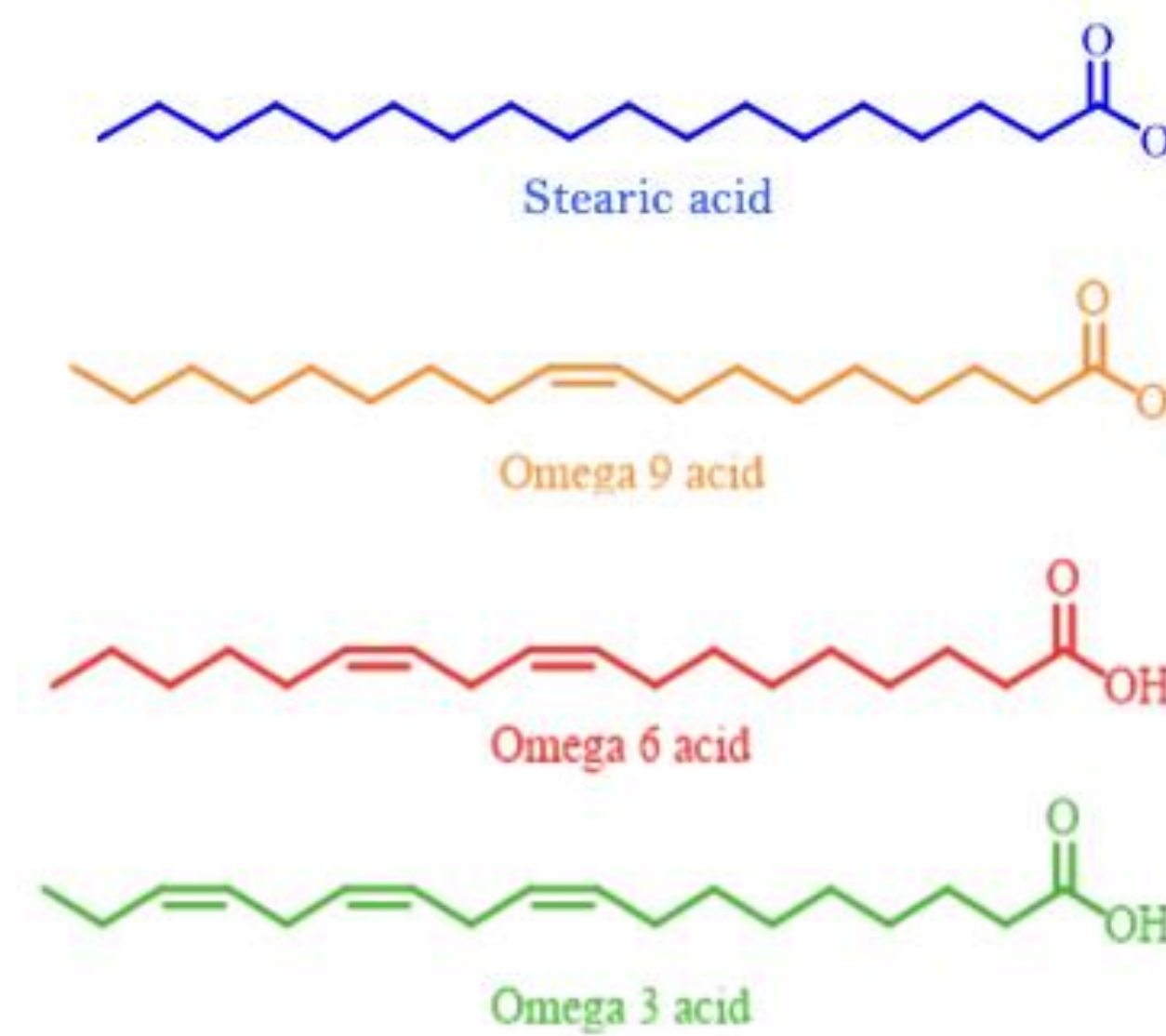
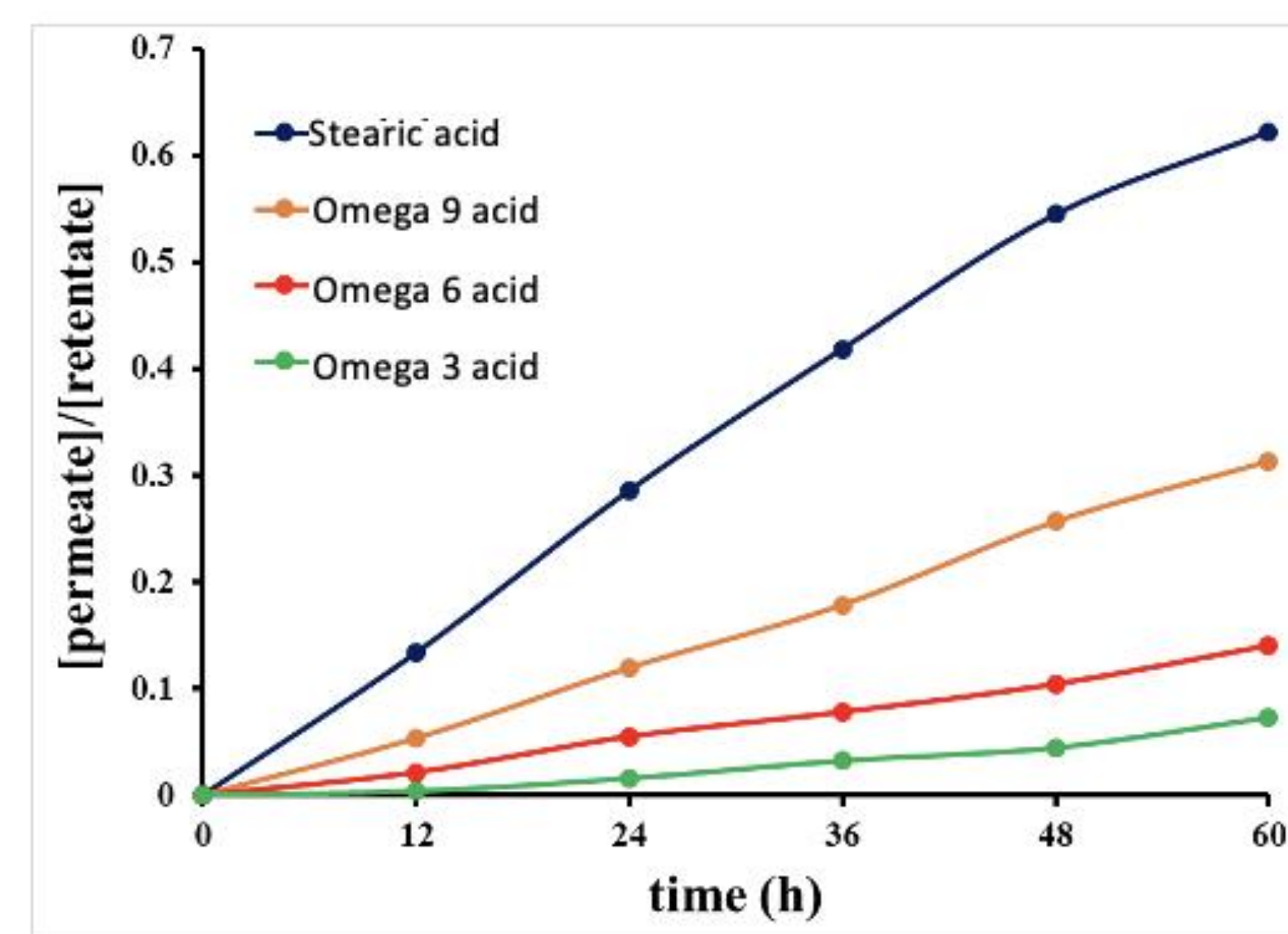
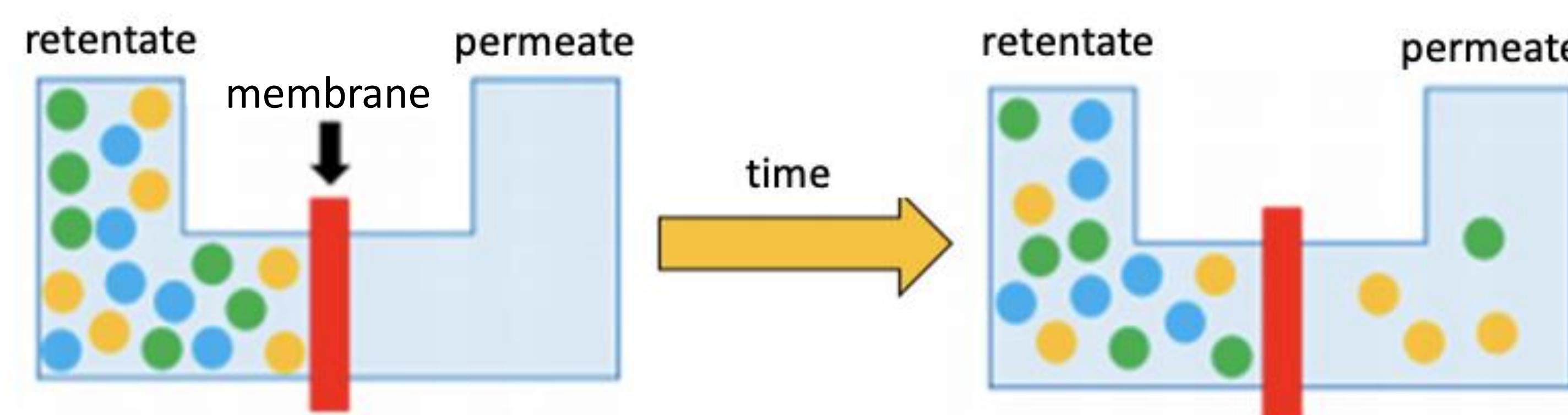
	Absolute flux {10 ⁻⁷ } (mol/h cm ²)				Flux of chemicals relative to Omega-3 acid			
	Stearic acid	Omega-9 acid	Omega-6 acid	Omega-3 acid	Stearic acid	Omega-9 acid	Omega-6 acid	Omega-3 acid
HCOF (1.3 nm)	6.7	3.7	2.4	1.8	3.7	2.0	1.3	1
TpPA COF (1.8 nm)	13.9	6.6	4.3	3.1	4.5	2.2	1.4	1
TpBD COF (2.4 nm)	15.1	11.3	6.4	5.2	2.9	2.1	1.2	1

As the pore size increases, the absolute fluxes also increase, but the selectivity decreases.

TpPA achieved the best separation; stearic acid's flux was 4.5x faster than that of Omega-3's.

Separation of fatty acids through COF(20)/epoxy membranes

We used a diffusion apparatus to run our nine separations.



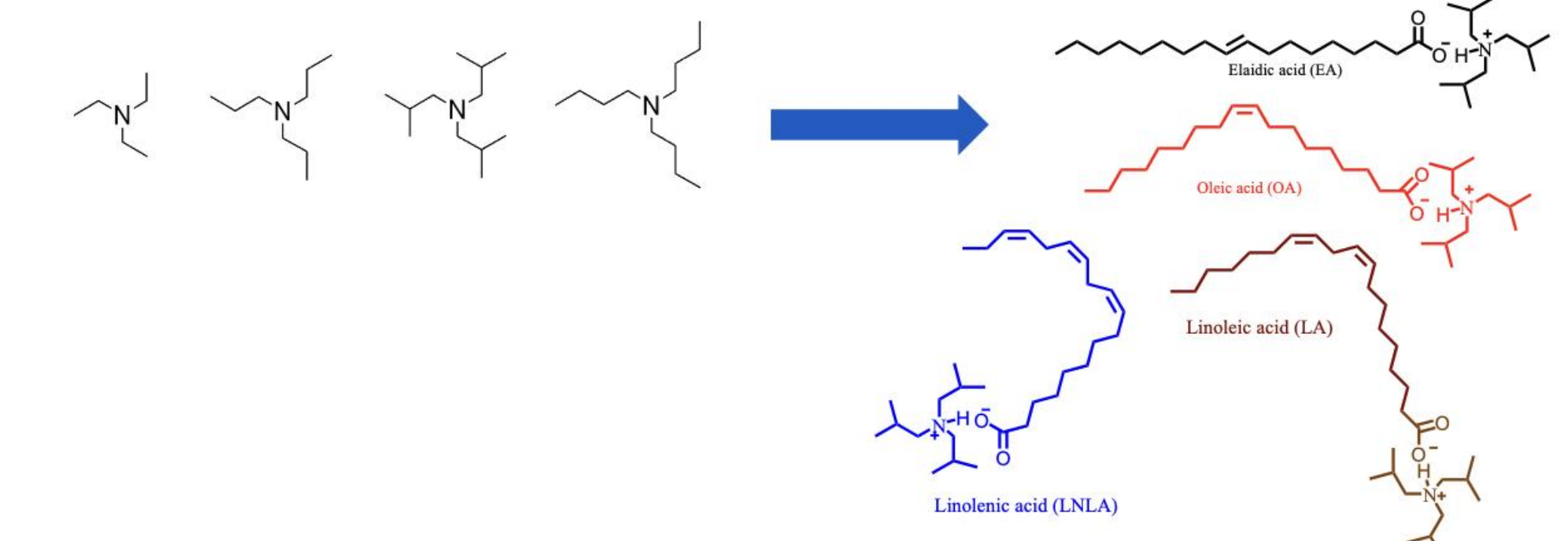
The flux of the fatty acids depends on their degree of saturation: acids with more double bonds have a higher curvature and critical area, leading to a slower flux.

Conclusions

The discovery that membranes can facilitate separation between fatty acids provides a highly promising alternative for industry: a cheap, efficient, and green method to obtain valuable starting materials that are otherwise wasted in daily usage. Our identification that TpPA COFs are the optimal membranes for these separations also reveal what pore size range is effective, and which other bigger or smaller pores do not work as effectively.

Future work

We are looking to add different types of amines with the fatty acids with the goal of increasing selectivity within our acids.



The amines will form a salt with the acids, which will increase the acid's size, which will then increase separation.

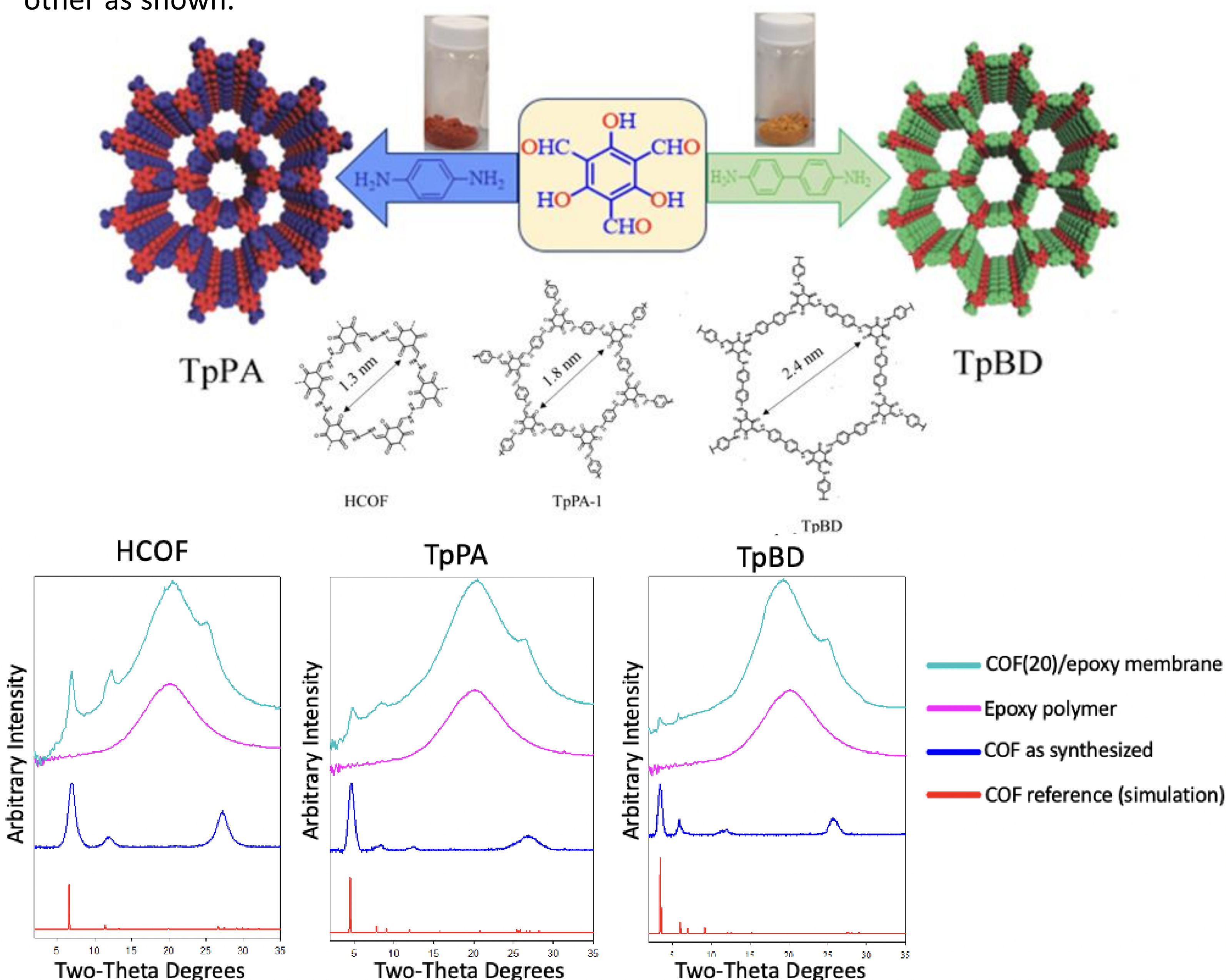
Acknowledgements

I would like to thank Professor Ned Bowden and Nimesh Pasan Ranasinghe, the graduate student who mentored me through the whole project, for this amazing opportunity and experience. I would also like to thank the Bowden research group for welcoming me into the group, and I wish them the best of luck in the future.



Synthesis of COFs with different pore sizes

Each COF forms 2D sheets with hexagonal pores, and the sheets stack on top of each other as shown.



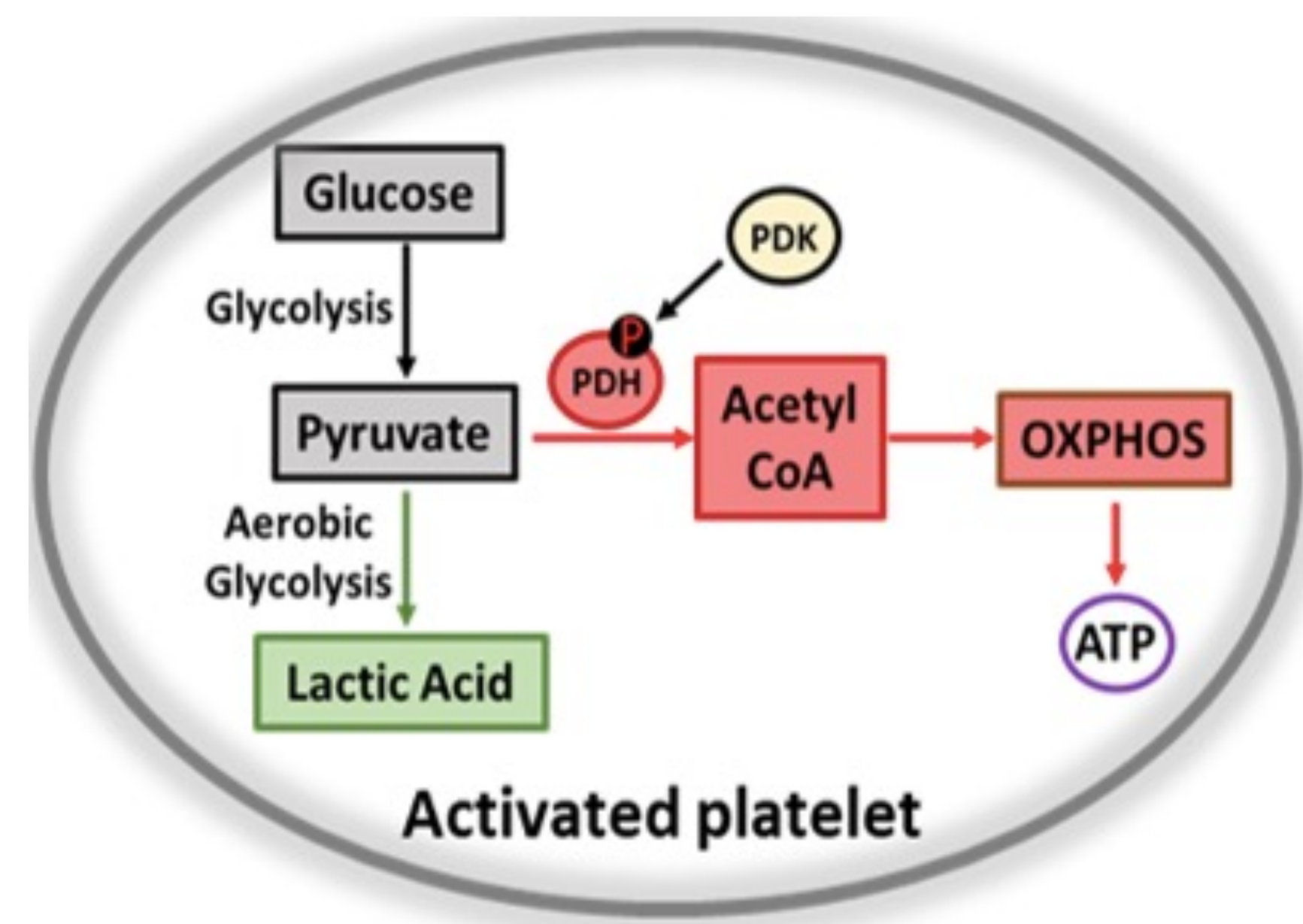
Targeting pyruvate dehydrogenase kinases inhibits thrombosis and platelet aggregation

Rebecca Xue¹, Manasa K. Nayak², PhD, Gagan D. Flora², PhD, Anil K. Chauhan², MTech, PhD

Blue Valley West High School¹, University of Iowa Medical Laboratories²

Introduction

- Platelets are disc-shaped cells present in blood and are involved in the formation of blood clots. Abnormal clotting blocks blood supply and causes heart attacks and ischemic stroke.
- Current antiplatelet treatments exist but cause unwanted side effects such as bleeding complications in thrombosis patients.
- Dichloroacetate, a known inhibitor of pyruvate dehydrogenase kinases (PDK) 1-4, inhibits platelet function and arterial thrombosis. (Nayak et al., 2018)
- **What effect does targeting PDK have on platelet function and arterial thrombosis?**



Methods

- Wild-type (PDK2^{+/+}, PDK4^{+/+}), double knockout (PDK2^{-/-}, PDK4^{-/-}) and single knockout mice (PDK2^{-/-} or PDK4^{-/-}) were used in the experiments.
- Various in vivo and in vitro techniques were used to observe platelet aggregation.

Results

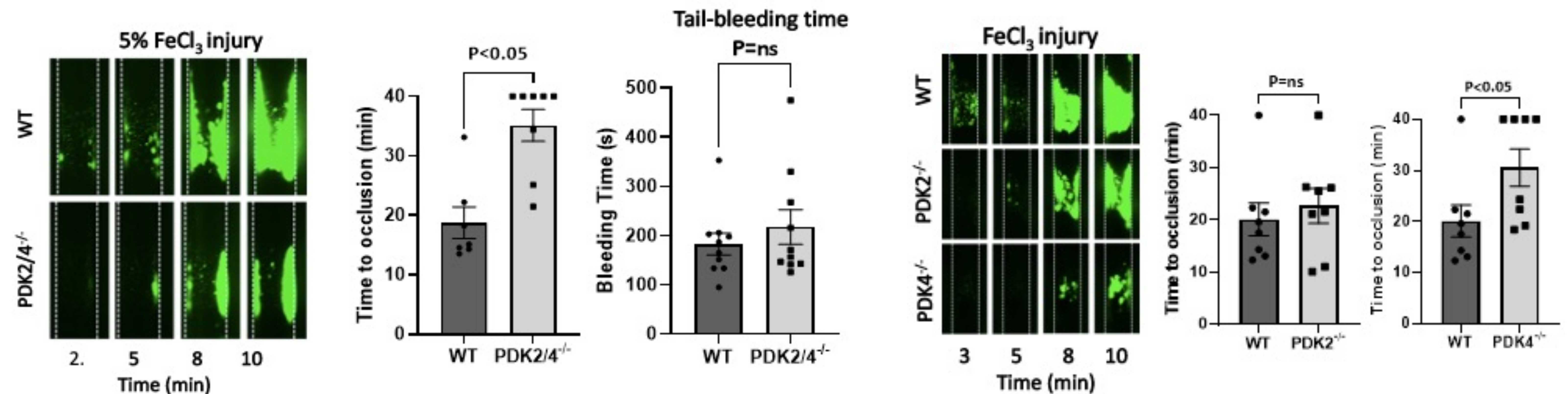


Figure 1: Arterial thrombosis is significantly inhibited in single KO and double KO mice.

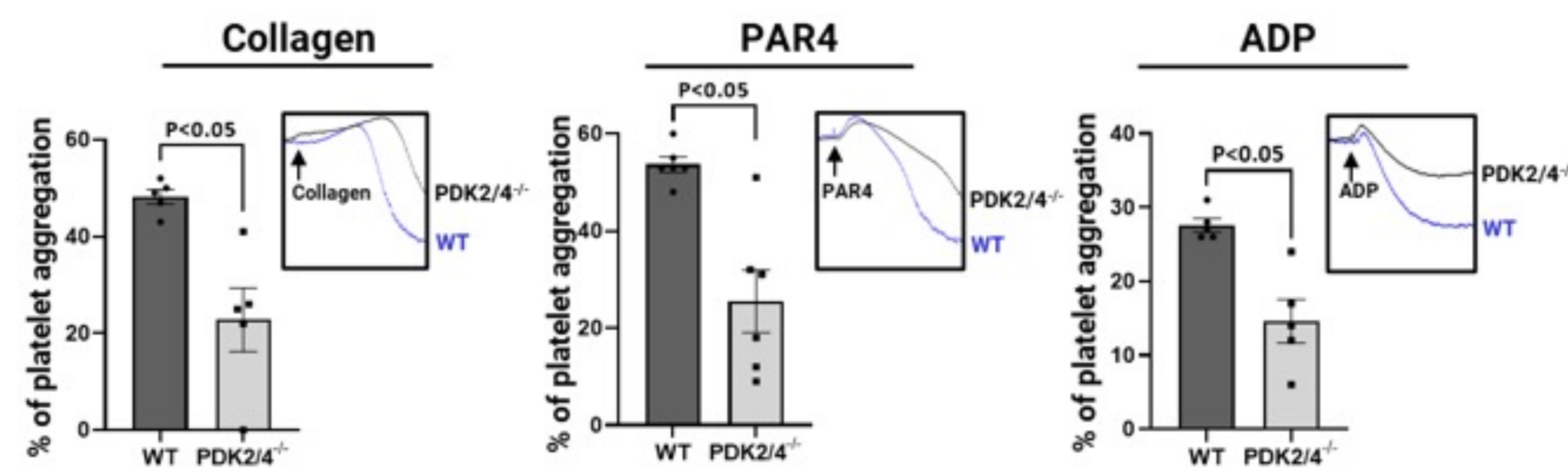


Figure 2: Platelet aggregation is significantly inhibited in double KO mice.

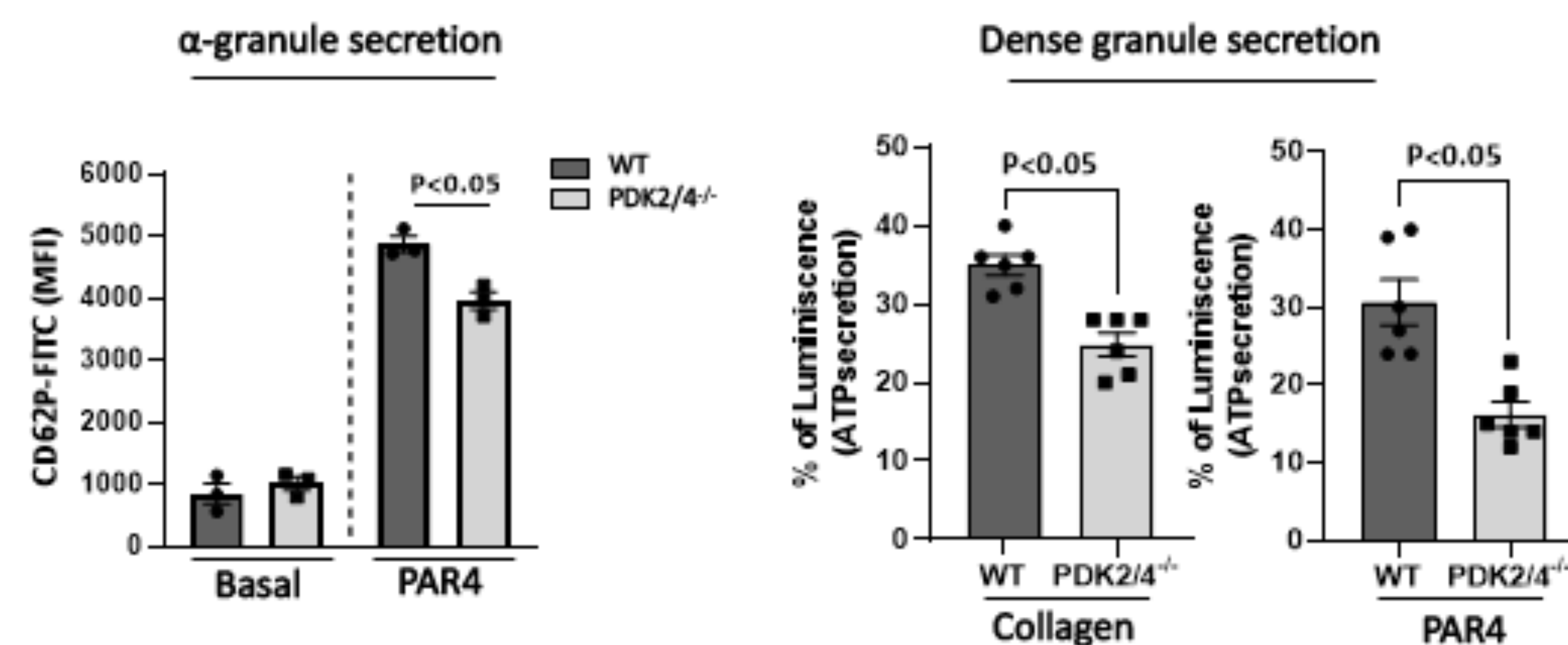


Figure 3: Platelet secretion is significantly inhibited in double KO mice.

Implications

- Inhibiting PDK should be further explored as a promising novel strategy for inhibiting platelet aggregation and arterial thrombosis.
- Future work should be done to determine the roles (if any) of PDK 1/3.

Acknowledgments

I would like to thank the Chauhan Lab for allowing me to have this opportunity, as well as Dr. Chauhan, Dr. Nayak, Dr. Flora, and Dr. Kumskova for their invaluable guidance.

References

Nayak, M. K., Dhanesha, N., Doddapattar, P., Rodriguez, O., Sonkar, V. K., Dayal, S., & Chauhan, A. K. (2018, August 14). Dichloroacetate, an inhibitor of pyruvate dehydrogenase kinases, inhibits platelet aggregation and arterial thrombosis.

Purpose Statement

We will infer the **sources of infection of SARS-CoV-2 Omicron and Delta variants** in Purdue University through phylogenetic analysis. We will use molecular clock and Bayesian coalescent approaches to reconstruct the phylogenetic tree sequences from Purdue University to identify the origin of closely related sequences. We will also investigate the virus's origins' **correlation with the university's COVID restriction policy**.

Introduction

- Severe acute respiratory syndrome coronavirus 2 (SARS-CoV-2) emerged in late 2019 and subsequently spread across the globe, including the United States. As of July 20, 2022, the virus has caused over a million deaths in the U.S. (Dong et al., 2020) despite widespread implementation of interventions directed at curbing transmission and limiting infection (i.e., masking, social distancing, and vaccination). Importantly, it remains unclear what effect these interventions had on the spread of SARS-CoV-2 in the U.S..
- Universities are particularly vulnerable to superspreading due to their large numbers of students, faculty, and staff, frequent social activities, communal living, and in-person instruction, all of which may facilitate efficient viral transmission to large numbers of individuals.
- Purdue University is a large public university in Indiana and is representative of large public universities across the U.S.. In response to the pandemic, Purdue implemented a plan to protect students that included masking, social distancing, suspension of university-associated travel, and frequent community surveillance. These measures changed over time as vaccination rates increased and SARS-CoV-2 incidence waxed and waned. The effect of these policies on the spread of virus into the university community remains unknown.
- Here, we attempt to identify the origins of SARS-CoV-2 Omicron and Delta variant sequences from the Purdue community as an example of a large public university. Recent study discovered the Gamma variant in Purdue entered primarily from Indiana and Illinois. With a more relaxed COVID policy, we want to compare the transmission routes of Omicron and Delta variants to that of Gamma's (Ciubotariu et al., 2022). This analysis builds a foundation for future analysis on the effects of mitigation policy on SARS-CoV-2's spread.

Methodology

1. Data collection

Viral genome sequences from Purdue were shared with us by the Carpi Lab (Purdue University). Additional sequences were downloaded from GISAID (<https://gisaid.org>), an open access website hosting virus sequence data. Using GISAID's AudacityInstant, we collected sequences closely related to a subset of SARS-CoV-2 sequences sampled from Purdue University.

We aligned our RNA sequences both manually using Seqotron and with NextAlign, a command-line tool, to ensure accurate homology between sequences.

2. Analysis and inferences

Reconstruction of the phylogenetic tree:

We used the Bayesian Markov chain Monte Carlo methods in BEAST to reconstruct the phylogenetic tree of our subset of Purdue sequences (Drummond & Rambaut, 2007). Our analysis used a HKY nucleotide substitution model, a gamma site heterogeneity model, strict molecular clock, a coalescent constant size tree prior, a UPGMA starting tree, and a Markov chain of length 100 million generations.

Phylogenetic analysis in a domestic migration context:

To estimate the number of introductions of Omicron and Delta variants to Purdue from different U.S. states, we used the Bayesian analysis of Tip Significance testing package (BaTS) to calculate the parsimony score (PS) of the posterior distribution of trees that BEAST produced (Parker et al., 2008).

Results

- Purdue sequences are nested within Indiana sequences, indicating this subset of sequences from Purdue were likely the product of local transmission.

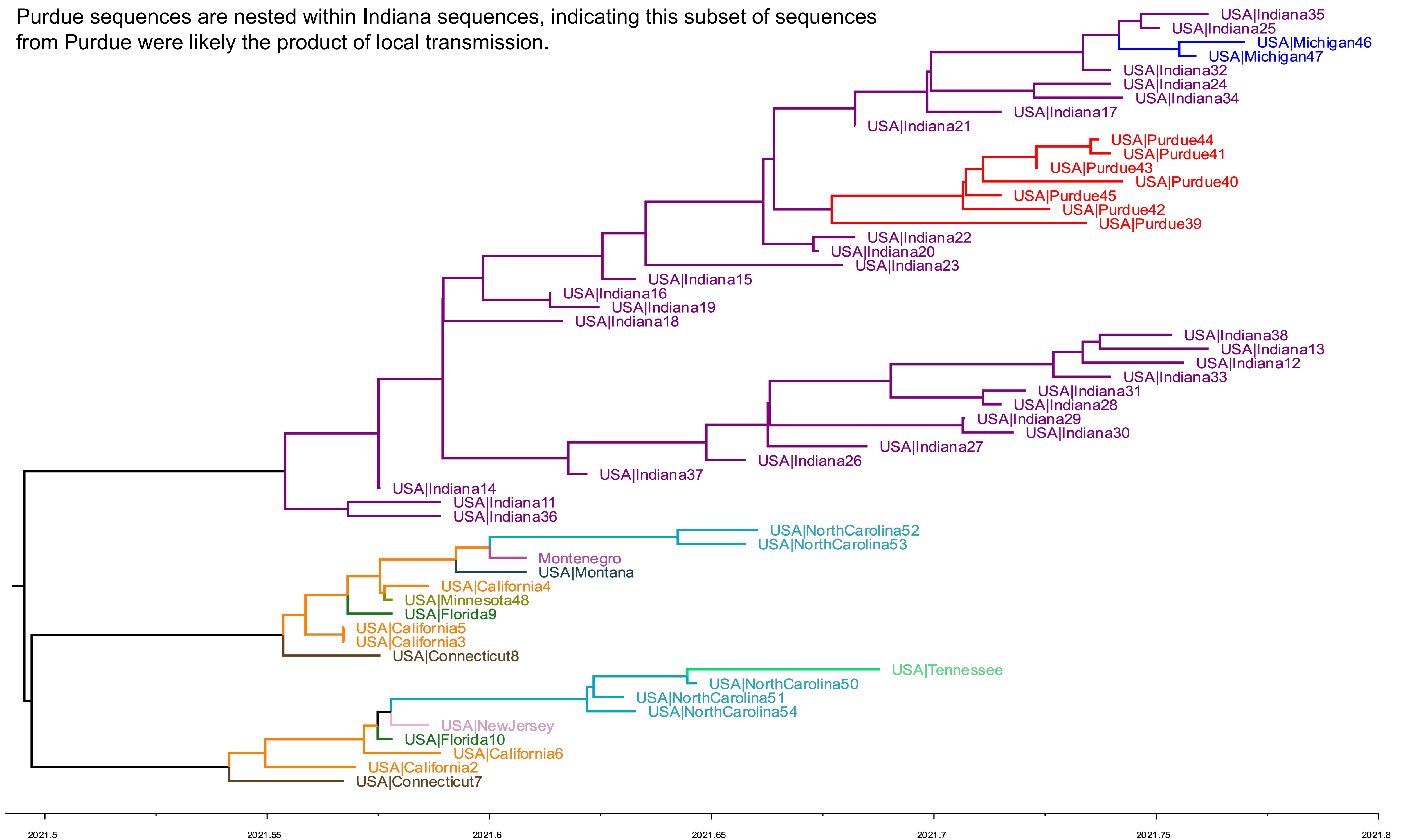


Fig 1. Time-informed Maximum Clade Credibility tree of Omicron and Delta genomes from Purdue and circulating Omicron and Delta genomes from 10 U.S. states and 1 other country.

- 12 pairwise estimates on parsimony scores (PS) to investigate Purdue sequences' association with other states and countries. The difference between the 3-state analysis and 2-state analysis of Purdue and Indiana is 1.003 while the difference for other state and countries is 0, indicating 1 introduction from Indiana to Purdue.

Discussion and Conclusions

- This project was a part of a study looking at a subset of over 700 Omicron and Delta genome sequences from Purdue. Ultimately, we will compare these 700 sequences' sources of infection and Gamma's sources of infection to infer about the efficacy of Purdue's COVID protocols.
- In the context of high vaccination rates and relaxed COVID restrictions, including the resumption of international travel, the subset of viruses analyzed here were still introduced to the university through **local transmission**. This is similar to a previous study of the introduction of Gamma variant viruses to Purdue, which found viruses mostly came from Indiana and Illinois. Interestingly, this occurred when there were lower vaccination rates and stricter COVID regulations in place, and presents a series of questions that require additional exploration: Why is it that when international travel resumed, the transmission routes stayed local? What factors contributed to this phenomenon – external factors like the high vaccination rate and/or intrinsic factors such as changes in SARS-CoV-2 infectiousness?

References

- Ciubotariu, I., Dorman, J., Perry, N. M., Gorenstein, L., Kattoor, J. J., Fola, A. A., Zine, A., Hendrix, G. K., Wilkes, R. P., Kitchen, A., & Carpi, G. (2022). Genomic Surveillance of SARS-CoV-2 in a University Community: Insights Into Tracking Variants, Transmission, and Spread of Gamma (P.1) Variant. *Open Forum Infect Dis*, 9(7), ofac268. <https://doi.org/10.1093/ofid/ofac268>
- Dong, E., Du, H., & Gardner, L. (2020). An interactive web-based dashboard to track COVID-19 in real time. *Lancet Infect Dis*, 20(5), 533-534. [https://doi.org/10.1016/S1473-3099\(20\)30120-1](https://doi.org/10.1016/S1473-3099(20)30120-1)
- Drummond, A. J., & Rambaut, A. (2007). BEAST: Bayesian evolutionary analysis by sampling trees. *BMC Evol Biol*, 7, 214. <https://doi.org/10.1186/1471-2148-7-214>
- Parker, J., Rambaut, A., & Pybus, O. G. (2008). Correlating viral phenotypes with phylogeny: accounting for phylogenetic uncertainty. *Infect Genet Evol*, 8(3), 239-246. <https://doi.org/10.1016/j.meegid.2007.08.001>

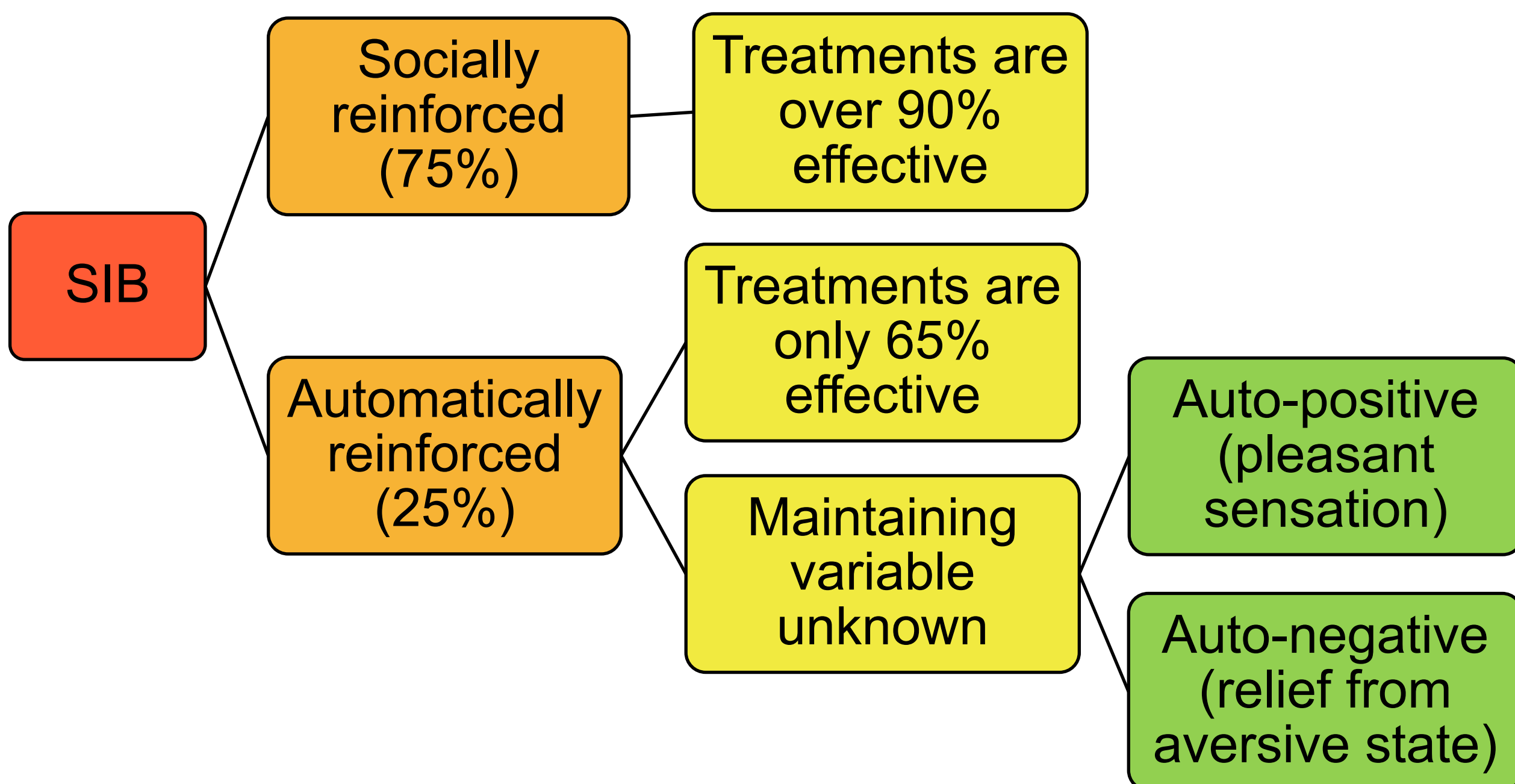
Differences in Indices of Happiness and Distress in Two Individuals with IDD and Automatically Reinforced Self Injurious Behavior (ASIB)

Sarah Yun¹, Matthew J. O'brien, PhD², Alex Pauls, MA², Kelly M. Schieltz, PhD²

¹Homestead High School, ²University of Iowa

Introduction

- Self injurious behavior (SIB) is common in individuals with intellectual developmental disabilities (IDD; Soke et al., 2016)
- It is the primary cause of emergency room visits among children with autism and leads to an increased risk of psychiatric hospitalization (Kalb et al., 2012)
- Automatically reinforced SIB (ASIB) is less understood and more resistant to treatment (Iwata et al., 1994)
- The purpose of this study was to identify different subtypes of automatically reinforced self injurious behavior (ASIB) using patterns of happiness (e.g. smiling) and distress (e.g. crying)
- Our hypothesis was that children with IDD would not show the same indices of emotion while engaging in ASIB

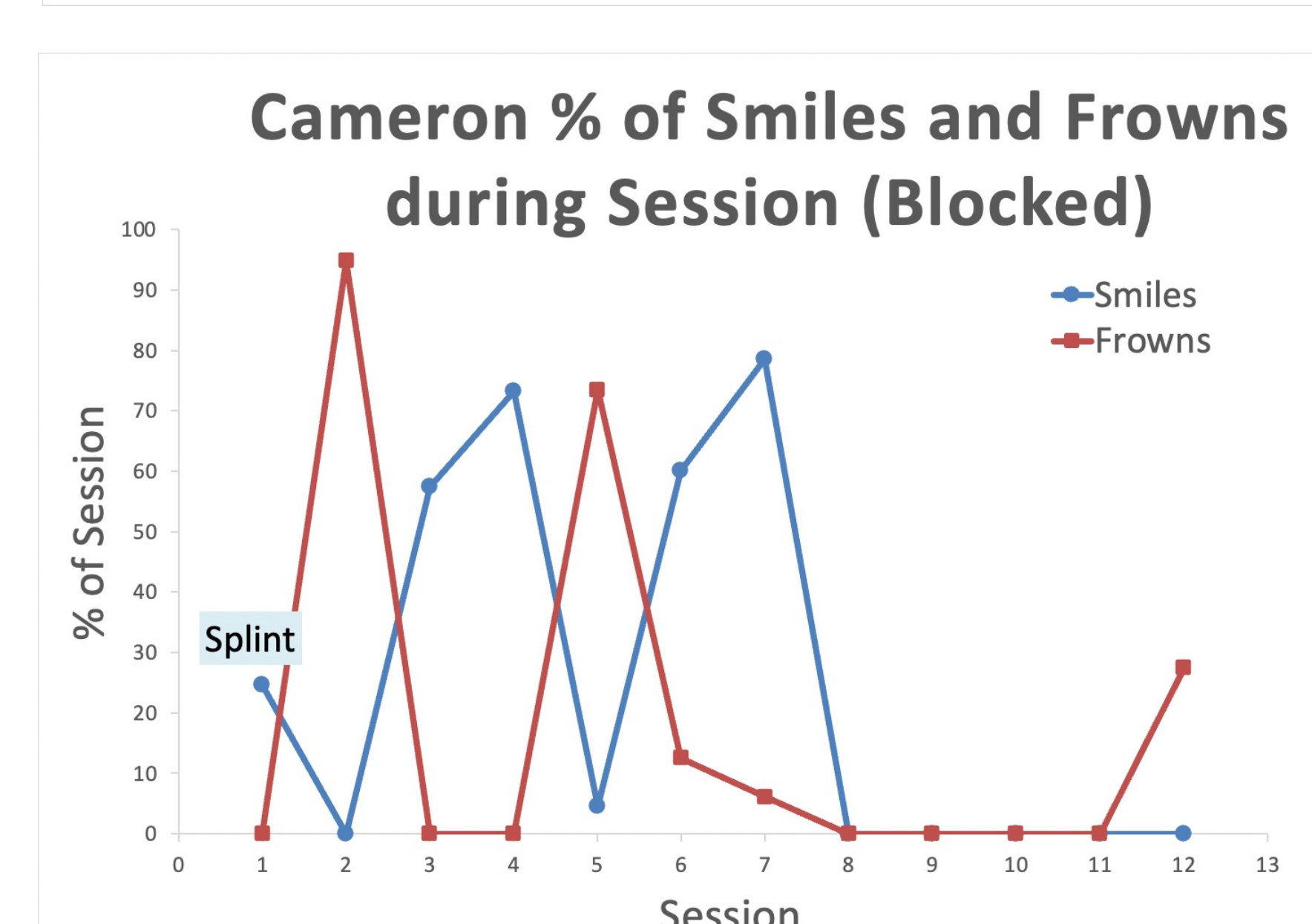
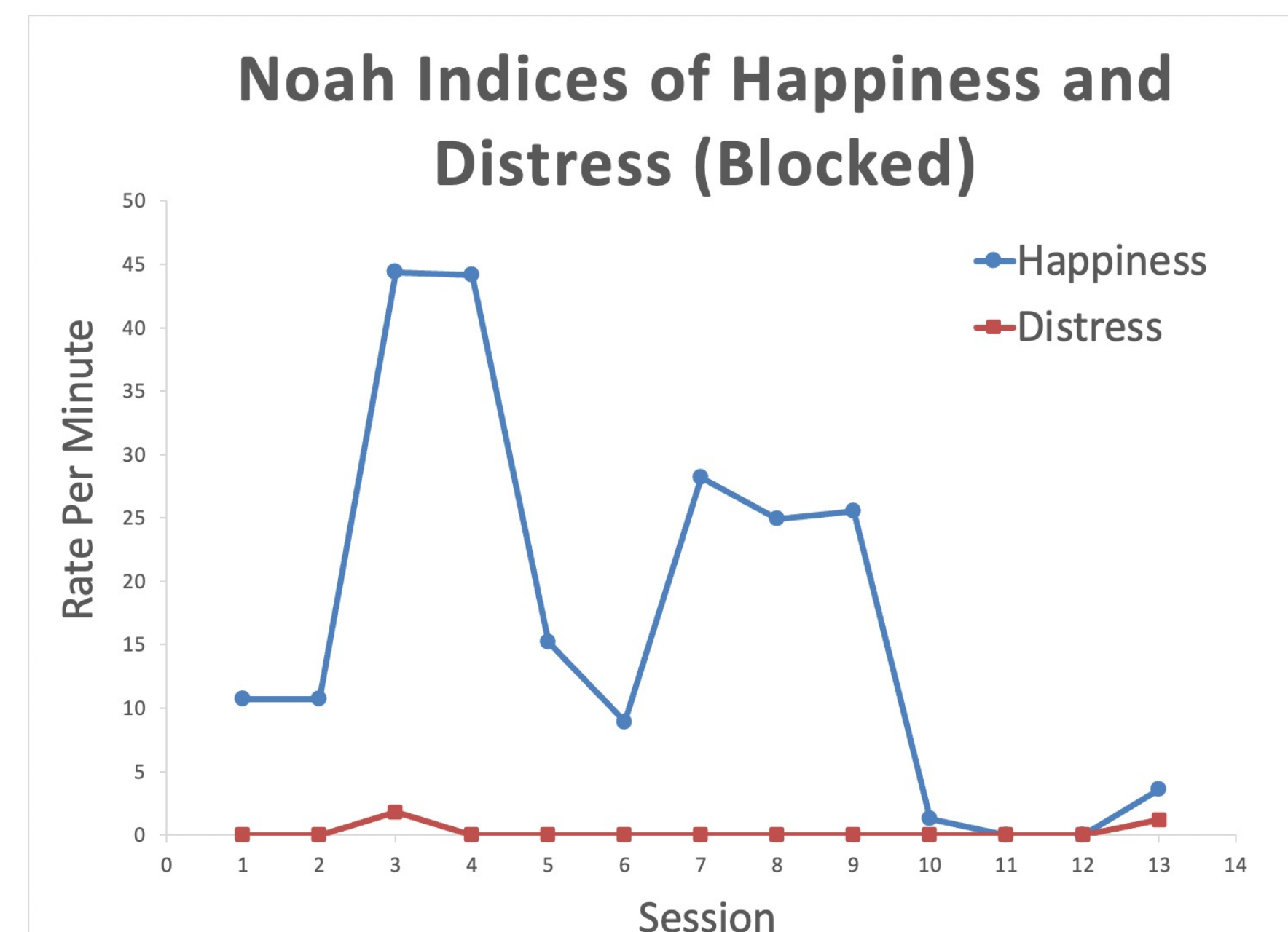
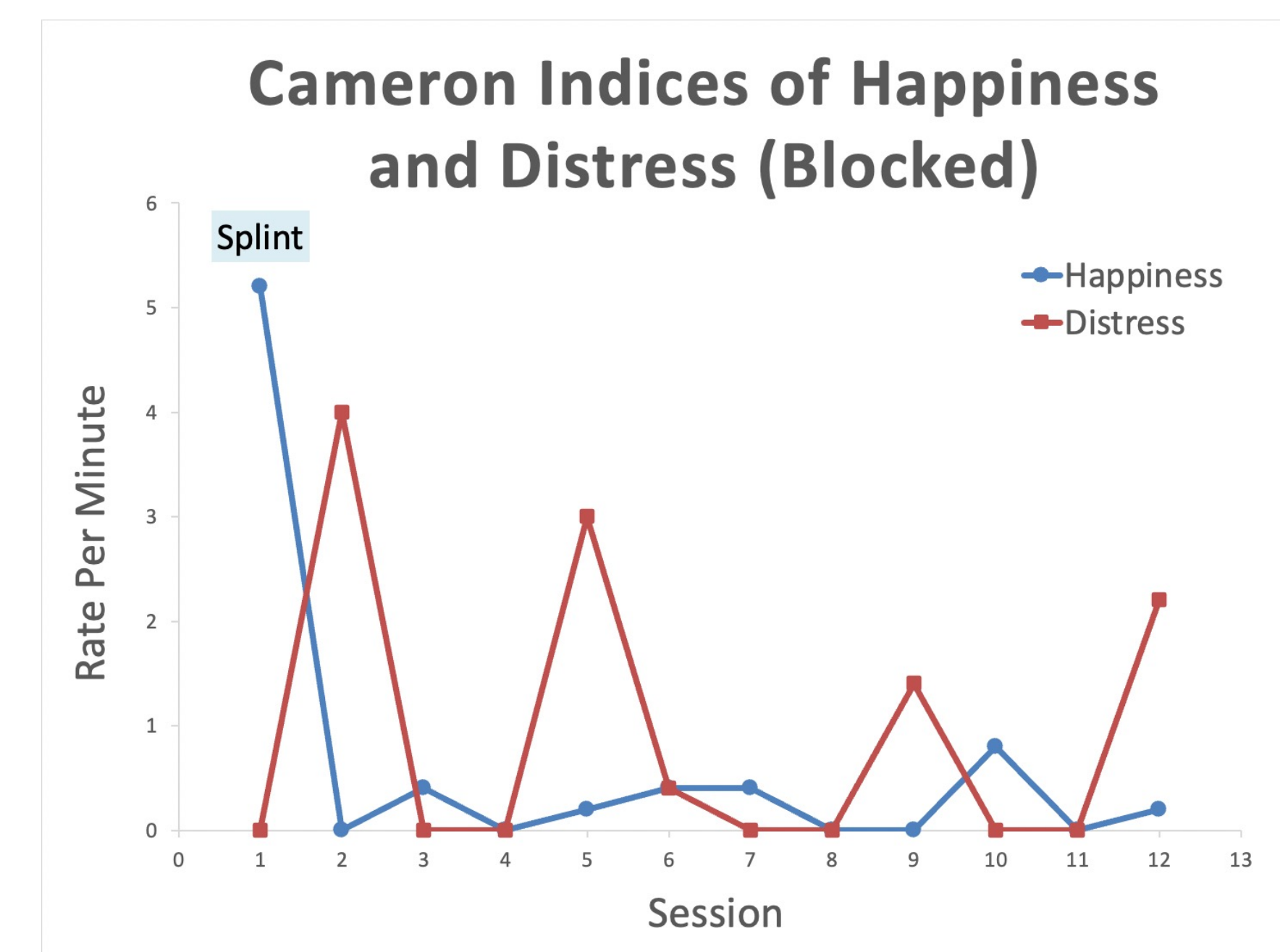
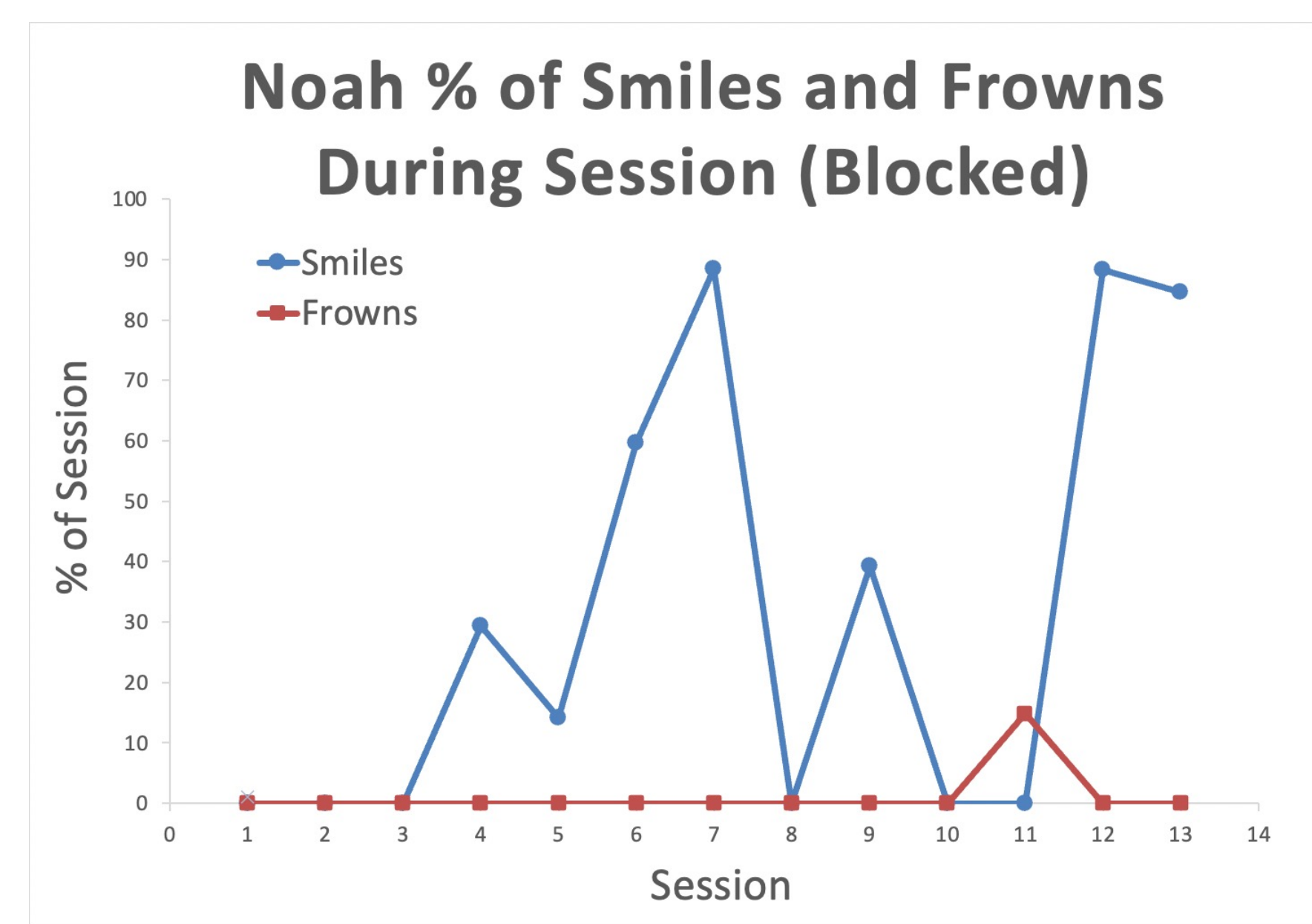
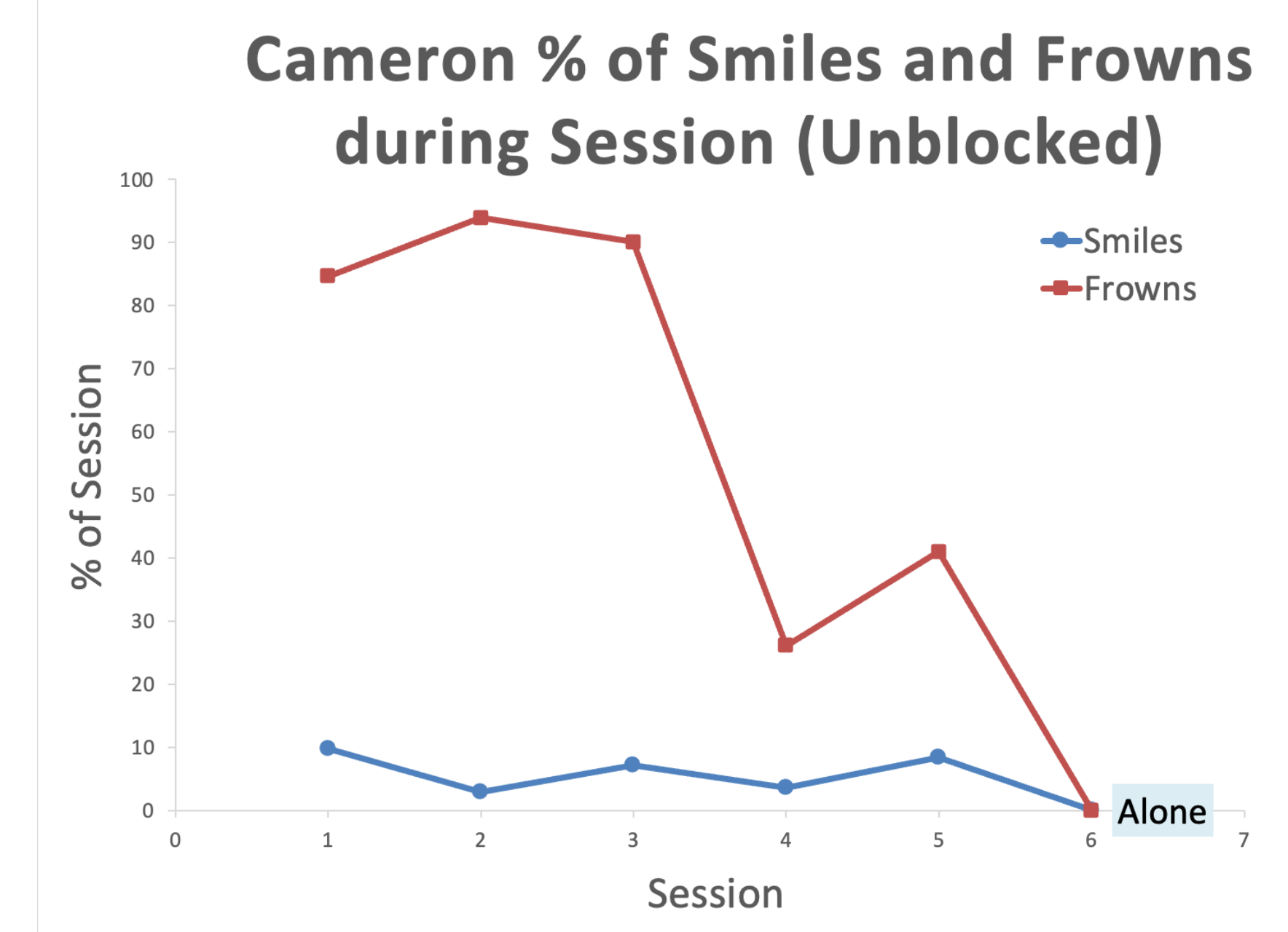
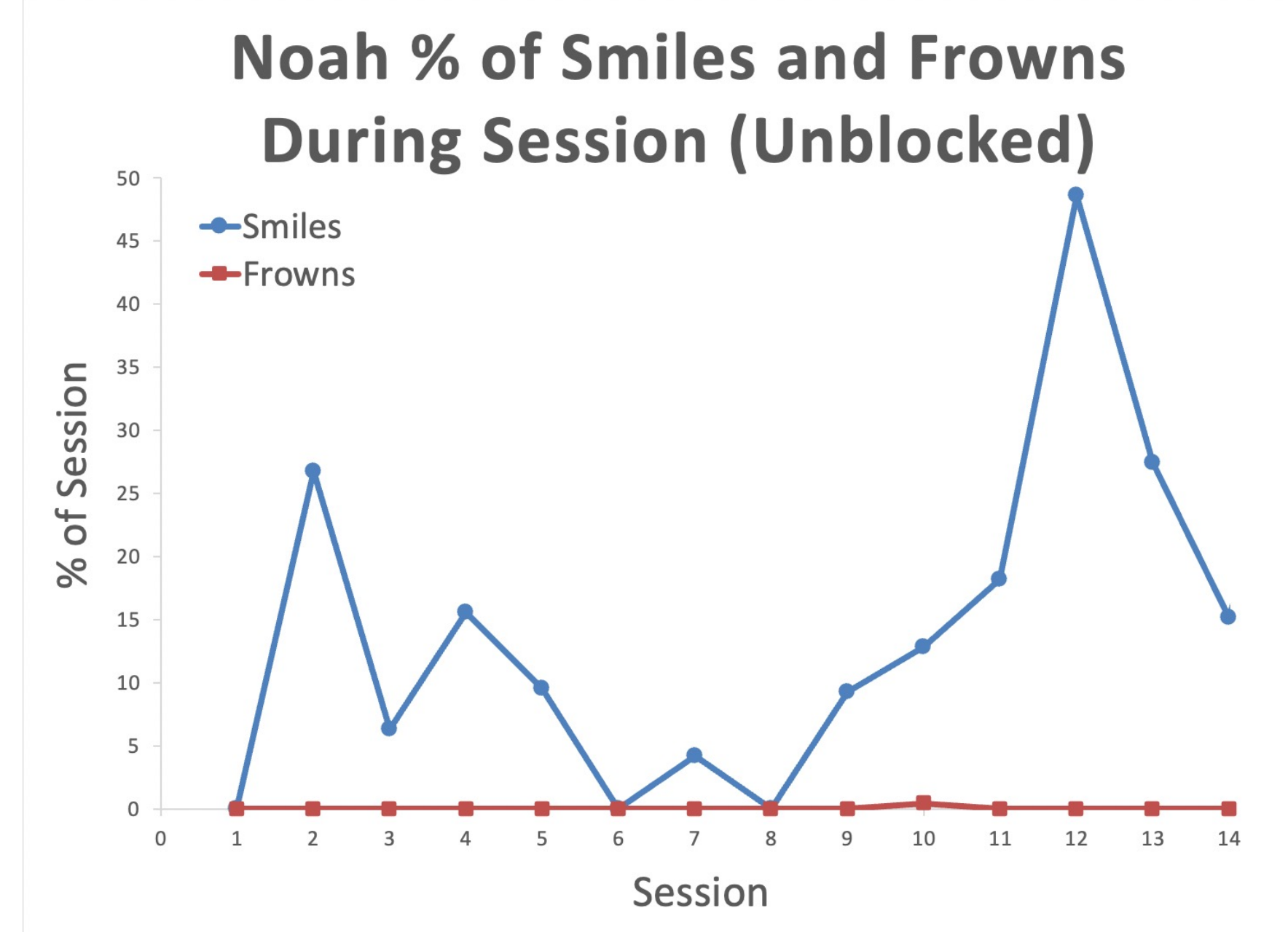
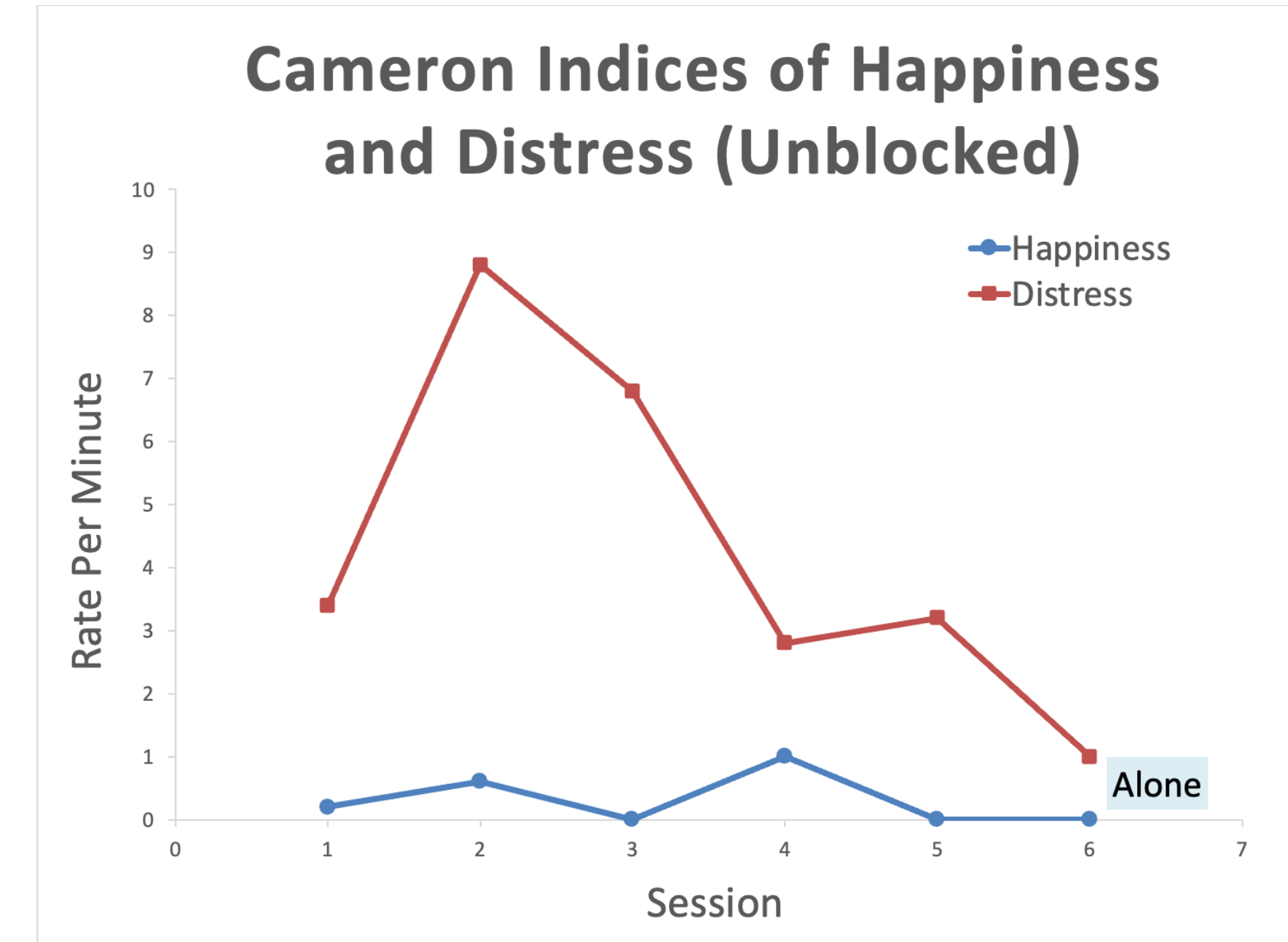
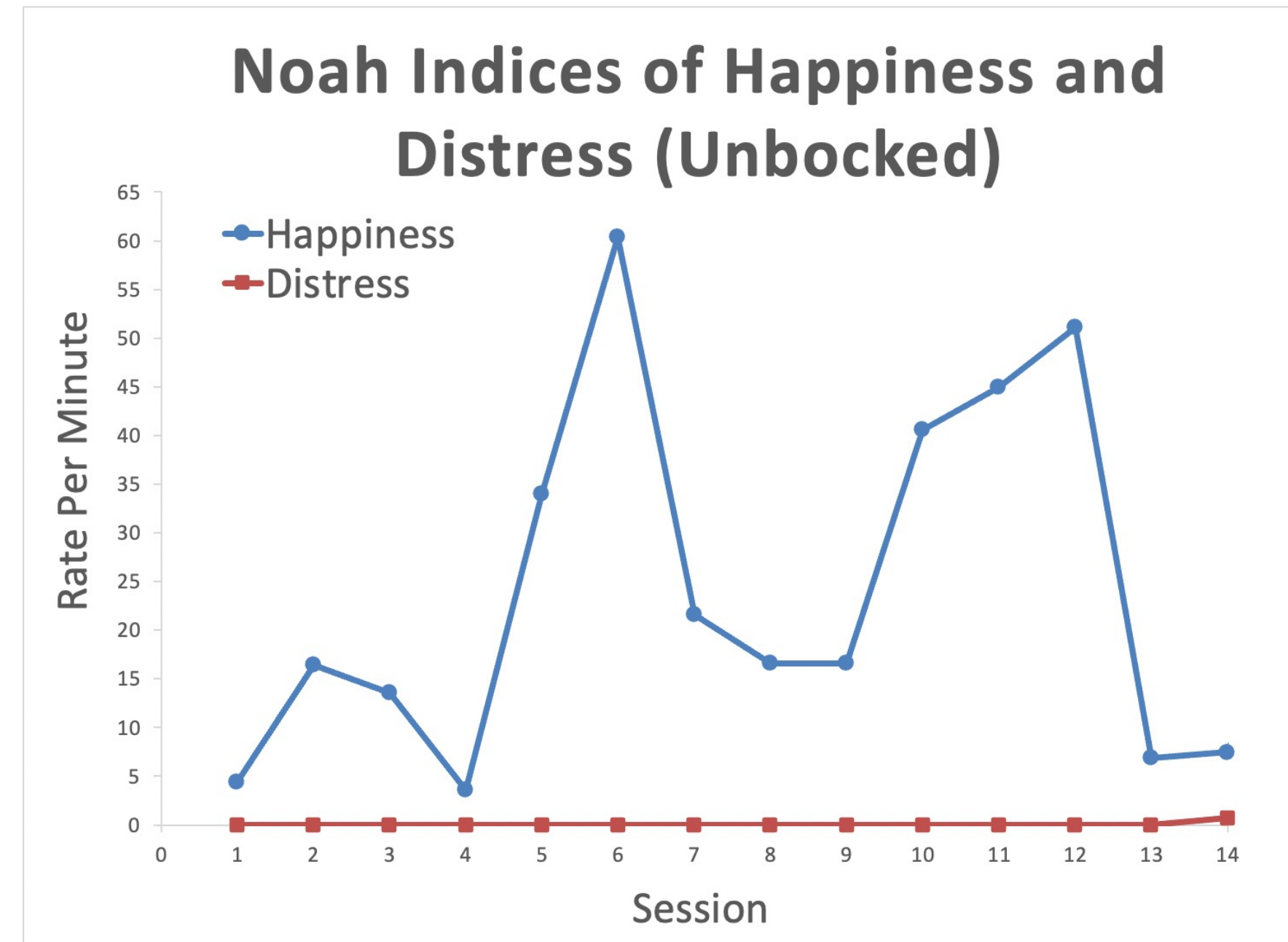


Methods

- Parent surveys were used to **individually define** indices for two patients with severe ASIB
- Recorded sessions of various stages of treatment were coded for indices using a behavioral event logging software

Noah	Cameron
Autism spectrum disorder Severe intellectual disability	Traumatic brain injury Moderate intellectual disability
Severe bilateral blindness, hearing loss, non-vocal	Underlying biomedical conditions (e.g. pancreatitis)
H1: auto-positive reinforcement (higher happiness than distress)	H2: auto-negative reinforcement (higher distress than happiness)

Results



Discussion

•Results consistent with hypothesis that individuals show clear differences in indices of happiness and distress while engaging in ASIB

	Noah	Cameron
Blocked	Higher indices of happiness slight increases in distress, but overall rates were remained extremely low	Slightly higher levels of distress, but no clear differentiation (overlap) % of smiles rose significantly
Unblocked	Higher indices of happiness, very low indices of distress	Higher indices of distress with clear differentiation (no overlap)
Class of Reinforcement (+ or -)	Suggests auto-positive reinforcement, especially due to sensory impairments	Suggests auto-negative reinforcement, to relieve aversive state caused by biomedical conditions

Conclusions

- Individuals display different patterns of emotion while engaging in ASIB, which suggests differences in underlying motivations
- Clinical practice would benefit from treating ASIB based on different functional categories for more effective treatment
- Indices of happiness and distress should be further explored as a potential method of subtyping ASIB for a larger IDD population

References

Iwata, B. A., Pace, G. M., Dorsey, M. F., Zarcone, J. R., Vollmer, T. R., Smith, R. G., Rodgers, T. A., Lerman, D. C., Shore, B. A., Mazaleski, J. L., Goh, H.-L., Cowdery, G. E., Kalsher, M. J., McCosh, K. C., & Willis, K. D. (1994). The functions of self-injurious behavior: An experimental-epidemiological analysis. *Journal of Applied Behavior Analysis*, 27(2), 215-240. <https://doi.org/10.1901/jaba.1994.27-215>

Kalb, L. G., Stuart, E. A., Freedman, B., Zablotsky, B., & Vasa, R. (2012). Psychiatric-related emergency department visits among children with an autism spectrum disorder. *Pediatric Emergency Care*, 28(12), 1269-1276. <https://doi.org/10.1097/pec.0b013e3182767d96>

Soke, G. N., Rosenberg, S. A., Hamman, R. F., Fingerlin, T., Robinson, C., Carpenter, L., ... & DiGiuseppe, C. (2016). Brief report: Prevalence of self-injurious behaviors among children with Autism Spectrum Disorder—A population-based study. *Journal of Autism and Developmental Disorders*, 46, 3607-3614. <https://doi.org/10.1007/s10803-016-2879-1>

Training Models to Analyze Reasons in Anti-Mask Tweets

Anne Zhang¹, Elizabeth North², Min Zhang³, Ling Tong³, Weiguo (Patrick) Fan³

¹Lexington High School

²Saint Andrew's School

³University of Iowa

IOWA

Introduction

The COVID-19 pandemic has had devastating impacts worldwide. An abundance of mitigation strategies like facial masks, social distancing, and vaccines, were developed to aid relief efforts.

- Our research group seeks to identify and analyze reasons why people would not wear masks or follow mask mandates.
- The virus's behavior in communities relies on the extent to which masks are available to and accepted by it. Understanding sources of people's stances is crucial in guiding public health officials to employ effective policies against the coronavirus.

Methods

- With 10,000 tweets against masks, reasons for each's position were identified, findings cross-checked, and data discrepancies sent for a third-party review.
- The text of our data was preprocessed by removing cases, numbers, punctuation, and urls, stemming, lemmatizing, and cleaning tokens, and removing stop words.
- Most common bigrams in our data were discovered (fig. 1).

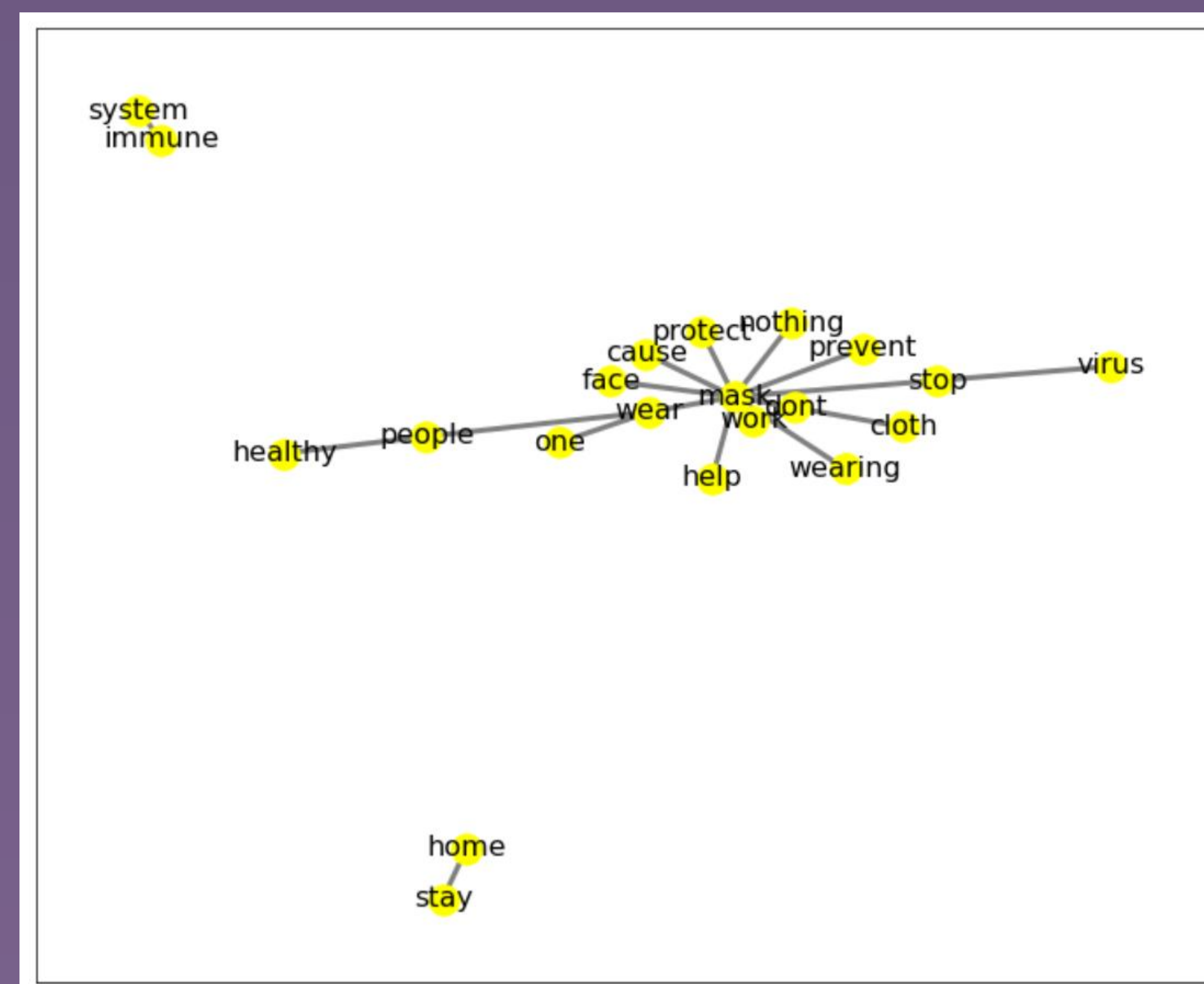


Figure 1: Network of prevalent bigrams

- Binary classification separated 10k tweets into reasons and no reasons.
- Via topic modelling with Latent Dirichlet allocation (LDA), trained a model to group tweets with most prominent similarities in types of reasoning.
- Tested LDA model to see what number of topics used would have optimal coherence score and decided with discretion on 7 categories (fig. 2).



Figure 4: Masks cause illness



Figure 5: Masks are unconstitutional

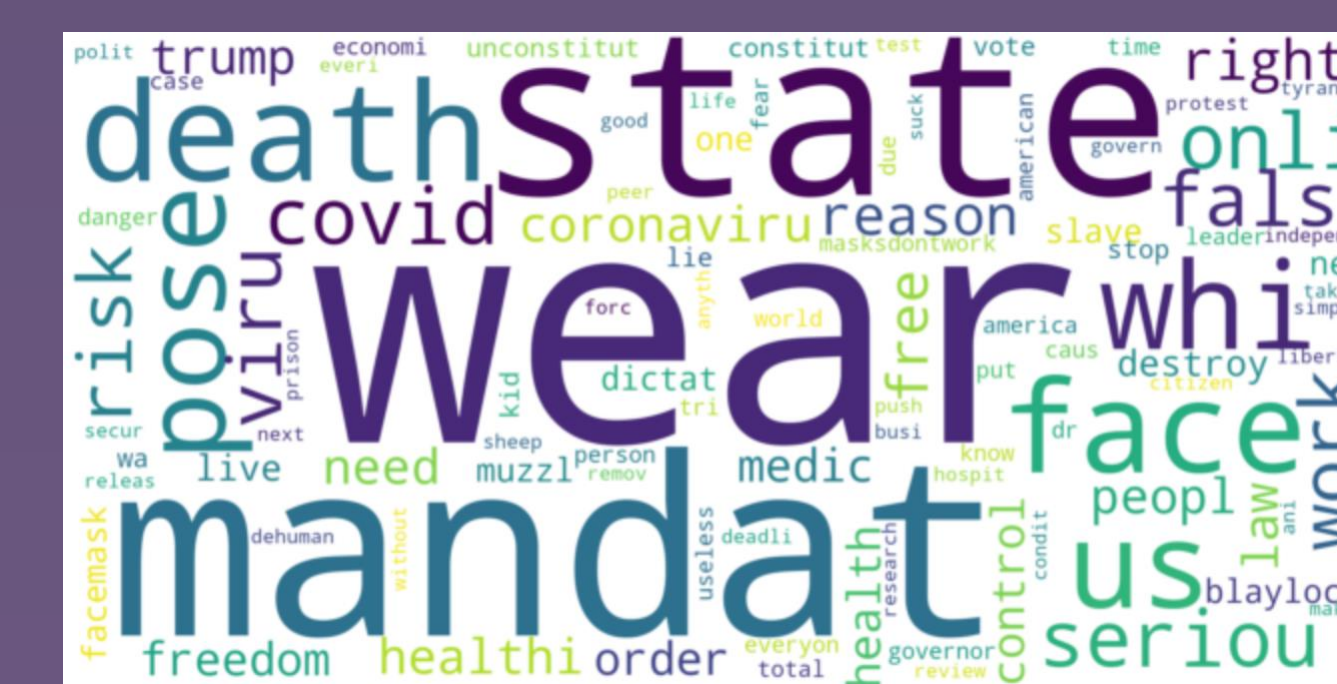


Figure 6: Masks are forced by the state



Figure 7: Masks violate our freedom



Figure 8: Masks don't work

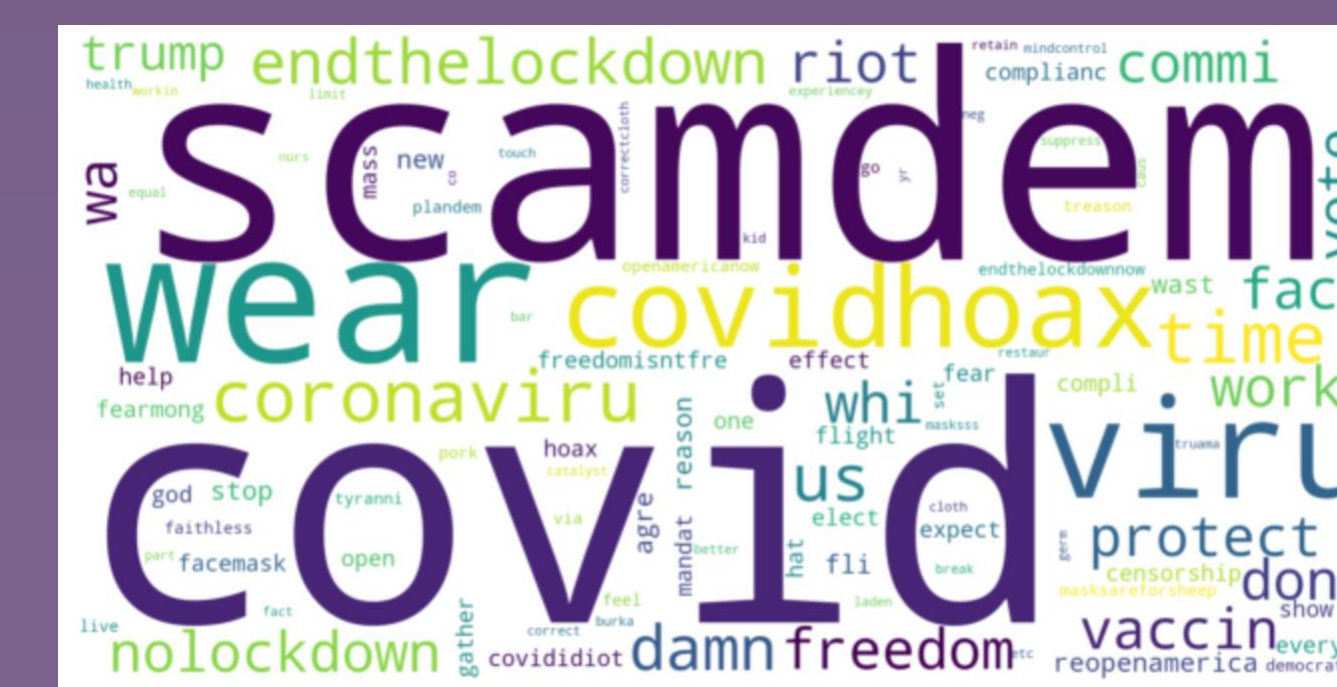


Figure 9: COVID is a hoax



Figure 10: Masks are used to control you

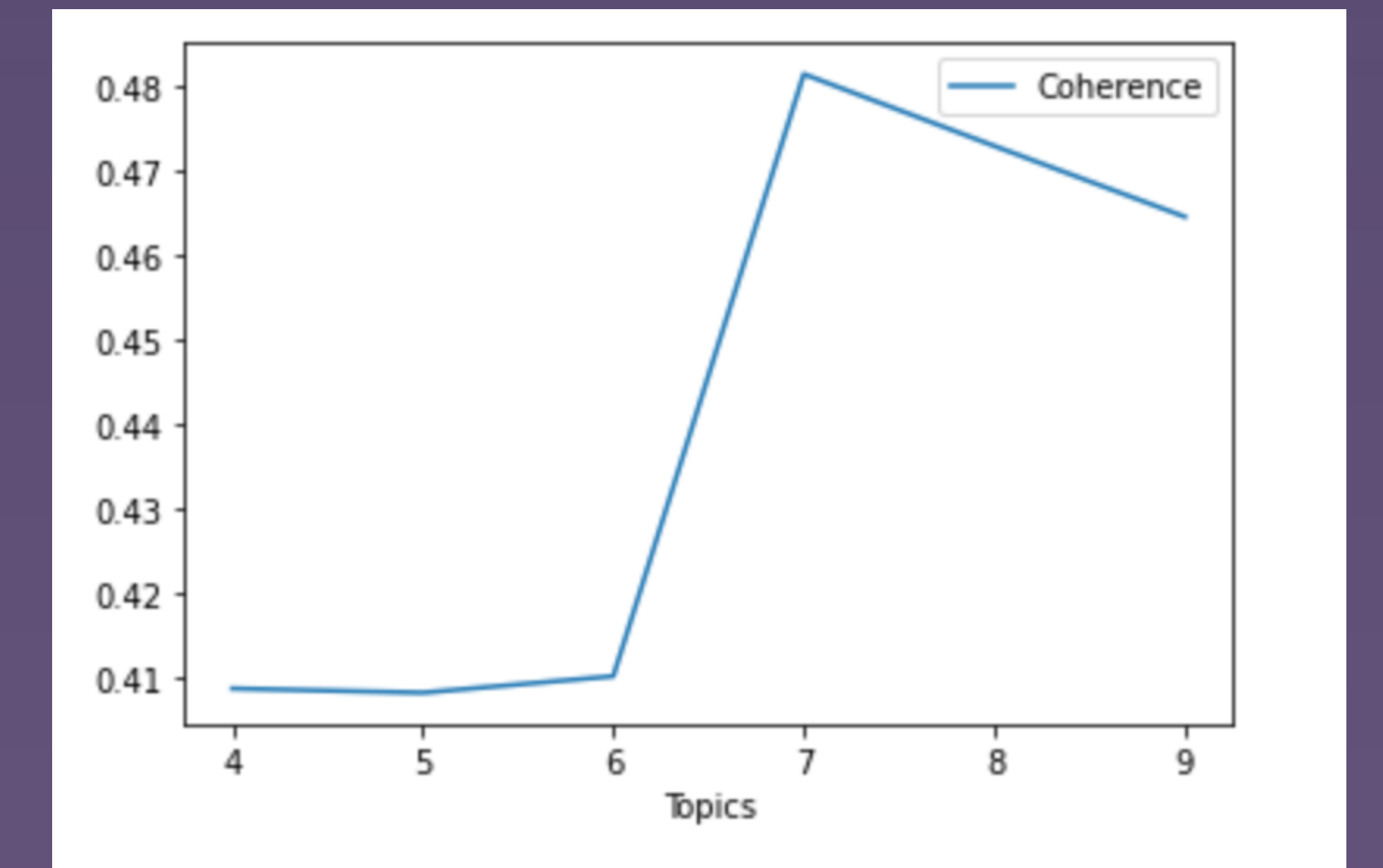


Figure 2: Number of topics vs. coherence

- Hyperparameters, alpha and beta, were adjusted accordingly. Each existing tweet was assigned a topic (fig. 3).

text_clean	label_final	reason_binary_label	topic0	topic1	topic2	topic3	topic4	topic5	topic6	assigned_topic	
the gov not has nothing to do with this...face...	against		1	0.623997	0.014305	0.304485	0.014299	0.014305	0.014306	0.014303	topic0
because a mask does not save lives!	against		1	0.071725	0.071438	0.071438	0.571093	0.071435	0.071437	0.071434	topic3
i refuse to wear a mask because i am not sick	against		1	0.855671	0.024079	0.024051	0.023971	0.024011	0.024018	0.023998	topic0

Figure 3: Topics assigned to text

Results

- After topic modelling, visualizations with term weighting of prominent words were created within each of 7 topics (fig. 4-10). We defined each topic with an overarching reason for attitudes against masks.
- When trained and tested following preprocessing and hyperparameter adjustment, decision tree model achieved accuracy rating of around 0.70.

Conclusion

- With further fine-tuning of our model, it is likely to be able to reach a higher accuracy rating in testing.
- Future plan is to run larger dataset of 1 million anti-masking tweets through the model to predict topics.
- Our hope is that it someday reliably assists in identifying reasoning, even past specific question posed.

Acknowledgments

I would like to thank Elizabeth North for being an incredible partner. I greatly appreciate Min Zhang and Ling Tong for their invaluable guidance and assistance throughout, as well as Dr. Weiguo (Patrick) Fan's support. Finally, I'm beyond grateful that the Secondary Student Training Program provided me with this opportunity to conduct research at their facilities.

Investigating Point Defects in Zeolitic Imidazolate Framework-7

Zhehao Zhang¹, Akalanka Ekanayake², Collin Hill², Alexei Tivanski²

¹The Webb Schools, Claremont, CA;

²Department of Chemistry, University of Iowa

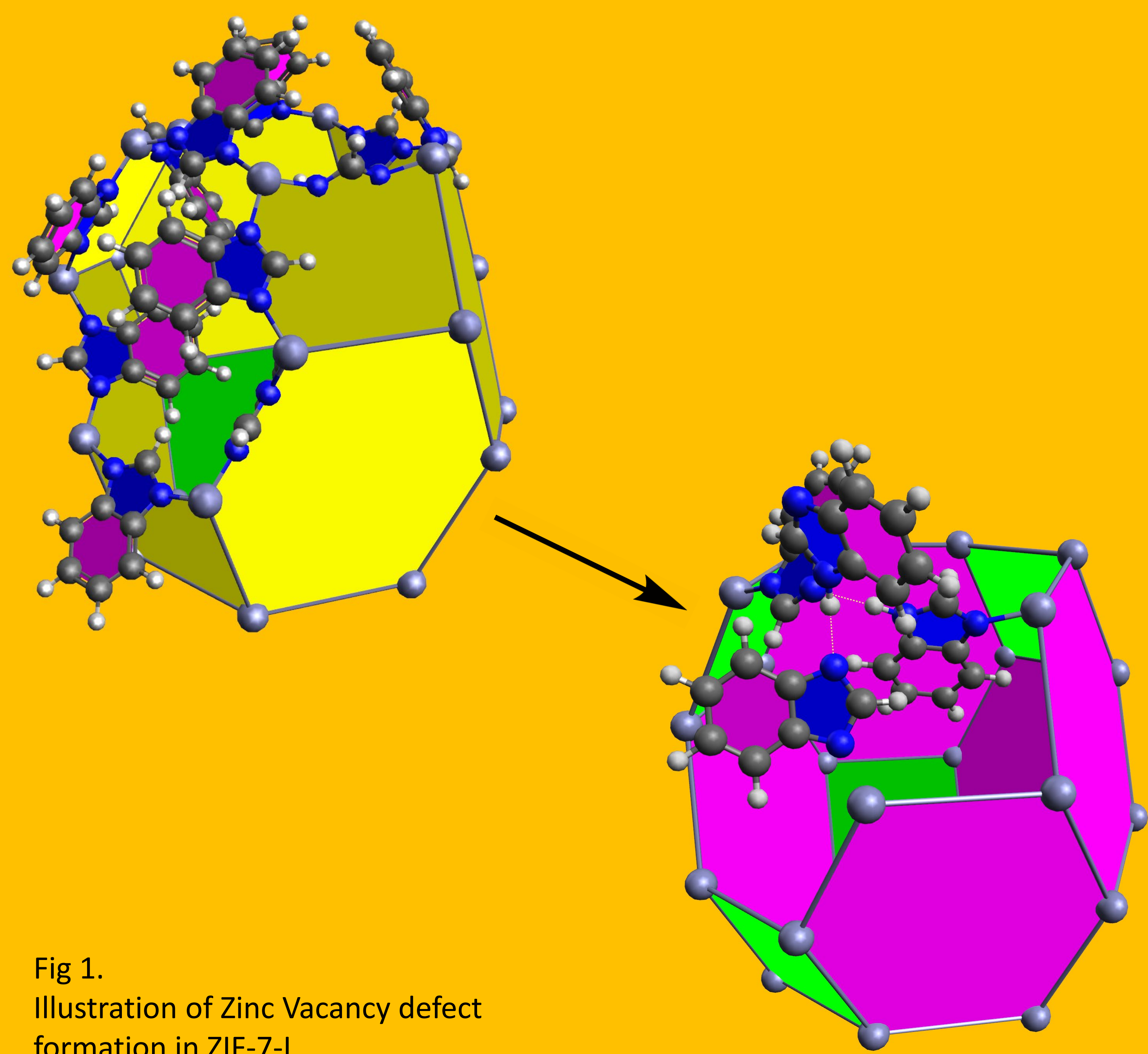


Fig 1. Illustration of Zinc Vacancy defect formation in ZIF-7-I

Background

Recently, the mechanism of the ZIF-7 gate-opening effect was determined: a benzimidazole linker rotation¹. It has also been found that there exists a size-dependency in this gate-opening effect², and our group also found that the ZIF-7 crystal size can affect the crystal's young's modulus. However, defects' effects are greatly overlooked in current simulations of ZIF-7, as they assume that ZIF-7 are perfect crystals^{1,3,4}, and we postulate that the overlooked defects could be the reason behind this size-dependency.

Methods

1. Compared PBE-DRSLL and variant with VWN correlation changed to PBE⁵ correlation
 - VWN⁶ correlation with DRSLL⁷ correction is too hard
 - PBE correlation with DRSLL correction is too soft, but error is less than VWN.
2. Optimized ZIF-7-I and ZIF-7-II structure
 - Lattice constants fixed to experimental values
 - used PBE correlation and PBE exchanged mixed with DRSLL Van der Waals exchange correction
3. Optimized defect-containing ZIF-7-I and ZIF-7-II structures
 - Used same functional as optimizing defect-free structures
 - formulated structures from perfect crystals, and then optimized within a 1x1x2 supercell

4. We will then find the transition state of defect formation with IRC to determine the kinetics of defect formation
5. Then, the Finite-deformation Nudged Elastic Band method⁸ will be employed to find the transition state energy of phase transition of defect-free and defected ZIF-7s to determine the effect of defects on the gate-opening effect
6. Also, we will measure the stress tensors during deformation of defected ZIF-7 to determine the effect of defects on the stiffness of the crystal.

Results

-Had begun the geometry optimization of different defect-containing ZIF-7-I and ZIF-7-II structures

-Determined that Zn leaving the structure and forming $Zn(NO_3)_2$ is a extremely thermodynamically feasible defect in ZIF-7-I, with $\Delta H = -144$ kJ, but maybe kinetically slow and entropy producing.

-Discovered when limiting the lattice constants to be fixed, ZIF-7-II optimization is converging extremely slowly, suggesting defect could drastically lower the barrier for phase change, and the energy minimum present for ZIF-7-II structure could be practically eliminated due to the defect

Table 1. Calculated Enthalpy change of zinc vacancy defect formation processes in ZIF-7-I

ZIF-7-I+2H ₂ O=	ZIF-7-I+2HNO ₃ =
ZnOH ₂ (s)+ZIF-7-I-VZn	Zn(NO ₃) ₂ (s)+ZIF-7-I-VZn
20.279158036962 kJ	-144.00427316956 kJ

Objectives

1. What are the **defect structures** of ZIF-7 and the **energetics** of their **formation processes**?
2. How would the **defects present in ZIF-7** affect the **gas adsorption** and **mechanical properties** of the crystal?



For extra supplementary information like input files for cp2k scan this QR code

Future Directions

Apart from continuing and finishing this work, there are a series of future directions this could apply in:

- Guiding and educating controlled defect formation, such as hydrolysis of ZIF-7, using mixed linkers to form defects, etc. to obtain crystals with defects that produce desired properties
- Could apply to defects' effects in other crystals with phase-changing properties

References

- Zhao, P., Fang, H., Mukhopadhyay, S., Li, A., Rudić, S., McPherson, I. J., Tang, C. C., Fairen-Jimenez, D., Tsang, S. C., & Redfern, S. A. (2019). Structural Dynamics of a metal-organic framework induced by CO₂ migration in its non-uniform porous structure. *Nature Communications*, 10(1). <https://doi.org/10.1038/s41467-019-08939-y>
- Cai, W., Lee, T., Lee, M., Cho, W., Han, D.-Y., Choi, N., Yip, A. C., & Choi, J. (2014). Thermal structural transitions and carbon dioxide adsorption properties of zeolitic imidazolate framework-7 (ZIF-7). *Journal of the American Chemical Society*, 136(22), 7961–7971. <https://doi.org/10.1021/ja5016298>
- Dixit, M., Major, D. T., & Pal, S. (2016). Hydrogen adsorption in zif-7: A DFT and ab-initio molecular dynamics study. *Chemical Physics Letters*, 651, 178–182. <https://doi.org/10.1016/j.cplett.2016.03.030>
- Zhang, Z., Yang, K. R., & Xu, X. (2019). Understanding the separation mechanism of C₂H₆/C₂H₄ on Zeolitic Imidazolate Framework zif-7 by periodic DFT investigations. *The Journal of Physical Chemistry C*, 124(1), 256–266. <https://doi.org/10.1021/acs.jpcc.9b04872>
- Perdew, J. P., Burke, K., & Ernzerhof, M. (1996). Generalized gradient approximation made simple. *Physical Review Letters*, 77(18), 3865–3868. <https://doi.org/10.1103/physrevlett.77.3865>
- Vosko, S. H., Wilk, L., & Nusair, M. (1980). Accurate spin-dependent electron liquid correlation energies for local spin density calculations: A critical analysis. *Canadian Journal of Physics*, 58(8), 1200–1211. <https://doi.org/10.1139/p80-159>
- Dion, M., Rydberg, H., Schröder, E., Langreth, D. C., & Lundqvist, B. I. (2004). Van der waals density functional for general geometries. *Physical Review Letters*, 92(24), 246401–246405. <https://doi.org/10.1103/physrevlett.92.246401>
- Ghasemi, A., Xiao, P., & Gao, W. (2019). Nudged elastic band method for solid-solid transition under finite deformation. *The Journal of Chemical Physics*, 151(5), 054110. <https://doi.org/10.1063/1.5113716>



Special thanks to the Tivanski group for guidance and inspiration, and the IT services for all the help with the Argon Cluster!

IOWA